

# World Journal of *Gastroenterology*

*World J Gastroenterol* 2022 August 7; 28(29): 3753-4018



**REVIEW**

- 3753 Mechanistic and functional extrapolation of SET and MYND domain-containing protein 2 to pancreatic cancer  
*Alshammari E, Zhang YX, Yang Z*

**MINIREVIEWS**

- 3767 Clinical challenge for gastroenterologists–Gastrointestinal manifestations of systemic mastocytosis: A comprehensive review  
*Elvevi A, Elli EM, Lucà M, Scaravaglio M, Pagni F, Ceola S, Ratti L, Invernizzi P, Massironi S*
- 3780 Structural changes of proteins in liver cirrhosis and consequential changes in their function  
*Gligorijević N, Minić S, Nedić O*
- 3793 Epidemiologic and socioeconomic factors impacting hepatitis B virus and related hepatocellular carcinoma  
*Gnyawali B, Pusateri A, Nickerson A, Jalil S, Mumtaz K*
- 3803 Endoscopic salvage therapy after failed biliary cannulation using advanced techniques: A concise review  
*Tsou YK, Pan KT, Lee MH, Lin CH*
- 3814 Enhanced endoscopic ultrasound imaging for pancreatic lesions: The road to artificial intelligence  
*Spadaccini M, Koleth G, Emmanuel J, Khalaf K, Facciorusso A, Grizzi F, Hassan C, Colombo M, Mangiavillano B, Fugazza A, Anderloni A, Carrara S, Repici A*

**ORIGINAL ARTICLE****Basic Study**

- 3825 Qingyi decoction attenuates intestinal epithelial cell injury *via* the calcineurin/nuclear factor of activated T-cells pathway  
*Wang GY, Shang D, Zhang GX, Song HY, Jiang N, Liu HH, Chen HL*
- 3838 High-fat diet aggravates colitis *via* mesenteric adipose tissue derived exosome metastasis-associated lung adenocarcinoma transcript 1  
*Chen D, Lu MM, Wang JH, Ren Y, Xu LL, Cheng WX, Wang SS, Li XL, Cheng XF, Gao JG, Kalyani FS, Jin X*
- 3854 Involvement of nitrergic neurons in colonic motility in a rat model of ulcerative colitis  
*Li YR, Li Y, Jin Y, Xu M, Fan HW, Zhang Q, Tan GH, Chen J, Li YQ*
- 3869 N-linked glycoproteomic profiling in esophageal squamous cell carcinoma  
*Liu QW, Ruan HJ, Chao WX, Li MX, Jiao YL, Ward DG, Gao SG, Qi YJ*

- 3886** HP0953 - hypothetical virulence factor overexpression and localization during *Helicobacter pylori* infection of gastric epithelium

*Arteaga-Resendiz NK, Rodea GE, Ribas-Aparicio RM, Olivares-Cervantes AL, Castelán-Vega JA, Olivares-Trejo JJ, Mendoza-Elizalde S, López-Villegas EO, Colín C, Aguilar-Rodea P, Reyes-López A, Salazar García M, Velázquez-Guadarrama N*

- 3903** Involvement of toll-like receptor 5 in mouse model of colonic hypersensitivity induced by neonatal maternal separation

*Mallaret G, Lashermes A, Meleine M, Boudieu L, Barbier J, Aissouni Y, Gelot A, Chassaing B, Gewirtz AT, Ardid D, Carvalho FA*

#### Case Control Study

- 3917** Comprehensive evaluation of microRNA as a biomarker for the diagnosis of hepatocellular carcinoma

*Malik J, Klammer M, Rolny V, Chan HLY, Piratvisuth T, Tanwandee T, Thongsawat S, Sukeepaisarnjaroen W, Esteban JJ, Bes M, Köhler B, Swiatek-de Lange M*

#### Retrospective Cohort Study

- 3934** Optimal timing of biliary drainage based on the severity of acute cholangitis: A single-center retrospective cohort study

*Lu ZQ, Zhang HY, Su CF, Xing YY, Wang GX, Li CS*

#### Retrospective Study

- 3946** Incidence and clinical characteristics of hypertriglyceridemic acute pancreatitis: A retrospective single-center study

*Lin XY, Zeng Y, Zhang ZC, Lin ZH, Chen LC, Ye ZS*

- 3960** Radiomics for differentiating tumor deposits from lymph node metastasis in rectal cancer

*Zhang YC, Li M, Jin YM, Xu JX, Huang CC, Song B*

- 3971** Effects of microwave ablation on serum Golgi protein 73 in patients with primary liver cancer

*Xu ZJ, Wei MJ, Zhang XM, Liu HG, Wu JP, Huang JF, Li YF, Huang ZJ, Yan YY*

#### Observational Study

- 3981** Evaluating the best treatment for multifocal hepatocellular carcinoma: A propensity score-matched analysis

*Risaliti M, Bartolini I, Campani C, Arena U, Xodo C, Adotti V, Rosi M, Taddei A, Muiasan P, Amedei A, Batignani G, Marra F*

- 3994** Structure of the myenteric plexus in normal and diseased human ileum analyzed by X-ray virtual histology slices

*Veress B, Peruzzi N, Eckermann M, Frohn J, Salditt T, Bech M, Ohlsson B*

#### META-ANALYSIS

- 4007** Recurrence rates after endoscopic resection of large colorectal polyps: A systematic review and meta-analysis

*Rotermund C, Djinbachian R, Taghiakbari M, Enderle MD, Eickhoff A, von Renteln D*

**ABOUT COVER**

Editorial Board Member of *World Journal of Gastroenterology*, Nikolaos Papadopoulos, MD, PhD, Consultant, The First Department of Internal Medicine, 417 Army Share Fund Hospital, Monis Petraki 10-12, Athens 11521, Greece. nipapmed@gmail.com

**AIMS AND SCOPE**

The primary aim of *World Journal of Gastroenterology* (WJG, *World J Gastroenterol*) is to provide scholars and readers from various fields of gastroenterology and hepatology with a platform to publish high-quality basic and clinical research articles and communicate their research findings online. WJG mainly publishes articles reporting research results and findings obtained in the field of gastroenterology and hepatology and covering a wide range of topics including gastroenterology, hepatology, gastrointestinal endoscopy, gastrointestinal surgery, gastrointestinal oncology, and pediatric gastroenterology.

**INDEXING/ABSTRACTING**

The WJG is now abstracted and indexed in Science Citation Index Expanded (SCIE, also known as SciSearch®), Current Contents/Clinical Medicine, Journal Citation Reports, Index Medicus, MEDLINE, PubMed, PubMed Central, Scopus, Reference Citation Analysis, China National Knowledge Infrastructure, China Science and Technology Journal Database, and Superstar Journals Database. The 2022 edition of Journal Citation Reports® cites the 2021 impact factor (IF) for WJG as 5.374; IF without journal self cites: 5.187; 5-year IF: 5.715; Journal Citation Indicator: 0.84; Ranking: 31 among 93 journals in gastroenterology and hepatology; and Quartile category: Q2. The WJG's CiteScore for 2021 is 8.1 and Scopus CiteScore rank 2021: Gastroenterology is 18/149.

**RESPONSIBLE EDITORS FOR THIS ISSUE**

Production Editor: *Ying-Yi Yuan*; Production Department Director: *Xiang Li*; Editorial Office Director: *Jia-Ru Fan*.

**NAME OF JOURNAL**

*World Journal of Gastroenterology*

**ISSN**

ISSN 1007-9327 (print) ISSN 2219-2840 (online)

**LAUNCH DATE**

October 1, 1995

**FREQUENCY**

Weekly

**EDITORS-IN-CHIEF**

Andrzej S Tarnawski

**EDITORIAL BOARD MEMBERS**

<http://www.wjgnet.com/1007-9327/editorialboard.htm>

**PUBLICATION DATE**

August 7, 2022

**COPYRIGHT**

© 2022 Baishideng Publishing Group Inc

**INSTRUCTIONS TO AUTHORS**

<https://www.wjgnet.com/bpg/gerinfo/204>

**GUIDELINES FOR ETHICS DOCUMENTS**

<https://www.wjgnet.com/bpg/GerInfo/287>

**GUIDELINES FOR NON-NATIVE SPEAKERS OF ENGLISH**

<https://www.wjgnet.com/bpg/gerinfo/240>

**PUBLICATION ETHICS**

<https://www.wjgnet.com/bpg/GerInfo/288>

**PUBLICATION MISCONDUCT**

<https://www.wjgnet.com/bpg/gerinfo/208>

**ARTICLE PROCESSING CHARGE**

<https://www.wjgnet.com/bpg/gerinfo/242>

**STEPS FOR SUBMITTING MANUSCRIPTS**

<https://www.wjgnet.com/bpg/GerInfo/239>

**ONLINE SUBMISSION**

<https://www.f6publishing.com>

## Mechanistic and functional extrapolation of SET and MYND domain-containing protein 2 to pancreatic cancer

Eid Alshammari, Ying-Xue Zhang, Zhe Yang

**Specialty type:** Oncology

**Provenance and peer review:**

Invited article; Externally peer reviewed.

**Peer-review model:** Single blind

**Peer-review report's scientific quality classification**

Grade A (Excellent): 0

Grade B (Very good): B, B

Grade C (Good): 0

Grade D (Fair): 0

Grade E (Poor): 0

**P-Reviewer:** Trna J, Czech Republic; Zafari N, Iran

**Received:** January 18, 2022

**Peer-review started:** January 18, 2022

**First decision:** April 11, 2022

**Revised:** April 24, 2022

**Accepted:** July 5, 2022

**Article in press:** July 5, 2022

**Published online:** August 7, 2022



**Eid Alshammari, Ying-Xue Zhang**, Department of Biochemistry, Microbiology, and Immunology, Wayne State University, Detroit, MI 48201, United States

**Zhe Yang**, Department of Biochemistry, Microbiology, and Immunology, Wayne State University School of Medicine, Detroit, MI 48201, United States

**Corresponding author:** Zhe Yang, PhD, Associate Professor, Department of Biochemistry, Microbiology, and Immunology, Wayne State University School of Medicine, 540 E Canfield St, Detroit, MI 48201, United States. [zyang@med.wayne.edu](mailto:zyang@med.wayne.edu)

### Abstract

Pancreatic ductal adenocarcinoma (PDAC) is one of the most lethal neoplasms worldwide and represents the vast majority of pancreatic cancer cases. Understanding the molecular pathogenesis and the underlying mechanisms involved in the initiation, maintenance, and progression of PDAC is an urgent need, which may lead to the development of novel therapeutic strategies against this deadly cancer. Here, we review the role of SET and MYND domain-containing protein 2 (SMYD2) in initiating and maintaining PDAC development through methylating multiple tumor suppressors and oncogenic proteins. Given the broad substrate specificity of SMYD2 and its involvement in diverse oncogenic signaling pathways in many other cancers, the mechanistic extrapolation of SMYD2 from these cancers to PDAC may allow for developing new hypotheses about the mechanisms driving PDAC tumor growth and metastasis, supporting a proposition that targeting SMYD2 could be a powerful strategy for the prevention and treatment of PDAC.

**Key Words:** Pancreatic ductal adenocarcinoma; Protein lysine methyltransferase; Histone/non-histone methylation; Oncogenic signaling pathways; Methyltransferase inhibitors

©The Author(s) 2022. Published by Baishideng Publishing Group Inc. All rights reserved.

**Core Tip:** The broad substrate specificity of SET and MYND domain-containing protein 2 (SMYD2) and its involvement in diverse oncogenic signaling pathways in numerous cancers have provided a wealth of information that could be extrapolated to the pancreatic ductal adenocarcinoma (PDAC) research field to expand our understanding of SMYD2 in PDAC development. This review not only discusses the known roles of SMYD2 in PDAC initiation and progression, but also aims to capitalize on a rich body of knowledge with respect to SMYD2's involvement in various signaling cascades to develop new hypotheses about the mechanisms of driving PDAC tumor growth and metastasis.

**Citation:** Alshammari E, Zhang YX, Yang Z. Mechanistic and functional extrapolation of SET and MYND domain-containing protein 2 to pancreatic cancer. *World J Gastroenterol* 2022; 28(29): 3753-3766

**URL:** <https://www.wjgnet.com/1007-9327/full/v28/i29/3753.htm>

**DOI:** <https://dx.doi.org/10.3748/wjg.v28.i29.3753>

## INTRODUCTION

Pancreatic cancer is one of the top ten leading causes of cancer-related mortality worldwide, accounting for about 448000 new cases and 441000 deaths in 2017[1]. Pancreatic cancer comprises several types of tumors that arise from the endocrine or exocrine components of the pancreas. The vast majority of pancreatic tumors arise from the exocrine cells, which make up the exocrine gland and the ducts of the pancreas. Pancreatic ductal adenocarcinoma (PDAC) is the most common and aggressive form of pancreatic cancer, which represents about 85% of pancreatic cancer cases[2]. The incidence and mortality rates of pancreatic cancer have dramatically increased over the past few decades and vary considerably across regions and populations, with the highest trends being recorded in developed countries[3]. Although the causes and mechanisms that initiate the formation and development of pancreatic cancer are still largely unknown, the variation in regions and populations may be attributed to the variance in some of the risk factors and the socioeconomic lifestyle identified for this disease, such as obesity, diabetes, and smoking. In the United States, the incidence of pancreatic cancer continues to increase, with an estimation of 60430 new cases and 48200 deaths in 2021, and it has become the fourth leading cause of cancer-related mortality[4]. Pancreatic cancer has the poorest prognosis among the top ten common cancers, with the current 5-year survival (OS) rate of just 10% [4], and it is expected to be the second most common cause of cancer death by 2030[5].

Diagnosis and treatment of PDAC are still challenging due to its multifactorial nature. It is predominantly diagnosed in advanced stages with unresectable tumors due to several reasons, including the lack of early detection methods, the lack of specific PDAC biomarkers and simple examinations, the retroperitoneal location of the pancreas, and the nonspecific symptoms due to its highly metastatic nature early in the disease course[6]. Also, PDAC incidence is significantly associated with age, with the highest incidence rates being in elderly people[1]. Given the poor overall health of the elderly, the surgical resection is not feasible for the majority of elderly PDAC patients, especially for those who have metastatic cancers that have spread to the nearby abdominal vessels and critical organs at diagnosis[7]. Only a small fraction of PDAC patients diagnosed in the early stage have resectable tumors. Although the surgery in combination with adjuvant therapy remains the only cure for PDAC patients, the overall survival rate of PDAC patients is poor, even for those PDAC populations who have undergone surgery [8-10]. PDAC patients, after surgical resection, usually develop acquired chemoresistance, with a high rate of recurrence due to the very heterogeneous biology of PDAC and the aggressive clinical behavior of this disease[6]. These factors may explain the high mortality in PDAC patients; therefore, it is of great importance to identify the molecular mechanism of PDAC pathogenesis and the involved signaling pathways in order to discover novel targets and potential biomarkers for PDAC diagnosis and therapy.

SET and MYND domain-containing protein 2 (SMYD2) has been linked with tumor progression, poor prognosis, or a worse malignant outcome in multiple human cancers including PDAC[11-16]. This protein belongs to a special class of protein lysine methyltransferases and is characterized by a conserved catalytic SET domain split by an MYND domain[11]. The MYND domain of SMYD2 is a zinc finger motif that facilitates the protein-protein interaction, while the SET domain, an evolutionarily conserved motif, catalyzes the transfer of methyl groups to lysine residues of target proteins using S-adenosylmethionine (SAM) as a donor substrate[12]. The carcinogenic potential of SMYD2 is exemplified by its ability to methylate a broad spectrum of proteins involved in cellular signaling, cell cycle control, and cell differentiation and proliferation[17-20]. SMYD2 is an epigenetic regulator that has histone lysine methyltransferase activity and can methylate histones H3K36 and H3K4[11,12]. Through the dimethylation of histone H3 at Lys36 (H3K36me<sub>2</sub>), SMYD2 was reported to downregulate gene transcription, which is further enhanced by Sin3A-mediated deacetylation to suppress cell proliferation [11]. On the other hand, methylation of histone H3K4 by SMYD2 is usually associated with gene activation, yet the exact underlying mechanism by which this SMYD2-mediated methylation regulates

cell proliferation is not well understood[12,21]. Several investigations revealed multiple nonhistone substrates of SMYD2, including the tumor suppressor p53, retinoblastoma-associated protein (RB), ER $\alpha$ , HSP90, PARP1, and PTEN (Table 1)[22-27]. For instance, the tumor suppressor p53 is an important nonhistone target that is monomethylated by SMYD2 at Lys370 located in the regulatory domain of p53, repressing the p53's transcriptional regulatory activity and promoting cancer initiation and growth[22]. It has also been shown that through its broad methyltransferase activity on nonhistone proteins, SMYD2 impacts various signaling pathways required for the development and progression of the malignancies [17,28-32]. These pathways include the critical signaling cascade RTK/Ras, the downstream signaling cascades of the RTK/Ras pathway, such as the mitogen-activated protein kinase (MAPK) pathway, and the PI3K/AKT pathway[16,27,28,30,31]. As dysregulation of these signaling pathways is an almost universal phenomenon in cancer, it is not surprising that SMYD2 overexpression has been linked with tumor development and progression in multiple human cancers, such as gastric cancer[33], esophageal squamous cell carcinoma[34], breast cancer[30], bladder cancer[23], colon cancer[31,35], colorectal cancer[36], hepatocellular carcinoma[14], acute lymphoblastic leukemia[37,38], hematopoietic leukemias [39], head and neck squamous cell carcinoma[15], lung adenocarcinoma[13], papillary thyroid carcinoma[40], cervical cancer[41,42], ovarian clear cell carcinoma[43,44], and renal cell carcinoma[45,46] (Table 2).

Because of SMYD2 overexpression in numerous human tumors (Figure 1A), understanding the molecular mechanisms of SMYD2 in cancer initiation and development, and validating its therapeutic potential as a drug target to inhibit abnormal cell proliferation, have gained increasing interest in recent years; currently, SMYD2 is one of the most extensively studied protein lysine methyltransferases in the context of cancer. However, the involvement of SMYD2 in PDAC initiation and progression has not yet been fully explored. The overexpression of SMYD2 has been reported in PDAC by a study that showed methylation of the human MAPK activated protein kinase 3 (MAPKAPK3) by SMYD2 promotes tumor growth and progression[16]. Another investigation identified that the SMYD2 Locus is among the active chromatin sites unique to the genomes of the adenocarcinoma of the pancreas (ASCP) and is associated with the active H3K4me1 histone mark[47]. These pioneering works, despite being limited in scope, demonstrate that SMYD2-mediated methylation of both histone and nonhistone proteins could also be an important tumorigenic event contributing to PDAC initiation and development. On the other hand, a rich body of knowledge available in many other human cancers with respect to the roles of SMYD2 in cell cycle control and various signaling cascades provides a wealth of information that could be extrapolated to the PDAC research field to expand our understanding of SMYD2 in PDAC development. Here, we review the known roles of SMYD2 in PDAC initiation and progression, and through capitalizing on the current knowledge about its known cancer-related functions in other human cancers, we propose there existing additional SMYD2-mediated methylation events involved in diverse signaling pathways that control and coordinate different cellular processes in PDAC.

## CURRENT EVIDENCE OF SMYD2 INVOLVEMENT IN PANCREATIC CANCER

One study aimed to investigate the function of SMYD2 in PDAC using mouse and cellular models found evidence that SMYD2 plays a pivotal role in the development of this deadly pancreatic cancer[16] (Figure 1B). In other human cancers, SMYD2 usually exerts its tumorigenic effects through methylating cell signaling-related proteins and through the effect of such methylation on the targets' activity, stability, or subcellular localization[13,27,42,48]. Such a methylation-oriented mechanism has been instrumental for the initial development of a mechanistic hypothesis of SMYD2 involvement in PDAC and for the subsequent success of establishing a novel link of SMYD2 to promoting PDAC growth and progression[16]. Using an *in vitro* protein-array system, which consists of about 9500 human proteins, 159 proteins were identified as SMYD2 substrates in this study. Among these hits, MAPKAPK3 was selected for further analysis due to being implicated in cancer and being linked to Ras signaling, a key driver of PDAC[16,49-52]. Although the roles of MAPKAPK3, like those of SMYD2, in PDAC were unknown at the time of the study, MAPKAPK3 has been known as a mediator in the MAPK/ERK cascade that is responsible for regulating a wide variety of stimulated cellular processes[53-55]. It has also been shown that MAPKAPK3, phosphorylated by ERK1/2, p38 kinase, and SAPK/JNK, plays a role in inflammation and stress responses[56-59]. Therefore, the identification of MAPKAPK3 as a new SMYD2 substrate suggested a novel regulatory axis in PDAC progression.

Further characterization confirmed that the SMYD2-MAPKAPK3 axis is required for efficient PDAC development and that SMYD2-mediated methylation of MAPKAPK3 is a key event during the K-Ras-driven transformation of PDAC cells *in vivo*[16]. Lys355 of MAPKAPK3 was identified as a site of methylation targeted by SMYD2 using a mutagenesis approach and an LC-MS/MS analysis. Specificity analyses using an MS approach showed that the related protein MAPKAPK2, which shares about 75% sequence identity with MAPKAPK3, as well as other MAPKAPK proteins, are not substrates of SMYD2. On the other hand, none of the eight active lysine methyltransferases, including SMYD3 and SET8, could methylate MAPKAPK3 *in vitro*. Co-expression of SMYD2 and MAPKAPK3 in PDAC cells identified MAPKAPK3-K355me1 in a SMYD2-dependent manner, demonstrating that only SMYD2 can

Table 1 Major SET and MYND domain-containing protein 2 nonhistone substrates

Substrate	Methylation site	Methylation effect	Affected pathways	Role of substrates in PDAC	Ref.
ALK	K1451; K1455; K1610	Promotes EML4-ALK phosphorylation and NSCLC cell growth	PI3K/ AKT; JAK/STAT; RTK/Ras	ALK rearrangement-positive cancer correlates with better response to chemotherapy	[28, 96]
$\beta$ -catenin	K133	Promotes $\beta$ -catenin nuclear translocation	Wnt/ $\beta$ -catenin/TCF	Mediates EMT; promotes cell proliferation, migration, and invasion	[48, 97]
BMPR2	Kinase domain	Stimulates BMPR2 kinase activity; SMAD1/5 phosphorylation; BMP pathway activation	BMP	Promotes tumor growth <i>via</i> GRB2/PI3K/ AKT pathway	[98, 99]
ER $\alpha$	K266	Suppresses ER $\alpha$ target gene activation	PI3K/ AKT; MAPK-ERK	ER $\alpha$ expression correlates with tumor progression; endocrine therapies	[100, 101]
EZH2	K307	Promotes EZH2 stability; cell proliferation; EMT;invasion in BC	RB-E2F	Linked to an aggressive phenotype	[102, 103]
HSP90AB1	K531; K574	Enhances dimerization; chaperone complex formation of HSP90AB1; promotes cancer cell proliferation	PI3K/ AKT	Targeting HSP90 decreases GEM chemoresistance	[25, 104]
MAPKAPK3	K355	Promotes pancreatic ductal adenocarcinoma	RTK/Ras; MAPK-ERK	Interacts with HSP27; mediates gemcitabine toxicity	[16]
p53	K370	Inhibits p53 and p53-mediated transcriptional regulation	p53	p53 methylation correlates with aggressive tumors; poor prognosis	[16, 22]
PARP1	K528	Enhances poly (ADP-ribosyl) ation enzymatic activity; promotes apoptotic escape of cancer cells	Base excision repair	Promotes tumorigenesis and resistance	[26, 105]
PTEN	K313	Inactivates PTEN; promotes BC cell proliferation	PI3K-AKT	Loss of PTEN enhances activation of PI3K-AKT; NF- $\kappa$ B and MYC; promotes tumor cell growth and survival	[27, 74]
RB	K810; K860	Enhances Ser 807/811 phosphorylation of RB1; enhances E2F transcriptional activity; cell cycle progression	RB-E2F pathway	Reduced expression of RB correlates with cancer progression	[23, 76,78]
STAT3	K685	Activates and phosphorylates STAT3; promotes cell proliferation and survival in triple-negative BC	JAK2/STAT3	Suppress apoptosis <i>via</i> regulation of BCL-2 family; promotes tumorigenesis	[30, 106]
P65	K310	Activates and phosphorylation p65; represses tumor cell apoptosis in triple-negative BC	NF- $\kappa$ B pathway	-	[30]

PDAC: Pancreatic ductal adenocarcinoma; MAPKAPK3: Mitogen-activated protein kinase activated protein kinase 3; RB: Retinoblastomaassociated protein; BC: Breast cancer; STAT3: Signal transducer and activator of transcription 3; BCL-2: B cell lymphoma-2.

monomethylate MAPKAPK3 at Lys355 both *in vitro* and *in vivo*. Moreover, depletion of SMYD2 led to a decreased expression of endogenous methylation of MAPKAPK3 at Lys355 in the human SW1990 PDAC cell line, indicating that SMYD2 is required for the physiological levels of MAPKAPK3-K355me1 in these cells. Additional experiments further confirmed MAPKAPK3 as a cancer-relevant cytoplasmic target of SMYD2, as determined by a decreased stromal response and a diminished inflammation in *K-Ras* mutant mice, as well as by the cytoplasmic co-localization of SMYD2 and MAPKAPK3 in human and murine PDAC cell lines[16].

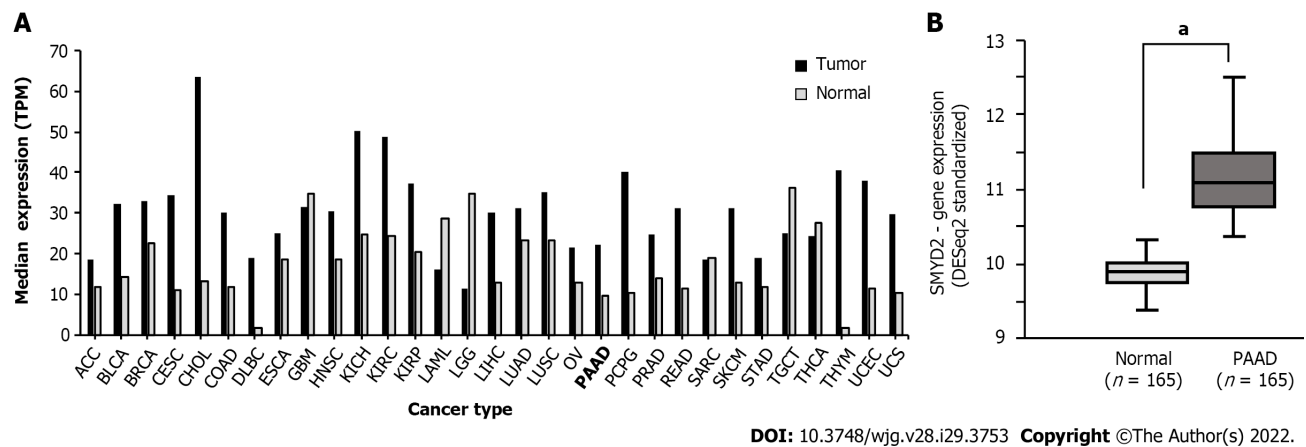
PDAC is one of the Ras-driven carcinomas, where *K-Ras* mutation is a key player in triggering the pancreatic intraepithelial neoplasia (PanIN) and tumor development[16,52]. The overexpression of SMYD2 in PDAC samples, as well as the methylation of the Ras-signaling kinase MAPKAPK3, support the idea that targeting the catalytic activity of SMYD2, or the SMYD2-MAPKAPK3 axis, may be therapeutic in the Ras-driven PDAC. SMYD2 expression was not detectable in normal pancreas tissue sections, while sections from murine and human PanIN and PDAC specimens revealed elevated expression of SMYD2[16]. Notably, an increase in the expression of SMYD2 is correlated with the cancer progression in samples from *K-Ras* mutant mice. Loss of SMYD2 resulted in a reduction in the acinar-to-ductal metaplasia (ADM)[16], an early event in PDAC development triggered by the activation of the RTK/Ras signaling pathway[60]. Consistently, a reduction in the development of the precancerous lesions PanINs and a decreased proliferation ability were also observed upon depletion of SMYD2, as determined by using MUC5AC, pERK1/2, Ki67, cleaved-Caspase-3, and  $\alpha$ SMA as markers for PanIN lesions, Ras pathway activation, proliferation, apoptosis, and stromal response, respectively. These

Table 2 SET and MYND domain-containing protein 2 involvement in human cancers

Cancer type	Findings	Ref.
Acute lymphoblastic leukemia	SMYD2 overexpression; worse OS and EFS; higher WBC counts; a higher percentage of high-risk disease; prognostic factor	[38]
Bladder cancer	Higher expression of SMYD2; promotes cell cycle progression of cancer cells; methylation of RB	[23]
Breast cancer	SMYD2 overexpression; worse RFS; prognostic factor	[107]
	SMYD2 overexpression; poor survival	[30]
Cervical cancer	Higher expression of SMYD2; worse OS; advanced FIGO stage; larger tumor size; poor prognosis	[41]
Chronic lymphocytic leukemia	Higher expression of SMYD2; high WBC counts; complex karyotype; tumor progression	[108]
Clear cell renal cell carcinoma	SMYD2 overexpression; worse OS and DFS; high TNM stage; early tumor relapse	[46]
Colon cancer	SMYD2 overexpression; upregulation MDR1/P-glycoprotein; poor prognosis; enhances oxaliplatin resistance	[31]
Colorectal cancer	SMYD2 overexpression; activates the Wnt/ $\beta$ -catenin pathway; worse OS and DFS; worse oncologic outcomes	[36]
Esophageal squamous cell carcinoma	Higher expression of SMYD2; worse OS; enhances venous invasion; higher pT category and recurrence	[34]
Gastric cancer	SMYD2 overexpression correlates with larger tumor size; aggressive invasion; more lymph node metastasis; recurrence; poor OS	[33]
Hematopoietic leukemias	Higher expression of SMYD2; promote Wnt- $\beta$ -Catenin signaling; poor OS	[39]
Hepatocellular carcinoma	SMYD2 overexpression correlates with tumor size; vascular invasion; differentiation; TNM stage; worse OS; poor prognosis	[14]
HPV-unrelated, non-multiple head and neck cancer	Higher expression of SMYD2; worse OS; prognostic biomarker	[15]
Lower-grade gliomas	Poor OS; prognostic biomarker	[109]
Lung adenocarcinoma	Overexpressed SMYD2 correlates with shorter OS and DFS; promotes proliferation, migration, and invasion of cancer cells	[13]
Non-small cell lung cancer	Overexpressed SMYD2 enhances cisplatin resistance; downregulates the p53 pathway	[32]
Ovarian clear cell carcinoma	Shorter OS and DSS; prognostic biomarker	[43]
Pancreatic cancer	SMYD2 overexpression; methylation of MAPKAPK3; enhances precancerous lesions; poor OS	[16]
Papillary thyroid carcinoma	SMYD2 overexpression correlates with PTC progression; poor prognosis and DFS; worse clinical outcomes	[40]
Renal cell tumor	Low expression of SMYD2 correlates with shorter DSS and DFS; prognostic biomarker	[45]

SMYD2: SET and MYND domain-containing protein 2; OS: Overall survival; EFS: Event-free survival; DFS: Disease-free survival; DSS: Disease-specific survival.

results have led to pharmacological inhibition experiments aimed to evaluate the therapeutic potential of targeting the SMYD2-MAPKAPK3 axis in Ras-driven pancreatic cancer[16]. The compound PF-3644022, which inhibits the kinase activity of MAPKAPK3, was found to suppress the expansion of PDAC cells in culture[16]. Also, treatment with PF-3644022 caused inhibition of PDAC growth in *K-Ras* mutant mice, as well as resulted in fewer PanIN, reduced cell proliferation, an elevated level of apoptosis, attenuation of the Ras pathway, and a reduced level of inflammatory cytokines. Treatment with the SMYD2 small molecule inhibitor BAY598[61] inhibited the methylation of MAPKAPK3 by SMYD2 and decreased the growth of *K-Ras/TP53* mutant PDAC cells, whereas the growth of *K-Ras/TP53/SMYD2* mutant cells was not significantly impacted. On the other hand, the chemotherapeutic gemcitabine had a stronger inhibitory effect on the clonal expansion of *K-Ras/TP53* mutant PDAC cells when combined with BAY598[16]. Gemcitabine also inhibits the growth of *K-Ras/TP53/SMYD2* mutant cells, suggesting that SMYD2 inhibition along with chemotherapy treatment cooperate to target PDAC cells. Such a notion was further supported by the fact that co-treatment of gemcitabine with either SMYD2 inhibition or its deletion resulted in much greater suppression of the growth of PDAC xenografts in mice when compared with any single-agent treatments. Another combination treatment with low-dose doxorubicin and BAY598 revealed similar results in inhibiting PDAC cell growth[16]. These studies together demonstrated that the efficacy of chemotherapy for the treatment of PDAC patients could be significantly improved by a combination of SMYD2 inhibition and effective chemotherapy agents, underscoring the therapeutic potential of targeting the SMYD2-MAPKAPK3 axis



**Figure 1 SET and MYND domain-containing protein 2 gene expression in cancer.** A: The gene expression profiles of SET and MYND domain-containing protein 2 (SMYD2) across 31 types of tumor samples and paired normal tissues from the Cancer Genome Atlas (TCGA) and the Genotype-Tissue Expression (GTEx) project, the analysis was performed using the Gene Expression Profiling Interactive Analysis (GEPIA2); B: Differences in SMYD2 expression between pancreatic ductal adenocarcinoma tissues and paired normal tissues. TPM: Transcripts per kilobase of exon per million mapped reads; ACC: Adrenocortical carcinoma; BLCA: Bladder urothelial carcinoma; BRCA: Breast invasive carcinoma; CESC: Cervical squamous cell carcinoma and endocervical adenocarcinoma; CHOL: Cholangiocarcinoma; COAD: Colon adenocarcinoma; DLBC: Lymphoid neoplasm diffuse large B-cell lymphoma; ESCA: Esophageal carcinoma; GBM: Glioblastoma multiforme; HNSC: Head and neck squamous cell carcinoma; KICH: Kidney chromophobe; KIRC: Kidney renal clear cell carcinoma; KIRP: Kidney renal papillary cell carcinoma; LAML: Acute myeloid leukemia; LGG: Lower grade glioma; LIHC: Liver hepatocellular carcinoma; LUAD: Lung adenocarcinoma; LUSC: Lung squamous cell carcinoma; OV: Ovarian serous cystadenocarcinoma; PAAD/PDAC: Pancreatic ductal adenocarcinoma; PCPG: Pheochromocytoma and paraganglioma; PRAD: Prostate adenocarcinoma; READ: Rectum adenocarcinoma; SARC: Sarcoma; SKCM: Skin cutaneous melanoma; STAD: Stomach adenocarcinoma; TGCT: Testicular germ cell tumors; THCA: Thyroid carcinoma; THYM: Thymoma; UCEC: Uterine corpus endometrial carcinoma; UCS: Uterine carcinosarcoma; *n*: Number of samples. <sup>a</sup>*P* < 0.001 is indicated by three asterisks.

in PDAC.

## FUNCTIONAL EXTRAPOLATION OF SMYD2 FROM OTHER CANCERS TO PANCREATIC CANCER

SMYD2 involvement in many other human cancers (Table 2) through regulating the oncogenic signaling pathways provides a conceptual foundation for extrapolating the known functions of SMYD2 to the less studied pancreatic cancer. SMYD2 is highly expressed in breast tumor tissues relative to normal breast tissues[30]. Inhibition of SMYD2 by RNAi-mediated knockdown or through the specific inhibitor AZ505 significantly decreased tumor growth *in vivo*, indicating that SMYD2 may be involved in the initiation and development of breast cancer (BC) *via* methylation of proteins required for BC cell survival. Indeed, the contribution of SMYD2 to BC development depends on its ability to methylate four protein targets including the NF- $\kappa$ B p65 subunit, signal transducer and activator of transcription 3 (STAT3), histone H3, and PTEN; the activation/inactivation of these protein targets by the methylation affects a wide range of cancer cell behaviors, including cell proliferation, migration, invasion, and survival (Figure 2). SMYD2-mediated methylation of the NF- $\kappa$ B p65 subunit resulted in NF- $\kappa$ B activation and repressed apoptosis of human breast cancer cells[30]. SMYD2-mediated methylation of STAT3 contributes to STAT3 activation in triple-negative breast cancer cells, which in turn increases SMYD2 expression, leading to increased methylation of H3K4 and H3K36 by SMYD2, thereby linking SMYD2 to several BC-associated signaling cascades, including JAK2/STAT3, ERK, and AKT signaling[11,27,30,62]. SMYD2-mediated methylation of PTEN at Lys313 was shown to downregulate the expression of PTEN and to suppress PTEN activity through inducing phosphorylation at serine 380 of PTEN[27,30]. PTEN is a dual lipid and protein phosphatase; as a negative regulator of PI3K/AKT signaling, it downregulates signal transduction initiated by growth factors and hormones through dephosphorylating phosphatidylinositol 3,4,5-triphosphate (PIP3) produced by PI3K[63]. Since PI3K/AKT signaling is a crucial intracellular pathway in human cancers and is frequently upregulated in multiple types of cancer including PDAC[64], the link of SMYD2 to this signaling pathway *via* the methylation-induced repression of PTEN activity suggests a possible new mechanism by which SMYD2 contributes to PDAC development. Several reports have shown the constitutive activation of Ras/ERK and PI3K/AKT signaling and PTEN downregulation being involved in the pathogenesis and progression of pancreatic cancer[65-70]. PTEN was shown to be abundantly expressed in the cytoplasm of non-tumor pancreatic tissues but to be significantly downregulated in PDAC tissues[71]. The downregulation of PTEN has been associated with a high rate of tumorigenesis and a poor prognosis for PDAC patients[71-73]. One important mechanism by which aberrant PTEN expression contributes to PDAC development is the activation of

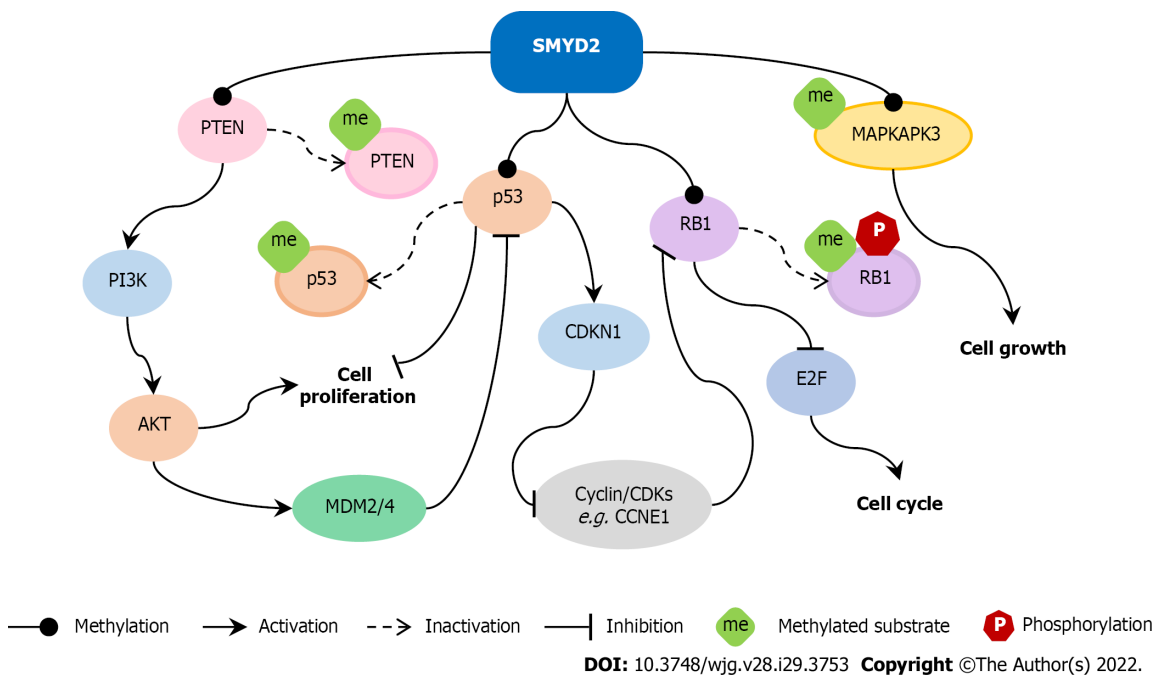


**Figure 2** A schematic model for SET and MYND domain-containing protein 2 driving pancreatic cancer development via methylation of nonhistone proteins. SET and MYND domain-containing protein 2 (SMYD2) can methylate several nonhistone proteins that may be involved in pancreatic cancer tumorigenesis, including p53, PTEN, retinoblastoma-associated protein (RB), and mitogen-activated protein kinase activated protein kinase 3 (MAPKAPK3). SMYD2 methylates and inactivates p53 to promote cell proliferation. PTEN is downregulated by SMYD2-mediated methylation, which promotes cell proliferation through activation of PI3K signaling. Methylation of RB by SMYD2 enhances RB phosphorylation, which allows E2F to disassociate from the RB-E2F complex and enhances E2F activity to promote cell cycle progression. SMYD2 impacts the RTK/Ras pathway through methylation of MAPKAPK3 to promote cell growth. MAPKAPK3: Mitogen-activated protein kinase activated protein kinase 3; RB: Retinoblastoma-associated protein.

the PI3K/AKT signaling pathway, which promotes PDAC cell growth, survival, and angiogenesis[74, 75]. Therefore, in addition to promoting PDAC growth *via* methylation of MAPKAPK3, it is possible that the tumor-promoting activity of SMYD2 in PDAC is attributable to its methyltransferase activity on PTEN, which subsequently causes the activation of the oncogenic PI3K/AKT signaling pathway. In order to prove this hypothesis, future investigation should be directed towards assessing whether Lys313 of PTEN, which is methylated by SMYD2 in BC, can be methylated by SMYD2 in the context of PDAC, and whether such methylation represses the tumor-suppressor activity of PTEN, leading to the activation of PI3K/AKT signaling.

Methylation of RB by SMYD2[76], which is involved in the development of bladder cancer[77], suggests another potential mechanism by which SMYD2 contributes to PDAC progression. SMYD2 is overexpressed in bladder cancer cell lines and primary bladder tumor samples and plays a role in promoting bladder cancer cell proliferation[23]. One mechanism for the SMYD2's bladder cancer-promoting role is the methylation of the tumor suppressor RB, which contributes to the hyperphosphorylation of RB, leading to RB inactivation, and thereby bypassing the regulatory action of RB on cell proliferation[23]. In the case of pancreatic cancer, RB protein levels were significantly lower in PDAC tumor tissues than those in adjacent normal tissues; the low protein levels of RB have been associated with PDAC progression[78]. Another study showed that RB depletion promotes PanIN and rapid malignant transformation in *K-Ras*-induced PDAC, being associated with an impaired p53 activity[79]. This result suggests the importance of RB function in suppressing PDAC progression through mediating the cellular senescence and enhancing p53 function. However, little is known about the methylation status of RB in pancreatic cancer, how such posttranslational modification regulates RB activity, and what are the downstream effects of the methylation on cellular functions and PDAC progression. Given the role of the SMYD2-mediated RB methylation in bladder cancer, one can speculate that there might exist an analogous cancer-promoting mechanism, where SMYD2 mediates the inactivation of RB through direct methylation of RB, resulting in bypassing cell cycle restrictions and promoting PDAC cell growth.

Because of the broad substrate specificity of SMYD2 (Table 1), with most of its substrates being tumor suppressors or oncogenic proteins, the mechanistic link of SMYD2 to PDAC proliferation is expected to be complex, involving the interconnected signaling pathways that regulate the cell cycle, apoptosis, as well as energy metabolism. The tumor suppressor p53 is another important methylation target of SMYD2[22], and this methylation has been shown to promote the tumorigenesis of cervical cancer through an alternative metabolic strategy, shifting the major production of cellular metabolism to lactate production[42]. p53 exerts its tumor-suppressive function in response to severe DNA damage and

inhibits the onset and progression of tumors[80]. p53 is a master regulator of the cell cycle and apoptosis and is involved in the regulation of metabolic pathways to maintain the metabolic homeostasis of cells [81,82]. It has been reported that SMYD2 monomethylates p53 at Lys370, which led to p53 inactivation by decreasing the binding activity of p53 to its target genes[22]. Loss-of-function and gain-of-function experiments revealed that SMYD2 depletion not only significantly reduced the p53K370me level but also increased the p53 reporter activity in cervical cancer cell lines; in contrast, overexpression of SMYD2 in the same cell lines led to an increased level of p53K370me[42]. It has also been shown that the knockdown of p53 in SMYD2-overexpressing cervical cancer cells compromised the increase in glucose uptake and lactate production induced by SMYD2[42]. Moreover, hijacking tumor glycolysis by the glucose analog 2-deoxy-D-glucose (2-DG) significantly repressed SMYD2-dependent tumor growth. These findings together indicate that SMYD2 is a positive glycolytic mediator and plays a promoting role in enhancing tumor growth in a glycolysis-dependent manner, likely through SMYD2-mediated methylation of p53 to promote aerobic glycolysis and tumorigenesis in cervical cancer[42]. Although the role of SMYD2-mediated p53 methylation in PDAC has not yet been explored, dysregulation of the p53 pathway is one of the primary molecular pathological events in PDAC, which promotes the development and progression of pancreatic tumors[83]. In a cohort of 272 PDAC patients, an aberrant alteration rate of the *TP53* gene was about 38% [84], consistent with earlier reports demonstrating 40% and 47% of PDAC samples having p53 mutations[85,86]. It was shown that the inactivation of p53 occurs during the progression of PanIN to invasive tumors[87], while activation of the mitochondrial p53 was shown to restore the apoptotic pathway and inhibit PDAC growth *in vitro* and *in vivo*[88]. These studies demonstrate that p53 dysfunction has a strong association with the progression of pancreatic cancer. As an upstream regulator of the p53 pathway, SMYD2 monomethylates p53 and deactivates the transcriptional activity of p53, and it is thus possible that its ability to block the p53-tumor suppressor activity is another mechanism by which SMYD2 contributes to PDAC progression. It would also be interesting to investigate whether SMYD2-mediated silencing of p53 is also involved in the metabolic reprogramming of pancreatic tumors and promotes the aerobic glycolysis of cancer cells.

## CURRENT CHALLENGES IN THE MOLECULAR THERAPEUTIC TARGETING OF SMYD2

Because of the tumor-promoting role of SMYD2 in numerous cancers including PDAC, the development of selective small-molecule inhibitors against SMYD2 could offer a substantial opportunity for targeted medicine with a broad therapeutic benefit. Great progress in crystal structure analysis of SMYD2 has allowed for the development of multiple selective and potent SMYD2 inhibitors over the past decade [89]. The first SMYD2 inhibitor AZ505 was identified in 2011 after screening over one million-compound library[90]. AZ505 is a competitive inhibitor and has high selectivity for SMYD2, with an inhibitory potency at  $IC_{50}$  of 0.12  $\mu$ M. This landmark discovery opened avenues for structure-based drug discovery for SMYD2 and led to the development of more potent SMYD2 inhibitors. A systematic structure-activity relationships (SAR) study on the AZ505 structure has identified the small molecule A893 as a highly selective SMYD2 inhibitor and being more potent in inhibiting p53 methylation than AZ505[91]. LLY507, another selective SMYD2 inhibitor, was developed and validated not only by a biochemical assay but also by the cell-based assays, and this inhibitor was found to strongly inhibit SMYD2-mediated p53 methylation in several cancer cell lines[92]. Using a modified high-throughput binding assay, BAY598 was identified as one of the most selective and potent SMYD2 inhibitors, with promising pharmacokinetic properties and capable of inducing SMYD2 inhibition *in vivo*[61]. BAY598 showed more than 100-fold selectivity towards SMYD2 relative to other SMYD proteins, and it had a preferred binding to the SMYD2-SAM substrate complex. In cell-based assays, BAY598 was able to inhibit the methylation of p53 by SMYD2, and it can also lead to a slight reduction of tumor area in mice[61]. Further studies identified additional potent and selective inhibitors with suitable pharmacokinetic properties, namely AZ931 and AZ506, though these inhibitors showed no effect on the proliferation of either *TP53* wild-type or *TP53*-deficient cell lines[93]. Recent studies presented new SMYD2 inhibitors, including EPZ033294, EPZ032597, MTF1497, and MTF9975[89,94]. It is noteworthy that EPZ033294 was the first SMYD2 inhibitor acting as a non-competitive inhibitor for the substrate peptide, with a low nanomolar inhibitory activity[94]. However, all these SMYD2 inhibitors are still at a research level and have not undergone clinical trials as therapeutic agents against tumors.

It is widely accepted that the cancer-promoting role of SMYD2 is dependent on its ability to methylate histone and nonhistone proteins, which has significant functions in the development and progression of malignancies. However, targeting the methyltransferase activity of SMYD2 has not yet achieved great outcomes in current cancer studies. This lack of success may be attributed to traditional SMYD2 inhibitors that usually inhibit the evolutionarily conserved cofactor binding site, as well as the complexity of the SMYD2 broad substrate specificity and its involvement in multiple signaling pathways that are essential for both normal and cancerous cells. Targeting the cofactor binding site of SMYD2 is a straightforward strategy, as the methyltransferase activity of SMYD2 relies on the methyl donor SAM being bound at the cofactor binding site. However, the highly conserved nature of this SAM binding site across the entire SET domain-containing protein lysine methyltransferase superfamily

makes designing a highly selective inhibitor with minimum cross-reactivity a challenge. Although a great selectivity has been achieved by some SMYD2 inhibitors, the current specificity analysis is limited to a handful number of SET domain-containing proteins that are closely related to SMYD2, and the full spectrum of the specificity profiles of these inhibitors across the genome is unknown. Consequently, some reports pointed out a potent inhibition of cell proliferation by some of the SMYD2 inhibitors, such as LLY507, being independent of SMYD2 inhibition, rather targeting several other unrelated enzymes to exert their inhibitory effects[94]. Similar conflicting data was also obtained about the effect of the SMYD2 inhibitor BAY598[61]. As a result of these conflicting data, some reports concluded that SMYD2 might not be required for *in vitro* cell line proliferation, though such a claim needs to be further studied [94]. The broad substrate specificity of SMYD2 represents another significant challenge in targeting SMYD2 for cancer therapy. In the past two decades, many nonhistone substrates of SMYD2 have been reported, suggesting that the functional impact of inhibiting SMYD2 will be very complex, involving different mechanisms and affecting various cellular pathways in both normal and pathological conditions. The lack of understanding of how SMYD2 inhibition affects the physiological behavior of normal cells is a major issue of current SMYD2 inhibitors. Another issue is that, for example, SMYD2 inhibition leading to the restoration of the p53 tumor suppressor activity has been well characterized, but how this inhibition affects the function of p53 gain-of-function mutants is unknown. Many mutant p53 proteins promote tumorigenesis through the gain-of-function mechanism[95]. The activity of such p53 mutants could be enhanced by targeting SMYD2 in a similar way as it does to wild-type p53, leading to unwanted outcomes and adverse effects. This is consistent with the evidence that SMYD2 is not always a poor prognostic marker for cancer patients, and the overexpression of SMYD2 has been shown to be a favorable prognostic marker for patients with renal cell tumors[45]. Nonetheless, given that the cancer-promoting role of SMYD2 has been confirmed in multiple types of cancers, it is worthwhile to continue to exploit SMYD2 as a drug target for cancer treatment, with more attention being paid to new inhibition strategies, such as targeting protein-protein interactions and targeting additional functional sites that are less conserved but have substrate-specific functions.

---

## CONCLUSION

---

In the past few decades, there have been huge improvements in our understanding of the complex molecular nature of pancreatic cancer and progress in the available therapy options, including surgery, chemotherapy, radiotherapy, immunotherapy, and targeted therapies. Although these therapy options have resulted in a slight improvement in the overall 5-year survival rate of patients, pancreatic cancer remains a difficult disease to treat. SMYD2 could be a promising target for the development of a novel PDAC therapy, given its involvement in diverse oncogenic signaling pathways to control multiple cellular processes like cell proliferation, apoptosis, and energy metabolism (Figure 2). SMYD2 is overexpressed in PDAC and serves as an important regulatory molecule through the interplay with the RTK/Ras signaling pathway and the PI3K-AKT signaling pathway to drive PDAC cell growth and metastasis. The projected role of SMYD2 in repressing the activity of the tumor suppressors p53 and PTEN in PDAC development further implies that SMYD2 is a key player in promoting the cell cycle, cell growth, and cell survival. Therefore, targeting SMYD2 could be a powerful strategy for the prevention and treatment of PDAC, in particular with consideration of tumor subtypes and genetic backgrounds.

---

## ACKNOWLEDGEMENTS

---

Thanks to Jacob Sobota for proofreading the article.

---

## FOOTNOTES

---

**Author contributions:** Alshammari E performed the majority of the writing, prepared the figures and tables; Zhang YX provided the input in writing the paper; Yang Z coordinated the writing of the paper and performed writing.

**Conflict-of-interest statement:** There are no conflicts of interest to report.

**Open-Access:** This article is an open-access article that was selected by an in-house editor and fully peer-reviewed by external reviewers. It is distributed in accordance with the Creative Commons Attribution NonCommercial (CC BY-NC 4.0) license, which permits others to distribute, remix, adapt, build upon this work non-commercially, and license their derivative works on different terms, provided the original work is properly cited and the use is non-commercial. See: <https://creativecommons.org/licenses/by-nc/4.0/>

**Country/Territory of origin:** United States

**ORCID number:** Eid Alshammari 0000-0002-8676-9480; Ying-Xue Zhang 0000-0001-8099-4225; Zhe Yang 0000-0001-9406-9516.

**S-Editor:** Chen YL

**L-Editor:** A

**P-Editor:** Chen YL

## REFERENCES

- GBD 2017 Pancreatic Cancer Collaborators.** The global, regional, and national burden of pancreatic cancer and its attributable risk factors in 195 countries and territories, 1990-2017: a systematic analysis for the Global Burden of Disease Study 2017. *Lancet Gastroenterol Hepatol* 2019; **4**: 934-947 [PMID: 31648972 DOI: 10.1016/S2468-1253(19)30347-4]
- Ryan DP,** Hong TS, Bardeesy N. Pancreatic adenocarcinoma. *N Engl J Med* 2014; **371**: 1039-1049 [PMID: 25207767 DOI: 10.1056/NEJMra1404198]
- Ilic M,** Ilic I. Epidemiology of pancreatic cancer. *World J Gastroenterol* 2016; **22**: 9694-9705 [PMID: 27956793 DOI: 10.3748/wjg.v22.i44.9694]
- Siegel RL,** Miller KD, Fuchs HE, Jemal A. Cancer Statistics, 2021. *CA Cancer J Clin* 2021; **71**: 7-33 [PMID: 33433946 DOI: 10.3322/caac.21654]
- Rahib L,** Smith BD, Aizenberg R, Rosenzweig AB, Fleshman JM, Matrisian LM. Projecting cancer incidence and deaths to 2030: the unexpected burden of thyroid, liver, and pancreas cancers in the United States. *Cancer Res* 2014; **74**: 2913-2921 [PMID: 24840647 DOI: 10.1158/0008-5472.CAN-14-0155]
- Oberstein PE,** Olive KP. Pancreatic cancer: why is it so hard to treat? *Therap Adv Gastroenterol* 2013; **6**: 321-337 [PMID: 23814611 DOI: 10.1177/1756283X13478680]
- Stathis A,** Moore MJ. Advanced pancreatic carcinoma: current treatment and future challenges. *Nat Rev Clin Oncol* 2010; **7**: 163-172 [PMID: 20101258 DOI: 10.1038/nrclinonc.2009.236]
- Ferrone CR,** Pieretti-Vanmarcke R, Bloom JP, Zheng H, Szymonifka J, Wargo JA, Thayer SP, Lauwers GY, Deshpande V, Mino-Kenudson M, Fernández-del Castillo C, Lillemoe KD, Warshaw AL. Pancreatic ductal adenocarcinoma: long-term survival does not equal cure. *Surgery* 2012; **152**: S43-S49 [PMID: 22763261 DOI: 10.1016/j.surg.2012.05.020]
- Stark AP,** Sacks GD, Rochefort MM, Donahue TR, Reber HA, Tomlinson JS, Dawson DW, Eibl G, Hines OJ. Long-term survival in patients with pancreatic ductal adenocarcinoma. *Surgery* 2016; **159**: 1520-1527 [PMID: 26847803 DOI: 10.1016/j.surg.2015.12.024]
- Strobel O,** Lorenz P, Hinz U, Gaida M, König AK, Hank T, Niesen W, Kaiser JÖR, Al-Saeedi M, Bergmann F, Springfield C, Berchtold C, Diener MK, Schneider M, Mehrabi A, Müller-Stich BP, Hackert T, Jager D, Büchler MW. Actual Five-year Survival After Upfront Resection for Pancreatic Ductal Adenocarcinoma: Who Beats the Odds? *Ann Surg* 2022; **275**: 962-971 [PMID: 32649469 DOI: 10.1097/SLA.0000000000004147]
- Brown MA,** Sims RJ 3rd, Gottlieb PD, Tucker PW. Identification and characterization of Smyd2: a split SET/MYND domain-containing histone H3 lysine 36-specific methyltransferase that interacts with the Sin3 histone deacetylase complex. *Mol Cancer* 2006; **5**: 26 [PMID: 16805913 DOI: 10.1186/1476-4598-5-26]
- Abu-Farha M,** Lambert JP, Al-Madhoun AS, Elisma F, Skerjanc IS, Figeys D. The tale of two domains: proteomics and genomics analysis of SMYD2, a new histone methyltransferase. *Mol Cell Proteomics* 2008; **7**: 560-572 [PMID: 18065756 DOI: 10.1074/mcp.M700271-MCP200]
- Wu L,** Kou F, Ji Z, Li B, Zhang B, Guo Y, Yang L. SMYD2 promotes tumorigenesis and metastasis of lung adenocarcinoma through RPS7. *Cell Death Dis* 2021; **12**: 439 [PMID: 33935284 DOI: 10.1038/s41419-021-03720-w]
- Zuo SR,** Zuo XC, He Y, Fang WJ, Wang CJ, Zou H, Chen P, Huang LF, Huang LH, Xiang H, Liu SK. Positive Expression of SMYD2 is Associated with Poor Prognosis in Patients with Primary Hepatocellular Carcinoma. *J Cancer* 2018; **9**: 321-330 [PMID: 29344279 DOI: 10.7150/jca.22218]
- Ohtomo-Oda R,** Komatsu S, Mori T, Sekine S, Hirajima S, Yoshimoto S, Kanai Y, Otsuji E, Ikeda E, Tsuda H. SMYD2 overexpression is associated with tumor cell proliferation and a worse outcome in human papillomavirus-unrelated nonmultiple head and neck carcinomas. *Hum Pathol* 2016; **49**: 145-155 [PMID: 26826421 DOI: 10.1016/j.humpath.2015.08.025]
- Reynold N,** Mazur PK, Stellfeld T, Flores NM, Lofgren SM, Carlson SM, Brambilla E, Hainaut P, Kaznowska EB, Arrowsmith CH, Khatri P, Stresemann C, Gozani O, Sage J. Coordination of stress signals by the lysine methyltransferase SMYD2 promotes pancreatic cancer. *Genes Dev* 2016; **30**: 772-785 [PMID: 26988419 DOI: 10.1101/gad.275529.115]
- Weirich S,** Schuhmacher MK, Kudithipudi S, Lungu C, Ferguson AD, Jeltsch A. Analysis of the Substrate Specificity of the SMYD2 Protein Lysine Methyltransferase and Discovery of Novel Non-Histone Substrates. *Chembiochem* 2020; **21**: 256-264 [PMID: 31612581 DOI: 10.1002/cbic.201900582]
- Olsen JB,** Cao XJ, Han B, Chen LH, Horvath A, Richardson TI, Campbell RM, Garcia BA, Nguyen H. Quantitative Profiling of the Activity of Protein Lysine Methyltransferase SMYD2 Using SILAC-Based Proteomics. *Mol Cell Proteomics* 2016; **15**: 892-905 [PMID: 26750096 DOI: 10.1074/mcp.M115.053280]
- Ahmed H,** Duan S, Arrowsmith CH, Barsyte-Lovejoy D, Schapira M. An Integrative Proteomic Approach Identifies Novel Cellular SMYD2 Substrates. *J Proteome Res* 2016; **15**: 2052-2059 [PMID: 27163177 DOI: 10.1021/acs.jproteome.6b00220]
- Yi X,** Jiang XJ, Fang ZM. Histone methyltransferase SMYD2: ubiquitous regulator of disease. *Clin Epigenetics* 2019; **11**: 112 [PMID: 31370883 DOI: 10.1186/s13148-019-0711-4]
- Sims RJ 3rd,** Nishioka K, Reinberg D. Histone lysine methylation: a signature for chromatin function. *Trends Genet* 2003; **19**: 629-639 [PMID: 14585615 DOI: 10.1016/j.tig.2003.09.007]

- 22 **Huang J**, Perez-Burgos L, Placek BJ, Sengupta R, Richter M, Dorsey JA, Kubicek S, Opravil S, Jenuwein T, Berger SL. Repression of p53 activity by Smyd2-mediated methylation. *Nature* 2006; **444**: 629-632 [PMID: 17108971 DOI: 10.1038/nature05287]
- 23 **Cho HS**, Hayami S, Toyokawa G, Maejima K, Yamane Y, Suzuki T, Dohmae N, Kogure M, Kang D, Neal DE, Ponder BA, Yamaue H, Nakamura Y, Hamamoto R. RB1 methylation by SMYD2 enhances cell cycle progression through an increase of RB1 phosphorylation. *Neoplasia* 2012; **14**: 476-486 [PMID: 22787429 DOI: 10.1593/neo.12656]
- 24 **Jiang Y**, Trescott L, Holcomb J, Zhang X, Brunzelle J, Sirinupong N, Shi X, Yang Z. Structural insights into estrogen receptor  $\alpha$  methylation by histone methyltransferase SMYD2, a cellular event implicated in estrogen signaling regulation. *J Mol Biol* 2014; **426**: 3413-3425 [PMID: 24594358 DOI: 10.1016/j.jmb.2014.02.019]
- 25 **Hamamoto R**, Toyokawa G, Nakakido M, Ueda K, Nakamura Y. SMYD2-dependent HSP90 methylation promotes cancer cell proliferation by regulating the chaperone complex formation. *Cancer Lett* 2014; **351**: 126-133 [PMID: 24880080 DOI: 10.1016/j.canlet.2014.05.014]
- 26 **Piao L**, Kang D, Suzuki T, Masuda A, Dohmae N, Nakamura Y, Hamamoto R. The histone methyltransferase SMYD2 methylates PARP1 and promotes poly(ADP-ribosyl)ation activity in cancer cells. *Neoplasia* 2014; **16**: 257-264, 264.e2 [PMID: 24726141 DOI: 10.1016/j.neo.2014.03.002]
- 27 **Nakakido M**, Deng Z, Suzuki T, Dohmae N, Nakamura Y, Hamamoto R. Dysregulation of AKT Pathway by SMYD2-Mediated Lysine Methylation on PTEN. *Neoplasia* 2015; **17**: 367-373 [PMID: 25925379 DOI: 10.1016/j.neo.2015.03.002]
- 28 **Wang R**, Deng X, Yoshioka Y, Vougiouklakis T, Park JH, Suzuki T, Dohmae N, Ueda K, Hamamoto R, Nakamura Y. Effects of SMYD2-mediated EML4-ALK methylation on the signaling pathway and growth in non-small-cell lung cancer cells. *Cancer Sci* 2017; **108**: 1203-1209 [PMID: 28370702 DOI: 10.1111/cas.13245]
- 29 **Jiang Y**, Holcomb J, Spellmon N, Yang Z. Purification of Histone Lysine Methyltransferase SMYD2 and Co-Crystallization with a Target Peptide from Estrogen Receptor  $\alpha$ . *Methods Mol Biol* 2016; **1366**: 207-217 [PMID: 26585137 DOI: 10.1007/978-1-4939-3127-9\_16]
- 30 **Li LX**, Zhou JX, Calvet JP, Godwin AK, Jensen RA, Li X. Lysine methyltransferase SMYD2 promotes triple negative breast cancer progression. *Cell Death Dis* 2018; **9**: 326 [PMID: 29487338 DOI: 10.1038/s41419-018-0347-x]
- 31 **Ren H**, Wang Z, Chen Y, Liu Y, Zhang S, Zhang T, Li Y. SMYD2-OE promotes oxaliplatin resistance in colon cancer through MDR1/P-glycoprotein via MEK/ERK/AP1 pathway. *Oncol Targets Ther* 2019; **12**: 2585-2594 [PMID: 31040701 DOI: 10.2147/OTT.S186806]
- 32 **Shang L**, Wei M. Inhibition of SMYD2 Sensitized Cisplatin to Resistant Cells in NSCLC Through Activating p53 Pathway. *Front Oncol* 2019; **9**: 306 [PMID: 31106145 DOI: 10.3389/fonc.2019.00306]
- 33 **Komatsu S**, Ichikawa D, Hirajima S, Nagata H, Nishimura Y, Kawaguchi T, Miyamae M, Okajima W, Ohashi T, Konishi H, Shiozaki A, Fujiwara H, Okamoto K, Tsuda H, Imoto I, Inazawa J, Otsuji E. Overexpression of SMYD2 contributes to malignant outcome in gastric cancer. *Br J Cancer* 2015; **112**: 357-364 [PMID: 25321194 DOI: 10.1038/bjc.2014.543]
- 34 **Komatsu S**, Imoto I, Tsuda H, Kozaki KI, Muramatsu T, Shimada Y, Aiko S, Yoshizumi Y, Ichikawa D, Otsuji E, Inazawa J. Overexpression of SMYD2 relates to tumor cell proliferation and malignant outcome of esophageal squamous cell carcinoma. *Carcinogenesis* 2009; **30**: 1139-1146 [PMID: 19423649 DOI: 10.1093/carcin/bgp116]
- 35 **Lai Y**, Yang Y. SMYD2 facilitates cancer cell malignancy and xenograft tumor development through ERBB2-mediated FUT4 expression in colon cancer. *Mol Cell Biochem* 2020 [PMID: 32342276 DOI: 10.1007/s11010-020-03738-2]
- 36 **Meng F**, Liu X, Lin C, Xu L, Liu J, Zhang P, Zhang X, Song J, Yan Y, Ren Z, Zhang Y. SMYD2 suppresses APC2 expression to activate the Wnt/ $\beta$ -catenin pathway and promotes epithelial-mesenchymal transition in colorectal cancer. *Am J Cancer Res* 2020; **10**: 997-1011 [PMID: 32266106]
- 37 **Sakamoto LH**, Andrade RV, Felipe MS, Motoyama AB, Pittella Silva F. SMYD2 is highly expressed in pediatric acute lymphoblastic leukemia and constitutes a bad prognostic factor. *Leuk Res* 2014; **38**: 496-502 [PMID: 24631370 DOI: 10.1016/j.leukres.2014.01.013]
- 38 **Zhang P**, Ruan J, Weng W, Tang Y. Overexpression of SET and MYND domain-containing protein 2 (SMYD2) is associated with poor prognosis in pediatric B lineage acute lymphoblastic leukemia. *Leuk Lymphoma* 2020; **61**: 437-444 [PMID: 31612757 DOI: 10.1080/10428194.2019.1675875]
- 39 **Brown MA**, Edwards MA, Alshiraihi I, Geng H, Dekker JD, Tucker HO. The lysine methyltransferase SMYD2 is required for normal lymphocyte development and survival of hematopoietic leukemias. *Genes Immun* 2020; **21**: 119-130 [PMID: 32115575 DOI: 10.1038/s41435-020-0094-8]
- 40 **Xu W**, Chen F, Fei X, Yang X, Lu X. Overexpression of SET and MYND Domain-Containing Protein 2 (SMYD2) Is Associated with Tumor Progression and Poor Prognosis in Patients with Papillary Thyroid Carcinoma. *Med Sci Monit* 2018; **24**: 7357-7365 [PMID: 30319138 DOI: 10.12659/MSM.910168]
- 41 **Sun JJ**, Li HL, Ma H, Shi Y, Yin LR, Guo SJ. SMYD2 promotes cervical cancer growth by stimulating cell proliferation. *Cell Biosci* 2019; **9**: 75 [PMID: 31548876 DOI: 10.1186/s13578-019-0340-9]
- 42 **Wang Y**, Jin G, Guo Y, Cao Y, Niu S, Fan X, Zhang J. SMYD2 suppresses p53 activity to promote glucose metabolism in cervical cancer. *Exp Cell Res* 2021; **404**: 112649 [PMID: 34015314 DOI: 10.1016/j.yexcr.2021.112649]
- 43 **Engqvist H**, Parris TZ, Kovács A, Rönnerman EW, Sundfeldt K, Karlsson P, Helou K. Validation of Novel Prognostic Biomarkers for Early-Stage Clear-Cell, Endometrioid and Mucinous Ovarian Carcinomas Using Immunohistochemistry. *Front Oncol* 2020; **10**: 162 [PMID: 32133296 DOI: 10.3389/fonc.2020.00162]
- 44 **Kojima M**, Sone K, Oda K, Hamamoto R, Kaneko S, Oki S, Kukita A, Kawata A, Honjoh H, Kawata Y, Kashiyama T, Sato M, Taguchi A, Miyamoto Y, Tanikawa M, Tsuruga T, Nagasaka K, Wada-Hiraike O, Osuga Y, Fujii T. The histone methyltransferase SMYD2 is a novel therapeutic target for the induction of apoptosis in ovarian clear cell carcinoma cells. *Oncol Lett* 2020; **20**: 153 [PMID: 32934721 DOI: 10.3892/ol.2020.12014]
- 45 **Pires-Luis AS**, Vieira-Coimbra M, Vieira FQ, Costa-Pinheiro P, Silva-Santos R, Dias PC, Antunes L, Lobo F, Oliveira J, Gonçalves CS, Costa BM, Henrique R, Jerónimo C. Expression of histone methyltransferases as novel biomarkers for renal cell tumor diagnosis and prognostication. *Epigenetics* 2015; **10**: 1033-1043 [PMID: 26488939 DOI: 10.1080/15592294.2015.1103578]

- 46 **Zhang Y**, Li C, Yang Z. Is MYND Domain-Mediated Assembly of SMYD3 Complexes Involved in Calcium Dependent Signaling? *Front Mol Biosci* 2019; **6**: 121 [PMID: 31737645 DOI: 10.3389/fmolb.2019.00121]
- 47 **Lenkiewicz E**, Malasi S, Hogenson TL, Flores LF, Barham W, Phillips WJ, Roesler AS, Chambers KR, Rajbhandari N, Hayashi A, Antal CE, Downes M, Grandgenett PM, Hollingsworth MA, Cridebring D, Xiong Y, Lee JH, Ye Z, Yan H, Hernandez MC, Leiting JL, Evans RM, Ordog T, Truty MJ, Borad MJ, Reya T, Von Hoff DD, Fernandez-Zapico ME, Barrett MT. Genomic and Epigenomic Landscaping Defines New Therapeutic Targets for Adenosquamous Carcinoma of the Pancreas. *Cancer Res* 2020; **80**: 4324-4334 [PMID: 32928922 DOI: 10.1158/0008-5472.CAN-20-0078]
- 48 **Deng X**, Hamamoto R, Vougiouklakis T, Wang R, Yoshioka Y, Suzuki T, Dohmae N, Matsuo Y, Park JH, Nakamura Y. Critical roles of SMYD2-mediated  $\beta$ -catenin methylation for nuclear translocation and activation of Wnt signaling. *Oncotarget* 2017; **8**: 55837-55847 [PMID: 28915556 DOI: 10.18632/oncotarget.19646]
- 49 **Dai S**, Xu S, Ye Y, Ding K. Identification of an Immune-Related Gene Signature to Improve Prognosis Prediction in Colorectal Cancer Patients. *Front Genet* 2020; **11**: 607009 [PMID: 33343640 DOI: 10.3389/fgene.2020.607009]
- 50 **Ren J**, Sun J, Li M, Zhang Z, Yang D, Cao H. MAPK Activated Protein Kinase 3 Is a Prognostic-Related Biomarker and Associated With Immune Infiltrates in Glioma. *Front Oncol* 2021; **11**: 793025 [PMID: 34938665 DOI: 10.3389/fonc.2021.793025]
- 51 **Tront JS**, Hoffman B, Liebermann DA. Gadd45a suppresses Ras-driven mammary tumorigenesis by activation of c-Jun NH2-terminal kinase and p38 stress signaling resulting in apoptosis and senescence. *Cancer Res* 2006; **66**: 8448-8454 [PMID: 16951155 DOI: 10.1158/0008-5472.CAN-06-2013]
- 52 **Waters AM**, Der CJ. KRAS: The Critical Driver and Therapeutic Target for Pancreatic Cancer. *Cold Spring Harb Perspect Med* 2018; **8** [PMID: 29229669 DOI: 10.1101/cshperspect.a031435]
- 53 **Shiryaev A**, Moens U. Mitogen-activated protein kinase p38 and MK2, MK3 and MK5: ménage à trois or ménage à quatre? *Cell Signal* 2010; **22**: 1185-1192 [PMID: 20227494 DOI: 10.1016/j.cellsig.2010.03.002]
- 54 **Djakiew D**. The p38 MAPK Pathway in Prostate Cancer. In: Tindall DJ, editor. Prostate Cancer: Biochemistry, Molecular Biology and Genetics. New York: Springer New York, 2013: 243-255 [DOI: 10.1007/978-1-4614-6828-8\_8]
- 55 **Sun Y**, Liu WZ, Liu T, Feng X, Yang N, Zhou HF. Signaling pathway of MAPK/ERK in cell proliferation, differentiation, migration, senescence and apoptosis. *J Recept Signal Transduct Res* 2015; **35**: 600-604 [PMID: 26096166 DOI: 10.3109/10799893.2015.1030412]
- 56 **Ludwig S**, Engel K, Hoffmeyer A, Sithanandam G, Neufeld B, Palm D, Gaestel M, Rapp UR. 3pK, a novel mitogen-activated protein (MAP) kinase-activated protein kinase, is targeted by three MAP kinase pathways. *Mol Cell Biol* 1996; **16**: 6687-6697 [PMID: 8943323 DOI: 10.1128/MCB.16.12.6687]
- 57 **McLaughlin MM**, Kumar S, McDonnell PC, Van Horn S, Lee JC, Livi GP, Young PR. Identification of mitogen-activated protein (MAP) kinase-activated protein kinase-3, a novel substrate of CSBP p38 MAP kinase. *J Biol Chem* 1996; **271**: 8488-8492 [PMID: 8626550 DOI: 10.1074/jbc.271.14.8488]
- 58 **Ronkina N**, Menon MB, Schwermann J, Tiedje C, Hitti E, Kotlyarov A, Gaestel M. MAPKAP kinases MK2 and MK3 in inflammation: complex regulation of TNF biosynthesis via expression and phosphorylation of tristetraprolin. *Biochem Pharmacol* 2010; **80**: 1915-1920 [PMID: 20599781 DOI: 10.1016/j.bcp.2010.06.021]
- 59 **Kyriakis JM**, Avruch J. Mammalian MAPK signal transduction pathways activated by stress and inflammation: a 10-year update. *Physiol Rev* 2012; **92**: 689-737 [PMID: 22535895 DOI: 10.1152/physrev.00028.2011]
- 60 **Beel S**, Kolloch L, Apken LH, Jürgens L, Bolle A, Sudhof N, Ghosh S, Wardelmann E, Meisterernst M, Steinestel K, Oeckinghaus A.  $\kappa$ B-Ras and Ral GTPases regulate acinar to ductal metaplasia during pancreatic adenocarcinoma development and pancreatitis. *Nat Commun* 2020; **11**: 3409 [PMID: 32641778 DOI: 10.1038/s41467-020-17226-0]
- 61 **Eggert E**, Hillig RC, Koehr S, Stöckigt D, Weiske J, Barak N, Mowat J, Brumby T, Christ CD, Ter Laak A, Lang T, Fernandez-Montalvan AE, Badock V, Weinmann H, Hartung IV, Barysyt-Lovejoy D, Szewczyk M, Kennedy S, Li F, Vedadi M, Brown PJ, Santhakumar V, Arrowsmith CH, Stellfeld T, Stresemann C. Discovery and Characterization of a Highly Potent and Selective Aminopyrazoline-Based in Vivo Probe (BAY-598) for the Protein Lysine Methyltransferase SMYD2. *J Med Chem* 2016; **59**: 4578-4600 [PMID: 27075367 DOI: 10.1021/acs.jmedchem.5b01890]
- 62 **Marotta LL**, Almendro V, Marusyk A, Shipitsin M, Schemme J, Walker SR, Bloushtain-Qimron N, Kim JJ, Choudhury SA, Maruyama R, Wu Z, Gönen M, Mulvey LA, Bessarabova MO, Huh SJ, Silver SJ, Kim SY, Park SY, Lee HE, Anderson KS, Richardson AL, Nikolskaya T, Nikolsky Y, Liu XS, Root DE, Hahn WC, Frank DA, Polyak K. The JAK2/STAT3 signaling pathway is required for growth of CD44<sup>+</sup>CD24<sup>-</sup> stem cell-like breast cancer cells in human tumors. *J Clin Invest* 2011; **121**: 2723-2735 [PMID: 21633165 DOI: 10.1172/JCI144745]
- 63 **Blanco-Aparicio C**, Renner O, Leal JF, Carnero A. PTEN, more than the AKT pathway. *Carcinogenesis* 2007; **28**: 1379-1386 [PMID: 17341655 DOI: 10.1093/carcin/bgm052]
- 64 **Manning BD**, Cantley LC. AKT/PKB signaling: navigating downstream. *Cell* 2007; **129**: 1261-1274 [PMID: 17604717 DOI: 10.1016/j.cell.2007.06.009]
- 65 **Chow JY**, Quach KT, Cabrera BL, Cabral JA, Beck SE, Carethers JM. RAS/ERK modulates TGFbeta-regulated PTEN expression in human pancreatic adenocarcinoma cells. *Carcinogenesis* 2007; **28**: 2321-2327 [PMID: 17638924 DOI: 10.1093/carcin/bgm159]
- 66 **Kennedy AL**, Adams PD, Morton JP. Ras, PI3K/Akt and senescence: Paradoxes provide clues for pancreatic cancer therapy. *Small GTPases* 2011; **2**: 264-267 [PMID: 22292129 DOI: 10.4161/sgtp.2.5.17367]
- 67 **Wong MH**, Xue A, Baxter RC, Pavlakis N, Smith RC. Upstream and Downstream Co-inhibition of Mitogen-Activated Protein Kinase and PI3K/Akt/mTOR Pathways in Pancreatic Ductal Adenocarcinoma. *Neoplasia* 2016; **18**: 425-435 [PMID: 27435925 DOI: 10.1016/j.neo.2016.06.001]
- 68 **Ebrahimi S**, Hosseini M, Shahidsales S, Maftouh M, Ferns GA, Ghayour-Mobarhan M, Hassanian SM, Avan A. Targeting the Akt/PI3K Signaling Pathway as a Potential Therapeutic Strategy for the Treatment of Pancreatic Cancer. *Curr Med Chem* 2017; **24**: 1321-1331 [PMID: 28176634 DOI: 10.2174/0929867324666170206142658]
- 69 **Ma J**, Sawai H, Matsuo Y, Ochi N, Yasuda A, Takahashi H, Wakasugi T, Funahashi H, Sato M, Takeyama H. IGF-1 mediates PTEN suppression and enhances cell invasion and proliferation via activation of the IGF-1/PI3K/Akt signaling

- pathway in pancreatic cancer cells. *J Surg Res* 2010; **160**: 90-101 [PMID: 19560785 DOI: 10.1016/j.jss.2008.08.016]
- 70 Si W, Liu X, Wei R, Zhang Y, Zhao Y, Cui L, Hong T. MTA2-mediated inhibition of PTEN leads to pancreatic ductal adenocarcinoma carcinogenicity. *Cell Death Dis* 2019; **10**: 206 [PMID: 30814496 DOI: 10.1038/s41419-019-1424-5]
- 71 Ni S, Wang H, Zhu X, Wan C, Xu J, Lu C, Xiao L, He J, Jiang C, Wang W, He Z. CBX7 suppresses cell proliferation, migration, and invasion through the inhibition of PTEN/Akt signaling in pancreatic cancer. *Oncotarget* 2017; **8**: 8010-8021 [PMID: 28030829 DOI: 10.18632/oncotarget.14037]
- 72 Chen S, He Z, Zhu C, Liu Y, Li L, Deng L, Wang J, Yu C, Sun C. TRIM37 Mediates Chemoresistance and Maintenance of Stemness in Pancreatic Cancer Cells via Ubiquitination of PTEN and Activation of the AKT-GSK-3 $\beta$ -Catenin Signaling Pathway. *Front Oncol* 2020; **10**: 554787 [PMID: 33194618 DOI: 10.3389/fonc.2020.554787]
- 73 Zhang Q, Li X, Li Y, Chen S, Shen X, Dong X, Song Y, Zhang X, Huang K. Expression of the PTEN/FOXO3a/PLZF signalling pathway in pancreatic cancer and its significance in tumourigenesis and progression. *Invest New Drugs* 2020; **38**: 321-328 [PMID: 31087222 DOI: 10.1007/s10637-019-00791-7]
- 74 Asano T, Yao Y, Zhu J, Li D, Abbruzzese JL, Reddy SA. The PI 3-kinase/Akt signaling pathway is activated due to aberrant Pten expression and targets transcription factors NF-kappaB and c-Myc in pancreatic cancer cells. *Oncogene* 2004; **23**: 8571-8580 [PMID: 15467756 DOI: 10.1038/sj.onc.1207902]
- 75 Ma J, Sawai H, Ochi N, Matsuo Y, Xu D, Yasuda A, Takahashi H, Wakasugi T, Takeyama H. PTEN regulates angiogenesis through PI3K/Akt/VEGF signaling pathway in human pancreatic cancer cells. *Mol Cell Biochem* 2009; **331**: 161-171 [PMID: 19437103 DOI: 10.1007/s11010-009-0154-x]
- 76 Saddic LA, West LE, Aslanian A, Yates JR 3rd, Rubin SM, Gozani O, Sage J. Methylation of the retinoblastoma tumor suppressor by SMYD2. *J Biol Chem* 2010; **285**: 37733-37740 [PMID: 20870719 DOI: 10.1074/jbc.M110.137612]
- 77 Malekzadeh K, Sobti RC, Nikbakht M, Shekari M, Hosseini SA, Tamandani DK, Singh SK. Methylation patterns of Rb1 and Casp-8 promoters and their impact on their expression in bladder cancer. *Cancer Invest* 2009; **27**: 70-80 [PMID: 19160091 DOI: 10.1080/07357900802172085]
- 78 Yue H, Na YL, Feng XL, Ma SR, Song FL, Yang B. Expression of p57kip2, Rb protein and PCNA and their relationships with clinicopathology in human pancreatic cancer. *World J Gastroenterol* 2003; **9**: 377-380 [PMID: 12532471 DOI: 10.3748/wjg.v9.i2.377]
- 79 Carrière C, Gore AJ, Norris AM, Gunn JR, Young AL, Longnecker DS, Korc M. Deletion of Rb accelerates pancreatic carcinogenesis by oncogenic Kras and impairs senescence in premalignant lesions. *Gastroenterology* 2011; **141**: 1091-1101 [PMID: 21699781 DOI: 10.1053/j.gastro.2011.05.041]
- 80 Lane DP. Cancer. p53, guardian of the genome. *Nature* 1992; **358**: 15-16 [PMID: 1614522 DOI: 10.1038/358015a0]
- 81 Oren M. Decision making by p53: life, death and cancer. *Cell Death Differ* 2003; **10**: 431-442 [PMID: 12719720 DOI: 10.1038/sj.cdd.4401183]
- 82 Liu J, Zhang C, Hu W, Feng Z. Tumor suppressor p53 and metabolism. *J Mol Cell Biol* 2019; **11**: 284-292 [PMID: 30500901 DOI: 10.1093/jmcb/mjy070]
- 83 Ansari D, Del Pino Bellido C, Bauden M, Andersson R. Centrosomal Abnormalities in Pancreatic Cancer: Molecular Mechanisms and Clinical Implications. *Anticancer Res* 2018; **38**: 1241-1245 [PMID: 29491046 DOI: 10.21873/anticancer.12345]
- 84 Shin SH, Kim SC, Hong SM, Kim YH, Song KB, Park KM, Lee YJ. Genetic alterations of K-ras, p53, c-erbB-2, and DPC4 in pancreatic ductal adenocarcinoma and their correlation with patient survival. *Pancreas* 2013; **42**: 216-222 [PMID: 23344532 DOI: 10.1097/MPA.0b013e31825b6ab0]
- 85 DiGiuseppe JA, Hruban RH, Goodman SN, Polak M, van den Berg FM, Allison DC, Cameron JL, Offerhaus GJ. Overexpression of p53 protein in adenocarcinoma of the pancreas. *Am J Clin Pathol* 1994; **101**: 684-688 [PMID: 8209852 DOI: 10.1093/ajcp/101.6.684]
- 86 Casey G, Yamanaka Y, Friess H, Kobrin MS, Lopez ME, Buchler M, Beger HG, Korc M. p53 mutations are common in pancreatic cancer and are absent in chronic pancreatitis. *Cancer Lett* 1993; **69**: 151-160 [PMID: 8513440 DOI: 10.1016/0304-3835(93)90168-9]
- 87 Norfadzilah MY, Pailoor J, Retneswari M, Chinna K, Noor LM. P53 expression in invasive pancreatic adenocarcinoma and precursor lesions. *Malays J Pathol* 2011; **33**: 89-94 [PMID: 22299208]
- 88 Cheng J, Okolotowicz KJ, Ryan D, Mose E, Lowy AM, Cashman JR. Inhibition of invasive pancreatic cancer: restoring cell apoptosis by activating mitochondrial p53. *Am J Cancer Res* 2019; **9**: 390-405 [PMID: 30906636]
- 89 Fabini E, Manoni E, Ferroni C, Rio AD, Bartolini M. Small-molecule inhibitors of lysine methyltransferases SMYD2 and SMYD3: current trends. *Future Med Chem* 2019; **11**: 901-921 [PMID: 30998113 DOI: 10.4155/fmc-2018-0380]
- 90 Ferguson AD, Larsen NA, Howard T, Pollard H, Green I, Grande C, Cheung T, Garcia-Arenas R, Cowen S, Wu J, Godin R, Chen H, Keen N. Structural basis of substrate methylation and inhibition of SMYD2. *Structure* 2011; **19**: 1262-1273 [PMID: 21782458 DOI: 10.1016/j.str.2011.06.011]
- 91 Sweis RF, Wang Z, Algire M, Arrowsmith CH, Brown PJ, Chiang GG, Guo J, Jakob CG, Kennedy S, Li F, Maag D, Shaw B, Soni NB, Vedadi M, Pappano WN. Discovery of A-893, A New Cell-Active Benzoxazinone Inhibitor of Lysine Methyltransferase SMYD2. *ACS Med Chem Lett* 2015; **6**: 695-700 [PMID: 26101576 DOI: 10.1021/acsmedchemlett.5b00124]
- 92 Nguyen H, Allali-Hassani A, Antonysamy S, Chang S, Chen LH, Curtis C, Emtage S, Fan L, Gheyti T, Li F, Liu S, Martin JR, Mendel D, Olsen JB, Pelletier L, Shatseva T, Wu S, Zhang FF, Arrowsmith CH, Brown PJ, Campbell RM, Garcia BA, Barsyte-Lovejoy D, Mader M, Vedadi M. LLY-507, a Cell-active, Potent, and Selective Inhibitor of Protein-lysine Methyltransferase SMYD2. *J Biol Chem* 2015; **290**: 13641-13653 [PMID: 25825497 DOI: 10.1074/jbc.M114.626861]
- 93 Cowen SD, Russell D, Dakin LA, Chen H, Larsen NA, Godin R, Throner S, Zheng X, Molina A, Wu J, Cheung T, Howard T, Garcia-Arenas R, Keen N, Pendleton CS, Pietenpol JA, Ferguson AD. Design, Synthesis, and Biological Activity of Substrate Competitive SMYD2 Inhibitors. *J Med Chem* 2016; **59**: 11079-11097 [PMID: 28002961 DOI: 10.1021/acs.jmedchem.6b01303]
- 94 Thomenius MJ, Totman J, Harvey D, Mitchell LH, Riera TV, Cosmopoulos K, Grassian AR, Klaus C, Foley M, Admirand EA, Jahic H, Majer C, Wigle T, Jacques SL, Gureasko J, Brach D, Lingaraj T, West K, Smith S, Rioux N,

- Waters NJ, Tang C, Raimondi A, Munchhof M, Mills JE, Ribich S, Porter Scott M, Kuntz KW, Janzen WP, Moyer M, Smith JJ, Chesworth R, Copeland RA, Boriack-Sjodin PA. Small molecule inhibitors and CRISPR/Cas9 mutagenesis demonstrate that SMYD2 and SMYD3 activity are dispensable for autonomous cancer cell proliferation. *PLoS One* 2018; **13**: e0197372 [PMID: 29856759 DOI: 10.1371/journal.pone.0197372]
- 95 **Oren M**, Rotter V. Mutant p53 gain-of-function in cancer. *Cold Spring Harb Perspect Biol* 2010; **2**: a001107 [PMID: 20182618 DOI: 10.1101/cshperspect.a001107]
- 96 **Ou K**, Liu X, Li W, Yang Y, Ying J, Yang L. ALK Rearrangement-Positive Pancreatic Cancer with Brain Metastasis Has Remarkable Response to ALK Inhibitors: A Case Report. *Front Oncol* 2021; **11**: 724815 [PMID: 34568053 DOI: 10.3389/fonc.2021.724815]
- 97 **Zhou P**, Li Y, Li B, Zhang M, Liu Y, Yao Y, Li D. NMIIA promotes tumor growth and metastasis by activating the Wnt/ $\beta$ -catenin signaling pathway and EMT in pancreatic cancer. *Oncogene* 2019; **38**: 5500-5515 [PMID: 30967633 DOI: 10.1038/s41388-019-0806-6]
- 98 **Gao S**, Wang Z, Wang W, Hu X, Chen P, Li J, Feng X, Wong J, Du JX. The lysine methyltransferase SMYD2 methylates the kinase domain of type II receptor BMPR2 and stimulates bone morphogenetic protein signaling. *J Biol Chem* 2017; **292**: 12702-12712 [PMID: 28588028 DOI: 10.1074/jbc.M117.776278]
- 99 **Wang Y**, Guo H, Zhang Z, Wang Q, Tian X, Yang Y. Inhibition of bone morphogenetic protein receptor 2 suppresses pancreatic ductal adenocarcinoma growth by regulating GRB2/PI3K/AKT axis. *Ann Transl Med* 2021; **9**: 557 [PMID: 33987255 DOI: 10.21037/atm-20-2194]
- 100 **Zhang X**, Tanaka K, Yan J, Li J, Peng D, Jiang Y, Yang Z, Barton MC, Wen H, Shi X. Regulation of estrogen receptor  $\alpha$  by histone methyltransferase SMYD2-mediated protein methylation. *Proc Natl Acad Sci U S A* 2013; **110**: 17284-17289 [PMID: 24101509 DOI: 10.1073/pnas.1307959110]
- 101 **Xue J**, Yao Y, Yao Q, Tian X, Feng Y, Su H, Kong D, Cui C, Yan L, Hao C, Zhou T. Important roles of estrogen receptor alpha in tumor progression and anti-estrogen therapy of pancreatic ductal adenocarcinoma. *Life Sci* 2020; **260**: 118302 [PMID: 32827543 DOI: 10.1016/j.lfs.2020.118302]
- 102 **Zeng Y**, Qiu R, Yang Y, Gao T, Zheng Y, Huang W, Gao J, Zhang K, Liu R, Wang S, Hou Y, Yu W, Leng S, Feng D, Liu W, Zhang X, Wang Y. Regulation of EZH2 by SMYD2-Mediated Lysine Methylation Is Implicated in Tumorigenesis. *Cell Rep* 2019; **29**: 1482-1498.e4 [PMID: 31693890 DOI: 10.1016/j.celrep.2019.10.004]
- 103 **Patil S**, Forster T, Reutlinger K, Kopp W, Verseemann L, Spitalieri J, Gaedcke J, Ströbel P, Singh SK, Ellenrieder V, Neeße A, Hessmann E. Chromatin-Independent Interplay of NFATc1 and EZH2 in Pancreatic Cancer. *Cells* 2021; **10** [PMID: 34943970 DOI: 10.3390/cells10123463]
- 104 **Giessrigl B**, Krieger S, Rosner M, Huttary N, Saiko P, Alami M, Messaoudi S, Peyrat JF, Maciuk A, Gollinger M, Kopf S, Kazlauskas E, Mazal P, Szekeres T, Hengstschläger M, Matulis D, Jäger W, Krupitza G. Hsp90 stabilizes Cdc25A and counteracts heat shock-mediated Cdc25A degradation and cell-cycle attenuation in pancreatic carcinoma cells. *Hum Mol Genet* 2012; **21**: 4615-4627 [PMID: 22843495 DOI: 10.1093/hmg/dds303]
- 105 **Xu F**, Sun Y, Yang SZ, Zhou T, Jhala N, McDonald J, Chen Y. Cytoplasmic PARP-1 promotes pancreatic cancer tumorigenesis and resistance. *Int J Cancer* 2019; **145**: 474-483 [PMID: 30614530 DOI: 10.1002/ijc.32108]
- 106 **Huang C**, Xie K. Crosstalk of Sp1 and Stat3 signaling in pancreatic cancer pathogenesis. *Cytokine Growth Factor Rev* 2012; **23**: 25-35 [PMID: 22342309 DOI: 10.1016/j.cytogfr.2012.01.003]
- 107 **Song J**, Liu Y, Chen Q, Yang J, Jiang Z, Zhang H, Liu Z, Jin B. Expression patterns and the prognostic value of the SMYD family members in human breast carcinoma using integrative bioinformatics analysis. *Oncol Lett* 2019; **17**: 3851-3861 [PMID: 30930987 DOI: 10.3892/ol.2019.10054]
- 108 **Oliveira-Santos W**, Rabello DA, Lucena-Araujo AR, de Oliveira FM, Rego EM, Pittella Silva F, Saldanha-Araujo F. Residual expression of SMYD2 and SMYD3 is associated with the acquisition of complex karyotype in chronic lymphocytic leukemia. *Tumour Biol* 2016; **37**: 9473-9481 [PMID: 26790435 DOI: 10.1007/s13277-016-4846-z]
- 109 **Yu H**, Zhang D, Lian M. Identification of an epigenetic prognostic signature for patients with lower-grade gliomas. *CNS Neurosci Ther* 2021; **27**: 470-483 [PMID: 33459509 DOI: 10.1111/cns.13587]

## Clinical challenge for gastroenterologists–Gastrointestinal manifestations of systemic mastocytosis: A comprehensive review

Alessandra Elvevi, Elena Maria Elli, Martina Lucà, Miki Scaravaglio, Fabio Pagni, Stefano Ceola, Laura Ratti, Pietro Invernizzi, Sara Massironi

**Specialty type:** Gastroenterology and hepatology

**Provenance and peer review:** Invited article; Externally peer reviewed.

**Peer-review model:** Single blind

**Peer-review report's scientific quality classification**

Grade A (Excellent): 0  
Grade B (Very good): B, B  
Grade C (Good): C  
Grade D (Fair): 0  
Grade E (Poor): 0

**P-Reviewer:** Bairwa DBL, India; Guo F, China; Piris-Villaespesa M, Spain

**Received:** December 3, 2021

**Peer-review started:** December 3, 2021

**First decision:** May 29, 2022

**Revised:** June 6, 2022

**Accepted:** July 11, 2022

**Article in press:** July 11, 2022

**Published online:** August 7, 2022



**Alessandra Elvevi, Martina Lucà, Miki Scaravaglio, Laura Ratti, Pietro Invernizzi, Sara Massironi,** Gastroenterology Division, San Gerardo Hospital, University of Milano – Bicocca School of Medicine, Monza 20900, Italy

**Elena Maria Elli,** Hematology Division and Bone Marrow Transplant Unit, San Gerardo Hospital, Monza 20900, Italy

**Fabio Pagni, Stefano Ceola,** Department of Medicine and Surgery, Section of Pathology, San Gerardo Hospital, University of Milano – Bicocca School of Medicine, Monza 20900, Italy

**Corresponding author:** Sara Massironi, MD, PhD, Gastroenterology Division, San Gerardo Hospital, University of Milano – Bicocca School of Medicine, Via G.B. Pergolesi 33, Monza 20900, Italy. [sara.massironi@libero.it](mailto:sara.massironi@libero.it)

### Abstract

Mastocytosis is a rare and heterogeneous disease characterized by various clinical and biological features that affect different prognoses and treatments. The disease is usually divided into 2 principal categories: cutaneous and systemic disease (SM). Clinical features can be related to mast cell (MC) mediator release or pathological MC infiltration. SM is a disease often hard to identify, and the diagnosis is based on clinical, biological, histological, and molecular criteria with different specialists involved in the patient's clinical work-up. Among all manifestations of the disease, gastrointestinal (GI) symptoms are common, being present in 14%-85% of patients, and can significantly impair the quality of life. Here we review the data regarding GI involvement in SM, in terms of clinical presentations, histological and endoscopic features, the pathogenesis of GI symptoms, and their treatment.

**Key Words:** Systemic mastocytosis; Gastrointestinal involvement; Gastrointestinal symptoms

©The Author(s) 2022. Published by Baishideng Publishing Group Inc. All rights reserved.

**Core Tip:** Gastrointestinal (GI) involvement is frequent in systemic disease (SM); GI symptoms are frequent (second in frequency only to itching), being the main culprits of chronic disorders, and are a major determinant of quality of life. GI symptoms could be secondary both to mast cell (MC) mediator release and MC infiltration in the GI tract, causing organ dysfunction. Diagnosis of GI involvement in SM is based on clinical and endoscopic suspicion and histologic demonstration of MC infiltration in GI mucosa, using immunohistochemistry (*i.e.*, CD117, tryptase, CD25). Symptomatic treatment is used to control mediators-release symptoms while cytoreductive therapies are necessary to reduce organ dysfunction secondary to MC infiltration and proliferation.

**Citation:** Elvevi A, Elli EM, Lucà M, Scaravaglio M, Pagni F, Ceola S, Ratti L, Invernizzi P, Massironi S. Clinical challenge for gastroenterologists—Gastrointestinal manifestations of systemic mastocytosis: A comprehensive review. *World J Gastroenterol* 2022; 28(29): 3767-3779

**URL:** <https://www.wjgnet.com/1007-9327/full/v28/i29/3767.htm>

**DOI:** <https://dx.doi.org/10.3748/wjg.v28.i29.3767>

## INTRODUCTION

Mastocytosis is a rare type of myeloid neoplasm characterized by clonal expansion and accumulation of morphologically and immune-phenotypically abnormal mast cells (MCs) in one or more organ systems [1]. Clinical presentation in mastocytosis patients is heterogeneous[1,2]. Cutaneous mastocytosis (CM) is the skin-limited presentation; it is most common in children, who experience spontaneous regression of skin lesions during their growth. Systemic mastocytosis (SM) is, on the contrary, a condition of MCs proliferation associated with extra-cutaneous involvement, and it is more frequent in adult patients. Neoplastic MCs form focal and/or diffuse infiltrates in various internal organs, including the bone marrow (BM), spleen, liver, and gastrointestinal (GI) tract[2-4]. Regardless of the type of SM, the BM is involved in virtually all patients.

In 2016, the World Health Organization (WHO) classification of SM identified 5 clinical variants with different prognoses: indolent SM (ISM), smoldering SM (SSM), aggressive SM (ASM), SM with associated hematological neoplasm (SM-AHN), and mast cell leukemia (MCL)[5,6]. Advanced SM (ASM, SM-AHN, and MCL) is generally associated with a poor outcome, whereas ISM patients usually have a comparable life expectancy in comparison with the general population[1,2].

In recent years, knowledge of the pathophysiology of mastocytosis has improved. Particularly, research has found that a recurrent activating D816V KIT mutation, located in the phosphor-transferase domain (PTD) of the receptor, is detectable in more than 80% of adult patients with SM[7,8]. Further genetic alterations, usually involved in myeloid malignances pathogenesis, are often found in advanced forms of SM. These mutations are associated with aggressive disease and poor prognosis[9].

For many years, mastocytosis has been considered an orphan disease, and this might be an explanation for the difficulty in estimating its prevalence. The reported prevalence of SM of 9.56 per 100000 persons[10] is probably underestimated; in the last few years, improved knowledge of the disease and availability of diagnostic tests suggested a higher prevalence, with the newer prevalence reported to be 21 per 100000 inhabitants in the adult population[11].

Mastocytosis diagnosis is based on the identification of atypical MCs in the affected tissue, according to the well-established WHO criteria, based on morphological, histological, cytofluorimetric, and molecular features[5,6] (Table 1). When the major and at least one minor SM criterion or three minor SM criteria are detected, the diagnosis SM is established. SM patients can be further sub-classified depending on the presence of B (organ involvement without organ failure) or C (organ involvement with organ dysfunction) findings, defining MCs burden or disease aggressiveness, respectively[1,5,6] (Table 2).

The severity of the symptoms associated with mastocytosis may vary from mild to life-threatening [2]. In general, symptoms occurring in SM are mainly due to the release of chemical mediators from the MCs, such as histamine, heparin, and eosinophil chemotactic factor, and thus produce symptoms associated with an allergic reaction, although a true allergic trigger may not be identified. In ASM, where MCs infiltration occurs, a decrease in blood cells (cytopenia), break-down of bones (osteolysis), swelling of the lymph nodes (lymphadenopathy), swelling of the liver (hepatomegaly), impaired liver function, ascites or portal hypertension, and malabsorption may occur[1,12,13].

Symptom-directed treatment should be considered in all SM patients[2]. Supportive therapies for SM are directed at MC's degranulation symptoms [histamine-receptors 1 (H1) and 2 (H2) antagonists, proton pump inhibitors (PPI), leukotriene antagonist, sodium cromolyn, corticosteroid], symptomatic skin disease (Psolarene plus ultraviolet A photo-chemotherapy, corticosteroids), and/or osteopenia/osteoporosis/pathologic fractures (bisphosphonate, cytokine/ immunomodulatory drugs) [2,14,15]. Treatment goals for ISM patients are primarily directed towards anaphylaxis prevention and

**Table 1 Systemic mastocytosis criteria according to World Health Organization 2016**

Major SM criterion	Multifocal dense infiltrates of MCs ( $\geq 15$ MCs in aggregates) in BM biopsies and/or in sections of other extracutaneous organ(s)
Minor SM criteria	(a) $> 25\%$ of all MCs are atypical cells (type I or type II) on BM smears or are spindle-shaped in MC infiltrates detected on sections of visceral organs (b) KIT point mutation at codon 816 in the BM or another extracutaneous organ (c) MCs in BM or blood or another extracutaneous organ exhibit CD2 and/or CD25 (d) Baseline serum tryptase level $>20$ ng/mL (in case of an unrelated myeloid neoplasm, item d is not valid as an SM criterion)

If at least 1 major and 1 minor or 3 minor systemic mastocytosis (SM) criteria are fulfilled, the diagnosis of SM can be established. BM: Bone marrow; MCs: Mast cells; SM: Systemic mastocytosis.

**Table 2 B and C Findings in systemic mastocytosis**

<b>B and C Findings in systemic mastocytosis</b>	
<b>B Findings</b>	
BM biopsy showing $> 30\%$ infiltration by MCs (focal, dense aggregates) and serum total tryptase level $> 200$ ng/mL	
Myeloproliferation or signs of dysplasia in non-MC lineage(s), no prominent cytopenias; criteria for AHN not met	
Hepatomegaly and/or splenomegaly on palpation without impairment of organ function and/or lymphadenopathy on palpation/imaging ( $> 2$ cm)	
<b>C Findings<sup>1</sup></b>	
Cytopenia(s): ANC $< 1 \times 10^9/L$ , Hb $< 10$ g/dL, or platelets $< 100 \times 10^9/L$	
Hepatomegaly on palpation with impairment of liver function, ascites, and/or portal hypertension	
Skeletal lesions: Osteolyses and/or pathologic fractures	
Palpable splenomegaly with hypersplenism	
Malabsorption with weight loss from gastrointestinal tract MC infiltrates	

<sup>1</sup>Must be attributable to the mast cell infiltrate. AHN: Associated hematological neoplasm; ANC: Absolute neutrophilic count; BM: Bone marrow; MCs: Mast cells.

symptom control/osteoporosis treatment. Patients with advanced SM frequently need MCs cytoreductive therapy to ameliorate disease-related organ dysfunction[2]. High response rates have been seen with small-molecules inhibitors that target mutant-KIT, including midostaurin (Food and Drug Administration and European Medicine Agency approved) or avapritinib (Food and Drug Administration approved)[2,16-19].

In this review, we sought to focus on clinical, pathophysiological, histological, and therapeutic aspects of GI tract involvement in SM.

## GI CLINICAL MANIFESTATIONS OF SM

GI involvement in the clinical presentation of SM has been reported to vary from 15% to 85%. The wide range of variability is probably due to variable definitions of GI symptoms and differences in the attention on GI involvement in the case series available in the literature[20]. However, among all clinical manifestations, GI symptoms appear to be second in frequency only to itching[21] and are the main culprits of chronic disorders being a major determinant of quality of life (QoL)[20-22].

GI symptoms can be varied and may be independent of a clear GI involvement with mastocytes' infiltration[23]. In addition, GI manifestations may occur in the absence of typical cutaneous manifestations, with GI dysfunction being observed in both cutaneous mastocytosis and SM[24]. Although the gastro-enteric tract involvement has been described in all SM variants, both the frequency and the type of GI symptoms vary according to the SM subtype.

GI symptoms associated with SM are often non-specific and mimic common conditions, such as irritable bowel syndrome, inflammatory bowel disease, or celiac disease, with recurrent abdominal pain, nausea, vomiting, gastro-esophageal reflux disease, diarrhea, and bloating, until more severe pictures characterized by long-standing, persistent, and intractable diarrhea with malabsorption occurs[23]. Also, peptic ulcer disease represents a GI manifestation of SM, causing gastro-duodenal ulceration in up

to 50% of cases[25], with possible severe GI bleeding sustained by the large amount of histamine released by mast cells (Table 3).

## **PATHOPHYSIOLOGY OF GI INVOLVEMENT**

From the pathophysiological point of view, these symptoms are caused by several mechanisms. Activation of MCs causes alteration in epithelial and neuromuscular function. MCs represent 2% of the cells present on the intestinal mucosa of the GI tract[26]: They are responsible for a series of regulatory functions concerning the barrier functions and vascular mucosal permeability, regulating the secretion of GI hormones, modulating peristalsis and the pain perception threshold, and regulating the endothelial barrier and chemotaxis of immune cells. They, therefore, intervene in the regulation of the inflammatory response and, as recently described, they drive the immune response by attracting both granulocytes and lymphocytes and triggering innate defense mechanisms, such as enhanced epithelial secretion, peristalsis, and alarm programs of the enteric nervous system[26,27].

Activated MCs release various inflammatory mediators, which determine intestinal motility alteration, visceral sensitivity alteration, and mucosal and epithelial gut barrier function alteration. Furthermore, MCs inflammatory mediators determine hypersecretion and increased motility, causing diarrhea and abdominal pain. In the more advanced and aggressive stages, there is a direct MC infiltration of the GI tract and the pathogenic mechanisms change. The GI tract can be involved in any phase of SM and the pathophysiological mechanisms are different. As well as reported for other extra-hematological manifestations of SM, in the initial and indolent forms of SM, the gut is a target of mediators released by MCs and functional disorders are more expressed, with mediator-related functional diarrhea, abdominal pain, and motor dyspepsia.

Thereafter, with the massive and persistent mediators' release, organic lesions appear, such as peptic disease. The main mediator released by MCs is histamine which exerts different effects on both the upper and lower gastrointestinal tract. Histamine interacts with H2 receptors, promoting the secretion of hydrochloric acid, resulting in gastroesophageal reflux disease, gastritis, and peptic ulcer.

The peptic ulcer due to the increase in histamine-related acid secretion is a condition not rarely observed in SM, and it is largely underestimated: It is reported in up to 40% of patients with SM. It does not correlate with circulating markers, in particular with circulating histamine; therefore, it has to be hypothesized with a low threshold of suspicion and then investigated with gastroscopy. Moreover, peptic ulcer bleeding in MS is also reported in up to 11% of patients[25]. Histamine also interacts with the H1 receptors, regulating the gut smooth muscle contraction, causing impaired peristalsis and motility disorders, clinically resulting in the dysmotility-like dyspepsia and functional diarrhea observed in patients in the early stages of SM.

Besides the GI effects of histamine, other transmitters are released in the course of SM, including prostaglandins and serotonin, which have various effects, including effects mainly on the neuromuscular junction of the GI tract, with consequently impaired motility and visceral hypersensitivity. Again, patients present with nausea, vomiting, and abdominal pain worsened by the reduction of the pain threshold. In the course of mastocytosis, diarrhea is often associated with flushing. Therefore, is important to distinguish "wet flushing", associated with profuse sweating, and "dry flushing", without sweating (Table 3). In SM, dry flushing is observed, whereas "wet flushing" is more related to physiological or para-physiological causes.

In the more advanced and aggressive stages of MS, the manifestations are mainly related to the gut MC infiltration of the GI wall, which impairs both the barrier functions and the absorbing functions, and the pathogenic mechanisms of diarrhea change from a functional to organic diarrhea. As the disease progresses, the clinical picture evolves into malabsorption, progressive caloric-protein malnutrition, vitamin deficiency, deterioration of the patient's condition, worsening of osteoporosis (already present in these patients), and finally anasarca, due to a complete impaired gut absorption and barrier function.

### ***Mast cell mediators-related GI abnormalities***

The release of a great amount of histamine and other peptides contained in MC granules has been implicated in the pathogenesis of a variety of functional GI manifestations in SM, including diarrhea, bloating, nausea, vomiting, abdominal pain, peptic ulcer disease, and related GI bleeding.

A recent multicenter French study analyzing a cohort of 83 patients affected by SM has demonstrated that GI symptoms are more frequent in SM patients compared to matched healthy subjects. Moreover, SM is correlated with a significantly greater risk of developing peptic ulcer disease, especially duodenal ulcers[28]. Diarrhea, bloating and abdominal pain have been reported as the most frequent SM-associated GI disturbances in several studies[20,22,25,29].

Abdominal pain has been described in different case series with a wide range of frequency from 12% to 100%. Of note, Cherner and colleagues[25] identified two different types of abdominal pain. The majority of SM patients suffered from an abdominal pain of dyspeptic nature, defined as an epigastric pain responsive to antacids and histamine type 2 receptor antagonists and with a high incidence of peptic disease on upper gastrointestinal endoscopic examination. A minority of patients complained of

**Table 3 Differential diagnosis between systemic mastocytosis and gastrointestinal diseases**

Symptoms	Differential diagnosis
Chronic diarrhea	Irritable bowel syndrome; Inflammatory bowel disease; Celiac disease; Thyreopathies ( <i>i.e.</i> hyperthyroidism, medullary thyroid cancer); Pancreatopathies
Epigastric pain, dyspepsia, heartburn	Functional dyspepsia; Peptic ulcer; Gastroesophageal reflux disease; H. pylori related gastritis; Zollinger-Ellison Syndrome
Flushing	Neuroendocrine neoplasms
Hepato-splenomegaly, portal hypertension	Cirrhosis; Non cirrhotic portal hypertension

non-dyspeptic pain associated with bloating that does not benefit from histamine 2 receptor antagonists and antacids and was associated with normal endoscopic investigations. While the pathogenesis of the first pain type may be easily correlated to increased acid secretion, the non-dyspeptic pain type is more likely related to intestinal motility disturbances and a lower pain threshold caused not only by an increased release of histamine but also by other mediators, such as serotonin, prostaglandins, and neuropeptides.

Functional diarrhea has been reported in several series of SM patients with a range from 14% to 100%. The presence of diarrhea has been described as an episodic increase in bowel movements with subsequent emission of liquid stool that may or may not be associated with a fecal weight > 200 g/d [20]. It may be related to increased gastric acid secretion with mechanisms similar to Zollinger Ellison syndrome and/or to increased bowel motility induced by prostaglandin D2 secretion, as there is evidence of cases of diarrhea responsive to aspirin administration[30]. In contrast, the presence of steatorrhea has been correlated with a condition of malabsorption characteristic of advanced mastocytosis with extensive mucosal and submucosal infiltration with MCs.

Nausea and vomiting have been described less frequently and usually as components of syndromic disorders that also include palpitations, flushing, abdominal cramps, and diarrhea, generally exacerbated by the ingestion of certain substances, such as alcohol and medications, or contact with inflammatory mediators, which stimulate MCs degranulation. The absence of specific colonic symptoms does not mean that the colon or rectum are not involved. In particular, rectal manometric studies show a lower distention threshold to induce pain or rectal urgency; patients complain of reduced rectal compliance or overactive rectal contractility.

### **Peptic ulcer disease**

One of the most common mediator-related clinical signs, which over time can generate organic lesions and GI organic damage, is related to gastric acid hypersecretion secondary to the hyper-histaminic state, which leads to dyspeptic pain and digestive ulcer disease.

A prospective study shows that peptic ulcers in SM are common, present in up to 50% of patients [25]. It is usually symptomatic and associated with gastric acid hypersecretion and elevated basal acid output (BAO)[31]. In some patients, BAO can reach the Zollinger-Ellison range, so that may even cause the signs and symptoms of the syndrome itself[20]. Of interest, a particular form of CM, the so-called *telangiectasia macularis eruptiva perstans*, also known as paucicellular mastocytosis, has been associated with peptic giant gastro-duodenal ulcers[32]. Other acid-related complications have been reported, such as ulcer perforation and severe esophagitis. Moreover, up to 11% of SM-affected patients will manifest peptic ulcer bleeding during the disease course. However, so far there has been no evidence of a consistent relationship between the level of serum histamine and the presence of ulcer disease or gastric acid output. However, despite the increased circulating histamine level, many patients have normal acid secretion and in some cases, even achlorhydria has been observed[31]. The variability in the response to circulating histamine may relate to partial inactivity of circulating histamine, differences between circulating histamine and gastric tissue histamine, and the intervention of unknown cofactors in the stimulation of oxyntic cells, as well as the theory of possible desensitization of parietal cells that can justify the rare cases of complete achlorhydria[20].

### **Mast cell infiltration-related GI abnormalities**

In patients with advanced SM, the B and C findings (Table 2) become prevalent to functional GI symptoms. B GI findings indicate organ involvement without organ dysfunction, while C GI-findings refer to the advanced stage where both organ infiltration and dysfunction coexist, being associated with a poor prognosis[6]. They include malabsorption, weight loss, and organomegaly (spleen, liver) until full-blown organ dysfunction leads to hepatic failure and ascites.

Malabsorption based on quantitative stool fat analysis, D-xylose, and Schilling tests has been found to occur in one-third of SM patients and is usually mild[32]. Thus, it is important to consider mastocytosis in the diagnostic work-up of chronic and intractable diarrhea, especially when the endoscopic presentation seems to be suggestive. Both the small and the large intestine can undergo permanent

alterations, which contribute to the genesis of diarrhea and malabsorption. Over time, patients could develop real intestinal malabsorption syndrome with vitamins A and D deficiency, overt osteomalacia and osteoporosis, protein-energy malnutrition, and anasarca. The whole gastrointestinal tract may be involved in SM with varying degrees.

Liver involvement in SM can range from an abnormal liver function test alone to hepatomegaly due to MC and eosinophil infiltrates in portal triads. Initial fibrosis can evolve in cirrhosis with worsening portal hypertension sustained by simultaneous splenomegaly, with or without hypersplenism, and ultimately ascites and upper digestive bleeding from esophageal varices. Of note, mastocytosis is one of the causes of non-cirrhotic portal hypertension[33], sustained by pre-sinusoidal and sinusoidal mechanisms through the infiltration of inflammatory mast cells within the portal vein and obstruction of the sinusoids[34]. In this setting, we can also observe vascular alterations, like portal hypertension, veno-occlusive disease (8%), and Budd-Chiari syndrome.

No studies have identified how many patients with SM develop portal hypertension, but in real medical practice, clinicians have to keep in mind that it can occur without associated advanced liver disease, further increasing the risk of upper GI bleeding. A study of 24 cases of SM involving the GI tract found only 3 patients with liver involvement; however, liver involvement correlates with more aggressive disease[23]. Moreover, as liver failure occurs, it contributes to worsening malnutrition and hypoalbuminemia that are already determined by intestinal insufficiency.

## ENDOSCOPIC FINDINGS IN SM

Even though no remarkable endoscopic findings could be found[4], there are several endoscopic pictures described in SM, and endoscopic findings could be secondary both to MC mediator release and to MC infiltration in the GI wall or liver.

### **Upper gastrointestinal endoscopy**

At upper GI endoscopy, peptic disease (esophagitis, esophageal strictures, peptic ulcer) is one of the most frequent findings in patients with SM[21].

According to the literature, upper GI involvement could be found in up to 40% of SM patients undergoing endoscopy[25] and may be sustained by chlorhydric acid hypersecretion. However, its pathogenesis is still uncertain: Peptic disease is thought to be secondary to gastric acid hypersecretion sustained by elevated histamine plasma levels, but data from literature are controversial: Hypersecretion of gastric acid does not seem to be consistently related to the level of serum histamine levels measured. It may, however, be possible that a relationship between tissue concentration of histamine and GI manifestations can exist[25].

While esophagitis and, when untreated, esophageal strictures are thought to be secondary to mediator release, esophageal varices could be accounted for SM endoscopic findings when liver infiltration is present; this infiltration determines intrahepatic portal hypertension with esophageal and gastric varices development[33-35].

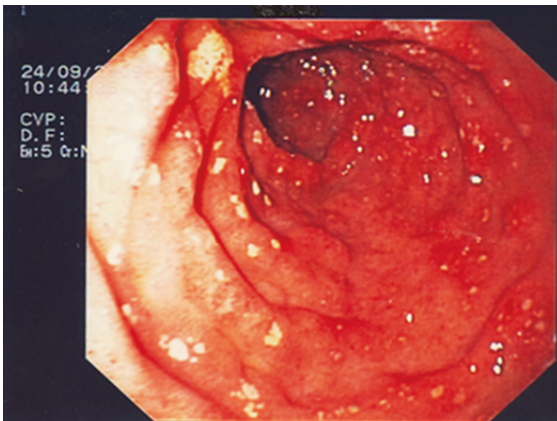
Exploration of the stomach and duodenum could show urticaria-like lesions in the antrum of the stomach, diffuse telangiectasia, multiple erosions of gastric and/or duodenal mucosa (Figure 1) and peptic ulcer; these findings are thought to be secondary to MCs mediators' release (*i.e.*, histamine, serotonin, prostaglandins, and neurotensin). When atypical mastocyte infiltration occurs, nodular mucosal lesion of the stomach and/or duodenum can be found[21,36,37].

### **Small bowel endoscopy and colonoscopy**

Small bowel, as well as other digestive tract components, could be involved by SM. From the review of literature, the most common findings during small bowel exploration are diffuse telangiectasia, thickened jejunal folds, scalloped folds, and diffuse nodularity[21,36]. As for the upper GI tract, diffuse telangiectasia and thickened jejunal folds are thought to be secondary to MC mediator release, while scalloped folds and diffuse nodularity are thought to be secondary to MC infiltration in the GI wall[21].

Colonoscopy in patients with SM can reveal diffuse telangiectasia and/or urticarial lesion, patchy mucosal erythema, as well as mucosal edema, mucosal friability, loss of vascular patterns, and diffuse nodularity. Moreover, adding indigo carmine dye spraying could be useful to enhance yellowish-white polypoid lesions and yellowish-white nodular or granular mucosal lesions[36,38,39].

As for the other GI tracts, mucosal erythema and edema, mucosal friability are thought to be secondary to MC mediator release, while loss of vascular patterns and nodular and /or polypoid lesions are thought to be secondary to MCs infiltration into the bowel wall[21]. Unfortunately, none of these endoscopic signs is specific for GI involvement of SM; hence, biopsy specimens of the GI wall should always be performed in order to have histological diagnostic confirmation of GI involvement.



DOI: 10.3748/wjg.v28.i29.3767 Copyright ©The Author(s) 2022.

**Figure 1** Endoscopic pictures of second portion of the duodenum. The mucosa appears to be erythematous, hyperemic, and covered with diffuse erosions.

## HISTOPATHOLOGICAL ASPECT IN SM

Mast cells (MCs) are unique granulated cells (approximately 20  $\mu\text{m}$ ) that are absent in peripheral blood. They develop *in situ* from CD34-positive or c-Kit-positive progenitor cells[40]. MCs are distributed throughout many tissues, including the gastrointestinal mucosa. They enable an immune function in response to a diversity of exogenous substances in the gut lumen[41].

Within the gut, two subpopulations can be distinguished: the mucosal reactive MCs, which may dramatically increase in response to immune stimuli and are dependent on T lymphocytes[42,43], and the submucosal MCs, which can act in the regulation of intestinal permeability, secretion, peristalsis, nociception, immunity, and angiogenesis[44]. The histologic appearances of the GI mucosa in SM patients are incompletely described[45]. Results of mucosal mast cell quantitation have similarly been mixed with some studies reporting increased, decreased, and normal numbers of mucosal mast cells in patients with SM compared with controls[46].

The mean normal value of MCs count in normal GI mucosa is yet to be validated in large patient cohorts; most studies consider a cutoff of 20 MCs per high-power field within the lamina propria, this value being 2 standard deviations above that found in the general population[47,48]. As MC infiltrate can be focal and mild, the diagnosis of mastocytosis in GI mucosal biopsies can be challenging; hence, multiple biopsies are necessary in order to improve diagnostic yield[28].

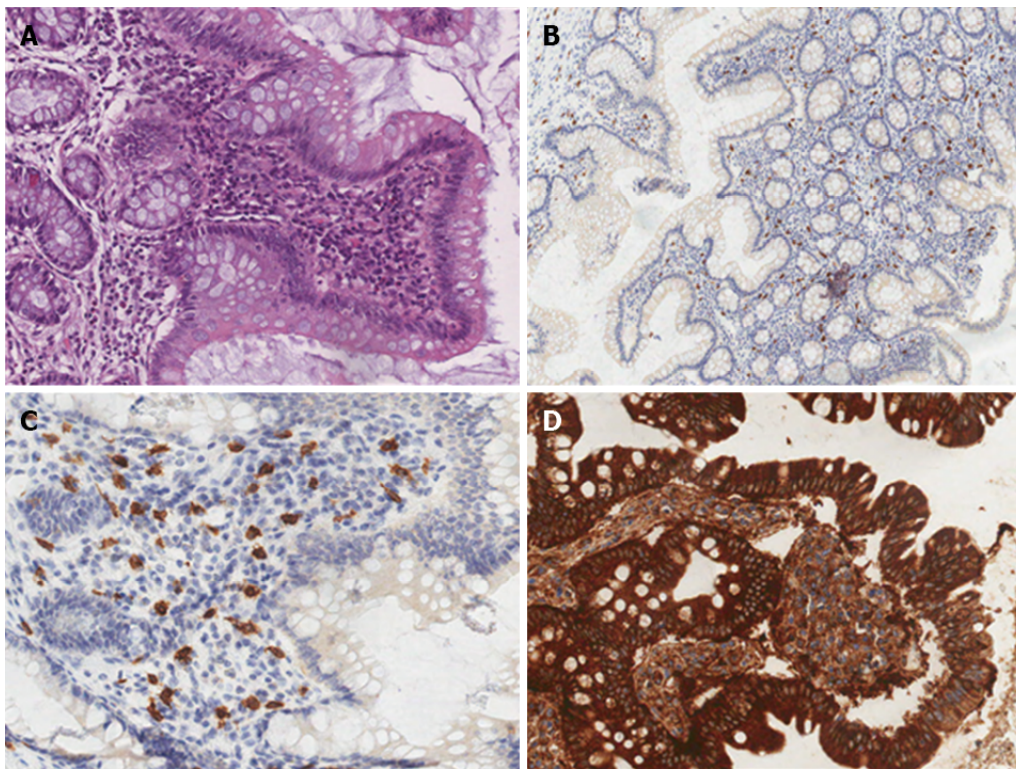
In almost all cases of SM involving the GI tract, the number of intramucosal MCs is substantially increased[23], and MCs group together forming pathognomonic compact micronodular or band-like infiltrate. Tiny clusters of cells, with a predominant sub-epithelial distribution, appear in different shapes, varying from rounded cells with a moderate amount of pale and eosinophilic cytoplasm to ovoid and spindle-shaped cells with scant cytoplasm. Those diagnostic infiltrates may be small but should consist at least of 15 clusterings[23].

Hematoxylin and eosin staining are not a definitive method for MCs detection, hence special staining is required, such as toluidine blue staining and immuno-histo-chemical panels using tryptase, CD117, and CD25[49]. Comparison between these techniques confirmed a stem cell factor receptor kit (testing for c-kit and CD117) is the most accurate technique[50]. CD117 is expressed on all types of MCs independent of maturation and activation status; in SM, c-Kit is often expressed in MCs in a mutated and constitutively activated form. In these patients, MCs aberrantly display CD25, a diagnostic marker of neoplastic MCs in all SM variants[51]. Therefore, CD117 is sensitive, but not specific for MCs; tryptase is less sensitive but more specific. Both CD117 and tryptase are not diagnostic of the neoplastic nature, whereas CD25 expression is considered a hallmark of MCs atypia[4] (Figure 2).

SM may involve other GI organs like the liver. The main site of liver involvement is the portal tract, where MCs may form groups of dense infiltrates within the fibrotic portal triads; because MCs are normally absent in the sinusoid, the presence of scattered MCs in liver sinusoids is also consistent with SM (Figure 3).

## TREATMENT OF GI SYMPTOMS

Symptom-directed treatments should be considered in all SM patients and are directed at MC degranulation symptoms (*i.e.* nausea, vomiting, abdominal pain, peptic disease, diarrhea)[2].



DOI: 10.3748/wjg.v28.i29.3767 Copyright ©The Author(s) 2022.

**Figure 2 Spectrum of histologic findings in patients with intestinal involvement of systemic mastocytosis.** A: A mild initial finding with mast cells arranged in sheets and micro aggregates (hematoxylin-eosin, × 10). A heavy eosinophil infiltrate frequently dominates the picture. Crypt architectural distortion, without any other evidence of inflammatory bowel disease. Scattered lymphocytes and plasma cells often accompanied the mast cell and eosinophil infiltrates; B-C: The mast cells show expression of c-kit (B; CD117, × 2) and tryptase (C; × 10); D: CD25 positive cells in a clearcut and spread duodenal mastocytosis (CD25, × 10).

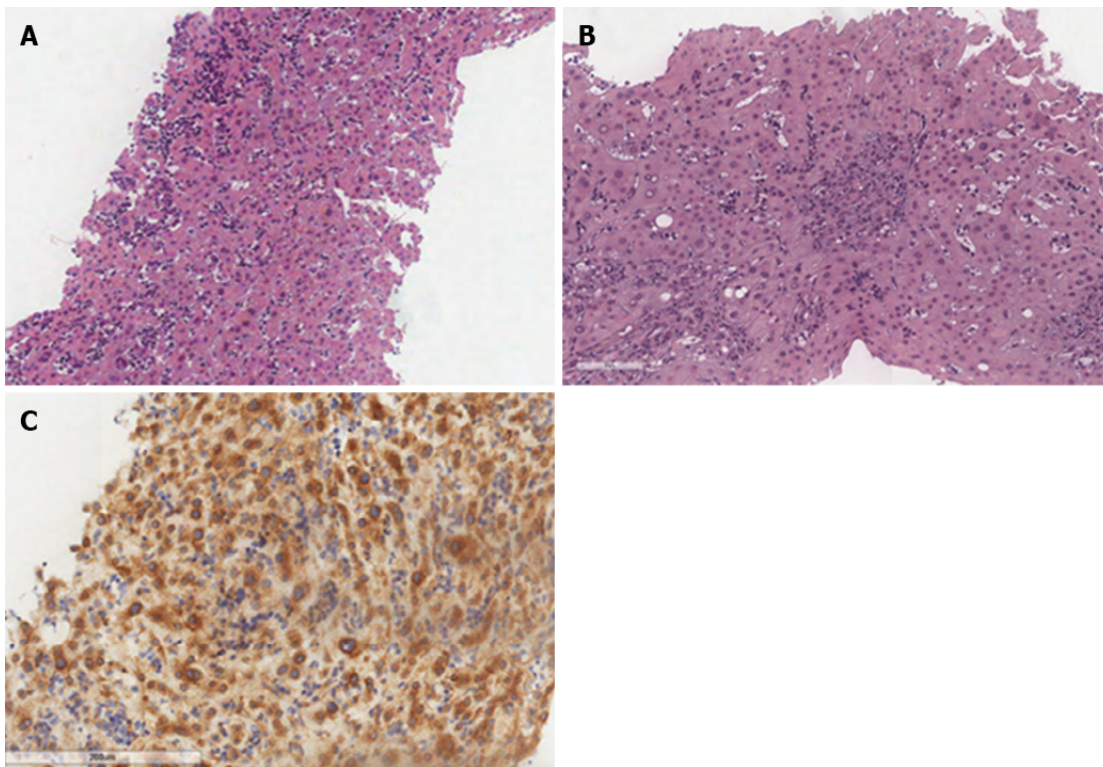
As first step, patients must recognize and avoid general and specific individual factors that trigger symptoms. These can commonly include physical factors such as heat, temperature changes, some forms of exercise, emotions, stress, sleep deprivation; diagnostic and therapeutic agents (such as opiates, NSAIDs, succinylcholine, and agents with tetrahydroisoquinoline, atracurium, rocuronium, and quinolones), foods, alcohol and Hymenoptera venoms[52].

Different symptomatic drugs have been proposed for the control of GI symptoms: H<sub>2</sub>- antagonists (*i.e.*, Famotidine 10 mg BID, Cimetidine 400 mg BID) are the first-line therapy[2]. They act as inverse agonists that combine with and stabilize the inactive conformation of the histamine-receptor, shifting the equilibrium toward the inactive state; in a concentration-dependent manner, they inhibit MC activation and histamine release. However, although, the mechanisms involved have not yet been delineated fully, downregulation of intracellular calcium ion accumulation seems to play a role[53]. Inactivation of histamine receptors reduces the histamine effect along the GI tract, hence reducing histamine-related symptoms (*i.e.*, diarrhea, abdominal pain, peptic disease).

When histamine-receptor blockers are poorly effective or ineffective, proton pump inhibitors (PPIs, *i.e.*, Omeprazole 20 mg/d, Rabeprazole 20 mg/d, Pantoprazole 40 mg/d) represent second-line therapy [2]. Hydrochloric acid is secreted by parietal cells in the oxyntic mucosa that lines the body and the fundus of the stomach as a response to different mediators (*i.e.*, histamine, gastrin, acetylcholine), that activate H<sup>+</sup>/K<sup>+</sup> ATP-ase (*i.e.*, the proton pump) that pumps hydrogen ions (protons) into the lumen in exchange for potassium ions. PPIs block this final step in gastric acid secretion by blocking H<sup>+</sup>/K<sup>+</sup> ATP-ase irreversibly. They are remarkably effective in the inhibition of gastric acid secretion[54]. Considering SM as a hypersecretory condition, it is clear that reducing hydrochloric acid secretion is beneficial in SM patients because it reduces peptic symptoms, peptic disease, and/or diarrhea.

Sodium cromolyn (100-200 mg QID 30 minutes before meals and bedtime) represents the third-line therapy when H<sub>2</sub> antagonists and PPIs are ineffective[2]. It works as an inhibitor of histamine release and cell membrane stabilizer: cromolyn sodium caused weak inhibition of histamine release. However, different studies have shown its action on other mediators involved in mast cells' degranulation by inhibiting prostaglandin D<sub>2</sub> release and TNF $\alpha$  release from mast cells, hence reducing MC degranulation and mediator release[55]. Reducing mediator release should help reduce GI symptoms.

Pardanani[2] has proposed systemic corticosteroid (*i.e.* prednisone 0.5-1 mg/kg/d starting dose; taper as feasible based on response/tolerance), as the fourth line of therapy for GI symptoms resistant to previous symptomatic therapies. Corticosteroids are potent anti-inflammatory drugs widely used in the treatment of allergic and inflammatory diseases. They also showed an in-vitro inhibition of MCs



DOI: 10.3748/wjg.v28.i29.3767 Copyright ©The Author(s) 2022.

**Figure 3** Frustules of hepatic parenchyma with substantially preserved structure, with trabeculae with 2-cell spinnerets with no significant steatosis, but focal balloon-like degeneration associated with biliary stasis phenomena. A: Biliary spaces with preserved ducts, with ductular regeneration and bilio-hepatocyte metaplasia (hematoxylin-eosin,  $\times 4$ ); B: Some phenomena of hepatitis with aggression of the biliary epithelium are observed (hematoxylin-eosin,  $\times 20$ ). Portal spaces enlarged due to the presence of mixed inflammatory infiltrates, mainly consisting of T lymphocytes (CD3 +) with initial fibrotic expansion and formation of porto-portal bridges; C: In this context, scattered CD117 +, tryptase + cells ( $\times 20$ ) referable to mast cells.

mediators' release. Systemic administration of corticosteroids has been used in patients with mastocytosis. While this treatment appears to improve control of some mediator-release symptoms, it has not been proven to reduce MC numbers significantly in patients with mastocytosis[56]. Of note, systemic corticosteroids have been useful in decreasing the malabsorption and ascites in some of these patients[57].

In advanced SM, treatments interfering with MC proliferation and survival are used[2]. GI symptoms secondary to organ infiltration could also benefit from cytoreductive therapies, such as 2-chlorodeoxyadenosine (cladribine or 2-CdA) or interferon-alfa[58]. In young and otherwise healthy ASM patients, allo-SCT is the only option for a sustained response[59]. Promising effects have been seen with the use of targeted therapy on mutated-KIT, which occurs in most SM patients[2]. Midostaurin (PKC412) is the first kit-inhibitor recent approved by the United States Food and Drug Administration (FDA) and European Medicines Agency (EMA) for the treatment of Advanced SM[16,17]. It has *in vitro* activity against kinase domain KIT mutants (D816Y and D816V). In the global Phase 2 CPKC412D2201 trial[18], 116 patients with advanced SM were enrolled; patients were treated with PKC412 at 100 mg BID. The overall response rate (ORR) per conventional criteria was 60% with 45% having a major response and 15% having a partial response, but it is often not sustained. In particular, concerning GI involvement, reversal of organ damage was reflected by normalization of hypoalbuminemia (58%), improvement in liver function test abnormalities (44%-58%), and/or reversion of weight loss (25%). Patients reported improvement of disease-related symptoms with treatment. Therefore, the most common drug side effects (all grades/grades 3-4) were nausea (79%/6%), vomiting (66%/6%), diarrhea (54%/3%), and fatigue (28%/9%), in addition to hematological toxicity, in terms of grade 3-4 of neutropenia, anemia, and thrombocytopenia, occurring in 24%, 41%, and 29% of patients, respectively.

Avapritinib[19], a KIT and PDGFRA inhibitor, showed promising results; other medications potentially effective for SM patients are under investigation[2]. Further optimization of treatment with tyrosine-kinase inhibitors in order to improve patients' quality of life is still needed.

## CONCLUSION

Mastocytosis is a rare and heterogeneous disease characterized by various biological and clinical

features with different prognosis and treatments. The disease is usually divided into 2 principal categories: CM and SM. Clinical features can be related to MCs mediators release or pathological MCs infiltration. The diagnosis of SM is based on clinical, biological, histological, and molecular criteria, according to WHO 2016 classification. A proper patient's workup requires a multidisciplinary approach including gastroenterologists, endoscopists, hematologists, and pathologists. Among all manifestations of the disease, GI symptoms are common, being present in 15%-85% of the patients and can significantly impair the quality of life. Here, we review the data regarding GI involvement in SM, in terms of clinical presentations, histological features, pathogenesis of GI symptoms and their treatment. The most frequent GI symptoms are abdominal pain, diarrhea, nausea, and vomiting. GI lesions may involve all the digestive tract, from the esophagus to the rectum. The histological diagnosis of GI involvement is difficult. The treatment of GI symptoms aims to prevent and limit MCs degranulation and/or its consequences and more rarely to control tumoral mast cells infiltration. The diagnosis of mastocytosis should be considered in the case of unexplained severe GI disorders.

---

## ACKNOWLEDGEMENTS

Massironi S and Invernizzi P are members of the European Reference Network on Hepatological Diseases (ERN RARE LIVER) and they thank AMAF Monza Onlus and AIRCS.

---

## FOOTNOTES

**Author contributions:** Elvevi A, Elli EM, and Massironi S designed the study; Elvevi A, Elli EM, Lucà M, and Scaravaglio M wrote the first draft of the paper; Pagni F, Ceola S, and Ratti L revised the paper and wrote the final version; Massironi S and Invernizzi P reviewed the paper for important intellectual content; all authors have read and approved the final manuscript.

**Conflict-of-interest statement:** All authors report no relevant conflict of interest for this article.

**Open-Access:** This article is an open-access article that was selected by an in-house editor and fully peer-reviewed by external reviewers. It is distributed in accordance with the Creative Commons Attribution NonCommercial (CC BY-NC 4.0) license, which permits others to distribute, remix, adapt, build upon this work non-commercially, and license their derivative works on different terms, provided the original work is properly cited and the use is non-commercial. See: <https://creativecommons.org/licenses/by-nc/4.0/>

**Country/Territory of origin:** Italy

**ORCID number:** Alessandra Elvevi 0000-0001-9841-2051; Elena Maria Elli 0000-0001-5576-5412; Martina Lucà 0000-0003-3787-6973; Miki Scaravaglio 0000-0003-2914-4908; Fabio Pagni 0000-0001-9625-1637; Stefano Ceola 0000-0002-5815-987X; Laura Ratti 0000-0003-0198-6433; Pietro Invernizzi 0000-0003-3262-1998; Sara Massironi 0000-0003-3214-8192.

**S-Editor:** Wu YXJ

**L-Editor:** Filipodia

**P-Editor:** Wu YXJ

---

## REFERENCES

- 1 **Horny H**, Akin C, Arber D, Peterson L, Tefferi A, Metcalfe D, Bennet J, Bain B, Escribano L, Valent P. WHO Classification of Tumours of Haematopoietic and Lymphoid Tissues. Revised 4th Ed. Lyon, France: IARC, 2017
- 2 **Pardanani A**. Systemic mastocytosis in adults: 2021 Update on diagnosis, risk stratification and management. *Am J Hematol* 2021; **96**: 508-525 [PMID: 33524167 DOI: 10.1002/ajh.26118]
- 3 **Valent P**, Akin C, Escribano L, Födinger M, Hartmann K, Brockow K, Castells M, Sperr WR, Kluin-Nelemans HC, Hamdy NA, Lortholary O, Robyn J, van Doormaal J, Sotlar K, Hauswirth AW, Arock M, Hermine O, Hellmann A, Triggiani M, Niedoszytko M, Schwartz LB, Orfao A, Horny HP, Metcalfe DD. Standards and standardization in mastocytosis: consensus statements on diagnostics, treatment recommendations and response criteria. *Eur J Clin Invest* 2007; **37**: 435-453 [PMID: 17537151 DOI: 10.1111/j.1365-2362.2007.01807.x]
- 4 **Zanelli M**, Pizzi M, Sanguedolce F, Zizzo M, Palicelli A, Soriano A, Bisagni A, Martino G, Caprera C, Moretti M, Masia F, De Marco L, Froio E, Foroni M, Bernardelli G, Alvarez de Celis MI, Giunta A, Merli F, Ascani S. Gastrointestinal Manifestations in Systemic Mastocytosis: The Need of a Multidisciplinary Approach. *Cancers (Basel)* 2021; **13** [PMID: 34282774 DOI: 10.3390/cancers13133316]
- 5 **Arber DA**, Orazi A, Hasserjian R, Thiele J, Borowitz MJ, Le Beau MM, Bloomfield CD, Cazzola M, Vardiman JW. The 2016 revision to the World Health Organization classification of myeloid neoplasms and acute leukemia. *Blood* 2016; **127**: 2391-2405 [PMID: 27069254 DOI: 10.1182/blood-2016-03-643544]

- 6 **Valent P**, Horny HP, Escribano L, Longley BJ, Li CY, Schwartz LB, Marone G, Nuñez R, Akin C, Sotlar K, Sperr WR, Wolff K, Brunning RD, Parwaresch RM, Austen KF, Lennert K, Metcalfe DD, Vardiman JW, Bennett JM. Diagnostic criteria and classification of mastocytosis: a consensus proposal. *Leuk Res* 2001; **25**: 603-625 [PMID: 11377686 DOI: 10.1016/s0145-2126(01)00038-8]
- 7 **Li Z**. New Insights into the Pathogenesis of Systemic Mastocytosis. *Int J Mol Sci* 2021; **22** [PMID: 34063170 DOI: 10.3390/ijms22094900]
- 8 **Garcia-Montero AC**, Jara-Acevedo M, Teodosio C, Sanchez ML, Nunez R, Prados A, Aldanondo I, Sanchez L, Dominguez M, Botana LM, Sanchez-Jimenez F, Sotlar K, Almeida J, Escribano L, Orfao A. KIT mutation in mast cells and other bone marrow hematopoietic cell lineages in systemic mast cell disorders: a prospective study of the Spanish Network on Mastocytosis (REMA) in a series of 113 patients. *Blood* 2006; **108**: 2366-2372 [PMID: 16741248 DOI: 10.1182/blood-2006-04-015545]
- 9 **Pardanani A**, Lasho T, Elala Y, Wassie E, Finke C, Reichard KK, Chen D, Hanson CA, Ketterling RP, Tefferi A. Next-generation sequencing in systemic mastocytosis: Derivation of a mutation-augmented clinical prognostic model for survival. *Am J Hematol* 2016; **91**: 888-893 [PMID: 27214377 DOI: 10.1002/ajh.24426]
- 10 **Cohen SS**, Skovbo S, Vestergaard H, Kristensen T, Møller M, Bindslev-Jensen C, Fryzek JP, Broesby-Olsen S. Epidemiology of systemic mastocytosis in Denmark. *Br J Haematol* 2014; **166**: 521-528 [PMID: 24761987 DOI: 10.1111/bjh.12916]
- 11 **Zanotti R**, Tanasi I, Bernardelli A, Orsolini G, Bonadonna P. Bone Marrow Mastocytosis: A Diagnostic Challenge. *J Clin Med* 2021; **10** [PMID: 33915965 DOI: 10.3390/jcm10071420]
- 12 **Alto WA**, Clarcq L. Cutaneous and systemic manifestations of mastocytosis. *Am Fam Physician* 1999; **59**: 3047-3054, 3059
- 13 **Nedoszytko B**. Mastocytosis in children and adults: clinical disease heterogeneity. Archives of medical science: AMS (e-pub ahead of print 20 November 2021)
- 14 **Orsolini G**, Viapiana O, Rossini M, Bonifacio M, Zanotti R. Bone Disease in Mastocytosis. *Immunol Allergy Clin North Am* 2018; **38**: 443-454 [PMID: 30007462 DOI: 10.1016/j.iac.2018.04.013]
- 15 **Brazzelli V**, Grassi S, Merante S, Grasso V, Ciccocioppo R, Bossi G, Borroni G. Narrow-band UVB phototherapy and psoralen-ultraviolet A photochemotherapy in the treatment of cutaneous mastocytosis: a study in 20 patients. *Photodermatol Photoimmunol Photomed* 2016; **32**: 238-246 [PMID: 27353865 DOI: 10.1111/phpp.12248]
- 16 **Growney JD**, Clark JJ, Adelsperger J, Stone R, Fabbro D, Griffin JD, Gilliland DG. Activation mutations of human c-KIT resistant to imatinib mesylate are sensitive to the tyrosine kinase inhibitor PKC412. *Blood* 2005; **106**: 721-724 [PMID: 15790786 DOI: 10.1182/blood-2004-12-4617]
- 17 **Gleixner KV**, Mayerhofer M, Aichberger KJ, Derdak S, Sonneck K, Böhm A, Gruze A, Samorapoompichit P, Manley PW, Fabbro D, Pickl WF, Sillaber C, Valent P. PKC412 inhibits in vitro growth of neoplastic human mast cells expressing the D816V-mutated variant of KIT: comparison with AMN107, imatinib, and cladribine (2CdA) and evaluation of cooperative drug effects. *Blood* 2006; **107**: 752-759 [PMID: 16189265 DOI: 10.1182/blood-2005-07-3022]
- 18 **Gotlib J**, Berubé C, Growney JD, Chen CC, George TI, Williams C, Kajiguchi T, Ruan J, Lilleberg SL, Durocher JA, Lichy JH, Wang Y, Cohen PS, Arber DA, Heinrich MC, Neckers L, Galli SJ, Gilliland DG, Coutre SE. Activity of the tyrosine kinase inhibitor PKC412 in a patient with mast cell leukemia with the D816V KIT mutation. *Blood* 2005; **106**: 2865-2870 [PMID: 15972446 DOI: 10.1182/blood-2005-04-1568]
- 19 **Bose P**, Verstovsek S. Avapritinib for Systemic Mastocytosis. *Expert Rev Hematol* 2021; **14**: 687-696 [PMID: 34289787 DOI: 10.1080/17474086.2021.1959315]
- 20 **Jensen RT**. Gastrointestinal abnormalities and involvement in systemic mastocytosis. *Hematol Oncol Clin North Am* 2000; **14**: 579-623 [DOI: 10.1016/S0889-8588(05)70298-7]
- 21 **Lee JK**, Whittaker SJ, Enns RA, Zetler P. Gastrointestinal manifestations of systemic mastocytosis. *World J Gastroenterol* 2008; **14**: 7005-7008 [PMID: 19058339 DOI: 10.3748/wjg.14.7005]
- 22 **Horan RF**, Austen KF. Systemic mastocytosis: retrospective review of a decade's clinical experience at the Brigham and Women's Hospital. *J Invest Dermatol* 1991; **96**: 5S-13S; discussion 13S [PMID: 16799602 DOI: 10.1111/1523-1747.ep12468899]
- 23 **Doyle LA**, Sepehr GJ, Hamilton MJ, Akin C, Castells MC, Hornick JL. A clinicopathologic study of 24 cases of systemic mastocytosis involving the gastrointestinal tract and assessment of mucosal mast cell density in irritable bowel syndrome and asymptomatic patients. *Am J Surg Pathol* 2014; **38**: 832-843 [PMID: 24618605 DOI: 10.1097/PAS.0000000000000190]
- 24 **Hamera L**, Santos AM, Prince SA, Chandrupatla S, Jordan J. Systemic Mastocytosis: A Rare Cause of Diarrhea. *Cureus* 2020; **12**: e9112 [PMID: 32670731 DOI: 10.7759/cureus.9112]
- 25 **Cherner JA**, Jensen RT, Dubois A, O'Dorisio TM, Gardner JD, Metcalfe DD. Gastrointestinal Dysfunction in Systemic Mastocytosis. *Gastroenterology* 1988; **95**: 657-667 [DOI: 10.1016/S0016-5085(88)80012-X]
- 26 **Bischoff SC**. Physiological and pathophysiological functions of intestinal mast cells. *Semin Immunopathol* 2009; **31**: 185-205 [PMID: 19533134 DOI: 10.1007/s00281-009-0165-4]
- 27 **Ciriza de Los Ríos C**, Castel de Lucas I, Canga Rodríguez-Valcárcel F, Diéguez Pastor MDC, de Las Cuevas Moreno N, Rey Díaz-Rubio E. Irritable bowel syndrome and basal serum tryptase: the correlation between subtype, severity and comorbidities. a pilot study. *Rev Esp Enferm Dig* 2021 [DOI: 10.17235/reed.2021.7697/2020]
- 28 **Sokol H**, Georgin-Lavialle S, Canioni D, Barete S, Damaj G, Soucie E, Bruneau J, Chandesris MO, Suarez F, Launay JM, Aouba A, Grandpeix-Guyodo C, Lanternier F, Grosbois B, de Gennes C, Cathébras P, Fain O, Hoyeau-Idrissi N, Dubreuil P, Lortholary O, Beaugerie L, Ranque B, Hermine O. Gastrointestinal manifestations in mastocytosis: a study of 83 patients. *J Allergy Clin Immunol* 2013; **132**: 866-73.e1 [PMID: 23890756 DOI: 10.1016/j.jaci.2013.05.026]
- 29 **Kirsch R**, Geboes K, Shepherd NA, de Hertogh G, Di Nicola N, Lebel S, Mickys U, Riddell RH. Systemic mastocytosis involving the gastrointestinal tract: clinicopathologic and molecular study of five cases. *Mod Pathol* 2008; **21**: 1508-1516 [PMID: 18931652 DOI: 10.1038/modpathol.2008.158]
- 30 **Poynard T**, Nataf C, Messing B, Modigliani R, Lecompte T, Nicolas P, Dray F, Ferme C. Secretory diarrhea and

- prostaglandin D2 overproduction in systemic mastocytosis. *N Engl J Med* 1982; **307**: 186 [DOI: [10.1056/NEJM198207153070315](https://doi.org/10.1056/NEJM198207153070315)]
- 31 **Cherner JA**. Gastric acid secretion in systemic mastocytosis. *N Engl J Med* 1989; **320**: 1562 [PMID: [2725591](https://pubmed.ncbi.nlm.nih.gov/2725591/)] DOI: [10.1056/NEJM198906083202320](https://doi.org/10.1056/NEJM198906083202320)]
- 32 **Arguedas MR**, Ferrante D. Systemic mastocytosis and giant gastroduodenal ulcer. *Gastrointest Endosc* 2001; **54**: 530-533 [PMID: [11577328](https://pubmed.ncbi.nlm.nih.gov/11577328/)] DOI: [10.1067/mge.2001.115320](https://doi.org/10.1067/mge.2001.115320)]
- 33 **McCarty TR**, Hung A, Mohanty A, Allen JI. Systemic Mastocytosis Complicated by Non-Cirrhotic Portal Hypertension and Variceal Bleeding. *ACG Case Rep J* 2017; **4**: e30 [PMID: [28286795](https://pubmed.ncbi.nlm.nih.gov/28286795/)] DOI: [10.14309/crj.2017.30](https://doi.org/10.14309/crj.2017.30)]
- 34 **Narayanan MN**, Liu Yin JA, Azzawi S, Warnes TW, Turck WP. Portal hypertension and ascites in systemic mastocytosis. *Postgrad Med J* 1989; **65**: 394-396 [PMID: [2608581](https://pubmed.ncbi.nlm.nih.gov/2608581/)] DOI: [10.1136/pgmj.65.764.394](https://doi.org/10.1136/pgmj.65.764.394)]
- 35 **Grundfest S**, Cooperman AM, Ferguson R, Benjamin S. Portal hypertension associated with systemic mastocytosis and splenomegaly. *Gastroenterology* 1980; **78**: 370-373 [DOI: [10.1016/0016-5085\(80\)90591-0](https://doi.org/10.1016/0016-5085(80)90591-0)]
- 36 **Scolapio JS**, Wolfe J 3rd, Malavet P, Woodward TA. Endoscopic findings in systemic mastocytosis. *Gastrointest Endosc* 1996; **44**: 608-610 [PMID: [8934172](https://pubmed.ncbi.nlm.nih.gov/8934172/)] DOI: [10.1016/s0016-5107\(96\)70019-6](https://doi.org/10.1016/s0016-5107(96)70019-6)]
- 37 **Mickys U**, Barakauskiene A, De Wolf-Peeters C, Geboes K, De Hertogh G. Aggressive systemic mastocytosis complicated by protein-losing enteropathy. *Dig Liver Dis* 2007; **39**: 693-697 [PMID: [16843741](https://pubmed.ncbi.nlm.nih.gov/16843741/)] DOI: [10.1016/j.dld.2006.06.003](https://doi.org/10.1016/j.dld.2006.06.003)]
- 38 **Bedeir A**, Jukic DM, Wang L, Mullady DK, Regueiro M, Krasinskas AM. Systemic mastocytosis mimicking inflammatory bowel disease: A case report and discussion of gastrointestinal pathology in systemic mastocytosis. *Am J Surg Pathol* 2006; **30**: 1478-1482 [PMID: [17063092](https://pubmed.ncbi.nlm.nih.gov/17063092/)] DOI: [10.1097/01.pas.0000213310.51553.d7](https://doi.org/10.1097/01.pas.0000213310.51553.d7)]
- 39 **Chrysakopoulos G**, Demonakou M, Papasavvas S, Koutsoumpas A, Mylonas G, Tzias V. Indolent systemic mastocytosis in a patient with ileocolitis. *Ann Gastroenterol* 2014; **27**: 270-272
- 40 **Okayama Y**, Kawakami T. Development, migration, and survival of mast cells. *Immunol Res* 2006; **34**: 97-115 [PMID: [16760571](https://pubmed.ncbi.nlm.nih.gov/16760571/)] DOI: [10.1385/IR:34:2:97](https://doi.org/10.1385/IR:34:2:97)]
- 41 **Shakoory B**, Fitzgerald SM, Lee SA, Chi DS, Krishnaswamy G. The role of human mast cell-derived cytokines in eosinophil biology. *J Interferon Cytokine Res* 2004; **24**: 271-281 [PMID: [15153310](https://pubmed.ncbi.nlm.nih.gov/15153310/)] DOI: [10.1089/107999004323065057](https://doi.org/10.1089/107999004323065057)]
- 42 **Irani AA**, Schechter NM, Craig SS, DeBlois G, Schwartz LB. Two types of human mast cells that have distinct neutral protease compositions. *Proc Natl Acad Sci USA* 1986; **83**: 4464-4468 [PMID: [3520574](https://pubmed.ncbi.nlm.nih.gov/3520574/)] DOI: [10.1073/pnas.83.12.4464](https://doi.org/10.1073/pnas.83.12.4464)]
- 43 **Irani AM**, Craig SS, DeBlois G, Elson CO, Schechter NM, Schwartz LB. Deficiency of the tryptase-positive, chymase-negative mast cell type in gastrointestinal mucosa of patients with defective T lymphocyte function. *J Immunol* 1987; **138**: 4381-4386
- 44 **Irani AM**, Goldstein SM, Wintroub BU, Bradford T, Schwartz LB. Human mast cell carboxypeptidase. Selective localization to MCTC cells. *J Immunol* 1991; **147**: 247-253
- 45 **Ammann RW**, Vetter D, Deyhle P, Tschen H, Sulser H, Schmid M. Gastrointestinal involvement in systemic mastocytosis. *Gut* 1976; **17**: 107-112 [PMID: [1261881](https://pubmed.ncbi.nlm.nih.gov/1261881/)] DOI: [10.1136/gut.17.2.107](https://doi.org/10.1136/gut.17.2.107)]
- 46 **Kleinschmidt S**, Harder J, Nolte I, Marsilio S, Hewicker-Trautwein M. Phenotypical characterization, distribution and quantification of different mast cell subtypes in transmural biopsies from the gastrointestinal tract of cats with inflammatory bowel disease. *Vet Immunol Immunopathol* 2010; **137**: 190-200 [PMID: [20646765](https://pubmed.ncbi.nlm.nih.gov/20646765/)] DOI: [10.1016/j.vetimm.2010.05.005](https://doi.org/10.1016/j.vetimm.2010.05.005)]
- 47 **Jakate S**, Demeo M, John R, Tobin M, Keshavarzian A. Mastocytic enterocolitis: increased mucosal mast cells in chronic intractable diarrhea. *Arch Pathol Lab Med* 2006; **130**: 362-367 [PMID: [16519565](https://pubmed.ncbi.nlm.nih.gov/16519565/)] DOI: [10.5858/2006-130-362-MEIMMC](https://doi.org/10.5858/2006-130-362-MEIMMC)]
- 48 **Akhavain M A**, Patel NR, Muniyappa PK, Glover SC. Allergic mastocytic gastroenteritis and colitis: an unexplained etiology in chronic abdominal pain and gastrointestinal dysmotility. *Gastroenterol Res Pract* 2012; **2012**: 950582 [PMID: [22577375](https://pubmed.ncbi.nlm.nih.gov/22577375/)] DOI: [10.1155/2012/950582](https://doi.org/10.1155/2012/950582)]
- 49 **Shukla SA**, Veerappan R, Whittimore JS, Ellen Miller L, Youngberg GA. Mast cell ultrastructure and staining in tissue. *Methods Mol Biol* 2006; **315**: 63-76 [PMID: [16110149](https://pubmed.ncbi.nlm.nih.gov/16110149/)] DOI: [10.1385/1-59259-967-2:063](https://doi.org/10.1385/1-59259-967-2:063)]
- 50 **Ramsay DB**, Stephen S, Borum M, Voltaggio L, Doman DB. Mast cells in gastrointestinal disease. *Gastroenterol Hepatol* 2010; **6**: 772-777
- 51 **Valent P**, Cerny-Reiterer S, Herrmann H, Mirkina I, George TI, Sotlar K, Sperr WR, Horny HP. Phenotypic heterogeneity, novel diagnostic markers, and target expression profiles in normal and neoplastic human mast cells. *Best Pract Res Clin Haematol* 2010; **23**: 369-378 [PMID: [21112036](https://pubmed.ncbi.nlm.nih.gov/21112036/)] DOI: [10.1016/j.beha.2010.07.003](https://doi.org/10.1016/j.beha.2010.07.003)]
- 52 **Castells M**, Butterfield J. Mast Cell Activation Syndrome and Mastocytosis: Initial Treatment Options and Long-Term Management. *J Allergy Clin Immunol Pract* 2019; **7**: 1097-1106 [PMID: [30961835](https://pubmed.ncbi.nlm.nih.gov/30961835/)] DOI: [10.1016/j.jaip.2019.02.002](https://doi.org/10.1016/j.jaip.2019.02.002)]
- 53 **Simons FE**, Simons KJ. Histamine and H1-antihistamines: celebrating a century of progress. *J Allergy Clin Immunol* 2011; **128**: 1139-1150.e4 [PMID: [22035879](https://pubmed.ncbi.nlm.nih.gov/22035879/)] DOI: [10.1016/j.jaci.2011.09.005](https://doi.org/10.1016/j.jaci.2011.09.005)]
- 54 **Spechler SJ**. Proton Pump Inhibitors: What the Internist Needs to Know. *Med Clin North Am* 2019; **103**: 1-14 [PMID: [30466666](https://pubmed.ncbi.nlm.nih.gov/30466666/)] DOI: [10.1016/j.mcna.2018.08.001](https://doi.org/10.1016/j.mcna.2018.08.001)]
- 55 **Leung KB**, Flint KC, Brostoff J, Hudspith BN, Johnson NM, Lau HY, Liu WL, Pearce FL. Effects of sodium cromoglycate and nedocromil sodium on histamine secretion from human lung mast cells. *Thorax* 1988; **43**: 756-761 [PMID: [2462755](https://pubmed.ncbi.nlm.nih.gov/2462755/)] DOI: [10.1136/thx.43.10.756](https://doi.org/10.1136/thx.43.10.756)]
- 56 **Marone G**, Spadaro G, Granata F, Triggiani M. Treatment of mastocytosis: pharmacologic basis and current concepts. *Leukemia Research* 2001; **25**: 583-594 [DOI: [10.1016/S0145-2126\(01\)00039-X](https://doi.org/10.1016/S0145-2126(01)00039-X)]
- 57 **Metcalfe DD**. Classification and diagnosis of mastocytosis: current status. *J Invest Dermatol* 1991; **96**: 2S-4S; discussion 4S, 60S [PMID: [16799601](https://pubmed.ncbi.nlm.nih.gov/16799601/)] DOI: [10.1111/1523-1747.ep12468882](https://doi.org/10.1111/1523-1747.ep12468882)]
- 58 **Lim KH**, Pardanani A, Butterfield JH, Li CY, Tefferi A. Cytoreductive therapy in 108 adults with systemic mastocytosis: Outcome analysis and response prediction during treatment with interferon-alpha, hydroxyurea, imatinib mesylate or 2-chlorodeoxyadenosine. *Am J Hematol* 2009; **84**: 790-794 [PMID: [19890907](https://pubmed.ncbi.nlm.nih.gov/19890907/)] DOI: [10.1002/ajh.21561](https://doi.org/10.1002/ajh.21561)]
- 59 **Ustun C**, Gotlib J, Popat U, Artz A, Litzow M, Reiter A, Nakamura R, Kluin-Nelemans HC, Verstovsek S, Gajewski J, Perales MA, George T, Shore T, Sperr W, Saber W, Kota V, Yavuz AS, Pullarkat V, Rogosheske J, Hogan W, Van Besien K, Hagglund H, Damaj G, Arock M, Horny HP, Metcalfe DD, Deeg HJ, Devine S, Weisdorf D, Akin C, Valent P.

Consensus Opinion on Allogeneic Hematopoietic Cell Transplantation in Advanced Systemic Mastocytosis. *Biol Blood Marrow Transplant* 2016; **22**: 1348-1356 [PMID: 27131865 DOI: 10.1016/j.bbmt.2016.04.018]

## Structural changes of proteins in liver cirrhosis and consequential changes in their function

Nikola Gligorijević, Simeon Minić, Olgica Nedić

**Specialty type:** Biochemistry and molecular biology

**Provenance and peer review:** Invited article; Externally peer reviewed.

**Peer-review model:** Single blind

**Peer-review report's scientific quality classification**

Grade A (Excellent): A  
Grade B (Very good): B, B  
Grade C (Good): 0  
Grade D (Fair): 0  
Grade E (Poor): 0

**P-Reviewer:** Costache RS, Romania; El-Shabrawi MH, Egypt; Pan Y, China

**Received:** January 13, 2022

**Peer-review started:** January 13, 2022

**First decision:** May 29, 2022

**Revised:** May 30, 2022

**Accepted:** June 30, 2022

**Article in press:** June 30, 2022

**Published online:** August 7, 2022



**Nikola Gligorijević, Olgica Nedić**, Department of Metabolism, University of Belgrade-Institute for the Application of Nuclear Energy, Belgrade 11080, Serbia

**Simeon Minić**, Centre of Excellence for Molecular Food Sciences and Department of Biochemistry, University of Belgrade-Faculty of Chemistry, Belgrade 11000, Serbia

**Corresponding author:** Nikola Gligorijević, PhD, Research Associate, Department of Metabolism, University of Belgrade-Institute for the Application of Nuclear Energy, Banatska 31b, Belgrade 11080, Serbia. [nikolag@inep.co.rs](mailto:nikolag@inep.co.rs)

### Abstract

The liver is the site of synthesis of the majority of circulating proteins. Besides initial polypeptide synthesis, sophisticated machinery is involved in the further processing of proteins by removing parts of them and/or adding functional groups and small molecules tailoring the final molecule to suit its physiological purpose. Posttranslational modifications (PTMs) design a network of molecules with the common protein ancestor but with slightly or considerably varying activity/localization/purpose. PTMs can change under pathological conditions, giving rise to aberrant or overmodified proteins. Undesired changes in the structure of proteins most often accompany undesired changes in their function, such as reduced activity or the appearance of new effects. Proper protein processing is essential for the reactions in living beings and crucial for the overall quality control. Modifications that occur on proteins synthesized in the liver whose PTMs are cirrhosis-related are oxidation, nitration, glycosylation, acetylation, and ubiquitination. Some of them predominantly affect proteins that remain in liver cells, whereas others predominantly occur on proteins that leave the liver or originate from other tissues and perform their function in the circulation. Altered PTMs of certain proteins are potential candidates as biomarkers of liver-related diseases, including cirrhosis. This review will focus on PTMs on proteins whose structural changes in cirrhosis exert or are suspected to exert the most serious functional consequences.

**Key Words:** Liver cirrhosis; Post-translational modifications; Circulation; Protein function; Protein structure; Chronic liver disease

©The Author(s) 2022. Published by Baishideng Publishing Group Inc. All rights reserved.

**Core Tip:** Chronic liver diseases and cirrhosis are accompanied by various metabolic disorders, some of which affect proteins. Besides changes in the concentration, structural alterations of proteins occur, mostly at the level of posttranslational modifications (PTMs). Five frequent cirrhosis-related PTMs are oxidation, nitration, glycosylation, acetylation, and ubiquitination. Some are more specific for the circulating proteins, whereas others are more specific for liver tissue-residing proteins. PTMs influence folding, stability, half-life, aggregation, and function of proteins. Modified proteins with altered function contribute to further progression of liver pathology. An overview of cirrhosis-related alterations of PTMs of specific proteins is the topic of this article.

**Citation:** Gligorijević N, Minić S, Nedić O. Structural changes of proteins in liver cirrhosis and consequential changes in their function. *World J Gastroenterol* 2022; 28(29): 3780-3792

**URL:** <https://www.wjgnet.com/1007-9327/full/v28/i29/3780.htm>

**DOI:** <https://dx.doi.org/10.3748/wjg.v28.i29.3780>

## INTRODUCTION

Liver cirrhosis is an end-stage condition of chronic liver disease[1]. The speed of progression from chronic disease to cirrhosis depends on multiple factors. Cirrhosis may develop due to toxic, infectious, immunopathological, or vascular processes. Alcoholic fatty liver disease (AFLD) and non-AFLD (NAFLD), and hepatitis B- and hepatitis C-induced diseases are the most common causes of cirrhosis, with AFLD being the most frequent.

The liver is the site of synthesis of the majority of circulating proteins. Besides initial polypeptide synthesis, sophisticated machinery is involved in the further processing of proteins by removing parts of them and/or adding functional groups and small molecules tailoring the final molecule to suit its physiological purpose. Changes that occur after formation of the polypeptide chain are known as cotranslations and posttranslational modifications (PTMs). PTMs enlarge the genome coding capacity by several orders of magnitude, designing a network of molecules with the common protein ancestor but with slightly or considerably varying activity/Localization/purpose. According to review articles of Ramazi and Zahiri[2] and Khoury *et al*[3], more than 400 different PTMs have been discovered to date.

When talking about PTMs, one should bear in mind the dynamic nature of the protein structure, which can be seen, among other ways, in different modifications at different moments of the protein lifespan. Each modification is expected to suit or respond to certain (patho)physiological needs of an organism. Furthermore, one protein can have more than one type of PTM simultaneously and at several molecular sites. Multiple PTMs are highly dependent on conformational and steric factors. A vast number of PTMs on proteins have been experimentally detected, but in the era of computational omics and bioinformatics, the prediction of PTMs based on the structure of proteins is an additional tool in the investigation of PTMs and their consequences on protein function.

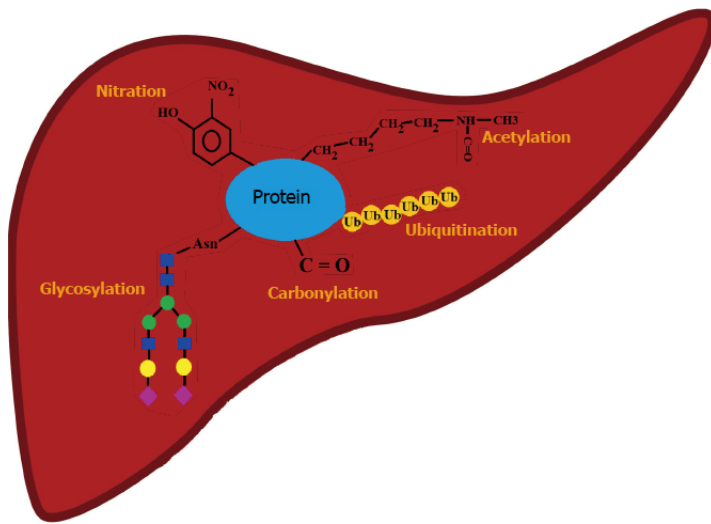
PTMs that occur under physiological conditions regulate the proper functioning of the organism. PTMs can, however, change under pathological conditions giving rise to aberrant or overmodified proteins. Undesired changes in protein structure most often accompany undesired changes in their function. Such modifications can reduce the initial activity of proteins or their lifespan with an overall outcome experienced as a decreased effect. Other modifications can, however, contribute to the appearance of new effects; these include misfolded proteins, previously unseen interactions, unusual molecular trafficking and localization, altered gene expression, creation of neoantigens, and stimulation of the immune system (which may lead to autoimmunity), protein aggregation followed by tissue deposition, prolonged half-life, impaired clearance and initiation of additional pathological processes. Thus, PTMs are essential for the reactions in living beings and crucial for the overall quality control.

Huang *et al*[4] reported more than 80 modification sites in proteins that were experimentally confirmed and named 24 major PTMs. Phosphorylation of the amino acid serine (Ser) is the most frequent modification, followed by phosphorylation of other amino acids, and then acetylation and ubiquitination. Lysine (Lys) is the amino acid that can be modified in the greatest number of different ways, resulting in as many as 15 types of altered species. Modifications that occur on proteins synthesized in the liver whose PTMs were found to be cirrhosis-related (Figure 1) are oxidation, nitration, glycosylation, acetylation, and ubiquitination[5-8].

## MECHANISMS UNDERLYING PTMS IN CIRRHOSIS

### Oxidation

Oxidative stress plays a major role in the development of liver pathology, regardless of etiology. The



DOI: 10.3748/wjg.v28.i29.3780 Copyright ©The Author(s) 2022.

Figure 1 Modifications that occur on proteins synthesized in the liver with evidence of cirrhosis-related posttranslational modifications.

liver, being a central organ of homeostasis, regulates metabolism, biosynthesis, and storage of carbohydrates, proteins, lipids, and vitamins. Due to such performances, it has intensive metabolic activity and is a site of a considerable free radical generation[9]. Any molecule possessing an unpaired electron is a free radical and is highly reactive. The most important free radicals produced by living organisms are reactive oxygen species (ROS) and reactive nitrogen species (RNS). Kupffer cells, neutrophils, and hepatocytes (mitochondria and cytochrome P450 enzymes) are involved in ROS generation during processes such as signal transduction, apoptosis, proliferation, growth, and defense against microorganisms[10]. Excessive quantities of ROS and RNS are toxic. They can induce tissue damage and are generally recognized as oxidative/nitrosative stress initiators. Cell type, intensity, and duration of the stress govern the outcome, which may be positive (beneficial) or negative (damaging). Some products of protein oxidation are chemically stable and present in large quantities, thus enabling their consideration as potential biomarkers of oxidative damage to be applied in clinical practice[11].

As mentioned before, cirrhosis usually occurs due to AFLD, NAFLD, and viral infection. The intersection point of all these conditions is oxidative stress. Alcohol in the case of AFLD, fatty acids in the case of NAFLD, and viral proteins in the case of hepatitis are the initiators of oxidative stress in these diseases. Different cellular compartments including mitochondria, cytoplasm, and endoplasmic reticulum are the sites of ROS production. Alterations in signaling pathways also play an important role in free radical induction. Detailed mechanisms underlining or assisting in oxidative stress generation in AFLD, NAFLD, and hepatitis B and C are reviewed in several papers[12-14]. Oxidation damages liver tissue by modifying proteins, DNA, and lipids. Once modified, these biomolecules gain altered structure, their function may be reduced to a different extent, their clearance rate may be increased or decreased, modified molecules may be involved in the activation of the immune system, or they alter signaling pathways contributing to further liver damage. Oxidative stress plays a role in both the initiation and progression of liver diseases[15].

### Nitration

Nitric oxide (NO) is a signaling molecule that can be synthesized in either enzymatically or non-enzymatically driven reactions in many cells. NO itself is not very reactive and has a short half-life. However, highly reactive peroxynitrite ion ( $\text{NO}_2^-$ ) may form in the reaction of NO with ROS. This ion can further react with tyrosine (Tyr) residues in a process called nitration, creating 3-nitroTyr[16], and with cysteine (Cys) residues in a reaction called S-nitrosylation, creating nitrosothiols[17]. Interaction with tryptophan (Trp) also occurs[18]. These nitration modifications affect not only proteins but also DNA and lipids. If not controlled, RNS may cause progressive damage to cells, tissues, and organs. Both ROS and RNS levels increase in liver diseases, as does the activity of inducible nitric oxide synthase. Mitochondria are particularly sensitive to nitro-oxidative damage since they have lower anti-oxidative capacity than the cytoplasm[19], rendering mitochondrial proteins and DNA vulnerable to nitration. Prolonged exposure of mitochondria to nitro-oxidation deteriorates their function, affecting both mitochondrial proteins and DNA[20-22].

When immunohistochemical detection of nitroproteins was performed in liver sections from patients with cirrhosis, a significant increase in nitrated proteins was observed[23]. Changes were more significant in patients with grade C (according to Child-Pugh classification) cirrhosis than in patients with grade A or B. A positive correlation was found between the level of nitrite and the level of nitroproteins with the progression of cirrhosis.

### Glycosylation

Glycosylation is one of the major posttranslational modifications that affects most secretory proteins. This modification introduces a higher level of diversity in the protein population due to the covalent addition of specific sugar moieties. Glycosylation influences both structural and functional properties of proteins. The overall glycome is affected by genetic and environmental factors, and changes may suggest the presence of inflammatory or other pathological events in the organism[24]. Glycosylation is an enzymatically regulated process that depends on several glycosyltransferases and glycosidases. Many factors including the activity of enzymes involved, substrate availability, and localization of enzymes within organelles affect the final glycosylation pattern of the protein. Unlike the genome and proteome, glycome is produced without a template. In the O-glycosylation of proteins, glycan attachment occurs at amino acid residues Ser and threonine (Thr). N-glycosylation involves asparagine (Asn) residues but only in a specific sequence, Asn-X-Ser/Thr, where X represents any amino acid except proline[25].

Several liver diseases are accompanied by alterations in protein glycosylation: NAFLD, liver fibrosis, cirrhosis, and hepatocellular carcinoma (HCC)[7,26-28]. A number of common glycosylation changes were noted as a general pattern in liver diseases, regardless of the disease type. They include increased fucosylation (Fuc), increased branching, and an appearance of a bisecting N-acetylglucosamine (GlcNAc). Additional analyses of the responsible glycosyltransferases documented that their levels were altered, underlining the mechanism of detected changes[7]. When the overall N-glycan structure was examined in immunoglobulin (Ig)G-deprived sera from patients with cirrhosis, two general trends emerged: an increase in bisecting GlcNAc structures and a decrease in fully galactosylated (Gal) bi- and triantennary N-glycans. The ratios of certain glycans were suggested to serve as potential biomarkers of a specific stage of liver fibrosis or cirrhosis[27]. Data reported in that study confirmed the correlation between the detected glycan changes and the levels of the corresponding glycosyltransferases.

### Acetylation

Acetylation is one of the key PTMs involved in the regulation of many proteins. It influences their stability, activity, localization, and interactions with other proteins. Metabolic pathways, including fatty acid metabolism and the Krebs cycle, are regulated by protein acetylation. This modification assumes the addition of an acetyl group from acetyl-coenzyme A on Lys residues[29]. Acetylation seems to play a significant role in liver diseases, as the pattern of protein acetylation in fatty liver is significantly different from the pattern in the healthy liver[30].

### Ubiquitination

Ubiquitin and its related pathways are closely connected to chronic liver disease. Dysfunctional ubiquitination was detected in liver tissue in different stages of chronic liver disease. Ubiquitin is a protein that consists of 76 amino acids and has seven Lys and N-terminal methionine (Met) residues that can form *iso*-peptide-linked ubiquitin chains. It binds to substrates by a three-step enzymatic mechanism involving activating enzyme (E1), conjugating enzyme (E2) and ligase (E3)[31]. Receptors with ubiquitin-binding domains can recognize ubiquitinated substrates[32]. On the other hand, deubiquitinases remove ubiquitin from modified molecules, making this PTM a reversible, dynamic process with a plethora of diverse cellular effects[33]. Ubiquitinated proteins may be taken by proteasome which destroys them, thus controlling their lifespan and activity.

Some of the aforementioned PTMs predominantly affect proteins that remain in liver cells (ubiquitination, acetylation, and nitration), whereas others predominantly occur on proteins that leave the liver and exert their functions in the circulation (oxidation and glycosylation). Additionally, there are proteins not originating from the liver whose structure changes in cirrhosis. Some of these modifications have the potential to serve as biomarkers of liver-related diseases.

This review mostly focuses on PTMs on the circulating proteins originating from the liver whose structural changes in cirrhosis exert the most serious functional consequences. Modifications of Igs and liver tissue proteins will be also briefly mentioned.

---

## PROTEINS FROM THE CIRCULATION AFFECTED BY SPECIFIC PTMS IN CIRRHOSIS

---

### Fibrinogen

Fibrinogen is a large, fibrillar glycoprotein with a molecular mass of 340 kDa. This protein is involved both in primary (interaction with platelets) and secondary hemostasis (fibrin formation). N-glycosylation analysis using lectin microarray with 15 Lectins demonstrated that cirrhosis induces changes in its glycans[34]. Based on the interactions with lectins *Pholiota squarrosa* (PhoSL), *Maackia amurensis* lectin I (MAL-I), *Maackia amurensis* lectin II (MAL-II), *Galanthus nivalis* lectin (GNL), *Phaseolus vulgaris* leucoagglutinin (PHA-L), and *Phaseolus vulgaris* lectin E (PHA-E), an increased content of the following carbohydrate moieties was observed: terminal  $\alpha$ -2,3 sialic acid (Sia) and  $\alpha$ -1,3 mannose (Man), a disaccharide composed of Gal and N-acetyl galactosamine (Gal $\beta$ -1,4GlcNAc) and tri/tetra-antennary

N-glycan structures. Core  $\alpha$ -1,6 (Fuc) and bi-antennary galactosylated N-glycans with the bisecting GlcNAc were, on the other hand, reduced. An increase in the number of Sia residues on fibrinogen as a consequence of cirrhosis was confirmed by several researchers[35,36]. Sialic acid is negatively charged and is a weak binding site for calcium ions[37]. Taking into consideration that advanced chronic liver disease is characterized by hypercalcemia[38], interactions between calcium ions and an increased number of Sia residues may be seen as a modulator of fibrinogen action in cirrhosis[37]. “Proper” glycosylation of fibrinogen is essential for its function. Alterations in this PTM may even lead to complete dysfunction of the protein[39-42].

Increased oxidation of fibrinogen from patients with cirrhosis was detected as well[34,43]. Dinitrophenyl-hydrazide (DNP)-reactive sites on fibrinogen were investigated using anti-DNP antibodies to analyze protein carbonyls and it was discovered that the A $\alpha$ -chain was dominantly carbonylated, followed by the B $\beta$ -chain. It seems that the  $\gamma$ -chain of fibrinogen is not carbonylated in patients with cirrhosis. Carbonylation affects the function of fibrinogen[44-46], as both A $\alpha$ - and B $\beta$ -chains contain cleavage sites for thrombin action. Oxidation of  $\alpha$ C domains on A $\alpha$ -chains also affects their mutual interaction and lateral association of fibrin monomers[47]. Generally, residues that may be affected by oxidation/carbonylation are located in all structural elements of fibrinogen. Thus, alterations in the secondary and tertiary structures of fibrinogen also accompany cirrhosis[34]. Reduced content of its  $\alpha$ -helical subunits was observed, which coincided with the formation of denser clots[46]. Although the structure of fibrinogen is altered in cirrhosis, Hugenholtz *et al*[43] did not detect significant structural changes in fibrin clots, even though clots formed from samples originating from patients with cirrhosis had reduced porosity. Subtle alterations, not visible by scanning electron microscopy, are most likely sufficient to influence porosity. Furthermore, carbonylated sites on fibrinogen are hydrophobic regions which prevent efficient liquid flow through the fibrin clot, increasing its resistance towards lysis by plasmin[36]. Overall, changes in fibrinogen structure due to cirrhosis are complex and lead to the formation of a molecule acquiring thrombogenic characteristics. Other factors that participate in coagulation or fibrinolysis are altered as well, defining a general pro-coagulant state in liver cirrhosis [48].

### Albumin

Albumin is the major plasma protein, constituting approximately 50% of the total protein content. It is a globular, single-chain,  $\alpha$ -helical protein, organized into three domains. This protein exhibits many physiological roles, such as maintenance of osmotic pressure and transport of various metal ions and biomolecules (fatty acids, metabolites, and drugs), providing anti-oxidative, anti-inflammatory, and hemostatic activities[49].

Cirrhosis is accompanied by reduced albumin concentration and its significant structural changes [49]. Oxidation of free Cys-34 residue is one of the most notable changes in albumin structure due to cirrhosis. This residue strongly contributes to the anti-oxidative capacity of albumin. Oxidized albumin differs from the native molecule pharmacokinetically and conformationally, negatively influencing its function[50]. Quantities of albumin oxidative forms, assessed by measuring the level of carbonyl groups and oxidation of free Cys-34 residue, correlate with the severity of liver failure[51]. Oxidative stress triggers the dimerization of albumin molecules (through free Cys residues) in patients with cirrhosis, with significant reduction in native albumin required for the physiological functions[52]. Furthermore, matrix-assisted laser desorption/ionization time of flight (MALDI-TOF) mass spectrometry (MS) detects cysteinylated Cys-34 in cirrhosis, followed by other molecular changes, such as truncation of N-terminal portion and glycosylation[53]. Oxidative stress also induces structural changes of the N-terminus and the reduced capacity of albumin to bind cobalt ions. Albumin modified in that way is called ischemia-modified albumin (IMA)[50]. The cobalt-binding assay revealed increased IMA levels in patients with advanced cirrhosis[54]. Additionally, the electron paramagnetic resonance study, using 16-doxyyl stearic acid as a spin probe, confirmed that the ligand-binding capacity of albumin is significantly reduced in cirrhosis[55]. A small-angle X-ray scattering study demonstrated that albumin in patients with liver disease has an altered, more open conformation compared to control samples[56]. To summarize, posttranslational alternations of albumin in cirrhosis influence its conformation, which further decreases its ligand binding.

Therefore, reduced level of serum albumin in patients with cirrhosis, as well as its substantial structural change, have important and clinically relevant consequences, such as alterations in the redox balance, hemostatic disorders, modifications in the transport of endogenous and exogenous ligands, acid-base imbalance, reduced detoxification capacity, and antioxidant activity[49].

### Transferrin

Human transferrin (Tf), an iron-binding protein, is a 76-kDa glycoprotein produced in the liver[57,58]. The Tf molecule contains two lobes at the N- and C-termini, and each binds one Fe<sup>3+</sup> ion[58]. Tf is stabilized by 19 intrachain disulfide bonds and is modified by three carbohydrate side chains; two of them are N-linked (Asn-413 and Asn-611) and the third one is O-linked (Ser-32)[57]. The glycosylation profile of Tf changes significantly in liver diseases. A carbohydrate-deficient Tf (CDT) is found in AFLD, and it is characterized by a loss of terminal sialic acids[59]. Lectin affinity electrophoresis of CDT also confirmed the absence of Asn-linked oligosaccharides in AFLD and cirrhosis[60]. Both Tf and iron

uptake capacity of deglycosylated Tf are significantly reduced by the human hepatoma cell line PLC/PRF/5[61], suggesting impaired function of Tf in liver cirrhosis. A less advanced liver disease can be discriminated from cirrhosis by studying disialotransferrin isoforms. Poor chromatographic resolution of disialotransferrin from trisialotransferrin (the so-called “di-tri bridging”) was seen for samples originating from patients with cirrhosis[62,63]. This abnormal pattern could be ascribed to the presence of higher mass disialotransferrin isoforms due to an increased branching and fucosylation of the carbohydrate moiety[64]. This phenomenon was not seen in less-advanced liver diseases[63].

Besides changes in the glycosylation profile, the lower concentration of Tf is also related to cirrhosis, and it represents a good indicator of the survival rate of patients[65]. Lower serum Tf concentration is accompanied by higher hepatic iron concentration and lipid peroxidation levels compared to healthy subjects. In this context, Tf exerts a protective role in maintaining liver function[66].

### **Hemopexin**

Hemopexin (HPX) is secreted mainly by hepatocytes and binds free heme in the circulation. The formed complex is cleared from the circulation by a hepatocyte-specific membrane receptor. The serum concentration of HPX does not significantly vary in liver diseases[67]. However, significant alterations in the glycosylation profile of HPX occur in patients with cirrhosis. Lectin chemiluminescence-linked immunosorbent assay demonstrated a higher level of N-glycosylation (fucosylation) in samples from patients with cirrhosis and HCC than in samples from patients with hepatitis and healthy individuals [68]. A study using liquid chromatography-tandem MS with multiple reaction monitoring (LC-MS/MS MRM) assay revealed a nearly five-fold increase in the sialylation of site-specific Oglycoforms of HPX in cirrhosis[67]. Since HPX is an important anti-oxidative protein, its altered N-glycosylation in cirrhosis possibly interferes with the redox balance in organisms.

### **Haptoglobin**

Haptoglobin (Hp) is a glycoprotein secreted by the liver into the plasma. Its major biological role is to capture released hemoglobin during intravascular hemolysis and prevent kidney damage by the released iron[69]. Hp is composed of two  $\alpha$  and two  $\beta$  chains linked by disulfide bonds in a quaternary structure[70,71]. All four N-glycosylation sites are located in the  $\beta$  subunit and glycoforms are known to create additional phenotypic variants[69,72]. Many studies have reported glycan changes of Hp in diseases. MALDI-TOF MS analyses revealed N-linked glycan alterations (increased fucosylation) of serum Hp  $\beta$  chain in patients with cirrhosis[69,71]. Zhu *et al*[73] applied a similar approach to distinguish the N-glycan profile of Hp in patients with cirrhosis from those with hypophosphatasia. A degree of bifucosylation was higher in samples from patients with an early-stage HCC than in samples from patients with cirrhosis, regardless of the etiology. Thus, monitoring alterations in the glycosylation profile of the Hp  $\beta$  chain may become a valuable approach for detection and distinction between HCC and cirrhosis. The observed changes of Hp at the N-glycosylation level most likely affect its functional properties, including interactions with binding partners, as was suggested in the case of progressive liver diseases[69].

### **Ferritin**

Ferritin plays an important role in storing intracellular iron and its segregation in a non-toxic form[74, 75]. It is a 24-mer globular protein that is made up of heavy (H) and light (L) subunits, with molecular masses of 21 kDa and 19 kDa, respectively[74]. Subunits surround the central hollow core, capable of binding up to 4500 iron ions[76]. Ferritin concentration in the circulation is relatively low (< 1  $\mu\text{g}/\text{mL}$ ) [74]. However, it is increased in conditions such as iron overload, infection, inflammation, malignancy, diabetes and liver diseases, including NAFLD and cirrhosis[77]. Besides changes in ferritin concentration, liver cirrhosis is also accompanied by the derangement of the ordered secondary structure of the protein[78].

Approximately 50%-80% of serum ferritin is glycosylated[79]. There is no strong evidence of the connection between ferritin glycosylation and cirrhosis. Some studies have reported a decrease in glycosylated ferritin in liver necrosis[79]. On the other hand, Chapman *et al*[80] demonstrated that the measurement of the fraction of glycosylated serum ferritin does not provide any advantage over the estimation of the total serum ferritin concentration in the assessment of iron stores in patients with liver cirrhosis.

### **Insulin-like growth factor binding protein 3**

Insulin-like growth factors (IGFs), namely IGF-I and IGF-II, are peptides that exert growth-promoting, endocrine and cytokine effects[81,82]. They are synthesized in many tissues locally, but the liver is the origin of IGFs that enter the circulation. IGF-I is the mediator of the growth hormone (GH) action. The activity of IGFs is regulated by a network of insulin-like growth factor binding proteins (IGFBPs) and is most often inhibited when IGFs are in complexes with IGFBPs. To perform their physiological roles, IGFs need to be released from complexes and interact with IGF receptors, which are predominantly found on cell membranes. IGFs are liberated from complexes by the proteolysis of IGFBPs. The synthesis of several IGFBPs occurs in the liver, under the control of GH. IGFBP-3 is the major binding

protein in the circulation and is synthesized in Kupffer cells. It forms ternary complexes with IGFs, which also contain an acid-labile subunit. These complexes are large (150 kDa), remain within blood vessels, and bind 75%-90% of the circulating IGFs, serving both as a reservoir and a guardian of the IGF activity.

IGFBP-3 has three N-glycosylation and two phosphorylation sites[83,84]. It is present in the circulation as two major glycoforms of 40 kDa and 44 kDa, although a non-glycosylated form (29 kDa) can also be detected. Diethylaminoethyl ion-exchange chromatography was shown to fractionate at least 12 IGFBP-3 species that are isoforms with different charges due to PTMs[85]. Three of these isoforms exhibited significant reactivity with lectin concanavalin A (Con A), specific for Man residues and to a lesser extent for glucose (Glc) and GlcNAc residues. In patients with alcoholic liver cirrhosis, two of these glycoforms had an increased reactivity with Con A, whereas the third one had decreased reactivity, compared to molecules originating from healthy persons. Furthermore, some differences were also detected between different stages of liver cirrhosis. IGFBP-3 from patients with Child score A stage exhibited similar isoform distribution and reactivity as in healthy persons. Child score B seems to be the turning point in the progression of cirrhosis, after which considerable changes in the concentration of IGFBP-3 and its structure occur. A reduced reactivity of IGFBP-3 due to cirrhosis was also noted with wheat germ agglutinin, specific for GlcNAc, and breadfruit lectin, specific for Gal and GalNAc residues[86]. These alterations affect the conformation of IGFBP-3 and its susceptibility to proteolytic cleavage, thus influencing its half-life and the entire mechanism that controls IGFs' activity. Since IGFBP-3 can also perform IGF-independent roles after binding to its cell surface or nuclear receptors, changes in IGFBP-3 glycosylation can contribute to the pathophysiology of several diseases such as diabetes, obesity, NAFLD, and cancer[87,88].

### **Sex hormone-binding globulin**

Sex hormone-binding globulin (SHBG) is a 90-kDa to 100-kDa homodimeric glycoprotein, mainly produced by the liver[89]. It is a transporter of sex hormones, capable of binding to them with high affinity[90]. SHBG is both N- and mucin-type O-glycosylated[90,91]. Comprehensive LC-MS/MS analysis revealed that fucosylation of N-glycoforms increases in liver cirrhosis. Additionally, the same pathology was related to an increase of the  $\alpha$ -2-6 sialylated glycoform of the O-glycopeptide of SHBG [67]. Glycosylation of SHBG does not seem to influence binding of steroid hormones[92]. However, it is suspected that higher content of sialic acid increases the half-life of SHBG[93], elevating the total concentration of this protein in patients with cirrhosis[94]. An increased concentration of SHBG may influence the equilibrium between protein-bound and free, physiologically active steroid hormones, particularly testosterone. Consequently, SHBG seems to play an important role in the occurrence of feminization in male non-alcoholic liver cirrhosis by reducing free testosterone level[95]. On the other hand, higher concentrations of this protein were reported to possibly exert protection against NAFLD [96]. The exact effect of altered glycosylation of SHBG on its function is still not known.

### **IgG**

IgGs are principle components of the defense system known as immunity. Although IgGs are not synthesized in the liver, their aberrant glycosylation has been linked to various liver diseases[97]. A study combining LC-MS/MS analysis with lectin fluorophore-linked immunosorbent assay identified changes in the glycosylation of anti-Gal IgG molecules in the sera of hepatitis C virus-infected individuals with fibrosis and cirrhosis[98]. The most prominent change was agalactosylation of heavy chains of anti-Gal IgG. The same study also revealed that truncation of Gal residues induced alterations in the tertiary structure of IgG molecules originating from patients with cirrhosis[98]. Yuan *et al*[97] confirmed agalactosylation of IgG molecules in cirrhosis and reported an increased degree of fucosylation in IgG1 and IgG3 glycoforms. Cirrhosis is also accompanied by Gal deficiency and decreased sialylation of IgA molecules, as well as by an increased amount of abnormally glycosylated polymeric IgA molecules[99]. Furthermore, concentrations of IgG and IgA are increased in the circulation of patients with cirrhosis[97]. Altered glycosylation could influence the ability of IgG to bind and activate complement system. It was discovered that alpha-Gal IgG antibodies from patients with cirrhosis have reduced complement-mediated killing ability[100]. This issue is important since bacterial infection is one of the major complications in patients with cirrhosis and alpha-Gal epitope is abundantly synthesized by bacteria.

---

## **LIVER TISSUE PROTEINS AFFECTED BY SPECIFIC PTMS IN CIRRHOSIS**

---

Proteins remaining in liver cells are mostly modified by ubiquitination, nitration and acetylation. Ubiquitination and associated processes play important roles in the development of cirrhosis affecting many proteins. E3 ubiquitin ligase promotes, for example, NF-E2-related factor 2 ubiquitination and degradation, disrupting the anti-oxidative pathway. The same ligase promotes the accumulation of extracellular matrix by inducing ubiquitination of procollagen1 to mature collagen1[101,102]. Sumoylation and neddylation, ubiquitin-like modifications, also play roles in liver cirrhosis. It was

discovered that *in vivo* reduction of neddylation ameliorates liver fibrosis[103]. Sumoylation affects, for example, promyelocytic leukemia protein and nuclear factor-kappa B (NF- $\kappa$ B)[104]. Modification of these proteins leads to cell proliferation and fibrosis in the liver. A detailed overview of ubiquitination and its implications in chronic liver disease is given in the 2021 review paper of Park *et al*[33].

Transcription factors, sterol regulatory element-binding transcription factor (SREBP), and carbohydrate-response element-binding protein (ChREBP) regulate fatty acid metabolism in the liver, promoting lipogenesis. These factors are active when acetylated. Sirtuins 1 and 3 (SIRT1 and SIRT3) are deacetylases that regulate their activity. High-fat diet and obesity reduce the expression of SIRT 1 and SIRT 3, thus promoting acetylation and activation of ChREBP and SREBP, followed by an increase in the uptake of fatty acids by the liver. Liver lipid load induces inflammation and the NF-kappa B pathway, and reduces mitophagy, altogether leading to mitochondrial and liver damage and advancement towards NAFLD. Calorie restriction and exercise upregulate SIRT1 and SIRT3, thus, preventing and ameliorating NAFLD[29]. ATP-citrate lyase, microtubules, heat shock protein 90 and CCAAT/enhancer binding protein  $\alpha$  are differently modified by acetylation in different liver diseases preceding cirrhosis. Aberrant acetylation of the mentioned proteins leads to their functional alterations and subsequently different metabolic responses, further contributing to the liver pathology[105-108].

There are many hepatic proteins with confirmed nitration status in liver diseases, whose functions are either augmented or reduced[109]. Decreased function of glutamine synthetase, 3-ketoacyl-CoA thiolase, aldehyde dehydrogenase 2, complexes I and V of oxidative phosphorylation, cytochrome p450 2E1 and B6, superoxide dismutase 1 and 2, and cluster of differentiation 95 contribute to decreased energy production, ROS leakage, steatosis, decreased anti-oxidant defense capacity, ethanol- and drug-induced toxicity, apoptosis and necrosis. Nitration of glutathione-S-transferase, however, potentiates the function of this enzyme, leading to an increased hepatic anti-oxidative defense capacity[110].

---

## CONCLUSION

---

Liver disease can progress from mild damage, over moderate with a certain degree of compensation, to severe, which cannot be compensated and may lead to organ failure. While still able to compensate for tissue damage, the liver produces scars of fibrotic tissue, which reduce its function. The persistent presence of agents and/or events that cause liver damage leads to decompensated cirrhosis, resulting in several pathological outcomes, including liver cancer, and finally, functional arrest.

Early diagnosis of chronic liver disease is critical since the etiology of the disease can be discovered in this stage. When cirrhosis progresses, the etiology of a disease is very hard to determine. Appropriate treatment administered on time can prevent and reverse the progression of cirrhosis which leads to irreversible changes. Avoiding or minimizing contributing harmful factors is recommended[1]. For example, persons with chronic liver disease should avoid alcohol intake and smoking[111]. On the other hand, consumption of coffee is associated with a slower progression of liver fibrosis[112]. There are no specific curative strategies targeting alterations in PTMs in cirrhosis.

Since oxidative stress is one of the causes involved in the etiology and development of liver diseases, supplementation of vitamins and minerals, which act as anti-oxidants and/or cofactors of enzymes and other molecules that participate in anti-oxidant defense, may be recommended. However, one should bear in mind that some substances are stored in the liver and may act as pro-disease agents[113]. For example, lipophilic vitamin A is stored in liver stellate cells. If overloaded with vitamin A, these cells start to produce collagen, leading to liver fibrosis. The beta-carotene form, however, causes no such effects and is safe to consume. Iron ions can induce oxidative stress by participation in the generation of free radicals. As already said, the liver is the site of iron storage, in association with the protein ferritin. Patients with alcoholic liver cirrhosis often have an increased intrahepatic iron concentration, which is highly correlated with mortality rates[114]. Thus, when considering management strategies to treat cirrhosis, one should have in mind the complexity and limitations of interconnected metabolic pathways.

---

## FOOTNOTES

---

**Author contributions:** Gligorijević N performed the literature search, writing and prepared the figure; Minic S performed the literature search and writing; Nedic O designed the outline, performed the literature search and coordinated the writing of the paper.

**Supported by** the Ministry of Education, Science and Technological Development of the Republic of Serbia, No. 451-03-9/2021-14/200019.

**Conflict-of-interest statement:** All authors report no relevant conflict of interest for this article.

**Open-Access:** This article is an open-access article that was selected by an in-house editor and fully peer-reviewed by

external reviewers. It is distributed in accordance with the Creative Commons Attribution NonCommercial (CC BY-NC 4.0) license, which permits others to distribute, remix, adapt, build upon this work non-commercially, and license their derivative works on different terms, provided the original work is properly cited and the use is non-commercial. See: <https://creativecommons.org/licenses/by-nc/4.0/>

**Country/Territory of origin:** Serbia

**ORCID number:** Nikola Gligorijević 0000-0002-8691-2486; Simeon Minić 0000-0002-7053-1216; Olgica Nedić 0000-0003-2042-0056.

**S-Editor:** Wu YXJ

**L-Editor:** A

**P-Editor:** Wu YXJ

## REFERENCES

- 1 **Wiegand J**, Berg T. The etiology, diagnosis and prevention of liver cirrhosis: part 1 of a series on liver cirrhosis. *Dtsch Arztebl Int* 2013; **110**: 85-91 [PMID: 23451000 DOI: 10.3238/arztebl.2013.0085]
- 2 **Ramazi S**, Zahiri J. Posttranslational modifications in proteins: resources, tools and prediction methods. *Database (Oxford)* 2021; **2021** [PMID: 33826699 DOI: 10.1093/database/baab012]
- 3 **Khoury GA**, Baliban RC, Floudas CA. Proteome-wide post-translational modification statistics: frequency analysis and curation of the swiss-prot database. *Sci Rep* 2011; **1** [PMID: 22034591 DOI: 10.1038/srep00090]
- 4 **Huang KY**, Lee TY, Kao HJ, Ma CT, Lee CC, Lin TH, Chang WC, Huang HD. dbPTM in 2019: exploring disease association and cross-talk of post-translational modifications. *Nucleic Acids Res* 2019; **47**: D298-D308 [PMID: 30418626 DOI: 10.1093/nar/gky1074]
- 5 **Osna NA**, Carter WG, Ganesan M, Kirpich IA, McClain CJ, Petersen DR, Shearn CT, Tomasi ML, Kharbanda KK. Aberrant post-translational protein modifications in the pathogenesis of alcohol-induced liver injury. *World J Gastroenterol* 2016; **22**: 6192-6200 [PMID: 27468209 DOI: 10.3748/wjg.v22.i27.6192]
- 6 **Karve TM**, Cheema AK. Small changes huge impact: the role of protein posttranslational modifications in cellular homeostasis and disease. *J Amino Acids* 2011; **2011**: 207691 [PMID: 22312457 DOI: 10.4061/2011/207691]
- 7 **Ramachandran P**, Xu G, Huang HH, Rice R, Zhou B, Lindpaintner K, Serie D. Serum Glycoprotein Markers in Nonalcoholic Steatohepatitis and Hepatocellular Carcinoma. *J Proteome Res* 2022; **21**: 1083-1094 [PMID: 35286803 DOI: 10.1021/acs.jproteome.1c00965]
- 8 **Lachiondo-Ortega S**, Mercado-Gómez M, Serrano-Maciá M, Lopitz-Otsoa F, Salas-Villalobos TB, Varela-Rey M, Delgado TC, Martínez-Chantar ML. Ubiquitin-Like Post-Translational Modifications (Ubl-PTMs): Small Peptides with Huge Impact in Liver Fibrosis. *Cells* 2019; **8** [PMID: 31817258 DOI: 10.3390/cells8121575]
- 9 **Arauz J**, Ramos-Tovar E, Muriel P. Redox state and methods to evaluate oxidative stress in liver damage: From bench to bedside. *Ann Hepatol* 2016; **15**: 160-173 [PMID: 26845593 DOI: 10.5604/16652681.1193701]
- 10 **Taub R**. Liver regeneration: from myth to mechanism. *Nat Rev Mol Cell Biol* 2004; **5**: 836-847 [PMID: 15459664 DOI: 10.1038/nrm1489]
- 11 **Kehm R**, Baldensperger T, Raupbach J, Höhn A. Protein oxidation - Formation mechanisms, detection and relevance as biomarkers in human diseases. *Redox Biol* 2021; **42**: 101901 [PMID: 33744200 DOI: 10.1016/j.redox.2021.101901]
- 12 **Galicía-Moreno M**, Gutiérrez-Reyes G. The role of oxidative stress in the development of alcoholic liver disease. *Rev Gastroenterol Mex* 2014; **79**: 135-144 [PMID: 24861526 DOI: 10.1016/j.rgm.2014.03.001]
- 13 **Ivanov AV**, Valuev-Elliston VT, Tyurina DA, Ivanova ON, Kochetkov SN, Bartosch B, Isagulians MG. Oxidative stress, a trigger of hepatitis C and B virus-induced liver carcinogenesis. *Oncotarget* 2017; **8**: 3895-3932 [PMID: 27965466 DOI: 10.18632/oncotarget.13904]
- 14 **Masarone M**, Rosato V, Dallio M, Gravina AG, Aglitti A, Loguercio C, Federico A, Persico M. Role of Oxidative Stress in Pathophysiology of Nonalcoholic Fatty Liver Disease. *Oxid Med Cell Longev* 2018; **2018**: 9547613 [PMID: 29991976 DOI: 10.1155/2018/9547613]
- 15 **Li S**, Tan HY, Wang N, Zhang ZJ, Lao L, Wong CW, Feng Y. The Role of Oxidative Stress and Antioxidants in Liver Diseases. *Int J Mol Sci* 2015; **16**: 26087-26124 [PMID: 26540040 DOI: 10.3390/ijms161125942]
- 16 **Radi R**. Protein tyrosine nitration: biochemical mechanisms and structural basis of functional effects. *Acc Chem Res* 2013; **46**: 550-559 [PMID: 23157446 DOI: 10.1021/ar300234c]
- 17 **Lamotte O**, Bertoldo JB, Besson-Bard A, Rosnoblet C, Aimé S, Hichami S, Terenzi H, Wendehenne D. Protein S-nitrosylation: specificity and identification strategies in plants. *Front Chem* 2014; **2**: 114 [PMID: 25750911 DOI: 10.3389/fchem.2014.00114]
- 18 **Nuriel T**, Hansler A, Gross SS. Protein nitrotryptophan: formation, significance and identification. *J Proteomics* 2011; **74**: 2300-2312 [PMID: 21679780 DOI: 10.1016/j.jprot.2011.05.032]
- 19 **Fernández-Checa JC**, Kaplowitz N, García-Ruiz C, Colell A. Mitochondrial glutathione: importance and transport. *Semin Liver Dis* 1998; **18**: 389-401 [PMID: 9875556 DOI: 10.1055/s-2007-1007172]
- 20 **Campello S**, Scorrano L. Mitochondrial shape changes: orchestrating cell pathophysiology. *EMBO Rep* 2010; **11**: 678-684 [PMID: 20725092 DOI: 10.1038/embor.2010.115]
- 21 **Mansouri A**, Fromenty B, Berson A, Robin MA, Grimbert S, Beaugrand M, Erlinger S, Pessayre D. Multiple hepatic mitochondrial DNA deletions suggest premature oxidative aging in alcoholic patients. *J Hepatol* 1997; **27**: 96-102 [PMID:

- 9252080 DOI: [10.1016/s0168-8278\(97\)80286-3](https://doi.org/10.1016/s0168-8278(97)80286-3)]
- 22 **Mansouri A**, Gaou I, De Kerguenec C, Amsellem S, Haouzi D, Berson A, Moreau A, Feldmann G, Lettéron P, Pessayre D, Fromenty B. An alcoholic binge causes massive degradation of hepatic mitochondrial DNA in mice. *Gastroenterology* 1999; **117**: 181-190 [PMID: [10381926](https://pubmed.ncbi.nlm.nih.gov/10381926/) DOI: [10.1016/s0016-5085\(99\)70566-4](https://doi.org/10.1016/s0016-5085(99)70566-4)]
  - 23 **Annie-Jeyachristy S**, Geetha A, Surendran R, Sundaram A, Lavanya K, Kumar SJ, Prakash SA. Level of nitrated proteins in the plasma, platelets and liver of patients with liver cirrhosis. *Redox Rep* 2009; **14**: 259-266 [PMID: [20003711](https://pubmed.ncbi.nlm.nih.gov/20003711/) DOI: [10.1179/135100009X12525712409616](https://doi.org/10.1179/135100009X12525712409616)]
  - 24 **Verhelst X**, Dias AM, Colombel JF, Vermeire S, Van Vlierberghe H, Callewaert N, Pinho SS. Protein Glycosylation as a Diagnostic and Prognostic Marker of Chronic Inflammatory Gastrointestinal and Liver Diseases. *Gastroenterology* 2020; **158**: 95-110 [PMID: [31626754](https://pubmed.ncbi.nlm.nih.gov/31626754/) DOI: [10.1053/j.gastro.2019.08.060](https://doi.org/10.1053/j.gastro.2019.08.060)]
  - 25 **Reily C**, Stewart TJ, Renfrow MB, Novak J. Glycosylation in health and disease. *Nat Rev Nephrol* 2019; **15**: 346-366 [PMID: [30858582](https://pubmed.ncbi.nlm.nih.gov/30858582/) DOI: [10.1038/s41581-019-0129-4](https://doi.org/10.1038/s41581-019-0129-4)]
  - 26 **Vanderschaeghe D**, Laroy W, Sablon E, Halfon P, Van Hecke A, Delanghe J, Callewaert N. GlycoFibroTest is a highly performant liver fibrosis biomarker derived from DNA sequencer-based serum protein glycomics. *Mol Cell Proteomics* 2009; **8**: 986-994 [PMID: [19181623](https://pubmed.ncbi.nlm.nih.gov/19181623/) DOI: [10.1074/mcp.M800470-MCP200](https://doi.org/10.1074/mcp.M800470-MCP200)]
  - 27 **Callewaert N**, Van Vlierberghe H, Van Hecke A, Laroy W, Delanghe J, Contreras R. Noninvasive diagnosis of liver cirrhosis using DNA sequencer-based total serum protein glycomics. *Nat Med* 2004; **10**: 429-434 [PMID: [15152612](https://pubmed.ncbi.nlm.nih.gov/15152612/) DOI: [10.1038/nm1006](https://doi.org/10.1038/nm1006)]
  - 28 **Malaguarnera G**, Bertino G, Vacante M, Malaguarnera M. Hepatocellular carcinoma markers in the omics era: the glycomic analysis. *Hepatobiliary Surg Nutr* 2014; **3**: 407-409 [PMID: [25568863](https://pubmed.ncbi.nlm.nih.gov/25568863/) DOI: [10.3978/j.issn.2304-3881.2014.07.04](https://doi.org/10.3978/j.issn.2304-3881.2014.07.04)]
  - 29 Nassir F. Role of acetylation in nonalcoholic fatty liver disease: a focus on SIRT1 and SIRT3. *Explor Med* 2020; **1**: 248-258. [DOI: [10.37349/emed.2020.00017](https://doi.org/10.37349/emed.2020.00017)]
  - 30 **Le-Tian Z**, Cheng-Zhang H, Xuan Z, Zhang Q, Zhen-Gui Y, Qing-Qing W, Sheng-Xuan W, Zhong-Jin X, Ran-Ran L, Ting-Jun L, Zhong-Qu S, Zhong-Hua W, Ke-Rong S. Protein acetylation in mitochondria plays critical functions in the pathogenesis of fatty liver disease. *BMC Genomics* 2020; **21**: 435 [PMID: [32586350](https://pubmed.ncbi.nlm.nih.gov/32586350/) DOI: [10.1186/s12864-020-06837-y](https://doi.org/10.1186/s12864-020-06837-y)]
  - 31 **Ciechanover A**. The unravelling of the ubiquitin system. *Nat Rev Mol Cell Biol* 2015; **16**: 322-324 [PMID: [25907614](https://pubmed.ncbi.nlm.nih.gov/25907614/) DOI: [10.1038/nrm3982](https://doi.org/10.1038/nrm3982)]
  - 32 **Dikic I**, Wakatsuki S, Walters KJ. Ubiquitin-binding domains - from structures to functions. *Nat Rev Mol Cell Biol* 2009; **10**: 659-671 [PMID: [19773779](https://pubmed.ncbi.nlm.nih.gov/19773779/) DOI: [10.1038/nrm2767](https://doi.org/10.1038/nrm2767)]
  - 33 **Park JS**, Ma H, Roh YS. Ubiquitin pathways regulate the pathogenesis of chronic liver disease. *Biochem Pharmacol* 2021; **193**: 114764 [PMID: [34529948](https://pubmed.ncbi.nlm.nih.gov/34529948/) DOI: [10.1016/j.bcp.2021.114764](https://doi.org/10.1016/j.bcp.2021.114764)]
  - 34 **Gligorijević N**, Minić S, Križáková M, Katrlík J, Nedić O. Structural changes of fibrinogen as a consequence of cirrhosis. *Thromb Res* 2018; **166**: 43-49 [PMID: [29655002](https://pubmed.ncbi.nlm.nih.gov/29655002/) DOI: [10.1016/j.thromres.2018.04.005](https://doi.org/10.1016/j.thromres.2018.04.005)]
  - 35 **Martinez J**, Palascak JE, Kwasniak D. Abnormal sialic acid content of the dysfibrinogenemia associated with liver disease. *J Clin Invest* 1978; **61**: 535-538 [PMID: [621288](https://pubmed.ncbi.nlm.nih.gov/621288/) DOI: [10.1172/JCI108964](https://doi.org/10.1172/JCI108964)]
  - 36 **Lisman T**, Ariëns RA. Alterations in Fibrin Structure in Patients with Liver Diseases. *Semin Thromb Hemost* 2016; **42**: 389-396 [PMID: [27071046](https://pubmed.ncbi.nlm.nih.gov/27071046/) DOI: [10.1055/s-0036-1572327](https://doi.org/10.1055/s-0036-1572327)]
  - 37 **Dang CV**, Shin CK, Bell WR, Nagaswami C, Weisel JW. Fibrinogen sialic acid residues are low affinity calcium-binding sites that influence fibrin assembly. *J Biol Chem* 1989; **264**: 15104-15108 [PMID: [2549051](https://pubmed.ncbi.nlm.nih.gov/2549051/) DOI: [10.1016/S0021-9258\(18\)63817-7](https://doi.org/10.1016/S0021-9258(18)63817-7)]
  - 38 **Kuchay MS**, Mishra SK, Farooqui KJ, Bansal B, Wasir JS, Mithal A. Hypercalcemia of advanced chronic liver disease: a forgotten clinical entity! *Clin Cases Miner Bone Metab* 2016; **13**: 15-18 [PMID: [27252737](https://pubmed.ncbi.nlm.nih.gov/27252737/) DOI: [10.11138/ccmbm/2016.13.1.015](https://doi.org/10.11138/ccmbm/2016.13.1.015)]
  - 39 **Marchi R**, Arocha-Piñango CL, Nagy H, Matsuda M, Weisel JW. The effects of additional carbohydrate in the coiled-coil region of fibrinogen on polymerization and clot structure and properties: characterization of the homozygous and heterozygous forms of fibrinogen Lima (Aalpha Arg141-->Ser with extra glycosylation). *J Thromb Haemost* 2004; **2**: 940-948 [PMID: [15140130](https://pubmed.ncbi.nlm.nih.gov/15140130/) DOI: [10.1111/j.1538-7836.2004.00730.x](https://doi.org/10.1111/j.1538-7836.2004.00730.x)]
  - 40 **Maekawa H**, Yamazumi K, Muramatsu S, Kaneko M, Hirata H, Takahashi N, Arocha-Piñango CL, Rodriguez S, Nagy H, Perez-Requejo JL. Fibrinogen Lima: a homozygous dysfibrinogen with an A alpha-arginine-141 to serine substitution associated with extra N-glycosylation at A alpha-asparagine-139. Impaired fibrin gel formation but normal fibrin-facilitated plasminogen activation catalyzed by tissue-type plasminogen activator. *J Clin Invest* 1992; **90**: 67-76 [PMID: [1634621](https://pubmed.ncbi.nlm.nih.gov/1634621/) DOI: [10.1172/JCI115857](https://doi.org/10.1172/JCI115857)]
  - 41 **Yamazumi K**, Shimura K, Terukina S, Takahashi N, Matsuda M. A gamma methionine-310 to threonine substitution and consequent N-glycosylation at gamma asparagine-308 identified in a congenital dysfibrinogenemia associated with posttraumatic bleeding, fibrinogen Asahi. *J Clin Invest* 1989; **83**: 1590-1597 [PMID: [2496144](https://pubmed.ncbi.nlm.nih.gov/2496144/) DOI: [10.1172/JCI114056](https://doi.org/10.1172/JCI114056)]
  - 42 **Sugo T**, Nakamikawa C, Takano H, Mimuro J, Yamaguchi S, Mosesson MW, Meh DA, DiOrto JP, Takahashi N, Takahashi H, Nagai K, Matsuda M. Fibrinogen Niigata with impaired fibrin assembly: an inherited dysfibrinogen with a Bbeta Asn-160 to Ser substitution associated with extra glycosylation at Bbeta Asn-158. *Blood* 1999; **94**: 3806-3813 [PMID: [10572095](https://pubmed.ncbi.nlm.nih.gov/10572095/) DOI: [10.1182/blood.V94.11.3806](https://doi.org/10.1182/blood.V94.11.3806)]
  - 43 **Hughenoltz GC**, Macrae F, Adelmeyer J, Dulfer S, Porte RJ, Lisman T, Ariëns RA. Procoagulant changes in fibrin clot structure in patients with cirrhosis are associated with oxidative modifications of fibrinogen. *J Thromb Haemost* 2016; **14**: 1054-1066 [PMID: [26833718](https://pubmed.ncbi.nlm.nih.gov/26833718/) DOI: [10.1111/jth.13278](https://doi.org/10.1111/jth.13278)]
  - 44 **Martinez M**, Weisel JW, Ischiropoulos H. Functional impact of oxidative posttranslational modifications on fibrinogen and fibrin clots. *Free Radic Biol Med* 2013; **65**: 411-418 [PMID: [23851017](https://pubmed.ncbi.nlm.nih.gov/23851017/) DOI: [10.1016/j.freeradbiomed.2013.06.039](https://doi.org/10.1016/j.freeradbiomed.2013.06.039)]
  - 45 **Xu YJ**, Qiang M, Zhang JL, Liu Y, He RQ. Reactive carbonyl compounds (RCCs) cause aggregation and dysfunction of fibrinogen. *Protein Cell* 2012; **3**: 627-640 [PMID: [22836718](https://pubmed.ncbi.nlm.nih.gov/22836718/) DOI: [10.1007/s13238-012-2057-y](https://doi.org/10.1007/s13238-012-2057-y)]
  - 46 **Becatti M**, Marcucci R, Bruschi G, Taddei N, Bani D, Gori AM, Giusti B, Gensini GF, Abbate R, Fiorillo C. Oxidative modification of fibrinogen is associated with altered function and structure in the subacute phase of myocardial infarction.

- Arterioscler Thromb Vasc Biol* 2014; **34**: 1355-1361 [PMID: 24790138 DOI: 10.1161/ATVBAHA.114.303785]
- 47 **Rosenfeld MA**, Vasilyeva AD, Yurina LV, Bychkova AV. Oxidation of proteins: is it a programmed process? *Free Radic Res* 2018; **52**: 14-38 [PMID: 29284315 DOI: 10.1080/10715762.2017.1402305]
- 48 **Zermatten MG**, Fraga M, Moradpour D, Bertaggia Calderara D, Aliotta A, Stirnimann G, De Gottardi A, Alberio L. Hemostatic Alterations in Patients With Cirrhosis: From Primary Hemostasis to Fibrinolysis. *Hepatology* 2020; **71**: 2135-2148 [PMID: 32090357 DOI: 10.1002/hep.31201]
- 49 **Bernardi M**, Ricci CS, Zaccherini G. Role of human albumin in the management of complications of liver cirrhosis. *J Clin Exp Hepatol* 2014; **4**: 302-311 [PMID: 25755577 DOI: 10.1016/j.jceh.2014.08.007]
- 50 **Carvalho JR**, Verdelho Machado M. New Insights About Albumin and Liver Disease. *Ann Hepatol* 2018; **17**: 547-560 [PMID: 29893696 DOI: 10.5604/01.3001.0012.0916]
- 51 **Oettl K**, Stadlbauer V, Petter F, Greilberger J, Putz-Bankuti C, Hallström S, Lackner C, Stauber RE. Oxidative damage of albumin in advanced liver disease. *Biochim Biophys Acta* 2008; **1782**: 469-473 [PMID: 18498776 DOI: 10.1016/j.bbadis.2008.04.002]
- 52 **Baldassarre M**, Domenicali M, Naldi M, Laggetta M, Giannone FA, Biselli M, Patrono D, Bertucci C, Bernardi M, Caraceni P. Albumin Homodimers in Patients with Cirrhosis: Clinical and Prognostic Relevance of a Novel Identified Structural Alteration of the Molecule. *Sci Rep* 2016; **6**: 35987 [PMID: 27782157 DOI: 10.1038/srep35987]
- 53 **Domenicali M**, Baldassarre M, Giannone FA, Naldi M, Mastroberroberto M, Biselli M, Laggetta M, Patrono D, Bertucci C, Bernardi M, Caraceni P. Posttranscriptional changes of serum albumin: clinical and prognostic significance in hospitalized patients with cirrhosis. *Hepatology* 2014; **60**: 1851-1860 [PMID: 25048618 DOI: 10.1002/hep.27322]
- 54 **Giannone FA**, Domenicali M, Baldassarre M, Bartoletti M, Naldi M, Laggetta M, Bertucci C, Colecchia A, Viale P, Bernardi M, Caraceni P. Ischaemia-modified albumin: a marker of bacterial infection in hospitalized patients with cirrhosis. *Liver Int* 2015; **35**: 2425-2432 [PMID: 25939693 DOI: 10.1111/liv.12860]
- 55 **Baldassarre M**, Naldi M, Zaccherini G, Bartoletti M, Antognoli A, Laggetta M, Gagliardi M, Tufoni M, Domenicali M, Waterstradt K, Paterini P, Baldan A, Leoni S, Bartolini M, Viale P, Trevisani F, Bernardi M, Caraceni P. Determination of Effective Albumin in Patients With Decompensated Cirrhosis: Clinical and Prognostic Implications. *Hepatology* 2021; **74**: 2058-2073 [PMID: 33710623 DOI: 10.1002/hep.31798]
- 56 **Paar M**, Fengler VH, Rosenberg DJ, Krebs A, Stauber RE, Oettl K, Hammel M. Albumin in patients with liver disease shows an altered conformation. *Commun Biol* 2021; **4**: 731 [PMID: 34127764 DOI: 10.1038/s42003-021-02269-w]
- 57 **Gomme PT**, McCann KB, Bertolini J. Transferrin: structure, function and potential therapeutic actions. *Drug Discov Today* 2005; **10**: 267-273 [PMID: 15708745 DOI: 10.1016/S1359-6446(04)03333-1]
- 58 **Kawabata H**. Transferrin and transferrin receptors update. *Free Radic Biol Med* 2019; **133**: 46-54 [PMID: 29969719 DOI: 10.1016/j.freeradbiomed.2018.06.037]
- 59 **Stibler H**. Carbohydrate-deficient transferrin in serum: a new marker of potentially harmful alcohol consumption reviewed. *Clin Chem* 1991; **37**: 2029-2037 [PMID: 1764777 DOI: 10.1093/clinchem/37.12.2029]
- 60 **Inoue T**, Yamauchi M, Ohkawa K. Structural studies on sugar chains of carbohydrate-deficient transferrin from patients with alcoholic liver disease using lectin affinity electrophoresis. *Electrophoresis* 1999; **20**: 452-457 [PMID: 10217151 DOI: 10.1002/(SICI)1522-2683(19990301)20:3<452::AID-ELPS452>3.0.CO;2-R]
- 61 **Hoefkens P**, Huijskes-Heins MI, de Jeu-Jaspars CM, van Noort WL, van Eijk HG. Influence of transferrin glycans on receptor binding and iron-donation. *Glycoconj J* 1997; **14**: 289-295 [PMID: 9111147 DOI: 10.1023/a:1018510309524]
- 62 **Arndt T**, van der Meijden BB, Wielders JP. Atypical serum transferrin isoform distribution in liver cirrhosis studied by HPLC, capillary electrophoresis and transferrin genotyping. *Clin Chim Acta* 2008; **394**: 42-46 [PMID: 18442477 DOI: 10.1016/j.cca.2008.03.033]
- 63 **Stewart SH**, Reuben A, Anton RF. Relationship of Abnormal Chromatographic Pattern for Carbohydrate-Deficient Transferrin with Severe Liver Disease. *Alcohol Alcohol* 2017; **52**: 24-28 [PMID: 27998920 DOI: 10.1093/alcalc/agw069]
- 64 **Landberg E**, Åström E, Kågedal B, Pålsson P. Disialo-trisialo bridging of transferrin is due to increased branching and fucosylation of the carbohydrate moiety. *Clin Chim Acta* 2012; **414**: 58-64 [PMID: 22902807 DOI: 10.1016/j.cca.2012.07.026]
- 65 **Viveiros A**, Finkenstedt A, Schaefer B, Mandorfer M, Scheiner B, Lehner K, Tobiasch M, Reiberger T, Tilg H, Edlinger M, Zoller H. Transferrin as a predictor of survival in cirrhosis. *Liver Transpl* 2018; **24**: 343-351 [PMID: 29149510 DOI: 10.1002/lt.24981]
- 66 **Yu Y**, Jiang L, Wang H, Shen Z, Cheng Q, Zhang P, Wang J, Wu Q, Fang X, Duan L, Wang S, Wang K, An P, Shao T, Chung RT, Zheng S, Min J, Wang F. Hepatic transferrin plays a role in systemic iron homeostasis and liver ferroptosis. *Blood* 2020; **136**: 726-739 [PMID: 32374849 DOI: 10.1182/blood.2019002907]
- 67 **Sanda M**, Benicky J, Wu J, Wang Y, Makambi K, Ahn J, Smith CI, Zhao P, Zhang L, Goldman R. Increased sialylation of site specific O-glycoforms of hemopexin in liver disease. *Clin Proteomics* 2016; **13**: 24 [PMID: 27688741 DOI: 10.1186/s12014-016-9125-x]
- 68 **Morota K**, Nakagawa M, Sekiya R, Hemken PM, Sokoll LJ, Elliott D, Chan DW, Dowell BL. A comparative evaluation of Golgi protein-73, fucosylated hemopexin,  $\alpha$ -fetoprotein, and PIVKA-II in the serum of patients with chronic hepatitis, cirrhosis, and hepatocellular carcinoma. *Clin Chem Lab Med* 2011; **49**: 711-718 [PMID: 21231906 DOI: 10.1515/CCLM.2011.097]
- 69 **Pompach P**, Brnakova Z, Sanda M, Wu J, Edwards N, Goldman R. Site-specific glycoforms of haptoglobin in liver cirrhosis and hepatocellular carcinoma. *Mol Cell Proteomics* 2013; **12**: 1281-1293 [PMID: 23389049 DOI: 10.1074/mcp.M112.023259]
- 70 **Bensi G**, Raugei G, Klefenz H, Cortese R. Structure and expression of the human haptoglobin locus. *EMBO J* 1985; **4**: 119-126 [PMID: 4018023 DOI: 10.1002/j.1460-2075.1985.tb02325.x]
- 71 **Zhang S**, Shu H, Luo K, Kang X, Zhang Y, Lu H, Liu Y. N-linked glycan changes of serum haptoglobin  $\beta$  chain in liver disease patients. *Mol Biosyst* 2011; **7**: 1621-1628 [PMID: 21380457 DOI: 10.1039/c1mb05020f]
- 72 **Polticelli F**, Bocedi A, Minervini G, Ascenzi P. Human haptoglobin structure and function--a molecular modelling study. *FEBS J* 2008; **275**: 5648-5656 [PMID: 18959750 DOI: 10.1111/j.1742-4658.2008.06690.x]

- 73 **Zhu J**, Lin Z, Wu J, Yin H, Dai J, Feng Z, Marrero J, Lubman DM. Analysis of serum haptoglobin fucosylation in hepatocellular carcinoma and liver cirrhosis of different etiologies. *J Proteome Res* 2014; **13**: 2986-2997 [PMID: 24807840 DOI: 10.1021/pr500128t]
- 74 **Orino K**, Watanabe K. Molecular, physiological and clinical aspects of the iron storage protein ferritin. *Vet J* 2008; **178**: 191-201 [PMID: 17764995 DOI: 10.1016/j.tvjl.2007.07.006]
- 75 **Wang W**, Knovich MA, Coffman LG, Torti FM, Torti SV. Serum ferritin: Past, present and future. *Biochim Biophys Acta* 2010; **1800**: 760-769 [PMID: 20304033 DOI: 10.1016/j.bbagen.2010.03.011]
- 76 **Fletcher LM**, Halliday JW, Powell LW. Interrelationships of alcohol and iron in liver disease with particular reference to the iron-binding proteins, ferritin and transferrin. *J Gastroenterol Hepatol* 1999; **14**: 202-214 [PMID: 10197487 DOI: 10.1046/j.1440-1746.1999.01836.x]
- 77 **Czaja AJ**. Review article: iron disturbances in chronic liver diseases other than haemochromatosis - pathogenic, prognostic, and therapeutic implications. *Aliment Pharmacol Ther* 2019; **49**: 681-701 [PMID: 30761559 DOI: 10.1111/apt.15173]
- 78 **Domschke W**, Meyer-Bertenrath JG. -Helical structures and iron contents of the ribosomal ferritin from normal, cirrhotic and cancerous human livers. *Digestion* 1971; **4**: 321-325 [PMID: 4329888 DOI: 10.1159/000197136]
- 79 **Cullis JO**, Fitzsimons EJ, Griffiths WJ, Tsochatzis E, Thomas DW; British Society for Haematology. Investigation and management of a raised serum ferritin. *Br J Haematol* 2018; **181**: 331-340 [PMID: 29672840 DOI: 10.1111/bjh.15166]
- 80 **Chapman RW**, Gorman A, Laulicht M, Hussain MA, Sherlock S, Hoffbrand AV. Binding of serum ferritin to concanavalin A in patients with iron overload and with chronic liver disease. *J Clin Pathol* 1982; **35**: 481-486 [PMID: 7085891 DOI: 10.1136/jcp.35.5.481]
- 81 **Annuziata M**, Granata R, Ghigo E. The IGF system. *Acta Diabetol* 2011; **48**: 1-9 [PMID: 21042815 DOI: 10.1007/s00592-010-0227-z]
- 82 **Jogie-Brahim S**, Feldman D, Oh Y. Unraveling insulin-like growth factor binding protein-3 actions in human disease. *Endocr Rev* 2009; **30**: 417-437 [PMID: 19477944 DOI: 10.1210/er.2008-0028]
- 83 **Firth SM**, Baxter RC. Characterisation of recombinant glycosylation variants of insulin-like growth factor binding protein-3. *J Endocrinol* 1999; **160**: 379-387 [PMID: 10076184 DOI: 10.1677/joe.0.1600379]
- 84 **Coverley JA**, Martin JL, Baxter RC. The effect of phosphorylation by casein kinase 2 on the activity of insulin-like growth factor-binding protein-3. *Endocrinology* 2000; **141**: 564-570 [PMID: 10650937 DOI: 10.1210/endo.141.2.7306]
- 85 **Nedić O**, Nikolić JA, Prisić S, Acimovic J, hajdukovic-Dragojlovic L. Reactivity of IGF binding protein-3 isoforms towards concanavalin A in healthy adults and subjects with cirrhosis. *Addict Biol* 2003; **8**: 81-88 [PMID: 12745420 DOI: 10.1080/1355621031000069927]
- 86 **Nedić O**, Nikolić JA, Hajduković-Dragojlović L, Todorović V, Masnikosa R. Alterations of IGF-binding proteins in patients with alcoholic liver cirrhosis. *Alcohol* 2000; **21**: 223-229 [PMID: 11091025 DOI: 10.1016/s0741-8329(00)00090-2]
- 87 **Cai Q**, Dozmorov M, Oh Y. IGFBP-3/IGFBP-3 Receptor System as an Anti-Tumor and Anti-Metastatic Signaling in Cancer. *Cells* 2020; **9** [PMID: 32443727 DOI: 10.3390/cells9051261]
- 88 **Arab JP**, Cabrera D, Sehrawat TS, Jalan-Sakrikar N, Verma VK, Simonetto D, Cao S, Yaqoob U, Leon J, Freire M, Vargas JI, De Assuncao TM, Kwon JH, Guo Y, Kostallari E, Cai Q, Kisseleva T, Oh Y, Arrese M, Huebert RC, Shah VH. Hepatic stellate cell activation promotes alcohol-induced steatohepatitis through Igfbp3 and SerpinA12. *J Hepatol* 2020; **73**: 149-160 [PMID: 32087348 DOI: 10.1016/j.jhep.2020.02.005]
- 89 **Luo J**, Chen Q, Shen T, Wang X, Fang W, Wu X, Yuan Z, Chen G, Ling W, Chen Y. Association of sex hormone-binding globulin with nonalcoholic fatty liver disease in Chinese adults. *Nutr Metab (Lond)* 2018; **15**: 79 [PMID: 30455723 DOI: 10.1186/s12986-018-0313-8]
- 90 **Yuan W**, Benicky J, Wei R, Goldman R, Sanda M. Quantitative Analysis of Sex-Hormone-Binding Globulin Glycosylation in Liver Diseases by Liquid Chromatography-Mass Spectrometry Parallel Reaction Monitoring. *J Proteome Res* 2018; **17**: 2755-2766 [PMID: 29972295 DOI: 10.1021/acs.jproteome.8b00201]
- 91 **Thaler MA**, Seifert-Klauss V, Luppá PB. The biomarker sex hormone-binding globulin - from established applications to emerging trends in clinical medicine. *Best Pract Res Clin Endocrinol Metab* 2015; **29**: 749-760 [PMID: 26522459 DOI: 10.1016/j.beem.2015.06.005]
- 92 **Luppá PB**, Thaler M, Schulte-Frohlinde E, Schreiegg A, Huber U, Metzger J. Unchanged androgen-binding properties of sex hormone-binding globulin in male patients with liver cirrhosis. *Clin Chem Lab Med* 2006; **44**: 967-973 [PMID: 16879062 DOI: 10.1515/CCLM.2006.186]
- 93 **Brenta G**, Bedecarras P, Schnitman M, Gurfinkiel M, Damilano S, Campo S, Pisarev MA. Characterization of sex hormone-binding globulin isoforms in hypothyroid women. *Thyroid* 2002; **12**: 101-105 [PMID: 11916278 DOI: 10.1089/105072502753522329]
- 94 **Kaymakoğlu S**, Okten A, Cakaloğlu Y, Boztaş G, Beşişik F, Taşçioğlu C, Yalçın S. Hypogonadism is not related to the etiology of liver cirrhosis. *J Gastroenterol* 1995; **30**: 745-750 [PMID: 8963392 DOI: 10.1007/BF02349641]
- 95 **Maruyama Y**, Adachi Y, Aoki N, Suzuki Y, Shinohara H, Yamamoto T. Mechanism of feminization in male patients with non-alcoholic liver cirrhosis: role of sex hormone-binding globulin. *Gastroenterol Jpn* 1991; **26**: 435-439 [PMID: 1916151 DOI: 10.1007/BF02782811]
- 96 **Price JC**, Wang R, Seaberg EC, Brown TT, Budoff MJ, Kingsley LA, Palella FJ Jr, Witt MD, Post WS, Lake JE, Thio CL. Sex Hormone-Binding Globulin Levels Are Inversely Associated With Nonalcoholic Fatty Liver Disease in HIV-Infected and -Uninfected Men. *Open Forum Infect Dis* 2019; **6**: ofz468 [PMID: 32128321 DOI: 10.1093/ofid/ofz468]
- 97 **Yuan W**, Sanda M, Wu J, Koomen J, Goldman R. Quantitative analysis of immunoglobulin subclasses and subclass specific glycosylation by LC-MS-MRM in liver disease. *J Proteomics* 2015; **116**: 24-33 [PMID: 25582524 DOI: 10.1016/j.jprot.2014.12.020]
- 98 **Mehta AS**, Long RE, Comunale MA, Wang M, Rodemich L, Krakover J, Philip R, Marrero JA, Dwek RA, Block TM. Increased levels of galactose-deficient anti-Gal immunoglobulin G in the sera of hepatitis C virus-infected individuals with fibrosis and cirrhosis. *J Virol* 2008; **82**: 1259-1270 [PMID: 18045939 DOI: 10.1128/JVI.01600-07]

- 99 **Tissandré E**, Morelle W, Berthelot L, Vrtovsnik F, Daugas E, Walker F, Lebrec D, Trawalé JM, Francoz C, Durand F, Moura IC, Paradis V, Moreau R, Monteiro RC. Both IgA nephropathy and alcoholic cirrhosis feature abnormally glycosylated IgA1 and soluble CD89-IgA and IgG-IgA complexes: common mechanisms for distinct diseases. *Kidney Int* 2011; **80**: 1352-1363 [PMID: 21866091 DOI: 10.1038/ki.2011.276]
- 100 **Lamontagne A**, Long RE, Comunale MA, Hafner J, Rodemich-Betesh L, Wang M, Marrero J, Di Bisceglie AM, Block T, Mehta A. Altered functionality of anti-bacterial antibodies in patients with chronic hepatitis C virus infection. *PLoS One* 2013; **8**: e64992 [PMID: 23750224 DOI: 10.1371/journal.pone.0064992]
- 101 **Wu T**, Zhao F, Gao B, Tan C, Yagishita N, Nakajima T, Wong PK, Chapman E, Fang D, Zhang DD. Hrd1 suppresses Nrf2-mediated cellular protection during liver cirrhosis. *Genes Dev* 2014; **28**: 708-722 [PMID: 24636985 DOI: 10.1101/gad.238246.114]
- 102 **Hasegawa D**, Fujii R, Yagishita N, Matsumoto N, Aratani S, Izumi T, Azakami K, Nakazawa M, Fujita H, Sato T, Araya N, Koike J, Tadokoro M, Suzuki N, Nagata K, Senoo H, Friedman SL, Nishioka K, Yamano Y, Itoh F, Nakajima T. E3 ubiquitin ligase synoviolin is involved in liver fibrogenesis. *PLoS One* 2010; **5**: e13590 [PMID: 21049091 DOI: 10.1371/journal.pone.0013590]
- 103 **Zou T**, Zhang J. Diverse and pivotal roles of neddylation in metabolism and immunity. *FEBS J* 2021; **288**: 3884-3912 [PMID: 33025631 DOI: 10.1111/febs.15584]
- 104 **Dai J**, Hu Y, Niu Q, Song G, Wang H, Li S. Role of PML SUMOylation in arsenic trioxide-induced fibrosis in HSCs. *Life Sci* 2020; **251**: 117607 [PMID: 32240679 DOI: 10.1016/j.lfs.2020.117607]
- 105 **Guo L**, Guo YY, Li BY, Peng WQ, Chang XX, Gao X, Tang QQ. Enhanced acetylation of ATP-citrate lyase promotes the progression of nonalcoholic fatty liver disease. *J Biol Chem* 2019; **294**: 11805-11816 [PMID: 31197036 DOI: 10.1074/jbc.RA119.008708]
- 106 **Groebner JL**, Girón-Bravo MT, Rothberg ML, Adhikari R, Tuma DJ, Tuma PL. Alcohol-induced microtubule acetylation leads to the accumulation of large, immobile lipid droplets. *Am J Physiol Gastrointest Liver Physiol* 2019; **317**: G373-G386 [PMID: 31373507 DOI: 10.1152/ajpgi.00026.2019]
- 107 **Yang Y**, Sangwung P, Kondo R, Jung Y, McConnell MJ, Jeong J, Utsumi T, Sessa WC, Iwakiri Y. Alcohol-induced Hsp90 acetylation is a novel driver of liver sinusoidal endothelial dysfunction and alcohol-related liver disease. *J Hepatol* 2021; **75**: 377-386 [PMID: 33675874 DOI: 10.1016/j.jhep.2021.02.028]
- 108 **Ding D**, Chen LL, Zhai YZ, Hou CJ, Tao LL, Lu SH, Wu J, Liu XP. Trichostatin A inhibits the activation of Hepatic stellate cells by Increasing C/EBP- $\alpha$  Acetylation in vivo and in vitro. *Sci Rep* 2018; **8**: 4395 [PMID: 29535398 DOI: 10.1038/s41598-018-22662-6]
- 109 **Abdelmegeed MA**, Song BJ. Functional roles of protein nitration in acute and chronic liver diseases. *Oxid Med Cell Longev* 2014; **2014**: 149627 [PMID: 24876909 DOI: 10.1155/2014/149627]
- 110 **Ji Y**, Neverova I, Van Eyk JE, Bennett BM. Nitration of tyrosine 92 mediates the activation of rat microsomal glutathione s-transferase by peroxynitrite. *J Biol Chem* 2006; **281**: 1986-1991 [PMID: 16314419 DOI: 10.1074/jbc.M509480200]
- 111 **Charatcharoenwitthaya P**, Karaketklang K, Aekplakorn W. Cigarette Smoking Increased Risk of Overall Mortality in Patients With Non-alcoholic Fatty Liver Disease: A Nationwide Population-Based Cohort Study. *Front Med (Lausanne)* 2020; **7**: 604919 [PMID: 33365321 DOI: 10.3389/fmed.2020.604919]
- 112 **Corrao G**, Zambon A, Bagnardi V, D'Amicis A, Klatsky A; Collaborative SIDECIR Group. Coffee, caffeine, and the risk of liver cirrhosis. *Ann Epidemiol* 2001; **11**: 458-465 [PMID: 11557177 DOI: 10.1016/s1047-2797(01)00223-x]
- 113 **Herrera JL**, Rodríguez R. Medical Care of the Patient With Compensated Cirrhosis. *Gastroenterol Hepatol (N Y)* 2006; **2**: 124-133 [PMID: 28286440]
- 114 **Harrison-Findik DD**. Role of alcohol in the regulation of iron metabolism. *World J Gastroenterol* 2007; **13**: 4925-4930 [PMID: 17854133 DOI: 10.3748/wjg.v13.i37.4925]

## Epidemiologic and socioeconomic factors impacting hepatitis B virus and related hepatocellular carcinoma

Bipul Gnyawali, Antoinette Pusateri, Ashley Nickerson, Sajid Jalil, Khalid Mumtaz

**Specialty type:** Gastroenterology and hepatology

**Provenance and peer review:** Invited article; Externally peer reviewed.

**Peer-review model:** Single blind

**Peer-review report's scientific quality classification**

Grade A (Excellent): 0  
Grade B (Very good): B, B  
Grade C (Good): 0  
Grade D (Fair): 0  
Grade E (Poor): 0

**P-Reviewer:** Liu DF, China; Venegas M, Chile

**Received:** January 18, 2022

**Peer-review started:** January 18, 2022

**First decision:** March 8, 2022

**Revised:** April 10, 2022

**Accepted:** July 11, 2022

**Article in press:** July 11, 2022

**Published online:** August 7, 2022



**Bipul Gnyawali**, Department of Medicine, Kettering Medical Center, Dayton, OH 45342, United States

**Antoinette Pusateri, Ashley Nickerson, Sajid Jalil, Khalid Mumtaz**, Department of Medicine, The Ohio State University, Columbus, OH 43210, United States

**Corresponding author:** Khalid Mumtaz, MBBS, MSc, Associate Professor, Department of Medicine, The Ohio State University, 395 W. 12<sup>th</sup> Avenue, 262 Suite, Columbus, OH 43210, United States. [khalid.mumtaz@osumc.edu](mailto:khalid.mumtaz@osumc.edu)

### Abstract

Chronic Hepatitis B is a highly prevalent disease worldwide and is estimated to cause more than 800000 annual deaths from complications such as cirrhosis and hepatocellular carcinoma (HCC). Although universal hepatitis B vaccination programs may have reduced the incidence and prevalence of chronic hepatitis B and related HCC, the disease still imposes a significant healthcare burden in many endemic regions such as Africa and the Asia-Pacific region. This is especially concerning given the global underdiagnosis of hepatitis B and the limited availability of vaccination, screening, and treatment in low-resource regions. Demographics including male gender, older age, ethnicity, and geographic location as well as low socioeconomic status are more heavily impacted by chronic hepatitis B and related HCC. Methods to mitigate this impact include increasing screening in high-risk groups according to national guidelines, increasing awareness and health literacy in vulnerable populations, and developing more robust vaccination programs in under-served regions.

**Key Words:** Hepatitis B; Epidemiology; Hepatocellular carcinoma; Socioeconomic status; Healthcare disparity; Hepatitis B vaccine

©The Author(s) 2022. Published by Baishideng Publishing Group Inc. All rights reserved.

**Core Tip:** While many studies in the past have analyzed the impact of various epidemiological and socioeconomic factors on viral hepatitis and hepatocellular carcinoma (HCC), this minireview is the first to adopt a global perspective in highlighting the impact of both epidemiologic and socioeconomic factors on current trends in chronic hepatitis B and related HCC. We highlight trends in incidence, prevalence and mortality of chronic hepatitis B seen throughout the world in the past few decades and the disparity in healthcare distribution and outcomes between different populations.

**Citation:** Gnyawali B, Pusateri A, Nickerson A, Jalil S, Mumtaz K. Epidemiologic and socioeconomic factors impacting hepatitis B virus and related hepatocellular carcinoma. *World J Gastroenterol* 2022; 28(29): 3793-3802

**URL:** <https://www.wjgnet.com/1007-9327/full/v28/i29/3793.htm>

**DOI:** <https://dx.doi.org/10.3748/wjg.v28.i29.3793>

## INTRODUCTION

In 2019, the World Health Organization (WHO) estimated the worldwide prevalence of chronic hepatitis B virus (HBV) to be around 296 million with the incidence of new HBV infection to be 1.5 million each year. HBV is more prevalent with high burden of disease in the regions of Africa, Western Pacific and South-East Asia compared to North America and Europe. Furthermore, fewer people in the African and South-East Asian regions knew about their HBV status and had access to treatment compared to the latter regions[1].

Hepatocellular carcinoma (HCC) in unsuspected HBV patients is a major cause of increased morbidity and mortality in low-income countries with limited resources[2,3]. While it may be too early to see the true impact of the global HBV vaccination initiative led by the WHO or treatment efforts for HBV-related HCC, evidence thus far demonstrates decreased burden of HBV and HCC in children and suggests treatment with antivirals can reduce HCC risk in some patients[4-8]. There continues to be great disparity in access to vaccines, treatment, and screening programs worldwide, however. Even where there is access, the risk of HCC in treated chronic HBV is not fully mitigated[9,10]. While concomitant liver diseases are certainly at play including co-infection with hepatitis C, aflatoxin exposure, metabolic syndrome, and alcohol use disorder, chronic HBV-related HCC has a significant global disease burden that disproportionately impacts people of different regions and demographics[9, 11]. The aim of this review is to examine the impact of epidemiologic and socioeconomic factors on chronic HBV-related HCC from a global perspective. Strategies to address the resulting disparities in disease outcomes will also be discussed.

## DEMOGRAPHIC FACTORS

### *Geographic variations*

There is significant global variation in the prevalence of chronic HBV between regions. As a result, the incidence and prevalence of HBV related HCC are also quite variable between regions and correlate with rate of HBV infection[12]. About 50%-80% of HCC can be linked to HBV worldwide, and the high-risk HCC regions represent 80% of the global burden of HCC[13]. Regions such as Africa, Southeast Asia, and the Western Pacific, are considered high-risk HCC regions owed partially due to high seroprevalence of chronic HBV which is estimated at 5%-10%. On the contrary, North America and Western Europe are low-risk HCC regions with an HBV prevalence of < 1%. The Middle East and the Indian subcontinent are intermediate-risk regions with HBV prevalence of 2%-5%[14]. Data illustrating the geographic distribution of chronic HBV by prevalence is seen in [Table 1](#) and [Figure 1](#).

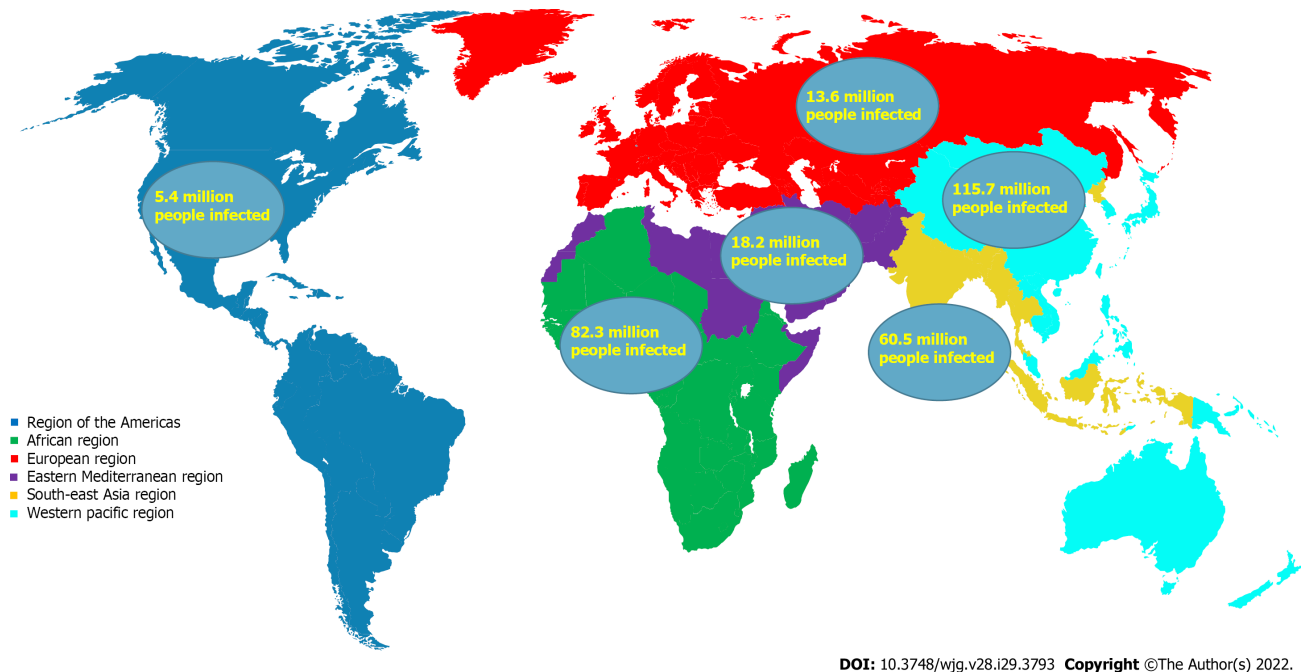
### *Asia and Africa*

Prevalence of HBV in Asia and Africa within high-risk regions is not uniform. In Africa, particularly West Africa and Sub-Saharan Africa, complications of chronic HBV including cirrhosis and HCC are frequent and fatal due to a relative lack of vaccination, surveillance and treatment[15]. Sub Saharan Africa had an estimated vaccination rate of less than 10% and fewer than 1% of HBV infections were diagnosed in 2019[9].

In East Asia, China has a high prevalence of HBV-related HCC, estimated to be 50% of the world's burden of HCC. Mongolia has the highest incidence rate of HCC in the world at 93.7 per 100000 with HBV being the predominant risk factor[9]. However, countries of low HCC incidence also exist in the Asia-Pacific region such as Japan, India, Singapore, and Pakistan. Interestingly, Japan has a low incidence of HBV where hepatitis C virus (HCV) is the major contributor of HCC, estimated to account for 80%-90% of cases[11,14,16].

**Table 1 Geographic distribution of Chronic hepatitis B virus by estimated disease burden in 2019**

Geographic region[22,40]	People living with hepatitis B infection
African region	82.3 million (62.1-114.7 million)
Region of the Americas	5.4 million (3.1-12.0 million) (2.1 million in Latin America and the Caribbean)
Eastern Mediterranean region	18.2 million (14.4-23.8 million)
European region	13.6 million (10.2-22.1 million)
South-East Asia region	60.5 million (45.3-120.9 million)
Western Pacific region	115.7 million (95.2-141.9 million)

**Figure 1 Geographic distribution of chronic hepatitis B virus.**

Data from Asian nations such as India, China, Thailand and Nepal show that there are evident disparities in HBV prevalence within population sub-groups[17,18]. Surveys of the Tibetan population in Nepal's Kathmandu valley showed prevalence of chronic HBV of 10%-20% compared to the overall prevalence of 0.9% in Nepal[18]. The general population of China has an estimated HBV prevalence of 6.89% while Western provinces have a higher prevalence at 8.92%[19]. The hill tribe of Chiang Rai province in Thailand see a significantly higher prevalence of chronic HBV at 26.6% while the overall prevalence in Thailand is 5.1% [17,20]. Although Southeast Asia as a region has a higher prevalence of HBV infection at 3.0%, there are variations in prevalence between ethnicities within the region. Given the relatively high prevalence rate of chronic HBV infection in Southeast Asia compared to Europe and the Americas, the incidence of liver cancer being highest in these regions is not surprising[11,21]. Some explanations for the disparities seen in the various regions and ethnic groups include unequal access to vaccines, limited health care programs, lack of health literacy, and elements of culture and religion that also serve a role[17,19,21].

### **United States**

Immigration from endemic countries is the main contributor to chronic HBV cases in the United States, which has a prevalence rate of 0.5% compared to 3.8% globally[21]. An estimated 70% of HBV infections in the United States are among foreign-born individuals with an estimated 730000 to 2.2 million living with chronic HBV[22]. Screening studies of foreign-born immigrants from Africa, the Middle East, and Asia have shown a higher chronic HBV prevalence rate of 10%-15% compared to 0.27%-0.50% for the general population[11,12,23,24]. Chronic HBV infection is disproportionately higher amongst Asian Americans in the United States[25]. Asian Americans comprise roughly 5%-6% of the population in the United States but 50% of the cases of chronic HBV[22].

Studies have also shown ethnic variation in HBV-related HCC within the United States, owing to differing sizes of immigrant populations from endemic countries. While rates of HCC in Asian and Pacific Islanders, once elevated are now declining, the incidence of HCC in Hispanics, Whites and African Americans continues to increase, driven mainly by HCV and non-alcoholic steatohepatitis (NASH) related cirrhosis[7,23,26-28]. Southern and Western states have the highest incidence rates of HCC in the United States[28]. While Asian Americans have the lowest mortality rates from HCC of all ethnicities, the highest mortality rates are seen in African Americans[29,30]. This apparent disparity may be partially explained by the etiology of HCC which include alcohol use disorder and HCV related cirrhosis, as well as health care disparities and access to quality care among African Americans. Recent studies show a disparity even after liver transplantation in patients with HCC, with African Americans consistently having worse survival than Asian Americans and White American patients[31].

### Europe

Western Europe, like the United States, has a growing diversity in its population. Most chronic HBV infections in Western European countries are due to migrant populations, with an HBV prevalence estimated to be around 4% for migrant populations and < 1% for the general population[23,27]. There is also a greater prevalence of cirrhosis and HCC in the foreign-born population[32]. A population-based study of HCC in England found a higher proportion of HCC in non-white ethnicities, particularly due to viral hepatitis-related HCC[33]. Similar findings are reported in studies of other low HCC risk countries such as Austria, Finland, Netherlands, Germany, the United Kingdom and Denmark in which migrant populations are over-represented in cases of chronic HBV and HCC[32,34].

### Latin America

There is a reported heterogeneous distribution in chronic HBV prevalence amongst Latin American countries. Owing to variation in the endemicity of HBV and underreporting, some studies report an estimated 7-12 million people infected in Central and South America and the Caribbean[35]. In contrast, a report by the Pan American Health Organization and the WHO in 2016 suggested chronic HBV seroprevalence in Latin America being 0.33% with an estimated 2.1 million infected in the general population. However, the variation in HBV serum antigen (HBsAg) seroprevalence ranged from 0.20% to 13.55% among the numerous countries[36].

In the majority of Latin America, HCV and alcoholic liver disease are the leading causes of HCC. HBV is more endemic to certain countries such as Brazil, Argentina, and Peru.

Systematic reviews and retrospective studies have shown HBV-related HCC accounting for 12%-14% of HCC in South and Central America with the countries Peru and Brazil having 20%-60% of their HCC cases related to HBV infection[37-39].

Although Latin American countries are more varied in HBV prevalence and range from low to high prevalence, overall HCC risk and burden is similarly as low as the rest of the Americas in a global context[11,36].

### Gender

Chronic HBV has a greater prevalence in males than females across all geographic regions[13]. Males also have a greater incidence, prevalence, and mortality from HCC than females across geographic location and age; studies have reported a 2 to 3 times increased risk of developing HCC in males compared to females[26,27,40,41].

Regions of higher chronic HBV prevalence such as sub-Saharan Africa and Southeast Asia, tend to also have a higher male to female ratio of HCC incidence. In the United States, both sexes have shown a trend of rising incidence rates of HCC since 1975, with HBV estimated to account for 10%-15% of HCC cases[42]. The gender disparity is not completely understood but is believed to be partially due to many overlapping risk factors that are more common in males, including alcoholism, diabetes, viral hepatitis, and tobacco use[43]. In the United States, heavy alcohol usage and tobacco use is much more common in males with both being independent risk factors for incidence of HCC[43,44]. In contrast, metabolic syndrome is more common in women, with one retrospective study reporting it accountable for 32% of HCC burden in the United States[27,44].

Despite controlling for other risk factors, male sex continues to remain an independent risk factor for HCC. Studies have linked higher testosterone levels to greater incidence of HCC in chronic HBV patients and estrogen replacement therapy to reduced risk of developing HCC[42,45,46]. Serum testosterone level has been associated with upregulated inflammatory activity while estrogen has shown to have an anti-inflammatory effect by inhibition of the NF- $\kappa$ B pathway[46-48]. Estrogen may be protective against development of HBV-related HCC through decreasing HBV RNA transcription which could explain higher viral loads seen in male carriers of HBV[12,47]. However, studies have failed to demonstrate a benefit in survival from hormonal therapy such as flutamide, an anti-androgen, and leuprorelin, a gonadotropin-releasing hormone agonist which has anti-androgen effects[48].

### Age

The average age of chronic HBV patients has continued to increase over time. A study comparing

chronic HBV patients derived from an insurance claims database of Medicaid and Medicare patients found that the median age had risen from 44.1 to 50.2 years for Medicaid patients and 48.1 to 51.8 for Medicare patients[49]. This trend has also been seen in studies from other countries. A large territory-wide cohort study conducted in Hong Kong found the mean age for Chronic HBV had increased from 41 in 2000-2004 to 55 in 2014-2017[50]. Chronic HBV is now presenting at an older median age due to longer life expectancy, under diagnosis of HBV, under screening, and delayed treatment[21,51]. There is also improved vaccine-induced immunity in the 20-49 years age group which is predicted to cause a continual upward shift in the median age of diagnosis[49].

In populations at low risk for HBV infection, such as in Western Europe and the United States where HBV is not endemic, HCC is rarely seen before the fourth decade of life with a mean age of diagnosis around 65 years[12]. In contrast, endemic regions such as Southeast Asia and sub-Saharan Africa, where > 80% of HCC cases occur, have mean ages of diagnosis about one decade earlier[42]. China has a mean age of diagnosis of HCC around 55-59 years[12]. In countries in Sub-Saharan Africa, mean age of diagnosis of HCC is 35-50 years, and found to be almost 20 years later in those Black Africans who migrate from a rural to city setting[12,52].

With the advent of the HBV vaccine in 1981, and the universal vaccination programs that began in the 1990s, there was a new focus on vaccination of newborns. As of 2020, 190 WHO member countries vaccinated newborns as part of their routine vaccination schedules, and global coverage with all 3 doses of HBV vaccine was estimated to be 83%[53]. This campaign also included recommendations to vaccinate high-risk adult populations, adolescents who had missed immunization, and advocated for societal awareness of the risks and consequences of HBV[22]. Asian males who are HBV carriers continue to present with HCC at a relatively young age[54]. This may be related to viral factors such as genotype. Genotype B is more commonly seen in the Asian demographic and has been associated with onset of HCC in patients under 50 years of age, with one study from Taiwan finding that more than 90% under 35 years of age had genotype B HBV[47,55]. Genotype C is associated with the highest risk of developing HCC in patients aged > 50 years[56]. Genotype F has been seen in Alaskan Native populations to have the greatest risk of developing HCC at a lower median age, with the annual incidence rate amongst men at 387/100000 and 63/100000 for women[57]. In contrast, genotypes A, D are less frequently associated with development of HCC and more common in North American and European populations[58].

### **Socioeconomic status**

Patients belonging to low socio-economic status are at significant disadvantage due to low health literacy, limited healthcare resources and access-including lack of insurance or ability to pay for care, especially for care of preventable diseases such as HBV. Hepatitis B is very infectious as it can be transmitted by contact with blood or bodily fluids, sexual intercourse and vertically from mother to baby. Vertical transmission is the most common mode of transmission in the developing world and can be dramatically reduced by HBV vaccination and use of anti-viral medications during third trimester [7]. Horizontal transmission seems to be more common in low prevalence regions[13,22]. While Hepatitis B viral load is considered one of the strongest predictors of HCC risk and can be managed with anti-viral medications, unfortunately, even in low-risk regions such as United States, roughly 3% of people currently living with chronic HBV are on treatment[14,21]. Several studies have shown the impact of socioeconomic status (SES) on health outcomes in cancer with populations of lower SES and less wealthy nations having significantly lower survival rates[32,59-61]. One retrospective analysis of European nations found nearly 20% variation in all-cancer relative survival between the least wealthy and most wealthy nations[61]. Similarly, low SES groups are associated with a variety of risk factors for poor outcomes in chronic HBV-related HCC. Despite 5-year survival rate for HCC in the United States increasing to 18% in 2019, the greatest benefits in survival and mortality are seen in groups with higher SES, while higher HCC incidence, later stage of diagnosis, and lower survival rates are seen in low-SES status groups[28,40]. Disadvantaged groups are typically minority ethnic groups such as African Americans and Hispanics as they tend to live in areas with the highest rates of family poverty, unemployment and high-school dropouts and thus may be associated with greater risk for HCC due to less access to screening and treatment[62].

Among patients with Medicaid insurance, the presence of comorbidities such as obesity, diabetes, alcohol, and tobacco use disorders combined with lower educational attainment contribute to liver disease such as alcoholic and NASH (ASH/NASH) and significantly overlap with liver disease from chronic HBV[63,64].

---

## **METHODS TO ADDRESS DISPARITIES**

---

### **Targeted screening and prevention**

Globally, chronic HBV and HCC cases are underdiagnosed. The 2016 Polaris Observatory study estimated that only 10% of infected people were diagnosed with HBV[51]. Chronic HBV infection is often asymptomatic and requires greater emphasis on screening, especially considering that HBV can

lead to HCC in patients without cirrhosis[13,42,65]. There is a geographic disparity in screening: About 2% of people with HBV knew their status in 2019 in Africa *vs* 22% in the Americas and 19% in the European region[21]. Additionally, there is likely underestimation of the true number of chronic HBV in the United States and other regions because high-risk populations have historically been under-represented in national surveys and surveillance studies, especially considering the large influx of yearly immigration to the US[24].

Early detection of tumors from screening in chronic HBV improves overall survival. A Randomized Controlled Trial study in Shanghai found that biannual screening in chronic HBV patients reduced HCC mortality by 37%[66]. An estimated 70% of liver cancer cases are preventable with risk factor modification and screening, thus judicious screening of high-risk populations with use of evidence-based guidelines can significantly reduce mortality from chronic HBV-related HCC[40]. The the American Association for the Study of Liver Diseases (AASLD) recommends HCC surveillance with ultrasound with or without AFP for all patients with diagnosed cirrhosis, and chronic HBV carriers who are high risk including African Americans older than 20 years, Asians older than 40 years, and those with family history of HCC. However, less than 1 in 5 high-risk patients are regularly screened[67]. Although greater than 90% of patients with acute HBV experience resolution of disease and the small minority develop chronic HBV infection, 40% of chronic HBV patients go on to develop cirrhosis, liver failure and HCC, and up to 25% of patients with chronic HBV end up dying from cirrhosis or HCC; thus HCC screening has been found cost-effective in patients with HBV even without cirrhosis when incidence of HCC is greater than 0.2% per year[67,68].

### Health literacy

Lack of health literacy is particularly apparent in vulnerable and underserved populations such as immigrant populations, Mexican Americans, and African Americans, who already disproportionately bear the burden of chronic HBV and HCC[69,70]. Increasing social awareness of risk factors and protective factors of chronic HBV can be an avenue to improve health literacy. Social media is used by much of the developed world. For example, World Hepatitis Day is an annual health education campaign led by the WHO in July that heavily utilizes social media to make a call to action to bolster efforts in prevention, screening, treatment and to spread awareness of viral hepatitis[71]. Culturally sensitive approaches are necessary with an increasingly diverse population of the United States, to effectively communicate with various ethnic groups. One such example is “photo novels” developed to cater to specific cultures which have been shown to be effective in increasing HBV awareness and screening in underserved populations[72].

In many developing countries, such as those in Sub-Saharan Africa and the Asia-Pacific region where the majority of global chronic HBV and HCC cases occur, there is limited knowledge of hepatitis B and the benefits of the HBV vaccine[1,11,12,73]. Only two percent of the patients in African and Southeast Asian regions were aware of their chronic HBV status in 2019[1]. There is a dire need for informational campaigns in these endemic regions to increase awareness and health education amongst vulnerable populations in addition to the national immunization programs that must be initiated at the federal level with support from international health organizations.

---

## CONCLUSION

Chronic HBV infection continues to have significant impact globally despite escalating vaccine coverage, screening techniques and availability of anti-viral medications. The close geographic relationship between endemic chronic HBV and increased burden of HCC remains to this day in Africa and the Asia-Pacific regions comprising the vast majority of HBV-related HCC in the world. HBV and HCC disproportionately affect certain ethnic groups within the United States and worldwide, many of which are of low SES. Men and the elderly are disproportionately affected at greater rates. To mitigate this largely preventable disease, enhanced access to screening, vaccinations, surveillance, and treatment must be achieved to reduce the burden of chronic HBV and HCC worldwide.

---

## FOOTNOTES

**Author contributions:** Gnyawali B and Mumtaz K contributed to the conception of the review; Gnyawali B and Pusateri A performed a review of the current literature; Gnyawali B drafted the manuscript; Pusateri A, Nickerson A, Mumtaz K, and Jalil S added key information and revised the manuscript; all authors read and approved the final manuscript.

**Conflict-of-interest statement:** There are no conflicts of interest to report.

**Open-Access:** This article is an open-access article that was selected by an in-house editor and fully peer-reviewed by external reviewers. It is distributed in accordance with the Creative Commons Attribution NonCommercial (CC BY-

NC 4.0) license, which permits others to distribute, remix, adapt, build upon this work non-commercially, and license their derivative works on different terms, provided the original work is properly cited and the use is non-commercial. See: <https://creativecommons.org/licenses/by-nc/4.0/>

**Country/Territory of origin:** United States

**ORCID number:** Bipul Gnyawali 0000-0003-4745-2787; Antoinette Pusateri 0000-0002-8458-7827; Ashley Nickerson 0000-0002-4494-9985; Sajid Jilil 0000-0001-6123-153X; Khalid Mumtaz 0000-0001-7868-6514.

**S-Editor:** Chen YL

**L-Editor:** A

**P-Editor:** Chen YL

## REFERENCES

- World Health Organization.** Global progress report on HIV, viral hepatitis and sexually transmitted infections, 2021: accountability for the global health sector strategies 2016–2021: actions for impact: web annex 2: data methods. July 15, 2021. [Cited 2 January 2022]. Available from: <https://www.who.int/publications/i/item/9789240027077> [DOI: 10.1093/med/9780198816805.003.0070]
- Beasley RP.** Rocks along the road to the control of HBV and HCC. *Ann Epidemiol* 2009; **19**: 231-234 [PMID: 19344859 DOI: 10.1016/j.annepidem.2009.01.017]
- Schweitzer A, Horn J, Mikolajczyk RT, Krause G, Ott JJ.** Estimations of worldwide prevalence of chronic hepatitis B virus infection: a systematic review of data published between 1965 and 2013. *Lancet* 2015; **386**: 1546-1555 [PMID: 26231459 DOI: 10.1016/S0140-6736(15)61412-X]
- Chang MH, Chen CJ, Lai MS, Hsu HM, Wu TC, Kong MS, Liang DC, Shau WY, Chen DS.** Universal hepatitis B vaccination in Taiwan and the incidence of hepatocellular carcinoma in children. Taiwan Childhood Hepatoma Study Group. *N Engl J Med* 1997; **336**: 1855-1859 [PMID: 9197213 DOI: 10.1056/nejm199706263362602]
- McMahon BJ, Bulkow LR, Singleton RJ, Williams J, Snowball M, Homan C, Parkinson AJ.** Elimination of hepatocellular carcinoma and acute hepatitis B in children 25 years after a hepatitis B newborn and catch-up immunization program. *Hepatology* 2011; **54**: 801-807 [PMID: 21618565 DOI: 10.1002/hep.24442]
- Ni YH, Chen DS.** Hepatitis B vaccination in children: the Taiwan experience. *Pathol Biol (Paris)* 2010; **58**: 296-300 [PMID: 20116181 DOI: 10.1016/j.patbio.2009.11.002]
- Petrick JL, McGlynn KA.** The changing epidemiology of primary liver cancer. *Curr Epidemiol Rep* 2019; **6**: 104-111 [PMID: 31259140 DOI: 10.1007/s40471-019-00188-3]
- Kuang XJ, Jia RR, Huo RR, Yu JJ, Wang JJ, Xiang BD, Li LQ, Peng Z, Zhong JH.** Systematic review of risk factors of hepatocellular carcinoma after hepatitis B surface antigen seroclearance. *J Viral Hepat* 2018; **25**: 1026-1037 [PMID: 29624821 DOI: 10.1111/jvh.12905]
- Petrick JL, Florio AA, Znaor A, Ruggieri D, Laversanne M, Alvarez CS, Ferlay J, Valery PC, Bray F, McGlynn KA.** International trends in hepatocellular carcinoma incidence, 1978-2012. *Int J Cancer* 2020; **147**: 317-330 [PMID: 31597196 DOI: 10.1002/ijc.32723]
- Vallet-Pichard A, Pol S.** Review article: immunisation against hepatitis B virus infection and the prevention of hepatocellular carcinoma. *Aliment Pharmacol Ther* 2021; **53**: 1166-1182 [PMID: 33909923 DOI: 10.1111/apt.16356]
- Bray F, Ferlay J, Soerjomataram I, Siegel RL, Torre LA, Jemal A.** Global cancer statistics 2018: GLOBOCAN estimates of incidence and mortality worldwide for 36 cancers in 185 countries. *CA Cancer J Clin* 2018; **68**: 394-424 [PMID: 30207593 DOI: 10.3322/caac.21492]
- El-Serag HB.** Epidemiology of viral hepatitis and hepatocellular carcinoma. *Gastroenterology* 2012; **142**: 1264-1273.e1 [PMID: 22537432 DOI: 10.1053/j.gastro.2011.12.061]
- Petruzzello A.** Epidemiology of Hepatitis B Virus (HBV) and Hepatitis C Virus (HCV) Related Hepatocellular Carcinoma. *Open Virol J* 2018; **12**: 26-32 [PMID: 29541276 DOI: 10.2174/1874357901812010026]
- Ringelhan M, McKeating JA, Protzer U.** Viral hepatitis and liver cancer. *Philos Trans R Soc Lond B Biol Sci* 2017; **372** [PMID: 28893941 DOI: 10.1098/rstb.2016.0274]
- Lemoine M, Thursz MR.** Battlefield against hepatitis B infection and HCC in Africa. *J Hepatol* 2017; **66**: 645-654 [PMID: 27771453 DOI: 10.1016/j.jhep.2016.10.013]
- Altekruse SF, McGlynn KA, Reichman ME.** Hepatocellular carcinoma incidence, mortality, and survival trends in the United States from 1975 to 2005. *J Clin Oncol* 2009; **27**: 1485-1491 [PMID: 19224838 DOI: 10.1200/JCO.2008.20.7753]
- Upala P, Apidechkul T, Tamornpark R, Chomchoei C, Yeemard F.** Seroprevalence and factors associated with hepatitis B infection among the hill tribe adult population in Thailand: a cross-sectional study. *BMC Infect Dis* 2020; **20**: 494 [PMID: 32650741 DOI: 10.1186/s12879-020-05221-1]
- Naveira MCM, Badal K, Dhakal J, Mayer NA, Pokharel B, Del Prado RF.** Seroprevalence of hepatitis B and C in Nepal: a systematic review (1973-2017). *Hepatol Med Policy* 2018; **3**: 10 [PMID: 30288333 DOI: 10.1186/s41124-018-0039-2]
- Wang H, Men P, Xiao Y, Gao P, Lv M, Yuan Q, Chen W, Bai S, Wu J.** Hepatitis B infection in the general population of China: a systematic review and meta-analysis. *BMC Infect Dis* 2019; **19**: 811 [PMID: 31533643 DOI: 10.1186/s12879-019-4428-y]
- Leroi C, Adam P, Khamduang W, Kawilapat S, Ngo-Giang-Huong N, Ongwandee S, Jiamsiri S, Jourdain G.** Prevalence of chronic hepatitis B virus infection in Thailand: a systematic review and meta-analysis. *Int J Infect Dis* 2016; **51**: 36-43

- [PMID: 27580678 DOI: 10.1016/j.ijid.2016.08.017]
- 21 **World Health Organization.** Global progress report on HIV, viral hepatitis and sexually transmitted infections. July 15, 2021. [Cited 2 January 2022]. Available from: <http://apps.who.int/iris/bitstream/handle/10665/342808/9789240030985-eng.pdf>
  - 22 **Nelson NP,** Easterbrook PJ, McMahon BJ. Epidemiology of Hepatitis B Virus Infection and Impact of Vaccination on Disease. *Clin Liver Dis* 2016; **20**: 607-628 [PMID: 27742003 DOI: 10.1016/j.cld.2016.06.006]
  - 23 **Chang ET,** Keegan TH, Gomez SL, Le GM, Clarke CA, So SK, Glaser SL. The burden of liver cancer in Asians and Pacific Islanders in the Greater San Francisco Bay Area, 1990 through 2004. *Cancer* 2007; **109**: 2100-2108 [PMID: 17385214 DOI: 10.1002/cncr.22642]
  - 24 **Cohen C,** Evans AA, London WT, Block J, Conti M, Block T. Underestimation of chronic hepatitis B virus infection in the United States of America. *J Viral Hepat* 2008; **15**: 12-13 [PMID: 18088239 DOI: 10.1111/j.1365-2893.2007.00888.x]
  - 25 **Kim HS,** Rotundo L, Yang JD, Kim D, Kothari N, Feurdean M, Ruhl C, Unalp-Arida A. Racial/ethnic disparities in the prevalence and awareness of Hepatitis B virus infection and immunity in the United States. *J Viral Hepat* 2017; **24**: 1052-1066 [PMID: 28581638 DOI: 10.1111/jvh.12735]
  - 26 **Petrick JL,** Kelly SP, Altekruse SF, McGlynn KA, Rosenberg PS. Future of Hepatocellular Carcinoma Incidence in the United States Forecast Through 2030. *J Clin Oncol* 2016; **34**: 1787-1794 [PMID: 27044939 DOI: 10.1200/JCO.2015.64.7412]
  - 27 **Ajayi F,** Jan J, Singal AG, Rich NE. Racial and Sex Disparities in Hepatocellular Carcinoma in the USA. *Curr Hepatol Rep* 2020; **19**: 462-469 [PMID: 33828937 DOI: 10.1007/s11901-020-00554-6]
  - 28 **Flores YN,** Datta GD, Yang L, Corona E, Devineni D, Glenn BA, Bastani R, May FP. Disparities in Hepatocellular Carcinoma Incidence, Stage, and Survival: A Large Population-Based Study. *Cancer Epidemiol Biomarkers Prev* 2021; **30**: 1193-1199 [PMID: 33737301 DOI: 10.1158/1055-9965.EPI-20-1088]
  - 29 **Li J,** Hansen BE, Peppelenbosch MP, De Man RA, Pan Q, Sprengers D. Factors associated with ethnical disparity in overall survival for patients with hepatocellular carcinoma. *Oncotarget* 2017; **8**: 15193-15204 [PMID: 28122352 DOI: 10.18632/oncotarget.14771]
  - 30 **Ren F,** Zhang J, Gao Z, Zhu H, Chen X, Liu W, Xue Z, Gao W, Wu R, Lv Y, Hu L. Racial disparities in the survival time of patients with hepatocellular carcinoma and intrahepatic cholangiocarcinoma between Chinese patients and patients of other racial groups: A population-based study from 2004 to 2013. *Oncol Lett* 2018; **16**: 7102-7116 [PMID: 30546445 DOI: 10.3892/ol.2018.9550]
  - 31 **Njei B,** Ditah I, Lim JK. Persistent racial disparities in survival among u.s. Adults with hepatocellular carcinoma after liver transplantation: the paradox of all-cause and cause-specific mortality. *Gastrointest Cancer Res* 2013; **6**: 73-74 [PMID: 23936546]
  - 32 **Koc ÖM,** Robaey G, Yildirim B, Posthouwer D, Hens N, Koek GH. The influence of ethnicity on disease outcome in patients with chronic hepatitis B infection. *J Med Virol* 2019; **91**: 623-629 [PMID: 30381836 DOI: 10.1002/jmv.25353]
  - 33 **Burton A,** Balachandrakumar VK, Driver RJ, Tataru D, Paley L, Marshall A, Alexander G, Rowe IA; HCC-UK/BASL/NCRAS Partnership, Palmer DH, Cross TJS. Regional variations in hepatocellular carcinoma incidence, routes to diagnosis, treatment and survival in England. *Br J Cancer* 2022; **126**: 804-814 [PMID: 34837073 DOI: 10.1038/s41416-021-01509-4]
  - 34 **Chu JJ,** Wörmann T, Popp J, Pätzelt G, Akmatov MK, Krämer A, Reintjes R. Changing epidemiology of hepatitis B and migration--a comparison of six Northern and North-Western European countries. *Eur J Public Health* 2013; **23**: 642-647 [PMID: 23132874 DOI: 10.1093/eurpub/cks067]
  - 35 **Roman S,** Jose-Abrego A, Fierro NA, Escobedo-Melendez G, Ojeda-Granados C, Martinez-Lopez E, Panduro A. Hepatitis B virus infection in Latin America: a genomic medicine approach. *World J Gastroenterol* 2014; **20**: 7181-7196 [PMID: 24966588 DOI: 10.3748/wjg.v20.i23.7181]
  - 36 **Organization PAH.** Hepatitis B and C in the Spotlight: A public health response in the Americas. 2016. [Cited 2 January 2022]. Available from: <https://iris.paho.org/bitstream/handle/10665.2/31449/9789275119297-eng.pdf?sequence=5&isAllowed=y>
  - 37 **de Martel C,** Maucort-Boulch D, Plummer M, Franceschi S. World-wide relative contribution of hepatitis B and C viruses in hepatocellular carcinoma. *Hepatology* 2015; **62**: 1190-1200 [PMID: 26146815 DOI: 10.1002/hep.27969]
  - 38 **Debes JD,** Chan AJ, Balderramo D, Kikuchi L, Gonzalez Ballerga E, Prieto JE, Tapias M, Idrovo V, Davalos MB, Cairo F, Barreyro FJ, Paredes S, Hernandez N, Avendaño K, Diaz Ferrer J, Yang JD, Carrera E, Garcia JA, Mattos AZ, Hirsch BS, Gonçalves PT, Carrilho FJ, Roberts LR. Hepatocellular carcinoma in South America: Evaluation of risk factors, demographics and therapy. *Liver Int* 2018; **38**: 136-143 [PMID: 28640517 DOI: 10.1111/liv.13502]
  - 39 **Chan AJ,** Balderramo D, Kikuchi L, Ballerga EG, Prieto JE, Tapias M, Idrovo V, Davalos MB, Cairo F, Barreyro FJ, Paredes S, Hernandez N, Avendaño K, Ferrer JD, Yang JD, Carrera E, Mattos AZ, Hirsch BS, Gonçalves PT, Carrilho FJ, Roberts LR, Debes JD. Early Age Hepatocellular Carcinoma Associated With Hepatitis B Infection in South America. *Clin Gastroenterol Hepatol* 2017; **15**: 1631-1632 [PMID: 28532694 DOI: 10.1016/j.cgh.2017.05.015]
  - 40 **American Cancer Society.** Cancer Facts and Figures 2019. 2019. [cited 14 Jan 2022]. Available from: <https://www.cancer.org/> [DOI: 10.1080/15398285.2012.701177]
  - 41 **Cook MB,** Dawsey SM, Freedman ND, Inskip PD, Wichner SM, Quraishi SM, Devesa SS, McGlynn KA. Sex disparities in cancer incidence by period and age. *Cancer Epidemiol Biomarkers Prev* 2009; **18**: 1174-1182 [PMID: 19293308 DOI: 10.1158/1055-9965.EPI-08-1118]
  - 42 **Mittal S,** El-Serag HB. Epidemiology of hepatocellular carcinoma: consider the population. *J Clin Gastroenterol* 2013; **47** Suppl: S2-S6 [PMID: 23632345 DOI: 10.1097/MCG.0b013e3182872f29]
  - 43 **Wu EM,** Wong LL, Hernandez BY, Ji JF, Jia W, Kwee SA, Kalathil S. Gender differences in hepatocellular cancer: disparities in nonalcoholic fatty liver disease/steatohepatitis and liver transplantation. *Hepatoma Res* 2018; **4** [PMID: 30687780 DOI: 10.20517/2394-5079.2018.87]
  - 44 **Welzel TM,** Graubard BI, Quraishi S, Zeuzem S, Davila JA, El-Serag HB, McGlynn KA. Population-attributable fractions of risk factors for hepatocellular carcinoma in the United States. *Am J Gastroenterol* 2013; **108**: 1314-1321 [PMID:

- 23752878 DOI: 10.1038/ajg.2013.160]
- 45 **Yip TC**, Wong GL, Chan HL, Tse YK, Liang LY, Hui VW, Lee HW, Lui GC, Kong AP, Wong VW. Elevated testosterone increases risk of hepatocellular carcinoma in men with chronic hepatitis B and diabetes mellitus. *J Gastroenterol Hepatol* 2020; **35**: 2210-2219 [PMID: 32343449 DOI: 10.1111/jgh.15079]
  - 46 **Hassan MM**, Botrus G, Abdel-Wahab R, Wolff RA, Li D, Twardy D, Phan AT, Hawk E, Javle M, Lee JS, Torres HA, Rashid A, Lenzi R, Hassabo HM, Abaza Y, Shalaby AS, Lacin S, Morris J, Patt YZ, Amos CI, Khaderi SA, Goss JA, Jalal PK, Kaseb AO. Estrogen Replacement Reduces Risk and Increases Survival Times of Women With Hepatocellular Carcinoma. *Clin Gastroenterol Hepatol* 2017; **15**: 1791-1799 [PMID: 28579181 DOI: 10.1016/j.cgh.2017.05.036]
  - 47 **Liu CJ**, Kao JH. Hepatitis B virus-related hepatocellular carcinoma: epidemiology and pathogenic role of viral factors. *J Chin Med Assoc* 2007; **70**: 141-145 [PMID: 17475593 DOI: 10.1016/S1726-4901(09)70346-6]
  - 48 **Zhang H**, Spencer K, Burley SK, Zheng XFS. Toward improving androgen receptor-targeted therapies in male-dominant hepatocellular carcinoma. *Drug Discov Today* 2021; **26**: 1539-1546 [PMID: 33561464 DOI: 10.1016/j.drudis.2021.02.001]
  - 49 **Nguyen MH**, Lim JK, Burak Ozbay A, Frayssé J, Liou I, Meyer N, Dusheiko G, Gordon SC. Advancing Age and Comorbidity in a US Insured Population-Based Cohort of Patients With Chronic Hepatitis B. *Hepatology* 2019; **69**: 959-973 [PMID: 30175482 DOI: 10.1002/hep.30246]
  - 50 **Lai JC**, Wong VW, Yip TC, Hui VW, Tse YK, Lee HW, Liang LY, Lui GC, Chan HL, Wong GL. Secular trend of treatment uptake in patients with chronic hepatitis B: A territory-wide study of 135 395 patients from 2000 to 2017. *J Gastroenterol Hepatol* 2021; **36**: 3487-3499 [PMID: 34404113 DOI: 10.1111/jgh.15664]
  - 51 **Lim JK**, Nguyen MH, Kim WR, Gish R, Perumalswami P, Jacobson IM. Prevalence of Chronic Hepatitis B Virus Infection in the United States. *Am J Gastroenterol* 2020; **115**: 1429-1438 [PMID: 32483003 DOI: 10.14309/ajg.0000000000000651]
  - 52 **Kew MC**. Epidemiology of hepatocellular carcinoma in sub-Saharan Africa. *Ann Hepatol* 2013; **12**: 173-182 [PMID: 23396727]
  - 53 **World Health Organization**. Immunization coverage. 15 July 2021. [cited 11 Jan 2022]. Available from: <https://www.who.int/publications> [DOI: 10.2471/blt.10.020910]
  - 54 **Goh MJ**, Kang W, Kim KM, Sinn DH, Gwak GY, Paik YH, Choi MS, Lee JH, Koh KC, Paik SW. Incidence and risk factors for development of hepatocellular carcinoma at young age in patients with chronic hepatitis B. *Scand J Gastroenterol* 2022; **57**: 70-77 [PMID: 34731072 DOI: 10.1080/00365521.2021.1988700]
  - 55 **Gomaa AI**, Khan SA, Toledano MB, Waked I, Taylor-Robinson SD. Hepatocellular carcinoma: epidemiology, risk factors and pathogenesis. *World J Gastroenterol* 2008; **14**: 4300-4308 [PMID: 18666317 DOI: 10.3748/wjg.14.4300]
  - 56 **Zhu RX**, Seto WK, Lai CL, Yuen MF. Epidemiology of Hepatocellular Carcinoma in the Asia-Pacific Region. *Gut Liver* 2016; **10**: 332-339 [PMID: 27114433 DOI: 10.5009/gnl15257]
  - 57 **Livingston SE**, Simonetti JP, McMahon BJ, Bulkow LR, Hurlburt KJ, Homan CE, Snowball MM, Cagle HH, Williams JL, Chulanov VP. Hepatitis B virus genotypes in Alaska Native people with hepatocellular carcinoma: preponderance of genotype F. *J Infect Dis* 2007; **195**: 5-11 [PMID: 17152003 DOI: 10.1086/509894]
  - 58 **Wong GL**, Chan HL, Yiu KK, Lai JW, Chan VK, Cheung KK, Wong EW, Wong VW. Meta-analysis: The association of hepatitis B virus genotypes and hepatocellular carcinoma. *Aliment Pharmacol Ther* 2013; **37**: 517-526 [PMID: 23305043 DOI: 10.1111/apt.12207]
  - 59 **Ohikere K**, Chitnis AS, Hahambis TA, Singal A, Wong RJ. Ethnic Minorities and Low Socioeconomic Status Patients With Chronic Liver Disease Are at Greatest Risk of Being Uninsured. *Gastroenterology Res* 2021; **14**: 313-323 [PMID: 35059065 DOI: 10.14740/gr1439]
  - 60 **Quaglia A**, Lillini R, Mamo C, Ivaldi E, Vercelli M; SEIH (Socio-Economic Indicators, Health) Working Group. Socio-economic inequalities: a review of methodological issues and the relationships with cancer survival. *Crit Rev Oncol Hematol* 2013; **85**: 266-277 [PMID: 22999326 DOI: 10.1016/j.critrevonc.2012.08.007]
  - 61 **Verdecchia A**, Baili P, Quaglia A, Kunkler I, Ciampichini R, Berrino F, Micheli A. Patient survival for all cancers combined as indicator of cancer control in Europe. *Eur J Public Health* 2008; **18**: 527-532 [PMID: 18417498 DOI: 10.1093/eurpub/ckn022]
  - 62 **Shebl FM**, Capo-Ramos DE, Graubard BI, McGlynn KA, Altekruse SF. Socioeconomic status and hepatocellular carcinoma in the United States. *Cancer Epidemiol Biomarkers Prev* 2012; **21**: 1330-1335 [PMID: 22669949 DOI: 10.1158/1055-9965.EPI-12-0124]
  - 63 **Yuan JM**, Govindarajan S, Arakawa K, Yu MC. Synergism of alcohol, diabetes, and viral hepatitis on the risk of hepatocellular carcinoma in blacks and whites in the U.S. *Cancer* 2004; **101**: 1009-1017 [PMID: 15329910 DOI: 10.1002/encr.20427]
  - 64 **Flores YN**, Yee HF Jr, Leng M, Escarce JJ, Bastani R, Salmerón J, Morales LS. Risk factors for chronic liver disease in Blacks, Mexican Americans, and Whites in the United States: results from NHANES IV, 1999-2004. *Am J Gastroenterol* 2008; **103**: 2231-2238 [PMID: 18671818 DOI: 10.1111/j.1572-0241.2008.02022.x]
  - 65 **Stewart SL**, Kwong SL, Bowlus CL, Nguyen TT, Maxwell AE, Bastani R, Chak EW, Chen MS Jr. Racial/ethnic disparities in hepatocellular carcinoma treatment and survival in California, 1988-2012. *World J Gastroenterol* 2016; **22**: 8584-8595 [PMID: 27784971 DOI: 10.3748/wjg.v22.i38.8584]
  - 66 **Zhang BH**, Yang BH, Tang ZY. Randomized controlled trial of screening for hepatocellular carcinoma. *J Cancer Res Clin Oncol* 2004; **130**: 417-422 [PMID: 15042359 DOI: 10.1007/s00432-004-0552-0]
  - 67 **Frenette CT**, Isaacson AJ, Bargellini I, Saab S, Singal AG. A Practical Guideline for Hepatocellular Carcinoma Screening in Patients at Risk. *Mayo Clin Proc Innov Qual Outcomes* 2019; **3**: 302-310 [PMID: 31485568 DOI: 10.1016/j.mayocpiqo.2019.04.005]
  - 68 **Chang MS**, Nguyen MH. Epidemiology of hepatitis B and the role of vaccination. *Best Pract Res Clin Gastroenterol* 2017; **31**: 239-247 [PMID: 28774405 DOI: 10.1016/j.bpg.2017.05.008]
  - 69 **Samant H**, Amiri HS, Zibari GB. Addressing the worldwide hepatocellular carcinoma: epidemiology, prevention and management. *J Gastrointest Oncol* 2021; **12**: S361-S373 [PMID: 34422400 DOI: 10.21037/jgo.2020.02.08]
  - 70 **Hyun S**, Ko O, Kim S, Ventura WR. Sociocultural barriers to hepatitis B health literacy in an immigrant population: a focus group study in Korean Americans. *BMC Public Health* 2021; **21**: 404 [PMID: 33632203 DOI: 10.1186/s12874-021-01400-0]

[10.1186/s12889-021-10441-4](https://doi.org/10.1186/s12889-021-10441-4)]

- 71 World Hepatitis Day - July 28, 2018. *MMWR Morb Mortal Wkly Rep* 2018; **67**: 773 [PMID: [30024865](https://pubmed.ncbi.nlm.nih.gov/30024865/) DOI: [10.15585/mmwr.mm6728a1](https://doi.org/10.15585/mmwr.mm6728a1)]
- 72 **Lee S**, Yoon H, Chen L, Juon HS. Culturally appropriate photonovel development and process evaluation for hepatitis B prevention in Chinese, Korean, and Vietnamese American communities. *Health Educ Behav* 2013; **40**: 694-703 [PMID: [23372031](https://pubmed.ncbi.nlm.nih.gov/23372031/) DOI: [10.1177/1090198112474003](https://doi.org/10.1177/1090198112474003)]
- 73 **Machmud PB**, Glasauer S, Gottschick C, Mikolajczyk R. Knowledge, Vaccination Status, and Reasons for Avoiding Vaccinations against Hepatitis B in Developing Countries: A Systematic Review. *Vaccines (Basel)* 2021; **9** [PMID: [34207829](https://pubmed.ncbi.nlm.nih.gov/34207829/) DOI: [10.3390/vaccines9060625](https://doi.org/10.3390/vaccines9060625)]

## Endoscopic salvage therapy after failed biliary cannulation using advanced techniques: A concise review

Yung-Kuan Tsou, Kuang-Tse Pan, Mu Hsien Lee, Cheng-Hui Lin

**Specialty type:** Gastroenterology and hepatology

**Provenance and peer review:** Invited article; Externally peer reviewed.

**Peer-review model:** Single blind

**Peer-review report's scientific quality classification**

Grade A (Excellent): 0  
Grade B (Very good): B  
Grade C (Good): C  
Grade D (Fair): 0  
Grade E (Poor): 0

**P-Reviewer:** Hou XH, China; Martino A, Italy

**Received:** February 13, 2022

**Peer-review started:** February 13, 2022

**First decision:** April 5, 2022

**Revised:** April 15, 2022

**Accepted:** July 5, 2022

**Article in press:** July 5, 2022

**Published online:** August 7, 2022



**Yung-Kuan Tsou, Mu Hsien Lee, Cheng-Hui Lin**, Department of Gastroenterology and Hepatology, Chang Gung Memorial Hospital, Taoyuan 333, Taiwan

**Yung-Kuan Tsou, Kuang-Tse Pan, Mu Hsien Lee, Cheng-Hui Lin**, Department of Medicine, Chang Gung University, Taoyuan 333, Taiwan

**Kuang-Tse Pan**, Department of Medical Imaging and Intervention, Chang Gung Memorial Hospital, Taoyuan 333, Taiwan

**Corresponding author:** Cheng-Hui Lin, MD, Doctor, Department of Gastroenterology and Hepatology, Chang Gung Memorial Hospital, No. 5 Fu-Shin Street, Kweishan, Taoyuan 333, Taiwan. [linchehui@adm.cgmh.org.tw](mailto:linchehui@adm.cgmh.org.tw)

### Abstract

Therapeutic endoscopic retrograde cholangiopancreatography (ERCP) begins with successful biliary cannulation. However, it is not always successful. The failure of the initial ERCP is attributed to two main aspects: the papilla/biliary orifice is endoscopically accessible, or it is inaccessible. When the papilla/biliary orifice is accessible, bile duct cannulation failure can occur even with advanced cannulation techniques, including double guidewire techniques, transpancreatic sphincterotomy, needle-knife precut papillotomy, or fistulotomy. There is currently no consensus on the next steps of treatment in this setting. Therefore, this review aims to propose and discuss potential endoscopic options for patients who have failed ERCP due to difficult bile duct cannulation. These options include interval ERCP, percutaneous-transhepatic-endoscopic rendezvous procedures (PTE-RV), and endoscopic ultrasound-assisted rendezvous procedures (EUS-RV). The overall success rate for interval ERCP was 76.3% (68%-79% between studies), and the overall adverse event rate was 7.5% (0-15.9% between studies). The overall success rate for PTE-RV was 88.7% (80.4%-100% between studies), and the overall adverse event rate was 13.2% (4.9%-19.2% between studies). For EUS-RV, the overall success rate was 82%-86.1%, and the overall adverse event rate was 13%-15.6%. Because interval ERCP has an acceptably high success rate and lower adverse event rate and does not require additional expertise, facilities, or other specialists, it can be considered the first choice for salvage therapy. EUS-RV can also be considered if local experts are available. For patients in urgent need of biliary drainage, PTE-RV should be considered.

**Key Words:** Difficult biliary cannulation; Endoscopic ultrasound; Rendezvous; Endoscopic retrograde cholangiopancreatography; Percutaneous transhepatic biliary drainage; Interval

©The Author(s) 2022. Published by Baishideng Publishing Group Inc. All rights reserved.

**Core Tip:** Three endoscopic salvage therapies are available for endoscopic retrograde cholangiopancreatography (ERCP) cannulation failure, but consensus is lacking. This review found that interval ERCP had an overall success rate of 76.3% and an adverse event rate of 7.5%. Percutaneous-transhepatic-endoscopic rendezvous procedure (PTE-RV) had an overall success rate of 88.7% and an adverse event rate of 13.2%. Endoscopic ultrasound-assisted rendezvous procedures (EUS-RV) had an overall success rate of 82%-86.1% and an adverse event rate of 13%-15.6%. Interval ERCP may be preferred, but EUS-RV may also be considered if a local expert is available. PTE-RV is reserved for patients requiring urgent biliary drainage.

**Citation:** Tsou YK, Pan KT, Lee MH, Lin CH. Endoscopic salvage therapy after failed biliary cannulation using advanced techniques: A concise review. *World J Gastroenterol* 2022; 28(29): 3803-3813

**URL:** <https://www.wjgnet.com/1007-9327/full/v28/i29/3803.htm>

**DOI:** <https://dx.doi.org/10.3748/wjg.v28.i29.3803>

## INTRODUCTION

Endoscopic retrograde cholangiopancreatography (ERCP) has become the treatment of choice for biliary tract diseases in recent decades. Selective biliary cannulation (SBC) is a critical step in the success of therapeutic ERCP; however, it is not always successful, even for experienced endoscopists[1]. The failure to achieve SBC during the initial ERCP can be attributed to two main aspects: an endoscopically inaccessible papilla/biliary orifice; and an endoscopically accessible papilla/biliary orifice but failed SBC with available cannulation methods. Management of initial ERCP failure constitutes a major clinical challenge for endoscopists. This review focuses on the endoscopic management of initial SBC failure in patients with an accessible papilla/biliary orifice.

When the major papilla is accessible, SBC typically begins with standard cannulation methods through a cannula or sphincterotome using either guidewire-assisted or contrast-guided techniques[2]. Using standard cannulation techniques, SBC fails in approximately 5% to 15% of cases[3]. This condition is often referred to as difficult biliary cannulation, although definitions have varied widely between endoscopists or studies[4,5]. In this case, depending on the experience or preference of the endoscopist, a variety of advanced techniques can be applied as a means of rescue. In general, when unintentional pancreatic guidewire insertion has been achieved, a double guidewire cannulation approach can be attempted[1]. Alternately or sequentially, transpancreatic sphincterotomy can be performed[6]. However, some endoscopists might prefer to perform needle-knife precut papillotomy (NKP) or needle-knife fistulotomy (NKF), especially after the placement of a pancreatic stent[2,7]. If the pancreatic duct is not cannulated, however, only NKP or NKF can be applied[4]. The application of these advanced technologies does not require additional facilities. Today, most qualified ERCP endoscopists can master at least some of these advanced cannulation techniques, so these procedures can often be performed by the same endoscopist during the same endoscopic session[8]. Despite these rescue techniques, failed biliary cannulation can occur[9]. Therefore, in this review, difficult biliary cannulation was defined as failure to achieve SBC using the advanced techniques described above[10,11]. In the setting of difficult bile duct cannulation, there is currently no consensus on the next steps in treatment[9]. Because endoscopic therapy has the advantage of a broader range of treatment options and no need for external drainage, this review aims to propose and discuss potential endoscopic options, alone or in combination with the percutaneous procedure, for patients who have failed initial ERCP due to difficult bile duct cannulation. These endoscopic options include interval ERCP, percutaneous-transhepatic-endoscopic rendezvous procedures (PTE-RV), and endoscopic ultrasound (EUS)-guided procedures. We also propose a potential treatment algorithm to provide practical advice.

## INTERVAL ERCP

In a literature search in early 2022, we were only able to find 7 studies (371 patients in total) reporting interval ERCP[9,12-17]. All of these studies were retrospective. There were no review/meta-analysis articles on this topic. However, when SBC cannot be achieved by advanced cannulation techniques,

**Table 1** Summary of studies on reporting interval endoscopic retrograde cholangiopancreatography

Ref.	Study design (patient number)	Percentage	Median time interval <sup>2</sup> (range)	Pre-cut during interval ERCP	Technical success rate	Factors associated with success	Overall complication rate
Kevans <i>et al</i> [12] (2010)	Retrospective (n = 19)	53% (19/36)	6 d (1-21 d)	0%	68% (13/19)	NA	0
Donnellan <i>et al</i> [13] (2012)	Retrospective (n = 51)	68% (51/75)	8 d (1-28 d)	NA	75% (38/51)	3 d <i>vs</i> 6 d (failure <i>vs</i> success)	3.9% (2/51)
Kim <i>et al</i> [14] (2012)	Retrospective (n = 69)	76% (69/91)	NA (1-3 d)	16% (11/69)	77% (53/69)	1 d <i>vs</i> 2-3 d (66% <i>vs</i> 88%)	15.9% (11/69)
Pavlidis <i>et al</i> [15] (2014)	Retrospective (n = 89)	82% (89/108)	4 d (IQR 3-6 d)	NA	78% (69/89)	NA	-
Colan-Hernandez <i>et al</i> [16] (2017)	Retrospective (n = 72)	64% (72/112)	7 d (IQR 5-11 d)	NA	75% (54/72)	≤ 4 d <i>vs</i> > 4 d (44% <i>vs</i> 79%)	4.2% (3/72)
Narayan <i>et al</i> [17] (2017)	Retrospective (n = 28)	76% (28/37)	3 d (3-4 d)	NA	79% (22/28)	NA	-
Lo <i>et al</i> [9] (2021)	Retrospective (n = 43)	38% (43/114)	4 d (1-20 d)	28% (12/43)	79% (34/43)	None	7.0% (3/43)
Overall	n = 371	-	-	-	76.3% (281/371)	-	7.5% (19/254)

<sup>1</sup>Number of study cases as a percentage of initial endoscopic retrograde cholangiopancreatography (ERCP) failures.

<sup>2</sup>Time interval between initial and interval ERCP.

ERCP: Endoscopic retrograde cholangiopancreatography; NA: Not available; IQR: Interquartile range.

such as NKP or NKF, these studies have shown that interval ERCP is a viable treatment option (Table 1) [9,12-17]. The overall success rate of interval ERCP was 76.3% (68%-79% between studies). The time interval between the initial ERCP and the interval ERCP varies greatly from study to study (median, 3-8 d) [9,12,13,15-17]. Three studies reported that 0%, 16%, and 28% of patients required a second precut procedure during the interval ERCP, respectively [9,12,14].

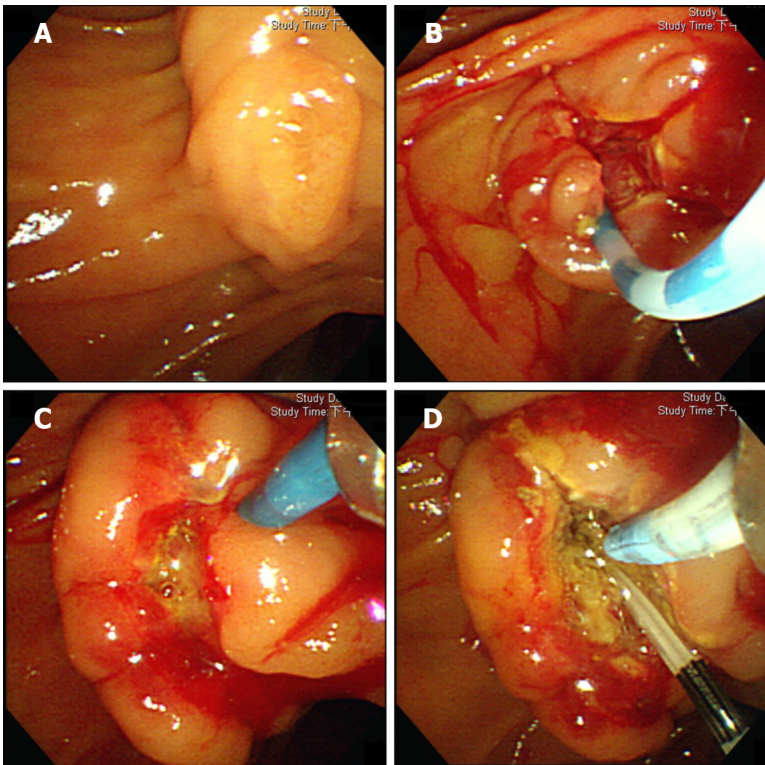
Interestingly, the timing to perform interval ERCP appeared to affect the success rate of interval ERCP [9,13,14,16]. The edema, tissue necrosis, and even bleeding of the major papilla caused by cannulation and/or NKP/F improved over time, resulting in an open and easily accessible papilla (Figures 1 and 2). Therefore, the success rate of interval ERCP could increase if it could be delayed for a couple of days. Donnellan *et al* [13] reported a significantly longer median time interval between initial and interval ERCP in the successful cannulation group compared to the failed cannulation group (6.0, 1-28 d *vs* 3.0, 1-8 d;  $P = 0.02$ ). Kim *et al* [14] studied only patients who received interval ERCP within 3 d [14]. They reported that the success rate of interval ERCP after one day was significantly lower than after 2-3 d (65.7% *vs* 88.2%,  $P = 0.027$ ). Except for the time interval, no other factor was significantly associated with the success of interval ERCP in their study. Colan-Hernandez *et al* [16] performed univariate and multivariate analyses of factors associated with interval ERCP cannulation failure. They found that the ERCP interval within 4 d after the initial precut was the only significant factor (cannulation success rate of 44.4% *vs* 79.4%,  $P = 0.024$  for univariate and 0.026 for multivariate analysis). However, in our study, we did not find any factors associated with interval ERCP failure in either the univariate or multivariate analysis [9].

Adverse events of interval ERCP were reported in five studies involving a total of 254 patients [9,12-14,16]. These adverse events included pancreatitis, bleeding, perforation, and cholangitis. The overall adverse event rate was 7.5% (0-15.9% between studies). Pancreatitis occurred in 1.6% (0-2.9%); all cases were mild. The bleeding rate was 2.8% (0-5.8%). Approximately half of the bleeding was mild, and the other half was moderate. The perforation rate was 1.2% (0-2.9%); all cases were mild. The cholangitis rate was 2.0% (0-4.7%). Two studies compared adverse event rates for initial and interval ERCP and found no significant difference [14,15].

In these studies, only 38%-82% of patients received interval ERCP when initial NKP/F failed to achieve SBC [9,12-17]. This result could reflect that some other salvage treatments, such as percutaneous or EUS-guided drainage, are still applicable in this situation [18].

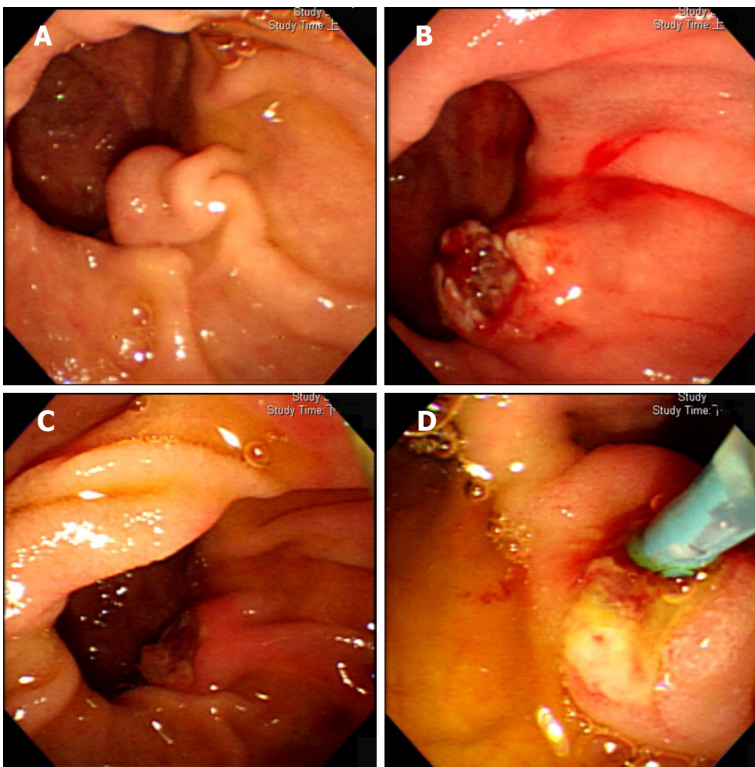
## PERCUTANEOUS-TRANSHEPATIC-ENDOSCOPIC RENDEZVOUS PROCEDURES

Percutaneous transhepatic biliary drainage (PTBD) remains possibly the most widely used salvage



DOI: 10.3748/wjg.v28.i29.3803 Copyright ©The Author(s) 2022.

**Figure 1** Interval endoscopic retrograde cholangiopancreatography, 1 d after the initial procedure. A: The original papilla in the initial endoscopic retrograde cholangiopancreatography (ERCP); B: Post-precut papilla, at the end of initial ERCP; C: post-precut papilla, at the beginning of interval ERCP. The papilla is swollen, edematous, and with mild oozing; D: Deep bile duct cannulation is unsuccessful during the interval ERCP, even after the placement of a pancreatic stent.



DOI: 10.3748/wjg.v28.i29.3803 Copyright ©The Author(s) 2022.

**Figure 2** Interval endoscopic retrograde cholangiopancreatography, 3 d after the initial procedure. A: The original papilla in the initial endoscopic retrograde cholangiopancreatography (ERCP); B: Post-precut papilla, at the end of initial ERCP; C: post-precut papilla, at the beginning of interval ERCP. Papillary edema due to pre-cut has disappeared; D: Deep bile duct cannulation is successful during the interval ERCP.

therapy in the setting of initial ERCP failure[19]. However, PTBD has some drawbacks, including a high rate of adverse events, decreased patient quality of life, and most importantly, providing of somewhat limited options for therapeutic maneuvers[3]. In addition, external drainage can cause discomfort and pain and often requires reintervention[20]. Therefore, an improved technique combining percutaneous and endoscopic approaches, known as percutaneous-transhepatic-endoscopic rendezvous procedures (PTE-RV), seems preferable to PTBD[21]. PTE-RV have been around for more than three decades[22]. They have several advantages over PTBD alone: (1) PTE-RV allow for transhepatic puncture using only small-caliber catheters, thereby reducing complications. Bokemeyer *et al*[21] reported significantly fewer complications with PTE-RV than in PTBD (16.6% *vs* 26.4%;  $P = 0.037$ ); (2) PTE-RV allow endoscopists to perform therapeutic ERCP in the usual manner through rendezvous access; and (3) Although PTBD is part of PTE-RV, once the biliary obstruction is resolved, the percutaneous access is closed[23].

PTE-RV can be executed as a one-stage procedure or a two-stage procedure[23]. The advantage of the one-stage procedure is that there is no need to insert a PTBD catheter. The two-stage procedure includes PTBD during the first session and internalization of the drain using an endoscope during the second session. These two steps are usually separated by a few hours to a few days[24]. Wayman *et al*[25] compared one-stage ( $n = 19$ ) and two-stage PTE-RV ( $n = 22$ ) and found that the technical success rates were comparable (94.7% *vs* 95.5%), but adverse events were more common in the two-stage group (37% *vs* 73%,  $P < 0.05$ ), mainly due to complications related to external drainage.

For the following purposes, we recommend the insertion of a percutaneously placed hydrophilic-coated catheter (*e.g.*, angiocatheter) before the endoscopic rendezvous procedure (Figure 3A). First, the hepatic capsule and parenchyma, which could be damaged by the antegrade-introduced guidewire (AGW), were protected. Second, to ensure percutaneous access, once the AGW is lost incidentally during PTE-RV, it can be reintroduced into the biliary tree. Third, to facilitate the movements of AGW. After the AGW is introduced into the duodenum, there are several ways to achieve SBC[23,26]. The first and most classic technique is to grasp the distal end of the AGW with a snare and then pull the wire through the working channel of the endoscope. Retrograde bile duct cannulation can then be achieved over the wire (Figure 3B). This technique is particularly useful for patients with tight biliary strictures since the guidewire can be secured at both sides of percutaneous and endoscopic routes to facilitate retrograde passage of a catheter or stent through the stricture (push-pull technique). However, this technique might be limited by the difficult capture of the AGW and laborious guidewire manipulation, the potential for kinking or accidental loss of the AGW during withdrawal, and the risk of hepatic capsule/parenchymal tearing during AGW manipulation. The second and parallel technique is to use a standard ERCP cannulation method alongside the AGW or the percutaneously introduced catheter (Figure 3C). The advantage of this technique is that it is simple and perhaps time saving while avoiding the limitations of classical techniques. However, in some cases, it can be difficult. In such cases, retrograde biliary cannulation can be performed after antegrade balloon dilation of the biliary orifice. The other adjunctive maneuvers include insertion of a retrograde guidewire into a percutaneously placed catheter exiting the ampulla or insertion of a sphincterotome into the AGW exiting the ampulla [26].

PTE-RV has been relatively less investigated. In a literature search in early 2022, we found no review/meta-analysis articles on this topic. We were only able to find six studies (441 patients in total) over the past decade; all of them were retrospective (Table 2)[21,23,24,26-28]. The reason for PTE-RV in the searched studies was the failure of the initial ERCP. All but one study on the management of biliary strictures after living-donor liver transplantation included patients with malignant biliary strictures[28], ranging from 38% to 100% of study patients. PTE-RV is effective, with a technical success rate of 88.7% (80.4%-100% between studies). PTE-RV is also safe, with an overall adverse event rate of 13.2% (4.9%-19.2% between studies). Most studies reported no deaths from procedure-related mortality, except for one study that reported a 3.5% mortality rate possibly related to the PTE-RV procedure[23,24,27,28].

## EUS-ASSISTED OR GUIDED BILIARY DRAINAGE

EUS-assisted or guided biliary drainage (EUS-BD) includes the EUS-assisted rendezvous technique (EUS-RV), EUS-guided choledochoduodenostomy (EUS-CDS), EUS-guided hepaticogastrostomy (EUS-HGS) and other procedures[29]. EUS-RV is designed to facilitate ERCP and does not involve tract dilation or stent placement and is therefore more physiologically and minimally invasive among the existing EUS-guided procedures[30]. Indications for EUS-RV include benign or potentially resectable malignant cases and unresectable malignant cases not suitable for other EUS-BD methods[31,32]. EUS-CDS and EUS-HGS involve direct transmural biliary drainage, so there could be some serious adverse events[33]. Therefore, both techniques are currently indicated for unresectable malignant cases[29-31, 33]. EUS-HGS and EUS-CDS are mainly used in patients in whom access to the papilla is not possible, such as in cases of duodenal obstruction or surgically altered anatomy. Therefore, they are beyond the scope of this review and are not included. However, indications for EUS-BD might change over time as technology advances, and improvements in devices/stents could increase technical success rates and reduce adverse event rates[34-37].

**Table 2** Summary of studies on reporting percutaneous-transhepatic-endoscopic rendezvous procedures

Ref.	Study design (patient number)	Malignant biliary obstruction	One-stage vs two-stage	Technical success rate	Adverse events	PTE-RV related mortality
Chivot <i>et al</i> [23] (2021)	Retrospective ( <i>n</i> = 84)	78.5%	One-stage	95.2% (80/84)	19% (16/84); Cholangitis: 9.5%; Pancreatitis: 3.5%; Hemorrhage: 2.3%; Pneumoperitoneum: 3.5%	3.5%
Bokemeyer <i>et al</i> [21] (2019)	Retrospective ( <i>n</i> = 163)	71.3%	NA	80.4% (131/163)	16.6% (27/163); Procedure-related complications: 8.6%; Drainage-related complications: 8%	NA
Yang <i>et al</i> [26] (2017)	Retrospective ( <i>n</i> = 42)	38%	Two-stage	92.9% (39/42)	7.1% (3/42)	NA
Tomizawa <i>et al</i> [24] (2014)	Retrospective ( <i>n</i> = 26)	91%	One-stage (73%) or two-stage	88% (23/26)	19.2% (5/26)	0
Neal <i>et al</i> [27] (2010)	Retrospective ( <i>n</i> = 106)	100%	Two-stage	92.5% (98/106)	4.9% (5/106)	0
Chang <i>et al</i> [28] (2010)	Retrospective ( <i>n</i> = 20)	0	Two-stage	100% (20/20)	10% (2/20); Pancreatitis: 5%; Cholangitis: 5%	0
Overall	441	-	-	88.7% (391/441)	13.2% (58/441)	-

PTE-RV: Percutaneous-transhepatic-endoscopic rendezvous procedures; NA: Not available.



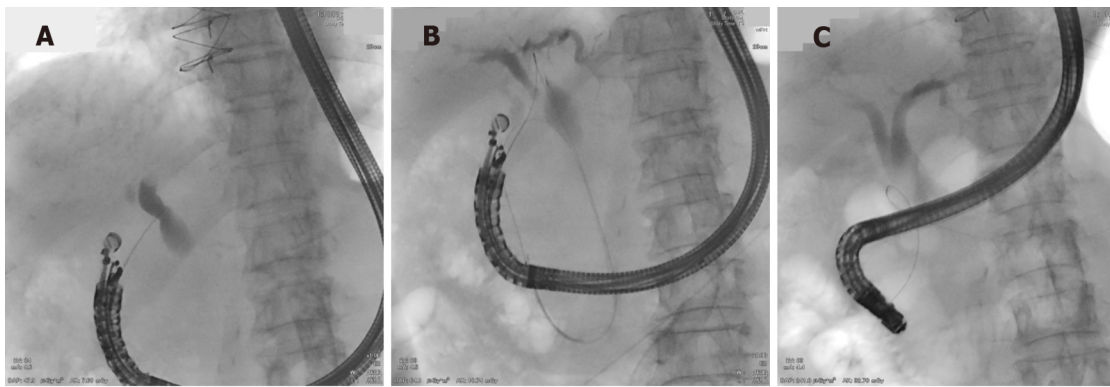
DOI: 10.3748/wjg.v28.i29.3803 Copyright ©The Author(s) 2022.

**Figure 3** Percutaneous-transhepatic-endoscopic rendezvous procedures. A: Placement of an angiocatheter to protect the liver capsule and parenchyma from guidewire damage; B: A metal stent is passed through the distal biliary stricture over the antegrade-introduced guidewire; C: Cannulation alongside the antegrade-introduced angiocatheter.

### EUS-assisted rendezvous technique

In EUS-RV, the bile duct is punctured under EUS guidance, followed by the introduction of an AGW into the duodenum (Figure 4). The EUS endoscope is then switched to a duodenoscope, with eventual ERCP (SBC is achieved over the AGW or in parallel to the AGW). There are three puncture routes for EUS-RV[11,31,38]: (1) The intrahepatic bile duct (IHBD) route: Either transesophageal puncture of B2 or transgastric puncture of B2 or B3 can be performed. If the target is the right IHBD, it can be punctured from the duodenal bulb (D1). Transgastric puncture of B2 is most frequently performed; (2) The extrahepatic bile duct (EHBD)/D1 route, with puncture from D1: In this route, the endoscope is usually in the push position (long position), and the proximal EHBD is punctured; and (3) The EHBD/second portion of the duodenum (D2) route, with puncture from D2. In this route, the endoscope is usually in a short position, and the distal EHBD is punctured.

Two studies proposing treatment algorithms suggested using the EHBD/D2 route as a first-line approach[10,31]. They reported that the EHBD/D2 route was feasible in 50%-62.5% of patients, with EUS-RV success rates of 100% in both studies. Iwashita *et al*[10] found that the EUS-RV success rate *via* the EHBD/D1 and IHBD routes was only 66.7%. Matsubara *et al*[31] found that the time between puncture and guidewire placement with the DEHBD/D2 route was significantly shorter than that with other methods (3.5 min *vs* 14.0 min,  $P = 0.014$ ). Therefore, EUS-RV *via* the EHBD/D2 route can be



DOI: 10.3748/wjg.v28.i29.3803 Copyright ©The Author(s) 2022.

**Figure 4** Endoscopic ultrasound-assisted rendezvous procedures. A: Under endoscopic ultrasound, the proximal extrahepatic bile duct is punctured through the duodenal bulb. The sonoendoscope is in a long position; B: The guidewire is delivered antegradely to the duodenum through the puncture route; C: Switch to a duodenoscope to grasp the antegradely introduced guidewire.

considered a first-line approach when feasible, although the route of access should be chosen on a patient-by-patient basis[10,31,32]. In the case of the IHBD approach, Iwashita *et al*[39] reported a hybrid rendezvous technique, in which a 6-French dilator was inserted into the biliary system for better guidewire manipulation, which could improve the technical success rate.

EUS-RV has been increasingly used in patients with SBC failure in initial ERCP[11,30]. A review by Tsuchiya *et al*[11] in 2016 (15 studies, 382 patients) reported that EUS-RV had an overall success rate of 82% (50%-100% between studies) and a complication rate of 13% (0-23% between studies). They also found that the IHBD puncture route had a lower success rate than the EHBD route (76% *vs* 85%). Therefore, in this review, we performed a literature search in Medline and included studies published after 2015 (7 studies, 177 patients; Table 3)[10,31,32,40-43]. The proportion of patients with malignant biliary obstruction was 43.5% (0-68.8% between studies). The results showed an overall EUS-RV success rate of 84.4% (78.6%-100% between studies) and a complication rate of 15.6% (6.3%-23.3% between studies) for EUS-RV. These results are similar to those in the aforementioned review article. Furthermore, we found that the IHBD puncture route also had a lower success rate than the EHBD route (74.2% *vs* 84.9%). The associated complications included pancreatitis (6.7%), cholangitis (1.7%), bile leak/peritonitis (3.3%), hematoma (0.6%), perforation (0.6%), pneumomediastinum (1.7%), aspiration pneumonia (0.6%), and gastric mucosal laceration (0.6%). In a recent meta-analysis (12 studies, 342 patients), Klair *et al*[30] further reported that, if only patients with normal anatomy (without surgical alterations) were included in the analysis, the technical success rate would have improved from 86.1% to 88.3%. The pooled clinical success rate was 80.8% (95%CI: 64.1-90.8). The pooled overall adverse event rate was 14% (95%CI: 10.5-18.4), including pancreatitis (7.2%), cholangitis (2.3%), bile leak (3.3%), bleeding (2.1%), perforation (2.7%), and peritonitis (2.3%). However, all of the studies included in this meta-analysis were retrospective.

Some unanswered questions remain; for example, does early switching to EUS-RV without spending too much time on advanced cannulation techniques improve technical success rates and reduce complication rates[44]? Further studies are required to clarify this issue.

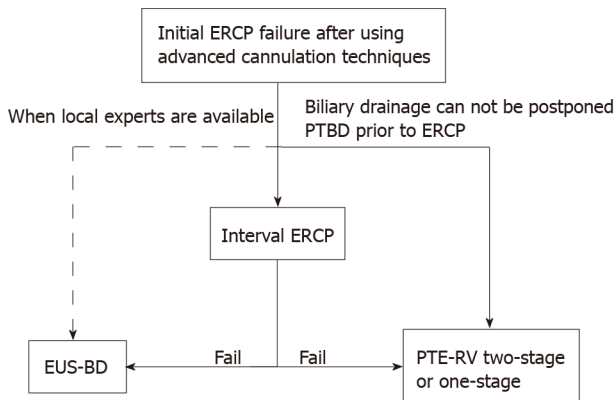
## CONCLUSION

Based on this review, interval ERCP appears to have the lowest technical success rate and overall complication rate of the three endoscopic salvage methods. Given the acceptably high success rates and low complication rates, and without the need for additional expertise, facilities (*e.g.*, EUS), or other specialists (*e.g.*, radiologists), interval ERCP can be considered the first choice when SBC is not feasible with advanced cannulation techniques[4]. In this way, more invasive alternative interventions can be avoided in approximately three-quarters of patients. However, the main limitation of interval ERCP is that it must be delayed by a few days to improve the success rate. Therefore, patients in urgent need of biliary drainage (*e.g.*, uncontrolled cholangitis) should undergo other, more invasive therapies. In this setting, since percutaneous biliary puncture is a more widespread technique than EUS-BD, and most ERCP endoscopists can perform rendezvous procedures, two-stage PTE-RV can be considered because PTBD can achieve early bile drainage. Of course, if both interventional radiologists and endoscopists are available, one-stage PTE-RV is welcome because it reduces complication rates. Another situation in which PTE-RV can be considered a first choice is when the patient has a PTBD drainage tube before the initial ERCP. EUS-BD is a relatively new technique and requires additional technical expertise/facilities, and as such, its use has been limited to some ERCP endoscopists at some advanced endoscopy centers.

**Table 3 Summary of studies on reporting endoscopic ultrasound-guided rendezvous procedures**

Ref.	Study design (patient number)	Malignant biliary obstruction	Success rate via EHBD	Success rate via IHBD	Overall technical success rate	Overall complication rate
Iwashita <i>et al</i> [10] (2016)	Prospective (n = 20)	60% (12/20)	86.7% (13/15)	75% (3/4)	80% (16/20)	15% (3/20); Hematoma (5%); Pancreatitis (10%)
Tang <i>et al</i> [40] (2016)	Retrospective (n = 25)	52% (13/25)	83.3% (20/24)	0 (0/1)	80% (20/25)	16% (4/25); Pancreatitis (12%); Cholangitis (4%)
Okuno <i>et al</i> [32] (2017)	Retrospective (n = 39)	62.5% (24/39)	84.6% (22/26)	68.8% (11/16)	78.6% (33/42)	16.7% (7/42); Pneumomediastinum (4.8%); Retroperitoneal perforation (2.4%); Cholangitis (2.4%); Peritonitis (4.8%); Pancreatitis (2.4%)
Nakai <i>et al</i> [41] (2017)	Retrospective (n = 30)	30% (9/30)	NA	NA	93.3% (28/30)	23.3% (7/30); Pancreatitis (10.0 %); Bile peritonitis (3.3 %); Cholangitis (3.3 %); Aspiration pneumonia (3.3 %); Gastric mucosa laceration (3.3 %)
Shiomi <i>et al</i> [42] (2018)	Prospective (n = 20)	40% (8/20)	83.3% (10/12)	87.5% (7/8)	85% (17/20)	15% (3/20); Biliary peritonitis (10%); Pancreatitis (5%)
Martinez <i>et al</i> [43] (2019)	Retrospective (n = 27)	0	81.5 % (22/27)	-	81.5 % (22/27)	11.1% (3/27); Pneumomediastinum (3.7%); Bile leak (3.7%); Pancreatitis (3.7%)
Matsubara <i>et al</i> [31] (2020)	Retrospective (n = 16)	68.8% (11/16)	93.3% (14/15)	100% (2/2 <sup>1</sup> )	100% (16/16)	6.3% (1/16); Pancreatitis (6.3%)
Overall	n = 177	43.5% (77/177)	84.9% (101/119)	74.2% (23/31)	84.4% (152/180)	15.6% (28/180); Pancreatitis (6.7%); Bile leak/peritonitis (3.3%); Cholangitis (1.7%); Pneumomediastinum (1.7%); Retroperitoneal perforation (0.6%); Hematoma (0.6%); Aspiration pneumonia (0.6%); Gastric mucosa laceration (0.6%)

<sup>1</sup>Including one patient had initial extrahepatic bile duct approach attempt.  
 NA: Not available; IHBD: Intrahepatic bile duct; EHBD: Extrahepatic bile duct.



DOI: 10.3748/wjg.v28.i29.3803 Copyright ©The Author(s) 2022.

**Figure 5 The proposed treatment algorithm.** ERCP: Endoscopic retrograde cholangiopancreatography; PTBD: Percutaneous transhepatic biliary drainage; PTE-RV: Percutaneous-transhepatic-endoscopic rendezvous procedure; EUS-BD: Endoscopic ultrasound-assisted or guided biliary drainage.

When local experts are available, EUS-BD could serve as a first-line salvage technique before considering PTBD, as recommended by recently issued ESGE guidelines[29]. If not, it might be performed in a second endoscopic session by another endoscopist with dual endoscopic techniques. Based on the current review, we propose a treatment algorithm to provide practical recommendations, as shown in Figure 5. Since there have been no comparative studies between treatments, the suggested practice should be validated by further studies.

**FOOTNOTES**

**Author contributions:** Tsou YK conceptualized and designed the review and wrote the manuscript; Pan KT was

responsible for the data acquisition/analysis of the percutaneous-transhepatic-endoscopic rendezvous procedures; Lee MH was responsible for the data acquisition/analysis of the endoscopic ultrasound-assisted or guided procedures; Lin CH contributed to revising and validating the manuscript.

**Conflict-of-interest statement:** There is no conflict of interest associated with any of the authors contributing their efforts to this manuscript.

**Open-Access:** This article is an open-access article that was selected by an in-house editor and fully peer-reviewed by external reviewers. It is distributed in accordance with the Creative Commons Attribution NonCommercial (CC BY-NC 4.0) license, which permits others to distribute, remix, adapt, build upon this work non-commercially, and license their derivative works on different terms, provided the original work is properly cited and the use is non-commercial. See: <https://creativecommons.org/licenses/by-nc/4.0/>

**Country/Territory of origin:** Taiwan

**ORCID number:** Yung-Kuan Tsou 0000-0002-7254-7369; Mu Hsien Lee 0000-0003-3664-5313; Cheng-Hui Lin 0000-0002-7856-2585.

**S-Editor:** Yan JP

**L-Editor:** A

**P-Editor:** Yan JP

## REFERENCES

- Berry R, Han JY, Tabibian JH. Difficult biliary cannulation: Historical perspective, practical updates, and guide for the endoscopist. *World J Gastrointest Endosc* 2019; **11**: 5-21 [PMID: 30705728 DOI: 10.4253/wjge.v11.i1.5]
- Reddy DN, Nabi Z, Lakhtakia S. How to Improve Cannulation Rates During Endoscopic Retrograde Cholangiopancreatography. *Gastroenterology* 2017; **152**: 1275-1279 [PMID: 28366733 DOI: 10.1053/j.gastro.2017.03.041]
- Chen Q, Jin P, Ji X, Du H, Lu J. Management of difficult or failed biliary access in initial ERCP: A review of current literature. *Clin Res Hepatol Gastroenterol* 2019; **43**: 365-372 [PMID: 30314736 DOI: 10.1016/j.clinre.2018.09.004]
- Testoni PA, Mariani A, Aabakken L, Arvanitakis M, Bories E, Costamagna G, Devière J, Dinis-Ribeiro M, Dumonceau JM, Giovannini M, Gyokeres T, Hafner M, Halttunen J, Hassan C, Lopes L, Papanikolaou IS, Tham TC, Tringali A, van Hooft J, Williams EJ. Papillary cannulation and sphincterotomy techniques at ERCP: European Society of Gastrointestinal Endoscopy (ESGE) Clinical Guideline. *Endoscopy* 2016; **48**: 657-683 [PMID: 27299638 DOI: 10.1055/s-0042-108641]
- Liao WC, Angsuwatcharakon P, Isayama H, Dhir V, Devereaux B, Khor CJ, Ponnudurai R, Lakhtakia S, Lee DK, Ratanachu-Ek T, Yasuda I, Dy FT, Ho SH, Makmun D, Liang HL, Draganov PV, Rerknimitr R, Wang HP. International consensus recommendations for difficult biliary access. *Gastrointest Endosc* 2017; **85**: 295-304 [PMID: 27720741 DOI: 10.1016/j.gie.2016.09.037]
- Zou XP, Leung JW, Li YH, Yao YL, Pei QS, Wu YL, He QB, Cao J, Ding XW. Comparison of sequential pancreatic duct guidewire placement technique and needle knife precut sphincterotomy for difficult biliary cannulation. *J Dig Dis* 2015; **16**: 741-746 [PMID: 26562073 DOI: 10.1111/1751-2980.12300]
- Kubota K, Sato T, Kato S, Watanabe S, Hosono K, Kobayashi N, Hisatomi K, Matsuhashi N, Nakajima A. Needle-knife precut papillotomy with a small incision over a pancreatic stent improves the success rate and reduces the complication rate in difficult biliary cannulations. *J Hepatobiliary Pancreat Sci* 2013; **20**: 382-388 [PMID: 22993078 DOI: 10.1007/s00534-012-0552-4]
- Barakat MT, Girotra M, Thosani N, Kothari S, Banerjee S. Escalating complexity of endoscopic retrograde cholangiopancreatography over the last decade with increasing reliance on advanced cannulation techniques. *World J Gastroenterol* 2020; **26**: 6391-6401 [PMID: 33244200 DOI: 10.3748/wjg.v26.i41.6391]
- Lo MH, Lin CH, Wu CH, Tsou YK, Lee MH, Sung KF, Liu NJ. Management of biliary diseases after the failure of initial needle knife precut sphincterotomy for biliary cannulation. *Sci Rep* 2021; **11**: 14968 [PMID: 34294788 DOI: 10.1038/s41598-021-94361-8]
- Iwashita T, Yasuda I, Mukai T, Iwata K, Ando N, Doi S, Nakashima M, Uemura S, Mabuchi M, Shimizu M. EUS-guided rendezvous for difficult biliary cannulation using a standardized algorithm: a multicenter prospective pilot study (with videos). *Gastrointest Endosc* 2016; **83**: 394-400 [PMID: 26089103 DOI: 10.1016/j.gie.2015.04.043]
- Tsuchiya T, Itoi T, Sofuni A, Tonozuka R, Mukai S. Endoscopic ultrasonography-guided rendezvous technique. *Dig Endosc* 2016; **28** Suppl 1: 96-101 [PMID: 26786389 DOI: 10.1111/den.12611]
- Kevans D, Zeb F, Donnellan F, Courtney G, Aftab AR. Failed biliary access following needle knife fistulotomy: is repeat interval ERCP worthwhile? *Scand J Gastroenterol* 2010; **45**: 1238-1241 [PMID: 20553113 DOI: 10.3109/00365521.2010.495418]
- Donnellan F, Enns R, Kim E, Lam E, Amar J, Telford J, Byrne MF. Outcome of repeat ERCP after initial failed use of a needle knife for biliary access. *Dig Dis Sci* 2012; **57**: 1069-1071 [PMID: 22147249 DOI: 10.1007/s10620-011-1982-6]
- Kim J, Ryu JK, Ahn DW, Park JK, Yoon WJ, Kim YT, Yoon YB. Results of repeat endoscopic retrograde cholangiopancreatography after initial biliary cannulation failure following needle-knife sphincterotomy. *J Gastroenterol Hepatol* 2012; **27**: 516-520 [PMID: 21913986 DOI: 10.1111/j.1440-1746.2011.06914.x]
- Pavlidis M, Barnabas A, Fernandopulle N, Bailey AA, Collier J, Phillips-Hughes J, Ellis A, Chapman R, Braden B. Repeat endoscopic retrograde cholangiopancreatography after failed initial precut sphincterotomy for biliary cannulation. *World J*

- Gastroenterol* 2014; **20**: 13153-13158 [PMID: 25278710 DOI: 10.3748/wjg.v20.i36.13153]
- 16 **Colan-Hernandez J**, Aldana A, Concepción M, Chavez K, Gómez C, Mendez-Bocanegra A, Martínez-Guillen M, Sendino O, Villanueva C, Llach J, Guarner-Argente C, Cárdenas A, Guarner C. Optimal timing for a second ERCP after failure of initial biliary cannulation following precut sphincterotomy: an analysis of experience at two tertiary centers. *Surg Endosc* 2017; **31**: 3711-3717 [PMID: 28127713 DOI: 10.1007/s00464-016-5410-z]
  - 17 **Narayan KS**, Gupta GK, Nijhawan S, Pandey S, Dhandhu BS, Puri S, Kumar A, Sharma D. Is it Worth to Repeat Endoscopic Retrograde Cholangiopancreatography after Failed Precut? *J Digest Endosc* 2017; **8**: 129-131
  - 18 **Téllez-Ávila FI**, Herrera-Mora D, Duarte-Medrano G, Lopez-Arce G, Lindoro-Barraza D, Casanova I, Elizondo-Rivera J, Ramírez-Luna M, Valdovinos-Andraca F. Biliary Drainage in Patients With Failed ERCP: Percutaneous Versus EUS-guided Drainage. *Surg Laparosc Endosc Percutan Tech* 2018; **28**: 183-187 [PMID: 29683996 DOI: 10.1097/SLE.0000000000000528]
  - 19 **Gupta K**, Mallery S, Hunter D, Freeman ML. Endoscopic ultrasound and percutaneous access for endoscopic biliary and pancreatic drainage after initially failed ERCP. *Rev Gastroenterol Disord* 2007; **7**: 22-37 [PMID: 17392627 DOI: 10.1111/j.1365-2982.2007.00981.x]
  - 20 **Nennstiel S**, Weber A, Frick G, Haller B, Meining A, Schmid RM, Neu B. Drainage-related Complications in Percutaneous Transhepatic Biliary Drainage: An Analysis Over 10 Years. *J Clin Gastroenterol* 2015; **49**: 764-770 [PMID: 25518004 DOI: 10.1097/MCG.0000000000000275]
  - 21 **Bokemeyer A**, Müller F, Niesert H, Brückner M, Bettenworth D, Nowacki T, Beyna T, Ullerich H, Lenze F. Percutaneous-transhepatic-endoscopic rendezvous procedures are effective and safe in patients with refractory bile duct obstruction. *United European Gastroenterol J* 2019; **7**: 397-404 [PMID: 31019708 DOI: 10.1177/2050640619825949]
  - 22 **Robertson DA**, Ayres R, Hacking CN, Shepherd H, Birch S, Wright R. Experience with a combined percutaneous and endoscopic approach to stent insertion in malignant obstructive jaundice. *Lancet* 1987; **2**: 1449-1452 [PMID: 2447457 DOI: 10.1016/s0140-6736(87)91141-x]
  - 23 **Chivot C**, Yzet C, Bouzerar R, Brazier F, Hakim S, Le Mouel JP, Nguyen-Khac E, Delcenserie R, Yzet T. Safety and efficacy of percutaneous transhepatic-endoscopic rendezvous procedure in a single session. *Surg Endosc* 2021; **35**: 3534-3539 [PMID: 32710212 DOI: 10.1007/s00464-020-07812-0]
  - 24 **Tomizawa Y**, Di Giorgio J, Santos E, McCluskey KM, Gelrud A. Combined interventional radiology followed by endoscopic therapy as a single procedure for patients with failed initial endoscopic biliary access. *Dig Dis Sci* 2014; **59**: 451-458 [PMID: 24271117 DOI: 10.1007/s10620-013-2913-5]
  - 25 **Wayman J**, Mansfield JC, Matthewson K, Richardson DL, Griffin SM. Combined percutaneous and endoscopic procedures for bile duct obstruction: simultaneous and delayed techniques compared. *Hepatogastroenterology* 2003; **50**: 915-918 [PMID: 12845949 DOI: 10.5172/rsj.351.15.2.119]
  - 26 **Yang MJ**, Kim JH, Hwang JC, Yoo BM, Kim SS, Lim SG, Won JH. Usefulness of combined percutaneous-endoscopic rendezvous techniques after failed therapeutic endoscopic retrograde cholangiography in the era of endoscopic ultrasound guided rendezvous. *Medicine (Baltimore)* 2017; **96**: e8991 [PMID: 29310413 DOI: 10.1097/MD.00000000000008991]
  - 27 **Neal CP**, Thomasset SC, Bools D, Sutton CD, Garcea G, Mann CD, Rees Y, Newland C, Robinson RJ, Dennison AR, Berry DP. Combined percutaneous-endoscopic stenting of malignant biliary obstruction: results from 106 consecutive procedures and identification of factors associated with adverse outcome. *Surg Endosc* 2010; **24**: 423-431 [PMID: 19565296 DOI: 10.1007/s00464-009-0586-0]
  - 28 **Chang JH**, Lee IS, Chun HJ, Choi JY, Yoon SK, Kim DG, You YK, Choi MG, Choi KY, Chung IS. Usefulness of the rendezvous technique for biliary stricture after adult right-lobe living-donor liver transplantation with duct-to-duct anastomosis. *Gut Liver* 2010; **4**: 68-75 [PMID: 20479915 DOI: 10.5009/gnl.2010.4.1.68]
  - 29 **van der Merwe SW**, van Wanrooij RLJ, Bronswijk M, Everett S, Lakhtakia S, Rimbas M, Hucl T, Kunda R, Badaoui A, Law R, Arcidiacono PG, Larghi A, Giovannini M, Khashab MA, Binmoeller KF, Barthet M, Perez-Miranda M, van Hooft JE. Therapeutic endoscopic ultrasound: European Society of Gastrointestinal Endoscopy (ESGE) Guideline. *Endoscopy* 2022; **54**: 185-205 [PMID: 34937098 DOI: 10.1055/a-1717-1391]
  - 30 **Klair JS**, Zafar Y, Ashat M, Bomman S, Murali AR, Jayaraj M, Law J, Larsen M, Singh DP, Rustagi T, Irani S, Ross A, Kozarek R, Krishnamoorthi R. Effectiveness and Safety of EUS Rendezvous After Failed Biliary Cannulation With ERCP: A Systematic Review and Proportion Meta-analysis. *J Clin Gastroenterol* 2021 [PMID: 34009843 DOI: 10.1097/MCG.0000000000001543]
  - 31 **Matsubara S**, Nakagawa K, Suda K, Otsuka T, Isayama H, Nakai Y, Oka M, Nagoshi S. A Proposed Algorithm for Endoscopic Ultrasound-Guided Rendezvous Technique in Failed Biliary Cannulation. *J Clin Med* 2020; **9** [PMID: 33260305 DOI: 10.3390/jcm9123879]
  - 32 **Okuno N**, Hara K, Mizuno N, Hijioka S, Tajika M, Tanaka T, Ishihara M, Hirayama Y, Onishi S, Niwa Y, Yamao K. Endoscopic Ultrasound-guided Rendezvous Technique after Failed Endoscopic Retrograde Cholangiopancreatography: Which Approach Route Is the Best? *Intern Med* 2017; **56**: 3135-3143 [PMID: 28943555 DOI: 10.2169/internalmedicine.8677-16]
  - 33 **Ogura T**, Higuchi K. Technical Review of Developments in Endoscopic Ultrasound-Guided Hepaticogastrostomy. *Clin Endosc* 2021; **54**: 651-659 [PMID: 33896154 DOI: 10.5946/ce.2021.020-KDDW]
  - 34 **Nakai Y**, Kogure H, Isayama H, Koike K. Endoscopic Ultrasound-Guided Biliary Drainage for Benign Biliary Diseases. *Clin Endosc* 2019; **52**: 212-219 [PMID: 30866611 DOI: 10.5946/ce.2018.188]
  - 35 **Han SY**, Kim SO, So H, Shin E, Kim DU, Park DH. EUS-guided biliary drainage versus ERCP for first-line palliation of malignant distal biliary obstruction: A systematic review and meta-analysis. *Sci Rep* 2019; **9**: 16551 [PMID: 31719562 DOI: 10.1038/s41598-019-52993-x]
  - 36 **Ginestet C**, Sanglier F, Hummel V, Rouchaud A, Legros R, Lepetit H, Dahan M, Carrier P, Loustaud-Ratti V, Sautereau D, Albouys J, Jacques J, Geyl S. EUS-guided biliary drainage with electrocautery-enhanced lumen-apposing metal stent placement should replace PTBD after ERCP failure in patients with distal tumoral biliary obstruction: a large real-life study. *Surg Endosc* 2022; **36**: 3365-3373 [PMID: 34606007 DOI: 10.1007/s00464-021-08653-1]
  - 37 **Karagyozov PI**, Tishkov I, Boeva I, Draganov K. Endoscopic ultrasound-guided biliary drainage-current status and future

- perspectives. *World J Gastrointest Endosc* 2021; **13**: 607-618 [PMID: 35070022 DOI: 10.4253/wjge.v13.i12.607]
- 38 **Dhir V**, Artifon EL, Gupta K, Vila JJ, Maselli R, Frazao M, Maydeo A. Multicenter study on endoscopic ultrasound-guided expandable biliary metal stent placement: choice of access route, direction of stent insertion, and drainage route. *Dig Endosc* 2014; **26**: 430-435 [PMID: 23941261 DOI: 10.1111/den.12153]
- 39 **Iwashita T**, Uemura S, Yoshida K, Mita N, Tezuka R, Yasuda I, Shimizu M. EUS-guided hybrid rendezvous technique as salvage for standard rendezvous with intra-hepatic bile duct approach. *PLoS One* 2018; **13**: e0202445 [PMID: 30133542 DOI: 10.1371/journal.pone.0202445]
- 40 **Tang Z**, Igbinomwanhia E, Elhanafi S, Othman MO. Endoscopic Ultrasound Guided Rendezvous Drainage of Biliary Obstruction Using a New Flexible 19-Gauge Fine Needle Aspiration Needle. *Diagn Ther Endosc* 2016; **2016**: 3125962 [PMID: 27822005 DOI: 10.1155/2016/3125962]
- 41 **Nakai Y**, Isayama H, Matsubara S, Kogure H, Mizuno S, Hamada T, Takahara N, Nakamura T, Sato T, Takeda T, Hakuta R, Ishigaki K, Saito K, Tada M, Koike K. A novel "hitch-and-ride" deep biliary cannulation method during rendezvous endoscopic ultrasound-guided ERCP technique. *Endoscopy* 2017; **49**: 983-988 [PMID: 28732390 DOI: 10.1055/s-0043-113444]
- 42 **Shiomi H**, Yamao K, Hoki N, Hisa T, Ogura T, Minaga K, Masuda A, Matsumoto K, Kato H, Kamada H, Goto D, Imai H, Takenaka M, Noguchi C, Nishikiori H, Chiba Y, Kutsumi H, Kitano M. Endoscopic Ultrasound-Guided Rendezvous Technique for Failed Biliary Cannulation in Benign and Resectable Malignant Biliary Disorders. *Dig Dis Sci* 2018; **63**: 787-796 [PMID: 29349694 DOI: 10.1007/s10620-018-4908-8]
- 43 **Martínez B**, Martínez J, Casellas JA, Aparicio JR. Endoscopic ultrasound-guided rendezvous in benign biliary or pancreatic disorders with a 22-gauge needle and a 0.018-inch guidewire. *Endosc Int Open* 2019; **7**: E1038-E1043 [PMID: 31404452 DOI: 10.1055/a-0918-5931]
- 44 **Yoon WJ**, Brugge WR. EUS-guided biliary rendezvous: EUS to the rescue. *Gastrointest Endosc* 2012; **75**: 360-361 [PMID: 22248604 DOI: 10.1016/j.gie.2011.09.024]

## Enhanced endoscopic ultrasound imaging for pancreatic lesions: The road to artificial intelligence

Marco Spadaccini, Glenn Koleth, James Emmanuel, Kareem Khalaf, Antonio Facciorusso, Fabio Grizzi, Cesare Hassan, Matteo Colombo, Benedetto Mangiavillano, Alessandro Fugazza, Andrea Anderloni, Silvia Carrara, Alessandro Repici

**Specialty type:** Gastroenterology and hepatology

**Provenance and peer review:** Invited article; Externally peer reviewed.

**Peer-review model:** Single blind

**Peer-review report's scientific quality classification**

Grade A (Excellent): 0

Grade B (Very good): B, B

Grade C (Good): 0

Grade D (Fair): 0

Grade E (Poor): 0

**P-Reviewer:** Pausawasdi N, Thailand; Tsoulfas G, Greece

**Received:** April 9, 2022

**Peer-review started:** April 9, 2022

**First decision:** May 9, 2022

**Revised:** June 7, 2022

**Accepted:** July 5, 2022

**Article in press:** July 5, 2022

**Published online:** August 7, 2022



**Marco Spadaccini, Glenn Koleth, Kareem Khalaf, Cesare Hassan, Matteo Colombo, Alessandro Fugazza, Andrea Anderloni, Silvia Carrara, Alessandro Repici,** Digestive Endoscopy Unit, Division of Gastroenterology, Humanitas Research Hospital and University, Milan 20800, Italy

**James Emmanuel,** Department of Gastroenterology and Hepatology, Queen Elizabeth, Kota Kinabalu 88200, Sabah, Malaysia

**Antonio Facciorusso,** Section of Gastroenterology, Department of Medical Sciences, University of Foggia, Foggia 71122, Italy

**Fabio Grizzi,** Department of Immunology and Inflammation, Humanitas Clinical and Research Hospital, Rozzano 20089, Italy

**Benedetto Mangiavillano,** Digestive Endoscopy Unit, Division of Gastroenterology, Humanitas Mater Domini, Castellanza 21053, Italy

**Corresponding author:** Marco Spadaccini, MD, Associate Specialist, Senior Researcher, Digestive Endoscopy Unit, Division of Gastroenterology, Humanitas Research Hospital and University, Via Manzoni 56, Milan 20800, Italy. [marco.spadaccini@humanitas.it](mailto:marco.spadaccini@humanitas.it)

### Abstract

Early detection of pancreatic cancer has long eluded clinicians because of its insidious nature and onset. Often metastatic or locally invasive when symptomatic, most patients are deemed inoperable. In those who are symptomatic, multi-modal imaging modalities evaluate and confirm pancreatic ductal adenocarcinoma. In asymptomatic patients, detected pancreatic lesions can be either solid or cystic. The clinical implications of identifying small asymptomatic solid pancreatic lesions (SPLs) of < 2 cm are tantamount to a better outcome. The accurate detection of SPLs undoubtedly promotes higher life expectancy when resected early, driving the development of existing imaging tools while promoting more comprehensive screening programs. An imaging tool that has matured in its reiterations and received many image-enhancing adjuncts is endoscopic ultrasound (EUS). It carries significant importance when risk stratifying cystic lesions and has substantial diagnostic value when combined with fine needle aspiration/biopsy (FNA/FNB). Adjuncts to EUS imaging include contrast-enhanced harmonic EUS and EUS-elastography, both having improved

the specificity of FNA and FNB. This review intends to compile all existing enhancement modalities and explore ongoing research around the most promising of all adjuncts in the field of EUS imaging, artificial intelligence.

**Key Words:** Pancreatic ductal adenocarcinoma; Pancreatic cancer; Endoscopic ultrasound; Contrast-enhanced endoscopic ultrasound; Endoscopic ultrasound contrast agents; Endoscopic ultrasound elastography; Artificial intelligence; Fractal analysis; Endoscopy; Imaging

©The Author(s) 2022. Published by Baishideng Publishing Group Inc. All rights reserved.

**Core Tip:** Several reviews have evaluated the use of contrast-enhanced endoscopic ultrasound (CE-EUS), EUS-elastography (EUS-E), and artificial intelligence in separation. Not many have reviewed all three modalities' strengths in a single article. This article elaborates on current methods and outcomes of CE-EUS and EUS-E while reviewing the impact of artificial intelligence on the field of EUS imaging.

**Citation:** Spadaccini M, Kolet G, Emmanuel J, Khalaf K, Facciorusso A, Grizzi F, Hassan C, Colombo M, Mangiavillano B, Fugazza A, Anderloni A, Carrara S, Repici A. Enhanced endoscopic ultrasound imaging for pancreatic lesions: The road to artificial intelligence. *World J Gastroenterol* 2022; 28(29): 3814-3824

**URL:** <https://www.wjgnet.com/1007-9327/full/v28/i29/3814.htm>

**DOI:** <https://dx.doi.org/10.3748/wjg.v28.i29.3814>

## INTRODUCTION

Pancreatic ductal adenocarcinoma (PDAC) is the 5<sup>th</sup> most fatal cancer globally, and those receiving a diagnosis have only a 6% 5-year survival rate[1]. Fortunately, early detection of a PDAC, especially when smaller than 1 cm, along with timely resection can aggrandize 5-year survival rates by up to 80.4% [2]. This disease's increasing incidence and mortality trend have brought different specialists (*i.e.* radiologists and gastroenterologists) together to create a framework to enhance early detection. Computed tomography (CT), magnetic resonance imaging (MRI), and endoscopic ultrasound (EUS) have all emerged as essentials in the multidisciplinary diagnostic approach of PDAC. EUS images of the pancreas are distinct from all modalities above because of their increased spatial resolution, making it 94% sensitive for PDAC detection[3]. Successive generations of EUS imaging transducers and post-processing software have markedly improved the spatial resolution of conventional B-mode EUS images. When used alone, it boasts a superior diagnostic accuracy over multidetector CT and MRI, singularly for solid pancreatic lesions (SPLs), but a meager specificity when differentiating pancreatic cancer from other pathologies[3,4]. However, with the advent of image-enhancing technologies such as contrast-enhanced EUS (CE-EUS) and EUS-elastography (EUS-E), there is evidence to suggest that even smaller SPLs are now detectable with good sensitivity and specificity[5-7]. Although promising, these advances' overarching impact in the face of early pancreatic cancer detection and diagnosing benign pancreatic diseases is still largely underwhelming. Pancreatic cancer remains a leading cause of death in industrialized populations, and the new case burden is estimated to grow steadily for the next 20 years [8]. Thus far, we know that the diagnostic accuracy of EUS, when coupled with EUS-guided tissue sampling, holds good outcomes, but reproducing its performance with ease remains a global challenge. The learning curve to master and competently perform an EUS examination is steep[9,10]. In this context, the introduction of artificial intelligence (AI), alone or in combination with existing enhanced EUS imaging technologies, may contribute to filling the gaps in accurately and consistently diagnosing pancreatic diseases[11]. This commentary highlights existing enhanced EUS imaging technologies while paving the way for AI, postulating its possible role in this arena.

## EUS-E

Elastography is an ultrasonographic tool to measure the stiffness of the desired study area. The desired study area for a suspicious pancreatic lesion is also known as a region of interest (ROI). Akin to the clinical aspect of palpating a mass by hand and describing its characteristics, elastography does this similarly, but instead for deeper structures[12]. The two types of elastography include strain elastography (SE) and sheer wave elastography (SWE). However, SWE is still unstable in its use to measure the elasticity of SPLs and will not be discussed further in this article[13].

The type of elastography used in EUS is quasi-static or SE. It measures tissue displacement from a compressive force generated internally by the patient's physiology like breathing and vascular pulsations or externally by the tip of the echoendoscope pressing against the GI wall[14]. The compressive force deforms the tissue momentarily. The amount the tissue deforms or the degree to which it gets displaced is known as strain. Softer or more elastic tissue, *i.e.* more benign, will have more displacement while stiffer, inelastic, and generally more malignant tissue, will have less strain[15]. The images can be seen side by side on the EUS display, with the EUS-E overlaid on the B mode image.

We present examples for PDAC (Figure 1A and B) and for a metastatic lymph node (Figure 1C). The color spectrum represents a qualitative measurement, blue being the hardest and red being the softest. Quantitative measurements are seen on the strain histogram or valued as the strain ratio (SR; the strain of the larger round-shaped ROI area A divided by the strain of smaller round-shaped region of surrounding normal tissue area B). Suggested surrounding normal homogenous tissue to be used as reference include either healthy surrounding pancreatic parenchyma (pSR) or healthy GI tract wall (wSR). Suggested elastography SR values are automatically computed and estimated using the built-in software found in the Olympus EU-ME2 processor and the Hitachi United States machines. However, the reference areas have yet to be standardized.

### Outcomes

One of the earliest prospective multicenter studies by Giovannini[16] evaluated the elastography of pancreatic masses from 121 patients on initial EUS referenced against final histological diagnoses. Elastography successfully demonstrated "intense blue" on qualitative measurement for all PDAC, endocrine tumors, pancreatic metastasis, and pancreatic sarcomas. According to his scoring system of 1 through 5 (5 being the stiffest and most intense blue), scores 1 and 2 had a negative predictive value (NPV) of 77.4%, whilst scores 3 and 4 had a positive predictive value (PPV) for malignancy of 92.8%[16].

In the interest of detecting smaller ductal adenocarcinomas (< 15 mm), which if resected earlier, have shown a 5-year survival mark in PDAC survivors to exceed 30%-60%, Ignee *et al*[7] evaluated SRs for SPLs of < 15 mm from 218 patients across 13 international centers. They found that EUS-E patterns of a small lesion (average size 11 ± 3 mm), if found to be soft, could confidently rule out malignancy (NPV 98%). Although PDAC was diagnosed in these small lesions with a sensitivity of 96%, elevated stiffness in a detected lesion had a specificity of only 67% with a PPV of 56% when diagnosing malignancy[7]. These small lesions' final etiological percentage breakdown was 66% benign, while 52% were neuroendocrine tumors (NETs). Notably, 36% of the NETs were stiff lesions, while 64% were soft compared to surrounding tissue. The remaining 23% were PDAC, 17% other entities, and 8% metastasis (which showed stiffness only 59% of the time)[7].

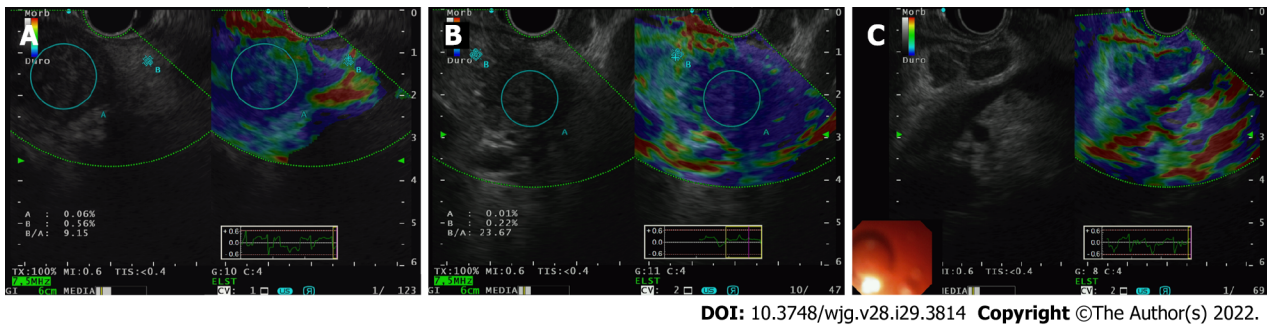
In 2012, Pei *et al*[17] and in 2013, Ying *et al*[18], the Asian groups conducted separate meta-analyses, but with additions to pooled data on the subject matter of EUS-E's diagnostic accuracy, a more recent meta-analysis of 17 studies analyzing 1544 lesions from 1537 patients was conducted in 2017. From their pooled results, EUS-E reported an accumulated sensitivity of 97% (95%CI: 95%-99%) and a specificity of 67% (95%CI: 59%-74%) for qualitative methods; 97% sensitivity (95%CI: 95%-98%) and 67% specificity (95%CI: 61%-73%) for Strain Histograms, and lastly, 98% specificity (95%CI: 96%-99%) and 62% sensitivity (95%CI: 56%-68%) for strain ratios, suggesting its value as a complement to EUS-guided tissue sampling, *i.e.* EUS-FNA[19].

Similarly, guidelines proposed by the European Federation of Societies for Ultrasound in Medicine and Biology (EFSUMB) advocate using elastography as a complementary tool for focal pancreatic lesion characterization[20]. When a EUS-FNA sample is negative, but the index of suspicion for malignancy remains, the EFSUMB recommends using elastography and CE-EUS for repeat tissue sampling or referring the patient directly to the surgeons for operative intervention without further delay[20]. We demonstrate the clinical application of EUS-E (with CE-EUS) to target FNB sampling in a patient with a degenerated intraductal papillary mucinous neoplasm (IPMN) under our surveillance (Figure 2). This patient had positive cytology, warranting early surgery. Although documented to be helpful in the diagnosis of early autoimmune pancreatitis due to an idiosyncratic distribution of tissue stiffness, the guidelines cannot recommend the use of elastography in differentiating advanced chronic pancreatitis from pancreatic cancer[20].

One of EUS-E's many inherent limitations is evident here: Its low specificity and inability to consistently distinguish between pancreatic diseases (inflammatory *vs* neoplastic) or even types of pancreatic malignancies.

Inbuilt elastography software reduces intra-observer variability by overcoming the selection bias of images by providing the operator with a real-time movie of all recorded frames. However, there remains significant inter-observer variability when differentiating NETs from normal pancreatic parenchyma, as both may appear green *i.e.* soft.

Here are a few other scenarios where misdiagnoses occur: (1) If the endoscopist places too much compressive pressure between the probe and the examined tissue; and (2) False image reconstruction due to the heterogeneity of the examined tissue *i.e.* in the case of pancreatic cancer where some areas within the lesion are either necrotic, fibrous from desmoplasia, or have become inhomogeneous from vessel infiltration.



DOI: 10.3748/wjg.v28.i29.3814 Copyright ©The Author(s) 2022.

**Figure 1 Endoscopic ultrasound-elastography.** A and B: Endoscopic ultrasound-elastography (EUS-E) use in demonstrating stiffness of pancreatic ductal adenocarcinoma tissue (encircled A) against normal pancreatic parenchyma (encircled B); C: EUS-E use in demonstrating stiffness of metastatic lymph nodes in patient from B. The nodes in B-mode when seen with elastography are blue, indicating that it's hard and potentially malignant.



DOI: 10.3748/wjg.v28.i29.3814 Copyright ©The Author(s) 2022.

**Figure 2 The clinical application of endoscopic ultrasound-elastography (with contrast-enhanced endoscopic ultrasound) to target fine needle biopsy sampling in a patient with a degenerated intraductal papillary mucinous neoplasm under our surveillance.** A: Case demonstration of a degenerated intraductal papillary mucinous neoplasm and combination use of endoscopic ultrasound-elastography (EUS-E) to direct fine needle biopsy (FNB) sampling. Pre-EUS-E, the area of concern was iso-echoic, resembling normal parenchyma; however, under EUS-E, the area is stiff (blue); B: Contrast use post-FNB showing hypo-enhancement of the area of concern, confirming the area previously highlighted by EUS-E; C: Post-EUS-E and contrast-enhanced EUS guided FNB sampling in the same patient, allowing targeted sampling of the hard area.

Other pitfalls include: (1) A lack of standardization of cut-off values for strain ratios, although some experts propose using parenchyma-to-lesion SR of  $> 9.10$  (PPV 89.7%; NPV 76.9%) or the gastric wall-to-lesion SR of  $> 16.2$  (PPV 86.5%; NPV 80%) [21]; (2) Border delineation once the lesion becomes larger [22]; (3) Inability to measure strain if the lesion is too far away from the probe, and lastly; and (4) Image acquisition when fluid is present, *i.e.* with cysts [22].

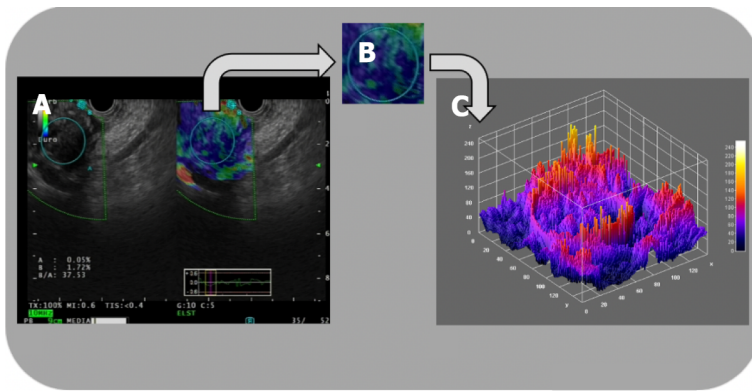
Carrara *et al* [21] demonstrated the use of fractal geometry analysis (Figure 3) to quantify the surface roughness of 2 tissues that share the same mechanical properties on elastography, and in doing so, overcome a significant limitation of EUS-E, but further trials are required [21]. Studies are also underway to evaluate the use of EUS-E in differentiating actual vessel wall infiltration by tumor tissue from that caused by an inflammatory reaction. The European Elastography Group, amongst others, is also designing and training deep learning platforms for future use in reducing inter-operator variability.

## CE-EUS IMAGING

CE-EUS imaging is a non-invasive technique that utilizes a contrast agent during a EUS examination to improve diagnostic imaging. Contrast use in ultrasound imaging was first pioneered in 1986 by Matsuda and Yabuuchi with the infusion of  $\text{CO}_2$  as a medium. Kato heralded its subsequent application into EUS in 1991, confined only to angiographic examinations [23]. In the mid-1990s, the use of Doppler function and sonicated serum albumin expanded the application of CE-EUS beyond the premise of angiographic studies [24].

In CE-EUS, the mechanical index (MI) alludes to the reaction of microbubbles in response to a stimulus in the form of an acoustic wave [25]. From this response, CE-EUS is typed into two: (1) Contrast-enhanced high-MI EUS (CEHMI-EUS), not requiring specific interpretive software; and (2) Contrast-enhanced low-MI EUS (CELMi-EUS), requiring a contrast-specific software mode.

A significant advantage of CELMI-EUS over CEHMI-EUS is its higher resolution and visibility of the contrast enhancer bubbles. In contrast, CEHMI-EUS's ability to display pancreatic macro-vessels (vessels with a diameter of approximately 0.2 mm and higher) comes at the expense of microbubble destruction



DOI: 10.3748/wjg.v28.i29.3814 Copyright ©The Author(s) 2022.

**Figure 3 Three-dimensional surface fractal dimension estimate.** A and B: Endoscopic ultrasound-elastography images (A) are used to highlight representative parenchymal regions (B) of solid pancreatic lesions; C: A computer-aided image analysis system generates an irregularly-shaped three-dimensional surface as a “shape matrix” of points with the column and row numbers proportional to the x and y coordinates and with the depth information z (x, y) stored as a matrix element. The three-dimensional fractal dimension, which is an index of the “surface roughness”, is automatically determined using the box-counting algorithm. The fractal dimension of a surface is expressed by a real number greater than 2 (the Euclidean dimension of a two-dimensional surface) and less than 3 (the Euclidean dimension of a solid). A surface with a higher surface fractal dimension is wrinkled than one with a lower dimension.

and, as a result, CEHMI-EUS's use for Doppler enhancement is preferred[26].

In collaboration with European experts in a recently issued guideline, the Asian Federation of Societies for Ultrasound in Medicine and Biology (AFSUMB) concluded that the MI should be between 0.2 and 0.4. They added that the 0.1 to 0.4 range used in published reports was influenced by several factors, including EUS probe type (radial or linear), image processing hardware, and software, phase-inversion harmonics, amplitude modulations, and focal points[27].

### **Contrast-enhanced harmonic EUS imaging**

Tissue harmonic imaging (THI) is an ultrasonographic technique, first introduced in 1997, that utilizes nonlinear propagation of ultrasound (US) waves to generate images that are superior in quality to the fundamental B-mode imaging mode[28]. This tool was incorporated into the EUS imaging arsenal approximately a decade later[29].

The two image processing techniques developed to generate harmonic images were the band filtering method and phase inversion method. The ability of harmonic imaging to improve signal-to-noise ratio and reduce artifacts produced by side lobes, grating lobes, and reverberation allowed it to outperform earlier imaging applications, such as Color Doppler and power Doppler, which were susceptible to motion artifacts[30]. Furthermore, this modality allowed for visualization of parenchymal perfusion and microvasculature of the pancreas[31].

AFSUMB, in their summary recommendations, alluded to the benefit of contrast-enhanced harmonic EUS (CH-EUS) for characterization of solid pancreatic masses, pancreatic cancer staging in patients with suspected major vessel involvement, identification of mural nodules in cystic pancreatic lesions, and detection of subtle pancreatic lesions[27].

Nevertheless, THI is saddled with certain intrinsic technical limitations. The narrow bandwidth decreases axial resolution when applying the band filtering method. This limitation gave rise to the conception of the phase inversion method. However, the latter method necessitates the transmission of two US pulses, thus decreasing the frame rate and raising the possibility of motion artifacts[30].

### **Contrast agents**

The first reported use of intravenous ultrasound contrast agents (UCAs) in ultrasonography was for image enhancement during echocardiography. Its adoption followed this in transabdominal ultrasonography before it was eventually introduced in EUS[32]. EFSUMB's recommendation on contrast for CE-EUS in non-liver applications highlighted its similarity to its use in transabdominal CEUS[33]. Worth noting is that the modalities, as mentioned earlier, represent the only imaging techniques that allow a dynamic observation of the CE phases[34]. UCAs are used to augment their ability in lesion characterization and intervention guidance.

During the evolutionary phase of CE-EUS, various agents were explored to advance the diagnostic performance of this modality. To render stability and durability, all commercially available agents are composed of gas-filled microbubbles encapsulated by a phospholipid or albumin shell. Each agent is aptly categorized based on its half-life and ability for transpulmonary passage[32].

The AFSUMB working group strongly recommends the following for use as UCAs: SonoVue (Lumason, sulfur hexafluoride micro-bubbles; Bracco, Milan, Italy; available in Europe, China, India, Korea, Hong Kong, New Zealand, Singapore, and Brazil); Definity (octafluoropropane microbubbles;

Bristol-Myers Squibb Medical Imaging, New York, NY, United States; available in the United States, Canada, and Australia), and Sonazoid (perfluorobutane microbubbles; GE Healthcare, Chicago, IL, United States; Daiichi Sankyo, Tokyo, Japan; available in Japan, South Korea, Taiwan and Norway). They further stated that neither of the agents had a superior diagnostic ability over the other[27].

### Outcomes

A significant emphasis has been placed on researching the adjunctive role of CE-EUS in evaluating solid pancreatic masses. The result is a wealth of data that supports its use in assessing the pancreas and related pathologies[33]. Mei *et al*[35] affirmed this in a recent meta-analysis ( $n = 1497$ ) to evaluate the accuracy of CE-EUS in discriminating between benign and malignant pancreatic masses with a reported pooled sensitivity, specificity, and diagnostic odds ratio of 0.91, 0.86, and 69.50, respectively[35].

Another meta-analysis that included 1139 patients across 12 studies highlighted that both high and low MI techniques had a 94% sensitivity and 89% specificity in differentiating pancreatic adenocarcinoma from other pathologies, with an area under the receiver operating characteristic curve of 0.9732. Subgroup analysis by excluding the outliers provided a sensitivity and specificity of 93%[36].

Săftoiu *et al*[37] analyzed the diagnostic accuracy of combining CE-EUS and elastography to differentiate focal pancreatic masses and highlighted its influence in decision making when confronted with a negative EUS-FNB result with a strong clinical suspicion of malignancy. A similar study by the same authors assessed the "synergistic" performance of CE-EUS with EUS-EG in 50 patients with a negative FNA of pancreatic masses. The results determined 19 to be pancreatic adenocarcinoma and 31 to be pseudo-tumoral chronic pancreatitis. CE-EUS reported a specificity of 100% and an accuracy of 93% in the cohort of 25 patients where EUS-EG demonstrated high lesion stiffness, diagnosing malignancy[38].

Buxbaum *et al*[39], in a prospective tandem-controlled trial involving 101 cases of focal pancreatic lesions, concluded that CE-EUS increased the diagnostic yield compared to conventional B-mode EUS with an odds ratio of 7.8 (95%CI: 2.7-30.2). Ninety-one percent of lesions were correctly characterized in the validation cohort, with an improved yield compared to unenhanced EUS[39]. In a real-life clinical setting, we demonstrate its use in a case of a degenerated IPMN showing how its use allows differentiation of tumor vegetation from mucus within a cyst (Figure 4).

---

## AI

AI can level the playing field for endoscopists globally by making this highly sensitive and specific, but technically challenging, diagnostic tool we know as EUS more user-friendly and quicker to master.

The existing image enhancing techniques, CH-EUS and EUS-E, are available to the endoscopist currently as stand-alone software plug-ins. They require prior training before use with a low to moderate learning curve to master given that the user is already proficient with an echoendoscope.

The potential of AI is seen here in its ability to harness the diagnostic power of EUS while unifying all existing and future image-enhancing techniques "under one roof." This unifying software can aid the endoscopist by highlighting areas of concern while prompting suitable image-enhancing methods.

This added edge of diagnostic confidence can help overcome lesion ambiguity and improve lesion specificity, regardless of the years of prior endosonographic training.

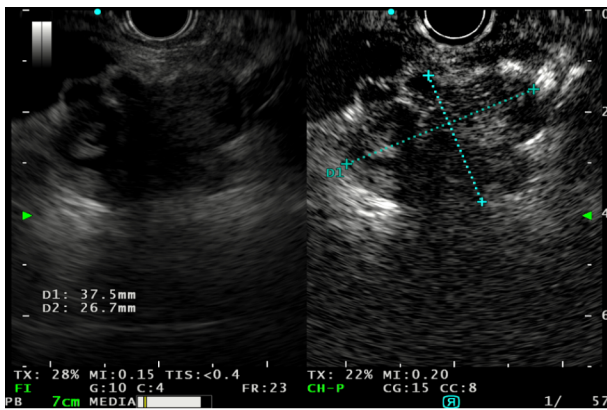
### Principle of AI

AI is a divaricate under the broader umbrella of computing methodology and information sciences. It utilizes autonomous properties from rapidly advancing technological developments in deep learning as a segue to mimic human behavior ultimately. Over the last decade, AI applications have quickly matured. Their iterations in the daily practice of various fields within medicine are expanding with success.

The development and training of computer-aided diagnosis (CAD) systems revolve around the aim of autonomously distinguishing features that the human eye and mind may unintentionally miss. Identifying and interpreting changes of varying subtleties, particularly in medical images, has been the high point of AI. The objectivity of a trained CAD system could potentially seek to overcome one of the most significant limitations of any physician or endoscopist: The lack of an intra- and inter-observer agreement. Suppose an AI system can distinguish between neoplastic and non-neoplastic lesions with near perfection after training, it would seem reasonable to imagine that the burden from pathological examinations may be considerably relieved very soon. Thus far, colonic adenoma detection and differentiation have gained tremendous attention from several CAD systems utilizing deep learning and Artificial Neural networks. Due to their promising results, these systems have gained popularity in day-to-day endoscopy usage[40-43].

### AI and EUS

The most common application of AI in EUS is creating machine learning architectures that extract EUS images and analyze them for their textures (boasting accuracy of up to 93%-94%) to create an artificial neural network that can ultimately serve as a clinical decision support tool. It can do one of 2 things: (1)



DOI: 10.3748/wjg.v28.i29.3814 Copyright ©The Author(s) 2022.

**Figure 4** Use of contrast-enhanced endoscopic ultrasound to study the evolution of a degenerated intraductal papillary mucinous neoplasm and the vegetations within, allowing differentiate between mucus and vegetations as only tumor vegetations will show inhomogeneous enhancement.

Using the station approach to familiarize the endoscopist with normal anatomy, as demonstrated by Kanno *et al*[44]; and (2) Non-invasively differentiating pancreatic parenchymal pathologies when EUS-FNB may not be clinically feasible or have a poor diagnostic yield in the case of cysts or AIP[40].

In 2008, two studies emerged providing the diagnostic ability of AI integrated EUS in reporting pancreatic diseases. Săftoiu *et al*[45] reported 68 cases in a prospective study using a neural network EUS to compare PDAC and chronic pancreatitis. The authors reported 95% accuracy in the system’s diagnostic ability. In the second study, Das *et al*[46] reviewed 319 images with a neural network system and performed a principal component analysis to compare acute and chronic pancreatitis, from pancreatic carcinoma. The study reported the area under the curve indicating the systems’ diagnostic ability to be 93%. In 2013, Zhu *et al*[47] studied 288 cases retrospectively with a support vector machine and reached an accuracy of 94%.

Additionally, Săftoiu *et al*[48], in a prospective multicenter study, reported 167 cases using a neural network system, reaching a diagnostic accuracy of 94%. Ozkan *et al*[49] reported an accuracy of 93% in reviewing 332 images in retrospect using a neural network. A deep learning architecture specific to EUS noteworthy of mentioning is one used to differentiate high-grade dysplasia *vs* malignancy for IPMN with an accuracy of 94%[42]. In a single-center retrospective study that trained a deep learning algorithm using 3970 still images, deep learning was superior to human ability in its diagnostic accuracy (95% *vs* 56%), proving an objective method such as this is more accurate in diagnosing malignancies of IPMN origin in comparison to conventional EUS features[42].

AI demonstrates its usefulness again in increasing diagnostic specificity using occlusion heatmap analysis to differentiate AIP from PDAC. The result is overcoming a delay in diagnosis, initiating immunosuppressive or chemoradiotherapy early, and preventing unwarranted resections (90% sensitive, 85% specific)[50]. It is worth mentioning that these studies use a cross-validation method with an internal control check, thus inflating the actuality of the diagnostic accuracy. In its applications to actual EUS fine-needle biopsy histopathological samples, AI was able to bring diagnostic clarity to difficult-to-analyze samples with an accuracy of 94.1% despite cellular paucity and contamination.

In centers with a lack of dedicated GI pathologists, AI software can quickly close this gap of diagnostic delay and eliminate repeat sampling at second or third centers[11]. One setback of AI is the black-box phenomenon, which can cause judgment errors without an explanatory basis. That said, a trained convolutional neural network model with extracted visual features from various pancreatic diseases, namely chronic pseudo-tumoral pancreatitis, NET, and PDAC, can accurately produce a real-time diagnosis[51].

## SUMMARY RECOMMENDATIONS

For a suspected pancreatic mass, we propose utilizing both EUS-E and CE-EUS to augment conventional B-mode imaging (Figure 5).

Their advantages in defining nodules and ambiguous ROIs allow FNA/FNB sampling precision, making them crucial adjuncts in day-to-day practice, whether for first encounters or follow-up visits.

Validation studies are still underway to evaluate promising non-contrast-based high-definition imaging modalities. The modalities are in-built into the echo processor for ease of microvasculature study. They carry great potential in supplementing and possibly surrogating UCAs in conditions, such as pregnancy or compromised cardiopulmonary status[52]. However, until then, EUS-E and CE-EUS

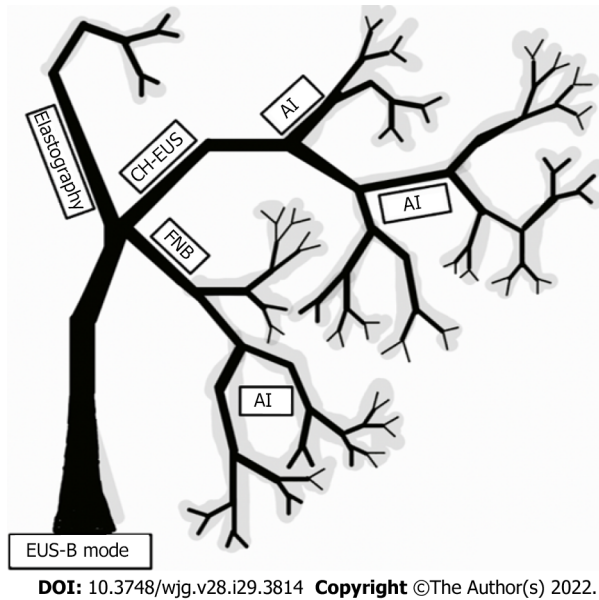


**Figure 5** Graphical representation of existing diagnostic applications to endoscopic ultrasound imaging in the form of a fractal tree, fractal analysis with artificial intelligence being the possible future of enhanced endoscopic ultrasound imaging. AI: Artificial intelligence; CH-EUS: Contrast-enhanced harmonic endoscopic ultrasound; FNB: Fine needle biopsy.

coupled with B-mode imaging will remain the choice stratagem in improving the early detection of pancreatic cancer.

## CONCLUSION

In the EUS world of greys, colors emerged from elastography and patterns from contrast use, improving the overall accuracy of pancreatic mass differentiation. AI could be the rainbow that bridges us to a more precise diagnosis.

## FOOTNOTES

**Author contributions:** Spadaccini M provided the outline; Koleth G with Spadaccini M performed most of the writing and equally contributed to this paper; Emmanuel J wrote on contrast-enhanced endoscopic ultrasound; Carrara S provided valuable oversight, all EUS pictures, and concluded the manuscript; Grizzi F provided the picture for fractal analysis; Khalaf K, Colombo M, Mangiavillano B, Fugazza A, Anderloni A, Facciorusso A, and Repici A provided input in writing the paper.

**Conflict-of-interest statement:** All the authors report no relevant conflicts of interest for this article.

**Open-Access:** This article is an open-access article that was selected by an in-house editor and fully peer-reviewed by external reviewers. It is distributed in accordance with the Creative Commons Attribution NonCommercial (CC BY-NC 4.0) license, which permits others to distribute, remix, adapt, build upon this work non-commercially, and license their derivative works on different terms, provided the original work is properly cited and the use is non-commercial. See: <https://creativecommons.org/licenses/by-nc/4.0/>

**Country/Territory of origin:** Italy

**ORCID number:** Marco Spadaccini 0000-0003-3909-9012; Glenn Koleth 0000-0002-2939-6876; James Emmanuel 0000-0001-7154-461X; Kareem Khalaf 0000-0002-5534-7533; Antonio Facciorusso 0000-0002-2107-2156; Fabio Grizzi 0000-0003-0925-742X; Cesare Hassan 0000-0001-7167-1459; Matteo Colombo 0000-0003-0715-8233; Benedetto Mangiavillano 0000-0003-0611-7448; Alessandro Fugazza 0000-0003-0485-4903; Andrea Anderloni 0000-0002-1021-0031; Silvia Carrara 0000-0003-4206-9463; Alessandro Repici 0000-0002-1621-6450.

**S-Editor:** Fan JR

**L-Editor:** Filipodia

**P-Editor:** Fan JR

## REFERENCES

- 1 **McGuigan A**, Kelly P, Turkington RC, Jones C, Coleman HG, McCain RS. Pancreatic cancer: A review of clinical diagnosis, epidemiology, treatment and outcomes. *World J Gastroenterol* 2018; **24**: 4846-4861 [PMID: 30487695 DOI: 10.3748/wjg.v24.i43.4846]
- 2 **Egawa S**, Toma H, Ohigashi H, Okusaka T, Nakao A, Hatori T, Maguchi H, Yanagisawa A, Tanaka M. Japan Pancreatic Cancer Registry; 30th year anniversary: Japan Pancreas Society. *Pancreas* 2012; **41**: 985-992 [PMID: 22750974 DOI: 10.1097/MPA.0b013e318258055c]
- 3 **Kitano M**, Yoshida T, Itonaga M, Tamura T, Hatamaru K, Yamashita Y. Impact of endoscopic ultrasonography on diagnosis of pancreatic cancer. *J Gastroenterol* 2019; **54**: 19-32 [PMID: 30406288 DOI: 10.1007/s00535-018-1519-2]
- 4 **Müller MF**, Meyenberger C, Bertschinger P, Schaer R, Marincek B. Pancreatic tumors: evaluation with endoscopic US, CT, and MR imaging. *Radiology* 1994; **190**: 745-751 [PMID: 8115622 DOI: 10.1148/radiology.190.3.8115622]
- 5 **Dietrich CF**, Ignee A, Frey H. Contrast-enhanced endoscopic ultrasound with low mechanical index: a new technique. *Z Gastroenterol* 2005; **43**: 1219-1223 [PMID: 16267707 DOI: 10.1055/s-2005-858662]
- 6 **Dietrich CF**, Sahai AV, D'Onofrio M, Will U, Arcidiacono PG, Petrone MC, Hocke M, Braden B, Burmester E, Möller K, Săftoiu A, Ignee A, Cui XW, Iordache S, Potthoff A, Iglesias-Garcia J, Fusaroli P, Dong Y, Jenssen C. Differential diagnosis of small solid pancreatic lesions. *Gastrointest Endosc* 2016; **84**: 933-940 [PMID: 27155592 DOI: 10.1016/j.gie.2016.04.034]
- 7 **Ignee A**, Jenssen C, Arcidiacono PG, Hocke M, Möller K, Săftoiu A, Will U, Fusaroli P, Iglesias-Garcia J, Ponnudurai R, Petrone MC, Braden B, Burmester E, Dong Y, Atkinson NS, Dietrich CF. Endoscopic ultrasound elastography of small solid pancreatic lesions: a multicenter study. *Endoscopy* 2018; **50**: 1071-1079 [PMID: 29689572 DOI: 10.1055/a-0588-4941]
- 8 **Rawla P**, Sunkara T, Gaduputi V. Epidemiology of Pancreatic Cancer: Global Trends, Etiology and Risk Factors. *World J Oncol* 2019; **10**: 10-27 [PMID: 30834048 DOI: 10.14740/wjon1166]
- 9 **Elfanagely Y**, Tse CS, Rich H, Hyder SM. Learning curves for EUS: single operators, endoscopy teams, and institutions. *Gastrointest Endosc* 2021; **93**: 989 [PMID: 33741097 DOI: 10.1016/j.gie.2020.10.031]
- 10 **Gonzalez JM**, Cohen J, Gromski MA, Saito K, Loundou A, Matthes K. Learning curve for endoscopic ultrasound-guided fine-needle aspiration (EUS-FNA) of pancreatic lesions in a novel ex-vivo simulation model. *Endosc Int Open* 2016; **4**: E1286-E1291 [PMID: 27995190 DOI: 10.1055/s-0042-118176]
- 11 **Tonozuka R**, Mukai S, Itoi T. The Role of Artificial Intelligence in Endoscopic Ultrasound for Pancreatic Disorders. *Diagnostics (Basel)* 2020; **11** [PMID: 33374181 DOI: 10.3390/diagnostics11010018]
- 12 **Faruk T**, Islam MK, Arefin S, Haq MZ. The Journey of Elastography: Background, Current Status, and Future Possibilities in Breast Cancer Diagnosis. *Clin Breast Cancer* 2015; **15**: 313-324 [PMID: 25858446 DOI: 10.1016/j.clbc.2015.01.002]
- 13 **Ohno E**, Kawashima H, Ishikawa T, Iida T, Suzuki H, Uetsuki K, Yashika J, Yamada K, Yoshikawa M, Gibo N, Aoki T, Kataoka K, Mori H, Yamamura T, Furukawa K, Nakamura M, Hirooka Y, Fujishiro M. Diagnostic performance of endoscopic ultrasonography-guided elastography for solid pancreatic lesions: Shear-wave measurements vs strain elastography with histogram analysis. *Dig Endosc* 2021; **33**: 629-638 [PMID: 32662150 DOI: 10.1111/den.13791]
- 14 **Sigrist RMS**, Liau J, Kaffas AE, Chammas MC, Willmann JK. Ultrasound Elastography: Review of Techniques and Clinical Applications. *Theranostics* 2017; **7**: 1303-1329 [PMID: 28435467 DOI: 10.7150/thno.18650]
- 15 **Giovannini M**. Endoscopic ultrasound elastography. *Pancreatol* 2011; **11** Suppl 2: 34-39 [PMID: 21464585 DOI: 10.1159/000323496]
- 16 **Giovannini M**. Contrast-enhanced endoscopic ultrasound and elastosonoendoscopy. *Best Pract Res Clin Gastroenterol* 2009; **23**: 767-779 [PMID: 19744639 DOI: 10.1016/j.bpg.2009.05.004]
- 17 **Pei Q**, Zou X, Zhang X, Chen M, Guo Y, Luo H. Diagnostic value of EUS elastography in differentiation of benign and malignant solid pancreatic masses: a meta-analysis. *Pancreatol* 2012; **12**: 402-408 [PMID: 23127527 DOI: 10.1016/j.pan.2012.07.013]
- 18 **Ying L**, Lin X, Xie ZL, Hu YP, Tang KF, Shi KQ. Clinical utility of endoscopic ultrasound elastography for identification of malignant pancreatic masses: a meta-analysis. *J Gastroenterol Hepatol* 2013; **28**: 1434-1443 [PMID: 23731128 DOI: 10.1111/jgh.12292]
- 19 **Lu Y**, Chen L, Li C, Chen H, Chen J. Diagnostic utility of endoscopic ultrasonography-elastography in the evaluation of solid pancreatic masses: a meta-analysis and systematic review. *Med Ultrason* 2017; **19**: 150-158 [PMID: 28440348 DOI: 10.11152/mu-987]
- 20 **Cosgrove D**, Piscaglia F, Bamber J, Bojunga J, Correas JM, Gilja OH, Klauser AS, Sporea I, Calliada F, Cantisani V, D'Onofrio M, Drakonaki EE, Fink M, Friedrich-Rust M, Fromageau J, Havre RF, Jenssen C, Ohlinger R, Săftoiu A, Schaefer F, Dietrich CF; EFSUMB. EFSUMB guidelines and recommendations on the clinical use of ultrasound elastography. Part 2: Clinical applications. *Ultraschall Med* 2013; **34**: 238-253 [PMID: 23605169 DOI: 10.1055/s-0033-1335375]
- 21 **Carrara S**, Di Leo M, Grizzi F, Correale L, Rahal D, Anderloni A, Auriemma F, Fugazza A, Preatoni P, Maselli R, Hassan C, Finati E, Mangiavillano B, Repici A. EUS elastography (strain ratio) and fractal-based quantitative analysis for the diagnosis of solid pancreatic lesions. *Gastrointest Endosc* 2018; **87**: 1464-1473 [PMID: 29329992 DOI: 10.1016/j.gie.2017.12.031]
- 22 **Hirche TO**, Ignee A, Barreiros AP, Schreiber-Dietrich D, Jungblut S, Ott M, Hirche H, Dietrich CF. Indications and limitations of endoscopic ultrasound elastography for evaluation of focal pancreatic lesions. *Endoscopy* 2008; **40**: 910-917 [PMID: 19009483 DOI: 10.1055/s-2008-107726]
- 23 **Kato T**, Tsukamoto Y, Naitoh Y, Hirooka Y, Furukawa T, Hayakawa T. Ultrasonographic and endoscopic ultrasonographic angiography in pancreatic mass lesions. *Acta Radiol* 1995; **36**: 381-387 [PMID: 7619616]
- 24 **Hirooka Y**, Naitoh Y, Goto H, Ito A, Taki T, Hayakawa T. Usefulness of contrast-enhanced endoscopic ultrasonography with intravenous injection of sonicated serum albumin. *Gastrointest Endosc* 1997; **46**: 166-169 [PMID: 9283869 DOI: 10.1016/s0016-5107(97)70067-1]

- 25 **Mohamed RM**, Yan BM. Contrast enhanced endoscopic ultrasound: More than just a fancy Doppler. *World J Gastrointest Endosc* 2010; **2**: 237-243 [PMID: [21160613](#) DOI: [10.4253/wjge.v2.i7.237](#)]
- 26 **Hocke M**, Dietrich CF. Advanced EUS Imaging for Pancreatic Diseases: CE-EUS (Low-MI, High-MI) and Real-Time Elastography, 3D. *Video J Encyc GI Endos* 2013; **1**: 537-539 [DOI: [10.1016/s2212-0971\(13\)70235-8](#)]
- 27 **Kitano M**, Yamashita Y, Kamata K, Ang TL, Imazu H, Ohno E, Hirooka Y, Fusaroli P, Seo DW, Napoléon B, Teoh AYB, Kim TH, Dietrich CF, Wang HP, Kudo M; Working group for the International Consensus Guidelines for Contrast-Enhanced Harmonic Endoscopic Ultrasound. The Asian Federation of Societies for Ultrasound in Medicine and Biology (AFSUMB) Guidelines for Contrast-Enhanced Endoscopic Ultrasound. *Ultrasound Med Biol* 2021; **47**: 1433-1447 [PMID: [33653627](#) DOI: [10.1016/j.ultrasmedbio.2021.01.030](#)]
- 28 **Anvari A**, Forsberg F, Samir AE. A Primer on the Physical Principles of Tissue Harmonic Imaging. *Radiographics* 2015; **35**: 1955-1964 [PMID: [26562232](#) DOI: [10.1148/rg.2015140338](#)]
- 29 **Alvarez-Sánchez MV**, Napoléon B. Contrast-enhanced harmonic endoscopic ultrasound imaging: basic principles, present situation and future perspectives. *World J Gastroenterol* 2014; **20**: 15549-15563 [PMID: [25400439](#) DOI: [10.3748/wjg.v20.i42.15549](#)]
- 30 **Ohno E**, Kawashima H, Hashimoto S, Goto H, Hirooka Y. Current status of tissue harmonic imaging in endoscopic ultrasonography (EUS) and EUS-elastography in pancreatobiliary diseases. *Dig Endosc* 2015; **27** Suppl 1: 68-73 [PMID: [25630752](#) DOI: [10.1111/den.12433](#)]
- 31 **Kitano M**, Sakamoto H, Matsui U, Ito Y, Maekawa K, von Schrenck T, Kudo M. A novel perfusion imaging technique of the pancreas: contrast-enhanced harmonic EUS (with video). *Gastrointest Endosc* 2008; **67**: 141-150 [PMID: [18155437](#) DOI: [10.1016/j.gie.2007.07.045](#)]
- 32 **Reddy NK**, Ionciă AM, Săftoiu A, Vilmann P, Bhutani MS. Contrast-enhanced endoscopic ultrasonography. *World J Gastroenterol* 2011; **17**: 42-48 [PMID: [21218082](#) DOI: [10.3748/wjg.v17.i1.42](#)]
- 33 **Săftoiu A**, Vilmann P, Bhutani MS. The role of contrast-enhanced endoscopic ultrasound in pancreatic adenocarcinoma. *Endosc Ultrasound* 2016; **5**: 368-372 [PMID: [28000627](#) DOI: [10.4103/2303-9027.190932](#)]
- 34 **D'Onofrio M**, Biagioli E, Gerardi C, Canestrini S, Rulli E, Crosara S, De Robertis R, Floriani I. Diagnostic performance of contrast-enhanced ultrasound (CEUS) and contrast-enhanced endoscopic ultrasound (ECEUS) for the differentiation of pancreatic lesions: a systematic review and meta-analysis. *Ultraschall Med* 2014; **35**: 515-521 [PMID: [25226455](#) DOI: [10.1055/s-0034-1385068](#)]
- 35 **Mei S**, Wang M, Sun L. Contrast-Enhanced EUS for Differential Diagnosis of Pancreatic Masses: A Meta-Analysis. *Gastroenterol Res Pract* 2019; **2019**: 1670183 [PMID: [30962802](#) DOI: [10.1155/2019/1670183](#)]
- 36 **Gong TT**, Hu DM, Zhu Q. Contrast-enhanced EUS for differential diagnosis of pancreatic mass lesions: a meta-analysis. *Gastrointest Endosc* 2012; **76**: 301-309 [PMID: [22703697](#) DOI: [10.1016/j.gie.2012.02.051](#)]
- 37 **Săftoiu A**, Iordache SA, Gheonea DI, Popescu C, Maloş A, Gorunescu F, Ciurea T, Iordache A, Popescu GL, Manea CT. Combined contrast-enhanced power Doppler and real-time sonoelastography performed during EUS, used in the differential diagnosis of focal pancreatic masses (with videos). *Gastrointest Endosc* 2010; **72**: 739-747 [PMID: [20674916](#) DOI: [10.1016/j.gie.2010.02.056](#)]
- 38 **Iordache S**, Costache MI, Popescu CF, Streba CT, Cazacu S, Săftoiu A. Clinical impact of EUS elastography followed by contrast-enhanced EUS in patients with focal pancreatic masses and negative EUS-guided FNA. *Med Ultrason* 2016; **18**: 18-24 [PMID: [26962549](#) DOI: [10.11152/mu.2013.2066.181.ich](#)]
- 39 **Buxbaum J**, Ko C, Varghese N, Lee A, Sahakian A, King K, Serna J, Lee H, Tchelepi H, Van Dam J, Duddalwar V. Qualitative and Quantitative Contrast-enhanced Endoscopic Ultrasound Improves Evaluation of Focal Pancreatic Lesions. *Clin Gastroenterol Hepatol* 2020; **18**: 917-925.e4 [PMID: [31499247](#) DOI: [10.1016/j.cgh.2019.08.054](#)]
- 40 **Kuwahara T**, Hara K, Mizuno N, Haba S, Okuno N, Koda H, Miyano A, Fumihara D. Current status of artificial intelligence analysis for endoscopic ultrasonography. *Dig Endosc* 2021; **33**: 298-305 [PMID: [33098123](#) DOI: [10.1111/den.13880](#)]
- 41 **Murakami D**, Yamato M, Arai M, Nishino T. Artificial intelligence in colonoscopy. *Lancet Gastroenterol Hepatol* 2021; **6**: 984-985 [PMID: [34774156](#) DOI: [10.1016/S2468-1253\(21\)00379-4](#)]
- 42 **Marya NB**, Powers PD, Chari ST, Gleeson FC, Leggett CL, Abu Dayyeh BK, Chandrasekhara V, Iyer PG, Majumder S, Pearson RK, Petersen BT, Rajan E, Sawas T, Storm AC, Vege SS, Chen S, Long Z, Hough DM, Mara K, Levy MJ. Utilisation of artificial intelligence for the development of an EUS-convolutional neural network model trained to enhance the diagnosis of autoimmune pancreatitis. *Gut* 2021; **70**: 1335-1344 [PMID: [33028668](#) DOI: [10.1136/gutjnl-2020-322821](#)]
- 43 **Zhang J**, Zhu L, Yao L, Ding X, Chen D, Wu H, Lu Z, Zhou W, Zhang L, An P, Xu B, Tan W, Hu S, Cheng F, Yu H. Deep learning-based pancreas segmentation and station recognition system in EUS: development and validation of a useful training tool (with video). *Gastrointest Endosc* 2020; **92**: 874-885.e3 [PMID: [32387499](#) DOI: [10.1016/j.gie.2020.04.071](#)]
- 44 **Kanno A**, Masamune A, Fujishima F, Iwashita T, Kodama Y, Katanuma A, Ohara H, Kitano M, Inoue H, Itoi T, Mizuno N, Miyakawa H, Mikata R, Irisawa A, Sato S, Notohara K, Shimosegawa T. Diagnosis of autoimmune pancreatitis by EUS-guided FNA using a 22-gauge needle: a prospective multicenter study. *Gastrointest Endosc* 2016; **84**: 797-804.e1 [PMID: [27068878](#) DOI: [10.1016/j.gie.2016.03.1511](#)]
- 45 **Săftoiu A**, Vilmann P, Gorunescu F, Gheonea DI, Gorunescu M, Ciurea T, Popescu GL, Iordache A, Hassan H, Iordache S. Neural network analysis of dynamic sequences of EUS elastography used for the differential diagnosis of chronic pancreatitis and pancreatic cancer. *Gastrointest Endosc* 2008; **68**: 1086-1094 [PMID: [18656186](#) DOI: [10.1016/j.gie.2008.04.031](#)]
- 46 **Das A**, Nguyen CC, Li F, Li B. Digital image analysis of EUS images accurately differentiates pancreatic cancer from chronic pancreatitis and normal tissue. *Gastrointest Endosc* 2008; **67**: 861-867 [PMID: [18179797](#) DOI: [10.1016/j.gie.2007.08.036](#)]
- 47 **Zhu M**, Xu C, Yu J, Wu Y, Li C, Zhang M, Jin Z, Li Z. Differentiation of pancreatic cancer and chronic pancreatitis using computer-aided diagnosis of endoscopic ultrasound (EUS) images: a diagnostic test. *PLoS One* 2013; **8**: e63820 [PMID: [23704940](#) DOI: [10.1371/journal.pone.0063820](#)]
- 48 **Săftoiu A**, Vilmann P, Dietrich CF, Iglesias-García J, Hocke M, Seicean A, Ignee A, Hassan H, Streba CT, Ionciă AM,

- Gheonea DI, Ciurea T. Quantitative contrast-enhanced harmonic EUS in differential diagnosis of focal pancreatic masses (with videos). *Gastrointest Endosc* 2015; **82**: 59-69 [PMID: 25792386 DOI: 10.1016/j.gie.2014.11.040]
- 49 **Ozkan M**, Cakiroglu M, Kocaman O, Kurt M, Yilmaz B, Can G, Korkmaz U, Dandil E, Eksi Z. Age-based computer-aided diagnosis approach for pancreatic cancer on endoscopic ultrasound images. *Endosc Ultrasound* 2016; **5**: 101-107 [PMID: 27080608 DOI: 10.4103/2303-9027.180473]
- 50 **Naito Y**, Tsuneki M, Fukushima N, Koga Y, Higashi M, Notohara K, Aishima S, Ohike N, Tajiri T, Yamaguchi H, Fukumura Y, Kojima M, Hirabayashi K, Hamada Y, Norose T, Kai K, Omori Y, Sukeda A, Noguchi H, Uchino K, Itakura J, Okabe Y, Yamada Y, Akiba J, Kanavati F, Oda Y, Furukawa T, Yano H. A deep learning model to detect pancreatic ductal adenocarcinoma on endoscopic ultrasound-guided fine-needle biopsy. *Sci Rep* 2021; **11**: 8454 [PMID: 33875703 DOI: 10.1038/s41598-021-87748-0]
- 51 **Udriștoiu AL**, Cazacu IM, Gruionu LG, Gruionu G, Iacob AV, Burtea DE, Ungureanu BS, Costache MI, Constantin A, Popescu CF, Udriștoiu Ș, Săftoiu A. Real-time computer-aided diagnosis of focal pancreatic masses from endoscopic ultrasound imaging based on a hybrid convolutional and long short-term memory neural network model. *PLoS One* 2021; **16**: e0251701 [PMID: 34181680 DOI: 10.1371/journal.pone.0251701]
- 52 **Hwang JS**, Seo DW, So H, Ko SW, Joo HD, Oh D, Song TJ, Park DH, Lee SS, Lee SK, Kim MH. Clinical utility of directional eFLOW compared with contrast-enhanced harmonic endoscopic ultrasound for assessing the vascularity of pancreatic and peripancreatic masses. *Pancreatology* 2022; **22**: 130-135 [PMID: 34753658 DOI: 10.1016/j.pan.2021.11.002]

## Basic Study

## Qingyi decoction attenuates intestinal epithelial cell injury via the calcineurin/nuclear factor of activated T-cells pathway

Guan-Yu Wang, Dong Shang, Gui-Xin Zhang, Hui-Yi Song, Nan Jiang, Huan-Huan Liu, Hai-Long Chen

**Specialty type:** Gastroenterology and hepatology**Provenance and peer review:**

Unsolicited article; Externally peer reviewed.

**Peer-review model:** Single blind**Peer-review report's scientific quality classification**Grade A (Excellent): 0  
Grade B (Very good): B, B  
Grade C (Good): C  
Grade D (Fair): D  
Grade E (Poor): 0**P-Reviewer:** Exbrayat JM, France; Ma W, China; Surbatovic M, Serbia**Received:** September 18, 2021**Peer-review started:** September 18, 2021**First decision:** December 4, 2021**Revised:** December 15, 2021**Accepted:** July 8, 2022**Article in press:** July 8, 2022**Published online:** August 7, 2022**Guan-Yu Wang, Dong Shang, Gui-Xin Zhang, Hai-Long Chen**, Department of General Surgery, The First Affiliated Hospital of Dalian Medical University, Dalian 116011, Liaoning Province, China**Guan-Yu Wang, Dong Shang, Gui-Xin Zhang, Nan Jiang, Huan-Huan Liu, Hai-Long Chen**, Institute of Integrative Medicine of Dalian Medical University, Dalian 116044, Liaoning Province, China**Hui-Yi Song**, Laboratory of Integrative Medicine, The First Affiliated Hospital of Dalian Medical University, Dalian 116011, Liaoning Province, China**Corresponding author:** Hai-Long Chen, PhD, Chief Physician, Department of General Surgery, The First Affiliated Hospital of Dalian Medical University, No. 222 Zhongshan Road, Dalian 116011, Liaoning Province, China. [hailongchen2014@yeah.net](mailto:hailongchen2014@yeah.net)**Abstract****BACKGROUND**

Recent studies have demonstrated that dysfunction of the intestinal barrier is a significant contributing factor to the development of severe acute pancreatitis (SAP). A stable intestinal mucosa barrier functions as a major anatomic and functional barrier, owing to the balance between intestinal epithelial cell (IEC) proliferation and apoptosis. There is some evidence that calcium overload may trigger IEC apoptosis and that calcineurin (CaN)/nuclear factor of activated T-cells (NFAT) signaling might play an important role in calcium-mediated apoptosis.

**AIM**

To investigate the potential mechanisms underlying the therapeutic effect of Qingyi decoction (QYD) in SAP.

**METHODS**

A rat model of SAP was created *via* retrograde infusion of sodium deoxycholate. Serum levels of amylase, tumor necrosis factor (TNF- $\alpha$ ), interleukin (IL)-6, D-lactic acid, and diamine oxidase (DAO); histological changes; and apoptosis of IECs were examined in rats with or without QYD treatment. The expression of the two subunits of CaN and NFAT in intestinal tissue was measured *via* quantitative real-time polymerase chain reaction and western blotting. For *in vitro* studies, Caco-2 cells were treated with lipopolysaccharide (LPS) and QYD serum, and then cell

viability and intracellular calcium levels were detected.

## RESULTS

Retrograde infusion of sodium deoxycholate increased the severity of pancreatic and intestinal pathology and the levels of serum amylase, TNF- $\alpha$ , and IL-6. Both the indicators of intestinal mucosa damage (D-lactic acid and DAO) and the levels of IEC apoptosis were elevated in the SAP group. QYD treatment reduced the serum levels of amylase, TNF- $\alpha$ , IL-6, D-lactic acid, and DAO and attenuated the histological findings. IEC apoptosis associated with SAP was ameliorated under QYD treatment. In addition, the protein expression levels of the two subunits of CaN were remarkably elevated in the SAP group, and the NFATc3 gene was significantly upregulated at both the transcript and protein levels in the SAP group compared with the control group. QYD significantly restrained CaN and NFATc3 gene expression in the intestine, which was upregulated in the SAP group. Furthermore, QYD serum significantly decreased the LPS-induced elevation in intracellular free Ca<sup>2+</sup> levels and inhibited cell death.

## CONCLUSION

QYD can exert protective effects against intestinal mucosa damage caused by SAP and the protective effects are mediated, at least partially, by restraining IEC apoptosis *via* the CaN/NFATc3 pathway.

**Key Words:** Severe acute pancreatitis; Intestinal epithelial cell; Apoptosis; Calcineurin/nuclear factor of activated T-cells pathway; Qingyi decoction

©The Author(s) 2022. Published by Baishideng Publishing Group Inc. All rights reserved.

**Core Tip:** This manuscript investigated the role of the calcineurin (CaN)/nuclear factor of activated T-cells (NFATc3) pathway in the apoptosis of intestinal epithelial cells (IECs) in severe acute pancreatitis (SAP) and the potential mechanisms underlying the therapeutic effect of Qingyi decoction (QYD). QYD significantly restrained CaN and NFATc3 gene expression in the intestine, ameliorated IEC apoptosis associated with SAP, and decreased the lipopolysaccharide-induced elevation in intracellular free Ca<sup>2+</sup> levels and cell death. These findings suggest that the protective effects of QYD might be mediated, at least partially, by downregulating IEC apoptosis *via* the CaN/NFATc3 pathway.

**Citation:** Wang GY, Shang D, Zhang GX, Song HY, Jiang N, Liu HH, Chen HL. Qingyi decoction attenuates intestinal epithelial cell injury *via* the calcineurin/nuclear factor of activated T-cells pathway. *World J Gastroenterol* 2022; 28(29): 3825-3837

**URL:** <https://www.wjgnet.com/1007-9327/full/v28/i29/3825.htm>

**DOI:** <https://dx.doi.org/10.3748/wjg.v28.i29.3825>

## INTRODUCTION

Severe acute pancreatitis (SAP) is a severe acute abdominal disease characterized by high morbidity and mortality that can occur as a consequence of systemic inflammatory response syndrome (SIRS) and multiple organ dysfunction syndrome (MODS)[1]. A considerable amount of literature has been published on SAP. These studies have demonstrated that dysfunction of the intestinal barrier is a significant contributing factor to the development of SAP. Disruption of the intestinal barrier can give rise to gut bacteria and endotoxin translocation, thus creating secondary infections, SIRS, and MODS, leading to SAP[2]. A stable intestinal mucosa barrier functions as a major anatomic and functional barrier, owing to the balance between intestinal epithelial cell (IEC) proliferation and apoptosis. Recent research has revealed that IEC apoptosis plays an essential role in the development of SAP, and increased IEC apoptosis has been confirmed to contribute to intestinal injury, mucosal atrophy, bacterial translocation, and barrier dysfunction in SAP[3-5].

As a ubiquitous second messenger, Ca<sup>2+</sup> has a significant impact on a variety of cellular processes in nearly all cell types. Calcineurin (CaN), a unique calcium-activated serine/threonine phosphatase, is a dominant factor in calcium-dependent signal transduction pathways. Nuclear factor of activated T-cells (NFAT) is a substrate phosphorylated by CaN, that is completely dependent on Ca<sup>2+</sup>/CaN signaling; thus, NFAT is remarkably responsive to intracellular Ca<sup>2+</sup> oscillations[6]. There is some evidence that calcium overload may trigger IEC apoptosis and that CaN/NFAT signaling might play an important role in calcium-mediated apoptosis[7,8].

Qingyidecoction (QYD), a Chinese herbal medicine consisting of Radix Bupleuri (Chaihu, *Bupleurum scorzonerifolium* Willd.), Scutellariae Radix (Huangqin, *Scutellaria baicalensis* Georgi.), Aucklandiae Radix (Muxiang, *Aucklandia lappa* Decne.), Rhizoma Corydalis (Yanhusuo, *Corydalis acropteryx* Fedde), Coptidis Rhizoma (Huanglian, *Coptis chinensis* Franch.), Radix Paeoniae Alba (Baishao, *Paeonia lactiflora* Pall.), Rhei Radix Et Rhizoma (Dahuang, *Rheum palmatum* L.) and Natrii Sulfas (Mangxiao, *Mirabilite*) has been widely utilized for several decades in the treatment of acute pancreatitis in China[9]. QYD, as an organic combination of many effective components, plays a multitarget role in acute pancreatitis treatment through multiple pathways, including protecting the intestinal barrier. The efficacy of QYD has been demonstrated to involve its ability to moderate endotoxin generation, restrict excessive neutrophil activation, minimize the release of inflammatory cytokines, and inhibit IEC apoptosis[10]. The present study aimed to investigate the role of the CaN/NFATc3 pathway in the apoptosis of IECs in SAP and explore the potential mechanisms underlying the therapeutic effect of QYD.

## MATERIALS AND METHODS

### **Animal preparation and experimental protocols**

Male Sprague-Dawley (SD) rats, 180-220 g, were obtained from the specific-pathogen-free Animal Center of Dalian Medical University. This study was approved by the Ethics Committee of Dalian Medical University. Thirty male SD rats were randomly divided into an SAP group, a QYD treatment group, and a control group, with ten rats per group. The SAP model was established using a method previously described[9]. The rats in the QYD group were gavaged with three doses of QYD (10 mL/kg body weight/dose, the First Affiliated Hospital of Dalian Medical University, Dalian, China) 0.5 h before and 6 and 12 h after surgery. The rats in the control group received only sham surgery[9]. The rats were anesthetized with 10% chloralhydrate *via* intraperitoneal injection at 3 mL per kg bodyweight 24 h post operation. Abdominal aorta blood samples and tissue samples were collected immediately.

### **Measurement of serum amylase, interleukin-6, tumor necrosis factor- $\alpha$ , D-lactic acid, and diamine oxidase**

Serum amylase was detected using a spectrophotometric method with a commercial kit (Jiancheng, Nanjing, China). Briefly, 0.5 mL of starch reagent and 0.10 mL of serum samples were added to a 5 mL graduated tube. After incubating for 7.5 min at 37 °C, 0.5 mL of iodine reagent and 3.0 mL water were added immediately. The absorbance was measured at 660 nm. Enzyme-linked immunosorbent assay (ELISA) kits for tumor necrosis factor (TNF- $\alpha$ ) (Lengton, Shanghai, China), D-lactic acid (Goybio, Shanghai, China), diamine oxidase (DAO) (Jiancheng, Nanjing, China), interleukin (IL)-6 (Lengton, Shanghai, China) were used to evaluate the levels in rat serum according to the manufacturer's instructions.

### **Histological examination**

Pancreatic and intestinal tissues were fixed in 10% formaldehyde. After dehydration in gradient alcohol and transparentizing in xylene, the tissues were embedded in paraffin and cut into 5  $\mu$ m thick slices. The slices were stained with hematoxylin and eosin for histological examination. The tissues were scored under an optical microscope (Leica, Solms, Germany) by a pathologist blinded to the experimental design. Five histopathological parameters (edema, inflammatory infiltration, hemorrhage, and acinar necrosis) of the pancreatic tissue were evaluated, each on a scale of 0-4 using a previously described method[11]. Mucosal injury, inflammatory infiltration, and hemorrhage were graded, each on a scale of 0-5, using a method described in a previous article to assess intestinal tissue[12].

### **Apoptosis detection**

Fixed rat intestinal sections with 10% formaldehyde were deparaffinized in xylene and rehydrated through a graded ethanol series. A terminal deoxynucleotidyl transferase-mediated dUTP nick-end labeling (TUNEL) assay kit (Keygen, Nanjing, China) was applied to assess apoptosis in intestinal tissue. Briefly, rat intestinal sections were treated with 50  $\mu$ L of the TUNEL reaction mixture and then incubated at 37 °C for 60 min. After rinsing with phosphate buffer solution, tissue sections were stained with 4',6-diamidino-2-phenylindole (DAPI) and observed with fluorescence microscopy.

### **Immunofluorescence analysis**

For immunofluorescence analysis, intestinal sections were incubated in a xylol-ethanol gradient to remove the paraffin. The slides were incubated with primary antibody against NFATc3 (Santa Cruz, CA, United States) and subsequently incubated with Alexa Fluor goat anti-rabbit immunoglobulin G (Life Technologies), and then observed using fluorescence microscopy following staining of the nuclei with DAPI (Sigma-Aldrich, St. Louis, MO). The specificity of the signals was monitored by blank staining without primary antibodies.

### Western blot analysis

Western blotting was performed as previously described[13]. Total protein from intestinal tissue was extracted with a protein extraction kit (KeyGen, Nanjing, China). Protein was separated by sodium dodecyl sulfate-polyacrylamide gel electrophoresis and then transferred onto a nitrocellulose membrane. After nonspecific binding was blocked, the membranes were incubated with primary antibodies against calcineurin A (CnA, 1:2000, Abcam, United Kingdom), calcineurin B (CnB, 1:500, Abcam, United Kingdom), and  $\beta$ -actin (1:1000). Immunoreactive proteins were visualized using enhanced chemiluminescence detection (Bioworld Technology, Nanjing, China). ImageJ software was used for statistical analyses of the band intensities normalized to  $\beta$ -actin.

### Quantitative real-time polymerase chain reaction

Total RNA extraction from intestinal tissue was performed with NAiso Plus (TaKaRa, Dalian, China), and then a PrimeScriptTMRT MasterMix kit (TaKaRa, Dalian, China) was used to synthesize cDNA. Quantitative real-time polymerase chain reaction (qRT-PCR) was carried out in a 7300 Real-time PCR System using a SYBR® Premix Ex Taq™II Kit (TaKaRa). The primer sequences were as follows: NFATC3 forward 5'-GGTGGCCATCCTGTGTGAA-3' and reverse 5'-CAGTAATGCGATGCACCTGGTAA-3';  $\beta$ -actin forward 5'-GGAGATTACTGCCCTGGCTCCTA-3' and reverse 5'-GACTCATCGTACTCCTGCTTGCTG-3'. The  $2^{-\Delta\Delta C_t}$  method was used for statistical analyses of the mRNA levels normalized to  $\beta$ -actin.

### Preparation of QYD serum

Drug-containing serum was prepared as described previously[14]. Ten SD rats were divided into two groups: A normal group and a QYD serum group. In the QYD serum group, QYD (the First Affiliated Hospital of Dalian Medical University, Dalian, China) was administered to SD rats *via* gavage at 10 mL/dose/kg body weight twice per day for 5 d. The rats in the normal group were treated with the same volume of saline. After 5 d of treatment, blood samples were extracted from the abdominal arteries. Under anesthesia, serum was isolated from both the normal group and the QYD group based on a previously described method[15].

### Cell experimental design

Caco-2 cells were randomly divided into the following groups: The rat serum group, in which the cells were treated with 10% normal rat serum for 24 h; the rat serum + lipopolysaccharide (LPS) group, in which the cells were exposed to 100 ng/mL LPS and 10% normal rat serum for 24 h; and the QYD serum + LPS group, in which the cells were treated with 100 ng/mL LPS and 10% QYD serum for 24 h.

### Cell viability analysis

Caco-2 cell viability was assessed using MTT assays (Sigma, St Louis, MO, United States). After incubation with MTT dye (5 mg/mL) for 4 h at 37 °C, DMSO (150  $\mu$ L/well) was added. The optical absorbance was evaluated with a microplate reader at 490 nm to measure cell viability.

### Measurement of intracellular calcium levels

Intracellular  $Ca^{2+}$  levels were monitored using the  $Ca^{2+}$ -sensitive fluorescent indicator Fluo-3. Fluo-3 can enter cells through the medium of lipophilic AM and combine with intracellular free  $Ca^{2+}$ . The fluorescence intensity of Fluo-3 is positively correlated with the concentration of intracellular free  $Ca^{2+}$ . Caco-2 cells were seeded in HBSS buffer with Fluo-3/AM at 5  $\mu$ mol/L for 30 min. The cells were washed twice in fresh HBSS and then treated with 0.5 mL of HBSS buffer. Finally, a confocal laser scanning microscope (BioRad Radiance 2100) was used to assess the fluorescence intensity.

### Statistical analysis

Data are expressed as the mean  $\pm$  SD. SPSS v16.0 software was used for data analysis. One-way ANOVA was applied to assess significant differences between groups;  $P < 0.05$  was considered to indicate a statistically significant difference.

## RESULTS

### Histological changes in the pancreas and intestine

As shown in Figure 1A, edema, inflammatory infiltration, hemorrhage, and acinar necrosis were observed in the pancreas as the characteristic morphological features of SAP. Interstitial edema, irregular villi, mucosal erosion, and inflammatory infiltration were exhibited in the SAP group, with necrosis and shedding of the intestinal epithelium. The pancreatic and intestinal histological scores were significantly higher according to the standards of Anthony and Chiu, respectively. However, QYD treatment significantly ameliorated the pancreatic and intestinal pathology caused by SAP (Figures 1B and 1C).

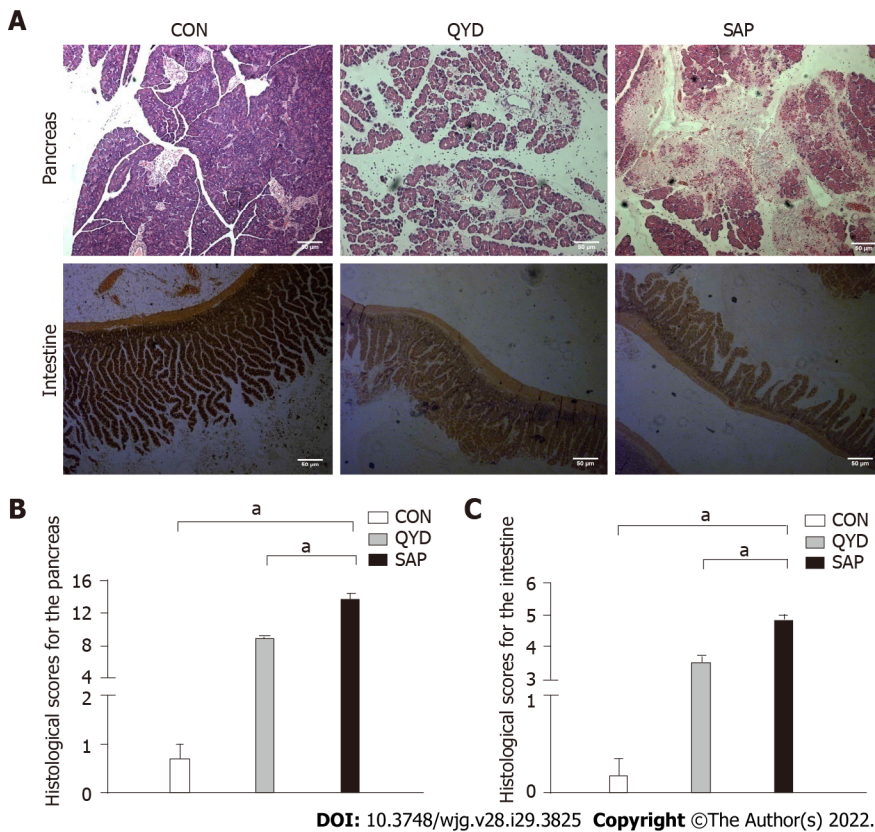


**Figure 1** Histological changes in pancreatic and intestinal tissues. A: Slight edema was detected [pancreas control (CON) group]; broad necrosis of acinar cells and interstitial edema were observed [pancreas severe acute pancreatitis (SAP) group]; only local necrosis, slight interstitial edema, and few inflammatory cell infiltrates were observed [pancreas Qingyi decoction (QYD) group]. Slight interstitial edema was detected (intestine CON group); irregular villi, mucosal erosion, and inflammatory infiltration were observed (intestine SAP group); edema and mild mucosal erosion were observed (intestine QYD group); B: Histological scores for the pancreas; C: Histological scores for the intestine. The histological scores for the pancreas and intestine were significantly ameliorated in the QYD treatment group compared with the SAP group. \* $P < 0.05$ , 100 ×. CON: Control; QYD: Qingyi decoction; SAP: Severe acute pancreatitis.

### Serum levels of amylase, IL-6, TNF- $\alpha$ , D-lactic acid and DAO

It can be seen from the data in **Figure 2** that the serum levels of amylase (**Figure 2A**), IL-6 (**Figure 2B**), and TNF- $\alpha$  (**Figure 2C**) were increased significantly in the SAP group compared with the control group. Consistent with previous research results, QYD treatment ameliorated the increases in amylase, IL-6, and TNF- $\alpha$  serum levels observed in the SAP group. D-lactic acid and DAO, which can serve as markers of intestinal barrier dysfunction and tissue injury, were significantly increased in the SAP group compared with the control group. However, the levels of serum D-lactic acid and DAO in the QYD group were significantly decreased compared with those in the SAP group (**Figures 3A** and **3B**).

### CnA and CnB expression in intestine

Following QYD treatment, the expression levels of CnA and CnB were detected *via* western blot analysis. The results, shown in **Figure 4A**, demonstrated that the expression levels of CnA and CnB were increased in the SAP group. The band intensities of CnA and CnB in the SAP group were 2.78 and 1.24, respectively, normalized to  $\beta$ -actin. QYD treatment significantly reduced the protein expression levels of CnA and CnB (**Figures 4B** and **4C**).

### NFATc3 expression in the intestine

Furthermore, we examined NFATc3 protein expression in intestinal tissues using immunofluorescence. NFATc3 was highly expressed in the SAP group compared with the control group but significantly downregulated under QYD treatment (**Figure 5A**). Semiquantitative analysis showed that the relative integral optical density (IOD) value was higher in the SAP group than in the control group. However, the relative IOD value was lower in the QYD group than in the SAP group (**Figure 5B**).

### Transcription of NFATc3 mRNA in intestinal tissue

Compared with the control group, qRT-PCR analysis revealed that the level of NFATc3 mRNA transcription was obviously increased in the SAP group. QYD treatment decreased the mRNA level compared with that in the SAP group (**Figure 6**).

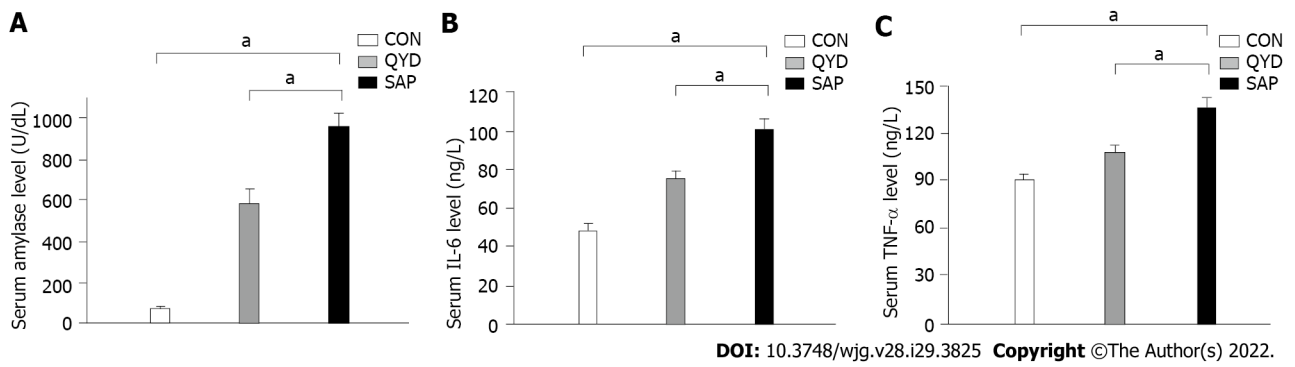


**Figure 2** Serum levels in the different experimental groups. A: Amylase; B: Interleukin-6; C: Tumor necrosis factor- $\alpha$ . <sup>a</sup>*P* < 0.05. CON: Control; QYD: Qingyi decoction; SAP: Severe acute pancreatitis; TNF: Tumor necrosis factor; IL: Interleukin.

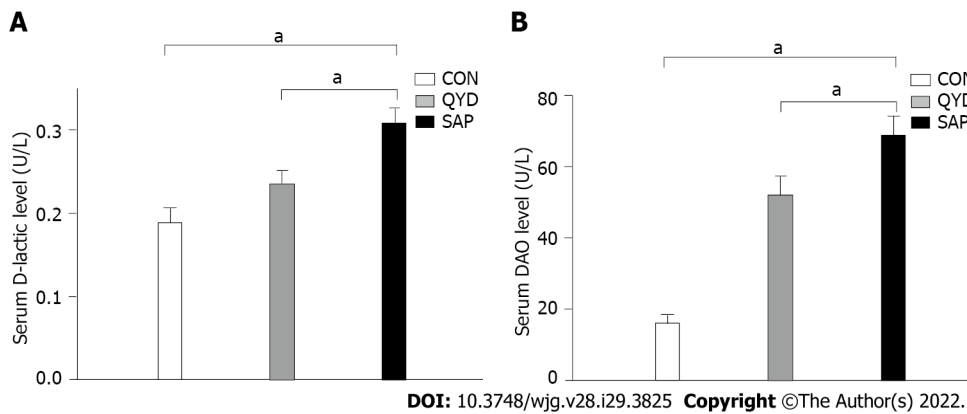


**Figure 3** Effect of Qingyi decoction on serum. A: D-lactic acid; B: Diamine oxidase. <sup>a</sup>*P* < 0.05. CON: Control; QYD: Qingyi decoction; SAP: Severe acute pancreatitis; DAO: Diamine oxidase.

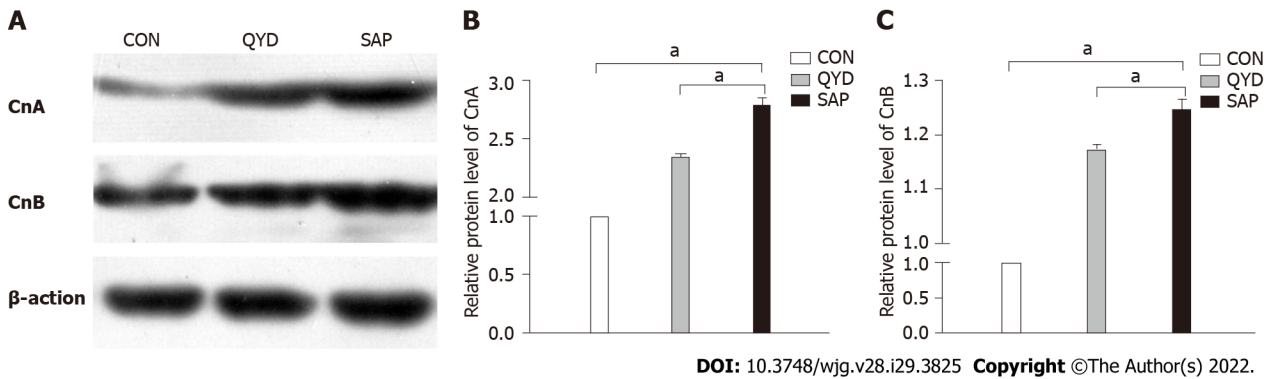


**Figure 4** Expression of calcineurin subunits in the intestine. A: Calcineurin A (CnA) and calcineurin B (CnB) protein expression in the intestine; B: Qingyi decoction (QYD) treatment significantly inhibited the elevated CnA protein expression in the intestine observed in the severe acute pancreatitis (SAP) group; C: QYD treatment significantly inhibited the elevated CnB protein expression in the intestine observed in the SAP group. <sup>a</sup>*P* < 0.05. CON: Control; QYD: Qingyi decoction; SAP: Severe acute pancreatitis; CnA: Calcineurin A; CnB: Calcineurin B.

**ICE apoptosis**

TUNEL staining results of rat intestinal tissue slices revealed that retrograde infusion of sodium deoxycholate increased ICE apoptosis compared with the control rats (Figure 7). However, compared with that in the SAP group, the level of ICE apoptosis in the QYD groups was significantly lower.

**Effect of QYD serum on cell viability and intracellular calcium**

A significant decline in cell viability after LPS treatment was verified by MTT assays (Figure 8), but QYD serum inhibited LPS-induced cell death. LPS induced a significant increase in Ca<sup>2+</sup> levels. Treatment with QYD serum significantly attenuated the increase in Ca<sup>2+</sup> levels caused by LPS-induced

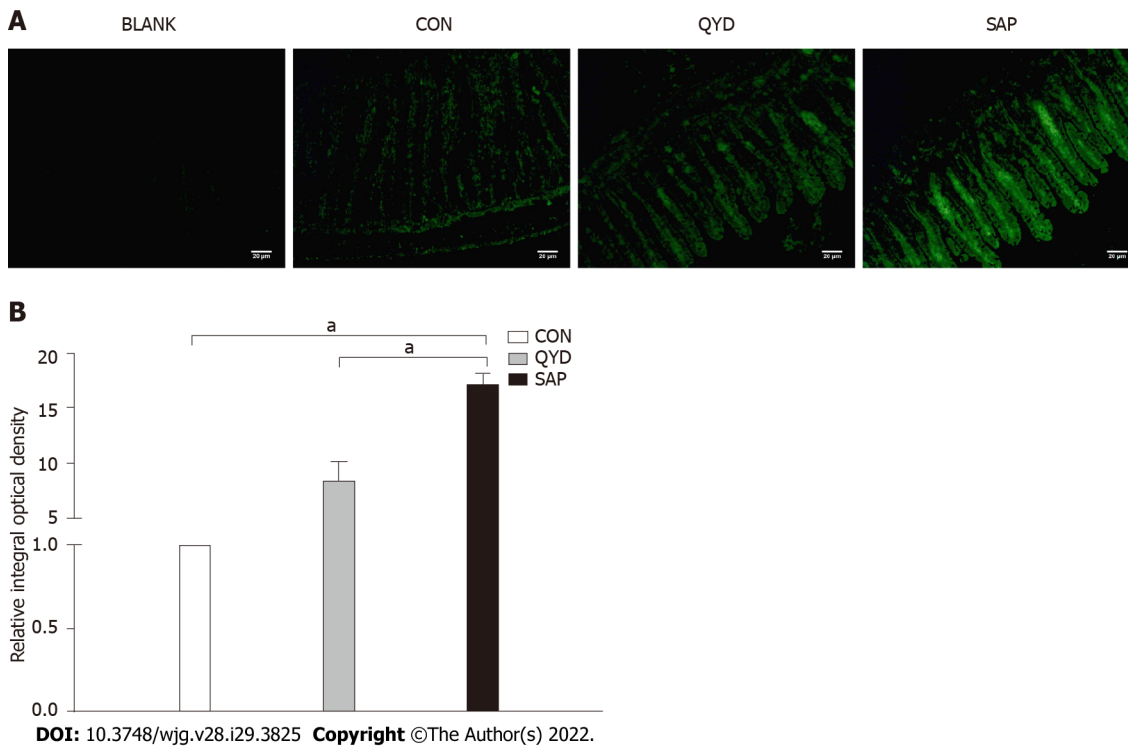


**Figure 5 Immunofluorescence and semiquantitative analysis of nuclear factor of activated T-cells c3 expression.** A: Immunofluorescence of nuclear factor of activated T-cells c3 (NFATc3) expression; B: Semiquantitative analysis of NFATc3 expression. NFATc3 was highly expressed in the severe acute pancreatitis group compared with the control group but significantly downregulated under Qingyi decoction treatment. <sup>a</sup>*P* < 0.05. BLANK: Control without primary antibody; CON: Control; QYD: Qingyi decoction; SAP: Severe acute pancreatitis.

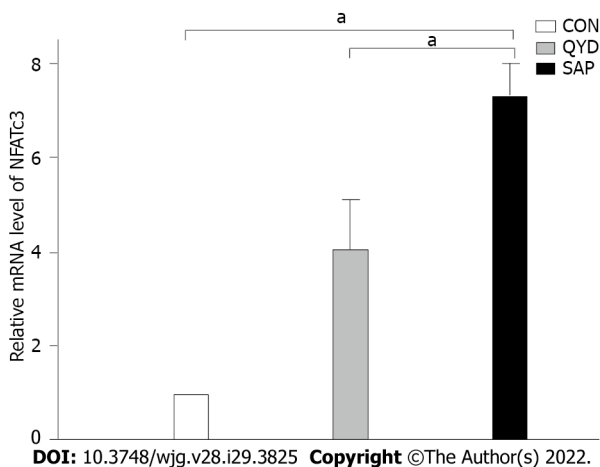


**Figure 6 The level of nuclear factor of activated T-cells c3 mRNA transcription in intestinal tissue.** <sup>a</sup>*P* < 0.05. CON: Control; QYD: Qingyi decoction; SAP: Severe acute pancreatitis; NFATc3: Nuclear factor of activated T-cells c3.

injury (Figure 9A). The relative mean optical density value was higher in the LPS group than in the control group, but QYD serum treatment decreased the relative mean optical density induced by LPS (Figure 9B).

## DISCUSSION

SAP refers to an acute abdominal disease characterized by rapid onset, rapid progression, and a high fatality rate. Prior studies have noted the importance of the intestinal barrier in the progression of SAP, which involves alterations in its mechanical, immune, chemical, and biological barriers[16]. Bacterial and/or endotoxin translocation from the gut lumen caused by intestinal barrier functional disturbance has a major influence on the prognosis of SAP[17]. The intestinal epithelium functions as the first barrier

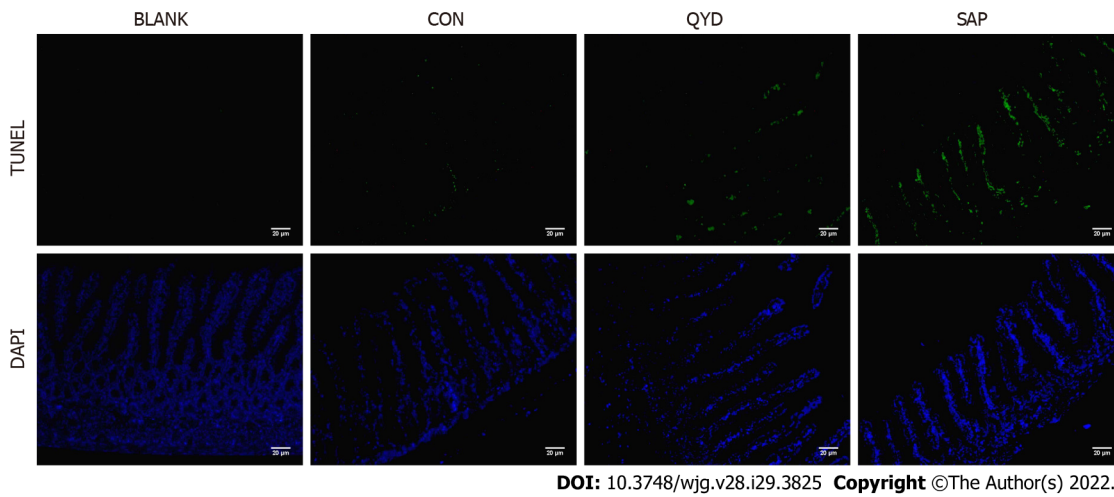


**Figure 7** Transferase-mediated dUTP nick-end labeling assay to assess intestinal epithelial cell apoptosis. Compared with that in the severe acute pancreatitis group, the level of intestinal epithelial cell apoptosis in the Qingyi decoction groups was significantly lower. 200 ×. BLANK: Control without primary antibody; CON: Control; QYD: Qingyi decoction; SAP: Severe acute pancreatitis. TUNEL: Transferase-mediated dUTP nick-end labeling; DAPI: 4',6-diamidino-2-phenylindole.

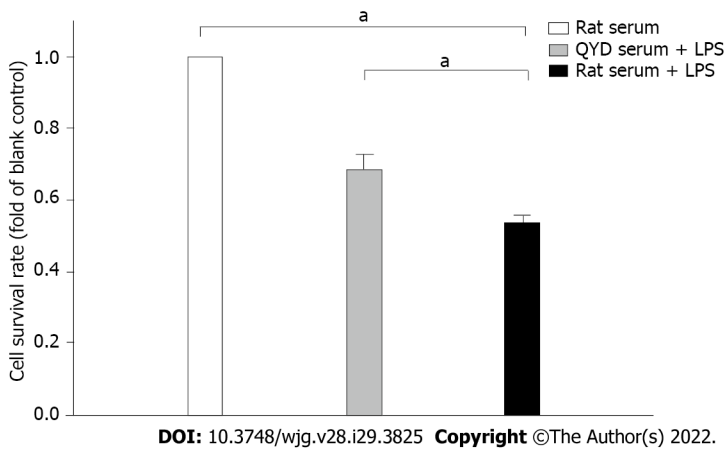
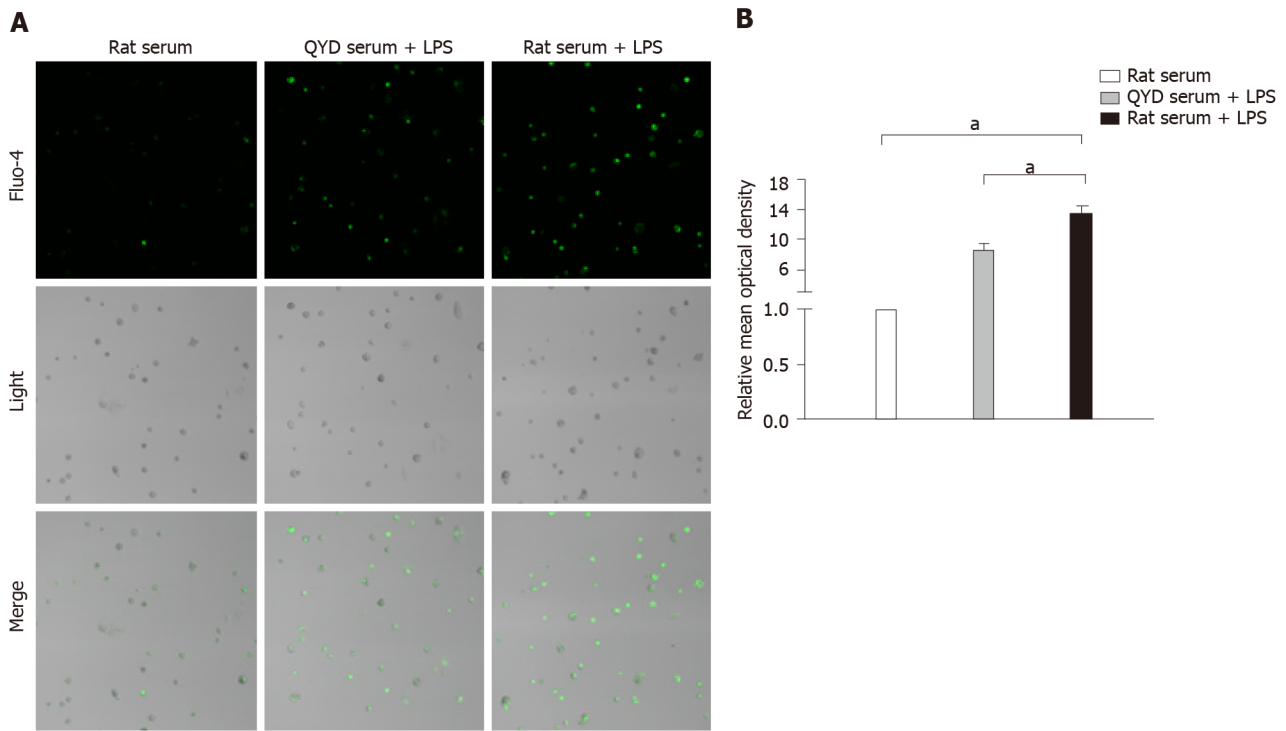


**Figure 8** Effect of Qingyi decoction serum on lipopolysaccharide-induced cell viability. <sup>a</sup>*P* < 0.05. QYD: Qingyi decoction; LPS: Lipopolysaccharide.

to defend against the invasion of overcrowded intestinal bacteria owing to intestinal motor dysfunction in SAP. Therefore, conservation and renovation of the intestinal epithelial function may have a positive effect on SAP and reduce SAP-mediated septic morbidity and mortality[18]. As a specific form of cell death in terms of its morphology and biochemistry, apoptosis has been thought of as a key factor in the physiological processes of IEC biology[19]. Recently, investigators have examined the effects of IEC apoptosis on intestinal integrity[18]. TNF- $\alpha$ , secreted from pancreatic acinar cells, monocytes and macrophages, not only mediates primary inflammation directly but also contributes to the occurrence of secondary inflammation[20,21]. High concentrations of TNF- $\alpha$  can be detected in serum as well as in pancreatic parenchyma, ascitic fluid, and lymphatic drainage in the early stages of AP. Many studies have confirmed that high serum levels of TNF- $\alpha$  are related to the severity of AP[22,23]. IL-6 is a phosphorylated glycoprotein of 185 amino acids encoded by the human IL-6 gene. The IL-6 gene has been mapped to human chromosome 7p21-24[24]. Current evidence has clarified that IL-6 is a vital cytokine in AP development; moreover, the serum level of IL-6 is associated with AP severity[25]. DAO is an intestinal mucosal enzyme that plays a key role in digestion and absorption and maintenance of the mucosal barrier. DAO activity in the mature upper villus cells of the intestinal mucosa is high, but it is very low in all other tissues under normal physiological conditions. However, DAO activity increases in the blood plasma and intestinal lumen when the intestinal mucosa is damaged[26,27]. D-lactic acid is a metabolite produced by the fermentation of intestinal bacteria. When the permeability of the intestinal mucosa increases as a result of infection with bacteria, D-lactic acid can enter the blood circulation and be detected in the peripheral blood. Consequently, D-lactic acid can be used as an early indicator of intestinal mucosa damage with high specificity[28]. In accordance with previous studies, the present results confirmed that retrograde infusion of sodium deoxycholate successfully created a rat model of SAP. Retrograde infusion of sodium deoxycholate increased the severity of pancreatic and intestinal



DOI: 10.3748/wjg.v28.i29.3825 Copyright ©The Author(s) 2022.

**Figure 9** Fluorescence images of  $[Ca^{2+}]_i$  changes and the relative mean optical density. A: Fluorescence images of  $Ca^{2+}$  changes measured using a confocal microscope; B: The relative mean optical density. Treatment with Qingyi decoction serum significantly attenuated the increase in  $Ca^{2+}$  levels observed in response to lipopolysaccharide-induced injury. <sup>a</sup> $P < 0.05$ . QYD: Qingyi decoction; LPS: Lipopolysaccharide.

pathology and the levels of serum amylase, TNF- $\alpha$ , and IL-6. Moreover, both the indicators of intestinal mucosa damage (D-lactic acid and DAO) and the levels of IEC apoptosis were elevated in the SAP group.

CaN, a serine/threonine phosphatase, can be defined as a central calcium-responsive signaling molecule that has a significant impact on immune responses. CaN contains two subunits, CnA (the large catalytic subunit) and CnB (the smaller regulatory subunit). As a result, the formation of a heterodimer determines the activity of CaN[29]. It is now well established based on a variety of studies that CaN is a significant contributing factor to the development of acute pancreatitis as a unique target of aberrant calcium signaling[30-32]. For example, bile acid-induced pancreatic injury, transient high ductal pressure-induced pancreatic inflammation, and pancreatic inflammation caused by radiocontrast agents are all dependent on CaN activation[31,33]. CaN can dephosphorylate several substrates; one of the most important of these substrates is NFATc[34]. CaN/NFAT signaling can accurately adjust gene expression to alter cell differentiation and development, dependent on its remarkable ability to sense  $Ca^{2+}$  oscillations in cells[35]. When phosphorylated, all NFAT members reside in the cytosol of resting cells. However, upon dephosphorylation in response to high intracellular levels of  $Ca^{2+}$ , cytosolic CaN binds to NFAT, leading to nuclear translocation and transcription. The calcium-CaN-activated NFAT family contains four members (NFATc1, NFATc2, NFATc3, and NFATc4), among which the NFATc3 gene has been identified to be expressed in mammalian intestinal tissues[36]. The effects of NFATc3 in AP were described in a report by Awla *et al*[37]. Their results demonstrated that NFATc3 could adjust to trypsinogen activation, inflammation, and pancreatic tissue damage during the process of AP. Consequently, NFATc3 activity might be a therapeutic target[37]. In this study, we found that the protein expression levels of the two subunits of CaN were remarkably elevated in the SAP group. Furthermore, we examined NFATc3 expression using qRT-PCR and immunofluorescence analyses. The results suggested that the NFATc3 gene was significantly upregulated at both the transcript and protein levels in the SAP group compared with the control group.

The therapeutic effects and associated mechanisms of QYD may lie in clearing fever, detoxifying, soothing the liver, regulating the flow of vital energy and removing obstructions, invigorating the circulation of blood, dissipating blood stasis, and dredging urination and defecation, according to traditional Chinese medicine's holistic thoughts[38]. QYD, as an organic combination of many effective components, plays a multitarget role in acute pancreatitis treatment through multiple pathways, including defending the intestinal barrier. It has been proven that QYD can suppress intestinal bacterial translocation, moderate inflammatory factor release, and prohibit intestinal mucosa destruction by inhibiting the expression of intestinal secreted phospholipase A2[39], suppressing the Toll-like receptor 4/nuclear factor-kappa B signaling pathway and stimulating Zona occludens 1 expression[9]. Serum

pharmacology, first brought forward by the famous Japanese medical scientist Masakazu Tashiro, was introduced into the field of TCM medical research in 1997[40]. Serum pharmacology can broadly be defined as a new experimental method in which the target drug is administered orally to experimental animals, and then the serum is separated for *in vitro* pharmacological testing after a certain period[41]. Currently, rabbits and rats are mainly chosen for the preparation of drug-containing serum as a result of their biological characteristics similar to those of humans[42]. After investigation of many of the pharmacokinetic parameters of TCM, an optimal medication plan (medicating 2 times a day, 3 d to 5 d continuously, and exsanguination 1 h after the last medication) was proven feasible. Owing to better reflecting the metabolism of TCM in the human body, serum pharmacology can provide new directions for pharmacological analysis of TCM[43]. In this study, the severity of SAP in the QYD group was attenuated compared with that in the untreated SAP group. In addition, the levels of IEC apoptosis declined in the QYD group relative to the untreated group. QYD significantly alleviated the upregulation of CaN and NFATc3 gene expression in the intestine in the SAP group. Further study indicated that QYD serum significantly decreased the LPS-induced elevation of intracellular free Ca<sup>2+</sup> levels and cell death.

## CONCLUSION

In summary, the results of this research demonstrated that the CaN/NFATc3 pathway might play a key role in IEC injury caused by SAP and that QYD can exert protective effects. Moreover, QYD can regulate CaN and NFATc3 gene expression. The findings suggest that the protective effects of QYD might be mediated, at least partially, by restraining IEC apoptosis *via* the CaN/NFATc3 pathway.

## ARTICLE HIGHLIGHTS

### Research background

Severe acute pancreatitis (SAP) is a severe acute abdominal disease characterized by high morbidity and mortality. A considerable amount of literature has demonstrated that intestinal barrier dysfunction is a significant contributory factor to SAP development. Qingyi decoction (QYD) has been used to treat acute pancreatitis in China for many years.

### Research motivation

The protective functions of QYD against intestinal mucosa injuries caused by SAP will provide new therapeutic information on SAP.

### Research objectives

To research the function and mechanism of QYD in treating intestinal mucosa injuries caused by SAP.

### Research methods

A rat model of SAP was created. Hematoxylin and eosin staining of pancreatic and intestinal tissue was performed. Enzyme-linked immunosorbent assay was used to estimate the concentrations of tumor necrosis factor (TNF- $\alpha$ ), interleukin (IL)-6, D-lactic acid, and diamine oxidase (DAO). Terminal deoxynucleotidyl transferase dUTP nick-end labeling was carried out to assess intestinal epithelial cell (IEC) apoptosis. Quantitative real-time polymerase chain reaction, western blotting, and immunofluorescence were used to determine the expression of calcineurin (CaN) and nuclear factor of activated T-cells (NFATc3). MTT and confocal laser scanning microscope were used to detect cell viability and intracellular calcium levels *in vitro* studies.

### Research results

In this study, the severity of SAP in the QYD group was attenuated. In addition, the levels of IEC apoptosis declined in the QYD group. QYD significantly restrained CaN and NFATc3 gene expression in the intestine. Further study indicated that QYD serum significantly decreased the lipopolysaccharide-induced elevation in intracellular free Ca<sup>2+</sup> levels and cell death.

### Research conclusions

This research demonstrated that the CaN/NFATc3 pathway might play a key role in IEC injury caused by SAP and that QYD can exert protective effects, at least partially, by restraining IEC apoptosis *via* the CaN/NFATc3 pathway.

### Research perspectives

This study provides insight into the function and mechanism of QYD in the treatment of intestinal

mucosa injuries caused by SAP *in vivo* and *in vitro* experiments, thereby providing theoretical support for the clinical application of QYD.

---

## FOOTNOTES

**Author contributions:** Wang GY, Shang D, and Chen HL designed the research; Wang GY, Jiang N, and Liu HH performed the research; Song HY, Wang GY and Zhang GX analyzed the data; Wang GY and Chen HL wrote the paper.

**Supported by** the National Key R and D Program of China, No. 2019YFE0119300; National Natural Science Foundation of China, No. 82074158; Project funded by China Postdoctoral Science Foundation, No. 2018M631793; Natural Science Foundation of Liaoning Province, No. 2019-ZD-0624; and Dalian Traditional Chinese Medicine-Related Scientific Research Project, No. 18Z2002.

**Institutional animal care and use committee statement:** This study was approved by the Animal Experimental Ethics Committee of Dalian Medical University (No. AEE19003).

**Conflict-of-interest statement:** All the authors report no relevant conflicts of interest for this article.

**Data sharing statement:** No additional data are available.

**ARRIVE guidelines statement:** The authors have read the ARRIVE guidelines, and the manuscript was prepared and revised according to the ARRIVE guidelines.

**Open-Access:** This article is an open-access article that was selected by an in-house editor and fully peer-reviewed by external reviewers. It is distributed in accordance with the Creative Commons Attribution Non Commercial (CC BY-NC 4.0) license, which permits others to distribute, remix, adapt, build upon this work non-commercially, and license their derivative works on different terms, provided the original work is properly cited and the use is non-commercial. See: <https://creativecommons.org/licenses/by-nc/4.0/>

**Country/Territory of origin:** China

**ORCID number:** Guan-Yu Wang 0000-0002-9982-8785; Dong Shang 0000-0001-6156-5214; Gui-Xin Zhang 0000-0003-0125-6609; Hui-Yi Song 0000-0003-3415-9223; Nan Jiang 0000-0002-0613-5729; Huan-Huan Liu 0000-0002-2023-8708; Hai-Long Chen 0000-0001-5547-5837.

**S-Editor:** Wang JJ

**L-Editor:** A

**P-Editor:** Wang JJ

---

## REFERENCES

- Zerem E. Treatment of severe acute pancreatitis and its complications. *World J Gastroenterol* 2014; **20**: 13879-13892 [PMID: 25320523 DOI: 10.3748/wjg.v20.i38.13879]
- Zhang JX, Dang SC, Yin K, Jiang DL. Protective effect of clodronate-containing liposomes on intestinal mucosal injury in rats with severe acute pancreatitis. *Hepatobiliary Pancreat Dis Int* 2011; **10**: 544-551 [PMID: 21947731 DOI: 10.1016/s1499-3872(11)60092-1]
- Yasuda T, Takeyama Y, Ueda T, Shinzeki M, Sawa H, Nakajima T, Kuroda Y. Breakdown of intestinal mucosa via accelerated apoptosis increases intestinal permeability in experimental severe acute pancreatitis. *J Surg Res* 2006; **135**: 18-26 [PMID: 16603187 DOI: 10.1016/j.jss.2006.02.050]
- Yasuda T, Takeyama Y, Ueda T, Shinzeki M, Kishi S, Sawa H, Nakajima T, Kuroda Y. Protective effect of caspase inhibitor on intestinal integrity in experimental severe acute pancreatitis. *J Surg Res* 2007; **138**: 300-307 [PMID: 17292420 DOI: 10.1016/j.jss.2006.09.022]
- McCarthy KM, Skare IB, Stankewich MC, Furuse M, Tsukita S, Rogers RA, Lynch RD, Schneeberger EE. Occludin is a functional component of the tight junction. *J Cell Sci* 1996; **109** (Pt 9): 2287-2298 [PMID: 8886979 DOI: 10.1242/jcs.109.9.2287]
- Sommerer C, Meuer S, Zeier M, Giese T. Calcineurin inhibitors and NFAT-regulated gene expression. *Clin Chim Acta* 2012; **413**: 1379-1386 [PMID: 21996081 DOI: 10.1016/j.cca.2011.09.041]
- Jia Z, Chen Q, Qin H. Ischemia-induced apoptosis of intestinal epithelial cells correlates with altered integrin distribution and disassembly of F-actin triggered by calcium overload. *J Biomed Biotechnol* 2012; **2012**: 617539 [PMID: 22701305 DOI: 10.1155/2012/617539]
- Shati AA. Doxorubicin-induces NFAT/Fas/FasL cardiac apoptosis in rats through activation of calcineurin and P38 MAPK and inhibition of mTOR signalling pathways. *Clin Exp Pharmacol Physiol* 2020; **47**: 660-676 [PMID: 31811646 DOI: 10.1111/1440-1681.13225]
- Zhang JW, Zhang GX, Chen HL, Liu GL, Owusu L, Wang YX, Wang GY, Xu CM. Therapeutic effect of Qingyi

- decoction in severe acute pancreatitis-induced intestinal barrier injury. *World J Gastroenterol* 2015; **21**: 3537-3546 [PMID: 25834318 DOI: 10.3748/wjg.v21.i12.3537]
- 10 **Yang DY**, Duan SB, Aili JT. [Effect of qingyi decoction in treating severe acute pancreatitis and its impacts on blood level of tumor necrosis factor-alpha, interleukin-6 and inteleukin-8]. *Zhongguo Zhong Xi Yi Jie He Za Zhi* 2009; **29**: 1122-1124 [PMID: 20214338]
  - 11 **Rongione AJ**, Kusske AM, Kwan K, Ashley SW, Reber HA, McFadden DW. Interleukin 10 reduces the severity of acute pancreatitis in rats. *Gastroenterology* 1997; **112**: 960-967 [PMID: 9041259 DOI: 10.1053/gast.1997.v112.pm9041259]
  - 12 **Chiu CJ**, Scott HJ, Gurd FN. Intestinal mucosal lesion in low-flow states. II. The protective effect of intraluminal glucose as energy substrate. *Arch Surg* 1970; **101**: 484-488 [PMID: 5311679 DOI: 10.1001/archsurg.1970.01340280036010]
  - 13 **Wang G**, Zhang J, Xu C, Han X, Gao Y, Chen H. Inhibition of SOCs Attenuates Acute Lung Injury Induced by Severe Acute Pancreatitis in Rats and PMVECs Injury Induced by Lipopolysaccharide. *Inflammation* 2016; **39**: 1049-1058 [PMID: 27025854 DOI: 10.1007/s10753-016-0335-1]
  - 14 **Guo SG**, Zhang W, Jiang T, Dai M, Zhang LF, Meng YC, Zhao LY, Niu JZ. Influence of serum collected from rat perfused with compound Biejia ruangan drug on hepatic stellate cells. *World J Gastroenterol* 2004; **10**: 1487-1494 [PMID: 15133859 DOI: 10.3748/wjg.v10.i10.1487]
  - 15 **Zhang GX**, Zhan C, Wang K, Han J, Shang D, Chen HI. Qingyi Decoction ameliorates acute biliary pancreatitis by targeting Gpbar1/NF-kb pathway. *Front Biosci (Landmark Ed)* 2019; **24**: 833-848 [PMID: 30844716 DOI: 10.2741/4754]
  - 16 **Nusrat A**, Parkos CA, Verkade P, Foley CS, Liang TW, Innis-Whitehouse W, Eastburn KK, Madara JL. Tight junctions are membrane microdomains. *J Cell Sci* 2000; **113** (Pt 10): 1771-1781 [PMID: 10769208 DOI: 10.1242/jcs.113.10.1771]
  - 17 **Chen X**, Zhao HX, Fu XS, Li CP, Zhong XL. Glucagonlike peptide 2 protects intestinal barrier in severe acute pancreatitis through regulating intestinal epithelial cell proliferation and apoptosis. *Pancreas* 2012; **41**: 1080-1085 [PMID: 22481288 DOI: 10.1097/MPA.0b013e31824966b0]
  - 18 **Wang X**, Wang B, Wu K, Xu M, Gong Z. Growth hormone downregulated the excessive apoptosis of ileal intestinal epithelial cells in rats during the early course of acute necrotizing pancreatitis. *Pancreas* 2002; **25**: 205-209 [PMID: 12142747 DOI: 10.1097/00006676-200208000-00016]
  - 19 **Jones BA**, Gores GJ. Physiology and pathophysiology of apoptosis in epithelial cells of the liver, pancreas, and intestine. *Am J Physiol* 1997; **273**: G1174-G1188 [PMID: 9435542 DOI: 10.1152/ajpgi.1997.273.6.G1174]
  - 20 **Malleo G**, Mazzon E, Siriwardena AK, Cuzzocrea S. TNF-alpha as a therapeutic target in acute pancreatitis--lessons from experimental models. *ScientificWorldJournal* 2007; **7**: 431-448 [PMID: 17450307 DOI: 10.1100/tsw.2007.98]
  - 21 **Wendling D**, Prati C. Paradoxical effects of anti-TNF- $\alpha$  agents in inflammatory diseases. *Expert Rev Clin Immunol* 2014; **10**: 159-169 [PMID: 24325385 DOI: 10.1586/1744666X.2014.866038]
  - 22 **Shen Y**, Cui N, Miao B, Zhao E. Immune dysregulation in patients with severe acute pancreatitis. *Inflammation* 2011; **34**: 36-42 [PMID: 20405190 DOI: 10.1007/s10753-010-9205-4]
  - 23 **Pooran N**, Indaram A, Singh P, Bank S. Cytokines (IL-6, IL-8, TNF): early and reliable predictors of severe acute pancreatitis. *J Clin Gastroenterol* 2003; **37**: 263-266 [PMID: 12960727 DOI: 10.1097/00004836-200309000-00013]
  - 24 **Talar-Wojnarowska R**, Gasiorowska A, Smolarz B, Romanowicz-Makowska H, Kulig A, Malecka-Panas E. Clinical significance of interleukin-6 (IL-6) gene polymorphism and IL-6 serum level in pancreatic adenocarcinoma and chronic pancreatitis. *Dig Dis Sci* 2009; **54**: 683-689 [PMID: 18661238 DOI: 10.1007/s10620-008-0390-z]
  - 25 **Hansen M**, Nielsen AR, Vilsbøll T, Lund A, Krarup T, Knop FK, Vestergaard H. Increased levels of YKL-40 and interleukin 6 in patients with chronic pancreatitis and secondary diabetes. *Pancreas* 2012; **41**: 1316-1318 [PMID: 22647735 DOI: 10.1097/MPA.0b013e31824d9b93]
  - 26 **Thompson JS**, Vaughan WP, Forst CF, Jacobs DL, Weekly JS, Rikkens LF. The effect of the route of nutrient delivery on gut structure and diamine oxidase levels. *JPEN J Parenter Enteral Nutr* 1987; **11**: 28-32 [PMID: 3102778 DOI: 10.1177/014860718701100128]
  - 27 **Bragg LE**, Thompson JS, West WW. Intestinal diamine oxidase levels reflect ischemic injury. *J Surg Res* 1991; **50**: 228-233 [PMID: 1900339 DOI: 10.1016/0022-4804(91)90183-m]
  - 28 **Smith SM**, Eng RH, Buccini F. Use of D-lactic acid measurements in the diagnosis of bacterial infections. *J Infect Dis* 1986; **154**: 658-664 [PMID: 3528318 DOI: 10.1093/infdis/154.4.658]
  - 29 **Rusnak F**, Mertz P. Calcineurin: form and function. *Physiol Rev* 2000; **80**: 1483-1521 [PMID: 11015619 DOI: 10.1152/physrev.2000.80.4.1483]
  - 30 **Orabi AI**, Wen L, Javed TA, Le T, Guo P, Sanker S, Ricks D, Boggs K, Eisses JF, Castro C, Xiao X, Prasad K, Esni F, Gittes GK, Husain SZ. Targeted inhibition of pancreatic acinar cell calcineurin is a novel strategy to prevent post-ERCP pancreatitis. *Cell Mol Gastroenterol Hepatol* 2017; **3**: 119-128 [PMID: 28090570 DOI: 10.1016/j.jcmgh.2016.08.006]
  - 31 **Mulli KA**, Wang D, Orabi AI, Sarwar S, Luo Y, Javed TA, Eisses JF, Mahmood SM, Jin S, Singh VP, Ananthanarayanan M, Perides G, Williams JA, Molken JD, Husain SZ. Bile acids induce pancreatic acinar cell injury and pancreatitis by activating calcineurin. *J Biol Chem* 2013; **288**: 570-580 [PMID: 23148215 DOI: 10.1074/jbc.M112.428896]
  - 32 **Shah AU**, Sarwar A, Orabi AI, Gautam S, Grant WM, Park AJ, Shah AU, Liu J, Mistry PK, Jain D, Husain SZ. Protease activation during *in vivo* pancreatitis is dependent on calcineurin activation. *Am J Physiol Gastrointest Liver Physiol* 2009; **297**: G967-G973 [PMID: 20501444 DOI: 10.1152/ajpgi.00181.2009]
  - 33 **Wen L**, Javed TA, Yimlamai D, Mukherjee A, Xiao X, Husain SZ. Transient High Pressure in Pancreatic Ducts Promotes Inflammation and Alters Tight Junctions via Calcineurin Signaling in Mice. *Gastroenterology* 2018; **155**: 1250-1263.e5 [PMID: 29928898 DOI: 10.1053/j.gastro.2018.06.036]
  - 34 **Macian F**. NFAT proteins: key regulators of T-cell development and function. *Nat Rev Immunol* 2005; **5**: 472-484 [PMID: 15928679 DOI: 10.1038/nri1632]
  - 35 **Müller MR**, Rao A. NFAT, immunity and cancer: a transcription factor comes of age. *Nat Rev Immunol* 2010; **10**: 645-656 [PMID: 20725108 DOI: 10.1038/nri2818]
  - 36 **Angulo C**, Alamillo E, Ascencio F, Reyes-Becerril M. Characterization of nuclear factor of activated T-cells-c3 (NFATc3) and gene expression of upstream-downstream signaling molecules in response to immunostimulants in Pacific red snapper

- cells. *Dev Comp Immunol* 2018; **78**: 149-159 [PMID: 28986213 DOI: 10.1016/j.dci.2017.10.001]
- 37 **Awla D**, Zetterqvist AV, Abdulla A, Camello C, Berglund LM, Spégel P, Pozo MJ, Camello PJ, Regnér S, Gomez MF, Thorlacius H. NFATc3 regulates trypsinogen activation, neutrophil recruitment, and tissue damage in acute pancreatitis in mice. *Gastroenterology* 2012; **143**: 1352-1360.e7 [PMID: 22841788 DOI: 10.1053/j.gastro.2012.07.098]
- 38 **HanSL**. Efficacy of Qingyi decoction in the treatment of severe acute pancreatitis: systematic review and meta-analysis. *J Pract Med* 2008
- 39 **Su S**, Liang T, Zhou X, He K, Li B, Xia X. Qingyi decoction attenuates severe acute pancreatitis in rats *via* inhibition of inflammation and protection of the intestinal barrier. *J Int Med Res* 2019; **47**: 2215-2227 [PMID: 30700190 DOI: 10.1177/0300060518809289]
- 40 **Zhang WX**, Feng M, Mao YL, Zhang WZ, Ni Y. Review on the Application of Serum Pharmacology of Traditional Chinese Medicine. *Drug Evaluation Res* 2019; **42**: 1448-1453
- 41 **Wu XW**, Hao YY, Nie CX, Ni Y, Hao XL, Liu C. An overview of methodology and research progress on application of serum pharmacology of traditional Chinese medicine. *Chin J Exp Tradit Med Form* 2019; **24**: 173-179
- 42 **Tao S**. Research on rapid discovery method of Chinese medicine effective substances based on chemometrics and immobilized enzyme. Zhejiang University, 2015
- 43 **Chen Q**, Huang L, Wang R, Pang C. Research Status of Serum Pharmacology and Serum Pharmacology of Traditional Chinese Medicine. *Agric Biotechnol* 2021; **10**: 126-128

## Basic Study

## High-fat diet aggravates colitis via mesenteric adipose tissue derived exosome metastasis-associated lung adenocarcinoma transcript 1

Dong Chen, Miao-Miao Lu, Jin-Hai Wang, Yue Ren, Ling-Ling Xu, Wei-Xin Cheng, Sai-Sai Wang, Xiao-Lin Li, Xiao-Fei Cheng, Jian-Guo Gao, Farhin Shaheed Kalyani, Xi Jin

**Specialty type:** Gastroenterology and hepatology

**Provenance and peer review:**

Unsolicited article; Externally peer reviewed.

**Peer-review model:** Single blind

**Peer-review report's scientific quality classification**

Grade A (Excellent): 0  
Grade B (Very good): B, B  
Grade C (Good): 0  
Grade D (Fair): D  
Grade E (Poor): 0

**P-Reviewer:** Chiu CC, Taiwan; Kao JT, Taiwan; Senousy M, Egypt

**Received:** December 4, 2021

**Peer-review started:** December 4, 2021

**First decision:** April 16, 2022

**Revised:** April 28, 2022

**Accepted:** July 6, 2022

**Article in press:** July 6, 2022

**Published online:** August 7, 2022



**Dong Chen, Jin-Hai Wang, Sai-Sai Wang, Xiao-Fei Cheng,** Department of Colorectal Surgery, The First Affiliated Hospital, College of Medicine, Zhejiang University, Hangzhou 310003, Zhejiang Province, China

**Miao-Miao Lu, Yue Ren, Ling-Ling Xu, Wei-Xin Cheng, Farhin Shaheed Kalyani,** Department of Medicine, Zhejiang University School of Medicine, Hangzhou 310003, Zhejiang Province, China

**Xiao-Lin Li,** Department of Emergency, The First Affiliated Hospital, College of Medicine, Zhejiang University, Hangzhou 310003, Zhejiang Province, China

**Jian-Guo Gao, Xi Jin,** Department of Gastroenterology, The First affiliated Hospital, College of Medicine, Zhejiang University, Hangzhou 310003, Zhejiang Province, China

**Corresponding author:** Xi Jin, MD, PhD, Doctor, Professor, Department of Gastroenterology, The First Affiliated Hospital, College of Medicine, Zhejiang University, No. 79 Qingchun Road, Hangzhou 310003, Zhejiang Province, China. [jxfl007@zju.edu.cn](mailto:jxfl007@zju.edu.cn)

**Abstract****BACKGROUND**

Obesity is associated with an increased risk of developing Crohn's disease (CD), higher disease activity, and comparatively worse clinical outcomes.

**AIM**

To investigate the role of mesenteric adipose tissue-derived exosomes in the pathogenesis of CD aggravation in obese individuals.

**METHODS**

First, we induced colitis in mice initiated on high-fat and normal diets and compared the severity of colitis. We then extracted and identified exosomes from mesenteric adipose tissue and determined the levels of metastasis-associated lung adenocarcinoma transcript 1 (MALAT1) in mesenteric adipose tissue-derived exosomes and the colon. Next, we demonstrated an interaction between MALAT1 and the miR-15a-5p/activating transcription factor 6 (ATF6) axis. Finally, we explored the effects of mesenteric adipose tissue-derived exosomes extracted from mice fed a high-fat or normal diet on the severity of 2,4,6-trinitrobenzenesulfonic acid (TNBS)-induced colitis and ATF6-related endoplasmic reticulum stress

pathways.

## RESULTS

High-fat diet was found to aggravate TNBS-induced colitis in mice. The expression of MALAT1 in mesenteric adipose tissue-derived exosomes of high-fat diet-fed mice increased. The increased expression of MALAT1 in colon tissue exacerbated TNBS-induced colitis and activated the ATF6 endoplasmic reticulum stress pathway. This effect was partially reversed by the reduced expression of MALAT1 and overexpression of miR-15a-5p.

## CONCLUSION

Mesenteric adipose tissue-derived exosome-encapsulated long noncoding RNAs MALAT1 targets the colon and aggravates TNBS-induced colitis in obese mice, which may potentially act on the miR-15a-5p/ATF6 axis and activate endoplasmic reticulum stress.

**Key Words:** Metastasis-associated lung adenocarcinoma transcript; Crohn's disease; miR-15a-5p; Mesenteric adipose tissue; Obesity; Colitis; Inflammatory bowel disease

©The Author(s) 2022. Published by Baishideng Publishing Group Inc. All rights reserved.

**Core Tip:** A higher visceral adipose tissue ratio has been associated with increased disease activity in patients with Crohn's disease. However, the mechanisms underlying this effect remain unclear. Our study indicates that a high-fat diet increases the mesenteric adipose tissue content and aggravates colitis in mice. Mesenteric adipose tissue-derived exosome long noncoding RNAs metastasis-associated lung adenocarcinoma transcript 1 can be absorbed by the colon, leading to the activation of the endoplasmic reticulum stress pathway by targeting the miR-15a-5p/activating transcription factor 6 axis to aggravate colitis.

**Citation:** Chen D, Lu MM, Wang JH, Ren Y, Xu LL, Cheng WX, Wang SS, Li XL, Cheng XF, Gao JG, Kalyani FS, Jin X. High-fat diet aggravates colitis *via* mesenteric adipose tissue derived exosome metastasis-associated lung adenocarcinoma transcript 1. *World J Gastroenterol* 2022; 28(29): 3838-3853

**URL:** <https://www.wjgnet.com/1007-9327/full/v28/i29/3838.htm>

**DOI:** <https://dx.doi.org/10.3748/wjg.v28.i29.3838>

## INTRODUCTION

Crohn's disease (CD) is a chronic relapsing inflammatory disease of the gastrointestinal tract that results from the interplay between genetic susceptibility and various environmental exposures[1]. The incidence of CD is higher in developed countries and urban areas than in developing and rural areas[2]. Similarly, the prevalence of CD is increasing in areas with rapid urbanization[3], paralleling the obesity epidemic, possibly in conjunction with western-style diets characterized by high fat content.

The conventional understanding is that CD is a chronic disease characterized by wasting, low weight, and malnutrition. Nevertheless, based on real world data, 15%-40% of patients with inflammatory bowel disease (IBD), including CD and ulcerative colitis (UC), are obese and 20%-40% are overweight [4]. Several studies have shown that obesity is associated with an increased risk of developing CD[5,6], a higher disease activity, and comparatively worse clinical outcomes[7]. For instance, Jain *et al*[8] observed that obesity was not only associated with an increased risk of persistent disease activity and relapse in patients with IBD but also with higher rates of anxiety, depression, fatigue, pain, and inferior social function scores. Although these studies on the association between obesity and the course of CD have some limitations, and the above-mentioned outcomes have not been observed consistently, accumulating evidence indicates that visceral adiposity better captures the association between obesity and CD than body mass index[4]. A higher baseline visceral adipose tissue/total fat mass ratio was found to be associated with increased disease activity[9]. Although the influence of obesity on the course of CD has been confirmed, the underlying mechanism remains elusive.

Significant expansion of adipose tissue is a common phenomenon in obese individuals. In addition to storing energy, adipose tissue is an endocrine organ that secretes various adipokines, lipokines, and exosomes, contributing to the state of chronic inflammation in obese individuals[10]. Localized mesenteric fat accumulation in CD patients, known as creeping fat, is not only related to overall obesity but also has a systemic pro-inflammatory effect[11]. Adipose tissue and visceral adipose tissue-derived endocrine hormones are involved in multiple diseases, including cancer[12], cardiovascular disease[13], and nonalcoholic steatohepatitis (NASH)[14]. Exosomes are extracellular vesicles secreted by various cells, including adipocytes[15]. Visceral adipose tissue-derived exosomes display tissue affinity, prefer-

entially targeting the colonic lamina propria[16]. Mesenteric adipose tissue can directly invade the lamina propria. Therefore, we hypothesized that obesity exacerbates IBD, partially due to mesenteric adipose tissue-derived exosomes.

Previous studies have indicated that exosomes contain multiple non-coding RNAs such as circular RNAs, long noncoding RNAs (lncRNAs), and microRNAs, which serve as messengers in cell-to-cell communication. Among these, lncRNAs are non-coding RNAs containing more than 200 nucleotides [17]. lncRNAs can interact with transcription factors to regulate transcription, bind to proteins to promote the formation of ribonucleoproteins, guide chromatin-modifying protein complexes targeting genes, and act as sponges for downstream microRNAs, participating in a variety of pathophysiological processes[18]. To our knowledge, few studies have explored the potential functions and mechanisms of adipocyte-derived exosomal lncRNAs in the exacerbation of CD.

The present study aimed to investigate the role of lncRNAs transferred by mesenteric adipose tissue-derived exosomes in obesity aggravated CD, and thereby assess the potential of these lncRNAs as therapeutic targets for the treatment of CD in this subpopulation.

## MATERIALS AND METHODS

### **Construction of obesity mouse model and colitis mouse model**

C57BL/6 mice (6-8 wk old) were purchased from Chengdu Dossy Experimental Animals Co.,Ltd. and fed either a normal diet (ND) (#D12451, Research Diets, United States) or a high-fat diet (HFD) (#D12492, Research Diets, United States) for 12 wk. To induce acute experimental colitis, 2,4,6-trinitrobenzenesulfonic acid (TNBS) (Beyotime, China; 100 µg/g, 175 µL) was injected into the colon for 4 d. The daily disease activity index (DAI) score was calculated in mice in accordance with a well-established method[19]. The body weight of the mice in each group was also recorded. On day 8, the mice were sacrificed for colon and mesenteric adipose tissue collection. Rectum tissue, 3 cm away from the anal margin, was collected for hematoxylin and eosin (HE) staining and inflammatory pathological score determination using the following steps. Briefly, mouse colon tissue was fixed in 10% formaldehyde, embedded in paraffin, sectioned, and stained with HE. Details of histological scoring have been described previously[20]. The remaining colon tissue was placed in liquid nitrogen for subsequent analyses. Mice were randomly divided into the following four groups ( $n = 6$  each): ND + control, HFD + control, normal diet + TNBS, and HFD + TNBS.

### **RNA Extraction and real-time reverse transcription-PCR**

Total RNA was isolated using Trizol (Invitrogen, United States) and reverse-transcribed into cDNA using the First Strand cDNA Synthesis Kit (TransGen, China), in accordance with the manufacturer's instructions. Real-time reverse transcription-PCR (qRT-PCR) was performed using the SYBR Premix Ex Taq qPCR kit (TaKaRa, Japan). Primer sequences used are listed in [Supplementary Table 1](#).

### **Enzyme linked immunosorbent assay and Western blotting**

The concentrations of mouse interleukin 1 $\beta$  (IL-1 $\beta$ ), tumor necrosis factor  $\alpha$  (TNF- $\alpha$ ), and interleukin 6 (IL-6) were detected using enzyme linked immunosorbent assay (ELISA) kits (Elabscience, China) according to the manufacturer's instructions. Additionally, total protein was isolated using radio-immune precipitation assay (RIPA) buffer (TaKaRa, Japan) supplemented with a protease inhibitor (Roche, Switzerland). After quantification using the BCA Protein Assay Kit (Thermo, United States), the proteins were separated by SDS-PAGE and transferred onto polyvinylidene fluoride (PVDF) membranes. The membranes were blocked and incubated overnight with antibodies against activating transcription factor 6 (ATF6) (ab227830, Abcam, United Kingdom), p-PERK (MA5-15033, Thermo, United States), p-IRE1 (CSB-RA00,7795A724phHU, CUSABIO, China), GRP78 (MA5-27687, Thermo, United States), p-EIF2 $\alpha$  (51995, CST, United States), CHOP (5554T, CST, United States), and GAPDH (ab8245, Abcam, United Kingdom) at 4 °C. The membranes were then incubated with HRP-conjugated secondary antibodies (Multi Sciences, China). Finally, the protein bands were detected using enhanced chemiluminescence (ECL) kits (Thermo, United States).

### **Isolation and primary culture of adipocytes**

Mesenteric adipose tissue (25 g) was isolated and placed into a sterile 50 mL polypropylene test tube containing 15 mL of collagenase [1 mg collagenase/1 mL phosphate balanced solution (PBS); 3 mL solution/1 g tissue]. After grinding, the solution was swirled for 20 s and the test tube was incubated at 37 °C in a rocking water bath at 100 rpm for 40 min. The solution was vortexed and filtered through a funnel containing a double gauze. Thereafter, the homogenate was centrifuged at 1000 rpm for 10 min, followed by collection of the top fat layer, which was washed three times with PBS. The precipitate was then resuspended in 10 mL of RBC lysis buffer (154 mmol/L NH<sub>4</sub>Cl, 10 mmol/L KHCO<sub>3</sub>, 1 mmol/L EDTA) in a water bath at 37 °C and 100 rpm for 5 min, followed by centrifugation at 1000 rpm for 10 min. The precipitates were resuspended in 10 mL of plate culture medium (DMEM, 0.1 mmol/L

penicillin, 0.06 mmol/L streptomycin, 10% HI-FBS, pH 7.4), swirled, spread on 100 mm culture dishes, and incubated at 37 °C. After 20 h, the cells were washed with 10 mL of PBS three times, and supplemented with 1 mL of trypsin. Finally, the cells were resuspended and subcultured for further analysis.

### **Isolation and confirmation of exosomes**

The supernatant of adipocytes was collected and centrifuged at 2000 × g for 30 min, followed by filtration through a 0.22 μm membrane to remove apoptotic cells, debris, and large particles. Exosomes were extracted from the filtrate according to the manufacturer's instructions as described previously [21]. For further confirmation, the diluted exosomes were subjected to NanoFCM (China) for transmission electron microscopy and size distribution analysis.

### **Luciferase reporter assay and RNA pull-down assay**

The luciferase reporter assay was performed using the Dual-Luciferase Reporter Assay System (Promega, United States), as described previously [22]. The RNA pull-down assay was performed using the Pierce Magnetic RNA-Protein Pull-Down Kit (Thermo, United States). Briefly, miR-15a-5p was biotinylated and transfected into the Caco-2 cells. Cultured cells were collected for lysis 48 h later. Thereafter, the RNA bound to miR-15a-5p was captured using Pierce nucleic acid-compatible streptavidin magnetic beads. Finally, qRT-PCR was performed to determine the expression of metastasis-associated lung adenocarcinoma transcript 1 (MALAT1).

### **Transfection of shMALAT1 and miR-15a-5p mimic**

Adipocytes were transfected with shMALAT1 and miR-15a-5p using Plko.1-EGFP-puro. ShMALAT1 was designed based on information from Thermo Fisher (<http://rnaidesigner.thermofisher.com/rnaidesigner/>). The sequence of shMALAT1 was 5'-TGTACTATCCCATCACTGAAG-3'.

### **Statistical analysis**

All data are presented as mean ± SD. Differences between two groups were analyzed using the Student's *t*-test. Two-way analysis of variance was used to compare the differences between multiple groups with two factors. All statistical analyses were performed using GraphPad 9.0.2 software, and *P* < 0.05 was considered to indicate a significant difference between groups.

## **RESULTS**

### **High-fat diet aggravated TNBS-induced colitis**

Accumulating evidence has shown that CD is more severe in obese individuals. We established a model of obesity in mice fed a HFD for 12 wk, while mice on a ND were used as controls. Thereafter, TNBS was used to induce colitis in the mice (Figure 1A). Compared with the control group, colon length was significantly shortened in the TNBS treatment group and the effect was further exacerbated by HFD (Figure 1B). To determine the degree of colitis activity index in different groups of mice, the DAI score was calculated daily for 8 d after starting TNBS treatment. HFD mice had a higher DAI score than the ND mice (Figure 1C). In addition, HFD significantly aggravated the TNBS-induced weight loss in mice (Figure 1D). To observe the degree of tissue damage in the mouse colon more intuitively, we used the colon tissue for HE staining and determined the histological injury scores (Figure 1E and F), which showed that HFD aggravated TNBS-induced colitis and tissue damage.

In addition, we measured the expression levels of pro-inflammatory cytokines in the colon tissues of mice in each group. The expression of TNF-α, IL-1β, and IL-6 in the colon of HFD mice treated with TNBS was significantly higher than that in ND mice treated with TNBS (Figure 1G-I). Notably, HFD itself increased the levels of pro-inflammatory cytokines in the colon of mice, which may be related to chronic inflammatory states in the body caused by obesity. These results suggest that HFD aggravates the severity of TNBS-induced colitis.

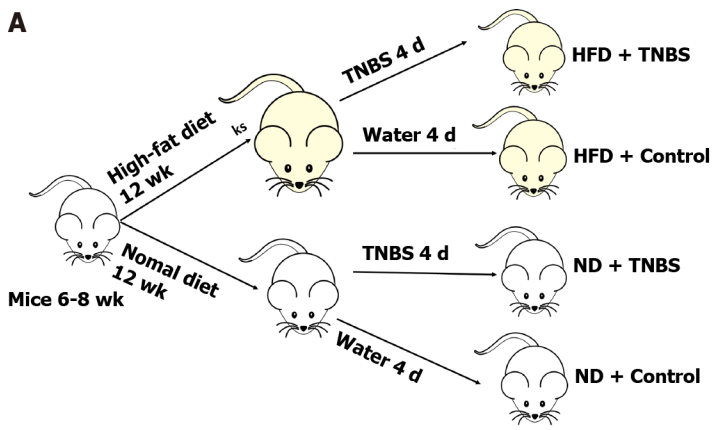
### **Successful extraction and identification of mesenteric adipose tissue derived exosomes (MAT-Exos)**

The mesenteric adipose tissue index was significantly increased in HFD mice (Figure 2A). MAT-Exos were isolated from mesenteric adipose tissue cultured in vitro, and the typical mitochondrial morphology was observed using transmission electron microscopy (Figure 2B). Using Western blotting, we demonstrated that the isolated exosomes expressed exosomal marker proteins CD63 and TSG101 and the adipocyte exosomal membrane protein HSP70 (Figure 2C). The properties of exosomes were further demonstrated by particle size analysis (Figure 2D). In summary, we successfully harvested and identified exosomes from mesenteric adipose tissue.

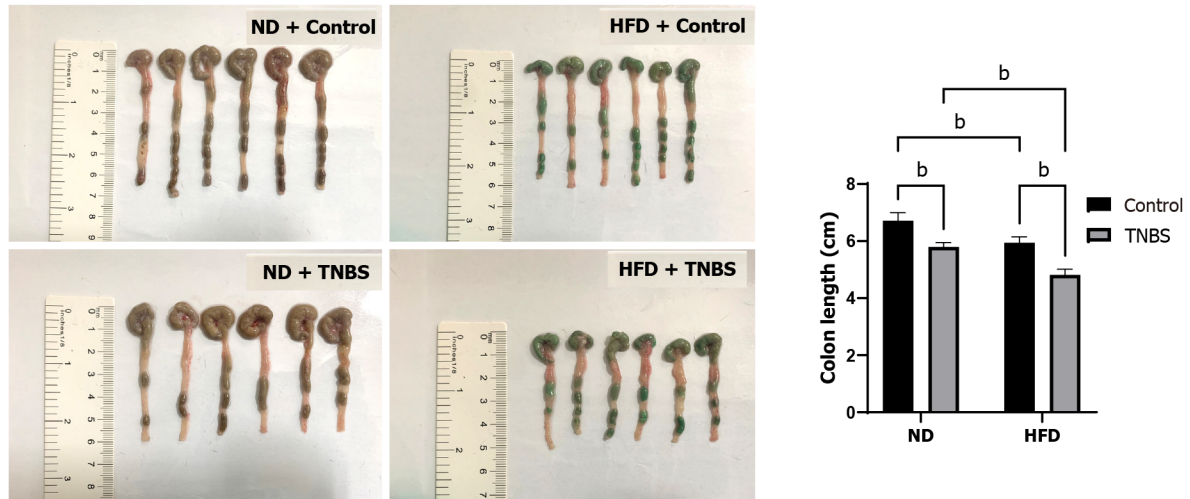
### **Partial contribution of MAT-Exo to increased colon lncRNA MALAT1 Levels in HFD-fed mice**

Existing literature indicates increased levels of lncRNA MALAT1 in HFD-fed mice [23]. In this study, the expression of lncRNA MALAT1 in MAT-Exos was found to be significantly increased in HFD-fed mice

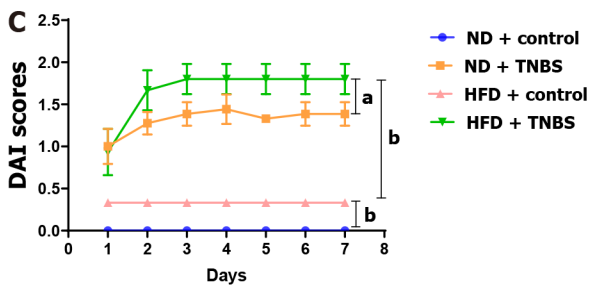
**A**



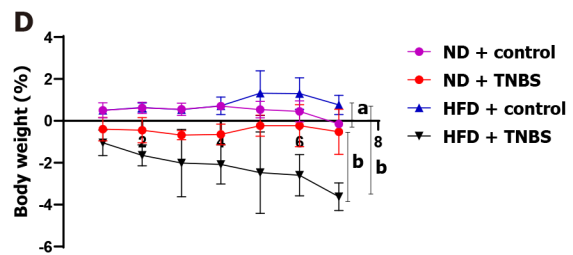
**B**



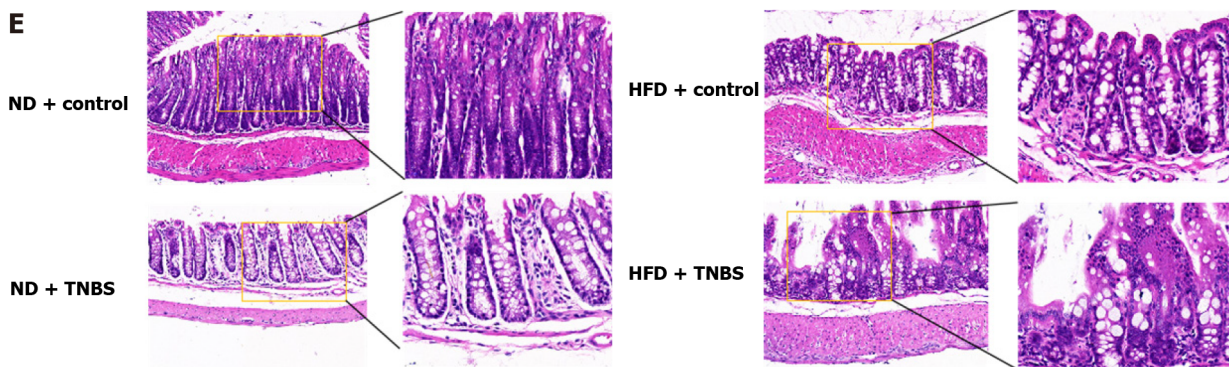
**C**



**D**



**E**



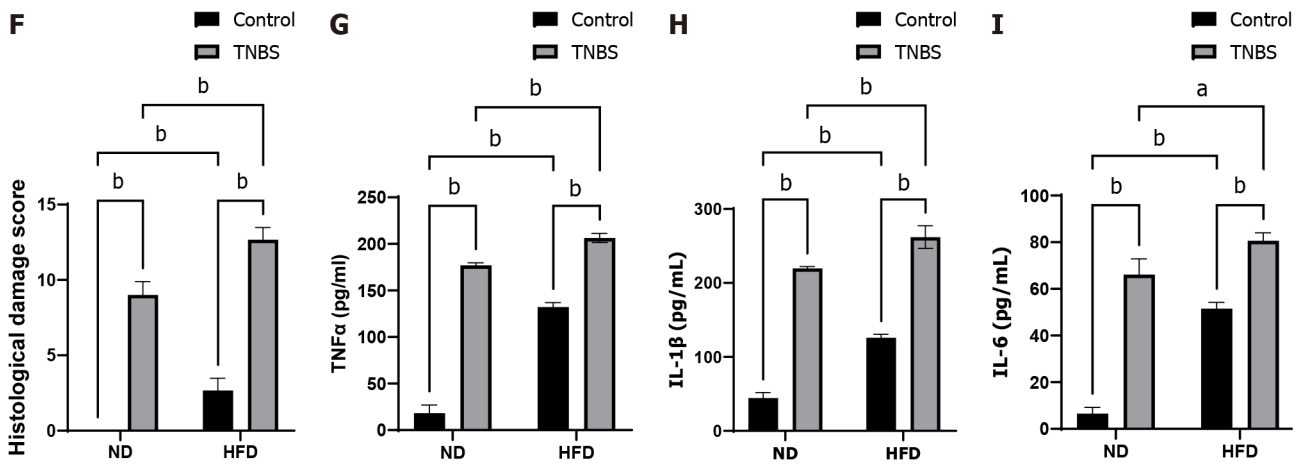


**Figure 1 High-fat diet aggravated colitis.** A: Experimental grouping process; B: Colon length of mice in each group; C: Disease activity index of mice in each group; D: Body weight change trend of mice in each group; E: Hematoxylin and eosin staining images of colon tissue; F: Histological damage score of colon tissue; G: Expression of tumor necrosis factor- $\alpha$  in colon tissue by enzyme linked immunosorbent assay (ELISA); H: Expression of interleukin-1 $\beta$  in colon tissue by ELISA; I: Expression of interleukin-6 (IL-6) in colon tissue by ELISA. DAI: Disease activity index; TNBS: 2,4,6-trinitrobenzenesulfonic acid; HFD: High-fat diet; ND: Normal diet; TNF- $\alpha$ : Tumor necrosis factor- $\alpha$ ; IL-1 $\beta$ : Interleukin-1 $\beta$ . <sup>a</sup>*P* < 0.05, <sup>b</sup>*P* < 0.01.

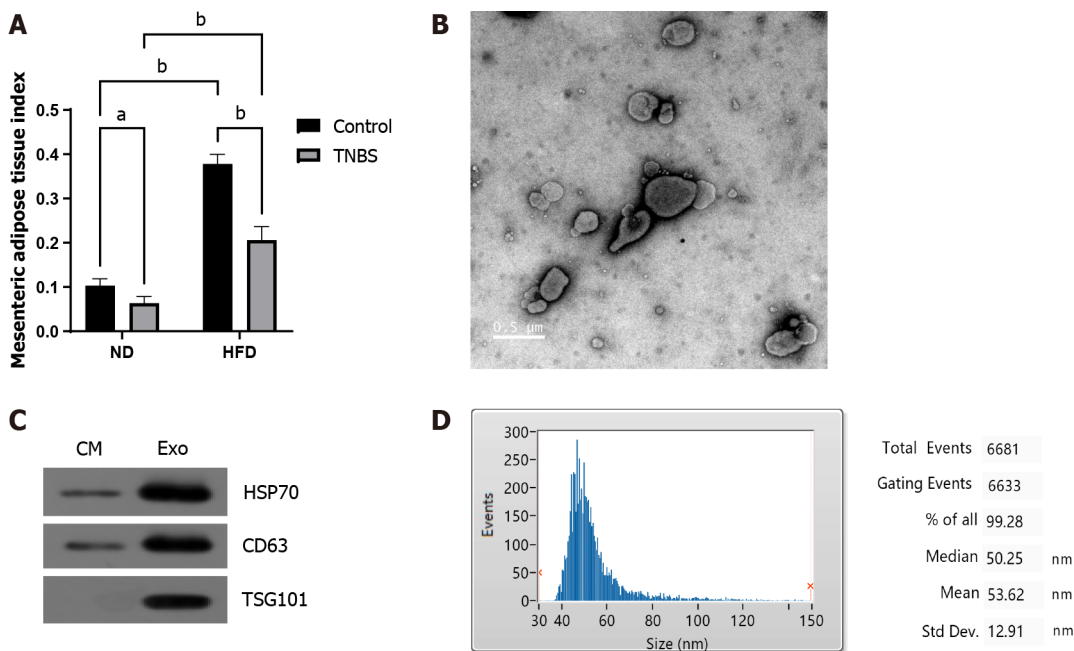


**Figure 2 Extraction and identification of exosomes derived from mesenteric adipose tissue.** A: Mesenteric adipose index of mice in each group; B: Images of exosomes observed under transmission electron microscopy; C: Western blotting to detect exosome marker proteins; D: Exosome particle size analysis. TNBS: 2,4,6-trinitrobenzenesulfonic acid; HFD: High-fat diet; ND: Normal diet. <sup>a</sup>*P* < 0.05, <sup>b</sup>*P* < 0.01.

using qRT-PCR (Figure 3A). The relative expression of lncRNA MALAT1 in mesenteric adipose and colon tissue in HFD mice treated with TNBS was significantly increased compared to that in ND mice treated with TNBS (Figure 3B and C). Therefore, we focused our attention on lncRNA MALAT1 and speculated that the increase in the relative expression of MALAT1 in the colon tissue of HFD mice may be partially attributed to exosomes from the mesenteric adipose tissue.

For further verification, MAT-Exos labeled with a PKH26 marker were incubated with Caco2 cells in vitro. PKH26 fluorescence in Caco2 cells was detected using a laser scanning confocal microscope, indicating that Caco2 cells can absorb MAT-Exos (Supplementary Figure 1). In addition, exosomes isolated from the mesenteric adipose tissue of HFD-fed and ND mice were injected into the mice *via* the tail vein, followed by lncRNA MALAT1 detection in the mouse colon tissue. MAT-Exos of HFD-fed mice increased the relative expression of lncRNA MALAT1 in the colon tissues of recipient mice (Figure 3D). We speculate that in HFD mice, the MAT-Exos-encapsulated lncRNA MALAT1 might target the colon to increase its local expression.

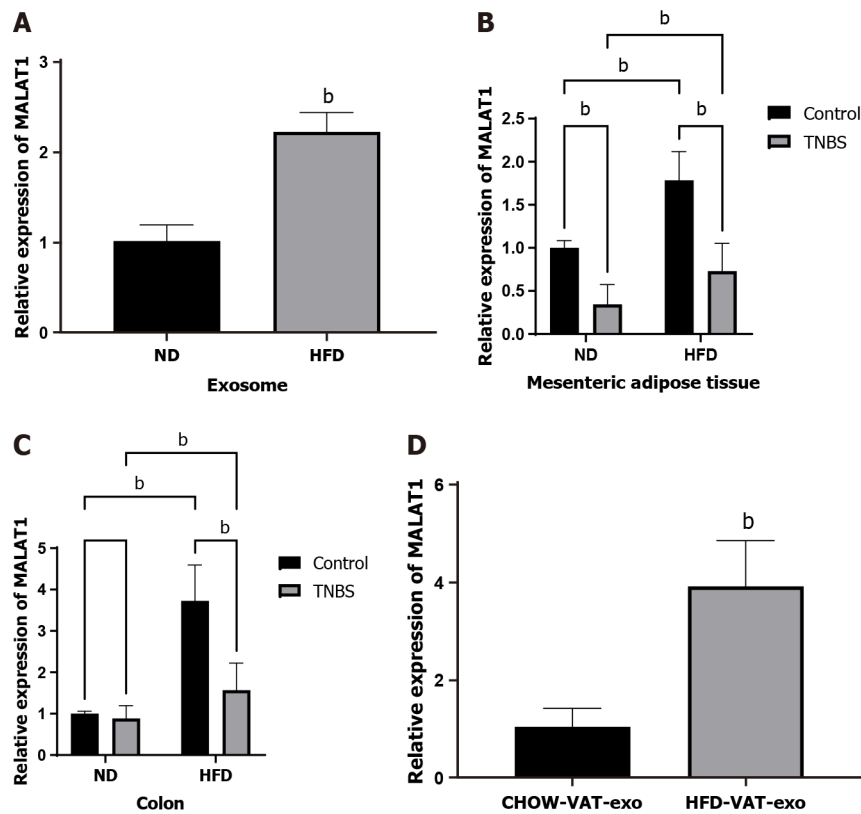


**Figure 3** Mesenteric adipose tissue derived exosomes from high-fat diet-fed mice increase the expression of long noncoding RNAs metastasis-associated lung adenocarcinoma transcript 1 in colon. **A:** Expression of metastasis-associated lung adenocarcinoma transcript 1 (MALAT1) in mesenteric adipose tissue derived exosomes (MAT-Exos) in each group; **B:** Expression of MALAT1 in mesenteric adipose tissue in each group; **C:** Expression of MALAT1 in colon in each group; **D:** Expression of MALAT1 in colon of normal mice after treated with MAT-Exo extracted from high-fat diet mice or normal diet mice. MALAT1: Metastasis-associated lung adenocarcinoma transcript 1; TNBS: 2,4,6-trinitrobenzenesulfonic acid; HFD: High-fat diet; ND: Normal diet. <sup>b</sup>*P* < 0.01.

### ***LncRNA MALAT1 targets the miR-15a-5p/ATF6 axis***

Numerous miRNAs with the ability to interact with lncRNA MALAT1 have been reported in literature [24], among which miR-15a-5p has attracted our attention. After searching miRDB (<http://mirdb.org>) [25] and TargetScan, we identified many potential mRNAs downstream of miR-15a-5p. Combining the literature review and bioinformatic prediction (Figure 4A), we chose ATF6 as the target mRNA of miR-15a-5p. ATF6 is an important molecule associated with endoplasmic reticulum (ER) stress [26] involved in gut homeostasis and IBD processes [27-29]. Western blotting was used to detect ATF6 expression in the colon tissues of mice in each group. The ATF6 levels in the colon tissues of ND mice treated with TNBS were higher than those in ND mice without TNBS treatment. In addition, HFD was found to upregulate the expression of ATF6 in the colon tissues (Figure 4B). Subsequently, we used a dual-luciferase assay to confirm the interaction between ATF6 and miR-15a-5p. Compared with the control group, miR-15a-5p reduced the relative expression of ATF6 when placed downstream of the wild-type 3' untranslated regions (3' UTRs), but not when it was downstream of the mutant 3' UTR, indicating a regulatory relationship between miR-15a-5p and ATF6 (Figure 4C). We then verified the interaction between miR-15a-5p and MALAT1 using RNA pull-down assays. We found that miR-15a-5p could bind to MALAT1, whereas the mutant miR-15a-5p could not pull down MALAT1 (Figure 4D). Based on these direct and indirect evidences, we can conclude that lncRNA MALAT1 can act on the miR-15a-5p/ATF6 axis.

### ***LncRNA MALAT1 binds miR-15a-5p to aggravate TNBS-induced colitis in HFD-fed mice***

We designed animal experiments to further demonstrate that mesenteric adipose tissue derived exosomes and their encapsulated lncRNA-MALAT1 can aggravate TNBS-induced colitis in HFD mice. First, MAT-Exos from HFD mice were isolated, and treated with either a short hairpin RNA targeting MALAT1 (shMALAT1) or a miR-15a-5p mimic before injection. MAT-Exos from ND mice were used as a control. Thereafter, the mice were randomly divided into four groups and treated with ND-MAT-Exos, HFD-MAT-Exos, HFD-MAT-Exos + shMALAT1, or HFD-MAT-Exos + miR-15a-5p mimic, *i.e.*, A, B, C, and D groups, respectively. Mice were injected with MAT-Exos (100 µg/mouse) *via* the tail vein on days 1, 4, and 8. On day 3, TNBS was administered to induce colitis. On day 9, the mice were sacrificed and the colon tissue was collected. Compared to MAT-Exos from ND mice, MAT-EXOSs from HFD mice significantly increased the body weight loss (Figure 5A), DAI (Figure 5D), and histological damage

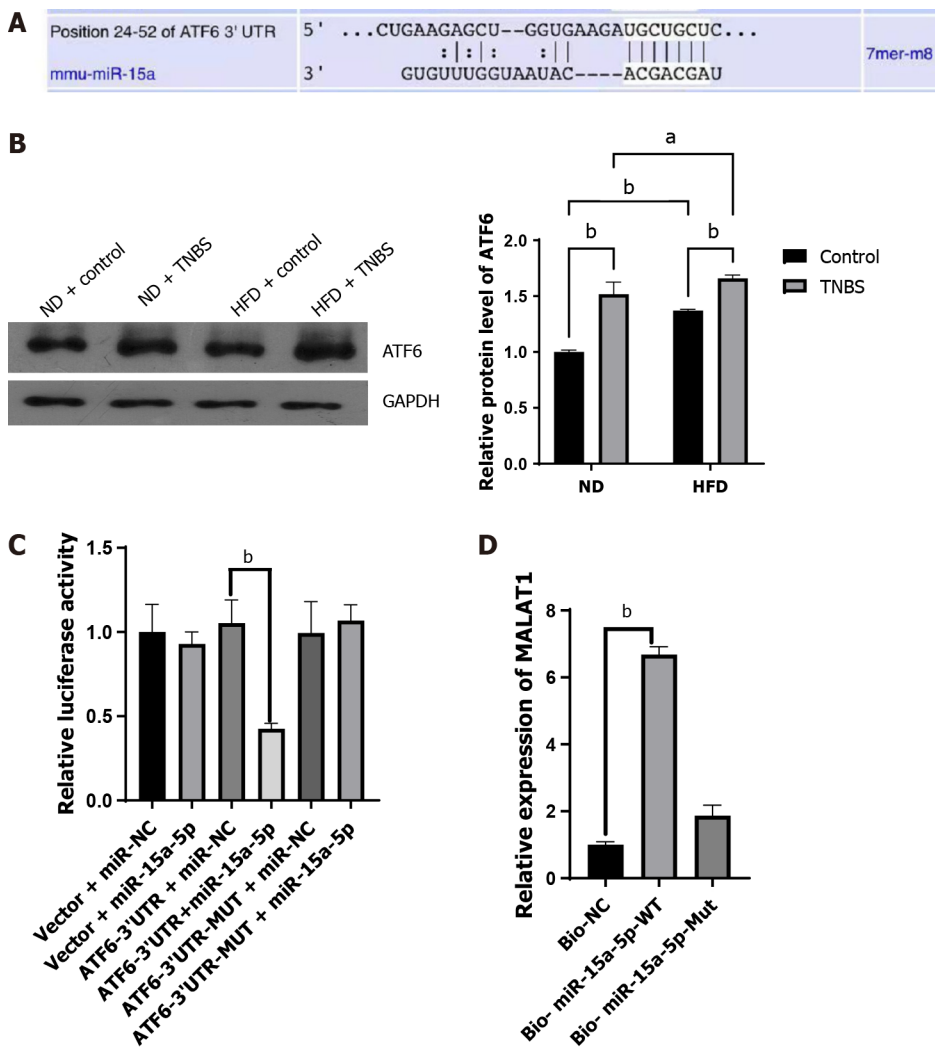


**Figure 4 Associations between metastasis-associated lung adenocarcinoma transcript 1 and miR-15a-5p/activating transcription factor 6.** A: Prediction of miR-15a-5p binding site on the 3' untranslated region of activating transcription factor 6 (ATF6); B: Western blotting to detect ATF6 protein; C: Dual luciferase report of miR-15a-5p and ATF6; D: RNA pull down analysis of miR-15a-5p and metastasis-associated lung adenocarcinoma transcript 1. ATF6: Activating transcription factor 6; TNBS: 2,4,6-trinitrobenzenesulfonic acid; HFD: High-fat diet; ND: Normal diet; 3' UTR: 3' untranslated region; WT: Wild type; Mut: Mutant. <sup>a</sup> $P < 0.05$ , <sup>b</sup> $P < 0.01$ .

score (Figure 5E and F), and decreased colon length (Figure 5B and C). Transfection with shMALAT1 to knockdown the expression of MALAT1 or treatment with the miR-15a-5p mimic to enhance the function of miR-15a-5p partially reversed the effects of MAT-Exos on HFD mice. In conclusion, lncRNA MALAT1 may sponge miR-15a-5p and aggravate TNBS-induced colitis in HFD mice.

#### ***LncRNA MALAT1 acted on the miR-15a-5p/ATF6 axis to exacerbate colitis in response to ER stress***

To further investigate whether lncRNA MALAT1 encapsulated within MAT-Exos of HFD mice aggravated TNBS-induced colitis *via* the miR-15a-5p/ATF6 axis, we detected the protein content of ATF6 in the colon tissue of mice in each group. MAT-Exos of HFD mice increased ATF6 expression in the colon tissue, whereas transfection with shMALAT1 or (A6) treatment with the miR-15a-5p mimic resulted in reduced expression of ATF6 in the colon tissue (Figure 6A). ATF6 is involved in IBD that develops in response to ER stress[30]. We further examined the expression of proteins associated with the ATF6-related ER stress pathway in the colon tissue. The expression of GRP78 and XBP-1 was increased in the colon of mice injected with MAT-Exos from HFD mice, a phenomenon that was antagonized by shMALAT1 and the miR-15a-5p mimic (Figure 6B; Supplementary Figure 2). In addition, the expression of other ER stress pathway related proteins, such as p-PERK, p-IRE1, p-eIF2 $\alpha$ , and CHOP, also increased upon injecting MAT-Exos into HFD mice (Figure 6B). Previous studies have shown that ER stress activates NF- $\kappa$ B signaling to induce an inflammatory response[31,32]. Therefore, we also detected inflammatory factors associated with the NF- $\kappa$ B pathway (Figure 6C) using ELISA. The observed changes were consistent with the expression of proteins associated with the ATF6-related ER stress pathway.

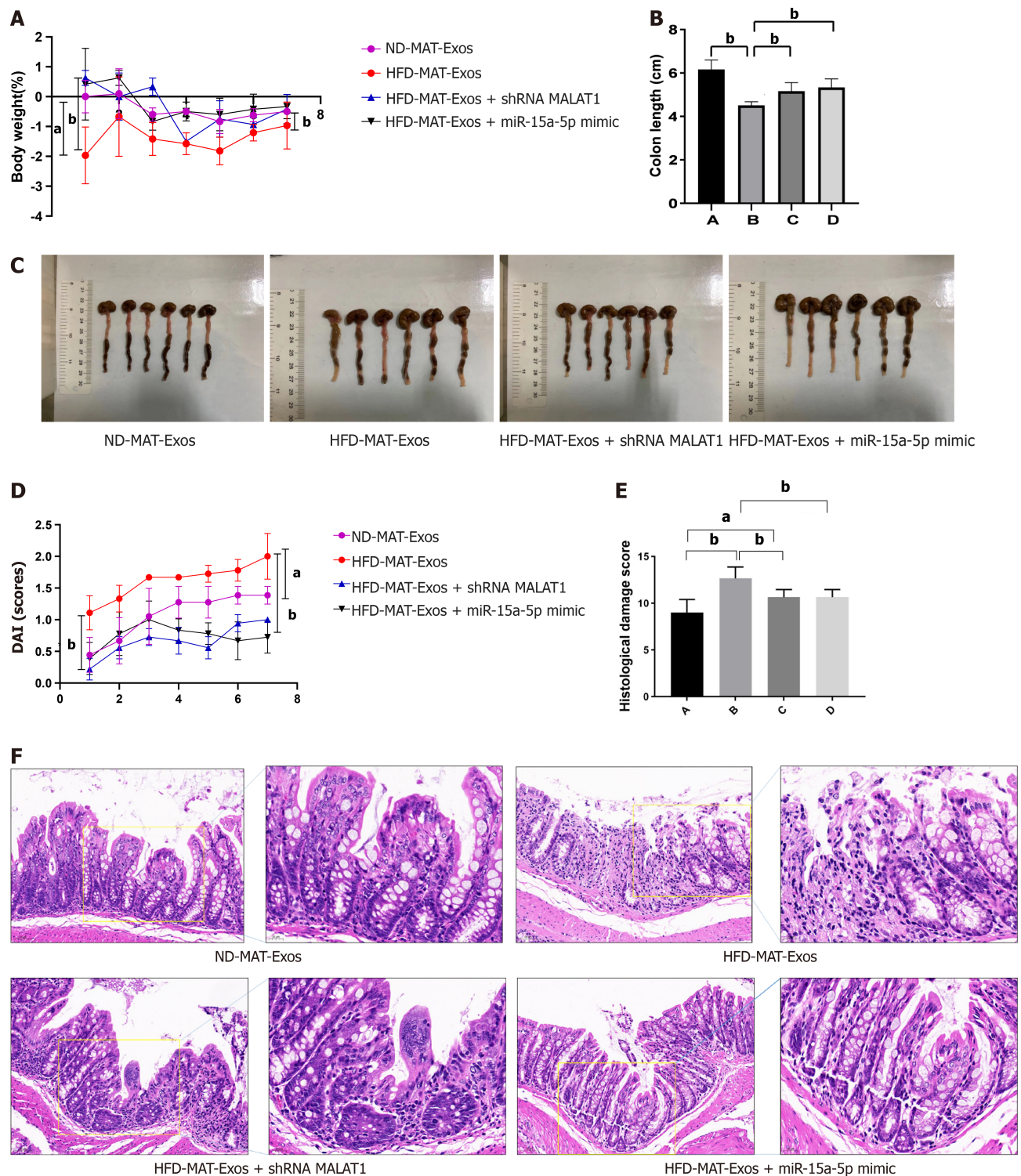


**Figure 5 Mesenteric adipose tissue derived exosomes of high-fat diet-fed mice aggravate 2,4,6-trinitrobenzenesulfonic acid solution-induced colitis, reversed by shMALAT1 and miR-15a-5p mimic.** A: Body weight change trend of mice in each group; B: Colon length of mice in each group; ND-MAT-Exos, HFD-MAT-Exos, HFD-MAT-Exos + shMALAT1, and HFD-MAT-Exos + miR-15a-5p mimic are labelled as A, B, C, and D groups, respectively; C: Colon image of mice in each group; D: Disease activity index of mice in each group; E: Histological damage score of colon tissue, ND-MAT-Exos, HFD-MAT-Exos, HFD-MAT-Exos + shMALAT1, and HFD-MAT-Exos + miR-15a-5p mimic are labelled as A, B, C, and D groups, respectively; F: Hematoxylin and eosin staining images of colon tissue. HFD: High-fat diet; ND: Normal diet; MAT-Exos: Mesenteric adipose tissue derived exosomes; MALAT1: Metastasis-associated lung adenocarcinoma transcript 1. <sup>a</sup>*P* < 0.05, <sup>b</sup>*P* < 0.01.

## DISCUSSION

Currently, almost one-third of the patients with IBD are obese and have a poor quality of life[8], great difficulty in inducing remission[33-35], increased risk of disease recurrence[8], and a higher burden of hospitalization and disease expenditure[36]. Therefore, it is necessary to explore the mechanism by

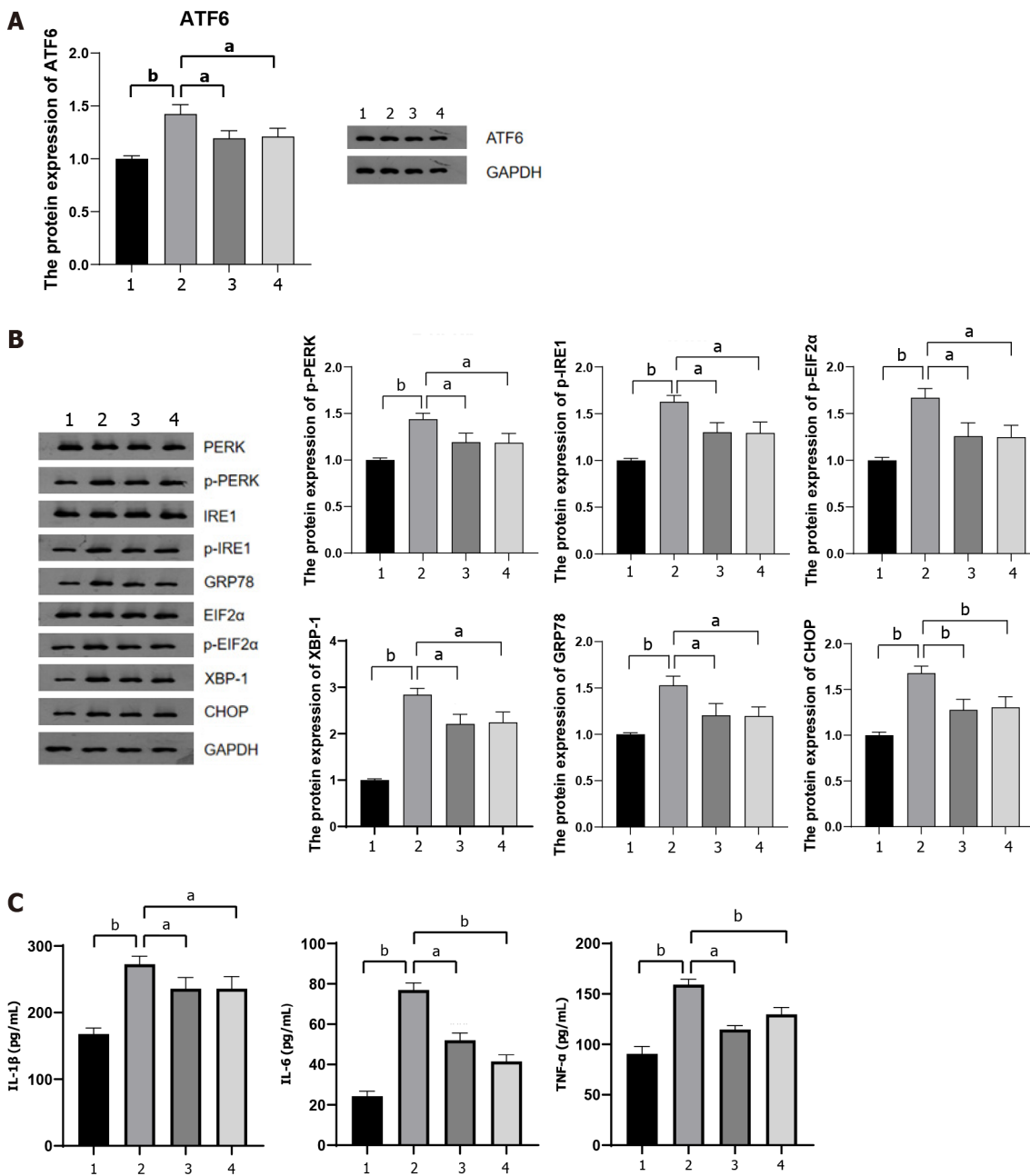


**Figure 6** Long noncoding RNAs metastasis-associated lung adenocarcinoma transcript 1 acted on the miR-15a-5p/activating transcription factor 6 axis to activate the endoplasmic reticulum stress signaling pathway. ND-MAT-Exos, HFD-MAT-Exos, HFD-MAT-Exos + shMALAT1, and HFD-MAT-Exos + miR-15a-5p mimic are labelled as 1, 2, 3, and 4 groups, respectively. A: The expression level of activating transcription factor 6 in colon tissue; B: The expression level of endoplasmic reticulum stress related proteins in colon tissue detected by Western blotting; C: The expression level of interleukin (IL)- $\beta$ , tumor necrosis factor  $\alpha$ , IL-6 in the colon tissue detected by enzyme linked immunosorbent assay. ATF-6: Activating transcription factor 6; IL: Interleukin; TNF- $\alpha$ : Tumor necrosis factor  $\alpha$ . <sup>a</sup> $P < 0.05$ , <sup>b</sup> $P < 0.01$ .

which obesity is induced in IBD to improve its treatment. Previous studies have shown that the increased severity of IBD in obese patients is related to increased intestinal permeability, intestinal microflora translocation, and changes in the intestinal microflora spectrum[37,38]. In addition, the increase in plasma leptin levels and decrease in adiponectin levels were also found to be involved in obesity-mediated IBD aggravation, but the mechanisms underlying these processes need further exploration[39]. In this study, we propose a novel mechanism through which obesity aggravates IBD *via* exosome-secreted lncRNAs.

First, we demonstrated that a high-fat diet could aggravate TNBS-induced colitis in mice and explored the underlying mechanisms. One of the main characteristics of obesity is the accumulation of adipose tissue. As adipose tissue is an endocrine organ, it plays an important role in a variety of metabolism-related diseases, especially visceral adipose tissue[40]. We focused our attention on the mesenteric adipose tissue, a type of visceral adipose tissue, as it is closest to the colon tissue and can communicate with the colon in various ways. In patients with CD, the lesion is often surrounded by a

special type of mesenteric adipose tissue called creeping fat, which is associated with the translocation of gut microbiota[41]. These findings suggest that the mesenteric adipose tissue may play an important role in IBD progression. We further found that TNBS treatment reduced the content of the mesenteric adipose tissue. However, the content of the mesenteric adipose tissue in HFD mice treated with TNBS was still significantly higher than that in ND mice treated with TNBS.

Exosomes serve as important means of intercellular communication. Previous reports have shown that exosomes secreted by visceral fat could target the colon tissue[16]. Therefore, we hypothesized that mesenteric-derived exosomes in obese mice may aggravate TNBS-induced colitis. Exosomes from the mesenteric adipose tissue were isolated and identified. Subsequently, exosomes extracted from the mesenteric adipose tissue of HFD and ND mice were separately injected into TNBS-treated ND mice *via* the tail vein. The results showed that exosomes from the mesenteric adipose tissue of HFD mice aggravated TNBS-induced colitis.

We then investigated the molecular mechanism by which exosomes derived from the mesenteric adipose tissue of HFD mice aggravated TNBS-induced colitis. A recent study indicated that visceral adipose tissue-derived exosomes can exacerbate colitis severity through proinflammatory noncoding RNAs such as miR-155[16]. In this study, we focused on the lncRNAs in exosomes. Using qRT-PCR, we identified that lncRNA expression is strongly associated with HFD in mesenteric adipose exosomes, as well as mesenteric adipose and colon tissues. In the same structures or tissues, the expression of MALAT1 was higher in TNBS-treated HFD mice than in TNBS-treated ND mice. An additional injection of MAT-Exos from HFD mice *via* the tail vein increased the relative expression of MALAT1 in the colon tissue, indicating that the increased expression of lncRNA MALAT1 in the colon tissue can be partially attributed to MAT-Exos arising from increased creeping fat. In fact, shMALAT1 partially reversed the effect of exosomes derived from the mesenteric adipose tissue in HFD mice, suggesting that exosomes derived from the mesenteric adipose tissue in HFD mice aggravated TNBS-induced enteritis in part due to the high expression of lncRNA MALAT1 in exosomes.

The mechanism by which lncRNA aggravates colitis was further investigated. We revealed that lncRNA MALAT1 could bind miR-15a-5p *in vivo*, and that the miR-15a-5p mimic could reverse the aggravation of colitis. Furthermore, the miR-15a-5p mimic and sh-MALAT1 reversed the HFD mice MAT-Exos-induced increase in the expression of ER stress-related proteins, including ATF6. We further verified the interaction between miR-15-5p and ATF6 using a dual-luciferase reporter assay. These results indicate that lncRNA MALAT1 may activate the ATF6-related ER stress signaling pathway by binding miR-15a-5p.

MALAT1 is abundantly expressed and highly conserved in 33 species of mammals, with the earliest study linking it to metastasis in non-small cell lung cancer[42]. However, recent studies have shown that MALAT1 plays an important role in a variety of tumors[18] as well as in a variety of autoimmune[43], infectious[44,45], and metabolism-related diseases[46]. Previous studies have shown that MALAT1 Levels are reduced in the plasma of patients with CD[47], suggesting that MALAT1 may be a protective factor with respect to the occurrence and development of CD. The results of our study indicated that TNBS treatment decreased the expression of MALAT1, in accordance with finding of previous reports, but the differences were not significant. Moreover, Li *et al*[48] indicated that MALAT1 targets intestinal epithelial cells and enhances the intestinal epithelial barrier, which plays a protective role by sequestering miR-146b-5p and maintaining the expression of AJC proteins, NUMB, and CLDN11 in IBD. However, they did not demonstrate an effect of MALAT1 overexpression on colitis *in vivo*.

Intriguingly, our study showed that obesity-induced increases in MALAT1 expression in colon tissue can aggravate colitis, suggesting that MALAT1 may be a double-edged sword with respect to IBD. Mechanistically, the contrary effect of MALAT1 in colitis was mainly due to the fact that exosomes derived from the mesenteric adipose tissue targeted the lamina propria of the colon rather than intestinal epithelial cells[16]. Many immune cells are distributed within the lamina propria of the colon, including dendritic cells, macrophages, and lymphoid cells, which supplement the barrier function of intestinal epithelial cells[49]. In addition, many adaptive immune system-related lymphocytes are recruited from peripheral circulation to the lamina propria and are involved in the onset and progression of IBD. LncRNA MALAT1 encapsulated in exosomes from the mesenteric adipose tissue may act on the abovementioned immune cells in the lamina propria and activate the ATF6-related ER stress pathway to promote the release of pro-inflammatory cytokines[50].

ER stress plays a role in the occurrence and development of metabolic syndrome-related diseases in the obese population[51]. Our study demonstrates that ER stress is one of the potential mechanisms by which obesity aggravates IBD, thereby highlighting the importance of weight loss in obese patients with IBD and the treatment of metabolic syndrome-related diseases. In addition, we preliminarily identified a new signaling pathway, namely, the MALAT1-miR-15a-5p/ATF6 axis, revealing a new regulatory mechanism, *i.e.*, the ATF6-related ER stress signaling pathway. Whether this signaling pathway plays a role in other tissues or diseases requires further investigation.

This study has several limitations that should be acknowledged. First, the effect of exosomes derived from the mesenteric adipose tissue was only studied in the colon as a whole, and the specific target cell types remain unclear and require further elucidation. Second, it would be more beneficial if the regulation of the lncRNAMALAT1-miR-15a-5p-ATF6 pathway could be confirmed in a more in-depth investigation. Finally, we speculated that the divergent effect of lncRNA MALAT1 on IBD severity may

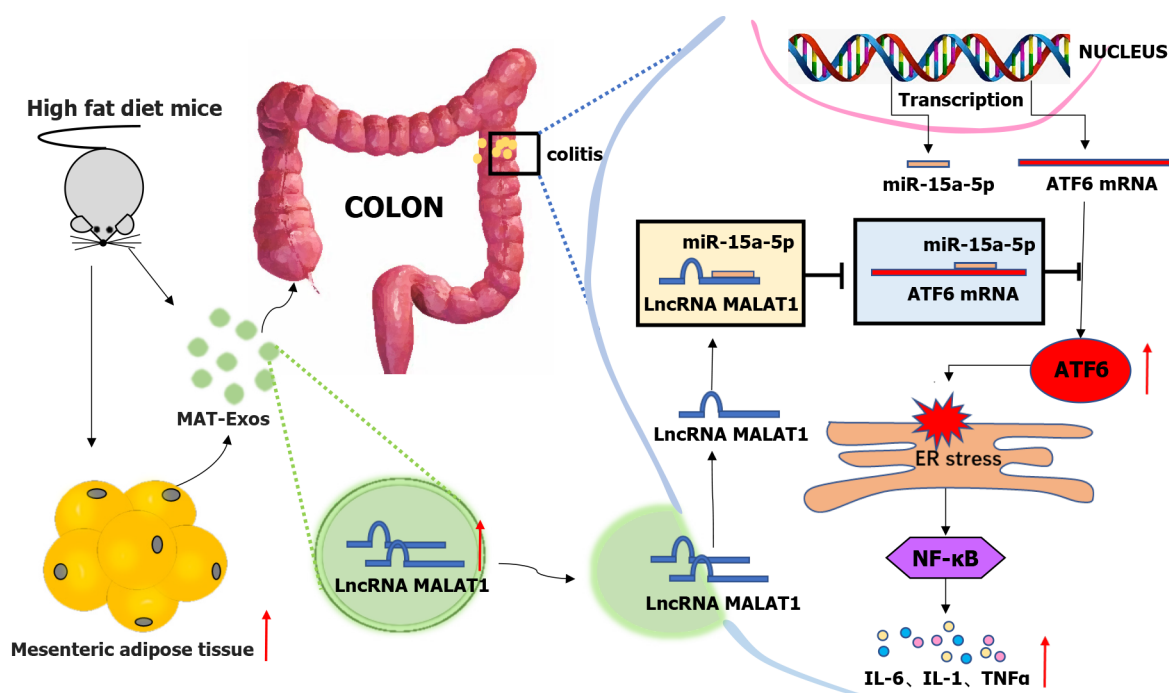


**Figure 7** Long non-coding RNA metastasis-associated lung adenocarcinoma transcript 1 encapsulated by mesenteric adipose tissue-derived exosomes targets the colon to aggravate colitis via the microRNA-15a-5p/activating transcription factor 6 axis in response to endoplasmic reticulum stress. ATF-6: Activating transcription factor 6; LncRNA: Long non-coding RNA; IL: Interleukin; TNF- $\alpha$ : Tumor necrosis factor- $\alpha$ ; ER: Endoplasmic reticulum; MAT-Exos: Mesenteric adipose tissue derived exosomes; MALAT1: Metastasis-associated lung adenocarcinoma transcript 1.

be due to its various targeting areas, where endogenous MALAT1 may exert its effect on intestinal epithelial cells, while extrinsic mesenteric adipose tissue-derived EXO-MALAT1 may act on the intestinal lamina propria through its gut-homing property. However, this theory requires further exploration in the future.

Overall, HFD increased the content of the mesenteric adipose tissue and associated EXO lncRNA MALAT1, which was then absorbed by the colon where it targeted the miR-15a-5p/ATF6 axis, thereby leading to the activation of the ER stress pathway. Further, downstream activation of the inflammatory factor signaling pathway may partially contribute to the aggravation of colitis in obese IBD patients.

## CONCLUSION

A higher visceral adipose-tissue ratio was associated with an increased disease activity in CD patients. But the underlining mechanism still remains elusive. Our study indicated that high-fat diet increased the content of mesenteric adipose tissue and aggravated colitis in mice. Mesenteric adipose tissue derived exosome lncRNA metastasis-associated lung adenocarcinoma transcript 1 can be absorbed by the colon leading to activation of the endoplasmic reticulum stress pathway by way of targeting the miR-15a-5p/ATF6 axis to aggravate colitis (Figure 7).

## ARTICLE HIGHLIGHTS

### Research background

Obesity is associated with an increased risk of developing Crohn's disease (CD), higher disease activity, and comparatively worse clinical outcomes, especially in CD patients with a high visceral adipose tissue ratio. However, the underlying mechanisms remain unclear.

### Research motivation

Exosomes contain multiple non-coding RNAs such as long non-coding RNAs (lncRNAs), which serve as messengers in cell-cell communication. Visceral adipose tissue derived exosomes display tissue affinity and preferentially target the colonic lamina propria. We hypothesized that obesity exacerbates inflammatory bowel disease, partially through mesenteric adipose tissue-derived exosomes.

### Research objectives

To investigate the role of mesenteric adipose tissue-derived exosomes in CD aggravation through obesity, thereby providing a potential therapeutic target for CD in this subpopulation.

### Research methods

A 2,4,6-trinitrobenzenesulfonic acid (TNBS) was used to induce colitis in mice fed a high-fat diet (HFD) and normal diet (ND). Exosomes from the mesenteric adipose tissue were extracted and identified, followed by the investigation of lncRNA metastasis-associated lung adenocarcinoma transcript 1 (MALAT1) expression. Luciferase reporter and RNA pull-down assays were performed to verify the interaction between MALAT1 and miR-15a-5p/activating transcription factor 6 (ATF6) axis. Finally, mesenteric adipose tissue-derived exosomes extracted from HFD-fed mice were isolated and treated with either a short hairpin RNA targeting MALAT1 (shMALAT) or an miR-15a-5p mimic before being injected into mice to explore their influence on TNBS-induced colitis.

### Research results

HFD can aggravate TNBS-induced colitis in mice, and increase the expression of MALAT1 in mesenteric adipose tissue-derived exosomes. Increased expression of MALAT1 in the colon tissue exacerbated TNBS-induced colitis and activated the ATF6-related endoplasmic reticulum stress pathway. Moreover, this effect was partially reversed by the reduced expression of MALAT1 and overexpression of miR-15a-5p.

### Research conclusions

Mesenteric adipose tissue-derived exosome-encapsulated lncRNA MALAT1 targets the colon and aggravates TNBS-induced colitis in obese mice, which may potentially act on the miR-15a-5p/ATF6 axis and induce endoplasmic reticulum stress.

### Research perspectives

Obesity-mediated aggravation of colitis might involve the mesenteric adipose tissue-derived exosome lncRNA MALAT1, but the specific cells of the intestine targeted by MALAT1 deserve further exploration.

---

## FOOTNOTES

**Author contributions:** Jin X designed the report; Chen D performed experiments and statistical analysis; Lu MM wrote the paper and assisted to design the report; Wang JH, Ren Y, Wang SS, Xu LL, Cheng XF, Cheng WX, Gao JG, and Li XL assisted to perform experiments and analyzed data; Kalyani FS assisted with paper writing; all authors had access to the study data and reviewed and approved the final manuscript.

**Supported by** the National Natural Science Foundation of China, No. 81770574; and the Natural Science Foundation of Zhejiang Province, No. LZ21H030002 and No. LY21H030005.

**Institutional animal care and use committee statement:** The study was reviewed and approved by the institutional review board of the Tab of Animal Experimental Ethical Inspection of the First Affiliated Hospital of Zhejiang University, NO. 2020-1101.

**Conflict-of-interest statement:** There are no conflicts of interest to report.

**Data sharing statement:** All the data included in this study are available upon request by contact with the corresponding author.

**ARRIVE guidelines statement:** The authors have read the ARRIVE guidelines, and the manuscript was prepared and revised according to the ARRIVE guidelines.

**Open-Access:** This article is an open-access article that was selected by an in-house editor and fully peer-reviewed by external reviewers. It is distributed in accordance with the Creative Commons Attribution NonCommercial (CC BY-NC 4.0) license, which permits others to distribute, remix, adapt, build upon this work non-commercially, and license their derivative works on different terms, provided the original work is properly cited and the use is non-commercial. See: <https://creativecommons.org/licenses/by-nc/4.0/>

**Country/Territory of origin:** China

**ORCID number:** Dong Chen 0000-0003-3892-9248; Miao-Miao Lu 0000-0002-9328-8239; Jin-Hai Wang 0000-0002-4640-7661; Yue Ren 0000-0001-9071-2738; Ling-Ling Xu 0000-0002-6668-3057; Wei-Xin Cheng 0000-0003-1764-0779; Sai-Sai Wang 0000-0002-5436-5385; Xiao-Lin Li 0000-0003-3682-3237; Xiao-Fei Cheng 0000-0003-3336-0996; Jian-Guo Gao 0000-

0002-9414-5395; Farhin Shaheed Kalyani 0000-0001-8276-8125; Xi Jin 0000-0001-9985-3035.

**S-Editor:** Chen YL**L-Editor:** A**P-Editor:** Yuan YY

---

## REFERENCES

- 1 **Torres J**, Mehandru S, Colombel JF, Peyrin-Biroulet L. Crohn's disease. *Lancet* 2017; **389**: 1741-1755 [PMID: 27914655 DOI: 10.1016/S0140-6736(16)31711-1]
- 2 **Molodecky NA**, Soon IS, Rabi DM, Ghali WA, Ferris M, Chernoff G, Benchimol EI, Panaccione R, Ghosh S, Barkema HW, Kaplan GG. Increasing incidence and prevalence of the inflammatory bowel diseases with time, based on systematic review. *Gastroenterology* 2012; **142**: 46-54.e42; quiz e30 [PMID: 22001864 DOI: 10.1053/j.gastro.2011.10.001]
- 3 **Ng SC**, Tang W, Ching JY, Wong M, Chow CM, Hui AJ, Wong TC, Leung VK, Tsang SW, Yu HH, Li MF, Ng KK, Kamm MA, Studd C, Bell S, Leong R, de Silva HJ, Kasturiratne A, Mufeena MNF, Ling KL, Ooi CJ, Tan PS, Ong D, Goh KL, Hilmi I, Pisespongsa P, Manatsathit S, Rerknimitr R, Aniwan S, Wang YF, Ouyang Q, Zeng Z, Zhu Z, Chen MH, Hu PJ, Wu K, Wang X, Simadibrata M, Abdullah M, Wu JC, Sung JY, Chan FKL; Asia-Pacific Crohn's and Colitis Epidemiologic Study (ACCESS) Study Group. Incidence and phenotype of inflammatory bowel disease based on results from the Asia-pacific Crohn's and colitis epidemiology study. *Gastroenterology* 2013; **145**: 158-165.e2 [PMID: 23583432 DOI: 10.1053/j.gastro.2013.04.007]
- 4 **Singh S**, Dulai PS, Zarrinpar A, Ramamoorthy S, Sandborn WJ. Obesity in IBD: epidemiology, pathogenesis, disease course and treatment outcomes. *Nat Rev Gastroenterol Hepatol* 2017; **14**: 110-121 [PMID: 27899815 DOI: 10.1038/nrgastro.2016.181]
- 5 **Khalili H**, Ananthakrishnan AN, Konijeti GG, Higuchi LM, Fuchs CS, Richter JM, Chan AT. Measures of obesity and risk of Crohn's disease and ulcerative colitis. *Inflamm Bowel Dis* 2015; **21**: 361-368 [PMID: 25563694 DOI: 10.1097/MIB.0000000000000283]
- 6 **Harpsoe MC**, Basit S, Andersson M, Nielsen NM, Frisch M, Wohlfahrt J, Nohr EA, Linneberg A, Jess T. Body mass index and risk of autoimmune diseases: a study within the Danish National Birth Cohort. *Int J Epidemiol* 2014; **43**: 843-855 [PMID: 24609069 DOI: 10.1093/ije/dyu045]
- 7 **Pringle PL**, Stewart KO, Peloquin JM, Sturgeon HC, Nguyen D, Sauk J, Garber JJ, Yajnik V, Ananthakrishnan AN, Chan AT, Xavier RJ, Khalili H. Body Mass Index, Genetic Susceptibility, and Risk of Complications Among Individuals with Crohn's Disease. *Inflamm Bowel Dis* 2015; **21**: 2304-2310 [PMID: 26181430 DOI: 10.1097/MIB.0000000000000498]
- 8 **Jain A**, Nguyen NH, Proudfoot JA, Martin CF, Sandborn WJ, Kappelman MD, Long MD, Singh S. Impact of Obesity on Disease Activity and Patient-Reported Outcomes Measurement Information System (PROMIS) in Inflammatory Bowel Diseases. *Am J Gastroenterol* 2019; **114**: 630-639 [PMID: 30865012 DOI: 10.14309/ajg.0000000000000197]
- 9 **Büning C**, von Kraft C, Hermsdorf M, Gentz E, Wirth EK, Valentini L, Haas V. Visceral Adipose Tissue in Patients with Crohn's Disease Correlates with Disease Activity, Inflammatory Markers, and Outcome. *Inflamm Bowel Dis* 2015; **21**: 2590-2597 [PMID: 26222339 DOI: 10.1097/MIB.0000000000000527]
- 10 **Scheja L**, Heeren J. The endocrine function of adipose tissues in health and cardiometabolic disease. *Nat Rev Endocrinol* 2019; **15**: 507-524 [PMID: 31296970 DOI: 10.1038/s41574-019-0230-6]
- 11 **Siegmund B**. Mesenteric fat in Crohn's disease: the hot spot of inflammation? *Gut* 2012; **61**: 3-5 [PMID: 22068165 DOI: 10.1136/gutjnl-2011-301354]
- 12 **Deng T**, Lyon CJ, Bergin S, Caligiuri MA, Hsueh WA. Obesity, Inflammation, and Cancer. *Annu Rev Pathol* 2016; **11**: 421-449 [PMID: 27193454 DOI: 10.1146/annurev-pathol-012615-044359]
- 13 **Packer M**. Epicardial Adipose Tissue May Mediate Deleterious Effects of Obesity and Inflammation on the Myocardium. *J Am Coll Cardiol* 2018; **71**: 2360-2372 [PMID: 29773163 DOI: 10.1016/j.jacc.2018.03.509]
- 14 **Schuster S**, Cabrera D, Arrese M, Feldstein AE. Triggering and resolution of inflammation in NASH. *Nat Rev Gastroenterol Hepatol* 2018; **15**: 349-364 [PMID: 29740166 DOI: 10.1038/s41575-018-0009-6]
- 15 **Sun Z**, Yang S, Zhou Q, Wang G, Song J, Li Z, Zhang Z, Xu J, Xia K, Chang Y, Liu J, Yuan W. Emerging role of exosome-derived long non-coding RNAs in tumor microenvironment. *Mol Cancer* 2018; **17**: 82 [PMID: 29678180 DOI: 10.1186/s12943-018-0831-z]
- 16 **Wei M**, Gao X, Liu L, Li Z, Wan Z, Dong Y, Chen X, Niu Y, Zhang J, Yang G. Visceral Adipose Tissue Derived Exosomes Exacerbate Colitis Severity via Pro-inflammatory MiRNAs in High Fat Diet Fed Mice. *ACS Nano* 2020; **14**: 5099-5110 [PMID: 32275391 DOI: 10.1021/acsnano.0c01860]
- 17 **Djebali S**, Davis CA, Merkel A, Dobin A, Lassmann T, Mortazavi A, Tanzer A, Lagarde J, Lin W, Schlesinger F, Xue C, Marinov GK, Khatun J, Williams BA, Zaleski C, Rozowsky J, Röder M, Kokocinski F, Abdelhamid RF, Alioto T, Antoshechkin I, Baer MT, Bar NS, Batut P, Bell K, Bell I, Chakraborty S, Chen X, Chhrast J, Curado J, Derrien T, Drenkow J, Dumais E, Dumais J, Dutttagupta R, Falconnet E, Fastuca M, Fejes-Toth K, Ferreira P, Foissac S, Fullwood MJ, Gao H, Gonzalez D, Gordon A, Gunawardena H, Howald C, Jha S, Johnson R, Kapranov P, King B, Kingswood C, Luo OJ, Park E, Persaud K, Preall JB, Ribeca P, Risk B, Robyr D, Sammeth M, Schaffer L, See LH, Shahab A, Skancke J, Suzuki AM, Takahashi H, Tilgner H, Trout D, Walters N, Wang H, Wrobel J, Yu Y, Ruan X, Hayashizaki Y, Harrow J, Gerstein M, Hubbard T, Reymond A, Antonarakis SE, Hannon G, Giddings MC, Ruan Y, Wold B, Carninci P, Guigó R, Gingeras TR. Landscape of transcription in human cells. *Nature* 2012; **489**: 101-108 [PMID: 22955620 DOI: 10.1038/nature11233]
- 18 **Amodio N**, Raimondi L, Juli G, Stamato MA, Caracciolo D, Tagliaferri P, Tassone P. MALAT1: a druggable long non-coding RNA for targeted anti-cancer approaches. *J Hematol Oncol* 2018; **11**: 63 [PMID: 29739426 DOI: 10.1038/nature11233]

- 10.1186/s13045-018-0606-4]
- 19 **Camuesco D**, Comalada M, Rodríguez-Cabezas ME, Nieto A, Lorente MD, Concha A, Zarzuelo A, Gálvez J. The intestinal anti-inflammatory effect of quercitrin is associated with an inhibition in iNOS expression. *Br J Pharmacol* 2004; **143**: 908-918 [PMID: 15533892 DOI: 10.1038/sj.bjp.0705941]
  - 20 **Wirtz S**, Popp V, Kindermann M, Gerlach K, Weigmann B, Fichtner-Feigl S, Neurath MF. Chemically induced mouse models of acute and chronic intestinal inflammation. *Nat Protoc* 2017; **12**: 1295-1309 [PMID: 28569761 DOI: 10.1038/nprot.2017.044]
  - 21 **Gao J**, Li X, Wang Y, Cao Y, Yao D, Sun L, Qin L, Qiu H, Zhan X. Adipocyte-derived extracellular vesicles modulate appetite and weight through mTOR signalling in the hypothalamus. *Acta Physiol (Oxf)* 2020; **228**: e13339 [PMID: 31278836 DOI: 10.1111/apha.13339]
  - 22 **Xie L**, Chen Z, Liu M, Huang W, Zou F, Ma X, Tao J, Guo J, Xia X, Lyu F, Wang H, Zheng C, Jiang J. MSC-Derived Exosomes Protect Vertebral Endplate Chondrocytes against Apoptosis and Calcification via the miR-31-5p/ATF6 Axis. *Mol Ther Nucleic Acids* 2020; **22**: 601-614 [PMID: 33230460 DOI: 10.1016/j.omtn.2020.09.026]
  - 23 **Liu SX**, Zheng F, Xie KL, Xie MR, Jiang LJ, Cai Y. Exercise Reduces Insulin Resistance in Type 2 Diabetes Mellitus via Mediating the lncRNA MALAT1/MicroRNA-382-3p/Resistin Axis. *Mol Ther Nucleic Acids* 2019; **18**: 34-44 [PMID: 31479923 DOI: 10.1016/j.omtn.2019.08.002]
  - 24 **Ji Q**, Cai G, Liu X, Zhang Y, Wang Y, Zhou L, Sui H, Li Q. MALAT1 regulates the transcriptional and translational levels of proto-oncogene RUNX2 in colorectal cancer metastasis. *Cell Death Dis* 2019; **10**: 378 [PMID: 31097689 DOI: 10.1038/s41419-019-1598-x]
  - 25 **Chen Y**, Wang X. miRDB: an online database for prediction of functional microRNA targets. *Nucleic Acids Res* 2020; **48**: D127-D131 [PMID: 31504780 DOI: 10.1093/nar/gkz757]
  - 26 **Hetz C**. The unfolded protein response: controlling cell fate decisions under ER stress and beyond. *Nat Rev Mol Cell Biol* 2012; **13**: 89-102 [PMID: 22251901 DOI: 10.1038/nrm3270]
  - 27 **Powell N**, Pantazi E, Pavlidis P, Tsakmaki A, Li K, Yang F, Parker A, Pin C, Cozzetto D, Minns D, Stolarczyk E, Saveljeva S, Mohamed R, Lavender P, Afzali B, Digby-Bell J, Tjir-Li T, Kaser A, Friedman J, MacDonald TT, Bewick GA, Lord GM. Interleukin-22 orchestrates a pathological endoplasmic reticulum stress response transcriptional programme in colonic epithelial cells. *Gut* 2020; **69**: 578-590 [PMID: 31792136 DOI: 10.1136/gutjnl-2019-318483]
  - 28 **Ma X**, Dai Z, Sun K, Zhang Y, Chen J, Yang Y, Tso P, Wu G, Wu Z. Intestinal Epithelial Cell Endoplasmic Reticulum Stress and Inflammatory Bowel Disease Pathogenesis: An Update Review. *Front Immunol* 2017; **8**: 1271 [PMID: 29118753 DOI: 10.3389/fimmu.2017.01271]
  - 29 **Kaser A**, Lee AH, Franke A, Glickman JN, Zeissig S, Tilg H, Nieuwenhuis EE, Higgins DE, Schreiber S, Glimcher LH, Blumberg RS. XBP1 Links ER stress to intestinal inflammation and confers genetic risk for human inflammatory bowel disease. *Cell* 2008; **134**: 743-756 [PMID: 18775308 DOI: 10.1016/j.cell.2008.07.021]
  - 30 **Stengel ST**, Fazio A, Lipinski S, Jahn MT, Aden K, Ito G, Wottawa F, Kuiper JWP, Coleman OI, Tran F, Bordoni D, Bernardes JP, Jentsch M, Luzius A, Bierwirth S, Messner B, Henning A, Welz L, Kakavand N, Falk-Paulsen M, Imm S, Hinrichsen F, Zilbauer M, Schreiber S, Kaser A, Blumberg R, Haller D, Rosenstiel P. Activating Transcription Factor 6 Mediates Inflammatory Signals in Intestinal Epithelial Cells Upon Endoplasmic Reticulum Stress. *Gastroenterology* 2020; **159**: 1357-1374.e10 [PMID: 32673694 DOI: 10.1053/j.gastro.2020.06.088]
  - 31 **Deng J**, Lu PD, Zhang Y, Scheuner D, Kaufman RJ, Sonenberg N, Harding HP, Ron D. Translational repression mediates activation of nuclear factor kappa B by phosphorylated translation initiation factor 2. *Mol Cell Biol* 2004; **24**: 10161-10168 [PMID: 15542827 DOI: 10.1128/MCB.24.23.10161-10168.2004]
  - 32 **Hu P**, Han Z, Couvillon AD, Kaufman RJ, Exton JH. Autocrine tumor necrosis factor alpha links endoplasmic reticulum stress to the membrane death receptor pathway through IRE1alpha-mediated NF-kappaB activation and down-regulation of TRAF2 expression. *Mol Cell Biol* 2006; **26**: 3071-3084 [PMID: 16581782 DOI: 10.1128/MCB.26.8.3071-3084.2006]
  - 33 **Puig L**. Obesity and psoriasis: body weight and body mass index influence the response to biological treatment. *J Eur Acad Dermatol Venereol* 2011; **25**: 1007-1011 [PMID: 21492252 DOI: 10.1111/j.1468-3083.2011.04065.x]
  - 34 **Bhalme M**, Sharma A, Keld R, Willert R, Campbell S. Does weight-adjusted anti-tumour necrosis factor treatment favour obese patients with Crohn's disease? *Eur J Gastroenterol Hepatol* 2013; **25**: 543-549 [PMID: 23337170 DOI: 10.1097/MEG.0b013e32835d1f15]
  - 35 **Harper JW**, Sinanan MN, Zisman TL. Increased body mass index is associated with earlier time to loss of response to infliximab in patients with inflammatory bowel disease. *Inflamm Bowel Dis* 2013; **19**: 2118-2124 [PMID: 23863401 DOI: 10.1097/MIB.0b013e32829cf401]
  - 36 **Flores A**, Burstein E, Cipher DJ, Feagins LA. Obesity in Inflammatory Bowel Disease: A Marker of Less Severe Disease. *Dig Dis Sci* 2015; **60**: 2436-2445 [PMID: 25799938 DOI: 10.1007/s10620-015-3629-5]
  - 37 **Martinez-Medina M**, Denizot J, Dreux N, Robin F, Billard E, Bonnet R, Darfeuille-Michaud A, Barnich N. Western diet induces dysbiosis with increased E coli in CEABAC10 mice, alters host barrier function favouring AIEC colonisation. *Gut* 2014; **63**: 116-124 [PMID: 23598352 DOI: 10.1136/gutjnl-2012-304119]
  - 38 **Lam YY**, Ha CW, Campbell CR, Mitchell AJ, Dinudom A, Oscarsson J, Cook DJ, Hunt NH, Caterson ID, Holmes AJ, Storlien LH. Increased gut permeability and microbiota change associate with mesenteric fat inflammation and metabolic dysfunction in diet-induced obese mice. *PLoS One* 2012; **7**: e34233 [PMID: 22457829 DOI: 10.1371/journal.pone.0034233]
  - 39 **Bilski J**, Mazur-Bialy AI, Brzozowski B, Magierowski M, Jasnos K, Krzysiek-Maczka G, Urbanczyk K, Ptak-Belowska A, Zwolinska-Wcislo M, Mach T, Brzozowski T. Moderate exercise training attenuates the severity of experimental rodent colitis: the importance of crosstalk between adipose tissue and skeletal muscles. *Mediators Inflamm* 2015; **2015**: 605071 [PMID: 25684862 DOI: 10.1155/2015/605071]
  - 40 **Kahn CR**, Wang G, Lee KY. Altered adipose tissue and adipocyte function in the pathogenesis of metabolic syndrome. *J Clin Invest* 2019; **129**: 3990-4000 [PMID: 31573548 DOI: 10.1172/JCI129187]
  - 41 **Spencer SP**, Sonnenburg JL. When Gut Microbiota Creep into Fat, the Fat Creeps Back. *Cell* 2020; **183**: 589-591 [PMID: 33125887 DOI: 10.1016/j.cell.2020.10.008]

- 42 **Ji P**, Diederichs S, Wang W, Böing S, Metzger R, Schneider PM, Tidow N, Brandt B, Buerger H, Bulk E, Thomas M, Berdel WE, Serve H, Müller-Tidow C. MALAT-1, a novel noncoding RNA, and thymosin beta4 predict metastasis and survival in early-stage non-small cell lung cancer. *Oncogene* 2003; **22**: 8031-8041 [PMID: [12970751](#) DOI: [10.1038/sj.onc.1206928](#)]
- 43 **Li GQ**, Fang YX, Liu Y, Meng FR, Wu X, Zhang CW, Zhang Y, Liu D, Gao B. MALAT1-Driven Inhibition of Wnt Signal Impedes Proliferation and Inflammation in Fibroblast-Like Synoviocytes Through CTNNB1 Promoter Methylation in Rheumatoid Arthritis. *Hum Gene Ther* 2019; **30**: 1008-1022 [PMID: [30909750](#) DOI: [10.1089/hum.2018.212](#)]
- 44 **Gu H**, Zhu Y, Zhou Y, Huang T, Zhang S, Zhao D, Liu F. LncRNA MALAT1 Affects *Mycoplasma pneumoniae* Pneumonia via NF- $\kappa$ B Regulation. *Front Cell Dev Biol* 2020; **8**: 563693 [PMID: [33134293](#) DOI: [10.3389/fcell.2020.563693](#)]
- 45 **Yong H**, Wu G, Chen J, Liu X, Bai Y, Tang N, Liu L, Wei J. lncRNA MALAT1 Accelerates Skeletal Muscle Cell Apoptosis and Inflammatory Response in Sepsis by Decreasing BRCA1 Expression by Recruiting EZH2. *Mol Ther Nucleic Acids* 2020; **19**: 97-108 [PMID: [31830649](#) DOI: [10.1016/j.omtn.2019.10.028](#)]
- 46 **Cremer S**, Michalik KM, Fischer A, Pfisterer L, Jaé N, Winter C, Boon RA, Muhly-Reinholz M, John D, Uchida S, Weber C, Poller W, Günther S, Braun T, Li DY, Maegdefessel L, Perisic Matic L, Hedin U, Soehnlein O, Zeiher A, Dimmeler S. Hematopoietic Deficiency of the Long Noncoding RNA MALAT1 Promotes Atherosclerosis and Plaque Inflammation. *Circulation* 2019; **139**: 1320-1334 [PMID: [30586743](#) DOI: [10.1161/CIRCULATIONAHA.117.029015](#)]
- 47 **Yarani R**, Mirza AH, Kaur S, Pociot F. The emerging role of lncRNAs in inflammatory bowel disease. *Exp Mol Med* 2018; **50**: 1-14 [PMID: [30523244](#) DOI: [10.1038/s12276-018-0188-9](#)]
- 48 **Li Y**, Zhu L, Chen P, Wang Y, Yang G, Zhou G, Li L, Feng R, Qiu Y, Han J, Chen B, He Y, Zeng Z, Chen M, Zhang S. MALAT1 Maintains the Intestinal Mucosal Homeostasis in Crohn's Disease via the miR-146b-5p-CLDN11/NUMB Pathway. *J Crohns Colitis* 2021; **15**: 1542-1557 [PMID: [33677577](#) DOI: [10.1093/ecco-jcc/jjab040](#)]
- 49 **Ramos GP**, Papadakis KA. Mechanisms of Disease: Inflammatory Bowel Diseases. *Mayo Clin Proc* 2019; **94**: 155-165 [PMID: [30611442](#) DOI: [10.1016/j.mayocp.2018.09.013](#)]
- 50 **So JS**. Roles of Endoplasmic Reticulum Stress in Immune Responses. *Mol Cells* 2018; **41**: 705-716 [PMID: [30078231](#) DOI: [10.14348/molcells.2018.0241](#)]
- 51 **Shan B**, Wang X, Wu Y, Xu C, Xia Z, Dai J, Shao M, Zhao F, He S, Yang L, Zhang M, Nan F, Li J, Liu J, Jia W, Qiu Y, Song B, Han JJ, Rui L, Duan SZ, Liu Y. The metabolic ER stress sensor IRE1 $\alpha$  suppresses alternative activation of macrophages and impairs energy expenditure in obesity. *Nat Immunol* 2017; **18**: 519-529 [PMID: [28346409](#) DOI: [10.1038/ni.3709](#)]

## Basic Study

## Involvement of nitrergic neurons in colonic motility in a rat model of ulcerative colitis

Yan-Rong Li, Yan Li, Yuan Jin, Mang Xu, Hong-Wei Fan, Qian Zhang, Guo-He Tan, Jing Chen, Yun-Qing Li

**Specialty type:** Gastroenterology and hepatology**Provenance and peer review:** Unsolicited article; Externally peer reviewed.**Peer-review model:** Single blind**Peer-review report's scientific quality classification**Grade A (Excellent): 0  
Grade B (Very good): B  
Grade C (Good): C  
Grade D (Fair): 0  
Grade E (Poor): 0**P-Reviewer:** Bernstein HG, Germany; Sahin Y, Turkey**Received:** December 16, 2021**Peer-review started:** December 16, 2021**First decision:** April 16, 2022**Revised:** April 27, 2022**Accepted:** July 6, 2022**Article in press:** July 6, 2022**Published online:** August 7, 2022**Yan-Rong Li, Yun-Qing Li**, Department of Human Anatomy, Basic Medical College, Guangxi Medical University, Nanning 530000, Guangxi Zhuang Autonomous Region, China**Yan-Rong Li**, Department of Gastroenterology, The First Affiliated Hospital of Jinzhou Medical University, Jinzhou 121000, Liaoning Province, China**Yan Li, Yuan Jin, Qian Zhang, Yun-Qing Li**, Department of Human Anatomy, Basic Medical College, Zunyi Medical University, Zunyi 563006, Guizhou Province, China**Mang Xu**, Department of Anatomy, Basic Medical College, Dali University, Dali 671000, Yunnan Province, China**Hong-Wei Fan**, Department of Anatomy, Histology and Embryology, Xuzhou Medical University, Xuzhou 221000, Jiangsu Province, China**Guo-He Tan**, Key Lab of Longevity and Aging-related Diseases of Chinese Ministry of Education, Guangxi Medical University, Nanning 530000, Guangxi Zhuang Autonomous Region, China**Guo-He Tan**, School of Basic Medical Sciences and Center for Translational Medicine, Guangxi Medical University, Nanning 530000, Guangxi Zhuang Autonomous Region, China**Jing Chen, Yun-Qing Li**, Department of Anatomy, Histology and Embryology and K. K. Leung Brain Research Centre, The Fourth Military Medical University, Xi'an 710032, Shaanxi Province, China**Yun-Qing Li**, Department of Human Anatomy, College of Preclinical Medical Sciences, Zhengzhou University, Zhengzhou 450001, Henan Province, China**Yun-Qing Li**, Key Laboratory of Brain Science Research and Transformation in Tropical Environment of Hainan Province, Hainan Medical University, Haikou 571199, Hainan Province, China**Corresponding author:** Yun-Qing Li, PhD, Professor, Department of Human Anatomy, Basic Medical College, Guangxi Medical University, No. 22 Shuang-Yong Road, Nanning 530000, Guangxi Zhuang Autonomous Region, China. [deptanat@fmmu.edu.cn](mailto:deptanat@fmmu.edu.cn)

## Abstract

## BACKGROUND

The mechanisms underlying gastrointestinal (GI) dysmotility with ulcerative colitis (UC) have not been fully elucidated. The enteric nervous system (ENS) plays an essential role in the GI motility. As a vital neurotransmitter in the ENS, the gas neurotransmitter nitric oxide (NO) may impact the colonic motility. In this study, dextran sulfate sodium (DSS)-induced UC rat model was used for investigating the effects of NO by examining the effects of rate-limiting enzyme nitric oxide synthase (NOS) changes on the colonic motility as well as the role of the ENS in the colonic motility during UC.

### AIM

To reveal the relationship between the effects of NOS expression changes in NOS-containing nitregic neurons and the colonic motility in a rat UC model.

### METHODS

Male rats ( $n = 8$ /each group) were randomly divided into a control (CG), a UC group (EG1), a UC + thrombin derived polypeptide 508 trifluoroacetic acid (TP508TFA; an NOS agonist) group (EG2), and a UC + NG-monomethyl-L-arginine monoacetate (L-NMMA; an NOS inhibitor) group (EG3). UC was induced by administering 5.5% DSS in drinking water without any other treatment (EG1), while the EG2 and EG3 were gavaged with TP508 TFA and L-NMMA, respectively. The disease activity index (DAI) and histological assessment were recorded for each group, whereas the changes in the proportion of colonic nitregic neurons were counted using immunofluorescence histochemical staining, Western blot, and enzyme linked immunosorbent assay, respectively. In addition, the contractile tension changes in the circular and longitudinal muscles of the rat colon were investigated *in vitro* using an organ bath system.

### RESULTS

The proportion of NOS-positive neurons within the colonic myenteric plexus (MP), the relative expression of NOS, and the NOS concentration in serum and colonic tissues were significantly elevated in EG1, EG2, and EG3 compared with CG rats. In UC rats, stimulation with agonists and inhibitors led to variable degrees of increase or decrease for each indicator in the EG2 and EG3. When the rats in EGs developed UC, the mean contraction tension of the colonic smooth muscle detected *in vitro* was higher in the EG1, EG2, and EG3 than in the CG group. Compared with the EG1, the contraction amplitude and mean contraction tension of the circular and longitudinal muscles of the colon in the EG2 and EG3 were enhanced and attenuated, respectively. Thus, during UC, regulation of the expression of NOS within the MP improved the intestinal motility, thereby favoring the recovery of intestinal functions.

### CONCLUSION

In UC rats, an increased number of nitregic neurons in the colonic MP leads to the attenuation of colonic motor function. To intervene NOS activity might modulate the function of nitregic neurons in the colonic MP and prevent colonic motor dysfunction. These results might provide clues for a novel approach to alleviate diarrhea symptoms of UC patients.

**Key Words:** Nitregic neurons; Nitric oxide; Nitric oxide synthase; Ulcerative colitis; Colonic motility; Colonic myenteric plexus

©The Author(s) 2022. Published by Baishideng Publishing Group Inc. All rights reserved.

**Core Tip:** This study focused on the effects of nitregic neurons in the myenteric plexus (MP) on colonic motor function in rats with ulcerative colitis (UC). The results suggest that an increased number of nitregic neurons in the colonic MP of the UC rats leads to reduced colon contractile function. Therefore, the regulation of the activity of nitregic neurons in the colonic MP through interference with the activities of nitric oxide synthase might be a novel potential and prospective way to reduce the diarrhea symptoms in UC patients.

**Citation:** Li YR, Li Y, Jin Y, Xu M, Fan HW, Zhang Q, Tan GH, Chen J, Li YQ. Involvement of nitregic neurons in colonic motility in a rat model of ulcerative colitis. *World J Gastroenterol* 2022; 28(29): 3854-3868

**URL:** <https://www.wjgnet.com/1007-9327/full/v28/i29/3854.htm>

**DOI:** <https://dx.doi.org/10.3748/wjg.v28.i29.3854>

## INTRODUCTION

Ulcerative colitis (UC) is a nonspecific inflammatory disorder of the intestine that primarily involves the rectum, sigmoid colon, and/or, the whole colon, in severe cases. Clinical features include recurrent episodes of abdominal pain, diarrhea, and mucopurulent stools[1]. Unfortunately, the disease course is permanent and causes great suffering to the patients. UC can occur at any age (mainly in young adults), and in recent years, its incidence has increased worldwide[2]. The etiology of UC is complex, and its pathogenesis might be related to genetics[3], immunological factors, psychiatric depression and anxiety [4], environmental factors[5], dietary allergy, intestinal flora[6], and other factors. Therefore, it leads to treatment difficulty and a prolonged treatment course, and recurs easily. Although current pharmacological treatments in the clinic might improve patient's symptoms, they still cannot achieve satisfactory results. In recent years, the research on the aspects of gastrointestinal (GI) motility disorders in UC patients has advanced, and the abnormal intestinal dynamics has become a focus of research on the pathogenesis of UC [7-9].

The enteric nervous system (ENS), including the submucous plexus (SP) and myenteric plexus (MP) [10,11], as an essential component of the peripheral nervous system (PNS), is independent of the central nervous system (CNS) and is involved in the regulation of intestinal secretion, absorption, and motility [12]. Neurons in the ENS, depending on their neurotransmission function, are divided into sensory neurons, motor neurons, and interneurons. Further, motor neurons are divided into excitatory and inhibitory ones, regulating the systolic and diastolic function of the intestine, respectively. Typically, the ENS plays a vital role in maintaining gut homeostasis; however, gut motility gets impaired once the relaxation and contraction functions of the gut become imbalanced.

As the primary inhibitory gas neurotransmitter within the ENS, nitric oxide (NO) regulates several GI functions, such as vascular permeability, mucosal defense, immune regulation, and GI motility[13]. Nitric oxide synthase (NOS), the rate-limiting enzyme of NO synthesis, is widely distributed in endothelial cells, macrophages, neuro-phagocytes, and neuronal cells. NOS can be divided into neural NOS (nNOS), endothelial NOS (eNOS), and inducible NOS (iNOS). Out of these, nNOS is located within the nervous tissue of both the CNS and PNS. NO is one of the major inhibitory neurotransmitters of non-adrenergic noncholinergic (NANC) nerves in the ENS and its release by NOS-positive neurons plays an essential role in stimulating GI secretion and relaxing GI smooth muscle. Changes in the NOS expression level cause alterations in GI motility; however, the impact of such changes in UC on colonic motility has not been clearly defined. Therefore, this study aimed to observe the changes of NOS within the colonic MP in dextran sulfate sodium (DSS)-induced UC rats, to further understand the underlying mechanisms of colonic motility in UC for delineating a new direction for the treatment of UC.

## MATERIALS AND METHODS

### Reagents

Dextran sulfate sodium (DSS; PC-99017), NG-monomethyl-L-arginine monoacetate (L-NMMA; PC-45273), and thrombin derived polypeptide 508 trifluoroacetic acid (TP508TFA; PC-50991) were purchased from PlantChemMed Co., Ltd (Shanghai, China). Rabbit Anti-HuD + HuC (ab184267) and Goat Anti-nNOS (ab1376) were purchased from Abcam (Cambridge, United Kingdom). Donkey Anti-Goat Alexa Fluor 488 (a11055) and Donkey Anti-Rabbit Alexa Fluor 594 (A21207) were purchased from Invitrogen Co., Ltd (Carlsbad, United States). Mouse Anti- $\beta$ -Actin monoclonal antibody (A1978) and Immobilon Forte western HRP substrate (Cat. No. WBLUF0020) were purchased from Merck KGaA (Darmstadt, Germany). HRP-Labeled Goat Anti-Rabbit IgG (H + L) (ZB-2306) and HRP-Labeled Goat Anti-Mouse IgG (H + L) (ZB-2305) were purchased from ZhongShan GoldBridge Biotechnology Co., Ltd (Beijing, China). SDS-PAGE Gel Preparation Kit (P0012A) was purchased from Beyotime Biotechnology Co., Ltd (Shanghai, China). BCA Protein Concentration Assay Kit (AR0146) was purchased from BOSTER Biological Technology Co., Ltd (Wuhan, China). NOS1/nNOS ELISA Kit (E-EL-R1438C) were purchased from Elabscience Biotechnology Co., Ltd (Wuhan, China). All other reagents and chemicals used in this study are commercially available.

### Animals and animal tests

Thirty-two 8-wk-old male Sprague-Dawley rats weighing  $200 \pm 20$  g were housed in a specific pathogen-free animal house. The animals were kept at a standard room temperature of  $24 \text{ }^\circ\text{C}$ , with 40%-60% relative humidity, 12 h light-dark alternation, and a standard laboratory diet containing 23% protein and water. All animals were provided by the Animal Center of the Fourth Military Medical University and divided into four major groups. All experimental procedures were conducted in accordance with the Principles of Laboratory Animal Care and approved by the University Ethics Committee and performed as per institutional guidelines. Efforts were made to minimize the number of animals used.

The rats were randomly divided into four groups ( $n = 8$ /each group), including the control (CG), UC (EG1), UC + NOS agonist TP508TFA (EG2), and UC + NOS inhibitor L-NMMA (EG3) groups. The CG group was housed as described above, whereas the animals in the three experimental groups (EG1-3)

were given tap water containing 5.5% DSS. The CG group was fed in the same way as the experimental groups except that DSS was not added in the tap water. All animals were given free access to water for 7 d, and the water was changed to tap water at day 15. Further, EG2 rats were treated with 3 mL of 0.01 mmol/L TP508 TFA i.g. daily for 15 d and EG3 rats were treated with 3 mL of 0.01 mmol/L L-NMMA i.g. daily for 15 d. Animals were regularly monitored for the general conditions, body weight, stool characteristics, occult blood, and hematochezia for the evaluation of the disease condition. The scoring criteria of the disease activity index (DAI) were as follows[14]: Body weight: No loss, 0 points; loss by 1%-5%, 1 point; loss by 6%-10%, 2 points; loss by 11%-15%, 3 points; loss by more than 15%, 4 points; stool characteristics: Normal (well-shaped), 0 points; bondless (mushy and semi-formed stool that does not adhere to the anus), 2 points; loose (watery stool that can adhere to the anus), 4 points; fecal occult blood or macroscopic hematochezia: Normal, 0 points; occult blood (+), 2 points; macroscopic hematochezia, 4 points. DAI score was calculated as equal to the average value of the sum of the above scores.

Rats in each group were individually subjected to the open field test on day 14 of the experiment. The rats were randomly placed into boxes with a height of 30-40 cm and a length of 100 cm on the bottom side. The box's inner walls were darkened, and the bottom surface was divided on the average 25 squares (4 cm × 4 cm) with a digital camera set 2 m above each side. The data was acquired automatically and recorded for 15 min. This technique was used to test the spontaneous activity of the animals and their anxious behavior in an open environment.

On the 15<sup>th</sup> day of the experiment, rats in each group were anesthetized with an intraperitoneal injection of 7% chloral hydrate (0.4 mL/100 g). The whole colon was removed to compare the colon length for rats in each group.

### **Histological evaluation of the colon**

Eight rats in each group were used for histological evaluation of the colon. Following the whole colon removal, the intestinal lumen was flushed using 0.01 mmol/L PBS buffer, and transected 6-9 cm from the anus. Colons were fixed in 4% paraformaldehyde, dehydrated in graded alcohols, and then embedded in the paraffin. The block was cut into 5 μm thick sections and hematoxylin-eosin stained. Afterwards, the slides were mounted with neutral gum and dried at 37 °C overnight. A whole slide was observed under a scanning biomicroscope (SLIDEVIEW VS200, Olympus, Tokyo, Japan). Histological changes were recorded based on the staining results, and the histological index (HI) scoring was performed, with the following criteria[15]: 0 points for no damage; 1 point for disappearance of basal 1/3 crypts; 2 points for disappearance of basal 2/3 crypts; 3 points disappearance of crypts with intact epithelial cells; and 4 points for crypt and epithelial cell disappearance.

### **Immunofluorescence histochemical staining**

The distal colons of eight rats in each group were dissected separately. The intestinal lumens were flushed in 0.01 mol/L PBS buffer, then a colonic strip with a width of approximately 0.5-1.0 cm was cut along the travel direction of the circular muscle (CM). Afterwards, the dissected colon was fixed in 4% paraformaldehyde. The mucosal layer was fixed upward and horizontally in PBS buffer (pH = 7.4). The mucosal, submucosal, and CM layers were removed with the help of filament forceps to preserve the longitudinal muscle (LM) layer. The tissues were blocked in 10% donkey serum for 30 min and then incubated with Rabbit-Anti-HuD + HuC (1: 500) and Goat-Anti-nNOS (1: 300) in a shaker overnight at 4 °C. Slides were incubated with Donkey Anti-Goat Alexa Fluor 488 (1: 500) and Donkey Anti-Rabbit Alexa Fluor 594 (1: 500) for 4 h. Eight different fields (approximately 1.0 cm × 1.0 cm) of the specimens were observed using confocal microscopy (FV-1000, Olympus, Tokyo, Japan) with the appropriate laser beams and filter settings for Alexa 488 (excitation, 488 nm; emission, 510-530 nm) and Alexa 594 (excitation, 543 nm; emission, 590-615 nm). Digital images were captured with an FV10-ASW 4.2 from Olympus, and these images eventually saved as TIFF files to calculate changes in the proportion of colon nitroergic neurons.

### **Western blot analysis**

Four rats in each group were anesthetized and perfused with pre-cooled PBS buffer, and the terminal colon was transected. The mucosa and submucosa were separated with silk tweezers. The muscle layer was put into a pre-cooled EP tube. The tissue was homogenized using an ultrasonic grinder, in the lysis buffer (RIPA: protease inhibitor: phosphatase inhibitors = 100:1:1). After standing for 10 min on ice, the supernatant was centrifuged at 12000 rpm (10008 × g) for 10 min. The protein concentration was measured using a BCA protein concentration assay kit and FC microplate reader (1410101, Thermo Fisher Scientific, Shanghai, China). The protein samples were kept at -80 °C for further use.

Gels were made using the SDS-PAGE gel preparation kit, and the samples were electrophoresed at a constant voltage of 80 and 120 V. Membrane transfer was achieved at a constant current of 300 mA. First, the PVDF membranes were blocked with Western blocking solution (P0252, Beyotime Biotechnology Co., Ltd., Shanghai, China) for 15 min and then incubated with Rabbit Anti-nNOS (1:1000) and Anti-β-Actin antibody (mouse monoclonal; 1:5000) on a shaker overnight at 4 °C. The PVDF membranes were then incubated with HRP-labeled Rabbit Anti-Goat IgG (H + L) (1:10000) and HRP-labeled Goat

Anti-Mouse IgG (H + L) (1:10000) for 2 h. After three rinses (10 min each) in TBST, the membranes were probed by Immobilon™ Western chemiluminescent HRP substrate (WBKLS0050, Merck KGaA, Darmstadt, Germany) and placed into ECL for the detection. The proteins were analyzed using Image-Pro Plus software (Image-Pro Plus Version 6.0, Media Cybernetics, Maryland, United States).

### ELISA

Whole blood from four rats in each group were kept for 2 h at room temperature and then centrifuged at 3800 rpm (1000 × g) for 20 min, followed by the removal of supernatant. Next, the terminal colon tissues were grounded and disrupted with an appropriate volume of PBS (usually at a weight to volume ratio of 1:9), homogenized using a glass homogenizer, and then centrifuged at 8460 rpm (5000 × g) for 5 to 10 min. Afterwards, the supernatant was collected. The NOS1/nNOS ELISA kit was used to determine the concentration of NOS in the colon as well as in the serum.

### *In vitro* gut colonic tension detection

Four rats in each group were used to explore the changes of *in vitro* gut colonic tension, including eight circular and eight longitudinal colon muscle strips. Rats were anesthetized, and the abdominal cavity was exposed. Then, the intestinal tube was carefully separated with the forceps and quickly freed. The colon was excised and placed in Krebs' fluid at 37 °C with a continuous supply of 95% O<sub>2</sub> and 5% CO<sub>2</sub> mixture. Then, 3 mm × 10 mm circular and LM strips were cut, where both ends were anchored to tension receptors and platinum rings at the lower end, respectively. The signals acquired by the tension receptors were recorded and processed with a multi-channel physiological signal acquisition and processing system (RM6240E, INSTRUMENT FACTORY, Chengdu, China). The mean amplitude of spontaneous contractions was recorded in circular and LM strips obtained from control and UC rats at rest, when the muscle strips were allowed to rest in the incubation solution for 30 min. After 10 min of recording, TP508TFA (1 × 10<sup>-4</sup> mol/L) was added to the bath of the UC group, and the mean amplitude changes of circular and LM strips were recorded, respectively. The liquid in the bath was replaced after 10 min, and the bath was washed. After resting for 30 min, L-NMMA (1 × 10<sup>-4</sup> mol/L) was added, and the corresponding mean amplitude changes were re-recorded.

### Statistical analysis

SPSS version 23.0 statistical software (SPSS Inc, Chicago, United States) was used for statistical analyses. Data are expressed as the mean ± SD, and comparisons between groups were performed by one-way ANOVA. A *P* value of < 0.05 was considered statistically significant.

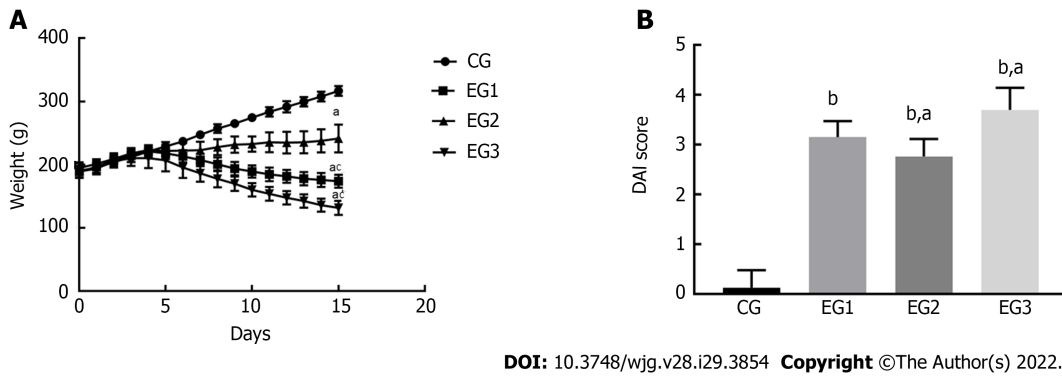
## RESULTS

### DAI scores

Sloth, anorexia, emaciation, decreased fur gloss, and higher stool frequency were found in all EG rats, with some developing mucopurulent bloody stools. From days 0 to 5, animals in all groups gained weight (CG group: 28.90 ± 2.43 g; EG1 group: 18.10 ± 3.23 g; EG2 group: 17.00 ± 6.17 g; EG3 group: 21.80 ± 3.63 g). The body weight of rats in each group was not significantly different (*P* > 0.05); however, the body weight of rats in the EG1-3 groups began to decrease from day 6. Until day 15, the CG group (116.60 ± 2.76 g) and EG2 group (58.60 ± 7.79 g) gained weight, while the EG1 group (26.00 ± 3.69 g) and EG3 group (60.40 ± 3.99 g) lost weight. The decrease in body weight was statistically significantly different between the EG groups and CG group (*P* < 0.05); the differences in weight change between the EG2-3 groups and EG1 group were also statistically significant (*P* < 0.05) (Figure 1A). As for the stool profiles of all the groups, two rats in the CG group exhibited bondless and loose stools without hematochezia. For the EG1 group, it took 3.25 ± 0.31 d to the occurrence of loose stools, 3.37 ± 0.37 d to fecal occult blood, and 4.12 ± 0.39 d to macroscopic hematochezia; the corresponding values in the EG2 and EG3 groups were 3.85 ± 0.50 d, 4.00 ± 0.37 d, and 4.62 ± 0.41 d, and 2.87 ± 0.29 d, 2.62 ± 0.26 d, and 3.37 ± 0.32 d, respectively. Regarding the DAI scores, no statistically significant differences was found from day 0 to day 5 for any group (*P* > 0.05). After day 5, the intergroup differences in DAI scores were significantly increased. The DAI scores were (0.12 ± 0.12), (3.15 ± 0.11), (2.67 ± 0.12), and (3.69 ± 0.15) for the CG, EG1, EG2 and EG3 groups, respectively, at day 15. Moreover, the scores were significantly different between the EG groups and CG group (*P* < 0.0001), and between the EG2-3 groups and EG1 group (*P* < 0.05) (Figure 1B).

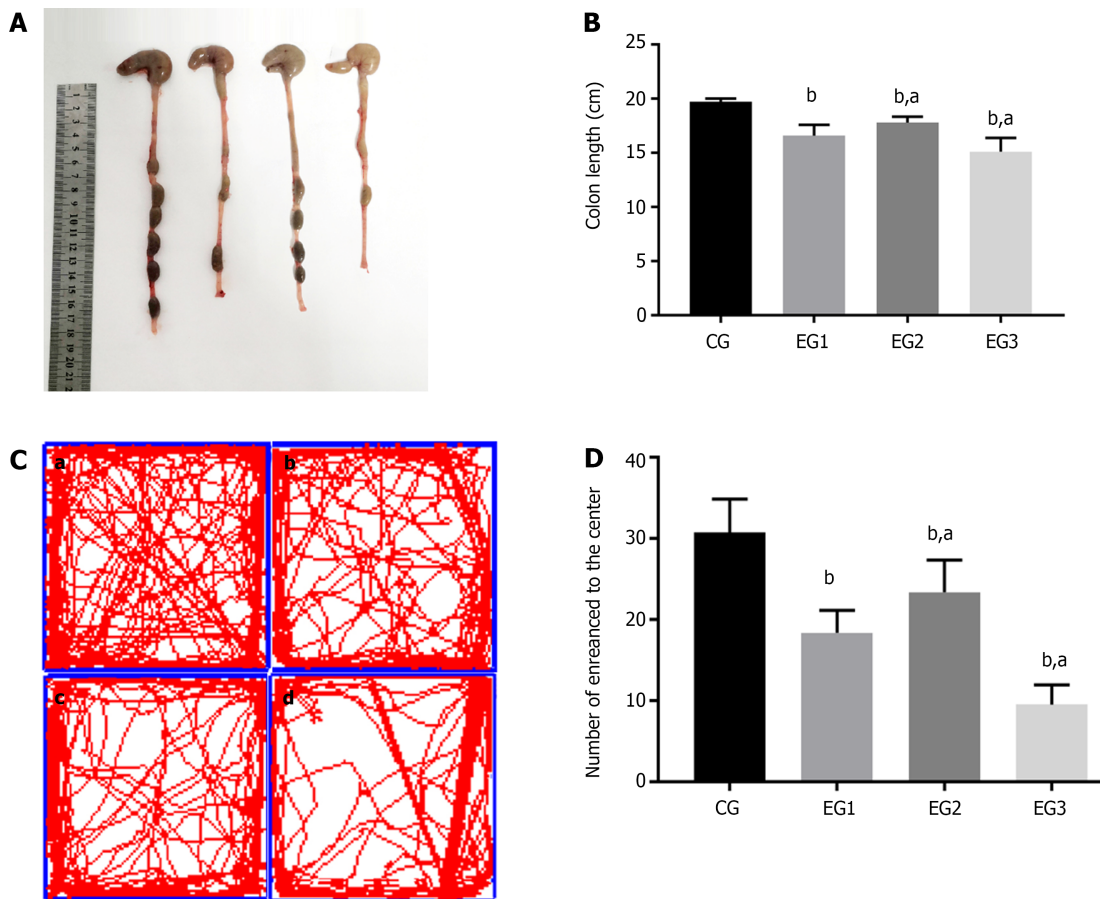
### Comparison of colon length and behavior

The colonic morphology of rats from each group was compared during the dissection (Figure 2A). Compared with the CG group, the colon length in the EG groups showed various degrees of shortening, and the differences were statistically significant (*P* < 0.0001). The difference was also significant between the EG2-3 groups and EG1 group (*P* < 0.05) (Figure 2B).



DOI: 10.3748/wjg.v28.i29.3854 Copyright ©The Author(s) 2022.

**Figure 1 Disease activity of animals in each group.** A: Body weight changes of rats. The differences in body weight were statistically significant between EG groups and CG group ( $^aP < 0.05$ ), and between EG2-3 groups and EG1 group ( $^bP < 0.05$ ); B: Disease activity index scores. The differences were significant between EG groups and CG group ( $^aP < 0.0001$ ), and between EG2-3 groups and EG1 group ( $^bP < 0.05$ ). CG: Control group; UC: Ulcerative colitis; NOS: Nitric oxide synthase; L-NMMA: NG-monomethyl-L-arginine monoacetate; EG1: UC group; EG2: UC + NOS agonist TP508TFA group; EG3: UC + NOS inhibitor L-NMMA group; DAI: Disease activity index.



DOI: 10.3748/wjg.v28.i29.3854 Copyright ©The Author(s) 2022.

**Figure 2 Colon length in each group and results of the open field test.** A: Colon length of rats in the four groups; B: Comparison of colon length in CG ( $19.71 \pm 0.11$  cm), EG1 ( $16.59 \pm 0.35$  cm), EG2 ( $17.80 \pm 0.19$  cm), and EG3 ( $15.11 \pm 0.44$  cm) groups. There were statistically significant differences between EG groups and CG group ( $^aP < 0.0001$ ), and between EG2-3 groups and EG1 group ( $^bP < 0.05$ ); C: Movement trajectories of rats. a: CG; b: EG1; c: EG2; d: EG3; D: Results of the open field test. There were statistically significant differences between EG groups and CG group ( $^aP < 0.0001$ ), and between EG2-3 groups and EG1 group ( $^bP < 0.05$ ). CG: Control group; UC: Ulcerative colitis; NOS: Nitric oxide synthase; L-NMMA: NG-monomethyl-L-arginine monoacetate; EG1: UC group; EG2: UC + NOS agonist TP508TFA group; EG3: UC + NOS inhibitor L-NMMA group.

On the 14th day of the experiment, the behavior of rats was examined using an open field test. The number of times that the rats passed through the center of an open box within 15 min period is shown as follows:  $30.75 \pm 1.46$  for the CG,  $18.38 \pm 0.98$  for EG1,  $23.38 \pm 1.40$  for EG2, and  $9.50 \pm 0.86$  for EG3 group. Differences were statistically significant between the EG groups and CG group ( $P < 0.0001$ ).

Additionally, the EG2-3 groups showed statistically significant differences compared with the EG1 group ( $P < 0.05$ ) (Figure 2C and D).

### **Colonic histological damage assessment**

The results of HE staining indicated that the colonic tissue structure of CG rats was normal, with the mucosal layer showing a well-arranged monolayer of columnar epithelial cells, clear intestinal glands, morphologically normal goblet cells, and no inflammatory cell infiltration. In the colon of EG1 rats, most crypts disappeared, with some broken or disappearing epithelia, accompanied by inflammatory cell infiltration. In the colon of EG2 rats, 1/3-2/3 of basal crypts disappeared, with the occasional destruction of epithelial cells. In the colon of EG3 rats, crypts completely disappeared, with some broken or disappearing epithelia, accompanied by massive inflammatory cell infiltration (Figure 3A). The HI scores for the colons of the rats in the CG, EG1, EG2, and EG3 groups were  $0.00 \pm 0.00$ ,  $3.07 \pm 0.25$ ,  $2.22 \pm 0.17$ , and  $3.71 \pm 0.14$ , respectively. The differences were statistically significant between the EG groups and CG group ( $P < 0.0001$ ), and between the EG2-3 groups and EG1 group ( $P < 0.05$ ) (Figure 3B).

### **Changes in proportion of NOS-positive colonic myenteric neurons**

The distal rat colons were double-stained by immunofluorescence histochemistry to observe the distribution and expression of NOS-positive neurons within the colonic MP. Within the colonic MP of rats, the proportion of these neurons in each group was counted. Enteric neurons exhibited a reticular distribution in the colonic MP (Figure 4B). NOS-positive neurons accounted for  $31.38 \pm 0.94\%$  in the CG group (Figure 4C) but were more distributed within the marginal side of the ganglia (Figure 4A). They were fusiform or star-shaped, and their nuclei were round with several elongated protrusions. The protrusions of these neurons were interconnected with each other to form a dense and complex neural network. In the EG1 group, the percentage of NOS-positive neurons in colonic neurons (Figure 4E) increased to  $42.25\% \pm 0.88\%$  under disease conditions (Figure 4F). The distribution of these neurons was no longer confined to the edges of the ganglia and began to appear elsewhere within the ganglia (Figure 4D). Moreover, the proportion of NOS-positive neurons in the EG2 group increased to  $51.75\% \pm 1.22\%$  (Figure 4I and H). These neurons in the ganglia were disorganized and widely distributed within the ganglia (Figure 4G). Compared with the EG1 group, the proportion of NOS-positive neurons in the EG3 group decreased to  $37.25\% \pm 1.09\%$  (Figure 4L and K), with their distribution within the ganglia being predominantly marginal (Figure 4J). The changes in the proportion of NOS-positive neurons to colonic neurons in the EG groups were statistically significant in comparison to the CG group ( $P < 0.0001$ ); however, the EG2 and EG3 groups were also significantly different from the EG1 group ( $P < 0.05$ ) (Figure 4M).

### **NOS protein expression level in colonic MP**

The expression level of NOS protein in the colonic MP of EG1 rats was higher than that in the CG group. The NOS expression in the EG2 rat colon was further increased, while the expression in the EG3 rat colon was lower than that in the EG1 group. The differences were statistically significant between the EG groups and CG group ( $P < 0.0001$ ) and between the EG2-3 groups and EG1 group ( $P < 0.05$ ) (Figure 5A and B).

### **Concentration of NOS in colonic myenteric tissue and serum**

The concentration of NOS was significantly increased in the colonic myenteric tissue in the EG groups compared with the CG group ( $P < 0.0001$ ); the EG2 group had a higher NOS concentration, whereas the EG3 group had a lower concentration than the EG1 group, and the difference between the EG2-3 groups and EG1 group was also statistically significant ( $P < 0.05$ ) (Figure 6A). In addition, serum concentrations of NOS were significantly increased in the EG group compared with the CG group ( $P < 0.0001$ ); however, the EG2 group had a significantly higher NOS concentration, whereas the EG3 group had a significantly lower concentration than the EG1 group ( $P < 0.05$ ) (Figure 6B).

### **Comparison of contraction tension of isolated rat colonic smooth muscle**

At rest, the contraction of the LM in the colon of CG rats appeared as a regular and sine wave-like curve with relatively neat amplitude (Figure 7A). In EGs rats, the contraction was significantly more frequent, with the increased amplitude (Figure 7B-D). The contraction tension of the LM of the colon was considerably more significant in EG rats than in CG rats ( $P < 0.0001$ ). However, the contraction tensions of the colonic LM were significantly weakened and increased in EG2 and EG3 rats, respectively, when compared with EG1 rats ( $P < 0.001$ ) (Figure 7E).

At rest, the contraction of the colonic CM in CG rats appeared as a regular and triangular wave-like curve. The amplitude was neat, with a contraction interval between the adjacent two waves (Figure 8A). In EGs rats, contraction of the CM of the colon was significantly accelerated, and its amplitude was increased (Figure 8B-D). The contraction tension of the colonic CM was significantly larger in EG rats than in CG rats ( $P < 0.0001$ ). The contraction tension of the colonic CM appeared significantly weakened and increased in EG1 rats compared with EG2 and EG3 rats, respectively ( $P < 0.0001$ ) (Figure 8E).

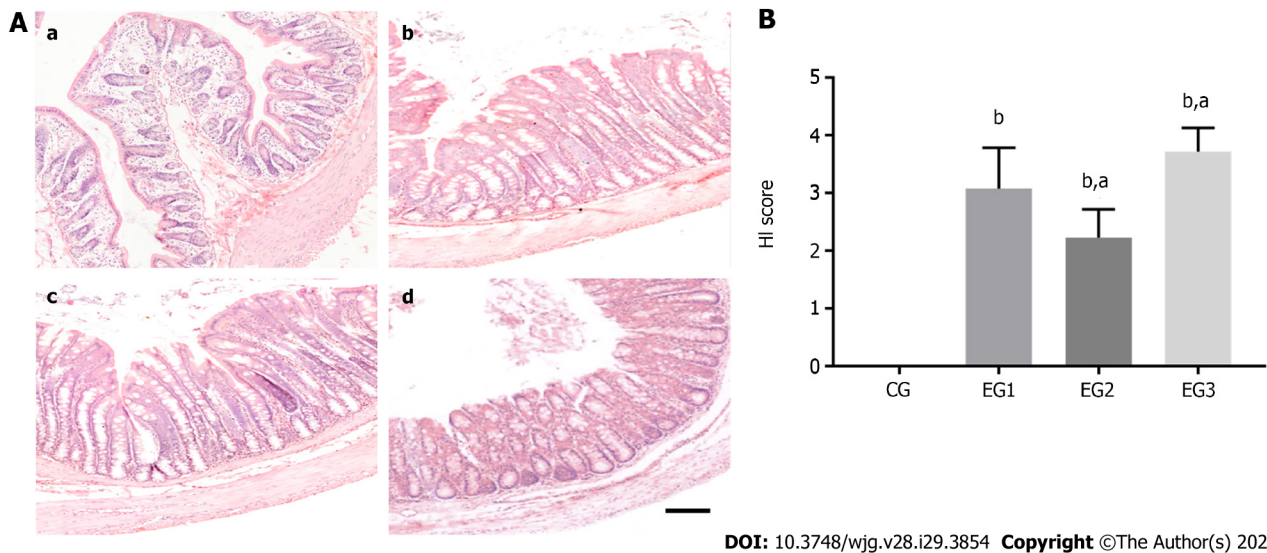


**Figure 3 Histological evaluation.** A: HE stained rat colon tissues. a: CG; b: EG1; c: EG2; d: EG3. Scale bar = 100  $\mu$ m; B: Comparison of colonic histological index scores showing statistically significant differences between EG groups and CG group ( $^*P < 0.0001$ ) and between EG2-3 groups and EG1 group ( $^*P < 0.05$ ). CG: Control group; UC: Ulcerative colitis; NOS: Nitric oxide synthase; L-NMMA: NG-monomethyl-L-arginine monoacetate; EG1: UC group; EG2: UC + NOS agonist TP508TFA group; EG3: UC + NOS inhibitor L-NMMA group; HI: Histological index.

## DISCUSSION

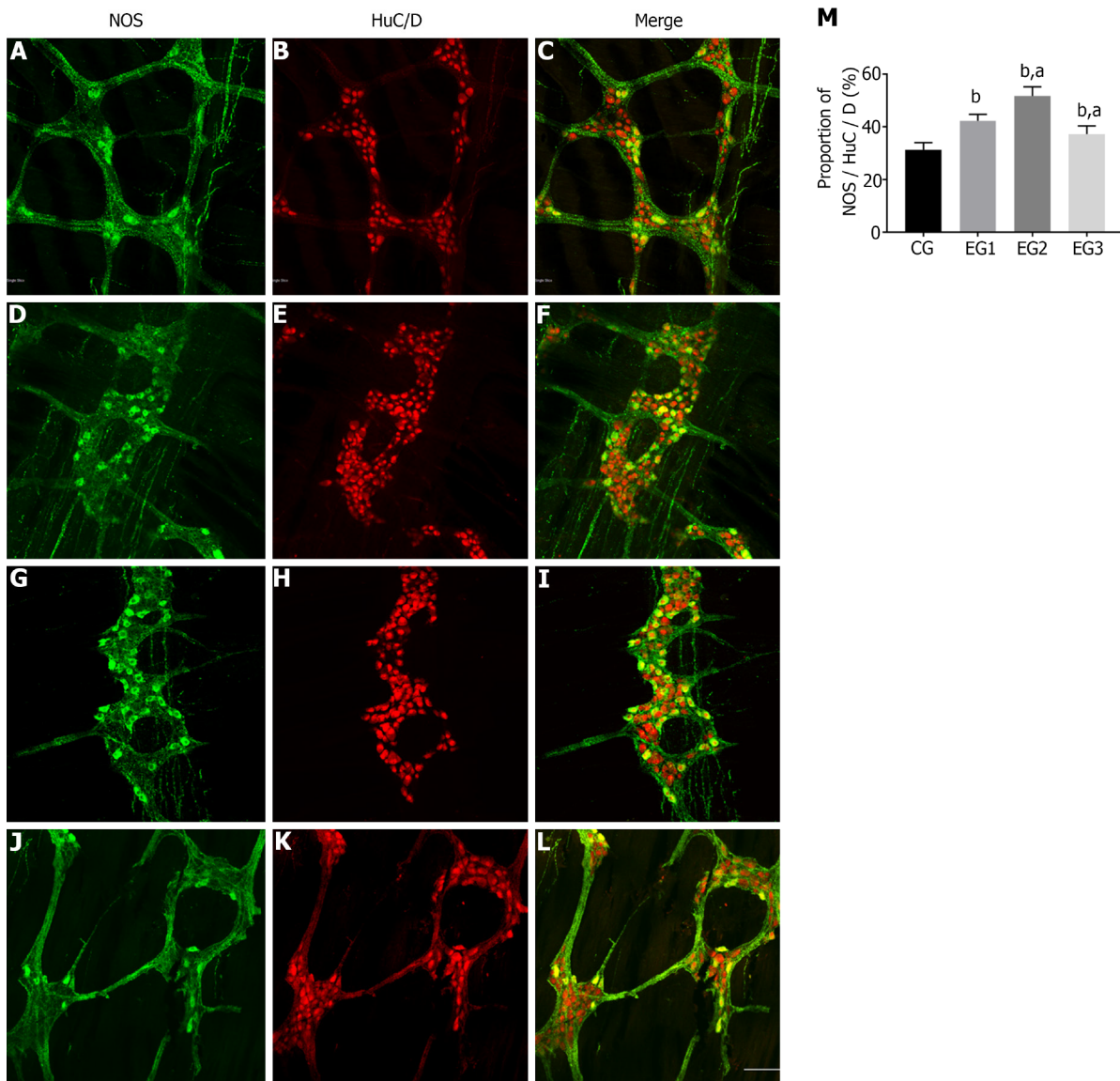
An increase or decrease in the number of neurons and/or neuronal degeneration in the ENS can lead to various diseases. For instance, congenital dysplasia of the ENS leads to congenital megacolon (Hirschsprung disease) and primary achalasia, whereas neurodegenerative ENS alterations can lead to the disorders such as Alzheimer, Huntington, and Parkinson diseases[16,17]. The secondary alterations in the ENS also result in inflammatory infiltrates or immune system pathologies such as irritable bowel syndrome[18], idiopathic enteric gangliosidosis[19], paraneoplastic syndrome[20], slow transit constipation[21], severe acute pancreatitis[22], diabetes mellitus[23,24], and UC[25].

The different types of ENS neurons have significantly different morphology and structure associated with the synthesis and secretion of neurotransmitters. However, by forming complex synaptic connections, these neurons participate in the structural basis that mainly underlies the relatively independent reflex activity of the gut and can also regulate the diverse motor and sensory activities of the digestive tract.

Despite the unclear etiology of UC, numerous studies have shown that its pathogenesis might be associated with the interactions between genetic susceptibility, environmental provoking factors, and immune-mediated tissue damage. Additionally, the relationship between abnormal intestinal motility and UC has also gained attention. Abnormal ENS is an important mechanism contributing to the abnormal colonic motility of UC, which is an important factor causing diarrhea in UC patients.

The onset of UC has a complex genetic background. Based on the gene polymorphism and heterogeneity, the impaired local barrier function of the intestinal mucosa can be the result of a combination of factors, such as altered epithelial permeability, neuroendocrine regulation, and intestinal flora translocation[26]. This, in turn, provokes the inflammatory response with symptoms such as abdominal pain, diarrhea, and colonic motor dysfunction. As the rate-limiting enzyme of NO synthesis in the body, NOS has three sub-types: iNOS, eNOS, and nNOS. Histological studies have identified intense focal iNOS expression by the inflamed bowel epithelium and in the mononuclear cell infiltrate in the intestinal tissues of both Crohn's disease and UC patients[27]. A great number of studies suggest that iNOS in the ENS may play a part in preventing activation of mast cells, reducing leukocyte adhesion to the endothelium and protecting the host from being invaded by colonic bacteria[28-30]. In normal and UC states, eNOS expression is limited to colonic vascular endothelium[31]. Baker *et al*[32] confirmed that during DSS-induced UC, eNOS KO mice suffered less tissue damage and inflammation than wild-type mice, suggesting that eNOS is essential for maintaining the integrity of the GI mucosa. nNOS is one of the specific markers for nitregic neurons within the ENS, the primary inhibitory neurons of the colonic MP[33]. By releasing inhibitory neurotransmitter NO, nitregic neurons can regulate GI motility. The changes in expression of nNOS in the colonic MP of UC rats indicate that nitregic neurons may be involved in NO-based neurotransmission and regulate GI motility in UC state.

Research has shown that NO is the second messenger in the smooth muscle cells (SMCs) or interstitial cells of Cajal (ICCs)[34]. NO is highly lipid-soluble and reaches target ICCs in a freely diffusible manner after synthesis. It binds to the soluble guanylyl cyclase in the cells to increase the enzymatic activity by altering its spatial configuration, which further leads to an increase in cyclic guanosine monophosphate



DOI: 10.3748/wjg.v28.i29.3854 Copyright ©The Author(s) 2022.

**Figure 4** Changes in the number of nitric oxide synthase-positive neurons in the colonic myenteric plexus. A-L: Immunofluorescent histochemical double-staining of the rat colonic myenteric plexus (MP) for nitric oxide synthase (NOS; green) and HuC/D (red) in CG (A-C), EG1 (D-F), EG2 (G-I), and EG3 (J-L) rats. Scale bar = 30 μm; M: Comparison of the proportion of NOS-positive neurons in the colonic MP showing statistically significant differences between EG groups and CG group (<sup>b</sup>*P* < 0.0001), and between EG2-3 groups and EG1 group (<sup>a</sup>*P* < 0.05). CG: Control group; UC: Ulcerative colitis; NOS: Nitric oxide synthase; L-NMMA: NG-monomethyl-L-arginine monoacetate; EG1: UC group; EG2: UC + NOS agonist TP508TFA group; EG3: UC + NOS inhibitor L-NMMA group; MP: myenteric plexus.

(cGMP) within the cells, activating the cGMP protein kinase-dependent calcium pumps, and therefore finally participates in intercellular information transmission[35]. Therefore, it could be concluded that as a messenger of information transmission between the NOS-positive neurons and GI SMCs, increased NO can reduce the Ca<sup>2+</sup> influx and directly promotes smooth muscle relaxation. In addition, studies have confirmed that NO can inhibit muscle contraction by inhibiting the release of excitatory transmitters[23,36]. Therefore, NO-mediated reduced contractility of the intestinal smooth muscle might be one of the important mechanisms contributing to colonic dysmotility[9,37].

In the present study, DSS was applied to induce the UC rat model successfully. For the first time, the finding of a secondary increase in NOS expression in the colonic MP of UC rats, combined with altered *in vitro* colonic contraction tension, suggests that the increased NOS expression is associated with the altered colonic motility in UC rats. Increasing (or decreasing) the number of NOS-positive neurons might enhance (or attenuate) the diastolic function of the colonic smooth muscle regulated by these neurons. However, the change in the number of NOS-positive neurons is often due to changes in the concentration and release of neurotransmitters caused by changes in the amount of NOS contained in neurons under pathological conditions, rather than caused by neuronal degeneration and regeneration. The results of *in vitro* studies of the colon using both agonists and inhibitors of NOS further confirmed that the altered NOS expression regulate the colonic motility in UC. A previous similar study

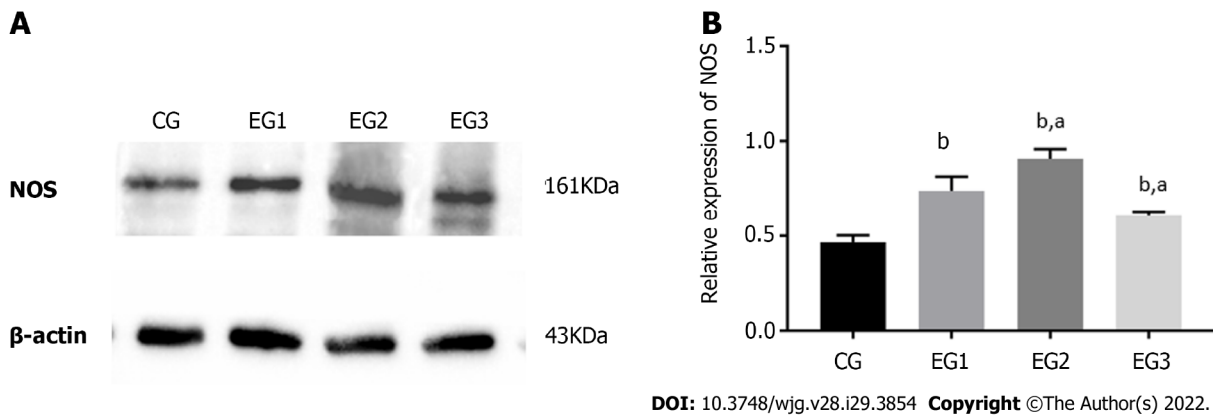


**Figure 5** Relative nitric oxide synthase protein expression in the colonic myenteric plexus. A: Western blot analysis of expression of nitric oxide synthase (NOS) in the colonic myenteric plexus (MP) of rats in the four groups; B: Comparison of the relative expression of NOS protein in the colonic MP of rats in the four groups showing statistically significant differences between EG groups and CG group ( $^bP < 0.0001$ ), and between EG2-3 groups and EG1 group ( $^aP < 0.05$ ). CG: Control group; UC: Ulcerative colitis; NOS: Nitric oxide synthase; L-NMMA: NG-monomethyl-L-arginine monoacetate; EG1: UC group; EG2: UC + NOS agonist TP508TFA group; EG3: UC + NOS inhibitor L-NMMA group; NOS: Nitric oxide synthase; MP: Myenteric plexus.

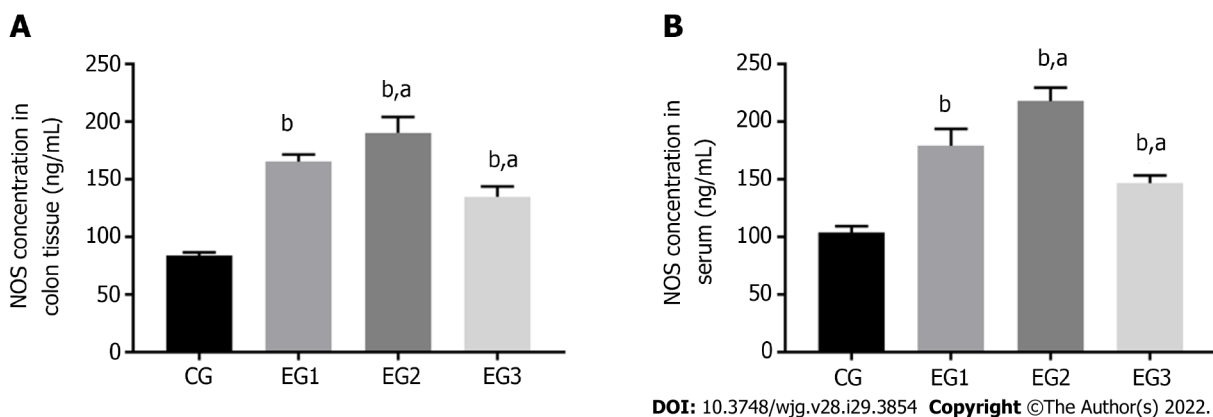


**Figure 6** Changes in nitric oxide synthase concentration in colonic myenteric tissue and serum. A: Comparison of nitric oxide synthase (NOS) concentration in colonic myenteric tissue of rats in the four groups showing statistically significant differences between EG groups and CG group ( $^bP < 0.0001$ ), and between EG2-3 groups and EG1 group ( $^aP < 0.05$ ); B: Comparison of NOS concentrations in the serum of rats in the four groups showing statistically significant differences between EG groups and CG group ( $^bP < 0.0001$ ), and between EG2-3 groups and CG group ( $^aP < 0.05$ ). CG: Control group; UC: Ulcerative colitis; NOS: Nitric oxide synthase; L-NMMA: NG-monomethyl-L-arginine monoacetate; EG1: UC group; EG2: UC + NOS agonist TP508TFA group; EG3: UC + NOS inhibitor L-NMMA group; NOS: Nitric oxide synthase.

demonstrated that the NOS expression and NO concentration within the muscular layer of the stomach and small intestine were increased in an animal model of chronic pancreatitis[38]. These results suggest that the reduced contractility of the gastric CM because of NO inhibition might be an important mechanism underlying gastric motor dysfunction in chronic pancreatitis[36,38]. Moreover, these findings can provide an interesting insight into the role of the ENS during GI dysmotility.

The initiation of colonic dysmotility in UC may be related to the structural alterations and abnormal number of ICCs, disturbed intestinal electrophysiology, changes in colonic pressure, and abnormal expression of gut-related neurotransmitters. Our present results have demonstrated that the increased NOS expression inhibits the contraction motility of the colonic smooth muscle. Therefore, appropriate adjustment of NOS levels can alter the expression of nitrenergic neurons, control the motor movement of the intestinal smooth muscle, and improve the UC colonic motor function. Of note, this could improve the symptoms of UC patients, providing a basis for the screening of novel agents against UC.

## CONCLUSION

The increased number of nitrenergic neurons in the colonic MP of UC rats, both *in vitro* and *in vivo*, diminishes the colonic motor function. In contrast, activation and inhibition of NOS activity could induce and diminish the colon motor function, respectively. Further, an increased number of nitrenergic neurons in the colonic MP of UC rats leads to reduced colon contractile function. Therefore, the

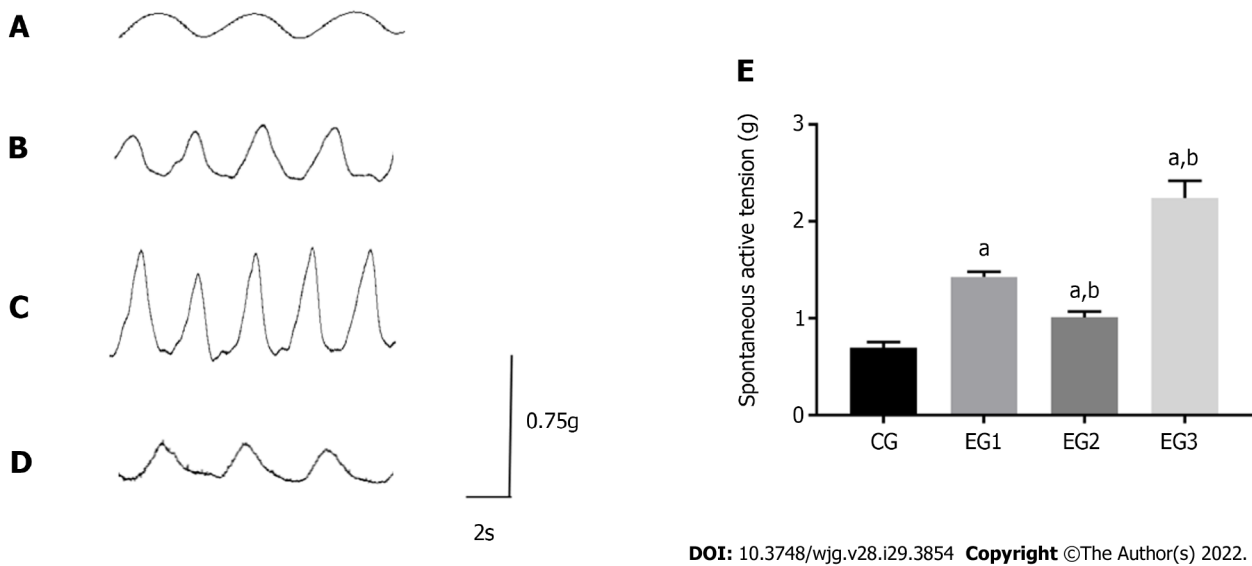


**Figure 7 Comparison of isolated colonic longitudinal muscle contraction tension.** A-D: Contraction amplitude of the colonic longitudinal muscle of CG (A), EG1 (B), EG2 (C), and EG3 (D) rats; E: Comparison of the contraction tension of the colonic longitudinal muscle among rats from the four groups: CG ( $0.69 \pm 0.02$  g), EG1 ( $1.42 \pm 0.02$  g), EG2 ( $2.24 \pm 0.07$  g), and EG3 ( $1.01 \pm 0.02$  g). All differences were statistically significant between EG groups and CG group ( $^*P < 0.0001$ ) and between EG2-3 groups and EG1 group ( $^*P < 0.001$ ). CG: Control group; UC: Ulcerative colitis; NOS: Nitric oxide synthase; L-NMMA: NG-monomethyl-L-arginine monoacetate; EG1: UC group; EG2: UC + NOS agonist TP508TFA group; EG3: UC + NOS inhibitor L-NMMA group; LM: Longitudinal muscle.

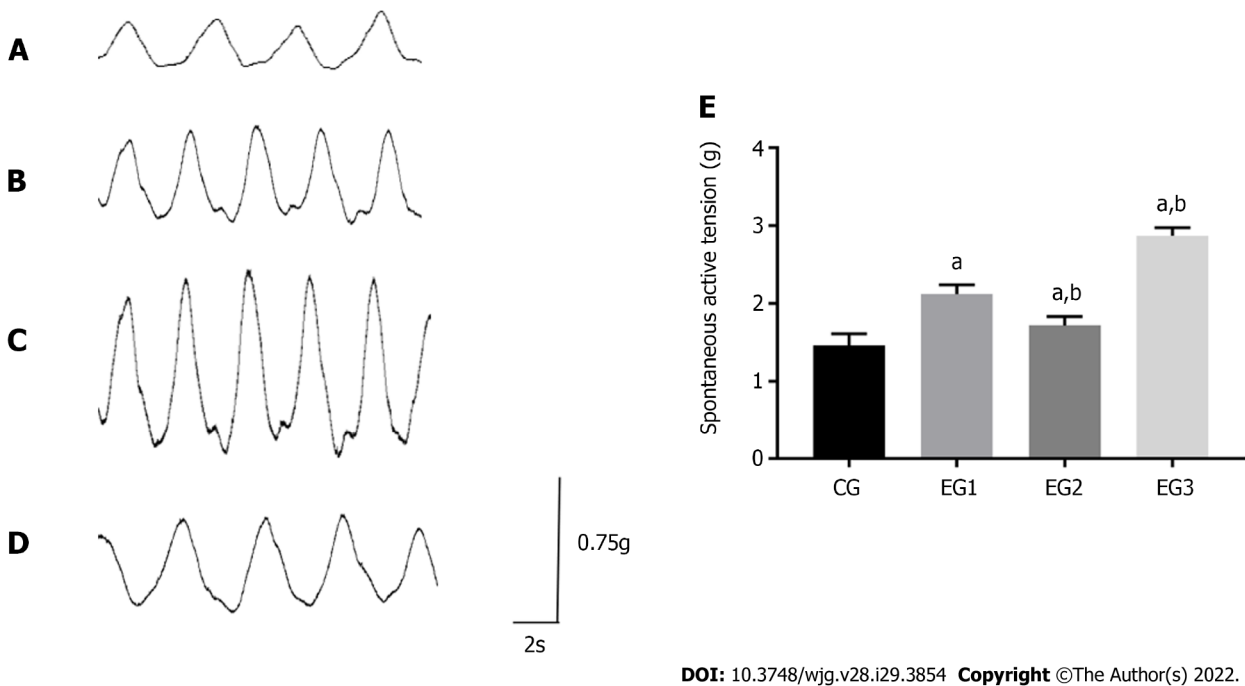


**Figure 8 Comparison of isolated colonic circular muscle contraction tension.** A-D: Contraction amplitude of the colonic circular muscle of CG (A), EG1 (B), EG2 (C), and EG3 (D) rats; E: Comparison of the contraction tension of the rat colonic circular muscle among the four groups: CG ( $1.46 \pm 0.06$  g), EG1 ( $2.12 \pm 0.49$  g), EG2 ( $2.87 \pm 0.04$  g), and EG3 ( $1.72 \pm 0.04$  g). All differences were statistically significant between EG groups and CG group ( $^*P < 0.0001$ ) and between EG2-3 groups and EG1 group ( $^*P < 0.0001$ ). CG: Control group; UC: Ulcerative colitis; NOS: Nitric oxide synthase; L-NMMA: NG-monomethyl-L-arginine monoacetate; EG1: UC group; EG2: UC + NOS agonist TP508TFA group; EG3: UC + NOS inhibitor L-NMMA group; CM: Circular muscle.

regulation of nitroergic neurons in the colonic MP through interference with the activity of NOS might be a novel potential and prospective way to reduce diarrhea symptoms in UC patients.

## ARTICLE HIGHLIGHTS

### Research background

Ulcerative colitis (UC) is a nonspecific inflammatory intestinal disorder with a complex etiology and poorly understood pathogenesis. The association between abnormal intestinal motility and UC has gained increasing attention over the past years. The enteric nervous system (ENS) regulates gut motility and based on their functions, has been divided into inhibitory and excitatory neurons, which mainly regulate the gut motility in terms of relaxation and contraction *via* different neurotransmitters. Nitroergic neurons are typical inhibitory neurons in the ENS and act through the neurotransmitter nitric oxide, which is synthesized by the rate-limiting enzyme nitric oxide synthase (NOS), whose expression changes might affect the motor function of the gut.

### Research motivation

UC is an intestinal disease with abdominal pain and diarrhea as the main symptoms, which are associated with abnormal gastrointestinal motility. Alterations in the amount of enteric neurotransmitters may change the number of enteric neurons. Nitroergic neurons are well-established enteric inhibitory neurons, and modification of its expression may interfere with its regulatory effect on intestinal motility and improve the symptoms of abdominal pain and diarrhea in UC.

### Research objectives

This study aimed to investigate the relationship between colonic NOS expression changes and colonic motility in dextran sulfate sodium (DSS)-induced UC rats, and to explore the effects of nitroergic neurons on colonic motility in UC rats to discover the potential mechanisms for the treatment of UC.

### Research methods

UC was induced in adult male rats with 5.5% DSS, and part of them were administered with NOS agonists and inhibitors. The rats were divided into control (CG), UC (EG1), UC + agonist (EG2), and UC + inhibitor (EG3) groups. The changes in tissue expression, relative protein expression, and concentration of NOS in rats were detected by immunofluorescence histochemical double staining, Western blot, and ELISA techniques, respectively. The effect of nitroergic neurons on colonic motility was examined by the changes in colonic circular muscle (CM) and longitudinal muscle (LM) contraction tension *in vitro*.

### Research results

Compared with CG rats, the proportion of NOS positive neurons within the colonic myenteric plexus (MP), the relative expression of NOS, and the concentration of NOS in both serum and colonic tissue were significantly higher in EG rats. After administration of NOS agonists and inhibitors, various degrees of increase and decrease were observed in EG2 and EG3 rats, respectively. The contraction amplitude and mean contraction tension of the CM and LM in rat colon after administration of agonists and inhibitors were attenuated and enhanced *in vitro*, respectively. For UC, regulating the expression of NOS within the MP may improve intestinal motility, thereby favoring the recovery of intestinal function.

### Research conclusions

Nitroergic neurons within the rat colonic MP are involved in the regulation of colonic motility. Increased NOS in the colonic MP of UC rats causes nitroergic neurons amplification, leading to decreased colonic contraction function. Modulation of NOS levels within colonic MP can alter nitroergic neuron expression and adjust the motor activity of the intestinal smooth muscle, which can further improve colonic motor function, moderate UC symptoms, and provide evidence for the development of new drugs against UC.

### Research perspectives

This study demonstrated increased NOS expression in the colonic MP of UC rats, with a possible corresponding increase in nitroergic neuron expression and a decrease in colonic contraction function in UC rats. Thus, by regulating the expression of NOS in the colonic MP, colonic motor function and interruption in the pathogenesis of UC can be achieved, thus providing a novel insight into the treatment of UC.

## FOOTNOTES

**Author contributions:** Li YQ and Chen J designed the study and edited the manuscript; Li YR, Li Y, Xu M, Jin Y, and Fan HW conducted the experiments; Li YR and Li Y completed the data analysis; Zhang Q and Tan GH provided language modification; Li YR and Li Y wrote the manuscript; all authors read and approved the final manuscript; and Li YR and Li Y contributed equally in carrying out this study and writing the manuscript.

**Supported by** National Natural Science Foundation of China, No. 31971112; Natural Science Foundation of Liaoning Province, No. 2021-MS-330; and Innovation Capability Support Program of Shaanxi, No. 2021TD-57.

**Institutional animal care and use committee statement:** All animal experiments conformed to the internationally accepted principles for the care and use of laboratory animals (licence No. SCXK (Shan) 2019-001, Animal Experiment Center, The Fourth Military Medical University, China; protocol No. IACUC-20211101, The Laboratory Animal Welfare and Ethics Committee at The Fourth Military Medical University, China).

**Conflict-of-interest statement:** All authors report no relevant conflicts of interest for this article.

**Data sharing statement:** No additional data are available.

**ARRIVE guidelines statement:** The authors have read the ARRIVE guidelines, and the manuscript was prepared and revised according to the ARRIVE guidelines.

**Open-Access:** This article is an open-access article that was selected by an in-house editor and fully peer-reviewed by external reviewers. It is distributed in accordance with the Creative Commons Attribution NonCommercial (CC BY-NC 4.0) license, which permits others to distribute, remix, adapt, build upon this work non-commercially, and license their derivative works on different terms, provided the original work is properly cited and the use is non-commercial. See: <https://creativecommons.org/licenses/by-nc/4.0/>

**Country/Territory of origin:** China

**ORCID number:** Yan-Rong Li 0000-0001-7830-1055; Yan Li 0000-0001-5089-8574; Yuan Jin 0000-0001-7184-2844; Mang Xu 0000-0003-1017-1455; Hong-Wei Fan 0000-0002-9546-593X; Qian Zhang 0000-0001-7249-4191; Guo-He Tan 0000-0002-1101-207X; Jing Chen 0000-0001-9971-1053; Yun-Qing Li 0000-0002-3707-3348.

**S-Editor:** Ma YJ

**L-Editor:** Wang TQ

**P-Editor:** Cai YX

## REFERENCES

- 1 **Kuehn F**, Hodin RA. Impact of Modern Drug Therapy on Surgery: Ulcerative Colitis. *Visc Med* 2018; **34**: 426-431 [PMID: 30675487 DOI: 10.1159/000493492]
- 2 **Hoffmann P**, Krisam J, Stremmel W, Gauss A. Real-World Outcomes of Vedolizumab Therapy in Ulcerative Colitis and Crohn's Disease at a Tertiary Referral Center. *Dig Dis* 2019; **37**: 33-44 [PMID: 30134234 DOI: 10.1159/000492322]
- 3 **Ponder A**, Long MD. A clinical review of recent findings in the epidemiology of inflammatory bowel disease. *Clin Epidemiol* 2013; **5**: 237-247 [PMID: 23922506 DOI: 10.2147/CLEP.S33961]
- 4 **Higuchi LM**, Khalili H, Chan AT, Richter JM, Bousvaros A, Fuchs CS. A prospective study of cigarette smoking and the risk of inflammatory bowel disease in women. *Am J Gastroenterol* 2012; **107**: 1399-1406 [PMID: 22777340 DOI: 10.1038/ajg.2012.196]
- 5 **Santana PT**, Rosas SLB, Ribeiro BE, Marinho Y, de Souza HSP. Dysbiosis in Inflammatory Bowel Disease: Pathogenic Role and Potential Therapeutic Targets. *Int J Mol Sci* 2022; **23** [PMID: 35408838 DOI: 10.3390/ijms23073464]
- 6 **Sundin J**, Aziz I, Nordlander S, Polster A, Hu YOO, Hugerth LW, Pennhag AAL, Engstrand L, Törnblom H, Simrén M, Öhman L. Evidence of altered mucosa-associated and fecal microbiota composition in patients with Irritable Bowel Syndrome. *Sci Rep* 2020; **10**: 593 [PMID: 31953505 DOI: 10.1038/s41598-020-57468-y]
- 7 **Bassotti G**, Antonelli E, Villanacci V, Nascimbeni R, Dore MP, Pes GM, Maconi G. Abnormal gut motility in inflammatory bowel disease: an update. *Tech Coloproctol* 2020; **24**: 275-282 [PMID: 32062797 DOI: 10.1007/s10151-020-02168-y]
- 8 **Li H**, Fan C, Lu H, Feng C, He P, Yang X, Xiang C, Zuo J, Tang W. Protective role of berberine on ulcerative colitis through modulating enteric glial cells-intestinal epithelial cells-immune cells interactions. *Acta Pharm Sin B* 2020; **10**: 447-461 [PMID: 32140391 DOI: 10.1016/j.apsb.2019.08.006]
- 9 **Głabaska D**, Guzek D, Grudzińska D, Lech G. Influence of dietary isoflavone intake on gastrointestinal symptoms in ulcerative colitis individuals in remission. *World J Gastroenterol* 2017; **23**: 5356-5363 [PMID: 28839435 DOI: 10.3748/wjg.v23.i29.5356]
- 10 **Costa M**, Spencer NJ, Brookes SJH. The role of enteric inhibitory neurons in intestinal motility. *Auton Neurosci* 2021; **235**: 102854 [PMID: 34329834 DOI: 10.1016/j.autneu.2021.102854]
- 11 **Schemann M**. Control of gastrointestinal motility by the "gut brain"--the enteric nervous system. *J Pediatr Gastroenterol Nutr* 2005; **41** Suppl 1: S4-S6 [PMID: 16131964 DOI: 10.1097/01.scs.0000180285.51365.55]
- 12 **Saldana-Morales FB**, Kim DV, Tsai MT, Diehl GE. Healthy Intestinal Function Relies on Coordinated Enteric Nervous System, Immune System, and Epithelium Responses. *Gut Microbes* 2021; **13**: 1-14 [PMID: 33929291 DOI: 10.1080/19490976.2021.1916376]
- 13 **Tse JKY**. Gut Microbiota, Nitric Oxide, and Microglia as Prerequisites for Neurodegenerative Disorders. *ACS Chem Neurosci* 2017; **8**: 1438-1447 [PMID: 28640632 DOI: 10.1021/acscchemneuro.7b00176]

- 14 **Sánchez-Fidalgo S**, Cárdeno A, Sánchez-Hidalgo M, Aparicio-Soto M, de la Lastra CA. Dietary extra virgin olive oil polyphenols supplementation modulates DSS-induced chronic colitis in mice. *J Nutr Biochem* 2013; **24**: 1401-1413 [PMID: 23337347 DOI: [10.1016/j.jnutbio.2012.11.008](https://doi.org/10.1016/j.jnutbio.2012.11.008)]
- 15 **Murano M**, Maemura K, Hirata I, Toshina K, Nishikawa T, Hamamoto N, Sasaki S, Saitoh O, Katsu K. Therapeutic effect of intracolonic administered nuclear factor kappa B (p65) antisense oligonucleotide on mouse dextran sulphate sodium (DSS)-induced colitis. *Clin Exp Immunol* 2000; **120**: 51-58 [PMID: 10759763 DOI: [10.1046/j.1365-2249.2000.01183.x](https://doi.org/10.1046/j.1365-2249.2000.01183.x)]
- 16 **Drossman DA**, Tack J, Ford AC, Szigethy E, Törnblom H, Van Oudenhove L. Neuromodulators for Functional Gastrointestinal Disorders (Disorders of Gut-Brain Interaction): A Rome Foundation Working Team Report. *Gastroenterology* 2018; **154**: 1140-1171.e1 [PMID: 29274869 DOI: [10.1053/j.gastro.2017.11.279](https://doi.org/10.1053/j.gastro.2017.11.279)]
- 17 **Filpa V**, Moro E, Protasoni M, Crema F, Frigo G, Giaroni C. Role of glutamatergic neurotransmission in the enteric nervous system and brain-gut axis in health and disease. *Neuropharmacology* 2016; **111**: 14-33 [PMID: 27561972 DOI: [10.1016/j.neuropharm.2016.08.024](https://doi.org/10.1016/j.neuropharm.2016.08.024)]
- 18 **Niesler B**, Kuerten S, Demir IE, Schäfer KH. Disorders of the enteric nervous system - a holistic view. *Nat Rev Gastroenterol Hepatol* 2021; **18**: 393-410 [PMID: 33514916 DOI: [10.1038/s41575-020-00385-2](https://doi.org/10.1038/s41575-020-00385-2)]
- 19 **Fornai M**, Pellegrini C, Antonioli L, Segnani C, Ippolito C, Barocelli E, Ballabeni V, Vegezzi G, Al Harraq Z, Blandini F, Levandis G, Cerri S, Blandizzi C, Bernardini N, Colucci R. Enteric Dysfunctions in Experimental Parkinson's Disease: Alterations of Excitatory Cholinergic Neurotransmission Regulating Colonic Motility in Rats. *J Pharmacol Exp Ther* 2016; **356**: 434-444 [PMID: 26582732 DOI: [10.1124/jpet.115.228510](https://doi.org/10.1124/jpet.115.228510)]
- 20 **Li S**, Fei G, Fang X, Yang X, Sun X, Qian J, Wood JD, Ke M. Changes in Enteric Neurons of Small Intestine in a Rat Model of Irritable Bowel Syndrome with Diarrhea. *J Neurogastroenterol Motil* 2016; **22**: 310-320 [PMID: 26645247 DOI: [10.5056/jnm15082](https://doi.org/10.5056/jnm15082)]
- 21 **De Giorgio R**, Barbara G, Stanghellini V, De Ponti F, Salvioli B, Tonini M, Velio P, Bassotti G, Corinaldesi R. Clinical and morphofunctional features of idiopathic myenteric ganglionitis underlying severe intestinal motor dysfunction: a study of three cases. *Am J Gastroenterol* 2002; **97**: 2454-2459 [PMID: 12358272 DOI: [10.1111/j.1572-0241.2002.06002.x](https://doi.org/10.1111/j.1572-0241.2002.06002.x)]
- 22 **Lin Z**, Liu Y, Zheng Q, Hu Q. Increased proportion of nitric oxide synthase immunoreactive neurons in rat ileal myenteric ganglia after severe acute pancreatitis. *BMC Gastroenterol* 2011; **11**: 127 [PMID: 22111589 DOI: [10.1186/1471-230X-11-127](https://doi.org/10.1186/1471-230X-11-127)]
- 23 **Dai Y**, Haque MM, Stuehr DJ. Restricting the conformational freedom of the neuronal nitric-oxide synthase flavoprotein domain reveals impact on electron transfer and catalysis. *J Biol Chem* 2017; **292**: 6753-6764 [PMID: 28232486 DOI: [10.1074/jbc.M117.777219](https://doi.org/10.1074/jbc.M117.777219)]
- 24 **Anitha M**, Gondha C, Sutliff R, Parsadianian A, Mwangi S, Sitaraman SV, Srinivasan S. GDNF rescues hyperglycemia-induced diabetic enteric neuropathy through activation of the PI3K/Akt pathway. *J Clin Invest* 2006; **116**: 344-356 [PMID: 16453021 DOI: [10.1172/JCI26295](https://doi.org/10.1172/JCI26295)]
- 25 **Gracie DJ**, Guthrie EA, Hamlin PJ, Ford AC. Bi-directionality of Brain-Gut Interactions in Patients With Inflammatory Bowel Disease. *Gastroenterology* 2018; **154**: 1635-1646.e3 [PMID: 29366841 DOI: [10.1053/j.gastro.2018.01.027](https://doi.org/10.1053/j.gastro.2018.01.027)]
- 26 **Leonardi I**, Paramsothy S, Doron I, Semon A, Kaakoush NO, Clemente JC, Faith JJ, Borody TJ, Mitchell HM, Colombel JF, Kamm MA, Iliev ID. Fungal Trans-kingdom Dynamics Linked to Responsiveness to Fecal Microbiota Transplantation (FMT) Therapy in Ulcerative Colitis. *Cell Host Microbe* 2020; **27**: 823-829.e3 [PMID: 32298656 DOI: [10.1016/j.chom.2020.03.006](https://doi.org/10.1016/j.chom.2020.03.006)]
- 27 **Singer II**, Kawka DW, Scott S, Weidner JR, Mumford RA, Riehl TE, Stenson WF. Expression of inducible nitric oxide synthase and nitrotyrosine in colonic epithelium in inflammatory bowel disease. *Gastroenterology* 1996; **111**: 871-885 [PMID: 8831582 DOI: [10.1016/s0016-5085\(96\)70055-0](https://doi.org/10.1016/s0016-5085(96)70055-0)]
- 28 **Kolios G**, Rooney N, Murphy CT, Robertson DA, Westwick J. Expression of inducible nitric oxide synthase activity in human colon epithelial cells: modulation by T lymphocyte derived cytokines. *Gut* 1998; **43**: 56-63 [PMID: 9771406 DOI: [10.1136/gut.43.1.56](https://doi.org/10.1136/gut.43.1.56)]
- 29 **Kubes P**. Inducible nitric oxide synthase: a little bit of good in all of us. *Gut* 2000; **47**: 6-9 [PMID: 10861252 DOI: [10.1136/gut.47.1.6](https://doi.org/10.1136/gut.47.1.6)]
- 30 **Vallance BA**, Deng W, De Grado M, Chan C, Jacobson K, Finlay BB. Modulation of inducible nitric oxide synthase expression by the attaching and effacing bacterial pathogen *Citrobacter rodentium* in infected mice. *Infect Immun* 2002; **70**: 6424-6435 [PMID: 12379723 DOI: [10.1128/IAI.70.11.6424-6435.2002](https://doi.org/10.1128/IAI.70.11.6424-6435.2002)]
- 31 **Vallance BA**, Dijkstra G, Qiu B, van der Waaij LA, van Goor H, Jansen PL, Mashimo H, Collins SM. Relative contributions of NOS isoforms during experimental colitis: endothelial-derived NOS maintains mucosal integrity. *Am J Physiol Gastrointest Liver Physiol* 2004; **287**: G865-G874 [PMID: 15217783 DOI: [10.1152/ajpgi.00187.2004](https://doi.org/10.1152/ajpgi.00187.2004)]
- 32 **Beck PL**, Xavier R, Wong J, Ezedi I, Mashimo H, Mizoguchi A, Mizoguchi E, Bhan AK, Podolsky DK. Paradoxical roles of different nitric oxide synthase isoforms in colonic injury. *Am J Physiol Gastrointest Liver Physiol* 2004; **286**: G137-G147 [PMID: 14665440 DOI: [10.1152/ajpgi.00309.2003](https://doi.org/10.1152/ajpgi.00309.2003)]
- 33 **Luo CX**, Zhu DY. Research progress on neurobiology of neuronal nitric oxide synthase. *Neurosci Bull* 2011; **27**: 23-35 [PMID: 21270901 DOI: [10.1007/s12264-011-1038-0](https://doi.org/10.1007/s12264-011-1038-0)]
- 34 **Bule M**, Palus K, Dąbrowski M, Calka J. Hyperglycaemia-Induced Downregulation in Expression of nNOS Intramural Neurons of the Small Intestine in the Pig. *Int J Mol Sci* 2019; **20** [PMID: 30987291 DOI: [10.3390/ijms20071681](https://doi.org/10.3390/ijms20071681)]
- 35 **Lalatta-Costerbosa G**, Clavenzani P, Petrosino G, Mazzoni M. An immunohistochemical study of the distribution of nitric oxide synthase-immunoreactive neurons and fibers in the reticular groove of suckling lambs. *J Anat* 2011; **218**: 439-448 [PMID: 21323665 DOI: [10.1111/j.1469-7580.2011.01345.x](https://doi.org/10.1111/j.1469-7580.2011.01345.x)]
- 36 **Tomuschat C**, O'Donnell AM, Coyle D, Dreher N, Kelly D, Puri P. NOS-interacting protein (NOSIP) is increased in the colon of patients with Hirschsprung's disease. *J Pediatr Surg* 2017; **52**: 772-777 [PMID: 28196663 DOI: [10.1016/j.jpedsurg.2017.01.046](https://doi.org/10.1016/j.jpedsurg.2017.01.046)]
- 37 **Huber A**, Saur D, Kurjak M, Schusdziarra V, Allescher HD. Characterization and splice variants of neuronal nitric oxide synthase in rat small intestine. *Am J Physiol* 1998; **275**: G1146-G1156 [PMID: 9815045 DOI: [10.1152/ajpgi.1998.275.5.G1146](https://doi.org/10.1152/ajpgi.1998.275.5.G1146)]

- 38 **Chen L**, Yu B, Luo D, Lin M. Enteric motor dysfunctions in experimental chronic pancreatitis: Alterations of myenteric neurons regulating colonic motility in rats. *Neurogastroenterol Motil* 2018; **30**: e13301 [PMID: [29520975](#) DOI: [10.1111/nmo.13301](#)]

## Basic Study

## N-linked glycoproteomic profiling in esophageal squamous cell carcinoma

Qi-Wei Liu, Hao-Jie Ruan, Wei-Xia Chao, Meng-Xiang Li, Ye-Lin Jiao, Douglas G Ward, She-Gan Gao, Yi-Jun Qi

**Specialty type:** Medicine, research and experimental

**Provenance and peer review:**

Unsolicited article; Externally peer reviewed.

**Peer-review model:** Single blind

**Peer-review report's scientific quality classification**

Grade A (Excellent): 0  
Grade B (Very good): 0  
Grade C (Good): C, C  
Grade D (Fair): 0  
Grade E (Poor): 0

**P-Reviewer:** Chen X, United States; Kashyap MK, India

**Received:** January 14, 2022

**Peer-review started:** January 14, 2022

**First decision:** April 12, 2022

**Revised:** April 26, 2022

**Accepted:** July 6, 2022

**Article in press:** July 6, 2022

**Published online:** August 7, 2022



**Qi-Wei Liu, Hao-Jie Ruan, Wei-Xia Chao, Meng-Xiang Li, She-Gan Gao, Yi-Jun Qi**, Henan Key Laboratory of Microbiome and Esophageal Cancer Prevention and Treatment; Henan Key Laboratory of Cancer Epigenetics; Cancer Hospital, The First Affiliated Hospital, College of Clinical Medicine, Henan University of Science and Technology, Luoyang 471003, Henan Province, China

**Ye-Lin Jiao**, Department of Pathology, The First People's Hospital of Luo Yang, Luoyang 471000, Henan Province, China

**Douglas G Ward**, Institute of Cancer and Genomic Sciences, College of Medical and Dental Sciences, University of Birmingham, Birmingham B15 2TT, United Kingdom

**Corresponding author:** Yi-Jun Qi, MD, PhD, Professor, Henan Key Laboratory of Microbiome and Esophageal Cancer Prevention and Treatment; Henan Key Laboratory of Cancer Epigenetics; Cancer Hospital, The First Affiliated Hospital, College of Clinical Medicine, Henan University of Science and Technology, No. 29 Jinghua Road, Luoyang 471003, Henan Province, China. [qiyijun@haust.edu.cn](mailto:qiyijun@haust.edu.cn)

**Abstract****BACKGROUND**

Mass spectrometry-based proteomics and glycomics reveal post-translational modifications providing significant biological insights beyond the scope of genomic sequencing.

**AIM**

To characterize the N-linked glycoproteomic profile in esophageal squamous cell carcinoma (ESCC) *via* two complementary approaches.

**METHODS**

Using tandem multilectin affinity chromatography for enrichment of N-linked glycoproteins, we performed N-linked glycoproteomic profiling in ESCC tissues by two-dimensional gel electrophoresis (2-DE)-based and isobaric tags for relative and absolute quantification (iTRAQ) labeling-based mass spectrometry quantitation in parallel, followed by validation of candidate glycoprotein biomarkers by Western blot.

**RESULTS**

2-DE-based and iTRAQ labeling-based quantitation identified 24 and 402 differentially expressed N-linked glycoproteins, respectively, with 15 in common, demonstrating the outperformance of iTRAQ labeling-based quantitation over 2-DE and complementarity of these two approaches. Proteomaps showed the distinct compositions of functional categories between proteins and glycoproteins with differential expression associated with ESCC. Western blot analysis validated the up-regulation of total procathepsin D and high-mannose procathepsin D, and the down-regulation of total haptoglobin, high-mannose clusterin, and GlcNAc/sialic acid-containing fraction of 14-3-3 $\zeta$  in ESCC tissues. The serum levels of glycosylated fractions of clusterin, proline-arginine-rich end leucine-rich repeat protein, and haptoglobin in patients with ESCC were remarkably higher than those in healthy controls.

### CONCLUSION

Our study provides insights into the aberrant N-linked glycoproteome associated with ESCC, which will be a valuable resource for future investigations.

**Key Words:** Esophageal squamous cell carcinoma; N-linked glycoprotein; Post-translational modification; Lectin; Cathepsin D; Haptoglobin; 14-3-3 $\zeta$

©The Author(s) 2022. Published by Baishideng Publishing Group Inc. All rights reserved.

**Core Tip:** The N-linked glycoproteome was comprehensively profiled by two-dimensional gel electrophoresis-based and isobaric tags for relative and absolute quantification (iTRAQ) labeling-based mass spectrometry quantitation in parallel after N-linked glycoprotein enrichment by a tandem of multilectin affinity chromatography. The iTRAQ labeling-based quantitative proteomic profiling outperformed protein spot intensity quantification used by two-dimensional gel electrophoresis. A total of 411 N-linked glycoproteins were identified, including 128 up-regulated and 283 down-regulated glycoproteins with differential expression, which provide the scientific community with a dataset of glycoproteins associated with esophageal squamous cell carcinoma for in-depth investigation.

**Citation:** Liu QW, Ruan HJ, Chao WX, Li MX, Jiao YL, Ward DG, Gao SG, Qi YJ. N-linked glycoproteomic profiling in esophageal squamous cell carcinoma. *World J Gastroenterol* 2022; 28(29): 3869-3885

**URL:** <https://www.wjgnet.com/1007-9327/full/v28/i29/3869.htm>

**DOI:** <https://dx.doi.org/10.3748/wjg.v28.i29.3869>

## INTRODUCTION

Esophageal cancer is a severe global health issue with 572000 new cases and 509000 deaths in 2018, half of which occur in China[1]. The two most common histological subtypes of esophageal cancer are esophageal squamous cell carcinoma (ESCC) and esophageal adenocarcinoma, with ESCC being the predominant histological subtype both in China and worldwide[2,3]. The long-term outcome of ESCC is correlated with clinical stage at diagnosis with the best outcome in the early stages[4-6]. Unfortunately, the current endoscopic screening for ESCC suffers from low patient compliance and high cost despite the fact that an early detection rate of 70% was achieved in a high-risk region in northern central China [7]. Furthermore, serum biomarkers for ESCC, including squamous cell carcinoma antigen, carcinoembryonic antigen, CYFRA21-1, and carbohydrate antigen 19-9, lack sufficient sensitivity and specificity for early detection[8-11]. The overall 5-year survival rate ranges from 15% to 25% because most cases of ESCC present at an advanced stage[6,12]. It is well accepted that novel biomarkers would hold great promise to improve the clinical outcome of ESCC.

Recent large-scale “omics” studies in ESCC have identified a myriad of aberrations at the levels of genome, epigenome, transcriptome, proteome, *etc.*, revealing the high molecular heterogeneity of ESCC [13-17]. Beyond the scope of other techniques, mass spectrometry (MS)-based proteomics has the ability to measure post-translational modifications that provide additional significant biological insights, for example, therapeutically targetable signaling proteins and pathways[18,19]. To date, comprehensive glycoproteomic studies of ESCC are lacking. Glycosylation is present on more than 50% of human proteins and aberrant glycosylation has been implicated in the development and progression of various cancers[20-24]. The sugar chains of glycoproteins are involved in numerous physiological and pathological functions including cell growth, adhesion, differentiation, migration, signal regulation, immune responses, and tumor invasion[20,25,26]. Notably, the clinical prognosis of cancer has been correlated with certain structures of glycans attached to proteins[27,28]. The bisecting GlcNAc structure

catalyzed by N-acetylglucosaminyltransferase III plays crucial roles in suppression of cancer metastasis, which contrasts with the tumor-promoting role of  $\beta$ 1, 6-branched N-glycan catalyzed by N-acetylglucosaminyltransferase V[29]. It has been reported that E-cadherin modified by complex N-glycans exhibits weakened adherens junctions, whereas high mannose or less N-glycans attached to E-cadherin produces stable adherens junctions[30]. Furthermore, N-acetylglucosaminyltransferase III modified  $\alpha$ 3 $\beta$ 1 integrin suppresses cell spreading and migration and focal adhesion kinase activity[31]. The fraction of ConA-binding procathepsin D in the serum of hepatocellular carcinoma patients is significantly increased and shows a sensitivity of 85% and specificity of 80% for hepatocellular carcinoma diagnosis [24]. Not surprisingly, over 50% of current cancer biomarkers are glycoproteins, such as AFP, AFP-L3, CA19-9, CA125, and CEA[32-35].

In this study, we used MS-based proteomic analysis to identify N-linked glycoproteins associated with ESCC after isolation of N-linked glycoproteins using tandem multilectin affinity chromatography. Our study unraveled a comprehensive landscape of N-linked glycosylation dysregulation associated with ESCC and bioinformatics analysis provided insights into the functional significance of such aberrant glycosylation. The glycosylated fractions of procathepsin D, clusterin, 14-3-3 $\zeta$ , proline-arginine-rich end leucine-rich repeat protein (PRELP), and haptoglobin may play important roles in malignant progression of ESCC and are potential diagnostic biomarkers for ESCC, suggesting that N-linked glycosylation aberrations may promote the malignant progression of ESCC.

## MATERIALS AND METHODS

### *Clinical samples*

All patients provided written informed consent, and the study was approved by the Ethics Committee of the Medical School, Henan University, China (ethics ref: 108) and conducted in accordance with the ethical guidelines of the 1975 Declaration of Helsinki. Forty-seven pairs of resected ESCC and adjacent normal esophageal mucosa tissue samples, and ten pre-operative serum samples were collected at Linzhou Cancer Hospital, Henan, China between 2010 and 2011 and stored in liquid nitrogen or at -70 °C prior to protein extraction. Among the tissue samples, 15 pairs served as a discovery set and the other 32 pairs as a validation set. All tissues were histopathologically confirmed as normal esophageal mucosa or ESCC. The adjacent non-cancerous samples were at least 3 cm distant from the edge of neoplastic mass. No patient in this study had received preoperative radiotherapy or chemotherapy.

### *Isolation of N-linked glycoproteins by lectin affinity chromatography*

Extraction of total tissue proteins and N-linked glycoproteins was performed as previously reported with modifications[24]. Briefly, the esophageal tissue was homogenized in lysis buffer (50 mmol/L Tris, 150 mmol/L NaCl, 1% NP-40, pH 7.2) supplemented with complete proteinase inhibitor cocktail (Roche Diagnostics GmbH, Mannheim, Germany) followed by centrifugation and supernatant collection. Enrichment of N-linked glycoproteins for three pairs of pooled protein samples from 15 ESCC and adjacent non-tumor tissues (five samples for each pair) was performed by tandem lectin affinity chromatography. The multilectin affinity chromatography used a combination of three agarose-bound lectins, Con A (Vector Laboratories, AL-1003), lentil lectin (LCH, Vector Laboratories, AL-1043), and snowdrop lectin (GNA, Vector Laboratories, AL-1243), and a combination of wheat germ agglutinin lectin (WGA, Vector Laboratories, AL-1023) and elderberry lectin (SNA, Vector Laboratories, AL-1303) for the first and second affinity chromatography, respectively. Sixty milligrams of pooled proteins were diluted with binding buffer (30 mmol/L Bis-Tris, 150 mmol/L NaCl, 1 mmol/L CaCl<sub>2</sub>, 1 mmol/L MnCl<sub>2</sub>, pH 7.2) and incubated with the lectins in the first affinity chromatography columns at room temperature for 2 h. After incubation, 200 mmol/L methyl- $\alpha$ -D-mannopyranoside was used for elution of high-mannose N-linked glycoproteins. The flowthrough of the first three-lectin column was subjected to the second chromatography for isolation of GlcNAc/sialic acid-containing N-linked glycoproteins using 200 mmol/L N-Acetyl-D-glucosamine as elution buffer. The eluted samples were desalted and concentrated by acetone precipitation.

### *Two-dimensional gel electrophoresis and image analysis*

Two-dimensional gel electrophoresis (2-DE) was performed as previously reported[24,36]. Fifty micrograms of glycoproteins were used for the first-dimension isoelectrofocusing electrophoresis using IPG strips with a linear pH range of 3-10, followed by the second dimension separation using 15% SDS-PAGE gels. Silver stained gels were scanned with an ImageScanner. Image analysis was carried out with ImageMaster 2-D Elite software 4.01.

### *In-gel digestion and MS identification*

The excised protein spots with differential expression were reduced with DTT, alkylated with iodoacetamide, dried in a speedvac, and digested with trypsin (12.5  $\mu$ g/mL in 50 mmol/L ammonium bicarbonate). LC-MS/MS analysis of tryptic peptides was performed using a Maxis Impact Q-TOF mass

spectrometer (BrukerDaltonics, Bremen, Germany). The MS/MS data were searched against the SwissProt human sequence database using MASCOT *via* Proteinscape (BrukerDaltonics, Bremen, Germany) and reverse database searching was used for estimating the false discovery rate. All proteins were identified by  $\geq 2$  unique peptides.

### **Isobaric tags for relative and absolute quantification labeling and MS identification**

Isobaric tags for relative and absolute quantification (iTRAQ) labeling of tryptic peptides was performed according to the protocol provided by the supplier. The iTRAQ labeled peptides derived from pooled protein samples of ten ESCC and adjacent non-tumor tissues as previously described in duplicate[37] were separated into 16 fractions by mixed-mode anion exchange/reverse-phase chromatography. Each fraction was dried, dissolved in 0.1% formic acid, and analyzed by LC-MS/MS using a Maxis Impact Q-TOF mass spectrometer (BrukerDaltonics, Bremen, Germany). Data were searched against the SwissProt human sequence database using MASCOT and expression ratios calculated by WARP-LC *via* Proteinscape (BrukerDaltonics, Bremen, Germany). The false discovery rate was estimated using a reverse database search strategy. All proteins were identified by  $\geq 2$  unique peptides. The data have been deposited at <https://www.iprox.cn/> with Project ID IPX0004371000.

### **Functional enrichment analysis**

Gene-set enrichment analyses of differentially expressed glycoproteins (DEGs) and previously identified differentially expressed proteins (DEPs)[37] were performed using Enrichment Map, which organizes the enriched gene-sets into a network with links representing the overlap of member genes [38]. The gene-sets with a *P* value  $< 0.001$  and false discovery rate  $< 5\%$  were selected for display in the enrichment map. To gain an insight into the functional makeup of DEGs and DEPs, Proteomap was used to visualize the functional distribution of DEGs or DEPs in cellular processes, including genetic information processing, metabolism, cellular processes, signaling, and others[39].

### **Western blot analysis**

Total tissue proteins were extracted using radioimmunoprecipitation assay lysis buffer, and glycoproteins were isolated by lectin affinity chromatography. Total proteins or glycoproteins were separated by SDS-PAGE and then transferred to PVDF membranes. The blots were blocked in 5% non-fat milk, incubated with primary antibodies and then corresponding secondary antibodies, and visualized using Supersignal West chemiluminescent substrate (Pierce Biotechnology, Rockford, IL, United States). Semi-quantitation of the band intensity was performed using image analysis software and corrected by reference to GAPDH. The antibodies used in this study were: Haptoglobin (1:2000, 16665-1-AP, Proteintech), cathepsin D (1:2500, ab75852, Abcam), clusterin (1:5000, 12289-1-AP, Proteintech), SOD3 (1:1500, T1799, Epitomics), PRELP (1:2000, AP6665b, Abgent), and 14-3-3- $\zeta$  (1:2500, ab85268, Abcam).

### **Statistical analysis**

All statistical analyses were performed with SPSS 24.0 software (SPSS, Chicago, IL, United States). Comparisons of quantitated protein band density between ESCC and adjacent non-cancerous tissues were done by paired Student's *t*-tests or Wilcoxon signed-rank sum tests. All statistical tests were two-sided, and *P*  $< 0.05$  was considered statistically significant.

## **RESULTS**

### **N-linked glycoprotein profiling by two-dimensional gel electrophoresis**

This study utilized two rounds of multilectin affinity chromatography to isolate N-linked glycoproteins. The first multilectin affinity column comprised Con A, LCH, and GNA lectins to isolate high-mannose N-linked glycoproteins, and the second affinity column included WGA and SNA lectins for GlcNAc/sialic acid-containing glycoprotein enrichment. 2-DE was used to separate the isolated N-linked glycoproteins. **Figure 1A** and **B** shows the representative 2-DE images of high-mannose glycoproteins isolated from ESCC and non-cancerous tissues. An average of  $742 \pm 45$  protein spots could be detected on each 2-DE gel analyzed by Image Master 2-D Elite. A total of 35 differential protein spots with  $\geq 1.5$  fold-changes in protein spot intensities (*P*  $< 0.05$ ) were identified, including 20 up-regulated and 15 down-regulated protein spots in ESCC compared with corresponding non-cancerous tissues, respectively. For GlcNAc/sialic acid-containing glycoprotein profiling, the patterns of protein spots on 2-DE gels were markedly different compared with those of high-mannose glycoproteins (**Figure 1C** and **D**). There were 23 protein spots with differential expression, including 5 up-regulated and 18 down-regulated protein spots in ESCC compared to non-cancerous tissues.

These protein spots were identified by LC-MS/MS of the trypsin-digested spots excised from preparative gels. The identities of proteins are shown in **Tables 1** and **2**, in which 22 proteins and 23 proteins were derived from the first and second lectin affinity chromatography, respectively. There

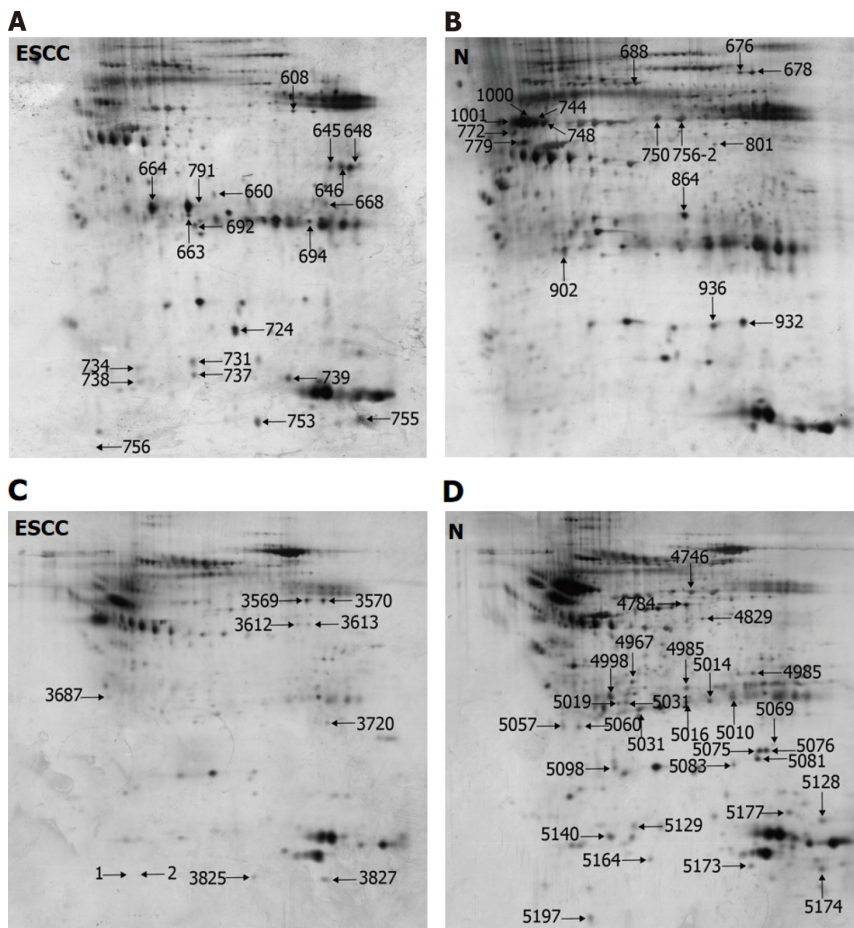
**Table 1 Summary of high-mannose N-linked glycoproteins in esophageal squamous cell carcinoma by 2-dimensional gel electrophoresis**

Spot No.	Accession	Protein identity (Theoretical MW/pI)	Ratio	P value	Scores	Unique Peptides	N-glycosylation sites
608	ENOA_HUMAN	Alpha-enolase (47.1/7.7)	2.2 (↑)	0.008	2050.2 (M:2050.2)	33	1 (102)
638	CATD_HUMAN	Cathepsin D (44.5/6.1)	2.6 (↑)	0.009	1351.8 (M:1351.8)	20	2 (134, 263)
645	G3P_HUMAN	Glyceraldehyde-3-phosphate dehydrogenase (36/9.3)	3.2 (↑)	0.009	319.9 (M:319.9)	4	0
646	G3P_HUMAN	Glyceraldehyde-3-phosphate dehydrogenase (36/9.3)	5.2 (↑)	0.002	611.5 (M:611.5)	10	0
648	G3P_HUMAN	Glyceraldehyde-3-phosphate dehydrogenase (36/9.3)	8.9 (↑)	0.009	730.1 (M:730.1)	14	0
660	CO1A2_HUMAN	Collagen alpha-2(I) chain (129.2/9.7)	1.7 (↑)	0.008	1207.8 (M:1207.8)	20	1 (207)
664	CATD_HUMAN	Cathepsin D (44.5/6.1)	12.5 (↑)	0.005	1337.1 (M:1337.1)	18	2 (134, 263)
668	ALDOA_HUMAN	Fructose-bisphosphate aldolase A (39.4/9.2)	1.6 (↑)	0.004	182.0 (M:182.0)	4	0
692	HSPB1_HUMAN	Heat shock protein beta-1 (22.8/6)	1.6 (↑)	0.009	1015.9 (M:1015.9)	15	0
694	TPIS_HUMAN	Triosephosphate isomerase (26.7/6.5)	1.8 (↑)	0.004	1277.6 (M:1277.6)	19	1 (233)
724	FABP5_HUMAN	Fatty acid-binding protein, epidermal (15.2/7.5)	2 (↑)	0.002	818.4 (M:818.4)	14	0
731	HPT_HUMAN	Haptoglobin (45.2/6.1)	2.1 (↑)	0.006	418.7 (M:418.7)	11	2 (207, 241)
734	HSPB1_HUMAN	Heat shock protein beta-1 (22.8/6)	1.5 (↑)	0.009	464.0 (M:464.0)	7	0
737	APOA1_HUMAN	Apolipoprotein A-I (30.8/5.5)	1.6 (↑)	0.002	200.4 (M:200.4)	4	0
738	COF1_HUMAN	Cofilin-1 (18.5/9.1)	1.5 (↑)	0.009	381.8 (M:381.8)	7	0
739	HBB_HUMAN	Hemoglobin subunit beta (16/6.9)	2.7 (↑)	0.008	720.5 (M:720.5)	10	0
753	CATD_HUMAN	Cathepsin D (44.5/6.1)	4.6 (↑)	0.009	702.0 (M:702.0)	13	2 (134, 263)
755	HBA_HUMAN	Hemoglobin subunit alpha (15.2/9.4)	3.9 (↑)	0.005	377.6 (M:377.6)	7	0
756	FIBB_HUMAN	Fibrinogen beta chain (55.9/9.3)	1.8 (↑)	0.009	3911.9 (M:3911.9)	55	0
791	FIBG_HUMAN	Fibrinogen gamma chain precursor (51.5/5.3)	1.5 (↑)	0.009	1356.7 (M:1356.7)	26	1 (78)
676	FIBB_HUMAN	Fibrinogen beta chain (55.9/9.3)	4.5 (↓)	0.006	1071.8 (M:1071.8)	18	0
678	CO3_HUMAN	Complement C3 (187/6)	6.2 (↓)	0.009	383.9 (M:383.9)	12	2 (85, 939)
688	HEMO_HUMAN	Hemopexin (51.6/6.6)	5.3 (↓)	0.002	698.2 (M:698.2)	13	2 (64, 240)
744	A1AT_HUMAN	Alpha-1-antitrypsin (46.7/5.3)	12.7 (↓)	0.009	784.8 (M:784.8)	14	3 (70, 107, 271)
748	HPT_HUMAN	Haptoglobin (45.2/6.1)	7.5 (↓)	0.008	1067.0 (M:1067.0)	19	2 (207, 241)
750	FIBB_HUMAN	Fibrinogen beta chain (55.9/9.3)	4.9 (↓)	0.009	3276.7 (M:3276.7)	48	0
772	A1AT_HUMAN	Alpha-1-antitrypsin (46.7/5.3)	1.8 (↓)	0.005	678.2 (M:678.2)	12	3 (70, 107, 271)
779	CLUS_HUMAN	Clusterin (52.5/5.9)	2.9 (↓)	0.009	619.3 (M:619.3)	10	3 (86, 103, 291)
801	FIBB_HUMAN	Fibrinogen beta chain (55.9/9.3)	2.1 (↓)	0.009	714.1 (M:714.1)	13	0
864	SODE_HUMAN	Extracellular superoxide dismutase [Cu-Zn] (25.8/6.2)	6.4 (↓)	0.004	798.6 (M:798.6)	12	1 (107)
902	APOA1_HUMAN	Apolipoprotein A-I (30.8/5.5)	4.3 (↓)	0.002	1206.2	24	0

					(M:1206.2)		
932	TRFE_HUMAN	Serotransferrin precursor (77/7)	3.8 (↓)	0.004	187.0 (M:187.0)	4	1 (630)
936	HPTR_HUMAN	Haptoglobin-related protein (39/6.7)	1.5 (↓)	0.002	226.4 (M:226.4)	4	1 (149)
1000	A1AT_HUMAN	Alpha-1-antitrypsin (46.7/5.3)	15.2 (↓)	0.006	1091.2 (M:1091.2)	20	3 (70, 107, 271)
1001	HPT_HUMAN	Haptoglobin (45.2/6.1)	9.8 (↓)	0.009	1054.6 (M:1054.6)	18	2 (207, 241)

**Table 2 Summary of sialic N-linked glycoproteins identified in esophageal squamous cell carcinoma by 2-dimensional gel electrophoresis**

Spot No.	Accession	Protein identity (Theoretical MW/pI)	Ratio	P value	Scores	Unique Peptides	N-glycosylation sites
3569	ENOA_HUMAN	Alpha-enolase (47.1/7.7)	2 (↑)	0.002	802.0 (M:802.0)	18	2 (17, 102)
3570	IGKC_HUMAN	Ig kappa chain C region (11.6/5.5)	2.4 (↑)	0.006	54.4 (M:54.4)	2	0
3612	TRFE_HUMAN	Serotransferrin (77/7)	1.5 (↑)	0.004	927.5 (M:927.5)	25	1 (630)
3687	KV305_HUMAN	Ig kappa chain V-III region WOL (11.7/9.5)	1.7 (↑)	0.009	125.4 (M:125.4)	2	0
3720	A1AT_HUMAN	Alpha-1-antitrypsin (46.7/5.3)	1.9 (↑)	0.002	49.3 (M:49.3)	2	3 (70, 107, 271)
4746	FIBB_HUMAN	Fibrinogen beta chain (55.9/9.3)	2.8 (↓)	0.004	817.3 (M:817.3)	17	0
4784	ACTB_HUMAN	Actin, cytoplasmic 1 (41.7/5.2)	3.4 (↓)	0.002	43.6 (M:43.6)	2	1 (12)
4948	HBB_HUMAN	Hemoglobin subunit beta (16/6.9)	1.8 (↓)	0.006	129.3 (M:129.3)	4	0
4967	ACTA_HUMAN	Actin, aortic smooth muscle (42/5.1)	1.7 (↓)	0.009	402.1 (M:402.1)	9	1 (14)
4985	FHR2_HUMAN	Complement factor H-related protein 2 (30.6/6)	2 (↓)	0.002	271.1 (M:271.1)	5	0
4998	1433Z_HUMAN	14-3-3 protein zeta/delta (27.7/4.6)	6.6 (↓)	0.009	62.1 (M:62.1)	2	2 (173, 224)
5010	FIBA_HUMAN	Fibrinogen alpha chain (94.9/5.6)	2.1 (↓)	0.002	83.3 (M:83.3)	3	3 (288, 419, 831)
5019	ACTH_HUMAN	Actin, gamma-enteric smooth muscle (41.8/5.2)	1.6 (↓)	0.009	92.7 (M:92.7)	3	1 (13)
5031	KV204_HUMAN	Ig kappa chain V-II region TEW (12.3/5.6)	1.5 (↓)	0.008	84.9 (M:84.9)	2	0
5057	CATB_HUMAN	Cathepsin B (37.8/5.9)	1.6 (↓)	0.009	84.8 (M:84.8)	2	2 (192, 289)
5069	FABP5_HUMAN	Fatty acid-binding protein, epidermal (15.2/7.5)	1.5 (↓)	0.005	88.7 (M:88.7)	2	0
5076	CRYAB_HUMAN	Alpha-crystallin B chain (20.1/6.9)	3.8 (↓)	0.009	240.1 (M:240.1)	6	0
5081	TAGL_HUMAN	Transgelin (22.6/9.4)	4.1 (↓)	0.009	134.7 (M:134.7)	3	0
5083	HSP71_HUMAN	Heat shock 70 kDa protein 1A/1B (70/5.4)	1.9 (↓)	0.004	105.8 (M:105.8)	3	1 (432)
5098	K1C17_HUMAN	Keratin, type I cytoskeletal 17 (48.1/4.8)	2.2 (↓)	0.002	198.2 (M:198.2)	5	0
5128	CYC_HUMAN	Cytochrome c (11.7/10.1)	2.6 (↓)	0.006	97.4 (M:97.4)	3	0
5164	S10A9_HUMAN	Protein S100-A9 (13.2/5.7)	1.7 (↓)	0.009	85.7 (M:85.7)	3	0
5173	S10A8_HUMAN	Protein S100-A8 (10.8/6.6)	1.5 (↓)	0.002	421.3 (M:421.3)	8	0



DOI: 10.3748/wjg.v28.i29.3869 Copyright ©The Author(s) 2022.

**Figure 1** Representative two-dimensional gel electrophoresis images of N-linked glycoproteins from esophageal squamous cell carcinoma (ESCC) and adjacent non-cancerous tissues (N), in which the denoted numbers represent protein spots with differential expression. A and B: Representative two-dimensional gel electrophoresis (2-DE) images of high-mannose glycoproteins from ESCC (A) and N (B); C and D: Representative 2-DE images of GlcNAc/sialic acid-containing glycoproteins from ESCC (C) and N (D). ESCC: Esophageal squamous cell carcinoma; N: Non-cancerous tissues.

were six proteins in common between these two isolated fractions. In agreement with our previous reports[24,36], many gel spots were identified as the same protein, indicating the presence of different proteoforms due to post-translational modifications. Using NetNGlyc (<http://www.cbs.dtu.dk/services/NetNGlyc>) to predict the glycosylation sites on proteins, 72.7% (16/22) of high-mannose N-linked glycoproteins and 56.5% (13/23) of GlcNAc/sialic acid-containing glycoproteins were found to have potential glycosylation sites, indicating some non-specific binding to lectins by non-glycosylated proteins.

#### ***N-linked glycoprotein profiling by iTRAQ labeling***

To comprehensively characterize the N-linked glycoproteome in ESCC, we further performed iTRAQ-based analysis of the N-linked glycoproteome in ESCC and non-cancerous tissues. One pair of protein pools from ten ESCC and matched non-cancerous tissues, respectively, were subjected to tandem lectin affinity chromatography enrichment, in-solution digestion with trypsin, iTRAQ labeling, and LC-MS/MS identification in duplicate. In total, 1464 and 1298 proteins from the first affinity column were identified in the two technical replicates (Figure 2A, Supplementary Tables 1 and 2). Using the cut-off criteria of  $\geq 2$  unique peptides and a fold-change of 1.5, 189 and 138 proteins with differential expression were identified from the first and second independent pools, respectively, with 65 proteins in common, resulting in identification of 262 differentially expressed proteins in total from the high-mannose binding lectin affinity chromatography, of which 203 (77.5%) have predicted N-linked glycosylation sites (Figure 2B). For N-linked glycoproteins enriched by the downstream GlcNAc/sialic acid binding lectin chromatography, two independent iTRAQ-labeled pools produced 1174 and 936 proteins following isolation of high-mannose glycoproteins (Figure 2C, Supplementary Tables 3 and 4). There were 237 of 1174 and 154 of 936 proteins with differential expression, respectively, with 74 proteins in common (Figure 2D). A total of 317 unique proteins, of which 246 (77.6%) were predicted to be N-linked glycoproteins, were identified from the GlcNAc/sialic acid binding lectin chromatography enrichment.

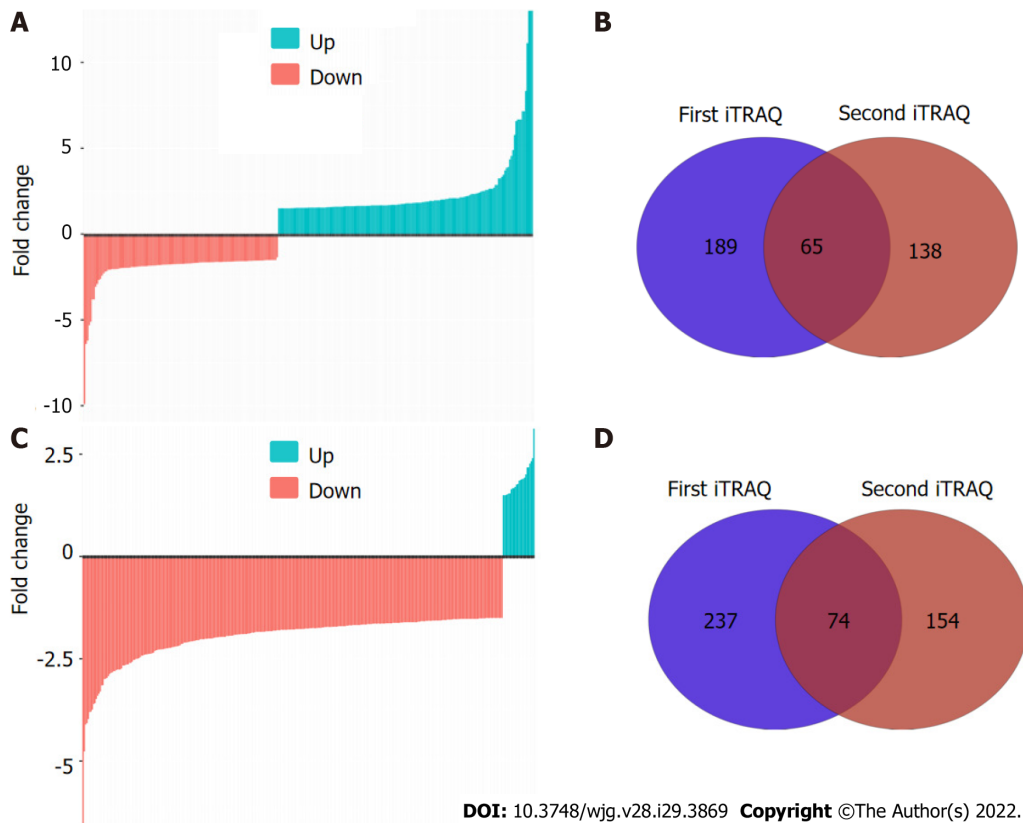


**Figure 2** N-linked glycoprotein profiling by isobaric tags for relative and absolute quantification labeling and liquid chromatography electrospray ionisation tandem mass spectrometry/mass spectrometry identification. A: Waterfall plot shows the differentially expressed high-mannose glycoproteins; B: Venn diagram depicts the unique and overlapped high-mannose glycoproteins identified from two independent replicates; C: Waterfall plot shows the differentially expressed GlcNAc/sialic acid-containing glycoproteins; D: Venn diagram depicts the unique and overlapped GlcNAc/sialic acid-containing glycoproteins identified from two independent replicates. iTRAQ: Isobaric tags for relative and absolute quantification.

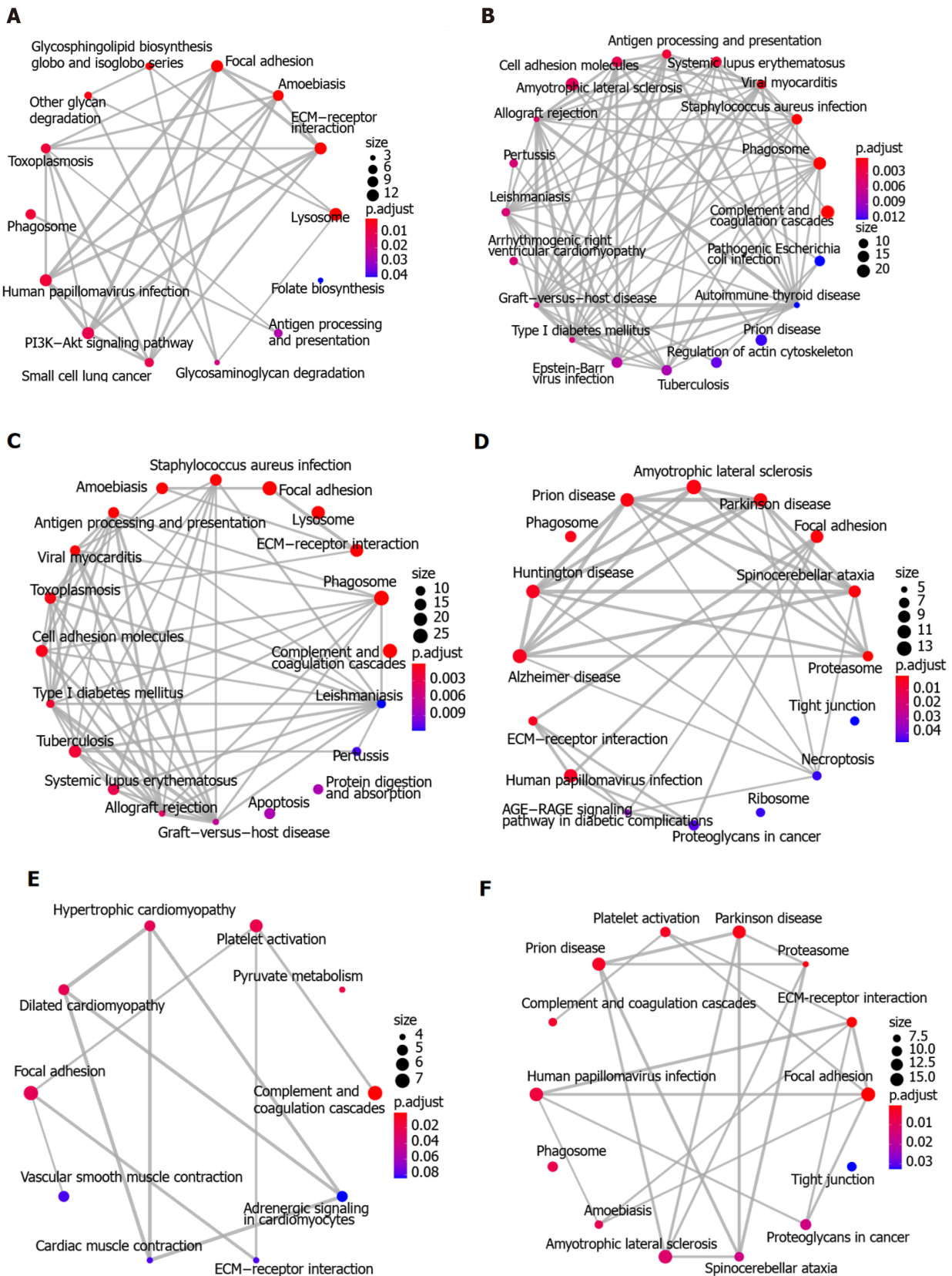
There were 58 overlapping glycoproteins found between 262 high-mannose glycoproteins and 317 GlcNAc/sialic acid-containing glycoproteins.

#### **Comparison of two-dimensional gel electrophoresis-based and iTRAQ labeling-based profiling**

In this study, two protocols for identifying N-linked glycoproteins based on different quantitative methods yielded quite different results. There were only 11 high-mannose glycoproteins and 4 GlcNAc/sialic acid-containing glycoproteins in common between 2-DE-based and iTRAQ-based glycoproteomic profiling. Our results demonstrate that iTRAQ-based quantitative proteomic profiling outperformed protein spot intensity quantification by 2-DE. There were, however, common glycoproteins found by both approaches. Therefore, the combination of these four fractions produced 411 unique N-linked glycoproteins. These findings indicate that a combination of these two complementary protocols could generate a more comprehensive landscape of N-linked glycoproteome implicated in ESCC because iTRAQ-based and 2-DE-based methods were able to isolate unique glycoproteins, thus providing a good representation of the N-linked glycoproteome.

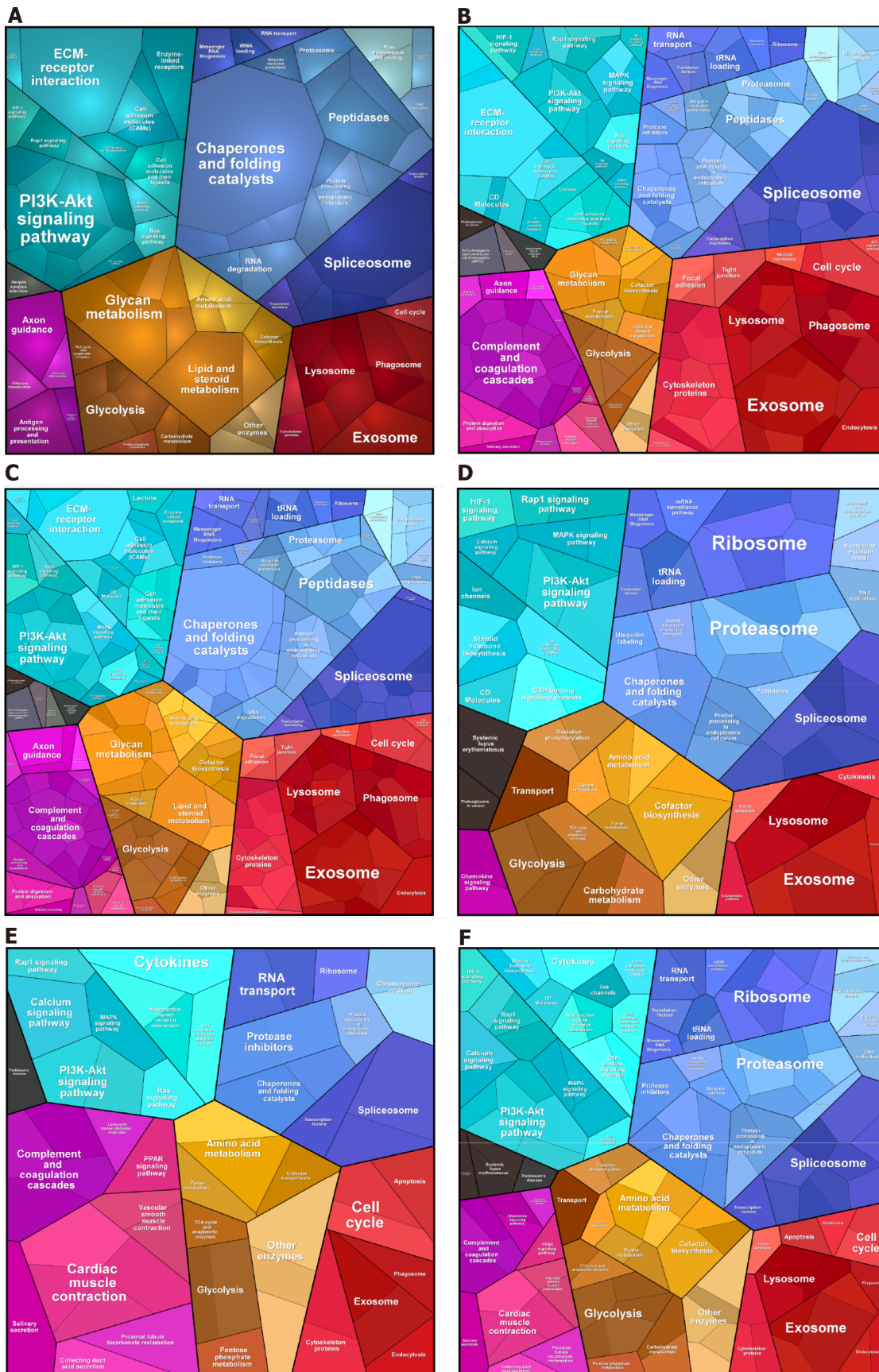
#### **Functional analysis of differentially expressed glycoproteins**

To explore the biological function of the 411 DEGs associated with ESCC, KEGG pathway enrichment analysis was initially performed using Enrichment Map. **Figure 3A-C** shows the 64 enriched pathways, which include complement and coagulation cascades, focal adhesion, ECM-receptor interaction, cellular interactions, immune response and infection, metabolism of fructose and mannose, glycolysis and gluconeogenesis, spliceosome, and PI3K-Akt and HIF-1 signaling pathways. In addition, proteomaps were constructed to visualize the composition of these DEGs in the five functional categories, which comprise genetic information processing, environmental information processing, cellular processes, metabolism, and organismal systems. **Figure 4A-C** shows that the genetic information processing accounts for the largest component of the DEGs, with protein processing, translation, and transcription being the biggest contributors to this functional category. In the category of signaling events, both the up-regulated and down-regulated DEGs were involved in PI3K-Akt, MAPK, Ras, Rap1, and HIF-1 signaling pathways (**Figure 4A** and **B**). The layouts of cellular process between up-regulated and down-regulated DEGs were different, with common components of exosome, lysosome, phagosome, cytoskeleton, and cell cycle, whereas the down-regulated DEGs are implicated in focal adhesion, tight



DOI: 10.3748/wjg.v28.i29.3869 Copyright ©The Author(s) 2022.

**Figure 3** Functional analyses of proteins and glycoproteins with differential expression using enrichment map. A-C: Kyoto encyclopedia of genes and genomes (KEGG) pathway enrichment analysis using enrichment map shows the significantly enriched biological pathways of up-regulated differentially expressed glycoproteins (DEGs), down-regulated DEGs, and total DEGs, respectively; D-F: KEGG pathway enrichment analysis using enrichment map shows the significantly enriched biological pathways of up-regulated DEPs, down-regulated DEPs, and total DEPs, respectively. KEGG: Kyoto encyclopedia of genes and genomes; DEGs: Differentially expressed glycoproteins; DEPs: Differentially expressed proteins.



DOI: 10.3748/wjg.v28.i29.3869 Copyright ©The Author(s) 2022.

**Figure 4** Functional analyses of proteins and glycoproteins with differential expression using Proteomap. A-C: Kyoto encyclopedia of genes and genomes (KEGG) pathway enrichment analysis using Proteomap shows the significantly enriched biological pathways of up-regulated differentially expressed glycoproteins (DEGs), down-regulated DEGs, and total DEGs, respectively; D-F: KEGG pathway enrichment analysis using Proteomap shows the significantly enriched biological pathways of up-regulated DEPs, down-regulated DEPs, and total DEPs, respectively. KEGG: Kyoto encyclopedia of genes and genomes; DEGs: differentially expressed glycoproteins; DEPs: differentially expressed proteins.

Differentially expressed glycoproteins; DEPs: Differentially expressed proteins.

junction, endocytosis, and p53 signaling pathway (Figure 4A and B). In glycolysis, there were more up-regulated than down-regulated DEGs. Notably, the complement and coagulation cascades in the immune system include exclusively down-regulated DEGs (Figure 4A and B).

### Functional comparison between glycoproteins and proteins with differential expression

Because there were only 82 overlapping proteins between DEGs and DEPs, the distinct subproteomes in each functional category may affect the structure of proteomaps. As shown in Figure 4, the compositions of proteomaps differ. In the category of genetic information processing, the chaperones, spliceosome, and peptidases are the predominant components in DEGs whereas the spliceosome, proteasome, and ribosome are the main contributors in DEPs. Although there are some signaling pathways (PI3K/Akt, MAPK, HIF1, Ras, and Rap1) in common in DEGs and DEPs, distinct components (neuroactive ligand-receptor interaction, calcium signaling pathway, GPT-binding signaling proteins, steroid hormone biosynthesis, and cytokines in DEPs *vs* NF kappa B pathway, FoxO pathway, ECM-receptor interaction, CD molecules, lectins, and enzyme-linked receptors in DEGs) are present in environment interaction (Figure 4C and F). Along with these differences, distinct compositions of the other three categories were found as well, in agreement with uniquely characterized proteomes. Likewise, Enrichment Map analysis showed that marked differences were found between DEGs and DEPs (Figure 3C and F). In the same line, there were remarkable distinctions between DEGs and DEPs identified using iTRAQ-based quantitation of Indian ESCC samples (data not shown)[40].

### Validation of potential glycoprotein biomarkers

Western blot analysis was performed to validate the differential expression of potential glycoprotein biomarkers for ESCC, including haptoglobin, cathepsin D, clusterin, superoxide dismutase 3 (SOD3), PRELP, and 14-3-3 $\zeta$ . Consistent with the corresponding protein spots of 748 and 1001 on 2-DE images, haptoglobin expression in ESCC was significantly down-regulated in tumor compared with adjacent non-cancerous tissues (Figure 5A). In contrast, the expression of procathepsin D instead of mature cathepsin D was remarkably enhanced in ESCC compared with the corresponding non-cancerous tissues (Figure 5B). There were no significant differences in the expression levels of the other four selected proteins (Supplementary Figure 1). These data suggest that the differential expression of glycoproteins identified in this study could be caused by up-regulation of protein expression, or up-regulation of N-linked glycosylation due to aberrant expression or activities of certain glycosyltransferases.

To assess the contribution of high-mannose or GlcNAc/sialic acid components attached to the selected glycoproteins, enrichment of corresponding glycoproteins *via* glycan chain binding to specific lectins was performed followed by Western blot detection. Consistent with the up-regulation of procathepsin D protein, the high-mannose subtype of procathepsin D was pronouncedly increased in ESCC as well (Figure 5C). In contrast to the expression pattern of total clusterin protein, the high-mannose fraction of clusterin was markedly down-regulated in ESCC as compared with non-cancerous tissues (Figure 5C). However, the glycosylated fractions of SOD3, PRELP, and haptoglobin did not show significant differences between ESCC and non-cancerous tissues after enrichment of high-mannose glycan structure of glycoproteins using lectin affinity chromatography. In agreement with the quantitative result of glycosylated 14-3-3 $\zeta$ , the GlcNAc/sialic acid-containing fraction of 14-3-3 $\zeta$  was strongly reduced in ESCC (Figure 5C).

### Serum levels of potential glycoprotein biomarkers

As isolation of N-linked glycoproteins from serum reduces the high-complexity of the serum proteome, we characterized the serum levels of potential glycoprotein biomarkers in patients with ESCC. As expected, the total protein levels of the six selected proteins were not significantly different in the serum of ESCC patients and healthy controls (Supplementary Figure 2). In contrast, the serum levels of glycosylated forms of clusterin, PRELP, and haptoglobin in ESCC patients were much higher than those of healthy controls (Figure 5D).

## DISCUSSION

Aberrant glycosylation of proteins, which is not correlated with mRNA levels, has been linked to a variety of cancers and reflects disease status and progression[20,41-44]. MS-based proteomics and glycomics hold considerable potential to identify novel glycosylation-based biomarkers. To the best of our knowledge, this study is the first to use tandem lectin affinity chromatography to enrich N-linked glycoproteins, followed by 2-DE-based and iTRAQ labeling-based proteomic quantitative profiling, and protein identification by MS. In total, 411 differentially expressed N-linked glycoproteins were

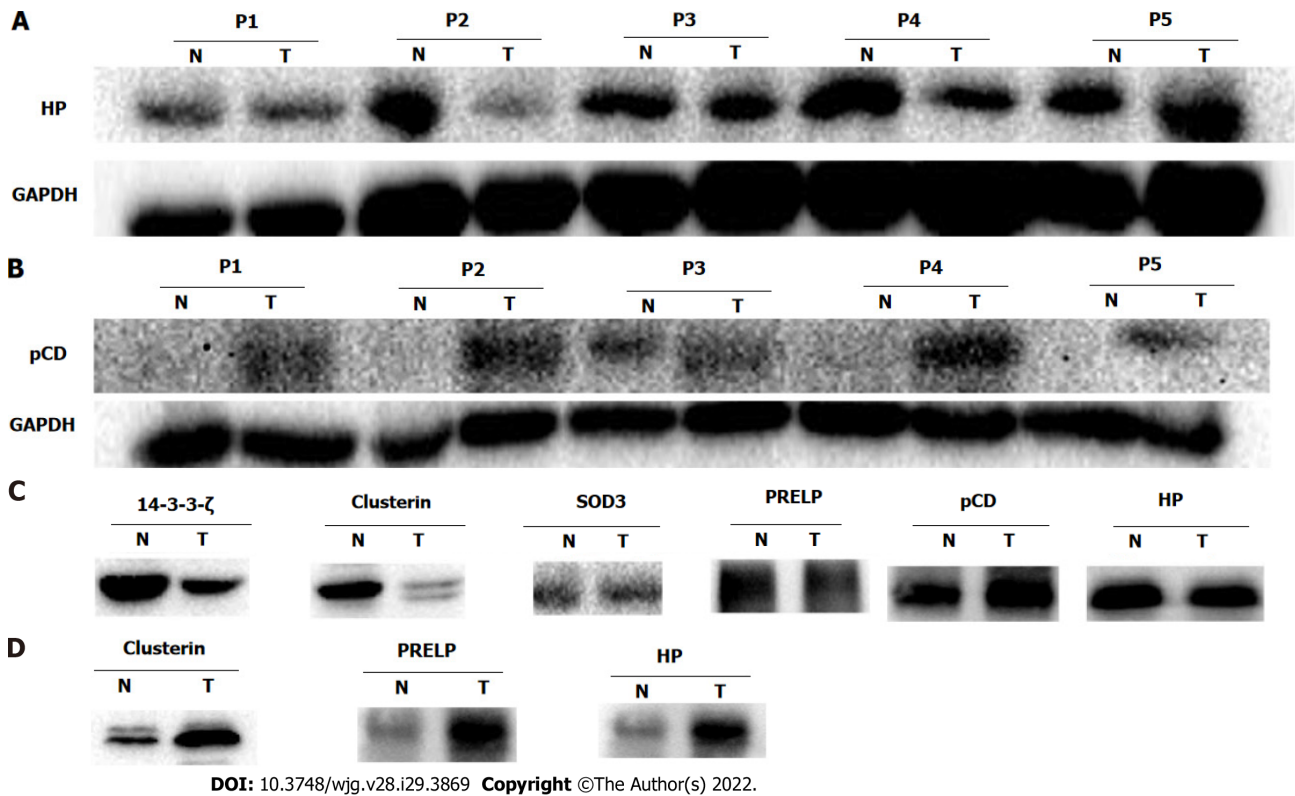


**Figure 5** Western blot validations of potential glycoprotein biomarkers. A and B: Representative Western blot results show haptoglobin (HP) (A) and procathepsin D (pCD) (B) with differential expression between esophageal squamous cell carcinoma (ESCC/T) and adjacent non-cancerous tissues (N); C: Representative Western blot results show the N-linked glycosylated fraction of HP, pCD, clusterin, superoxide dismutase 3 (SOD3), proline-arginine-rich end leucine-rich repeat protein (PRELP), and 14-3-3 $\zeta$  in ESCC/T and N enriched by corresponding lectins; D: Representative Western blot results show the N-linked glycosylated fractions of clusterin, PRELP, and HP in serum of patients with ESCC/T and healthy controls. The results are representative of three independent experiments. ESCC/T: Esophageal squamous cell carcinoma; HP: Haptoglobin; pCD: Procathepsin D; SOD3: Superoxide dismutase 3; PRELP: Proline-arginine-rich end leucine-rich repeat protein.

identified, including 128 up-regulated and 283 down-regulated DEGs. These DEGs provide the scientific community a dataset of glycoproteins associated with ESCC for in-depth investigation.

Depending on the linkage of carbohydrate to the protein backbone, glycoproteins fall into two main types, N-glycosylated and O-glycosylated, in which glycans are covalently attached to the amide nitrogen of asparagine residues and to the hydroxyl group of serine or threonine residues, respectively [45]. Lectins are defined as proteins that bind to the particular oligosaccharide epitope structures attached to proteins or lipids *via* selective affinities [46]. Due to these natural features, lectins are frequently used to isolate glycoproteins from a variety of origins, in particular from blood, to reduce sample complexity and to enrich low-abundance proteins. Using three lectins in parallel, *i.e.*, ConA, WGA, and Jacalin, a total of 423 proteins were fractionated from membrane proteins, among which 202 (71%) have predicted N-linked glycosylation sites [47]. As expected, there were unique and shared proteins enriched by these three lectins. To comprehensively isolate N-linked glycoproteins involved in ESCC, five lectins allocated to two sequential affinity chromatographies were used in this study to increase the coverage of captured N-linked glycoproteins. In addition, two complementary methods for quantitative profiling of enriched glycoproteins were used. In total, 262 and 317 nonredundant DEPs were identified by iTRAQ labeling-based profiling from the first and second lectin affinity chromatography, respectively. 2-DE-based MS/MS profiling led to fewer DEPs being identified compared with the iTRAQ labeling-based approach. Under a high stringency of selection criteria (foldchange  $\geq 1.5$ , unique peptides  $\geq 2$ ), 519 proteins were identified in total, of which 402 (77.5%) carry predicted N-linked glycosylation sites. Identification of a large number of proteins without predicated glycosylation sites indicates the existence of non-specific binding to certain lectins needing further in-depth study to elucidate.

Functional analysis based on KEGG pathway annotations by Proteomap revealed that there were striking differences in the compositions of DEGs distributed in five functional entities. In line with previous findings, the DEGs in genetic information processing account for the largest fraction of N-linked glycoproteome, supporting the survival and rapid growth of cancer cells [39]. In further support of this, a number of signaling pathways, including PI3K-Akt, MAPK, Rap1, and HIF-1 pathways, which play important roles in oncogenesis and progression, were significantly enriched. In metabolism, glycolysis was significantly enriched in DEGs identified in this study. The increased rate of glucose

metabolism and aerobic glycolysis, also known as the Warburg effect, are recognized hallmarks of cancer[48]. In agreement with this, HIF signaling proteins were over-represented in ESCC and may contribute to increased glycolysis. Besides energy generation, aerobic glycolysis enhances rapid growth and unlimited proliferation of cancer cells through providing precursors for certain biosynthetic processes as well as alteration of the tumor microenvironment[49]. Moreover, extracellular lactate has inhibitory effects on human cytotoxic T lymphocytes[50,51]. Furthermore, metabolic phenotype of cancer stem cell seems distinct from bulk cancer cells and is characterized by glycolysis and/or XoPhos [49]. The increased expression of fructose-bisphosphate aldolase A, triosephosphate isomerase, alpha-enolase, all-trans-retinol dehydrogenase [NAD(+)] ADH1B, and glyceraldehyde-3-phosphate dehydrogenase in ESCC may contribute to the progression of ESCC *via* increased glycolysis and could serve as therapeutic targets for the management of ESCC. All together, these distinct functional categories and related effector molecules may represent potential therapeutic targets in ESCC.

Cathepsin D, a lysosomal protease, is expressed in nearly all cells and tissues of mammals. However, pro-cathepsin D but not mature cathepsin D is reportedly associated with the development and progression of a variety of cancers[52]. In line with up-regulation of ConA-binding cathepsin D and procathepsin D, glycosylated procathepsin D was increased in ESCC as well, suggesting it as a potential biomarker for ESCC. In addition, we also demonstrated that both total haptoglobin and N-linked haptoglobin in serum were differentially expressed in ESCC, as seen in other malignancies[41,53,54]. Although there were no alterations in the levels of total protein expression, the high-mannose clusterin and sialic acid glycoforms of 14-3-3 $\zeta$  were down-regulated in ESCC but need further study to characterize their glycan moieties. After probing the serum levels of these candidate biomarkers, we provide several potential biomarkers for ESCC diagnosis. Additionally, our findings reveal that differential protein expression is a confounding factor for identification of aberrant glycosylation.

The current study has several limitations. First, the main limitation is that sample pooling used in this study may cause a loss of inter-individual information. However, this is partly compensated by the validation of candidate biomarkers using individual tissue samples. Second, affinity chromatography comprising multiple lectins for glycoprotein isolation yielded different subglycoproteomes. Further studies should characterize the composition and structure of glycans associated with proteins. Nevertheless, our study represents, to our knowledge, the first study to characterize the glycoproteome associated with ESCC, and thus provides the scientific community a resource of glycoproteins for in-depth investigation.

## CONCLUSION

In conclusion, this study catalogued a total of 411 N-linked glycoproteins implicated in ESCC after glycoprotein enrichment using two stage multilectin affinity chromatography and MS/MS identification. Proteomap analysis revealed the distribution of differential glycoproteins in five functional categories. A preliminary validation demonstrated the differential expression of glycoprotein biomarker candidates, including total procathepsin D and haptoglobin in ESCC, high-mannose fractions of procathepsin D, clusterin and sialiated 14-3-3 $\zeta$  in ESCC, and glycosylated fractions of clusterin, PRELP, and haptoglobin in serum. Consequently, this study yielded a comprehensive landscape of N-linked glycoproteome associated with ESCC for further characterization.

## ARTICLE HIGHLIGHTS

### Research background

Recent large-scale “omics” studies in esophageal squamous cell carcinoma (ESCC) have identified a myriad of aberrations at the levels of genome, epigenome, transcriptome, proteome, *etc.*, revealing the high molecular heterogeneity of ESCC. However, protein post-translational modifications, such as glycosylation and phosphorylation, which provide additional significant biological insights, are missing.

### Research motivation

The sugar chains of glycoproteins are involved in numerous physiological and pathological conditions. More than 50% of current cancer biomarkers are glycoproteins.

### Research objectives

To identify N-linked glycoproteins associated with ESCC after isolation of N-linked glycoproteins using tandem multilectin affinity chromatography.

### Research methods

N-linked glycoproteins were isolated from ESCC and adjacent non-tumor tissue samples using multilectin affinity chromatography. Two-dimensional gel electrophoresis (2-DE)-based and isobaric tags for relative and absolute quantification (iTRAQ) labeling-based mass spectrometry quantitation were performed in parallel to profile the N-linked glycoproteome in ESCC, followed by validation of candidate glycoprotein biomarkers using Western blot.

### Research results

A total of 411 differentially expressed N-linked glycoproteins (DEGs) with potential glycosylation sites on proteins were identified by 2-DE-based and iTRAQ labeling-based quantitation, demonstrating the outperformance of iTRAQ labeling-based quantitation over 2-DE. These DEGs exhibited distinctive compositions in functional categories from differentially expressed proteins in ESCC. Western blot analysis validated the up-regulation of total procathepsin D and high-mannose procathepsin D, and the down-regulation of total haptoglobin, high-mannose clusterin, and GlcNAc/sialic acid-containing fraction of 14-3-3 $\zeta$  in ESCC tissues. The serum levels of glycosylated fractions of clusterin, proline-arginine-rich end leucine-rich repeat protein, and haptoglobin in patients with ESCC were remarkably higher than those in healthy controls.

### Research conclusions

This study identified the aberrant N-linked glycoproteome associated with ESCC, which will be a valuable resource for future investigations.

### Research perspectives

In-depth characterization of the composition and structure of glycans associated with proteins can shed more lights on biological insights and clinical relevance of the identified DEGs in ESCC.

---

## FOOTNOTES

**Author contributions:** Qi YJ and Gao SG designed and coordinated the study; Liu QW, Ruan HJ, Chao WX, Li MX, Jiao YL, and Ward DG performed the experiments, and acquired and analyzed the data; Qi YJ and Ward DG wrote the manuscript; and all authors approved the final version of the article.

**Supported by** National Natural Science Foundation of China, No. 81072039 and No. 81872037.

**Institutional review board statement:** The study was approved by the Ethics Committee of the Medical School, Henan University, China (ethics ref: 108) and conducted in accordance with the ethical guidelines of the 1975 Declaration of Helsinki.

**Conflict-of-interest statement:** All authors report no relevant conflicts of interest for this article.

**Data sharing statement:** No additional data are available.

**Open-Access:** This article is an open-access article that was selected by an in-house editor and fully peer-reviewed by external reviewers. It is distributed in accordance with the Creative Commons Attribution NonCommercial (CC BY-NC 4.0) license, which permits others to distribute, remix, adapt, build upon this work non-commercially, and license their derivative works on different terms, provided the original work is properly cited and the use is non-commercial. See: <https://creativecommons.org/licenses/by-nc/4.0/>

**Country/Territory of origin:** China

**ORCID number:** Qi-Wei Liu 0000-0002-7874-4056; Hao-Jie Ruan 0000-0002-3201-3864; Wei-Xia Chao 0000-0003-0700-658X; Meng-Xiang Li 0000-0002-6987-545X; Ye-Lin Jiao 0000-0002-4920-0738; Douglas G Ward 0000-0002-2328-1445; She-Gan Gao 0000-0002-7720-8729; Yi-Jun Qi 0000-0003-0239-5862.

**S-Editor:** Ma YJ

**L-Editor:** Wang TQ

**P-Editor:** Qi WW

---

## REFERENCES

- 1 **Bray F**, Ferlay J, Soerjomataram I, Siegel RL, Torre LA, Jemal A. Global cancer statistics 2018: GLOBOCAN estimates of incidence and mortality worldwide for 36 cancers in 185 countries. *CA Cancer J Clin* 2018; **68**: 394-424 [PMID: 30207593 DOI: 10.3322/caac.21492]

- 2 **Abnet CC**, Arnold M, Wei WQ. Epidemiology of Esophageal Squamous Cell Carcinoma. *Gastroenterology* 2018; **154**: 360-373 [PMID: 28823862 DOI: 10.1053/j.gastro.2017.08.023]
- 3 **Song Y**, Li L, Ou Y, Gao Z, Li E, Li X, Zhang W, Wang J, Xu L, Zhou Y, Ma X, Liu L, Zhao Z, Huang X, Fan J, Dong L, Chen G, Ma L, Yang J, Chen L, He M, Li M, Zhuang X, Huang K, Qiu K, Yin G, Guo G, Feng Q, Chen P, Wu Z, Wu J, Zhao J, Luo L, Fu M, Xu B, Chen B, Li Y, Tong T, Wang M, Liu Z, Lin D, Zhang X, Yang H, Zhan Q. Identification of genomic alterations in oesophageal squamous cell cancer. *Nature* 2014; **509**: 91-95 [PMID: 24670651 DOI: 10.1038/nature13176]
- 4 **Zeng H**, Zheng R, Guo Y, Zhang S, Zou X, Wang N, Zhang L, Tang J, Chen J, Wei K, Huang S, Wang J, Yu L, Zhao D, Song G, Shen Y, Yang X, Gu X, Jin F, Li Q, Li Y, Ge H, Zhu F, Dong J, Guo G, Wu M, Du L, Sun X, He Y, Coleman MP, Baade P, Chen W, Yu XQ. Cancer survival in China, 2003-2005: a population-based study. *Int J Cancer* 2015; **136**: 1921-1930 [PMID: 25242378 DOI: 10.1002/ijc.29227]
- 5 **Wang GQ**, Jiao GG, Chang FB, Fang WH, Song JX, Lu N, Lin DM, Xie YQ, Yang L. Long-term results of operation for 420 patients with early squamous cell esophageal carcinoma discovered by screening. *Ann Thorac Surg* 2004; **77**: 1740-1744 [PMID: 15111177 DOI: 10.1016/j.athoracsur.2003.10.098]
- 6 **Pennathur A**, Gibson MK, Jobe BA, Luketich JD. Oesophageal carcinoma. *Lancet* 2013; **381**: 400-412 [PMID: 23374478 DOI: 10.1016/S0140-6736(12)60643-6]
- 7 **He Z**, Liu Z, Liu M, Guo C, Xu R, Li F, Liu A, Yang H, Shen L, Wu Q, Duan L, Li X, Zhang C, Pan Y, Cai H, Ke Y. Efficacy of endoscopic screening for esophageal cancer in China (ESECC): design and preliminary results of a population-based randomised controlled trial. *Gut* 2019; **68**: 198-206 [PMID: 29306867 DOI: 10.1136/gutjnl-2017-315520]
- 8 **Kosugi S**, Nishimaki T, Kanda T, Nakagawa S, Ohashi M, Hatakeyama K. Clinical significance of serum carcinoembryonic antigen, carbohydrate antigen 19-9, and squamous cell carcinoma antigen levels in esophageal cancer patients. *World J Surg* 2004; **28**: 680-685 [PMID: 15383868 DOI: 10.1007/s00268-004-6865-y]
- 9 **Mealy K**, Feely J, Reid I, McSweeney J, Walsh T, Hennessy TP. Tumour marker detection in oesophageal carcinoma. *Eur J Surg Oncol* 1996; **22**: 505-507 [PMID: 8903494 DOI: 10.1016/s0748-7983(96)92998-4]
- 10 **Shimada H**, Nabeya Y, Okazumi S, Matsubara H, Miyazawa Y, Shiratori T, Hayashi H, Gunji Y, Ochiai T. Prognostic significance of CYFRA 21-1 in patients with esophageal squamous cell carcinoma. *J Am Coll Surg* 2003; **196**: 573-578 [PMID: 12691934 DOI: 10.1016/s1072-7515(02)01905-1]
- 11 **Zheng X**, Xing S, Liu XM, Liu W, Liu D, Chi PD, Chen H, Dai SQ, Zhong Q, Zeng MS, Liu WL. Establishment of using serum YKL-40 and SCCA in combination for the diagnosis of patients with esophageal squamous cell carcinoma. *BMC Cancer* 2014; **14**: 490 [PMID: 25001061 DOI: 10.1186/1471-2407-14-490]
- 12 **Enzinger PC**, Mayer RJ. Esophageal cancer. *N Engl J Med* 2003; **349**: 2241-2252 [PMID: 14657432 DOI: 10.1056/NEJMra035010]
- 13 **Cui Y**, Chen H, Xi R, Cui H, Zhao Y, Xu E, Yan T, Lu X, Huang F, Kong P, Li Y, Zhu X, Wang J, Zhu W, Ma Y, Zhou Y, Guo S, Zhang L, Liu Y, Wang B, Xi Y, Sun R, Yu X, Zhai Y, Wang F, Yang J, Yang B, Cheng C, Liu J, Song B, Li H, Wang Y, Zhang Y, Cheng X, Zhan Q, Liu Z. Whole-genome sequencing of 508 patients identifies key molecular features associated with poor prognosis in esophageal squamous cell carcinoma. *Cell Res* 2020; **30**: 902-913 [PMID: 32398863 DOI: 10.1038/s41422-020-0333-6]
- 14 **Gao YB**, Chen ZL, Li JG, Hu XD, Shi XJ, Sun ZM, Zhang F, Zhao ZR, Li ZT, Liu ZY, Zhao YD, Sun J, Zhou CC, Yao R, Wang SY, Wang P, Sun N, Zhang BH, Dong JS, Yu Y, Luo M, Feng XL, Shi SS, Zhou F, Tan FW, Qiu B, Li N, Shao K, Zhang LL, Xue Q, Gao SG, He J. Genetic landscape of esophageal squamous cell carcinoma. *Nat Genet* 2014; **46**: 1097-1102 [PMID: 25151357 DOI: 10.1038/ng.3076]
- 15 **Li J**, Chen Z, Tian L, Zhou C, He MY, Gao Y, Wang S, Zhou F, Shi S, Feng X, Sun N, Liu Z, Skogerboe G, Dong J, Yao R, Zhao Y, Sun J, Zhang B, Yu Y, Shi X, Luo M, Shao K, Li N, Qiu B, Tan F, Chen R, He J. LncRNA profile study reveals a three-lncRNA signature associated with the survival of patients with oesophageal squamous cell carcinoma. *Gut* 2014; **63**: 1700-1710 [PMID: 24522499 DOI: 10.1136/gutjnl-2013-305806]
- 16 **Cancer Genome Atlas Research Network**; Analysis Working Group: Asan University; BC Cancer Agency; Brigham and Women's Hospital; Broad Institute; Brown University; Case Western Reserve University; Dana-Farber Cancer Institute; Duke University; Greater Poland Cancer Centre; Harvard Medical School; Institute for Systems Biology; KU Leuven; Mayo Clinic; Memorial Sloan Kettering Cancer Center; National Cancer Institute; Nationwide Children's Hospital; Stanford University; University of Alabama; University of Michigan; University of North Carolina; University of Pittsburgh; University of Rochester; University of Southern California; University of Texas MD Anderson Cancer Center; University of Washington; Van Andel Research Institute; Vanderbilt University; Washington University; Genome Sequencing Center: Broad Institute; Washington University in St. Louis; Genome Characterization Centers: BC Cancer Agency; Broad Institute; Harvard Medical School; Sidney Kimmel Comprehensive Cancer Center at Johns Hopkins University; University of North Carolina; University of Southern California Epigenome Center; University of Texas MD Anderson Cancer Center; Van Andel Research Institute; Genome Data Analysis Centers: Broad Institute; Brown University; Harvard Medical School; Institute for Systems Biology; Memorial Sloan Kettering Cancer Center; University of California Santa Cruz; University of Texas MD Anderson Cancer Center; Biospecimen Core Resource: International Genomics Consortium; Research Institute at Nationwide Children's Hospital; Tissue Source Sites: Analytic Biologic Services; Asan Medical Center; Asterand Bioscience; Barretos Cancer Hospital; BioreclamationIVT; Botkin Municipal Clinic; Chonnam National University Medical School; Christiana Care Health System; Cureline; Duke University; Emory University; Erasmus University; Indiana University School of Medicine; Institute of Oncology of Moldova; International Genomics Consortium; Invidumed; Israelitisches Krankenhaus Hamburg; Keimyung University School of Medicine; Memorial Sloan Kettering Cancer Center; National Cancer Center Goyang; Ontario Tumour Bank; Peter MacCallum Cancer Centre; Pusan National University Medical School; Ribeirão Preto Medical School; St. Joseph's Hospital & Medical Center; St. Petersburg Academic University; Tayside Tissue Bank; University of Dundee; University of Kansas Medical Center; University of Michigan; University of North Carolina at Chapel Hill; University of Pittsburgh School of Medicine; University of Texas MD Anderson Cancer Center; Disease Working Group: Duke University; Memorial Sloan Kettering Cancer Center; National Cancer Institute; University of Texas MD Anderson Cancer Center; Yonsei University College of

- Medicine; Data Coordination Center: CSRA Inc; Project Team: National Institutes of Health. Integrated genomic characterization of oesophageal carcinoma. *Nature* 2017; **541**: 169-175 [PMID: 28052061 DOI: 10.1038/nature20805]
- 17 **Cao W**, Lee H, Wu W, Zaman A, McCorkle S, Yan M, Chen J, Xing Q, Sinnott-Armstrong N, Xu H, Sailani MR, Tang W, Cui Y, Liu J, Guan H, Lv P, Sun X, Sun L, Han P, Lou Y, Chang J, Wang J, Gao Y, Guo J, Schenk G, Shain AH, Biddle FG, Collisson E, Snyder M, Bivona TG. Multi-faceted epigenetic dysregulation of gene expression promotes esophageal squamous cell carcinoma. *Nat Commun* 2020; **11**: 3675 [PMID: 32699215 DOI: 10.1038/s41467-020-17227-z]
  - 18 **Zhang B**, Whiteaker JR, Hoofnagle AN, Baird GS, Rodland KD, Paulovich AG. Clinical potential of mass spectrometry-based proteogenomics. *Nat Rev Clin Oncol* 2019; **16**: 256-268 [PMID: 30487530 DOI: 10.1038/s41571-018-0135-7]
  - 19 **Gao Q**, Zhu H, Dong L, Shi W, Chen R, Song Z, Huang C, Li J, Dong X, Zhou Y, Liu Q, Ma L, Wang X, Zhou J, Liu Y, Boja E, Robles AI, Ma W, Wang P, Li Y, Ding L, Wen B, Zhang B, Rodriguez H, Gao D, Zhou H, Fan J. Integrated Proteogenomic Characterization of HBV-Related Hepatocellular Carcinoma. *Cell* 2019; **179**: 561-577.e22 [PMID: 31585088 DOI: 10.1016/j.cell.2019.08.052]
  - 20 **Ohtsubo K**, Marth JD. Glycosylation in cellular mechanisms of health and disease. *Cell* 2006; **126**: 855-867 [PMID: 16959566 DOI: 10.1016/j.cell.2006.08.019]
  - 21 **Mechref Y**, Hussein A, Bekesova S, Pungpapong V, Zhang M, Dobrolecki LE, Hickey RJ, Hammoud ZT, Novotny MV. Quantitative serum glycomics of esophageal adenocarcinoma and other esophageal disease onsets. *J Proteome Res* 2009; **8**: 2656-2666 [PMID: 19441788 DOI: 10.1021/pr8008385]
  - 22 **Sethi MK**, Hancock WS, Fanayan S. Identifying N-Glycan Biomarkers in Colorectal Cancer by Mass Spectrometry. *Acc Chem Res* 2016; **49**: 2099-2106 [PMID: 27653471 DOI: 10.1021/acs.accounts.6b00193]
  - 23 **Li CW**, Lim SO, Xia W, Lee HH, Chan LC, Kuo CW, Khoo KH, Chang SS, Cha JH, Kim T, Hsu JL, Wu Y, Hsu JM, Yamaguchi H, Ding Q, Wang Y, Yao J, Lee CC, Wu HJ, Sahin AA, Allison JP, Yu D, Hortobagyi GN, Hung MC. Glycosylation and stabilization of programmed death ligand-1 suppresses T-cell activity. *Nat Commun* 2016; **7**: 12632 [PMID: 27572267 DOI: 10.1038/ncomms12632]
  - 24 **Qi YJ**, Ward DG, Pang C, Wang QM, Wei W, Ma J, Zhang J, Lou Q, Shimwell NJ, Martin A, Wong N, Chao WX, Wang M, Ma YF, Johnson PJ. Proteomic profiling of N-linked glycoproteins identifies ConA-binding procathepsin D as a novel serum biomarker for hepatocellular carcinoma. *Proteomics* 2014; **14**: 186-195 [PMID: 24259486 DOI: 10.1002/pmic.201300226]
  - 25 **Alper J**. Glycobiology. Turning sweet on cancer. *Science* 2003; **301**: 159-160 [PMID: 12855785 DOI: 10.1126/science.301.5630.159]
  - 26 **Varki A**. Biological roles of oligosaccharides: all of the theories are correct. *Glycobiology* 1993; **3**: 97-130 [PMID: 8490246 DOI: 10.1093/glycob/3.2.97]
  - 27 **Hakomori S**. Tumor malignancy defined by aberrant glycosylation and sphingo(glyco)lipid metabolism. *Cancer Res* 1996; **56**: 5309-5318 [PMID: 8968075 DOI: 10.1097/00002820-199612000-00006]
  - 28 **Kobata A**. A retrospective and prospective view of glycopathology. *Glycoconj J* 1998; **15**: 323-331 [PMID: 9613818 DOI: 10.1023/a:1006961532182]
  - 29 **Xu Q**, Isaji T, Lu Y, Gu W, Kondo M, Fukuda T, Du Y, Gu J. Roles of N-acetylglucosaminyltransferase III in epithelial-to-mesenchymal transition induced by transforming growth factor  $\beta$ 1 (TGF- $\beta$ 1) in epithelial cell lines. *J Biol Chem* 2012; **287**: 16563-16574 [PMID: 22451656 DOI: 10.1074/jbc.M111.262154]
  - 30 **Liwosz A**, Lei T, Kukuruzinska MA. N-glycosylation affects the molecular organization and stability of E-cadherin junctions. *J Biol Chem* 2006; **281**: 23138-23149 [PMID: 16682414 DOI: 10.1074/jbc.M512621200]
  - 31 **Zhao Y**, Nakagawa T, Itoh S, Inamori K, Isaji T, Kariya Y, Kondo A, Miyoshi E, Miyazaki K, Kawasaki N, Taniguchi N, Gu J. N-acetylglucosaminyltransferase III antagonizes the effect of N-acetylglucosaminyltransferase V on  $\alpha$ 3 $\beta$ 1 integrin-mediated cell migration. *J Biol Chem* 2006; **281**: 32122-32130 [PMID: 16940045 DOI: 10.1074/jbc.M607274200]
  - 32 **Kim JH**, Jun KH, Jung H, Park IS, Chin HM. Prognostic Value of Preoperative Serum Levels of Five Tumor Markers (Carcinoembryonic Antigen, CA19-9, Alpha-fetoprotein, CA72-4, and CA125) in Gastric Cancer. *Hepatogastroenterology* 2014; **61**: 863-869 [PMID: 26176088 DOI: 10.5754/hge131018]
  - 33 **Terzi H**, Kale E, Kale A, Turkay U, Chong GO, Lee YS. New method: Are tumor markers in vaginal-washing fluid significant in the diagnosis of primary ovarian carcinoma? *Eur J Gynaecol Oncol* 2015; **36**: 560-563 [PMID: 26513883 DOI: 10.12892/ejgo2743.2015]
  - 34 **Zhang D**, Yu M, Xu T, Xiong B. Predictive value of serum CEA, CA19-9 and CA125 in diagnosis of colorectal liver metastasis in Chinese population. *Hepatogastroenterology* 2013; **60**: 1297-1301 [PMID: 23933921 DOI: 10.5754/hge121125]
  - 35 **Kumada T**, Nakano S, Takeda I, Kiriya S, Sone Y, Hayashi K, Katoh H, Endoh T, Sassa T, Satomura S. Clinical utility of Lens culinaris agglutinin-reactive alpha-fetoprotein in small hepatocellular carcinoma: special reference to imaging diagnosis. *J Hepatol* 1999; **30**: 125-130 [PMID: 9927159 DOI: 10.1016/s0168-8278(99)80016-6]
  - 36 **Qi Y**, Chiu JF, Wang L, Kwong DL, He QY. Comparative proteomic analysis of esophageal squamous cell carcinoma. *Proteomics* 2005; **5**: 2960-2971 [PMID: 15986332 DOI: 10.1002/pmic.200401175]
  - 37 **Gao SG**, Liu RM, Zhao YG, Wang P, Ward DG, Wang GC, Guo XQ, Gu J, Niu WB, Zhang T, Martin A, Guo ZP, Feng XS, Qi YJ, Ma YF. Integrative topological analysis of mass spectrometry data reveals molecular features with clinical relevance in esophageal squamous cell carcinoma. *Sci Rep* 2016; **6**: 21586 [PMID: 26898710 DOI: 10.1038/srep21586]
  - 38 **Merico D**, Isserlin R, Stueker O, Emili A, Bader GD. Enrichment map: a network-based method for gene-set enrichment visualization and interpretation. *PLoS One* 2010; **5**: e13984 [PMID: 21085593 DOI: 10.1371/journal.pone.0013984]
  - 39 **Liebermeister W**, Noor E, Flamholz A, Davidi D, Bernhardt J, Milo R. Visual account of protein investment in cellular functions. *Proc Natl Acad Sci U S A* 2014; **111**: 8488-8493 [PMID: 24889604 DOI: 10.1073/pnas.1314810111]
  - 40 **Pawar H**, Kashyap MK, Sahasrabudhe NA, Renuse S, Harsha HC, Kumar P, Sharma J, Kandasamy K, Marimuthu A, Nair B, Rajagopalan S, Maharudraiah J, Premalatha CS, Kumar KV, Vijayakumar M, Chaerkady R, Prasad TS, Kumar RV, Pandey A. Quantitative tissue proteomics of esophageal squamous cell carcinoma for novel biomarker discovery. *Cancer Biol Ther* 2011; **12**: 510-522 [PMID: 21743296 DOI: 10.4161/cbt.12.6.16833]
  - 41 **Zhang Y**, Zhu J, Yin H, Marrero J, Zhang XX, Lubman DM.ESI-LC-MS Method for Haptoglobin Fucosylation Analysis

- in Hepatocellular Carcinoma and Liver Cirrhosis. *J Proteome Res* 2015; **14**: 5388-5395 [PMID: 26503433 DOI: 10.1021/acs.jproteome.5b00792]
- 42 **Darebna P**, Novak P, Kucera R, Topolcan O, Sanda M, Goldman R, Pompach P. Changes in the expression of N- and O-glycopeptides in patients with colorectal cancer and hepatocellular carcinoma quantified by full-MS scan FT-ICR and multiple reaction monitoring. *J Proteomics* 2017; **153**: 44-52 [PMID: 27646713 DOI: 10.1016/j.jprot.2016.09.004]
- 43 **Ahn JM**, Sung HJ, Yoon YH, Kim BG, Yang WS, Lee C, Park HM, Kim BJ, Lee SY, An HJ, Cho JY. Integrated glycoproteomics demonstrates fucosylated serum paraoxonase 1 alterations in small cell lung cancer. *Mol Cell Proteomics* 2014; **13**: 30-48 [PMID: 24085812 DOI: 10.1074/mcp.M113.028621]
- 44 **Lin Z**, Yin H, Lo A, Ruffin MT, Anderson MA, Simeone DM, Lubman DM. Label-free relative quantification of alpha-2-macroglobulin site-specific core-fucosylation in pancreatic cancer by LC-MS/MS. *Electrophoresis* 2014; **35**: 2108-2115 [PMID: 24285556 DOI: 10.1002/elps.201300376]
- 45 **Christiansen MN**, Chik J, Lee L, Anugraham M, Abrahams JL, Packer NH. Cell surface protein glycosylation in cancer. *Proteomics* 2014; **14**: 525-546 [PMID: 24339177 DOI: 10.1002/pmic.201300387]
- 46 **Ghosh D**, Krokhn O, Antonovici M, Ens W, Standing KG, Beavis RC, Wilkins JA. Lectin affinity as an approach to the proteomic analysis of membrane glycoproteins. *J Proteome Res* 2004; **3**: 841-850 [PMID: 15359739 DOI: 10.1021/pr049937f]
- 47 **Lee A**, Kolarich D, Haynes PA, Jensen PH, Baker MS, Packer NH. Rat liver membrane glycoproteome: enrichment by phase partitioning and glycoprotein capture. *J Proteome Res* 2009; **8**: 770-781 [PMID: 19125615 DOI: 10.1021/pr800910w]
- 48 **Hanahan D**, Weinberg RA. Hallmarks of cancer: the next generation. *Cell* 2011; **144**: 646-674 [PMID: 21376230 DOI: 10.1016/j.cell.2011.02.013]
- 49 **Ganapathy-Kanniappan S**. Molecular intricacies of aerobic glycolysis in cancer: current insights into the classic metabolic phenotype. *Crit Rev Biochem Mol Biol* 2018; **53**: 667-682 [PMID: 30668176 DOI: 10.1080/10409238.2018.1556578]
- 50 **Fischer K**, Hoffmann P, Voelkl S, Meidenbauer N, Ammer J, Edinger M, Gottfried E, Schwarz S, Rothe G, Hoves S, Renner K, Timischl B, Mackensen A, Kunz-Schughart L, Andreesen R, Krause SW, Kreutz M. Inhibitory effect of tumor cell-derived lactic acid on human T cells. *Blood* 2007; **109**: 3812-3819 [PMID: 17255361 DOI: 10.1182/blood-2006-07-035972]
- 51 **Kumagai S**, Koyama S, Itahashi K, Tanegashima T, Lin YT, Togashi Y, Kamada T, Irie T, Okumura G, Kono H, Ito D, Fujii R, Watanabe S, Sai A, Fukuoka S, Sugiyama E, Watanabe G, Owari T, Nishinakamura H, Sugiyama D, Maeda Y, Kawazoe A, Yukami H, Chida K, Ohara Y, Yoshida T, Shinno Y, Takeyasu Y, Shirasawa M, Nakama K, Aokage K, Suzuki J, Ishii G, Kuwata T, Sakamoto N, Kawazu M, Ueno T, Mori T, Yamazaki N, Tsuboi M, Yatabe Y, Kinoshita T, Doi T, Shitara K, Mano H, Nishikawa H. Lactic acid promotes PD-1 expression in regulatory T cells in highly glycolytic tumor microenvironments. *Cancer Cell* 2022; **40**: 201-218.e9 [PMID: 35090594 DOI: 10.1016/j.ccell.2022.01.001]
- 52 **Choi H**, Ko Y, Lee CY. Pro-cathepsin D as a diagnostic marker in differentiating malignant from benign pleural effusion: a retrospective cohort study. *BMC Cancer* 2020; **20**: 825 [PMID: 32867726 DOI: 10.1186/s12885-020-07327-w]
- 53 **Okuyama N**, Ide Y, Nakano M, Nakagawa T, Yamanaka K, Moriwaki K, Murata K, Ohigashi H, Yokoyama S, Eguchi H, Ishikawa O, Ito T, Kato M, Kasahara A, Kawano S, Gu J, Taniguchi N, Miyoshi E. Fucosylated haptoglobin is a novel marker for pancreatic cancer: a detailed analysis of the oligosaccharide structure and a possible mechanism for fucosylation. *Int J Cancer* 2006; **118**: 2803-2808 [PMID: 16385567 DOI: 10.1002/ijc.21728]
- 54 **Park SY**, Yoon SJ, Jeong YT, Kim JM, Kim JY, Bernert B, Ullman T, Itzkowitz SH, Kim JH, Hakomori SI. N-glycosylation status of beta-haptoglobin in sera of patients with colon cancer, chronic inflammatory diseases and normal subjects. *Int J Cancer* 2010; **126**: 142-155 [PMID: 19551866 DOI: 10.1002/ijc.24685]

## Basic Study

**HP0953 - hypothetical virulence factor overexpression and localization during *Helicobacter pylori* infection of gastric epithelium**

Nancy K Arteaga-Resendiz, Gerardo E Rodea, Rosa María Ribas-Aparicio, Alma L Olivares-Cervantes, Juan Arturo Castellán-Vega, José de Jesús Olivares-Trejo, Sandra Mendoza-Elizalde, Edgar O López-Villegas, Christian Colín, Pamela Aguilar-Rodea, Alfonso Reyes-López, Marcela Salazar García, Norma Velázquez-Guadarrama

**Specialty type:** Gastroenterology and hepatology

**Provenance and peer review:** Invited article; Externally peer reviewed

**Peer-review model:** Single blind

**Peer-review report's scientific quality classification**

Grade A (Excellent): 0  
Grade B (Very good): B  
Grade C (Good): C, C  
Grade D (Fair): 0  
Grade E (Poor): 0

**P-Reviewer:** Keikha M, Iran; Kirkik D, Turkey; Mi Y, China

**Received:** January 29, 2022

**Peer-review started:** January 29, 2022

**First decision:** April 10, 2022

**Revised:** April 26, 2022

**Accepted:** July 11, 2022

**Article in press:** July 11, 2022

**Published online:** August 7, 2022



**Nancy K Arteaga-Resendiz, Gerardo E Rodea, Alma L Olivares-Cervantes, Sandra Mendoza-Elizalde, Christian Colín, Pamela Aguilar-Rodea, Norma Velázquez-Guadarrama,** Laboratorio de Investigación en Enfermedades Infecciosas, Hospital Infantil de México Federico Gómez, Mexico City 06720, Mexico

**Nancy K Arteaga-Resendiz, Rosa María Ribas-Aparicio, Juan Arturo Castellán-Vega,** Posgrado en Biomedicina y Biotecnología Molecular, Laboratorio de Producción y Control de Biológicos, Escuela Nacional de Ciencias Biológicas, Instituto Politécnico Nacional, Mexico City 11340, Mexico

**José de Jesús Olivares-Trejo,** Laboratorio de Adquisición de Hierro, Universidad Autónoma de la Ciudad México, Posgrado Ciencias Genómica, Mexico City 03100, Mexico

**Edgar O López-Villegas,** Laboratorio Central de Microscopía, Escuela Nacional de Ciencias Biológicas, Instituto Politécnico Nacional, Mexico City 11340, Mexico

**Alfonso Reyes-López,** Centro de estudios económicos y sociales en salud, Hospital Infantil de México Federico Gómez, Mexico City 06720, Mexico

**Marcela Salazar García,** Laboratorio de Investigación en Biología del Desarrollo y Teratogénesis Experimental, Hospital Infantil de México Federico Gómez, Mexico City 06720, Mexico

**Corresponding author:** Norma Velázquez-Guadarrama, PhD, Research Scientist, Laboratorio de Investigación en Enfermedades Infecciosas, Hospital Infantil de México Federico Gómez, Dr. Márquez 162, Col. Doctores, Alcaldía Cuauhtémoc, Mexico City 06720, Mexico.

[normave@himfg.edu.mx](mailto:normave@himfg.edu.mx)

**Abstract****BACKGROUND**

The high prevalence and persistence of *Helicobacter pylori* (*H. pylori*) infection, as well as the diversity of pathologies related to it, suggest that the virulence factors used by this microorganism are varied. Moreover, as its proteome contains 340 hypothetical proteins, it is important to investigate them to completely understand the mechanisms of its virulence and survival. We have previously

reported that the hypothetical protein HP0953 is overexpressed during the first hours of adhesion to inert surfaces, under stress conditions, suggesting its role in the environmental survival of this bacterium and perhaps as a virulence factor.

### AIM

To investigate the expression and localization of HP0953 during adhesion to an inert surface and against gastric (AGS) cells.

### METHODS

Expression analysis was performed for HP0953 during *H. pylori* adhesion. HP0953 expression at 0, 3, 12, 24, and 48 h was evaluated and compared using the Kruskal-Wallis equality-of-populations rank test. Recombinant protein was produced and used to obtain polyclonal antibodies for immunolocalization. Immunogold technique was performed on bacterial sections during adherence to inert surfaces and AGS cells, which was analyzed by transmission electron microscopy. HP0953 protein sequence was analyzed to predict the presence of a signal peptide and transmembrane helices, both provided by the ExPASy platform, and using the GLYCOPP platform for glycosylation sites. Different programs, *via*, I-TASSER, RaptorX, and HAlign-Kbest, were used to perform three-dimensional modeling.

### RESULTS

HP0953 exhibited its maximum expression at 12 h of infection in gastric epithelium cells. Immunogold technique revealed HP0953 localization in the cytoplasm and accumulation in some peripheral areas of the bacterial body, with greater expression when it is close to AGS cells. Bioinformatics analysis revealed the presence of a signal peptide that interacts with the transmembrane region and then allows the release of the protein to the external environment. The programs also showed a similarity with the Tip-alpha protein of *H. pylori*. Tip-alpha is an exotoxin that penetrates cells and induces tumor necrosis factor alpha production, and HP0953 could have a similar function as posttranslational modification sites were found; modifications in turn require enzymes located in eukaryotic cells. Thus, to be functional, HP0953 may necessarily need to be translocated inside the cell where it can trigger different mechanisms producing cellular damage.

### CONCLUSION

The location of HP0953 around infected cells, the probable posttranslational modifications, and its similarity to an exotoxin suggest that this protein is a virulence factor.

**Key Words:** Hypothetical protein HP0953; Adherence; *Helicobacter pylori*; Glycocalyx; Virulence factor; Persistence

©The Author(s) 2022. Published by Baishideng Publishing Group Inc. All rights reserved.

**Core Tip:** The high prevalence and persistence of *Helicobacter pylori* infection and the diverse pathologies associated with it suggest that the virulence factors of this microorganism are varied. Moreover, its proteome contains 340 hypothetical proteins, so it is crucial to investigate them to elucidate the mechanisms of its virulence and survival. We studied the hypothetical protein HP0953, its location around infected cells, and the probable posttranslational modifications. Its similarity to an exotoxin suggests that HP0953 is a virulence factor.

**Citation:** Arteaga-Resendiz NK, Rodea GE, Ribas-Aparicio RM, Olivares-Cervantes AL, Castelán-Vega JA, Olivares-Trejo JJ, Mendoza-Elizalde S, López-Villegas EO, Colín C, Aguilar-Rodea P, Reyes-López A, Salazar García M, Velázquez-Guadarrama N. HP0953 - hypothetical virulence factor overexpression and localization during *Helicobacter pylori* infection of gastric epithelium. *World J Gastroenterol* 2022; 28(29): 3886-3902

**URL:** <https://www.wjgnet.com/1007-9327/full/v28/i29/3886.htm>

**DOI:** <https://dx.doi.org/10.3748/wjg.v28.i29.3886>

## INTRODUCTION

The estimated prevalence of *Helicobacter pylori* (*H. pylori*) infection is 70% in developing countries and 30%-40% in the United States and other industrialized countries[1]. However, not all people infected with this bacterium have symptoms. *H. pylori* has been associated with gastroduodenal diseases and it is

considered the major risk factor for the development of gastric cancer[2]. *H. pylori* colonizes the gastric mucosa, adhering to the mucous epithelial cells and to the mucous layer that covers the gastric epithelium. Adherence to gastric cells is the first step in establishing an infection and for successful colonization, the bacterium releases various effector proteins/toxins[3-5].

Upon colonization, the pathogenic mechanism of *H. pylori* is mediated by virulence factors such as flagella and the ability to form a biofilm (both *in vitro* and *in vivo*)[6]. Biofilm formation enhances the ability of microorganisms to survive in a hostile environment, which would cause and exacerbate infections, rather than extend them, resulting in chronicity[7]. The glycocalyx participates in adhesion to inert surfaces, allowing biofilm formation but also participates in cell attachment; the major components of the glycocalyx are glycans and may contain digestive proteins or secreted virulence factors[8,9]. *H. pylori* secretes various virulence factors, including urease, cag pathogenicity island proteins, hemagglutinin, Lewis antigens (Le<sup>x</sup> and Le<sup>y</sup>), BabA CagA, and VacA[10-12]. All these virulence factors have been extensively investigated elsewhere.

Furthermore, *H. pylori* contains hypothetical proteins, some of which are secreted particularly in the context of interactions with the host. The bacterium uses a set of secreted and translocated proteins to adapt itself to the mucosal environment[13]. *H. pylori* possesses a relatively small genome of < 1.6 Mb [14,15] compared with other gram-negative prokaryotes, such as *Escherichia coli*, whose genome is > 4.5 Mb[16]. Despite its small size, an ineligible fraction of *H. pylori* proteins, possibly 30%-40%, are annotated as “hypothetical proteins”. Using bioinformatics tools, Naqvi *et al*[17] and Zanotti and Cendron[18] respectively analyzed 340 hypothetical proteins of *H. pylori* 26695. The function of some of these proteins can be hypothesized based on a weak homology with proteins of other bacteria, whereas most proteins do not exhibit similarities with others, and their function cannot be predicted[17,18].

HP0953 is a hypothetical and uncharacterized protein of *H. pylori* secretome; it lacks conserved domains but, interestingly, is present in all *H. pylori* strains whose genomes have been sequenced, as well as in *H. acinonychis* that colonizes the gastric mucosa of large felines. The closely related *H. hepaticus* and *Campylobacter jejuni* lack HP0953 homologs, suggesting that HP0953 is unique to the gastric *Helicobacter* species[11]. Moreover, we previously observed that this protein is overexpressed during adhesion to inert surfaces under stress conditions. Most of the possible effects of secreted proteins on the host have yet to be discovered. In addition, secreted factors represent eligible proteins for identifying promising targets for the development of new antimicrobial drugs[17,18].

In recent years, there has been an increasing importance on *H. pylori*; on the one hand when it is present, it is associated with gastric disease, and on the other hand, it is associated with gastroduodenal reflux, food allergy, and asthma when it is absent[19]. This dual role in the human microbiota emphasizes the need for further characterization of the hypothetical proteins already described. In this study, the location of the protein is determined for the first time, inside and outside the bacterium, and we predict some biochemical characteristics, through *in silico* analysis that contribute toward understanding the importance of this hypothetical protein to the microorganism in the establishment of infection, its role in such infection, or colonization of the host.

---

## MATERIALS AND METHODS

---

### ***In silico* analysis of HP0953 protein**

We obtained the amino acid sequence of HP0953 (accession number NP\_207745) from the National Center for Biotechnology Information database[20]. Then, we used the Pfam database to analyze the HP0953 sequence and search for conserved domains or homologous regions present in other proteins [21].

### **Signal peptide prediction**

The amino acid sequence of HP0953 was analyzed using the SignalP-4.1 tool provided by the ExPASy platform to predict the presence of a signal peptide[22].

### **Prediction of transmembrane helices and glycosylation sites**

The amino acid sequence previously obtained was analyzed to predict transmembrane helices using the TM pred tool provided by the ExPASy platform[23,24]. The glycosylation sites were investigated using the GLYCOPP platform[25].

### **Three-dimensional modeling of HP0953 protein**

To explore the remote homologs that could be used as a template for modeling, we used the HHpred tool that uses the HMM comparison[26]. Different programs such as I-TASSER[27], RaptorX[28], and HHalign-Kbest[29] were used to perform three-dimensional (3D) modeling.

### **Strain, cell culture, and extraction of genomic DNA from *H. pylori***

*H. pylori* strain 26695 was cultured on Casman agar (Dibico; Mexico) supplemented with 5% sheep

erythrocytes and incubated in an atmosphere of 50 mL/L CO<sub>2</sub> and 37 °C for 48 h. The culture was harvested for infected human against gastric (AGS) cell-line assay and genomic DNA extraction. Genomic DNA extraction was performed according to the protocol established for the Wizard kit (Promega; United States) by its manufacturer.

### **Amplification and purification of HP0953**

HP0953 was amplified by polymerase chain reaction (PCR) using *H. pylori* genomic DNA as the template. To amplify the complete gene, 50 µL of reaction mixture was prepared as follows: 1.25 U polymerase GoTaq<sup>®</sup>, 0.2 mmol/L dATP, 0.2 mmol/L dGTP, 0.2 mmol/L dCTP, 0.2 mmol/L dTTP, 1.5 mmol/L MgCl<sub>2</sub> (Promega), HP0953F oligonucleotide (25 pmol) (5'-GGGGGATCCATG-GTTTAAATCGCTCTTTTAGGGGTG-3'), HP0953R oligonucleotide (25 pmol) (5'-GGGGTCGACCCT-TAACGCACAAACGCTACC-3'), and *H. pylori* 26695 DNA (250 ng). For amplification of the gene without the signal peptide, the same PCR was performed substituting the oligonucleotide HP0953F by HP095WSPF (5'-GGGGGATCCGTCCTCTGATTTAAAGGGCATG-3'). The amplification cycle consisted of 94 °C for 1 min, followed by 30 cycles at 94 °C for 30 s, 68.4 °C for 30 s, 72 °C for 1 min, and a final step at 72 °C for 7 min. Both PCR products (555 and 474 bp) were purified using the protocol established by Promega for using the Wizard<sup>®</sup> SV gel and the PCR Clean-Up System (Promega).

### **Cloning of the complete and without-signal peptide hp0953**

Complete HP0953 and its version without the signal peptide were inserted into the vector pJET1.2 (Thermo Scientific; Lithuania) according to the manufacturer's instructions to obtain the recombinant pJET-HP0953 and pJET-HP0953WSP plasmids, respectively. Chemically competent DH5α cells of *Escherichia coli* (*E. coli*) were transformed with each plasmid by thermal shock [30,31]. The recombinant colonies were selected in LB agar (Sigma-Aldrich; MO) containing 100 µg/mL ampicillin. The plasmids were extracted using the illustra<sup>™</sup> plasmidPrep Mini Spin Kit (GE Healthcare; United Kingdom).

The pJET-HP0953 and pJET-HP0953WSP plasmids were digested with the fast restriction enzymes BamHI and Sal I according to the manufacturer's instructions (Thermo Scientific) to free both versions of HP0953. Restriction products were purified using the protocol established by Promega for the Wizard<sup>®</sup> SV gel and the PCR Clean-Up System. DNA fragments were ligated into the expression vectors pET28a(+) (Novagen, United States) for the complete HP0953 and pGEX-6p-2 (GE Healthcare) for the version without the signal peptide. The vectors were digested with the same enzymes and treated with alkaline phosphatase (Thermo Scientific). The Rapid DNA Ligation Kit (Thermo Scientific) was used to obtain the recombinant pET-HP0953 and pGEX-HP0953WSP plasmids. Chemically competent DH5α cells of *E. coli* were transformed with each plasmid by thermal shock. The recombinant colonies were selected in LB agar containing 50 µg/mL kanamycin for pET-HP0953 or 100 µg/mL ampicillin for pGEX-HP0953WSP. The plasmids were extracted using the illustra<sup>™</sup> plasmidPrep Mini Spin Kit (GE Healthcare) and analyzed by PCR. DNA inserts in the recombinant plasmids were characterized by sequencing; for this purpose, PCRs were performed as described earlier using the following primers: T7F (5'-TAATACGACTCACTATAGGG-3') and T7R (5'-GCTAGTTATTGCTCAGCG-3') for pET-HP0953 and HP095WSPF (5'-GGGGGATCCGTCCTCTGATTTAAAGGGCATG-3') and HP0953R (5'-GGGGTCGACCCTTAACGCACAAACGCTACC-3') for pGEX-HP0953WSP. The annealing temperature was 68.4 °C for pET-HP0953 and 60 °C for pGEX-HP0953WSP. The PCR products were purified as described earlier and sequenced by Synthesis and Sequencing Unit, Institute of Biotechnology, Universidad Nacional Autónoma de México. Chemically competent BL21 pLysS cells of *E. coli* were transformed with each recombinant plasmid and the empty plasmids by thermal shock [31]. The recombinant colonies were selected in LB agar containing the corresponding antibiotic.

### **Expression and purification of HP0953 protein**

The HP0953 protein was expressed according to the manufacturer's instructions for pET28a(+) and pGEX-6p-2 vectors using 1 mmol/L IPTG (Sigma-Aldrich) and incubating the *E. coli* pET28a(+)/pET-HP0953-transformed cells for 16 h at 30 °C to obtain the recombinant protein His-HP0953 and the *E. coli* pGEX-6p-2/pGEX-HP0953WSP-transformed cells for 3 h at 37 °C to obtain the recombinant protein GST-HP0953WSP. The inclusion bodies were extracted as described in the inclusion body preparation method without solubilizing the inclusion bodies in a denaturing agent [32]. The cell pellet was resuspended in 1 mL of 4 × sample buffer. Aliquots were collected throughout the process and analyzed by sodium dodecyl sulfate-polyacrylamide gel electrophoresis (SDS-PAGE) and western blot assays. The inclusion bodies were electrophoresed on SDS-PAGE, and the recombinant protein band was purified by electroelution. The glutathione-S-transferase (GST)-HP0953WSP recombinant protein was used to produce polyclonal antibodies, as described later, and the His-HP0953 protein was used to purify antibodies.

### **Production of polyclonal anti-GST-HP0953WSP**

Anti-GST-HP0953WSP antibodies were obtained by immunization of a New Zealand rabbit (2 mo age) according to the Howard and Bethell method [33] (approved by the Bioethics Committee of the Hospital Infantil de México Federico Gómez).

### Purification of polyclonal anti-HP0953

Purification of polyclonal antibody was performed by immunoabsorption. The His-HP0953 protein was subjected to SDS-PAGE on preparative gels. The bands were transferred onto a polyvinylidene fluoride (PVDF) membrane (Millipore; United States), which was blocked with 0.5% bovine serum albumin (BSA) and washed with phosphate buffer solution (PBS)-Tween. Serum was diluted 1:100 in PBS-Tween, incubated with the membrane for 2 h under stirring at room temperature, and washed with PBS-Tween; then, the membrane was incubated with 0.02 M glycine-HCl (pH 2.2) for 10 min at room temperature. Finally, 1 M Tris base (pH 9.1) was added. The antibody was recovered and stored at -20 °C. Nonpurified antisera and purified antibodies were tested against a total extract of *H. pylori*, and the two purified recombinant proteins were evaluated by western blotting using the same PVDF membrane, which was stripped between each test[34].

### Construction of plasmid pBlue-5CM3 for site-directed mutagenesis of the HP0953 gene in *H. pylori*

The chloramphenicol resistance gene was obtained from the pLysS plasmid of the *E. coli* BL21 (DE3) pLysS strain by PCR, for which 50 µL of reaction mix was prepared, consisting of 1 × HF Fusion buffer (Thermo Scientific); 0.2 mmol/L each of dATP, dGTP, dCTP, and dTTP (Promega); 6 pmol each of primer CMF (5'-GGG AGATCTTTACGCCCCGCCCTG-3') and CMR (5'-GGGCATATGATG-GAGAAAAAATCACTGG-3'); plasmid pLysS (250 ng); and Phusion DNA Polymerase (1 U) (Thermo Scientific). The CMF and CMR primers contain restriction sites for *Bgl*III and *Nde*I, respectively. The amplification program consisted of initial denaturation at 98 °C for 30 s; 35 cycles of denaturation at 98 °C for 10 s, primer annealing at 65 °C for 30 s, and extension at 72 °C for 1 min; and a final extension at 72 °C for 7 min.

The 5' and 3' fragments of the HP0953 gene were obtained from the plasmid pJET-HP0953, constructed above by PCR. To amplify the 5' fragment, 50 µL of the reaction mixture was prepared, consisting of GoTaq DNA polymerase (Promega) (1.25 U); 0.2 mmol/L each of dATP, dGTP, dCTP, and dTTP; 1.5 mmol/L MgCl<sub>2</sub> (Promega); primer HP0953F (25 pmol) (5'-GGGGGATCCATG-GTTTTAATCGCTCTTTAGGGGTG-3'); primer HP0953R (5'-GGGAGATCTCATGGAATTGCTCCAT-GAAGCG-3'); and plasmid DNA from pJET-HP0953 (250 ng). The amplification program consisted of initial denaturation at 94 °C for 1 min; 35 cycles of denaturation at 94 °C for 30 s, primer annealing at 68.4 °C for 30 s, and extension at 72 °C for 30 s; and a final extension at 72 °C for 7 min. To amplify the 3' fragment, PCR was performed under the same conditions but using the primers HP0953F (5'-GGGCATATGAGTCCGAGCAGACGACTACG-3') and HP0953R (5'-GGGGTTCGACCTACCT-TAACGCACAAACGCTACC-3'). Amplicons of 304 and 248 bp were obtained, respectively.

We subjected 5 µL of each amplification product to 1.5% agarose gel electrophoresis at 85 volts for 75 min. Then, we stained the gel with ethidium bromide (Sigma-Aldrich) and observed the bands under ultraviolet light. Upon confirmation of the amplified product, the remainder was purified using a Wizard SV Gel and PCR Clean-up System, as per the manufacturer's protocol. Each fragment was inserted into a pJET1.2 vector. The ligation reaction of each fragment in the pJET1.2 vector consisted of 1 × reaction buffer, 0.15 pmol purified PCR product (5' fragment, 3' fragment, or chloramphenicol resistance gene; 0.15 pmol), pJET1.2/Blunt Cloning Vector (0.05 pmol), and T4 DNA ligase (5 U). The reaction mixture was incubated at 22 °C for 20 min.

After ligation, we used heat shock treatment to transform 50 µL of competent *E. coli* DH5α cells with each plasmid[31]. Then, they were centrifuged at 5000 × g for 1 min, the supernatant was decanted, and the pellet was resuspended in the residual medium. Subsequently, the bacterial suspension was seeded on LB agar plates containing ampicillin (100 µg/mL; Sigma-Aldrich) and incubated at 37 °C for 18-24 h to select the recombinant clones. Following incubation, we selected five colonies from the plate and resuspended them in 2 mL of LB broth (Sigma-Aldrich) containing ampicillin (100 µg/mL), and the plasmid was extracted using the alkaline lysis method[35]. We quantified the plasmid DNA using an Epoch microplate spectrophotometer (Biotek Instruments, Inc.; United States) and stored it at -20 °C.

We performed three PCR assays to verify the sequence of the cloned fragments. Each PCR reaction was performed in a final volume of 20 µL, consisting of 1 × HF Fusion buffer (Thermo Scientific); 0.2 mmol/L each of dATP, dGTP, dCTP, and dTTP (Thermo Scientific); primer pJET1.2F (0.2 µM) (5'-CGACTCACTATAGGGAGAGCGGC-3') (Thermo Scientific); primer pJET1.2R (0.2 µM) (5'-AAGAACATCGATTTTCCATGGCAG-3') (Thermo Scientific); plasmid DNA (100 ng/µL) (pJET-CM, pJET-5' or pJET-3'); and Phusion DNA polymerase (Thermo Scientific) (0.4 U). The amplification program consisted of initial denaturation at 98 °C for 30 s; 35 cycles of 98 °C for 10 s, 68 °C for 30 s, and 72 °C for 30 s; and a final extension at 72 °C for 7 min. The PCR products were sequenced by Macrogen (Seoul, Korea).

The 5' fragments, 3' fragments, and the chloramphenicol resistance gene were obtained from the plasmids previously constructed by enzymatic digestion. *Bam*HI and *Bgl*III were used for the 5' fragment, *Nde*I and *Sal*I for the 3' fragment, and *Bgl*III and *Nde*I for the chloramphenicol resistance gene, according to the above-described digestion protocols. The fragments were inserted into the pBluescript II KS+ vector (Agilent Technologies, Inc.; United States), which allows for the synthesis of ssDNA and has an ampicillin resistance gene to facilitate selection following the above-described protocols.

*E. coli* XL1-blue MRF' cells were transformed with the constructed vector (pBlue-5CM3) using heat shock treatment and selected following culture on LB agar plates (Sigma-Aldrich) with 100 µg/mL of ampicillin[31]. The plasmid was extracted using alkaline lysis[35], and fragment insertion was verified by automated sequencing. *H. pylori* was transformed with the plasmid using electroporation[36]. The mutant *H. pylori* strain was cultured on Casman agar supplemented with 5% sheep erythrocytes and incubated in an atmosphere of 50 mL/L CO<sub>2</sub> at 37 °C for 48 h.

#### **Identification of HP0953 in *H. pylori***

The purified antibody was used for identifying the protein HP0953 in *H. pylori* 26695 by western blotting. A total extract obtained from *H. pylori* adhesion test (see below) was used, and soluble and insoluble fractions were separated according to the inclusion body preparation method[32]. These fractions were subjected to SDS-PAGE (50 mg of protein) and transferred onto a PVDF membrane, where western blotting was performed using the purified antibody diluted 1:2 in PBS-Tween and incubated overnight under stirring at 4 °C and the secondary antibody diluted 1:10000 [anti-rabbit immunoglobulin G (IgG) horseradish peroxidase (HRP)-conjugated antibody] (Santa Cruz Biotechnology; United States)[34]. Washing was done with TBST (2 mmol/L Tris, 15 mmol/L NaCl, 0.1% Tween 20, pH 7.6). Finally, the membrane was visualized using Immobilon Western Chemiluminescent HRP substrate (Millipore).

#### **Adhesion test of *H. pylori***

A suspension ( $6 \times 10^8$ ) of *H. pylori* 26695 culture in Brucella broth (Dibico) supplemented with 1% yeast extract was prepared. Next, 50 mL of the suspension was placed in cell culture bottles and incubated at 37 °C in an atmosphere of 50 mL/L CO<sub>2</sub> for 0, 1, 3, 12, and 24 h; these time points are the first hours of biofilm formation where adherence occurs. After the incubation period, the supernatant was removed, and the bottle walls were scraped to obtain adherent cells, which were resuspended in 1 mL of sterile 1 × PBS.

#### **Thawing and seeding of AGS cells**

First, 1 mL of AGS cell suspension was placed in a 15 mL conical tube. Subsequently, 2 mL of DMEM-F12 (Gibco, Life Technologies; United States) medium was added for washing by centrifugation at 1500 rpm for 5 min. A second washing step was performed, and the cells were resuspended again in DMEM-F12 medium. Next, 1 mL of the cell suspension was taken to seed into cell culture bottles. The bottles were incubated in a CO<sub>2</sub> chamber for 24 h at 37 °C.

#### **AGS cell infection assay by *H. pylori***

The gene expression assay during biofilm formation was performed in duplicate in ten cell culture bottles of 225 mL each. A suspension of *H. pylori* (strain 26695, previously cultured for 24 h in a plate with Casman medium) was prepared in DMEM-F12 culture medium. The cells were washed by centrifugation at 3000 rpm for 15 min. After washing, the cell pellet was used to prepare a bacterial suspension in 300 mL of DMEM-F12 culture medium inside a flask until the growth level reached similar to that in tube number 2 on the McFarland scale. To each bottle, 30 mL of the bacterial suspension similar to McFarland tube 2 suspension was added, and then 20 mL of DMEM-F12 medium without the bacteria was added to complete 50 mL. One bottle was not infected with the bacterial strain and was used as the control for the transmission electron microscopy (TEM) assay. The bottles were incubated at 3, 12, 24, and 48 h post-infection. Time 0 was taken as the culture of the bacterial strain with no contact with AGS cells for the expression assay. After each time point of incubation, the supernatant was discarded, and 1 mL of sterile 1 × PBS was added for washing the cells. Subsequently, the wall of the bottle was scraped with a gendarme to detach the cells and remove the adhered biofilm. Each sample was processed for RNA extraction assay. An aliquot was taken for use in TEM, and the remainder was centrifuged at 7000 rpm for 15 min. The test was conducted in triplicate.

#### **Immunogold technique for TEM**

First, 500 µL of the samples obtained from the adhesion test was centrifuged at 2500 rpm for 10 min and fixed with 4% paraformaldehyde (MP Biomedicals; United States) in 1 × PBS (pH 7.4) for 1 h at 4 °C. Then, three washes were performed with 1 × PBS (pH 7.4), and the sample was dehydrated by adding 50% ethanol (Merck; IRL) for 10 min, followed by two washes with 70% ethanol for 15 min at room temperature. The inclusion was done using the LR-White method as described by Vázquez and Echeverría[37], and ultrathin sections of 60-90 nm were obtained. The sections were placed on nickel grids, blocked with 5% BSA for 20 min, and incubated with the purified polyclonal antibody overnight at 4 °C. The sample was then washed with TBST and incubated with the secondary antibody (goat anti-rabbit IgG coupled to 10-nm colloidal gold particles, 1:5, Sigma-Aldrich) diluted in deionized water for 1 h at room temperature. The grids were rinsed with TBST. Finally, they were observed under a transmission electron microscope (JEM 1010 JEOL Ltd. Japan) equipped with a TEM Imaging Systems AMT (Woburn; United States).

Table 1 Prediction of glycosylation sites

Position	Residue	Residue score	Prediction
Probable N-linked glycosylation sites			
68	NNK	-0.20374993	Non-glycosylated
69	NKY	-0.11718906	Non-glycosylated
80	NAK	-0.46398761	Non-glycosylated
113	NIS	0.031759513	Potentially glycosylated
120	NYL	-0.12578944	Non-glycosylated
130	NTY	-0.42088241	Non-glycosylated
134	NLK	-0.028092183	Non-glycosylated
164	NLN	0.45527702	Potentially glycosylated
166	NDN	-0.14904342	Non-glycosylated
168	NEI	0.2906731	Potentially glycosylated
Probable O-linked glycosylation sites			
15	S	0.3493683	Potentially glycosylated
16	S	-0.20711247	Non-glycosylated
18	S	-0.033164353	Non-glycosylated
20	S	-0.066886402	Non-glycosylated
23	S	0.33910492	Potentially glycosylated
33	S	-0.58418843	Non-glycosylated
40	S	-0.76207501	Non-glycosylated
43	S	0.16899016	Potentially glycosylated
78	T	-0.75721234	Non-glycosylated
84	S	-0.20144186	Non-glycosylated
107	S	-0.2527357	Non-glycosylated

There are three probable N-linked and six probable O-linked glycosylation sites.

### Quantitative SYBR-Green real time-PCR analysis for *hp0953* expression during *H. pylori* infection of AGS cells

Expression analysis was performed by real time-PCR (RT-qPCR). The glutamate racemase (*glmM*) gene was used as an internal control for the bacterial cell, and the  $\beta$ -globin gene was used as an internal control for human AGS cells. *HP0953* expression was evaluated at different time points (0, 3, 12, 24, and 48 h). Time 0 was taken as the culture of the bacterial strain with no contact with AGS cells.

Gene-specific primers were developed for *HP0953* and *glmM* using the Primer3 software, v.0.4.0[38, 39]. The sequences of all the primers were as follows: *HP0953* (5'-CATATGCCGAGCAGACGACTACG-3'; 5'-GTTCGACCTACCTTAACGCACAAACGCTACC-3'), *glmM* (5'-ACCGACGCTCTCACCCACTT-3'; 5'-AGCGCGAGCCACAACCCTTT-3'). Total RNA was isolated from the AGS cell cultures with and without *H. pylori* at a multiplicity of infection of 1:100. RNA was extracted using TRIzol® Reagent (Ambion RNA, Life Technologies; United States), followed by phenol:chloroform extraction. The quality and amount of the resulting RNA were evaluated using a Nano-Drop spectrophotometer (The Epoch™ Multi-Volume Spectrophotometer System; United States) at 260 and 280 nm, respectively.

Reverse transcription reaction and SYBR-Green PCR were performed as described below. To initiate the first-strand cDNA synthesis, 1 mg of total RNA was treated with 500  $\mu$ L of DNase I (10 U/mL; Invitrogen; United States). Then, it was incubated for 30 min at 37 °C and 5 min at 75 °C with 4  $\mu$ L of 5 × RT buffer, 2  $\mu$ L of 25 mmol/L MgCl<sub>2</sub>, 2  $\mu$ L of 10 mmol/L dNTP mix, 2  $\mu$ L of 50 mmol/L random hexamer primers, 1  $\mu$ L of RNase inhibitor (20 U/ $\mu$ L), and sufficient H<sub>2</sub>O for a final volume of 20  $\mu$ L. The mixture was then incubated for 10 min at 25 °C and 30 min at 48 °C with 2  $\mu$ L of MultiScribe reverse transcriptase (50 U/mL; Applied Biosystems; United States). The reaction was terminated by heating the sample at 95 °C for 10 min. Aliquots of 200 ng of cDNA were used in the SYBR-Green PCR analysis according to the manufacturer's protocol. RT-PCR amplification was performed in triplicate under the

following conditions: 2 min at 50 °C (for UNG activation) and 10 min at 95 °C (for polymerase activation), followed by 40 cycles of denaturation and alignment/extension at 95 °C for 15 s and 60 °C for 1 min, respectively, using the Stratagene Mx3005p qPCR System and MxPro-Mx3005p software (Santa Clara; United States). Relative quantification of HP0953 RNA expression was performed using the comparative CT method. The  $\Delta$  Ct (difference in CT values) between HP0953 and the *glmM* internal control and the  $\Delta \Delta$  Ct were calculated to normalize the differences in cDNA concentrations for each reaction. The RNA expression level was calculated using the equation  $2^{-(\Delta\Delta Ct)}$  [40]. The Kruskal-Wallis equality-of-populations rank test was used to compare the expression of the gene at all study time points. Differences were considered to be significant when the *P* value was < 0.05.

## RESULTS

### *In silico* analysis of HP0953 protein features

*In silico* analyses allow us to foresee probable protein maturation. The analysis conducted using the SignalP 4.1 tool revealed that HP0953 protein loses a signal peptide after excision between amino acids 21 and 22 which could lead to extracellular release (Figure 1). This region is also believed to present a transmembrane helix (Figure 2). The protein modifications provided us an insight into their probable function. Tables 1 and 2 show the predicted modification sites for HP0953. There are three predicted N-linked glycosylation sites in amino acid positions 113, 164, and 168 and six predicted O-linked glycosylation sites in positions 15, 23, 43, 111, 115, and 183. Moreover, there are four predicted myristoylation sites in positions 12-17, 29-34, 73-78, and 182-187 and one predicted prenylation site in the position 185-188.

To predict the structural model, we used different programs such as I-TASSER, RaptorX, and HHalign-Kbest, the latter being the one that generated a better quality model (Figures 3 and 4). The HHpred program disclosed a similarity with the Tip-alpha protein of *H. pylori*; thus, it was used as a template for modeling. Additionally, no conserved domains were found or matches with other proteins.

### Site-directed mutagenesis of HP0953 gene

Plasmid pBlue-5CM3 was constructed for HP0953 site-directed mutagenesis (Supplementary Figure 1). Sequencing the *Dhp0953::Cm* Blue-5CM3 construction multiple cloning site corresponded to inserted HP0953 and *Cm* cassette. However, we were unable to propagate the *H. pylori*-transformed strain.

### HP0953 is detected in the insoluble fraction of *H. pylori* protein extract

For *H. pylori* HP0953 protein identification, insoluble and soluble fractions were obtained and resolved by SDS-PAGE assay. HP0953 protein was not detected in the soluble fraction, and its total concentration was very low in the insoluble fraction (data not shown). Interestingly, HP0953 was expressed constitutively at all the tested time points (Figure 5).

### HP0953 is located in the cytoplasm and the peripheral zone of *H. pylori*

Protein location is indicative of its function. HP0953 was identified in the insoluble fraction of *H. pylori* lysates, which probably implies that the function of HP0953 is elicited in the vicinity of the outer membrane. To examine this hypothesis, we performed the immunogold technique on bacterial sections that were analyzed by TEM. The micrographs showed that HP0953 protein is located in the cytoplasm and accumulated in some peripheral areas of the bacterial body (Figure 6A), as well as in bacteria-bacteria contact areas (Figures 6B, 6C and 6D). Furthermore, there was a large accumulation of the protein in the bacterial debris (Figure 6E). Interestingly, the presence of this protein was also observed in the area of the glycocalyx that covers *H. pylori* (Figure 7), and accumulated where said coating spreads, producing a type of net, perhaps indicating the formation of a biofilm. Interestingly, a large amount of HP0953 protein was secreted during the infection of gastric cells because it was found in the *H. pylori*-AGS cell contact area (Figure 8).

### Higher expression of HP0953 is required in the early stages of *H. pylori*-AGS cell interaction

RT-qPCR was performed to elucidate the behavior of HP0953 during the contact of *H. pylori* with AGS cells. Figure 9 shows a comparison of the expression ratios of the treated and untreated cultures. HP0953 expression was observed at all the tested time points; however, higher expression values were observed after 12 h of infection. *glmM* was the prokaryotic constitutive gene that was used as an internal control (Figure 9).

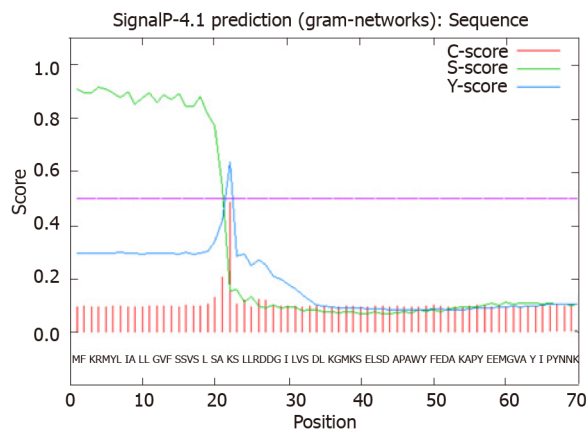
## DISCUSSION

The high prevalence of *H. pylori* infection and its significant persistence in the gastrointestinal tract in the population with limited economic resources, as well as the diversity of related pathologies, the

**Table 2 Prediction of posttranslational modification sites**

Position	Residue	Prediction
PS00008 MYRISTYL N-myristoylation site		
12-17	GVfsSV	N-myristoylation site
29-34	GilvSD	N-myristoylation site
73-78	GleqAT	N-myristoylation site
182-187	GSvcAL	N-myristoylation site
PS00005 PKC_PHOSPHO_SITE Protein Kinase C phosphorylation site		
20-22	SaK	MOD_RES 20 phosphoserine [condition: S]
PS00001 ASN_GLYCOSYLATION N-glycosylation site		
113-116	NISY	CARBOHYD 113 N-linked (GlcNAc) asparagine [condition: N]
PS00294 PRENYLATION Prenyl group binding site (CAAX box)		
185-188	CALr	Prenyl group binding site (CAAX box)

There are four predicted myristoylation sites, one predicted protein kinase C phosphorylation site, one predicted glycosylation site, and one predicted prenylation site.



# Measure	Position	Value	Cutoff	signal peptide?
max. C	22	0.486		
max. Y	22	0.635		
max. S	4	0.916		
mean S	1-21	0.858		
D	1-21	0.740	0.570	YES

Name = Sequence SP = 'YES' Cleavage site between pos. 21 and 22: LSA-KS D = 0.740 D-cutoff = 0.570 Network = Signal1P-noTM  
**DOI: 10.3748/wjg.v28.i29.3886 Copyright ©The Author(s) 2022.**

**Figure 1 Prediction of a signal peptide for HP0953 protein.** The green line that represents the S-score indicates a high probability that the first 20 amino acids conform a signal peptide that can be removed by a cut between amino acids 20 and 21, as marked by the tallest red line indicating the C-score.

environment, and the genetics of the host, suggest that the pathogenicity mechanisms used by this microorganism are numerous. The different bacterial strains express variations in their virulence factors, including those associated with the colonization process (*e.g.*, urease, flagella, a chemotaxis system, and adhesins), immune response evaders (*e.g.*, lipopolysaccharide and flagella; CagA and the type IV secretion system, VacA; gamma-glutamyl transpeptidase, and catalase superoxide dismutase), and disease inducers (*e.g.*, VacA, BabA, IceA, HtrA, CagA, and the type IV secretion system, DupA, and OipA)[41]. Furthermore, the *H. pylori* proteome consists of 340 proteins that are described as hypothetical, implying that their structure or function is unknown, thus indicating that some proteins may be related to pathogenicity mechanisms or are important to adapt to the surrounding environment. The HP0953 protein exhibited its maximum expression at the first 12 h of infection in a culture of gastric epithelium cells; this finding along with its location near the infected cells and the predicted prenylation and myristoylation sites suggest that it is an important protein during the bacterium’s colonization phase of the gastric epithelium.

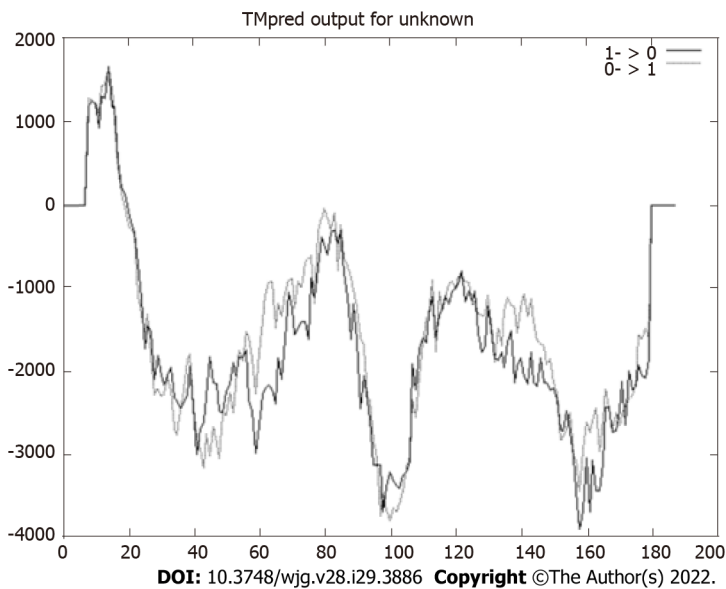


**Figure 2 Prediction of transmembrane helices.** Values > 0 indicate the probable presence of transmembrane helices, as observed in the region constituted by the first 25 amino acids. The HP0953 protein could be anchored to the membrane to be subsequently secreted.

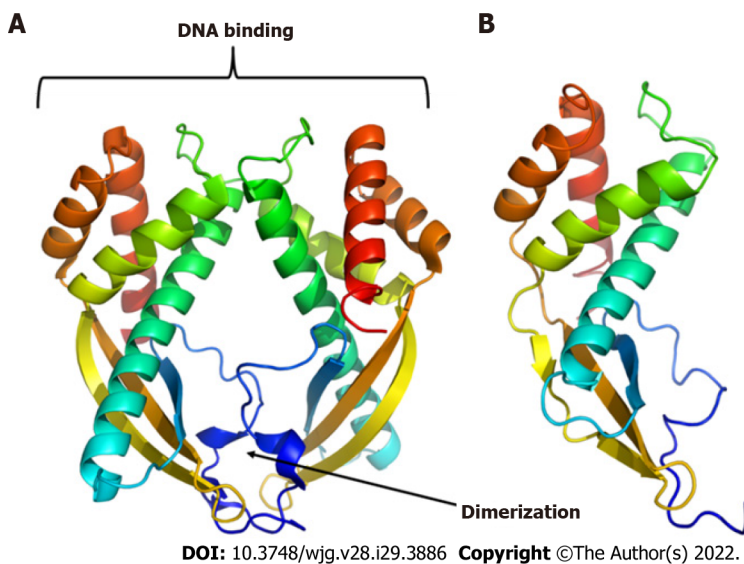


**Figure 3 Three-dimensional models of proteins.** A: Tip-alpha protein from *Helicobacter pylori* (*H. pylori*); B: HP0953 protein from *H. pylori*. Tip-alpha acquires a dimer arrangement that could also be present in the HP0953 protein due to its structural similarity in the position of the alpha helices and beta sheets.

Although various studies, such as those conducted by Naqvi *et al*[17] in 2016 and Park *et al*[42] in 2012, have performed *in silico* analyses to determine the probable structures and functions of the hypothetical proteins of *H. pylori*, none of them evaluated the probable function of HP0953[17,42]. Furthermore, the bioinformatics analysis performed in this study highlighted the presence of a signal peptide that may anchor at the transmembrane region and then allow the release of the protein to the external environment after its excision. The analyses also revealed some probable glycosylation sites, which suggests that HP0953 is a protein from the glycocalyx. The glycocalyx is defined as any glycoprotein-associated polysaccharide that contains bacterial surface structures and is distant from the outer membrane or cell wall surface[43]. Bacterial glycocalyx generally has protection functions that allow bacterial survival and persistence in the natural environment and cell attachment[44].

Different modification patterns are found within the HP0953 sequence, such as the myristoylation pattern. This modification is essential for the removal of membrane proteins[45]; the existence of these putative sites provides an idea about its pathogenicity. Importantly, these bacteria lack the enzyme N-myristoyl transferase (NMT) required for producing this modification; hence, the proteins that are myristoylated are processed by the NMT of their eukaryotic hosts[46]. NMT is a suitable therapeutic target in opportunistic infections in humans; in fact, it has been associated with carcinogenesis, in

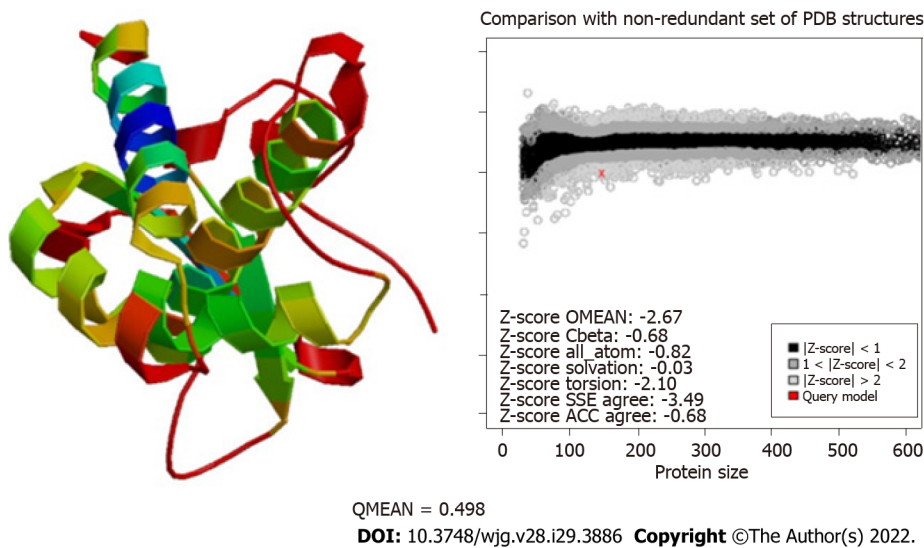


**Figure 4 Evaluation of the modeling quality of HP0953.** The QMEAN for this protein was 0.498, which indicates that the obtained model is acceptable. PDB: Protein Data Bank; SSE: Secondary Structure Element; ACC: Solvent Accessibility.

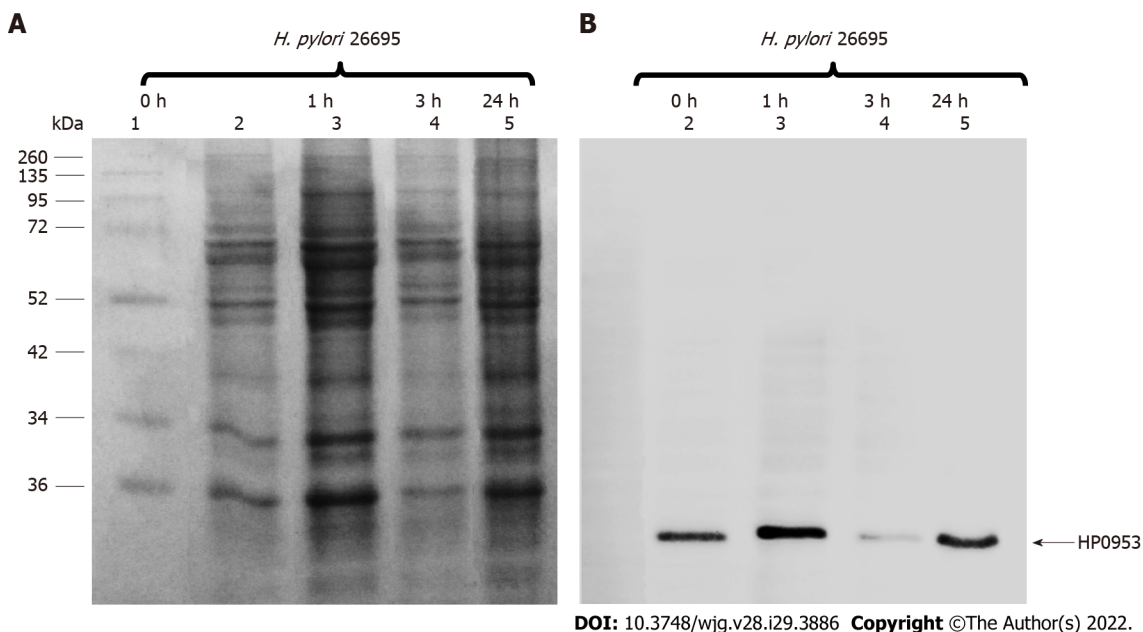
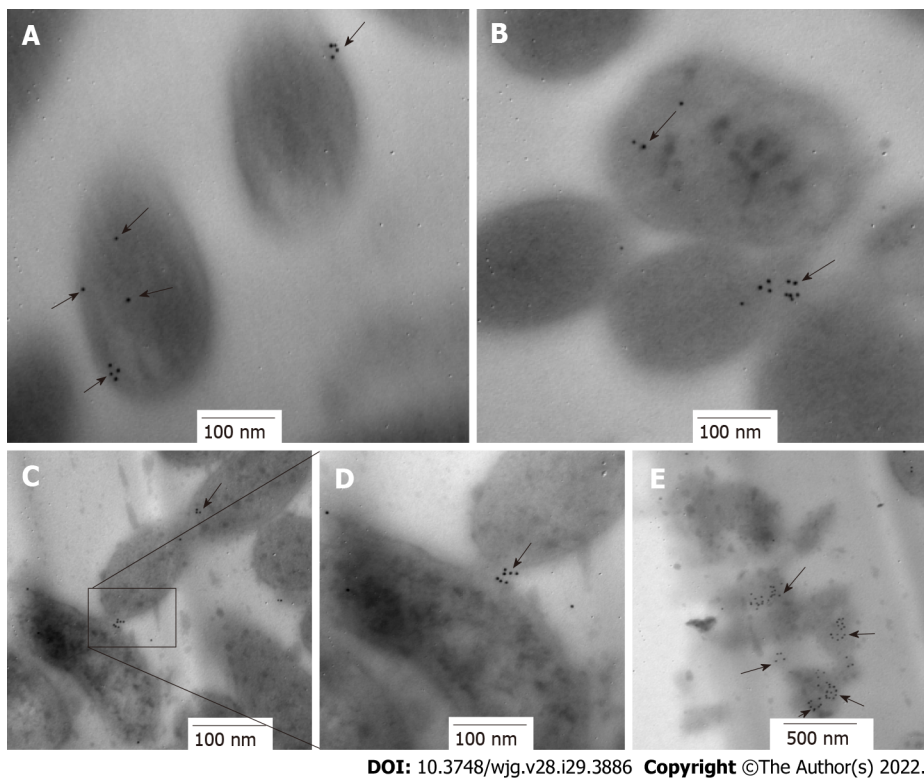


**Figure 5 Location of the hypothetical protein HP0953 in the insoluble fraction of *Helicobacter pylori* 26695.** A: Sulfate-polyacrylamide gel electrophoresis 16% gel stained with Coomassie blue; B: Western blot with an arrow showing the band corresponding to the expected molecular weight. Lanes: (1) Molecular weight marker and (2-5) insoluble fractions of *Helicobacter pylori* 26695 from samples collected at 0, 1, 3, and 24 h of incubation during biofilm formation. The arrow indicates the presence of the native HP0953 protein. *H. pylori*: *Helicobacter pylori*.

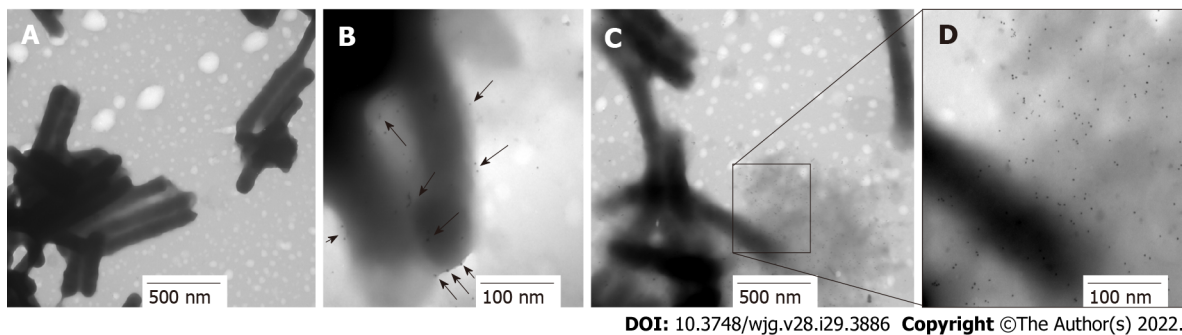
particular colon cancer[47]. Myristoylation has been suggested to occur as part of the secretory machinery[48,49]. Hypothetical patterns of prenylation were also detected, which is a class of modification involving the addition of isoprenoids or geranylgeranyl, and it is involved in membrane interactions due to the hydrophobicity of these lipids[50]. This modification is often a step to target the affected proteins to specific membranes[51]. As this modification was predicted in HP0953 by the ProtComB tool, it could be relevant for its function.

Extracellular proteins can play a vital role in bacterial pathogenesis[11], which correlates with our findings of the similarity between the HP0953 protein and the Tip-alpha protein, which is described as the only virulence factor secreted by all *H. pylori* strains[52]. Moreover, its overexpression has been related to the development of gastric cancer. Tip-alpha is an exotoxin that penetrates cells and induces the production of tumor necrosis factor alpha[53]. HP053 protein could have a similar function because probable posttranslational modification sites related to bacterial pathogenesis were also found. It has been reported that some bacteria secrete effectors through the type III or type IV secretion systems, mimicking the functions of eukaryotic proteins to evade the defense systems. Subsequently, they



DOI: 10.3748/wjg.v28.i29.3886 Copyright ©The Author(s) 2022.

**Figure 6 Immunolocalization of HP0953 protein in *Helicobacter pylori* bacterial transmission electron microscopy sections.** A and B: 100000 ×; C: 75000 ×; D: 150000 ×; E: 60000 ×. The black arrows show the location of HP0953 protein. Immunogold technique, primary antibody (polyclonal rabbit anti-HP0953), secondary antibody (goat anti-rabbit immunoglobulin G coupled to 10-nm colloidal gold particles). (JEM 1010 JEOL Ltd. Tokyo, Japan) microscope equipped with a TEM Imaging Systems AMT (Woburn, MA, United States).



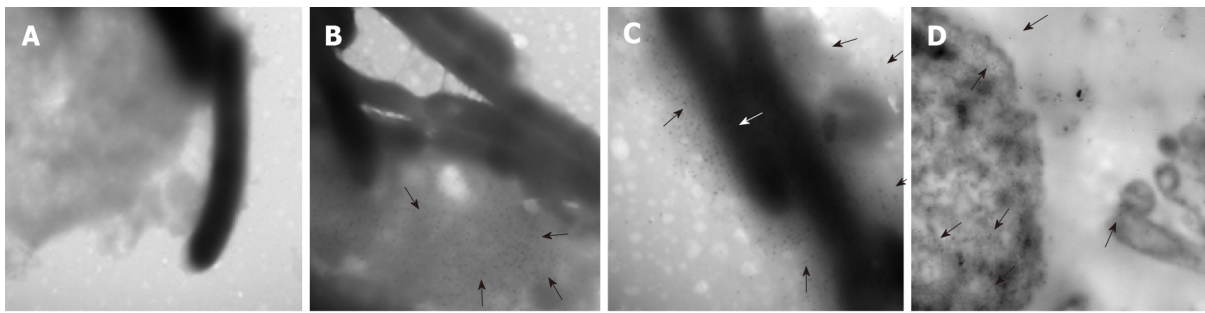
DOI: 10.3748/wjg.v28.i29.3886 Copyright ©The Author(s) 2022.

**Figure 7 Immunolocalization of HP0953 protein in whole bacteria.** A: *Helicobacter pylori* (*H. pylori*) incubated with the secondary antibody alone, 20000 ×; B-D: Complete immunogold technique for *H. pylori*; B: 100000 ×; C: 30000 ×; D: 100000 ×. Black arrows indicate the location of HP0953 protein. Immunogold technique, primary antibody (polyclonal rabbit anti-HP0953), secondary antibody (goat anti-rabbit immunoglobulin G coupled to 10-nm colloidal gold particles).

undergo a posttranslational modification mediated by the same host enzymes to become biologically active[54], stimulating or inhibiting the immune response, interfering signaling pathways, affecting T-cell activation, or whatever their function may be[55]. Among these posttranslational modifications are myristoylation and prenylation[56,57], which were also detected in the *in silico* analysis conducted in this study. These modifications added lipid residues that allow the protein to anchor to the cell membrane to exert some unknown function.

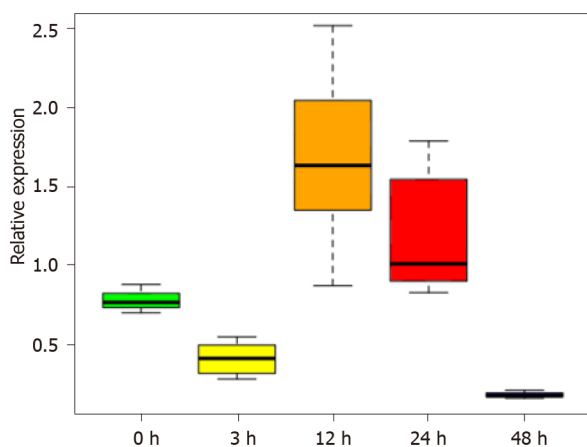
HP0953 lacks homologous proteins outside *H. pylori*, and this absence limits comparisons and the elucidation of its potential role. X-ray crystallography analysis can be performed to determine its 3D structure, which could then be used in comparisons with other proteins in the database. However, it was observed that HP0953 is an insoluble protein, which makes it difficult to purify in its native form.

The persistence of *H. pylori* in an environment where there are peristaltic movements and cell shedding is mediated by a variety of adhesins present on the bacterial surface[10,58], and the adhesion of *H. pylori* can be achieved by a connection of the plasma membrane through filamentous materials. However, it is known that glycocalyx preferentially adheres to the surfaces of biomaterials and compromised tissues, forming biofilms[55]. Research on biofilm composition has shown that a



DOI: 10.3748/wjg.v28.i29.3886 Copyright ©The Author(s) 2022.

**Figure 8 Location of HP0953 protein during against gastric cell infection by *Helicobacter pylori*.** A: Against gastric (AGS) cell at 3 h of infection by *Helicobacter pylori* (*H. pylori*), incubated with the secondary antibody alone, 40000 ×; B: Complete immunogold technique for AGS cells at 3 h of infection by *H. pylori*, 40000 ×; C: Complete immunogold technique for AGS cells at 3 h of infection by *H. pylori*, 50000 ×; D: Complete immunogold technique for AGS cells at 12 h of infection by *H. pylori*, 40000 ×. White arrows indicate the location of HP0953 protein.



DOI: 10.3748/wjg.v28.i29.3886 Copyright ©The Author(s) 2022.

**Figure 9 Expression of HP0953 increases significantly after 12 h of infection of against gastric cells.** The Kruskal-Wallis equality-of-populations rank test was used to compare the expression of the gene at all study time points.  $P = 0.0006$ .

pericellular matrix, also known as the glycocalyx, develops to preserve and concentrate the lytic enzymes secreted by bacteria, which, in turn, increases their metabolic efficiency[8]. This suggests that the hypothetical protein HP0953 could be involved in lytic processes by being present in the glycocalyx and concentrated in the bacterial debris; however, functionality studies are still required to elucidate the role of this protein in the persistence of *H. pylori* in the human stomach. Smith *et al*[11] suggested that this protein could be involved in the survival of the bacterium in the gastric environment based on their finding that it is also present in *H. acinonychis*, which colonizes the gastric mucosa of felines. Nevertheless, other closely related  $\epsilon$ -proteobacteria, such as *H. hepaticus* and *C. jejuni*, lack sequences that are homologous to HP0953, thus suggesting that this protein is unique to the gastric *Helicobacter* species[11], suggesting an important role of HP0953 in *H. pylori* gastric pathogenesis.

In our previous study, we observed the overexpression of HP0953 protein during the first hours of adherence to inert surfaces and AGS cells[59], suggesting its involvement in the survival of *H. pylori* in the environment or in its pathogenic mechanisms. In the present study, we found that initial levels of HP0953 expression become diminished, perhaps as a result of the adaptation of *H. pylori* to its environment. The levels of HP0953 rise after 3 h, indicating that this protein is required for the interaction of *H. pylori* with AGS cells, and the maximum level of HP0953 expression occurred 12 h after the infection of AGS cells. Genetic regulation in pathogens allows for fluctuation in the expression of constitutive genes following initial contact with the target cells[60,61]. The immunogold assay demonstrated that HP0953 protein was located in the cytoplasm, accumulated in some peripheral areas of the bacterial body, and exhibited a greater expression when it is close to AGS cells. These data suggest that HP0953 protein is synthesized in the cytoplasm and subsequently exported to the outer membrane, where it is involved in adhesion functions as its agglomeration was detected at the binding sites between the bacterium and in the space between the bacterium and gastric cells. Similarly, the immunogold assay of HP0953 protein in the whole bacterium revealed that the protein was primarily located in the bacterial coat or glycocalyx, which is consistent with the finding reported by Smith *et al* [11], who investigated the proteins secreted by *H. pylori* and found that HP0953 protein was a

component of this set of proteins.

Furthermore, we altered *HP0953* to obtain a mutant strain. Unfortunately, we were unable to propagate the resultant *HP0953* mutant clone, but we are continuing with our efforts to modify the methodology to obtain a mutant strain that can be successfully propagated. Further studies are necessary to determine the structure and function of hypothetical proteins of *H. pylori*, such as *HP0953*, which may be associated with the disease pathology.

## CONCLUSION

*HP0953* protein exhibited its maximum expression during the first 12 h of infection in a culture of gastric epithelium cells. This finding indicated its location surrounding the infected cells, and the predicted presence of prenylation and myristoylation sites suggests that *HP0953* is a relevant protein during the bacterium's colonization phase of the gastric epithelium. *HP0953* was also found to be strikingly similar to an exotoxin, possibly associating it with the development of gastric cancer.

## ARTICLE HIGHLIGHTS

### Research background

*Helicobacter pylori* (*H. pylori*) is a bacterium of clinical relevance. Approximately 50% of the worldwide human population is colonized by this bacterium, where up to 3% can develop gastric cancer. Several environmental conditions such as the genetic predisposition of the host, and bacterial virulence factors are directly associated.

### Research motivation

*H. pylori* is a bacterium associated with gastric diseases. This microorganism owns more than 200 hypothetical proteins with functions yet unknown. Some of them could be related to the disease or adaptation to gastric microenvironment. However, in a short-term future, they can be considered as therapeutic targets.

### Research objectives

The objective was to characterize the hypothetical protein *HP0953*, such as structure, location, and expression, to determine if it is a virulence factor employed by *H. pylori* during infection of against gastric (AGS) cells.

### Research methods

Several bioinformatic platforms (SignalP, ExPasy, GLYCOPP, I-Tasser) were employed to predict some features of the hypothetical protein *HP0953*, such as peptide-signaling, three-dimensional structure, and possible post-translational modifications. *HP0953* was located during *H. pylori* infection to AGS cells by transmission electron microscopy, employing a specific antibody for said protein and immunogold technique. The expression of *HP0953* during the infection of AGS cell cultures by the bacterium was evaluated by real-time polymerase chain reaction.

### Research results

The hypothetical protein *HP0953* was observed in the cytoplasm and embedded in the glycocalyx secreted by the bacterium, as well as in the space between the bacterium and the AGS cell. The overexpression of the protein was observed at 12 h of infection. *HP0953* was predicted to possess a signal peptide, which can interact with transmembranal regions for its secretion. Additionally, the *HP0953* protein acts as like an exotoxin, which can then undergo post-translational modifications, which might then require the eukaryotic cell to be carried out.

### Research conclusions

The hypothetical protein *HP0953* is a protein located in the periphery of infected cells. It is overexpressed during infection. The *in silico* analysis revealed prenylation and myristoylation sites. These findings suggest that the protein has a relevant function during the colonization or infection of *H. pylori* into gastric epithelium.

### Research perspectives

Propagate a *H. pylori* modified strain, which lacks the *HP0953* protein. The study will define its functions and establish a new precedent for the study of the pathogenesis of the disease, and its relevance in the adaptation process in the gastric microenvironment.

---

## ACKNOWLEDGEMENTS

---

The authors would like to acknowledge Alejandra S Rodríguez for her skillful technical assistance.

---

## FOOTNOTES

---

**Author contributions:** Arteaga-Resendiz NK, Rodea GE, Olivares-Cervantes AL, and Colín C performed the experiments, and acquired and analyzed data; Arteaga-Resendiz NK, Rodea GE, Colín C, Olivares-Cervantes AL, Aguilar-Rodea P, Ribas-Aparicio RM, López-Villegas EO, Olivares-Trejo JJ, and Velázquez-Guadarrama N interpreted the data; Reyes-López A and Arteaga-Resendiz NK statistical data analyzed; Rodea GE, Ribas-Aparicio RM, Mendoza-Elizalde S, Salazar García M and Velázquez-Guadarrama N wrote the manuscript; and all authors approved the final version of the article.

**Supported by** the Federal Funds, HIM/2009/037. SSA851 and HIM / 2014/012. SSA 1098; the grant from Secretaría de Investigación y Posgrado, SIP 20161878; and the Instituto Politécnico Nacional by Consejo Nacional de Ciencia y Tecnología, CB-222180.

**Institutional review board statement:** The study was reviewed and approved by the Ethics, Biosafety and Scientific committees at the Health Institute approved the experiment (HIM/2009/037. SSA851 and HIM/2014/012. SSA 1098).

**Institutional animal care and use committee statement:** Animal care was performed under national and institutional policies (NOM-062-ZOO-1999).

**Conflict-of-interest statement:** All the authors report no relevant conflicts of interest for this article.

**Data sharing statement:** No additional data are available.

**ARRIVE guidelines statement:** The authors have read the ARRIVE guidelines, and the manuscript was prepared and revised according to them.

**Open-Access:** This article is an open-access article that was selected by an in-house editor and fully peer-reviewed by external reviewers. It is distributed in accordance with the Creative Commons Attribution NonCommercial (CC BY-NC 4.0) license, which permits others to distribute, remix, adapt, build upon this work non-commercially, and license their derivative works on different terms, provided the original work is properly cited and the use is non-commercial. See: <https://creativecommons.org/licenses/by-nc/4.0/>

**Country/Territory of origin:** Mexico

**ORCID number:** Nancy K Arteaga-Resendiz [0000-0003-0777-4212](https://orcid.org/0000-0003-0777-4212); Gerardo E Rodea [0000-0003-1165-0511](https://orcid.org/0000-0003-1165-0511); Rosa María Ribas-Aparicio [0000-0002-1141-2794](https://orcid.org/0000-0002-1141-2794); Alma L Olivares-Cervantes [0000-0001-8209-4896](https://orcid.org/0000-0001-8209-4896); Juan Arturo Castelán-Vega [0000-0003-1102-2101](https://orcid.org/0000-0003-1102-2101); José de Jesús Olivares-Trejo [0000-0002-4225-4493](https://orcid.org/0000-0002-4225-4493); Sandra Mendoza-Elizalde [0000-0002-0255-4125](https://orcid.org/0000-0002-0255-4125); Edgar O López-Villegas [0000-0002-9995-2145](https://orcid.org/0000-0002-9995-2145); Christian Colín [0000-0002-8796-9978](https://orcid.org/0000-0002-8796-9978); Pamela Aguilar-Rodea [0000-0002-1522-2138](https://orcid.org/0000-0002-1522-2138); Alfonso Reyes-López [0000-0002-6249-3678](https://orcid.org/0000-0002-6249-3678); Marcela Salazar García [0000-0001-5318-8148](https://orcid.org/0000-0001-5318-8148); Norma Velázquez-Guadarrama [0000-0002-3620-7260](https://orcid.org/0000-0002-3620-7260).

**Corresponding Author's Membership in Professional Societies:** Hospital Infantil de México Federico Gómez, 11217.

**S-Editor:** Wang JJ

**L-Editor:** A

**P-Editor:** Wang JJ

---

## REFERENCES

---

- 1 **Connor BA.** *Helicobacter pylori*. In: Centers for Disease Control and Prevention. CDC Yellow Book 2020: Health Information for International Travel. New York: Oxford University Press, 2017
- 2 **Cheok YY, Lee CYQ, Cheong HC, Vadivelu J, Looi CY, Abdullah S, Wong WF.** An Overview of *Helicobacter pylori* Survival Tactics in the Hostile Human Stomach Environment. *Microorganisms* 2021; **9** [PMID: [34946105](https://pubmed.ncbi.nlm.nih.gov/34946105/) DOI: [10.3390/microorganisms9122502](https://doi.org/10.3390/microorganisms9122502)]
- 3 **Huang Y, Wang QL, Cheng DD, Xu WT, Lu NH.** Adhesion and Invasion of Gastric Mucosa Epithelial Cells by *Helicobacter pylori*. *Front Cell Infect Microbiol* 2016; **6**: 159 [PMID: [27921009](https://pubmed.ncbi.nlm.nih.gov/27921009/) DOI: [10.3389/fcimb.2016.00159](https://doi.org/10.3389/fcimb.2016.00159)]
- 4 **Wizenty J, Tacke F, Sigal M.** Responses of gastric epithelial stem cells and their niche to *Helicobacter pylori* infection. *Ann Transl Med* 2020; **8**: 568 [PMID: [32775369](https://pubmed.ncbi.nlm.nih.gov/32775369/) DOI: [10.21037/atm.2020.02.178](https://doi.org/10.21037/atm.2020.02.178)]
- 5 **Sharndama HC, Mba IE.** *Helicobacter pylori*: an up-to-date overview on the virulence and pathogenesis mechanisms. *Braz J Microbiol* 2022; **53**: 33-50 [PMID: [34988937](https://pubmed.ncbi.nlm.nih.gov/34988937/) DOI: [10.1007/s42770-021-00675-0](https://doi.org/10.1007/s42770-021-00675-0)]
- 6 **Yonezawa H, Osaki T, Kamiya S.** Biofilm Formation by *Helicobacter pylori* and Its Involvement for Antibiotic Resistance.

- Biomed Res Int* 2015; **2015**: 914791 [PMID: 26078970 DOI: 10.1155/2015/914791]
- 7 **Percival SL**, Suleman L. Biofilms and Helicobacter pylori: Dissemination and persistence within the environment and host. *World J Gastrointest Pathophysiol* 2014; **5**: 122-132 [PMID: 25133015 DOI: 10.4291/wjgp.v5.i3.122]
  - 8 **Gristina AG**, Costerton JW. Bacterial adherence and the glycocalyx and their role in musculoskeletal infection. *Orthop Clin North Am* 1984; **15**: 517-535 [PMID: 6472832]
  - 9 **Argüeso P**, Woodward AM, AbuSamra DB. The Epithelial Cell Glycocalyx in Ocular Surface Infection. *Front Immunol* 2021; **12**: 729260 [PMID: 34497615 DOI: 10.3389/fimmu.2021.729260]
  - 10 **Liu Y**, Hidaka E, Kaneko Y, Akamatsu T, Ota H. Ultrastructure of Helicobacter pylori in human gastric mucosa and H. pylori-infected human gastric mucosa using transmission electron microscopy and the high-pressure freezing-freeze substitution technique. *J Gastroenterol* 2006; **41**: 569-574 [PMID: 16868805 DOI: 10.1007/s00535-006-1813-2]
  - 11 **Smith TG**, Lim JM, Weinberg MV, Wells L, Hoover TR. Direct analysis of the extracellular proteome from two strains of Helicobacter pylori. *Proteomics* 2007; **7**: 2240-2245 [PMID: 17533641 DOI: 10.1002/pmic.200600875]
  - 12 **Chmiela M**, Kupcinskas J. Review: Pathogenesis of Helicobacter pylori infection. *Helicobacter* 2019; **24** Suppl 1: e12638 [PMID: 31486234 DOI: 10.1111/hel.12638]
  - 13 **Alzahrani S**, Lina TT, Gonzalez J, Pinchuk IV, Beswick EJ, Reyes VE. Effect of Helicobacter pylori on gastric epithelial cells. *World J Gastroenterol* 2014; **20**: 12767-12780 [PMID: 25278677 DOI: 10.3748/wjg.v20.i36.12767]
  - 14 **Tomb JF**, White O, Kerlavage AR, Clayton RA, Sutton GG, Fleischmann RD, Ketchum KA, Klenk HP, Gill S, Dougherty BA, Nelson K, Quackenbush J, Zhou L, Kirkness EF, Peterson S, Loftus B, Richardson D, Dodson R, Khalak HG, Glodek A, McKenney K, Fitzgerald LM, Lee N, Adams MD, Hickey EK, Berg DE, Gocayne JD, Utterback TR, Peterson JD, Kelley JM, Cotton MD, Weidman JM, Fujii C, Bowman C, Wattley L, Wallin E, Hayes WS, Borodovsky M, Karp PD, Smith HO, Fraser CM, Venter JC. The complete genome sequence of the gastric pathogen Helicobacter pylori. *Nature* 1997; **388**: 539-547 [PMID: 9252185 DOI: 10.1038/41483]
  - 15 **Baltrus DA**, Amieva MR, Covacci A, Lowe TM, Merrell DS, Ottemann KM, Stein M, Salama NR, Guillemin K. The complete genome sequence of Helicobacter pylori strain G27. *J Bacteriol* 2009; **191**: 447-448 [PMID: 18952803 DOI: 10.1128/JB.01416-08]
  - 16 **Blattner FR**, Plunkett G 3rd, Bloch CA, Perna NT, Burland V, Riley M, Collado-Vides J, Glasner JD, Rode CK, Mayhew GF, Gregor J, Davis NW, Kirkpatrick HA, Goeden MA, Rose DJ, Mau B, Shao Y. The complete genome sequence of Escherichia coli K-12. *Science* 1997; **277**: 1453-1462 [PMID: 9278503 DOI: 10.1126/science.277.5331.1453]
  - 17 **Naqvi AA**, Anjum F, Khan FI, Islam A, Ahmad F, Hassan MI. Sequence Analysis of Hypothetical Proteins from Helicobacter pylori 26695 to Identify Potential Virulence Factors. *Genomics Inform* 2016; **14**: 125-135 [PMID: 27729842 DOI: 10.5808/GI.2016.14.3.125]
  - 18 **Zanotti G**, Cendron L. Structural and functional aspects of the Helicobacter pylori secretome. *World J Gastroenterol* 2014; **20**: 1402-1423 [PMID: 24587618 DOI: 10.3748/wjg.v20.i6.1402]
  - 19 **Otero LL**, Ruiz VE, Perez Perez GI. Helicobacter pylori: the balance between a role as colonizer and pathogen. *Best Pract Res Clin Gastroenterol* 2014; **28**: 1017-1029 [PMID: 25439068 DOI: 10.1016/j.bpg.2014.09.003]
  - 20 **National Center of Biotechnology Information**. Protein. [cited 8 July 2021]. Available from: <https://www.ncbi.nlm.nih.gov/protein>
  - 21 **Mistry J**, Chuguransky S, Williams L, Qureshi M, Salazar GA, Sonnhammer ELL, Tosatto SCE, Paladin L, Raj S, Richardson LJ, Finn RD, Bateman A. Pfam: The protein families database in 2021. *Nucleic Acids Res* 2021; **49**: D412-D419 [PMID: 33125078 DOI: 10.1093/nar/gkaa913]
  - 22 **Petersen TN**, Brunak S, von Heijne G, Nielsen H. SignalP 4.0: discriminating signal peptides from transmembrane regions. *Nat Methods* 2011; **8**: 785-786 [PMID: 21959131 DOI: 10.1038/nmeth.1701]
  - 23 **Siss Institute of Bioinformatics**. ExPASy. [cited 8 July 2021]. Available from: <https://www.expasy.org/>
  - 24 **Hofmann K**, Stoffel W. TMbase - A database of membrane spanning proteins segments. *Biol Chem* 1993; **374**: 166
  - 25 **GlycoPP V2.0** A webserver for glycosites prediction in procaryotes. [cited 8 July 2021]. Available from: <https://datascience.imtech.res.in/alkarao/glycopp2/>
  - 26 **Zimmermann L**, Stephens A, Nam SZ, Rau D, Kübler J, Lozajic M, Gabler F, Söding J, Lupas AN, Alva V. A Completely Reimplemented MPI Bioinformatics Toolkit with a New HHpred Server at its Core. *J Mol Biol* 2018; **430**: 2237-2243 [PMID: 29258817 DOI: 10.1016/j.jmb.2017.12.007]
  - 27 **Zhang Lab**. I-TASSER Protein Structure  $\alpha$  Function Predictions. [cited 9 May 2021]. Available from: <https://zhanggroup.org/I-TASSER/>
  - 28 **RaptorX**. RaptorX: Protein Structure and Function Prediction Powered by Deep Learning. [cited 4 November 2016]. Available from: <http://raptorx.uchicago.edu/>
  - 29 **HHalign-Kbest**: A service for optimized model generation through sub optimal HMM-HMM sequence alignment. [cited 4 November 2016]. Available from: <https://bioserv.rpbs.univ-paris-diderot.fr/services/HHalign-Kbest/>
  - 30 **Vosshall L**. Hanahan competent cell protocol. [cited 8 July 2021]. Available from: <https://www.rockefeller.edu/research/uploads/www.rockefeller.edu/sites/8/2018/10/Hanahan.pdf>
  - 31 **Froger A**, Hall JE. Transformation of plasmid DNA into E. coli using the heat shock method. *J Vis Exp* 2007; **253** [PMID: 18997900 DOI: 10.3791/253]
  - 32 **Hyvonen M**. Inclusion body preparation. [cited 8 July 2021]. Available from: <https://hyvonen.bioc.cam.ac.uk/wp-content/uploads/2017/09/ib.pdf>
  - 33 **Howard GC**, Bethell DR. Polyclonal antibodies, In: Basic Methods in Antibody Production and Characterization. Florida, USA: CRC Press, 2000: 31-48
  - 34 **Abcam**. Western blot membrane stripping for restaining protocol. [cited 8 July 2021]. Available from: <https://docs.abcam.com/pdf/protocols/western-blot-membrane-stripping-for-restaining-protocol.pdf>
  - 35 **Birnboim HC**, Doly J. A rapid alkaline extraction procedure for screening recombinant plasmid DNA. *Nucleic Acids Res* 1979; **7**: 1513-1523 [PMID: 388356 DOI: 10.1093/nar/7.6.1513]
  - 36 **Ge Z**, Taylor DE. H. pylori DNA Transformation by Natural Competence and Electroporation. In: Clayton CL, Mobley

- HLT. *Helicobacter pylori* Protocols. New Jersey: Humana Press, 1997: 145-152
- 37 **Vázquez NG**, Echeverría O. Introducción a la microscopía Electrónica Aplicada a las Ciencias Biológicas. Facultad de Ciencias de la Universidad Nacional Autónoma de México. México: Fondo de Cultura Económica, 2000: 148-151
  - 38 **Untergasser A**, Cutcutache I, Koressaar T, Ye J, Faircloth BC, Remm M, Rozen SG. Primer3--new capabilities and interfaces. *Nucleic Acids Res* 2012; **40**: e115 [PMID: 22730293 DOI: 10.1093/nar/gks596]
  - 39 **Koressaar T**, Remm M. Enhancements and modifications of primer design program Primer3. *Bioinformatics* 2007; **23**: 1289-1291 [PMID: 17379693 DOI: 10.1093/bioinformatics/btm091]
  - 40 **Pfaffl MW**. A new mathematical model for relative quantification in real-time RT-PCR. *Nucleic Acids Res* 2001; **29**: e45 [PMID: 11328886 DOI: 10.1093/nar/29.9.e45]
  - 41 **Chang WL**, Yeh YC, Sheu BS. The impacts of *H. pylori* virulence factors on the development of gastroduodenal diseases. *J Biomed Sci* 2018; **25**: 68 [PMID: 30205817 DOI: 10.1186/s12929-018-0466-9]
  - 42 **Park SJ**, Son WS, Lee BJ. Structural analysis of hypothetical proteins from *Helicobacter pylori*: an approach to estimate functions of unknown or hypothetical proteins. *Int J Mol Sci* 2012; **13**: 7109-7137 [PMID: 22837682 DOI: 10.3390/ijms13067109]
  - 43 **Luong P**, Dube DH. Dismantling the bacterial glycocalyx: Chemical tools to probe, perturb, and image bacterial glycans. *Bioorg Med Chem* 2021; **42**: 116268 [PMID: 34130219 DOI: 10.1016/j.bmc.2021.116268]
  - 44 **Ogata M**, Araki K, Ogata T. An electron microscopic study of *Helicobacter pylori* in the surface mucous gel layer. *Histol Histopathol* 1998; **13**: 347-358 [PMID: 9589892 DOI: 10.14670/HH-13.347]
  - 45 **Hayashi N**, Titani K. N-myristoylated proteins, key components in intracellular signal transduction systems enabling rapid and flexible cell responses. *Proc Jpn Acad Ser B Phys Biol Sci* 2010; **86**: 494-508 [PMID: 20467215 DOI: 10.2183/pjab.86.494]
  - 46 **Maurer-Stroh S**, Eisenhaber F. Myristoylation of viral and bacterial proteins. *Trends Microbiol* 2004; **12**: 178-185 [PMID: 15051068 DOI: 10.1016/j.tim.2004.02.006]
  - 47 **Wright MH**, Heal WP, Mann DJ, Tate EW. Protein myristoylation in health and disease. *J Chem Biol* 2010; **3**: 19-35 [PMID: 19898886 DOI: 10.1007/s12154-009-0032-8]
  - 48 **Simon SM**, Aderem A. Myristoylation of proteins in the yeast secretory pathway. *J Biol Chem* 1992; **267**: 3922-3931 [PMID: 1740440]
  - 49 **Yuan M**, Song ZH, Ying MD, Zhu H, He QJ, Yang B, Cao J. N-myristoylation: from cell biology to translational medicine. *Acta Pharmacol Sin* 2020; **41**: 1005-1015 [PMID: 32203082 DOI: 10.1038/s41401-020-0388-4]
  - 50 **Palsuledesai CC**, Distefano MD. Protein prenylation: enzymes, therapeutics, and biotechnology applications. *ACS Chem Biol* 2015; **10**: 51-62 [PMID: 25402849 DOI: 10.1021/cb500791f]
  - 51 **Hildebrandt D**. Heterogeneous Prenyl Processing of the Heterotrimeric G protein Gamma Subunits. *The Enzymes* 2011; **29**: 97-124 [DOI: 10.1016/B978-0-12-381339-8.00006-8]
  - 52 **Tosi T**, Cioci G, Jouravleva K, Dian C, Terradot L. Structures of the tumor necrosis factor alpha inducing protein Tipalpha: a novel virulence factor from *Helicobacter pylori*. *FEBS Lett* 2009; **583**: 1581-1585 [PMID: 19401200 DOI: 10.1016/j.febslet.2009.04.033]
  - 53 **Mahant S**, Chakraborty A, Som A, Mehra S, Das K, Mukhopadhyay AK, Gehlot V, Bose S, Das R. The Synergistic Role of Tip  $\alpha$ , Nucleolin and Ras in *Helicobacter pylori* Infection Regulates the Cell Fate Towards Inflammation or Apoptosis. *Curr Microbiol* 2021; **78**: 3720-3732 [PMID: 34468852 DOI: 10.1007/s00284-021-02626-2]
  - 54 **Al-Quadan T**, Price CT, London N, Schueler-Furman O, AbuKwaik Y. Anchoring of bacterial effectors to host membranes through host-mediated lipidation by prenylation: a common paradigm. *Trends Microbiol* 2011; **19**: 573-579 [PMID: 21983544 DOI: 10.1016/j.tim.2011.08.003]
  - 55 **Ismail S**, Hampton MB, Keenan JI. *Helicobacter pylori* outer membrane vesicles modulate proliferation and interleukin-8 production by gastric epithelial cells. *Infect Immun* 2003; **71**: 5670-5675 [PMID: 14500487 DOI: 10.1128/IAI.71.10.5670-5675.2003]
  - 56 **Popa CM**, Tabuchi M, Valls M. Modification of Bacterial Effector Proteins Inside Eukaryotic Host Cells. *Front Cell Infect Microbiol* 2016; **6**: 73 [PMID: 27489796 DOI: 10.3389/fcimb.2016.00073]
  - 57 **Hicks SW**, Galán JE. Exploitation of eukaryotic subcellular targeting mechanisms by bacterial effectors. *Nat Rev Microbiol* 2013; **11**: 316-326 [PMID: 23588250 DOI: 10.1038/nrmicro3009]
  - 58 **Vázquez-Jiménez FE**, Torres J, Flores-Luna L, Cerezo SG, Camorlinga-Ponce M. Patterns of Adherence of *Helicobacter pylori* Clinical Isolates to Epithelial Cells, and its Association with Disease and with Virulence Factors. *Helicobacter* 2016; **21**: 60-68 [PMID: 25908566 DOI: 10.1111/hel.12230]
  - 59 **Arteaga-Resendiz NK**, Velázquez-Guadarrama N, Rivera-Gutiérrez S, Olivares Trejo J J, Méndez-Tenorio A, Valencia Mayoral P, López-Villegas E O, Rodríguez-Leviz A, Viguera J C, Arellano-Galindo J, Girón J, Torres-López J. In silico analysis of proteins potentially involved in fimbrial biogenesis in *Helicobacter pylori*. *Bol Med Hosp Infant Mex* 2013; **70**: 78-88
  - 60 **De la Cruz MA**, Ares MA, von Bargen K, Panunzi LG, Martínez-Cruz J, Valdez-Salazar HA, Jiménez-Galicia C, Torres J. Gene Expression Profiling of Transcription Factors of *Helicobacter pylori* under Different Environmental Conditions. *Front Microbiol* 2017; **8**: 615 [PMID: 28443084 DOI: 10.3389/fmicb.2017.00615]
  - 61 **Kitamoto S**, Nagao-Kitamoto H, Kuffa P, Kamada N. Regulation of virulence: the rise and fall of gastrointestinal pathogens. *J Gastroenterol* 2016; **51**: 195-205 [PMID: 26553054 DOI: 10.1007/s00535-015-1141-5]

## Basic Study

## Involvement of toll-like receptor 5 in mouse model of colonic hypersensitivity induced by neonatal maternal separation

Geoffroy Mallaret, Amandine Lashermes, Mathieu Meleine, Ludivine Boudieu, Julie Barbier, Youssef Aissouni, Agathe Gelot, Benoit Chassaing, Andrew T Gewirtz, Denis Ardid, Frederic Antonio Carvalho

**Specialty type:** Gastroenterology and hepatology

**Provenance and peer review:**

Unsolicited article; Externally peer reviewed.

**Peer-review model:** Single blind

**Peer-review report's scientific quality classification**

Grade A (Excellent): 0  
Grade B (Very good): B  
Grade C (Good): C  
Grade D (Fair): 0  
Grade E (Poor): 0

**P-Reviewer:** Ghannam WM, Egypt; Plaza MA, Spain

**Received:** March 15, 2022

**Peer-review started:** March 15, 2022

**First decision:** May 29, 2022

**Revised:** June 9, 2022

**Accepted:** July 5, 2022

**Article in press:** July 5, 2022

**Published online:** August 7, 2022



**Geoffroy Mallaret, Mathieu Meleine, Ludivine Boudieu, Julie Barbier, Youssef Aissouni, Agathe Gelot, Denis Ardid,** Department of Pharmacology, UMR 1107 NeuroDol, University of Clermont Auvergne, Clermont-Ferrand 63000, France

**Amandine Lashermes,** Department of Microbiology, Université Paris-Saclay, National Research Institute for Agriculture, Food and the Environment, AgroParisTech, Micalis Institute, Jouy-en-Josas 78350, France

**Benoit Chassaing,** Team “Mucosal Microbiota in Chronic Inflammatory Diseases”, INSERM U1016, CNRS UMR 8104, Université Paris Cité, Paris 75014, France

**Andrew T Gewirtz,** Center for Inflammation, Institute for Biomedical Sciences, Georgia State University, Atlanta, GA30033, United States

**Frederic Antonio Carvalho,** Department of Pharmacology, INSERM 1107 NeuroDOL/University of Clermont Auvergne, Clermont-Ferrand 63000, France

**Corresponding author:** Frederic Antonio Carvalho, PhD, Academic Research, Department of Pharmacology, INSERM 1107 NeuroDOL/University of Clermont Auvergne, 28 Place Henri Dunant, Clermont-Ferrand 63000, France. [frederic.carvalho@inserm.fr](mailto:frederic.carvalho@inserm.fr)

**Abstract****BACKGROUND**

Chronic abdominal pain is the most common cause for gastroenterology consultation and is frequently associated with functional gastrointestinal disorders including irritable bowel syndrome and inflammatory bowel disease. These disorders present similar brain/gut/microbiota triad alterations, associated with abnormal intestinal permeability, intestinal dysbiosis and colonic hypersensitivity (CHS). Intestinal dysbiosis can alter colon homeostasis leading to abnormal activation of the innate immunity that promotes CHS, perhaps involving the toll-like receptors (TLRs), which play a central role in innate immunity.

**AIM**

To understand the mechanisms between early life event paradigm on intestinal permeability, fecal microbiota composition and CHS development in mice with TLRs expression in colonocytes.

## METHODS

Maternal separation model (NMS) CHS model, which mimics deleterious events in childhood that can induce a wide range of chronic disorders during adulthood were used. Colonic sensitivity of NMS mice was evaluated by colorectal distension (CRD) coupled with intracolonic pressure variation (IPV) measurement. Fecal microbiota composition was analyzed by 16S rRNA sequencing from weaning to CRD periods. TLR mRNA expression was evaluated in colonocytes. Additionally, the effect of acute intrarectal instillation of the TLR5 agonist flagellin (FliC) on CHS in adult naive wildtype mice was analyzed.

## RESULTS

Around 50% of NMS mice exhibited increased intestinal permeability and CHS associated with intestinal dysbiosis, characterized by a significant decrease of species richness, an alteration of the core fecal microbiota and a specific increased relative abundance of flagellated bacteria. Only TLR5 mRNA expression was increased in colonocytes of NMS mice with CHS. Acute intrarectal instillation of FliC induced transient increase of IPV, reflecting transient CHS appearance.

## CONCLUSION

Altogether, these data suggest a pathophysiological continuum between intestinal dysbiosis and CHS, with a role for TLR5.

**Key Words:** Chronic abdominal pain; Colonic hypersensitivity; Toll-like receptors; Intestinal microbiota; Early life events

©The Author(s) 2022. Published by Baishideng Publishing Group Inc. All rights reserved.

**Core Tip:** Neonatal maternal separation (NMS) model mimic deleterious events in childhood, which can induce a wide range of chronic disorders during adulthood. Herein, around 50% of NMS mice exhibited increased intestinal permeability and colonic hypersensitivity (CHS) associated with intestinal dysbiosis. Only toll-like receptor 5 (TLR5) mRNA expression was increased in colonocytes of NMS mice with CHS and acute intrarectal instillation of flagellin transiently increased intracolonic pressure variations, reflecting transient CHS appearance. Together, those findings suggest a pathophysiological continuum between intestinal permeability, intestinal dysbiosis and CHS, with a previously undescribed role for TLR5 in CHS.

**Citation:** Mallaret G, Lashermes A, Meleine M, Boudieu L, Barbier J, Aissouni Y, Gelot A, Chassaing B, Gewirtz AT, Ardid D, Carvalho FA. Involvement of toll-like receptor 5 in mouse model of colonic hypersensitivity induced by neonatal maternal separation. *World J Gastroenterol* 2022; 28(29): 3903-3916

**URL:** <https://www.wjgnet.com/1007-9327/full/v28/i29/3903.htm>

**DOI:** <https://dx.doi.org/10.3748/wjg.v28.i29.3903>

## INTRODUCTION

Irritable bowel syndrome (IBS) is one of the major chronic gastrointestinal disorders, strongly related to stress. It is characterized by abdominal pain, changes in bowel habits and increased intestinal permeability without macroscopic organic alterations. Such changes has been hypothesized to trigger impairment of life's quality and the development of comorbidities such as anxiety and depression[1]. A worldwide prevalence of 3%-5% has been reported and today, efficient pharmacological treatments are limited to relieve symptoms[2]. Colonic hypersensitivity (CHS), frequently associated with abdominal pain, has been described as the main cause of medical consultation in IBS patients with a prevalence ranging from 33% to 90%[3]. This symptom is defined by an altered sensation in response to colorectal stimuli and is clinically revealed by enhanced perception of mechanical triggers applied to the bowel. The common hypothesis is that CHS may result from colonic homeostasis changes and/or alterations of the brain-gut connection. In fact, the brain-gut axis has been shown to be impacted by inflammation and immunological factors, psychological factors, dysregulation of the hypothalamic-pituitary-adrenal (HPA) axis, abnormal activation of the vagus nerve and the enteric nervous system and intestinal dysbiosis[4].

Qualitative and/or quantitative alterations of the intestinal microbiota has been characterized in most of the functional gastrointestinal disorders including IBS[5]. Despite the numerous studies carried out, data on specific bacterial groups altered in IBS patients are still inconclusive. However, *Enterobacteriaceae*

family, *Lactobacillaceae* family, and *Bacteroides* genus seem to be increased in patients with IBS compared with controls, whereas uncultured *Clostridiales* I, *Faecalibacterium* and *Bifidobacterium* genus were decreased in IBS patients[6]. Furthermore, it has been described that some IBS patients with chronic abdominal pain present specific intestinal microbiota dysbiosis, allowing considerations of the gut microbiota as a potential therapeutic target[7].

In healthy conditions, the interaction between gut microbiota and pattern recognition receptors (PRRs), especially local toll-like receptors (TLRs), allow maintenance of intestinal barrier in a homeostatic state. Indeed, TLRs, mostly present on the membrane of immune and epithelial cells, identify pathogen-associated molecular patterns (PAMPs) and induce intracellular signaling cascade resulting in the production of cytokines and chemokines important for colonic homeostasis. The mammalian TLRs family consists of 13 members (TLR1-10 in humans, TLR1-9 and TLR11-13 in mice) and each TLR responds to distinct PAMPs leading to the activation of specific signaling pathway. For example, TLR4 recognizes lipopolysaccharide (LPS) and TLR5, which is expressed in the basolateral membrane of the intestinal epithelium, detects flagellin (FliC)[8]. In a dysbiotic state, alterations in the signature of microbial molecules sensed by the host can lead to abnormal activation state of the immune system and induce a low-grade intestinal inflammation[9].

The breakdown of the symbiotic relationship between TLRs and gut microbiota could contribute to the development of various multifactorial intestinal diseases, such as IBS. Previous studies have reported modifications of TLRs expression and activation in intestinal biopsies of IBS patients[10-15]. Furthermore, a preclinical study assessed the effect of neonatal maternal separation (NMS) in rats on TLRs expression, showing an upregulation of TLRs in colonic mucosa[16]. In this context, because of correlation between IBS and early life adverse events[17], this study investigated the impact of NMS paradigm on intestinal permeability, fecal microbiota composition and CHS development in mice as well as the association with TLRs expression.

## MATERIALS AND METHODS

### Animals

Seven-week-old wild type C57Bl/6J males and females mice were purchased from Janvier Laboratories (Le Genest Saint Isle, France). They were mated to obtain male pups for the NMS protocol. After birth, wild-type C57Bl/AJ pups were isolated from their mother from post-natal days P2 to P14, three hours per day (from 9:00 a.m. to 12:00 p.m.). These mice were named NMS mice. Pups were then left with their mothers up to weaning (P21) (Figure 1A). Control wild-type C57Bl/AJ pups were co-housed in the animal facility and were called non-handled (NH) mice. In addition, ten-week-old wild type C57Bl/6J males were purchased from Janvier Laboratories and used for FliC intrarectal instillation experiment. Animals were given access to food and water *ad libitum* and housed with a 12 h light-dark cycle. All experiments were performed on twelve-week-old male mice and were performed according to the ethical guidelines set out by the International Association for the Study of Pain (IASP), complied with the European Union regulation and were approved by ethics committees: The local committees C2EA-02 of Clermont-Ferrand (approvals CE110-12 and CE111-12).

### Colorectal distension test

Colorectal distension test (CRD) was performed using the non-invasive manometric method described [18]. A miniaturized pressure transducer catheter (Mikro-Tip SPR-254; Millar Instruments, Houston, TX, United States) equipped with a custom-made balloon (length: 1.5 cm) prepared from a polyethylene plastic bag which avoid any colonic compliance effect. On the day of the experiment, the mice were accustomed to the holding device for 1 h before the CRD. Then, under mild anesthetic (2.5% isoflurane), the balloon was inserted into the rectum such that the distal end of the balloon was 5 mm from the anal margin. Subsequently, the animals were placed in the holding device and allowed to recover for 30 min prior to CRD. The balloon was connected to an electronic barostat (Distender Series II, G&J Electronics, Toronto, Canada) and a preamplifier (PCU-2000 Dual Channel Pressure Control Unit, Millar Instruments, Houston, TX, United States) connected to the PowerLab interface (AD Instruments, Dunedin, New Zealand). The barostat enabled the control of the balloon pressure. The distension protocol consisted of a set of increasing distension pressures (20, 40, 60, 80 and 100 mmHg), each of which was repeated twice, which was applied for 20 s with a 4 min inter-pressure interval. The signal was acquired and analyzed using LabChart 7 software (AD Instruments, Dunedin, New Zealand). After intracolonic pressure recording for each animals along the CRD protocols and signal treatment as previously described[18], intracolonic pressure variation (IPV), reflecting the colonic sensitivity, was calculated as previously described[19] for each distension pressure. Briefly, IPV was calculated by subtracting the integral (area under the curve) of the treated signal corresponding to the 20 s preceding the CRD from the integral (area under the curve) of the treated signal during the 20 s of CRD stimulation. Therefore, two groups of NMS mice were defined: NMS non-sensitized (NMS NS) and NMS sensitized (NMS S) mice. The NMS S animals are distinguished according to the area under the curve (AUC) value in response to the distention pressures from 60 to 100 mmHg during CRD procedure

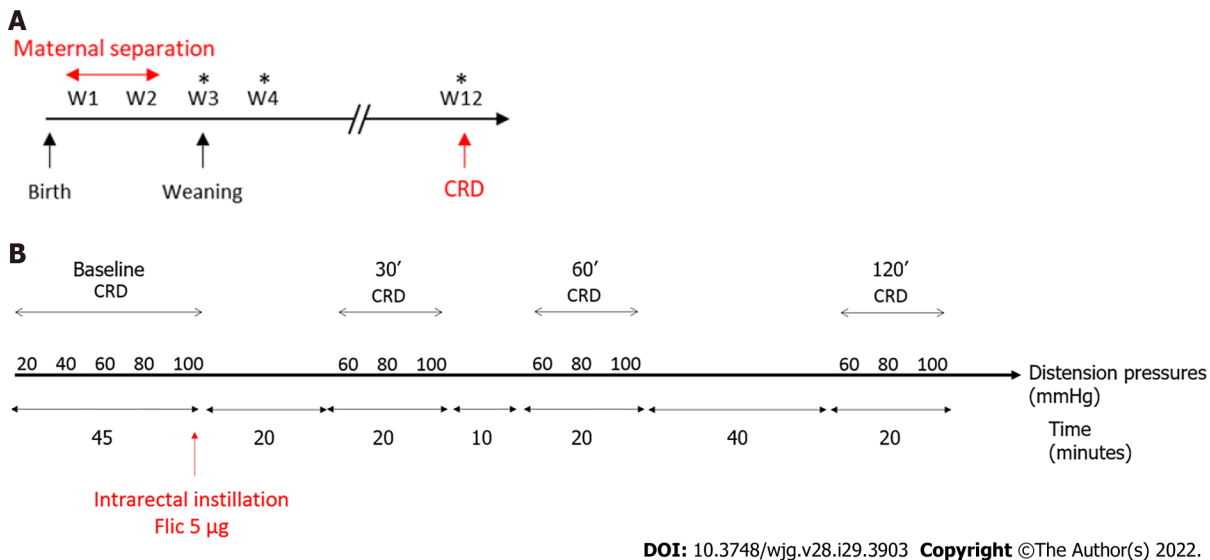


**Figure 1** Time course protocols used in this study. A: Time course protocol for neonatal maternal separation experiment; B: Time course protocol for flagellin intrarectal instillation experiment. \*Feces sample collection for Next Generation Sequencing; CRD: Colorectal distension test.

[20]. Briefly, if this value is higher than the average AUC of the NH control animals plus twice the SEM value ( $AUC_{NMS} \geq AUC_{NH} + 2 \times SEM_{NH}$ ), this mouse is considered as hypersensitive and are placed in the NMS S group. Others are considered as NMS NS. For FliC intrarectal instillation experiment, the distension protocol was the same before intrarectal instillation and, only a set of distension pressure 60, 80 and 100 mmHg was used 30 min, 60 min and 120 min after intrarectal instillation.

#### ***In vivo* intestinal permeability**

*In vivo* intestinal permeability was assessed using fluorescein dextran (FITC- dextran 3000-5000 Da, TdB Consultancy AB, Uppsala, Sweden) as previously described[21]. Briefly, before CRD, NMS and NH mice were orally gavaged with 0.6 g/g body weight of FITC-dextran and blood samples were obtained from the retro-orbital venous plexus 3 h after this administration. Plasma FITC levels were determined by fluorometry at 488 nm using a microplate reader (Tecan, Lyon, France).

#### **Fecal pellets collection, DNA extraction and microbiota sequencing**

Fecal pellets were collected from mice at week 3, 4 and 12 and stored at  $-80^{\circ}\text{C}$  prior to DNA extraction. Bacterial DNA was extracted from fecal bacteria following the protocol of NucleoSpin® Soil kit (Macherey-Nagel, Düren, Germany). DNA concentrations and purity were then assessed using Take3 micro-volume plate and Epoch Microplate Spectrophotometer (BioTek, Winooski, VT, United States). The 16S rRNA gene V4 variable region polymerase chain reaction (PCR) primers 515/806 with barcode on the forward primer were used in a 30 cycles PCR using the HotStarTaq Plus Master Mix Kit (Qiagen®, Germantown, MD, United States). Next generation sequencing (NGS) was performed at Molecular Research DNA (MR DNA - Shallowater, TX, United States) on a MiSeq following the manufacturer's guidelines. Sequences data analysis was performed using the quantitative insights into microbial ecology pipeline (QIIME)[22]. The analysis was carried out on the core microbiota *i.e.* the operational taxonomic units (OTUs) present in the fecal microbiota of 90% of the mice.

#### **FliC intrarectal instillation**

FliC from wildtype *Salmonella enterica* serovar typhimurium (SL3201, fljB<sup>-</sup>) was provided by Pr. A. Gewirtz (Center for Inflammation, Georgia State University, Atlanta, GA, United States). Briefly, FliC was purified through sequential cation- and anion-exchange chromatography and purity was verified as described previously[8]. Intrarectal instillation was performed under mild anesthetic (2.5% isoflurane) using orogastric feeding tube and inserted 2.5 cm up the colon (Figure 1B). At this point, 50 μL of FliC diluted in PBS, corresponding to 5 μg was slowly administered over 30 s while pressure was applied to the anal area to prevent leakage. Following the injection of the solution, the tube was slowly removed and the rectal pressure was maintained for a further 30 s.

#### **Colonocytes extraction**

Following mice euthanasia, fragments of colon (3-4 cm) were flushed and opened longitudinally along the mesentery and homogenized in cold PBS to remove feces. Then, these fragments were incubated into HBSS containing EDTA solution (2 mmol/L) 30 min at  $37^{\circ}\text{C}$  with strong agitation every 10 min. After HBSS/EDTA incubation, colons were removed and samples were centrifuged at 2000 g for 10 min.

Then, HBSS/EDTA was removed and colonocytes were deep-frozen in liquid nitrogen and stored at -80 °C for further analysis.

### **RNA extraction, reverse transcription and quantitative PCR**

Total RNA from mice colonocytes was extracted using the RNeasy Plus Mini Kit (Qiagen®, Germantown, MD, United States) according to the manufacturer's protocol. After RNA extraction, reverse transcription was performed with the High Capacity cDNA RT Kit (Applied Biosystems, Foster City, CA, United States) with 500 ng of RNA, followed by a qPCR using LightCycler FastStart DNA Master SYBR Green Kit (Roche Applied Science, Penzberg, Germany). The primers used for TLRs expression analysis are described in Table 1. All results were normalized to the *HPRT* gene. Samples were tested in duplicate, and the average values were used for quantification by using  $2^{-\Delta\Delta Ct}$  method.

### **Fecal FliC and LPS load quantification**

FliC and LPS were quantified using human embryonic kidney (HEK)-Blue-mTLR5 and HEK-Blue-mTLR4 cells, respectively (Invivogen, San Diego, California, United States). Fecal material was resuspended in PBS to a final concentration of 100 mg/mL and homogenized for 10 s using a Mini-Beadbeater-24 without the addition of beads to avoid bacteria disruption. The samples were then centrifuged at 8000 g for 2 min and the resulting supernatant was serially diluted and applied to mammalian cells. Purified *Escherichia coli* FliC and LPS (Sigma, St Louis, Missouri, United States) were used for standard curve determination using HEK-Blue-mTLR5 and HEK-Blue-mTLR4 cells, respectively. After 24 h of stimulation, cell culture supernatant was applied to QUANTI-Blue medium (Invivogen, San Diego, California, United States) and alkaline phosphatase activity was measured at 620 nm after 30 min.

### **Statistical analysis**

Statistical analyses were performed with Prism 7 software (GraphPad, La Jolla, CA, United States). The Kolmogorov-Smirnov test has been used to check if data follow a normal distribution. One-way ANOVA, Kruskal-Wallis test or two-way ANOVA (more than two groups) were used for intergroup-comparisons with Tukey's, Dunn's and Dunnett's test for the post-hoc analysis. Correlation was assessed using Pearson's test. ANOSIM method followed by Monte-Carlo permutation test was performed to assess the significance of beta-diversity analysis of fecal microbiota using the QIIME. A *P* value  $\leq 0.05$  was considered statistically significant.

## **RESULTS**

### **NMS paradigm induces CHS and intestinal permeability increase in a subset of mice**

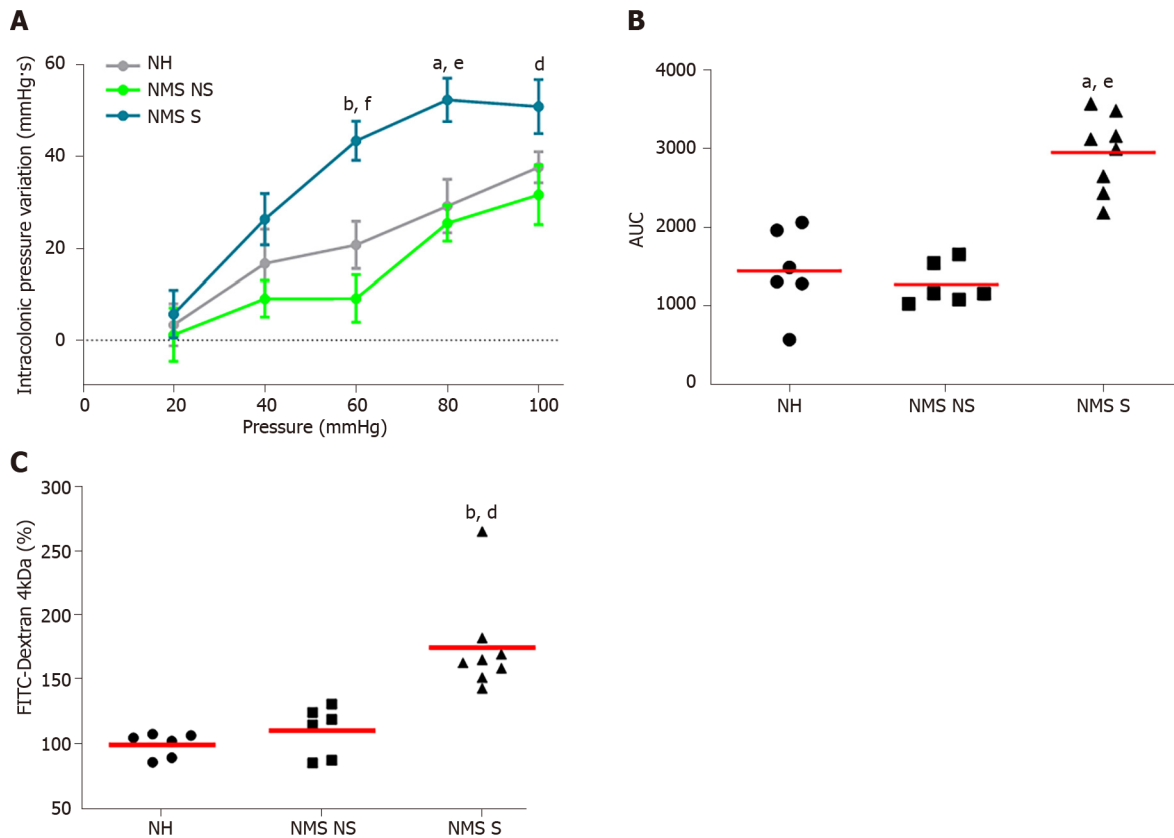
In order to evaluate colonic sensitivity, a CRD test was performed on twelve-week-old NH or NMS mice (Figure 1A). As previously described[23], among NMS mice only a subset developed CHS in comparison to NH mice. Therefore, two groups of NMS mice were defined: NMS NS and NMS S mice. In fact, colorectal distension assessment revealed significant increase of IPV for the highest distension pressures 60, 80 and 100 mmHg in the NMS S group in comparison to NMS NS and NH groups (Figure 2A). Analysis of the areas under the curve (AUC) for each mouse confirmed this significant difference between NH, NMS NS and NMS S groups (Figure 2B). Intestinal permeability assessment revealed significant increase of FITC-Dextran plasma levels in the NMS S group compared to NH and NMS NS groups (Figure 2C).

### **Fecal microbiota dysbiosis is associated with CHS in neonatal maternal separated mice**

Illumina sequencing of the 16S rRNA gene was performed on fecal pellets DNA extracts from NH, NMS NS and NMS S mice at W3, W4 and W12 (just before the CRD test) according to the time course protocol for NMS experiment (Figure 1A). Alpha-diversity analysis (number of observed OTUs) of the core fecal microbiota revealed no statistical difference between NH, NMS NS and NMS S animals at week 3, before weaning (Figure 3A-left panel). However, a significant decrease of species richness appeared at W4 in NMS S mice in comparison to NH or NMS NS animals and persisted at adulthood (W12, time point of CRD test), even if NMS NS and NMS S mice were co-housed in the same cage during all the experiment (Figure 3A-middle and right panels). In addition, a significant decrease of the observed OTUs number was present in NMS NS at adulthood (W12) in comparison to NH mice. Principal coordinates analysis based on unweighted UniFrac distances confirmed the alteration of the core fecal microbiota. It enabled to significantly (ANOSIM method followed by the Monte-Carlo permutation test, *P* < 0.05) identify the three animals' groups from W3 to W12 (Figure 3B). The taxonomic analysis of the fecal core microbiota composition in the NMS S group revealed in twelve weeks old mice a decreased relative abundance of bacteria belonging to the phylum *Bacteroidetes* and an increase in *Firmicutes* in comparison to the NMS NS group (Figure 3C). At lower taxonomic levels, NMS S mice were characterized by a decreased abundance of bacteria from the genera *Allobaculum* and *Barnesiella* compared to

Table 1 Primers used for toll-like receptors expression analysis

Gene	5'-3' Forward	5'-3' Reverse
tlr2	ACCAAGATCCAGAAGAGCCA	CATCACCGGTCAGAAAACAA
tlr3	GCGTTGCGAAGTGAAGAACT	TTCAAGAGGAGGGCGAATAA
tlr4	TTCAGAACTTCAGTGGCTGG	TGTTAGTCCAGAGAACTTCTCG
tlr5	GCAGGATCATGGCATGTCAAC	ATCTGGGTGAGGTTACAGCCT
tlr9	AACCGCCACTTCTATAACCAG	GTAAGACAGAGCAAGGCAGG
hprt	TGCTGACCTGCTGGATTA	AGTTGAGAGATCATGTCCAC



DOI: 10.3748/wjg.v28.i29.3903 Copyright ©The Author(s) 2022.

**Figure 2 Neonatal maternal separation induces colonic hypersensitivity and increases intestinal permeability in mice.** A: Intracolonic pressure variation (IPV) in response to colorectal distension in non-handled (NH), neonatal maternal separated non-sensitized (NMS NS) and neonatal maternal separated sensitized (NMS S) mice; B: Area under the curve (AUC) of the IPV relative to colorectal distension for each NH, NMS NS and NMS S mouse; C: FITC-dextran 4 kDa plasmatic concentrations, 3 h after oral gavage with 15 mg of FITC-dextran of NH, NMS NS and NMS S mice. Values are expressed as a percentage of FITC-dextran per mL of plasma in comparison to the NH group mean. NH:  $n = 6$ ; NMS NS:  $n = 6$ ; NMS S:  $n = 8$ . <sup>a</sup> $P < 0.05$  and <sup>b</sup> $P < 0.01$  vs NH group; and <sup>d</sup> $P < 0.05$ , <sup>e</sup> $P < 0.01$  and <sup>f</sup> $P < 0.001$  vs NMS NS group. For IPV to CRD test, dots represent means and error bars represent SEM. For AUC and FITC-dextran, each dot represents one mouse and red lines represent means.

control NH mice, and a decreased abundance of bacteria from the genera *Bacteroides* compared to NMS NS mice. The relative abundances of *Lachnospirillum*, *Clostridium* and *Lactobacillus* were increased in these NMS animals with CHS in comparison to NMS mice without CHS. Surprisingly, the relative abundance of *Lactobacillus* was decreased in NMS NS animals compared to NH group (Figure 3D).

#### CHS induced by NMS exposure increased fecal level of FliC and is related to TLR5 overexpression in colonocytes

To understand potential mechanisms between fecal microbiota dysbiosis and CHS induced by NMS, quantification of two different PAMPs, FliC and LPS, was performed in feces from twelve-week-old NH, NM NS and NMS S mice. Exposure to NMS paradigm increased significantly fecal level of FliC (Figure 4A) rather than fecal LPS which is not significant better between different animal (Figure 4B).

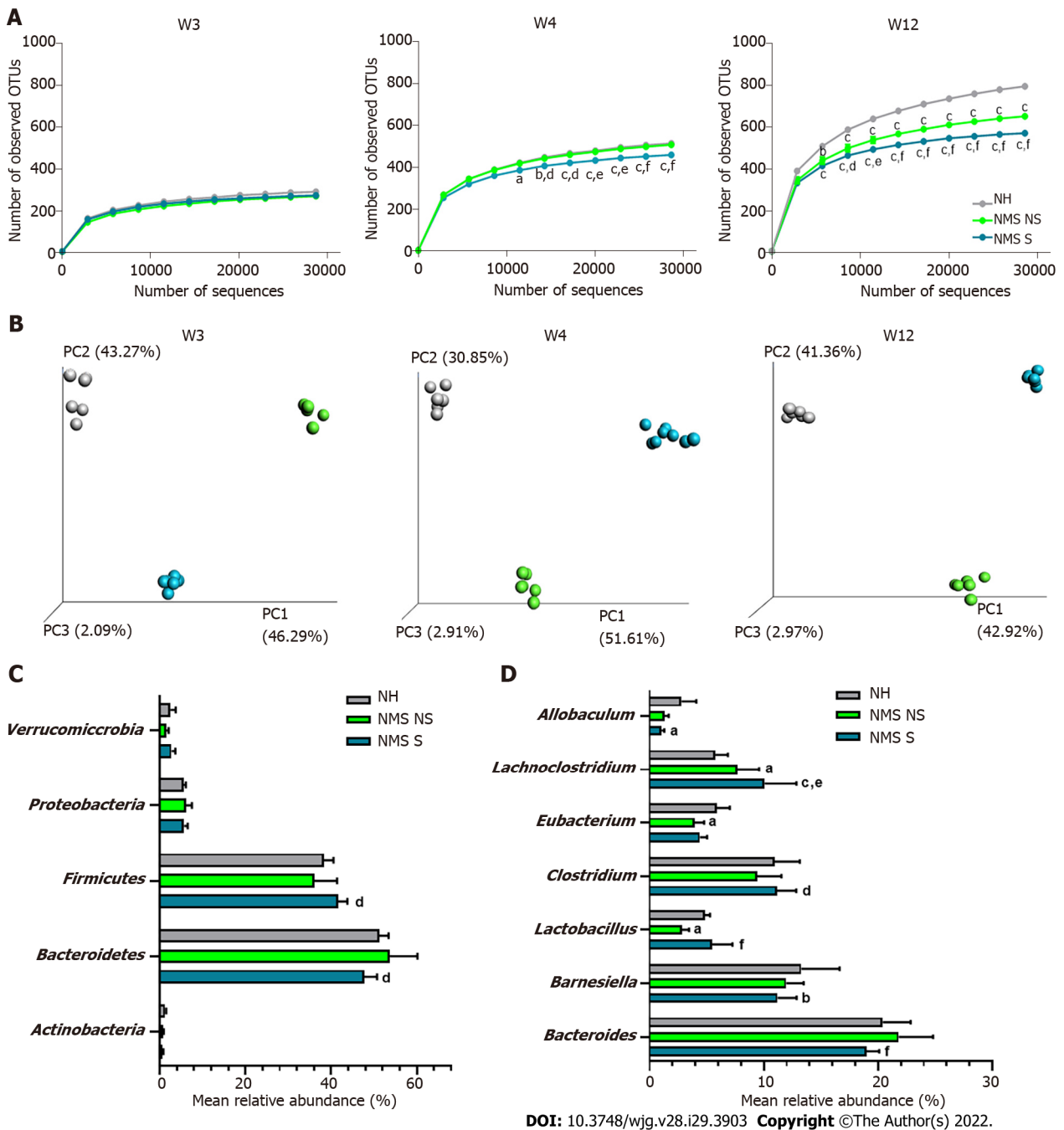
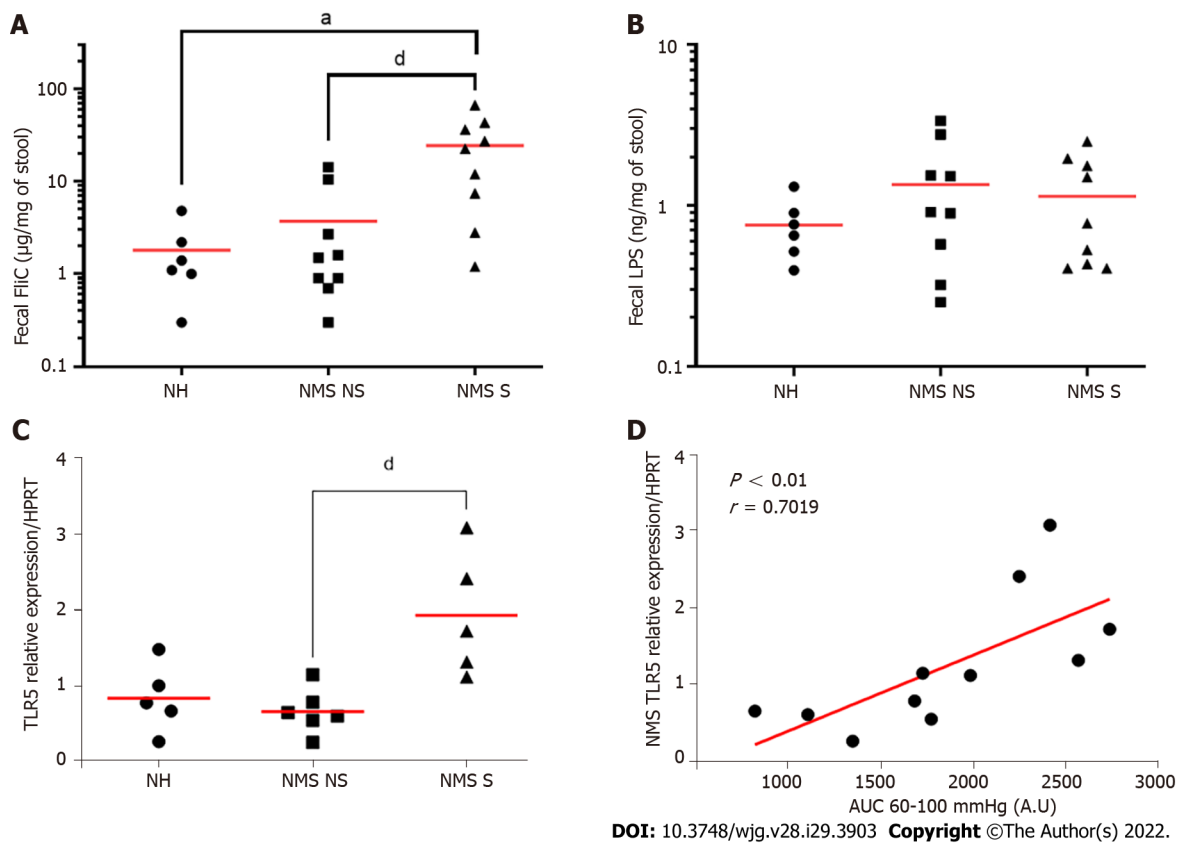


**Figure 3 Neonatal maternal separation paradigm induces alterations of core fecal microbiota related to colonic hypersensitivity.** A: Alpha-diversity analysis of the core microbiota. Number of observed operational taxonomic units according to the number of sequences per samples of fecal samples from non-handled (NH), neonatal maternal separated non-sensitized (NMS NS) and neonatal maternal separated sensitized (NMS S) mice at week 3 (W3), week 4 (W4) and week 12 (W12); B: Beta-diversity analysis of the core microbiota. Principal coordinates analysis (PCoA) of unweighted UniFrac distances of NH, NMS NS and NMS S mice at W3, W4 and W12; C and D: Mean relative abundances of bacterial phyla (C) and genera (D) significantly altered by the NMS paradigm between NH, NMS NS and NMS S mice at W12. NH:  $n = 6$ ; NMS NS:  $n = 6$ ; NMS S:  $n = 8$ .  $^aP < 0.05$ ,  $^bP < 0.01$  and  $^cP < 0.001$  vs NH or  $^dP < 0.05$ ,  $^eP < 0.01$  and  $^fP < 0.001$  vs NMS NS groups respectively. For alpha-diversity analysis, dots represent means and error bars represent SEM. For PCoA analysis each dot represents one mouse.

As TLRs are the main receptors of PAMPs, the TLRs mRNA expression in colonocytes from NH, NMS NS and NMS S mice was quantified in adult (W12) mice. As previously described, three mouse groups were defined, based on the CHS (Supplementary Figure 1A and B). In those mouse groups, the TLR2, 3, 4 and 9 mRNA were not modified between NH, NMS NS and NMS S animals (Supplementary Figure 1C), whereas TLR5 mRNA expression is significantly increased only in NMS S subgroup (NH:  $0.836 \pm 0.200$ , NMS NS:  $0.662 \pm 0.120$ , NMS S:  $1.925 \pm 0.363$ ,  $P < 0.05$  vs NMS NS) (Figure 4C). AUC corresponding to the IPV for highest colorectal distension pressures (60, 80 and 100 mmHg) significantly correlated with the mRNA expression level of TLR5 in colonocytes of NMS mice ( $P < 0.01$ ) (Figure 4D).



DOI: 10.3748/wjg.v28.i29.3903 Copyright ©The Author(s) 2022.

**Figure 4 Neonatal maternal separation induced colonic hypersensitivity is associated with increased flagellin fecal content and colonocytes toll-like receptor 5 expression.** A: Levels of fecal flagellin (FliC) assayed with toll-like receptor 5 (TLR5) reporter cells; B: Levels of fecal lipopolysaccharide assayed with TLR4 reporter cells; C: Colonocytes mRNA expression of TLR5 in non-handled (NH), neonatal maternal separated non-sensitized (NMS NS) and neonatal maternal separated sensitized (NMS S) mice at week 12. Values are expressed as relative expression of TLR5 mRNA compared to *HPRT* expression; D: Correlation between NMS colonocytes TLR5 expression and area under the curve (AUC) corresponding of the intracolonic pressure variation (IPV) for highest colorectal distension pressures (60, 80 and 100 mmHg). A and B: NH:  $n = 6$ ; NMS NS:  $n = 9$ ; NMS S:  $n = 9$ . <sup>a</sup> $P < 0.05$  vs NH group; and <sup>d</sup> $P < 0.05$  vs NMS NS group. C and D: NH:  $n = 5$ ; NMS NS:  $n = 6$ ; NMS S:  $n = 5$ . <sup>d</sup> $P < 0.05$  vs NMS NS. For FliC quantification TLR5 mRNA relative expression, each dot represents one mouse and red lines represent means and for correlation between TLR5 expression and AUC of IPV, each dot represents one mouse and red line represents the linear regression curve.

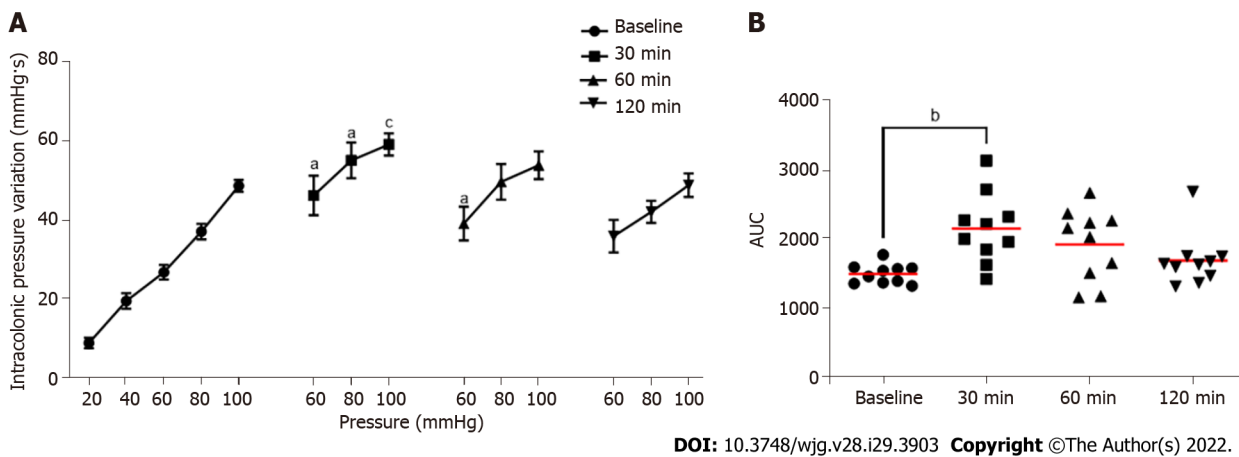
### ***FliC* intrarectal instillation is associated with a transient increase of colonic sensitivity**

Intrarectal instillation of FliC, agonist of the receptor TLR5, significantly increased IPV at the 60, 80 and 100 mmHg distension pressure 30 min and 60 min post-instillation (Figure 5A). The increase in the response to CRD test was transient and did not persist 120 min after FliC instillation. AUC confirmed this significant increase of IPV 30 min after intrarectal instillation of FliC (Figure 5B).

## **DISCUSSION**

Abdominal pain, frequently associated with CHS, has been shown to be a common feature of IBS patients. It also strongly impacts on patient's quality of life, leading to an important rate of consultation in Gastroenterology[24]. According to clinical studies, 33% to 90% of IBS patients exhibit CHS[3,25]. IBS presents a poorly first line treatment efficacy, especially regarding the treatment of abdominal pain[26]. Thus, in accordance with the aim of our study, a better characterization of mechanisms associated with CHS is important for the establishment of new potential pharmacological targets.

The etiology of this condition, resulting in various symptoms, remains unclear even if biological, psychological and social factors seem to be involved. Indeed, several studies reported an increased risk of IBS associated with early adverse life events[17,27-29]. These events refer to traumatic experience during childhood such as physical, sexual or emotional abuse as well as discordant relationship with primary caretaker. Using NMS stress animal model[30], our study demonstrates the impact of early adverse life events on colonic sensitivity of adult mice. Interestingly, only a subset of NMS mice presented CHS, revealed by CRD test, compared to control non-handled mice. These results were consistent with data obtained in previous studies carried out in both rats and mice[23,31,32].



DOI: 10.3748/wjg.v28.i29.3903 Copyright ©The Author(s) 2022.

**Figure 5 Evaluation of the impact of intrarectal instillation of flagellin on colonic sensitivity.** A: Intracolonic pressure variation (IPV) in response to colorectal distension in males mice before (Baseline) and after (30, 60 and 120 min) intrarectal instillation of flagellin (5  $\mu$ g); B: Area under the curve (AUC) of the IPV relative to highest colorectal distension pressures (60, 80 and 100 mmHg). For each mouse and each time point,  $n = 10$ . <sup>a</sup> $P < 0.05$ , <sup>b</sup> $P < 0.01$  and <sup>c</sup> $P < 0.001$  respect to Baseline. For IPV to colorectal distension test, dots represent means and error bars represent SEM. For AUC, each dot represents one mouse and red lines represent means.

Many studies reported an association between activation of the HPA axis, the major neuroendocrine system regulating various bodily processes in response to psychological or physical stressors, and intestinal permeability increase[33,34]. Furthermore, alteration of the intestinal barrier is a key clinical feature of IBS and it has been related to CHS[35]. In our study, assessment of intestinal permeability was carried out by measurement of FITC-dextran plasma level. Only NMS animals with CHS exhibited high plasmatic levels of FITC-dextran, suggesting that NMS paradigm induced CHS is associated with altered intestinal barrier. This result is in accordance with previous reports showing increased intestinal permeability following NMS paradigm or chronic stress exposure[34,36,37]. In addition, the link between the weakness of the intestinal mucosa barrier and CHS has been demonstrated in a mouse model of post-infectious IBS[20].

Consistent studies reported intestinal dysbiosis in IBS patients[6]. The main distinguishing feature of IBS patients compared to healthy volunteers is on one hand the increased abundance of bacteria belonging to the *Firmicutes* phylum and on the other hand, the decreases abundance of bacteria belongs to the *Bacteroidetes* phylum. Implication of the intestinal microbiota in CHS and associated chronic abdominal pain was also suggested[38]. In the present study, the characterization of the fecal microbiota composition using high-throughput sequencing of the 16S rRNA revealed the presence of a dysbiotic state making it possible to discriminate NH, NMS NS and NMS S mice. Indeed, the beta-diversity analyses showed that the composition of the fecal microbiota is different between NMS and NH control mice but also between NMS NS and NMS S mice while these animals came from the same litters and were co-housed. Changes in intestinal microbiota composition associated with NMS and CHS appeared very early, before weaning the animals (week 3) and persisted over time up to 12 wk. These alterations in the fecal microbiota composition were also characterized by a decreased bacterial richness in NMS S mice from week 4 to week 12. In general, this decrease was associated with a physiological disorder in the host, which seemed to be in agreement with the results obtained in this model[39]. A reduction in the bacterial diversity of the intestinal microbiota has notably been demonstrated in IBD and IBS patients but also in stress animal models[40-44]. *Clostridium* and *Lachnospirillum*, flagellated bacteria, are among the genera whose abundance was increased in NMS S mice, at W12, the time of colonic sensitivity assessment, compared to NMS mice without CHS. Studies carried out in animals subjected to stress during the neonatal period have also shown an increase in the relative abundance of the *Clostridium* genus[43,45,46]. Furthermore and interestingly, Luna et al[47] highlighted an increased relative abundance of different species of *Clostridium* and *Lachnospirillum* within the mucosa-associated microbiota in children with an autistic disorder associated with functional gastrointestinal disorders and in particular abdominal pain. These findings suggest an implication of the intestinal microbiota in the development of CHS in the NMS model.

In a dysbiotic state, particularly associated with an increase in intestinal permeability, alterations in the signature of microbial molecules sensed by the host can lead to a different activation state of the immune system[9]. Indeed, PAMPs, such as LPS or FliC, are sensed by PRRs including TLRs, which are expressed on the host cell surface or in the cytosolic compartment of numerous cell types. In this context, the aim of our study was to characterize the expression of different TLRs in colonocytes from our different animal subgroups after NMS paradigm. It is important to note that NMS paradigm is not associated with a modification of the intestinal inflammation status[23,36]. An increased TLR5 expression was observed only in animals presenting CHS after NMS paradigm, moreover, correlation

between gene expression of TLR5 and AUC from 60 to 100 mmHg (corresponding to nociceptive stimulation) in NMS mice. These findings are in line with some reports showing upregulation of TLRs in IBS patient's colonic biopsies[10-12,15]. An increased expression of some TLRs was also observed in NMS model but without association with visceral pain[11]. Few publications have indicated TLRs implication in animal pain model, especially inflammatory and neuropathic pain[48,49]. In visceral pain context, Tramullas *et al*[50] in 2014 demonstrated involvement of TLR4 in visceral sensitivity in a chronic stress model. Furthermore, Luczynski *et al*[51] demonstrated increased colonic sensitivity to colorectal distention in germ free mice, associated with an increase of TLRs expression in spinal cord. Finally, in 2018, a study published by Zhou *et al*[52] established TLR4 implication in inflammatory visceral pain in animals with high-fat diet. Following the demonstration of FliC increase in NMS S mice fecal content and the upregulation of TLR5 expression in the NMS S mouse colonocytes, the effect of FliC was assessed on visceral sensitivity in naïve animals. We highlighted a transient increase of colonic sensitivity between 30 min and 60 min after FliC intra-rectal instillation. These results are the first to demonstrate potential FliC and TLR5 involvement in CHS in a non-inflammatory IBS-like animal model. Indeed, only Das *et al*[53] have shown that TLR5 signaling mediates hypersensitivity in a model of allodynia and that sensitivity was reversed by blocking TLR5 with a specific antagonist. Moreover, Dlugosz *et al*[54] has found a significantly higher serum level of antibodies to FliC patients with IBS. Our data, associated with the results of previous studies suggest that TLR5, through its activation by FliC, could play a key role in CHS induced by dysbiosis related to the NMS paradigm and more generally, in the pathophysiology of IBS.

## CONCLUSION

In conclusion, our results demonstrated the association of fecal dysbiosis, characterized especially by an increased abundance of flagellated bacteria, with impaired intestinal permeability, increased TLR5 expression and induced CHS. Taken together, TLR5 signaling upon recognition of FliC is relevant in visceral pain through both direct and indirect mechanisms, and application of TLR5-specific antagonists could potentially reversed CHS in non-inflammatory visceral pain context[23,36].

## ARTICLE HIGHLIGHTS

### Research background

Chronic abdominal pain associated to irritable bowel syndrome (IBS) is strongly related to stress and is the most common cause for gastroenterology consultation. Brain/gut/microbiota dialogue alterations are suspected to be involved in colonic hypersensitivity (CHS), responsible for chronic abdominal pain. It is also associated with abnormal intestinal permeability and intestinal dysbiosis, which can alter colon homeostasis leading to abnormal activation of the innate immunity that promotes CHS, perhaps involving the toll-like receptors (TLRs), which play a central role in innate immunity.

### Research motivation

The breakdown of the relationship between TLRs and gut microbiota could contribute to the development of IBS. Thus, because of correlation between IBS and early life adverse events, our study investigated the impact of neonatal maternal separation (NMS) paradigm on intestinal homeostasis, fecal microbiota composition and CHS development in mice as well as the association with TLRs expression.

### Research objectives

A better characterization of mechanisms associated with CHS is important for the establishment of new potential pharmacological targets.

### Research methods

In our study, we used a referenced CHS animal model, the NMS paradigm, which mimics deleterious events in childhood that can induce a wide range of chronic disorders during adulthood. In addition, we have evaluated colonic sensitivity of NMS mice by colorectal distension (CRD) coupled with intracolonic pressure variation measurement. Fecal microbiota composition was analyzed by 16S rRNA sequencing from weaning to CRD periods. TLR mRNA expression was evaluated in colonocytes.

### Research results

This study, based on the preclinical mouse model of NMS, demonstrated that around 50% of NMS mice exhibited increased intestinal permeability and CHS associated with intestinal dysbiosis. In particular, a significant increased amount of flagellated bacteria was observed in the NMS mice with CHS. In

association, only *tlr5* mRNA expression was increased in colonocytes of NMS mice with CHS.

### Research conclusions

Taken together, our results suggest a pathophysiological continuum between intestinal dysbiosis and CHS, with a role for TLR5.

### Research perspectives

TLR5 signaling upon recognition of flagellin is relevant in visceral pain through both direct and indirect mechanisms, and application of TLR5-specific antagonists could potentially reversed CHS in non-inflammatory visceral pain context.

---

## ACKNOWLEDGEMENTS

The authors would like to acknowledge Abdelkrim Alloui (Animal facilities) for animal care.

---

## FOOTNOTES

**Author contributions:** Mallaret G and Lashermes A contributed equally to this article; Study concept and design done by Mallaret G, Lashermes A, Ardid D and Carvalho FA; Acquisition of data done by Mallaret G, Lashermes A, Barbier J, Aissouni Y, Chassaing B; Analysis and interpretation of data done by Mallaret G, Lashermes A, Chassaing B, Gewirtz AT, Ardid D and Carvalho FA; Drafting of the manuscript done by Mallaret G, Lashermes A, Meleine M, Boudieu L and Carvalho FA; Obtained funding done by Ardid D and Carvalho FA; Study supervision done by Gewirtz AT, Ardid D and Carvalho FA.

**Supported by** the Region Auvergne-Rhône-Alpes and FEDER, No. Thématiques émergentes and Pack Ambition Recherche; the French Government IDEX-ISITE Initiative, No. 16-IDEX-0001-CAP 20-25; the Ministère de la Recherche et de la Technologie, INSERM and University of Clermont Auvergne, No. UMR1071.

**Institutional animal care and use committee statement:** All experiments were performed according to the ethical guidelines set out by the International Association for the Study of Pain, complied with the European Union regulation and were approved by ethics committees: the local committees C2EA-02 of Clermont-Ferrand (approvals CE110-12 and CE111-12).

**Conflict-of-interest statement:** All authors have nothing to disclose.

**Data sharing statement:** All sequencing raw data have been deposited in European Nucleotide Archive (ENA) under accession number PRJEB50651.

**ARRIVE guidelines statement:** The authors have read the ARRIVE guidelines, and the manuscript was prepared and revised according to the ARRIVE guidelines.

**Open-Access:** This article is an open-access article that was selected by an in-house editor and fully peer-reviewed by external reviewers. It is distributed in accordance with the Creative Commons Attribution NonCommercial (CC BY-NC 4.0) license, which permits others to distribute, remix, adapt, build upon this work non-commercially, and license their derivative works on different terms, provided the original work is properly cited and the use is non-commercial. See: <https://creativecommons.org/licenses/by-nc/4.0/>

**Country/Territory of origin:** France

**ORCID number:** Geoffroy Mallaret 0000-0002-3658-3418; Amandine Lashermes 0000-0002-8241-464X; Mathieu Meleine 0000-0002-0925-087X; Ludivine Boudieu 0000-0002-4774-9313; Julie Barbier 0000-0001-7177-3236; Youssef Aissouni 0000-0002-9264-7690; Agathe Gelot 0000-0002-7884-6968; Benoit Chassaing 0000-0002-4285-769X; Andrew T Gewirtz 0000-0002-6338-7578; Denis Ardid 0000-0003-4320-7338; Frederic Antonio Carvalho 0000-0003-1592-2369.

**S-Editor:** Zhang H

**L-Editor:** A

**P-Editor:** Yu HG

---

## REFERENCES

- 1 **Kopczyńska M, Mokros Ł, Pietras T, Małecka-Panas E.** Quality of life and depression in patients with irritable bowel syndrome. *Prz Gastroenterol* 2018; **13**: 102-108 [PMID: 30002768 DOI: 10.5114/pg.2018.75819]

- 2 **Sperber AD**, Bangdiwala SI, Drossman DA, Ghoshal UC, Simren M, Tack J, Whitehead WE, Dumitrascu DL, Fang X, Fukudo S, Kellow J, Okeke E, Quigley EMM, Schmulson M, Whorwell P, Archampong T, Adibi P, Andresen V, Benninga MA, Bonaz B, Bor S, Fernandez LB, Choi SC, Corazziari ES, Francisconi C, Hani A, Lazebnik L, Lee YY, Mulak A, Rahman MM, Santos J, Setshedi M, Syam AF, Vanner S, Wong RK, Lopez-Colombo A, Costa V, Dickman R, Kanazawa M, Keshteli AH, Khatun R, Maleki I, Poitras P, Pratap N, Stefanyuk O, Thomson S, Zeevenhoooven J, Palsson OS. Worldwide Prevalence and Burden of Functional Gastrointestinal Disorders, Results of Rome Foundation Global Study. *Gastroenterology* 2021; **160**: 99-114.e3 [PMID: 32294476 DOI: 10.1053/j.gastro.2020.04.014]
- 3 **Farzaei MH**, Bahramsoltani R, Abdollahi M, Rahimi R. The Role of Visceral Hypersensitivity in Irritable Bowel Syndrome: Pharmacological Targets and Novel Treatments. *J Neurogastroenterol Motil* 2016; **22**: 558-574 [PMID: 27431236 DOI: 10.5056/jnm16001]
- 4 **Watanabe S**, Radman-Livaja M, Rando OJ, Peterson CL. A histone acetylation switch regulates H2A.Z deposition by the SWR-C remodeling enzyme. *Science* 2013; **340**: 195-199 [PMID: 23580526 DOI: 10.1126/science.1229758]
- 5 **Enck P**, Mazurak N. Dysbiosis in Functional Bowel Disorders. *Ann Nutr Metab* 2018; **72**: 296-306 [PMID: 29694952 DOI: 10.1159/000488773]
- 6 **Pittayanon R**, Lau JT, Yuan Y, Leontiadis GI, Tse F, Surette M, Moayyedi P. Gut Microbiota in Patients With Irritable Bowel Syndrome-A Systematic Review. *Gastroenterology* 2019; **157**: 97-108 [PMID: 30940523 DOI: 10.1053/j.gastro.2019.03.049]
- 7 **Jalanka-Tuovinen J**, Salonen A, Nikkilä J, Immonen O, Kekkonen R, Lahti L, Palva A, de Vos WM. Intestinal microbiota in healthy adults: temporal analysis reveals individual and common core and relation to intestinal symptoms. *PLoS One* 2011; **6**: e23035 [PMID: 21829582 DOI: 10.1371/journal.pone.0023035]
- 8 **Gewirtz AT**, Navas TA, Lyons S, Godowski PJ, Madara JL. Cutting edge: bacterial flagellin activates basolaterally expressed TLR5 to induce epithelial proinflammatory gene expression. *J Immunol* 2001; **167**: 1882-1885 [PMID: 11489966 DOI: 10.4049/jimmunol.167.4.1882]
- 9 **Levy M**, Kolodziejczyk AA, Thaiss CA, Elinav E. Dysbiosis and the immune system. *Nat Rev Immunol* 2017; **17**: 219-232 [PMID: 28260787 DOI: 10.1038/nri.2017.7]
- 10 **Brint EK**, MacSharry J, Fanning A, Shanahan F, Quigley EM. Differential expression of toll-like receptors in patients with irritable bowel syndrome. *Am J Gastroenterol* 2011; **106**: 329-336 [PMID: 21102570 DOI: 10.1038/ajg.2010.438]
- 11 **McKernan DP**, Gaszner G, Quigley EM, Cryan JF, Dinan TG. Altered peripheral toll-like receptor responses in the irritable bowel syndrome. *Aliment Pharmacol Ther* 2011; **33**: 1045-1052 [PMID: 21453321 DOI: 10.1111/j.1365-2036.2011.04624.x]
- 12 **Belmonte L**, Beutheu Youmba S, Bertiaux-Vandaële N, Antonietti M, Lecleire S, Zalar A, Gourcerol G, Leroi AM, Déchelotte P, Coëffier M, Ducrotté P. Role of toll like receptors in irritable bowel syndrome: differential mucosal immune activation according to the disease subtype. *PLoS One* 2012; **7**: e42777 [PMID: 23028414 DOI: 10.1371/journal.pone.0042777]
- 13 **Dlugosz A**, Zakikhany K, Acevedo N, D'Amato M, Lindberg G. Increased Expression of Toll-Like Receptors 4, 5, and 9 in Small Bowel Mucosa from Patients with Irritable Bowel Syndrome. *Biomed Res Int* 2017; **2017**: 9624702 [PMID: 28246611 DOI: 10.1155/2017/9624702]
- 14 **Koçak E**, Akbal E, Köklü S, Ergül B, Can M. The Colonic Tissue Levels of TLR2, TLR4 and Nitric Oxide in Patients with Irritable Bowel Syndrome. *Intern Med* 2016; **55**: 1043-1048 [PMID: 27150852 DOI: 10.2169/internalmedicine.55.5716]
- 15 **Shukla R**, Ghoshal U, Ranjan P, Ghoshal UC. Expression of Toll-like Receptors, Pro-, and Anti-inflammatory Cytokines in Relation to Gut Microbiota in Irritable Bowel Syndrome: The Evidence for Its Micro-organic Basis. *J Neurogastroenterol Motil* 2018; **24**: 628-642 [PMID: 30347939 DOI: 10.5056/jnm18130]
- 16 **McKernan DP**, Nolan A, Brint EK, O'Mahony SM, Hyland NP, Cryan JF, Dinan TG. Toll-like receptor mRNA expression is selectively increased in the colonic mucosa of two animal models relevant to irritable bowel syndrome. *PLoS One* 2009; **4**: e8226 [PMID: 20011045 DOI: 10.1371/journal.pone.0008226]
- 17 **Bradford K**, Shih W, Vidlock EJ, Presson AP, Naliboff BD, Mayer EA, Chang L. Association between early adverse life events and irritable bowel syndrome. *Clin Gastroenterol Hepatol* 2012; **10**: 385-90.e1 [PMID: 22178460 DOI: 10.1016/j.cgh.2011.12.018]
- 18 **Larauche M**, Gourcerol G, Million M, Adelson DW, Taché Y. Repeated psychological stress-induced alterations of visceral sensitivity and colonic motor functions in mice: influence of surgery and postoperative single housing on visceromotor responses. *Stress* 2010; **13**: 343-354 [PMID: 20536336 DOI: 10.3109/10253891003664166]
- 19 **Picard E**, Carvalho FA, Agosti F, Bourinet E, Ardid D, Eschalier A, Daulhac L, Mallet C. Inhibition of Ca<sub>v</sub>3.2 calcium channels: A new target for colonic hypersensitivity associated with low-grade inflammation. *Br J Pharmacol* 2019; **176**: 950-963 [PMID: 30714145 DOI: 10.1111/bph.14608]
- 20 **Lashermes A**, Boudieu L, Barbier J, Sion B, Gelot A, Barnich N, Ardid D, Carvalho FA. Adherent-Invasive E. coli enhances colonic hypersensitivity and P2X receptors expression during post-infectious period. *Gut Microbes* 2018; **9**: 26-37 [PMID: 28806140 DOI: 10.1080/19490976.2017.1361091]
- 21 **Tambuwalla MM**, Cummins EP, Lenihan CR, Kiss J, Stauch M, Scholz CC, Fraisl P, Lasitschka F, Mollenhauer M, Saunders SP, Maxwell PH, Carmeliet P, Fallon PG, Schneider M, Taylor CT. Loss of prolyl hydroxylase-1 protects against colitis through reduced epithelial cell apoptosis and increased barrier function. *Gastroenterology* 2010; **139**: 2093-2101 [PMID: 20600011 DOI: 10.1053/j.gastro.2010.06.068]
- 22 **Caporaso JG**, Bittinger K, Bushman FD, DeSantis TZ, Andersen GL, Knight R. PyNAST: a flexible tool for aligning sequences to a template alignment. *Bioinformatics* 2010; **26**: 266-267 [PMID: 19914921 DOI: 10.1093/bioinformatics/btp636]
- 23 **Meleine M**, Boudieu L, Gelot A, Muller E, Lashermes A, Matricon J, Silberberg C, Theodorou V, Eschalier A, Ardid D, Carvalho FA. Comparative effects of  $\alpha$ 2 $\delta$ -1 ligands in mouse models of colonic hypersensitivity. *World J Gastroenterol* 2016; **22**: 7111-7123 [PMID: 27610021 DOI: 10.3748/wjg.v22.i31.7111]
- 24 **Lovell RM**, Ford AC. Effect of gender on prevalence of irritable bowel syndrome in the community: systematic review and meta-analysis. *Am J Gastroenterol* 2012; **107**: 991-1000 [PMID: 22613905 DOI: 10.1038/ajg.2012.131]

- 25 **Kanazawa M**, Palsson OS, Thiwan SI, Turner MJ, van Tilburg MA, Gangarosa LM, Chitkara DK, Fukudo S, Drossman DA, Whitehead WE. Contributions of pain sensitivity and colonic motility to IBS symptom severity and predominant bowel habits. *Am J Gastroenterol* 2008; **103**: 2550-2561 [PMID: 18684175 DOI: 10.1111/j.1572-0241.2008.02066.x]
- 26 **Camilleri M**, Boeckxstaens G. Dietary and pharmacological treatment of abdominal pain in IBS. *Gut* 2017; **66**: 966-974 [PMID: 28232472 DOI: 10.1136/gutjnl-2016-313425]
- 27 **Ju T**, Naliboff BD, Shih W, Presson AP, Liu C, Gupta A, Mayer EA, Chang L. Risk and Protective Factors Related to Early Adverse Life Events in Irritable Bowel Syndrome. *J Clin Gastroenterol* 2020; **54**: 63-69 [PMID: 30575634 DOI: 10.1097/MCG.0000000000001153]
- 28 **Park SH**, Vidlock EJ, Shih W, Presson AP, Mayer EA, Chang L. Adverse childhood experiences are associated with irritable bowel syndrome and gastrointestinal symptom severity. *Neurogastroenterol Motil* 2016; **28**: 1252-1260 [PMID: 27061107 DOI: 10.1111/nmo.12826]
- 29 **Whitehead WE**, Crowell MD, Robinson JC, Heller BR, Schuster MM. Effects of stressful life events on bowel symptoms: subjects with irritable bowel syndrome compared with subjects without bowel dysfunction. *Gut* 1992; **33**: 825-830 [PMID: 1624167 DOI: 10.1136/gut.33.6.825]
- 30 **Moloney RD**, O'Mahony SM, Dinan TG, Cryan JF. Stress-induced visceral pain: toward animal models of irritable-bowel syndrome and associated comorbidities. *Front Psychiatry* 2015; **6**: 15 [PMID: 25762939 DOI: 10.3389/fpsy.2015.00015]
- 31 **Botschuijver S**, Welting O, Levin E, Maria-Ferreira D, Koch E, Montijn RC, Seppen J, Hakvoort TBM, Schuren FHJ, de Jonge WJ, van den Wijngaard RM. Reversal of visceral hypersensitivity in rat by Menthacarin®, a proprietary combination of essential oils from peppermint and caraway, coincides with mycobiome modulation. *Neurogastroenterol Motil* 2018; **30**: e13299 [PMID: 29383802 DOI: 10.1111/nmo.13299]
- 32 **Yi L**, Zhang H, Sun H, Zhou L, Chen Y, Xuan L, Jiang Y, Xu S. Maternal Separation Induced Visceral Hypersensitivity from Childhood to Adulthood. *J Neurogastroenterol Motil* 2017; **23**: 306-315 [PMID: 28238254 DOI: 10.5056/jnm16089]
- 33 **de Punder K**, Pruijboom L. Stress induces endotoxemia and low-grade inflammation by increasing barrier permeability. *Front Immunol* 2015; **6**: 223 [PMID: 26029209 DOI: 10.3389/fimmu.2015.00223]
- 34 **Kelly JR**, Kennedy PJ, Cryan JF, Dinan TG, Clarke G, Hyland NP. Breaking down the barriers: the gut microbiome, intestinal permeability and stress-related psychiatric disorders. *Front Cell Neurosci* 2015; **9**: 392 [PMID: 26528128 DOI: 10.3389/fncel.2015.00392]
- 35 **Camilleri M**, Madsen K, Spiller R, Greenwood-Van Meerveld B, Verne GN. Intestinal barrier function in health and gastrointestinal disease. *Neurogastroenterol Motil* 2012; **24**: 503-512 [PMID: 22583600 DOI: 10.1111/j.1365-2982.2012.01921.x]
- 36 **Miquel S**, Martín R, Lashermes A, Gillet M, Meleine M, Gelot A, Eschalier A, Ardid D, Bermúdez-Humarán LG, Sokol H, Thomas M, Theodorou V, Langella P, Carvalho FA. Anti-nociceptive effect of *Faecalibacterium prausnitzii* in non-inflammatory IBS-like models. *Sci Rep* 2016; **6**: 19399 [PMID: 26775847 DOI: 10.1038/srep19399]
- 37 **Rincel M**, Olier M, Minni A, Monchaux de Oliveira C, Matime Y, Gaultier E, Grit I, Helbling JC, Costa AM, Lépina Y, Moisan MP, Layé S, Ferrier L, Parnet P, Theodorou V, Darnaudéry M. Pharmacological restoration of gut barrier function in stressed neonates partially reverses long-term alterations associated with maternal separation. *Psychopharmacology (Berl)* 2019; **236**: 1583-1596 [PMID: 31147734 DOI: 10.1007/s00213-019-05252-w]
- 38 **Moloney RD**, Johnson AC, O'Mahony SM, Dinan TG, Greenwood-Van Meerveld B, Cryan JF. Stress and the Microbiota-Gut-Brain Axis in Visceral Pain: Relevance to Irritable Bowel Syndrome. *CNS Neurosci Ther* 2016; **22**: 102-117 [PMID: 26662472 DOI: 10.1111/cns.12490]
- 39 **Mosca A**, Leclerc M, Hugot JP. Gut Microbiota Diversity and Human Diseases: Should We Reintroduce Key Predators in Our Ecosystem? *Front Microbiol* 2016; **7**: 455 [PMID: 27065999 DOI: 10.3389/fmicb.2016.00455]
- 40 **Frank DN**, St Amand AL, Feldman RA, Boedeker EC, Harpaz N, Pace NR. Molecular-phylogenetic characterization of microbial community imbalances in human inflammatory bowel diseases. *Proc Natl Acad Sci U S A* 2007; **104**: 13780-13785 [PMID: 17699621 DOI: 10.1073/pnas.0706625104]
- 41 **Lepage P**, Häslér R, Spehlmann ME, Rehman A, Zvirbliene A, Begun A, Ott S, Kupcinskis L, Doré J, Raedler A, Schreiber S. Twin study indicates loss of interaction between microbiota and mucosa of patients with ulcerative colitis. *Gastroenterology* 2011; **141**: 227-236 [PMID: 21621540 DOI: 10.1053/j.gastro.2011.04.011]
- 42 **Pozuelo M**, Panda S, Santiago A, Mendez S, Accarino A, Santos J, Guarner F, Azpiroz F, Manichanh C. Reduction of butyrate- and methane-producing microorganisms in patients with Irritable Bowel Syndrome. *Sci Rep* 2015; **5**: 12693 [PMID: 26239401 DOI: 10.1038/srep12693]
- 43 **Moussaoui N**, Jacobs JP, Larauche M, Biraud M, Million M, Mayer E, Taché Y. Chronic Early-life Stress in Rat Pups Alters Basal Corticosterone, Intestinal Permeability, and Fecal Microbiota at Weaning: Influence of Sex. *J Neurogastroenterol Motil* 2017; **23**: 135-143 [PMID: 27829577 DOI: 10.5056/jnm16105]
- 44 **Tap J**, Derrien M, Törnblom H, Brazeilles R, Cools-Portier S, Doré J, Störstrud S, Le Nevé B, Öhman L, Simrén M. Identification of an Intestinal Microbiota Signature Associated With Severity of Irritable Bowel Syndrome. *Gastroenterology* 2017; **152**: 111-123.e8 [PMID: 27725146 DOI: 10.1053/j.gastro.2016.09.049]
- 45 **Zhou XY**, Li M, Li X, Long X, Zuo XL, Hou XH, Cong YZ, Li YQ. Visceral hypersensitive rats share common dysbiosis features with irritable bowel syndrome patients. *World J Gastroenterol* 2016; **22**: 5211-5227 [PMID: 27298564 DOI: 10.3748/wjg.v22.i22.5211]
- 46 **Murakami T**, Kamada K, Mizushima K, Higashimura Y, Katada K, Uchiyama K, Handa O, Takagi T, Naito Y, Itoh Y. Changes in Intestinal Motility and Gut Microbiota Composition in a Rat Stress Model. *Digestion* 2017; **95**: 55-60 [PMID: 28052282 DOI: 10.1159/000452364]
- 47 **Luna RA**, Oezguen N, Balderas M, Venkatachalam A, Runge JK, Versalovic J, Veenstra-VanderWeele J, Anderson GM, Savidge T, Williams KC. Distinct Microbiome-Neuroimmune Signatures Correlate With Functional Abdominal Pain in Children With Autism Spectrum Disorder. *Cell Mol Gastroenterol Hepatol* 2017; **3**: 218-230 [PMID: 28275689 DOI: 10.1016/j.jcmgh.2016.11.008]
- 48 **Lacagnina MJ**, Watkins LR, Grace PM. Toll-like receptors and their role in persistent pain. *Pharmacol Ther* 2018; **184**: 145-158 [PMID: 28987324 DOI: 10.1016/j.pharmthera.2017.10.006]

- 49 **Nicotra L**, Loram LC, Watkins LR, Hutchinson MR. Toll-like receptors in chronic pain. *Exp Neurol* 2012; **234**: 316-329 [PMID: 22001158 DOI: [10.1016/j.expneurol.2011.09.038](https://doi.org/10.1016/j.expneurol.2011.09.038)]
- 50 **Tramullas M**, Finger BC, Moloney RD, Golubeva AV, Moloney G, Dinan TG, Cryan JF. Toll-like receptor 4 regulates chronic stress-induced visceral pain in mice. *Biol Psychiatry* 2014; **76**: 340-348 [PMID: 24331544 DOI: [10.1016/j.biopsych.2013.11.004](https://doi.org/10.1016/j.biopsych.2013.11.004)]
- 51 **Luczynski P**, Tramullas M, Viola M, Shanahan F, Clarke G, O'Mahony S, Dinan TG, Cryan JF. Microbiota regulates visceral pain in the mouse. *Elife* 2017; **6**: e25887 [PMID: 28629511 DOI: [10.7554/eLife.25887](https://doi.org/10.7554/eLife.25887)]
- 52 **Zhou SY**, Gilliland M 3rd, Wu X, Leelasinjaroen P, Zhang G, Zhou H, Ye B, Lu Y, Owyang C. FODMAP diet modulates visceral nociception by lipopolysaccharide-mediated intestinal inflammation and barrier dysfunction. *J Clin Invest* 2018; **128**: 267-280 [PMID: 29202473 DOI: [10.1172/JCI92390](https://doi.org/10.1172/JCI92390)]
- 53 **Das N**, Dewan V, Grace PM, Gunn RJ, Tamura R, Tzarum N, Watkins LR, Wilson IA, Yin H. HMGB1 Activates Proinflammatory Signaling via TLR5 Leading to Allodynia. *Cell Rep* 2016; **17**: 1128-1140 [PMID: 27760316 DOI: [10.1016/j.celrep.2016.09.076](https://doi.org/10.1016/j.celrep.2016.09.076)]
- 54 **Dlugosz A**, Nowak P, D'Amato M, Mohammadian Kermani G, Nyström J, Abdurahman S, Lindberg G. Increased serum levels of lipopolysaccharide and anti-flagellin antibodies in patients with diarrhea-predominant irritable bowel syndrome. *Neurogastroenterol Motil* 2015; **27**: 1747-1754 [PMID: 26387872 DOI: [10.1111/nmo.12670](https://doi.org/10.1111/nmo.12670)]

## Case Control Study

# Comprehensive evaluation of microRNA as a biomarker for the diagnosis of hepatocellular carcinoma

Juliane Malik, Martin Klammer, Vinzent Rolny, Henry Lik-Yuen Chan, Teerha Piratvisuth, Tawesak Tanwandee, Satawat Thongsawat, Wattana Sukeepaisarnjaroen, Juan Ignacio Esteban, Marta Bes, Bruno Köhler, Magdalena Swiatek-de Lange

**Specialty type:** Oncology

**Provenance and peer review:**

Unsolicited article; Externally peer reviewed.

**Peer-review model:** Single blind

**Peer-review report's scientific quality classification**

Grade A (Excellent): A

Grade B (Very good): 0

Grade C (Good): C

Grade D (Fair): 0

Grade E (Poor): 0

**P-Reviewer:** Elkady N, Egypt;

Sahin TT, Turkey

**Received:** January 28, 2022

**Peer-review started:** January 28, 2022

**First decision:** April 10, 2022

**Revised:** May 20, 2022

**Accepted:** July 11, 2022

**Article in press:** July 11, 2022

**Published online:** August 7, 2022



**Juliane Malik, Martin Klammer, Vinzent Rolny, Magdalena Swiatek-de Lange**, Roche Diagnostics GmbH, Penzberg 82377, Germany

**Henry Lik-Yuen Chan**, Faculty of Medicine, The Chinese University of Hong Kong, Hong Kong 999077, China

**Teerha Piratvisuth**, NKC Institute of Gastroenterology and Hepatology, Songklanagarind Hospital, Hat Yai 90112, Thailand

**Tawesak Tanwandee**, Division of Gastroenterology, Faculty of Medicine, Siriraj Hospital, Mahidol University, Bangkok 10700, Thailand

**Satawat Thongsawat**, Department of Internal Medicine, Maharaj Nakorn Chiang Mai Hospital, Chiang Mai University, Chiang Mai 50200, Thailand

**Wattana Sukeepaisarnjaroen**, Faculty of Medicine, Srinagarind Hospital, Khon Kaen University, Khon Kaen 40000, Thailand

**Juan Ignacio Esteban**, Liver Unit, Vall d'Hebron University Hospital, Barcelona 08035, Spain

**Marta Bes**, Transfusion Safety Laboratory, Banc de Sang i Teixits, Barcelona 08005, Spain

**Bruno Köhler**, Department of Medical Oncology, National Center for Tumor Diseases, University Hospital Heidelberg, Heidelberg 69120, Germany

**Bruno Köhler**, Liver Cancer Center Heidelberg, University Hospital Heidelberg, Heidelberg 69120, Germany

**Corresponding author:** Juliane Malik, PhD, Roche Diagnostics GmbH, Nonnenwald 2, Penzberg 82377, Germany. [juliane.malik@roche.com](mailto:juliane.malik@roche.com)

## Abstract

### BACKGROUND

Hepatocellular carcinoma (HCC) is the most common type of primary liver cancer. Current guidelines for HCC management recommend surveillance of high-risk patients every 6 mo using ultrasonography. Serum biomarkers, like alpha-fetoprotein (AFP), protein induced by vitamin K absence/antagonist-II

(PIVKA-II) and lectin-reactive AFP, show suboptimal performance for detection of HCC, which is crucial for successful resection or treatment. Thus, there is a significant need for new biomarkers to aid early diagnosis of HCC. Studies have shown that the expression level of human microRNAs (miRNAs), a small, non-coding RNA species released into the blood, can serve as an early marker for various diseases, including HCC.

#### AIM

To evaluate the diagnostic role of miRNAs in HCC as single markers, signatures or in combination with known protein biomarkers.

#### METHODS

Our prospective, multicenter, case-control study recruited 660 participants (354 controls with chronic liver disease and 306 participants with HCC) and employed a strategy of initial screening by two independent methods, real-time quantitative PCR ( $n = 60$ ) and next-generation sequencing ( $n = 100$ ), to assess a large number of miRNAs. The results from the next-generation sequencing and real-time quantitative PCR screening approaches were then combined to select 26 miRNAs (including two putative novel miRNAs). Those miRNAs were analyzed for their diagnostic potential as single markers or in combination with other miRNAs or established protein biomarkers AFP and PIVKA-II *via* real-time quantitative PCR in training ( $n = 200$ ) and validation cohorts ( $n = 300$ ).

#### RESULTS

We identified 26 miRNAs that differentiated chronic liver disease controls from (early) HCC *via* two independent discovery approaches. Three miRNAs, miR-21-5p (miR-21), miR-320a and miR-186-5p, were selected by both methods. In the training cohort, only miR-21, miR-320d and miR-423 could significantly distinguish ( $Q < 0.05$ ) between the HCC and chronic liver disease control groups. In the multivariate setting, miR-21 with PIVKA-II was selected as the best combination, resulting in an area under the curve of 0.87 for diagnosis and area under the curve of 0.74 for early diagnosis of HCC. In the validation cohort, only miR-21 and miR-423 could be confirmed as potential HCC biomarkers. A combination of miRNAs did not perform better than any single miRNA. Improvement of PIVKA-II performance through combination with miRNAs could not be confirmed in the validation panel. Two putative miRs, put-miR-6 and put-miR-99, were tested in the training and validation panels, but their expression could only be detected in very few samples and at a low level (cycle threshold between 31.24 and 34.97).

#### CONCLUSION

miRNAs alone or as a signature in combination with protein biomarkers AFP and PIVKA-II do not improve the diagnostic performance of the protein biomarkers.

**Key Words:** Carcinoma; Hepatocellular; MicroRNAs; Biomarkers; Alpha-fetoprotein; Protein induced by vitamin K absence-II; Diagnosis

©The Author(s) 2022. Published by Baishideng Publishing Group Inc. All rights reserved.

**Core Tip:** Hepatocellular carcinoma (HCC) is the most common type of primary liver cancer and has a high mortality rate, making early diagnosis essential for better treatment outcomes. Studies have shown microRNAs to be early markers for HCC; we evaluated the potential diagnostic role of microRNAs alone and in combination with known protein biomarkers (alpha-fetoprotein, protein induced by vitamin K absence/antagonist-II) in samples from HCC-affected individuals and controls using real-time quantitative PCR and next-generation sequencing. MiR-21 and miR-423 demonstrated significant differential expression between the HCC and control groups. MicroRNAs alone or as a signature in combination with protein biomarkers did not improve diagnostic performance of the protein biomarkers.

**Citation:** Malik J, Klammer M, Rolny V, Chan HLY, Piratvisuth T, Tanwandee T, Thongsawat S, Sukepaisarnjaroen W, Esteban JI, Bes M, Köhler B, Swiatek-de Lange M. Comprehensive evaluation of microRNA as a biomarker for the diagnosis of hepatocellular carcinoma. *World J Gastroenterol* 2022; 28(29): 3917-3933

**URL:** <https://www.wjgnet.com/1007-9327/full/v28/i29/3917.htm>

**DOI:** <https://dx.doi.org/10.3748/wjg.v28.i29.3917>

## INTRODUCTION

According to the World Health Organization report of cancer cases worldwide, hepatocellular carcinoma (HCC) was the sixth most common cancer in terms of new cases and the fourth most common cause of cancer-related deaths in 2018[1]. HCC accounts for 85%-90% of all primary liver cancers[2], and in most cases develops in cirrhotic livers. Cirrhosis arises as a consequence of chronic liver injury and inflammation caused by viral and non-viral factors. About 70% of all HCC cases are caused by viral liver infections like hepatitis B virus (HBV) and hepatitis C virus (HCV)[3]. Approximately 80% of HCC cases occur in eastern Asia and sub-Saharan Africa, where the dominant risk factor is chronic infection with HBV and exposure to aflatoxin B1. In contrast, the main risk factors for HCC development in North America, Europe and Japan are infection with HCV or alcohol misuse, diabetes and obesity[4]. The mortality rate of HCC is high, with 5-year overall survival rates of 19.5%[5].

Limited treatment options exist for patients with HCC when diagnosed at advanced stages, so early detection is crucial to reduce mortality. If diagnosed early, treatment options such as resection, local ablation and liver transplantation are available and increase the 5-year overall survival rate for very early HCC [Barcelona-Clinic Liver Cancer (BCLC) stage 0] to 70%-90% and for early HCC (BCLC stage A) to 50%-70%. Intermediate to end-stage HCCs are unresectable and have a median survival of 16 mo for intermediate HCC (BCLC stage B), 6 mo for advanced HCC (BCLC stage C) and 3-4 mo for end-stage HCC (BCLC stage D)[6].

HCC is often asymptomatic, making its early diagnosis challenging. Major international guidelines recommend surveillance of high-risk patients [patients with severe chronic liver disease (CLD) such as chronic HBV or HCV infections, alcohol abuse or non-alcoholic steatohepatitis, leading to cirrhosis of the liver) at 6-mo intervals using abdominal ultrasound (US) with (The Asian Pacific Association for the Study of the Liver, American Association for the Study of Liver Diseases) or without (European Association for the Study of the Liver-European Organisation for Research and Treatment of Cancer) measurement of alpha-fetoprotein (AFP) levels in serum[7-9]. Japanese guidelines on HCC management propose the use of US and measurement of AFP, lectin-reactive AFP and protein induced by vitamin K absence/antagonist-II (PIVKA-II; also known as des-gamma-carboxy prothrombin) for routine follow-up in patients at high risk for developing HCC[10]. Other recommended imaging methods are computed tomography (CT) and magnetic resonance imaging; however, these are very cost-intensive, not easily accessible and have potential adverse effects like radiation exposure (CT)[6-8,11]. US use is also not without problems, as its performance is operator-dependent[12] and is limited in the setting of non-alcoholic steatohepatitis[13]. Adjunctive use of AFP may improve HCC detection rates. Although it has limited sensitivity for early-stage HCC, its addition to US improved sensitivity from 45% to 63% ( $P = 0.002$ )[11,14]. PIVKA-II is more sensitive but less specific than AFP for diagnosis of HCC in patients affected by chronic HCV infection[15]. Thus, there is a great need for new, non-invasive diagnostic tools to improve the detection of early HCC and eliminate operator-dependent variability.

MicroRNAs (miRNAs) are small (approximately 22 nucleotides), non-coding RNA molecules that post-transcriptionally modify gene regulation by base-pairing to mRNA[16]. The target mRNA is then either degraded (complementary or near-perfect complementary binding) or the translation is inhibited (partial complementarity), thus inhibiting protein expression[17].

In the cancer research field, the role of miRNAs has been discussed extensively. In the context of human cancers, miRNAs are associated with cell proliferation, genomic instability, tissue invasion, metastasis, angiogenesis, evasion of apoptosis and immune response. They can also act as oncogenes or tumor suppressor genes[18]. Clinical applications of miRNAs have been studied in various malignant tumors, such as lung, breast and prostate cancers[19]. Primarily, miRNAs from serum and plasma are of particular interest for diagnosis of cancer and the study of disease prognosis. The main advantage of miRNA-based diagnosis is the high stability of these molecules in blood and other biological fluids that can be easily sampled[20-22].

In HCC, the role of miRNAs for diagnosis and therapy has been exhaustively analyzed, although with contradictory results[23]. The expression of several miRNAs in different HCC tumor tissue samples was both elevated and decreased compared with a control group (non-tumorous tissue) in different studies[24]. Additionally, numerous circulating miRNA candidates or signatures composed of several miRNAs have been published as biomarker candidates for HCC (*e.g.*, hsa-miR-206, hsa-miR-141-3p and hsa-miR-433-3p)[25]. In some cases, both increases and decreases in the expression of the same miRNA (*e.g.*, hsa-miR-143, hsa-miR-155, hsa-miR-195) have been reported[26]. While previous studies have given some indication that miRNAs may be useful biomarkers for HCC, no miRNA has been found as a reliable biomarker in the diagnosis of early-stage HCC. To date, studied cohorts have been small, or control cohorts contained only one group of patients with a disease having a high risk for HCC [27], only healthy individuals[28] or did not include patients with early HCC[29]. A large cohort is necessary to obtain statistically significant results[30], and an HCC biomarker should show high sensitivity and specificity in patients at risk for HCC (including those with HBV, HCV and cirrhosis).

The aim of this study was to identify and clinically validate potential miRNAs for the early detection of HCC in human plasma samples through a comprehensive, prospective, multicenter, case-control study. To this end, a large cohort including 660 HCC (early and late stage) and CLD patients was studied. The potential improvement of the diagnostic performance of already established protein

biomarkers for HCC (AFP and PIVKA-II) in combination with miRNA biomarkers was also assessed.

## MATERIALS AND METHODS

### **Patient sample collection**

Between 2014 and 2016, EDTA-plasma samples from 354 CLD controls, including HBV and HCV with and without cirrhosis, and 306 HCC (early and late stage) patients were provided by the following institutions: Maharaj Nakorn Chiang Mai Hospital, Chiang Mai, Thailand; Siriraj Hospital, Bangkok, Thailand; Songklanagarind Hospital, Hat Yai, Thailand; Srinagarind Hospital, Khon Kaen, Thailand; Prince of Wales Hospital, Shatin, Hong Kong; NCT University Hospital Heidelberg, Heidelberg, Germany; and Vall d'Hebron University Hospital, Barcelona, Spain. Full inclusion and exclusion criteria have been previously described[31].

Written informed consent was obtained from all participants. The study was conducted in full conformance with the principles of the Declaration of Helsinki and with approval of independent ethics committees. Plasma samples were collected before treatment (surgery, percutaneous ethanol injection, chemotherapy, radiotherapy) according to the appropriate standard operating procedures and stored at -70 °C until analysis. Repeated freeze-thaw cycles were avoided. HCC diagnosis was verified using imaging (ultrasonography, CT, magnetic resonance imaging) or biopsy, followed by histopathological analysis.

### **Description and clinical data of patients**

The demographic and clinical characteristics of the study participants are presented in **Supplementary Table 1**. All diagnosed HCC cases were classified according to BCLC guidelines upon sample collection. Early-stage HCC was defined as BCLC 0 and A and late-stage HCC as BCLC B, C and D. CLD controls were individuals with HBV or HCV with or without cirrhosis. Some patients had additional underlying diseases, which were not considered when distributing them into the four groups. All clinical data, including the patients' diagnoses, were blinded to laboratory operators to avoid measurement bias.

### **Study design**

CLD and HCC patient samples were randomly distributed into four panels: a screening panel for real-time quantitative (RT-q) PCR ( $n = 60$ ), a screening panel for next-generation sequencing (NGS) ( $n = 100$ ), a training panel ( $n = 200$ ) and a validation panel ( $n = 300$ ) (**Supplementary Table 1**). Comparisons were made for: (1) All HCC (early + late stages) *vs* controls (HBV and HCV, with and without cirrhosis); (2) Early HCC *vs* controls; and (3) Early HCC *vs* cirrhosis (**Figure 1**).

### **miRNA isolation**

The following methods for miRNA isolation from plasma were validated: TaqMan miRNA ABC Purification Kit, mirVana PARIS Kit (both LifeTechnologies, Carlsbad, CA, United States) and the miRCURY RNA Isolation Kit-Biofluids (Exiqon, Vedbaek, Denmark). The best performance for the isolation of small RNA was found using the last method; therefore, all isolation experiments were performed using the miRCURY RNA Isolation Kit-Biofluids. The starting material was 250  $\mu$ L of EDTA-plasma per patient. Handling was according to the manufacturer's protocol with the following adaption: after adding the protein precipitation solution and subsequent centrifugation, only 200  $\mu$ L of supernatant was transferred into a new tube; the remaining volume was discarded. For quality control, spike-ins UniSp2, UniSp4 and UniSp5 from the miRCURY Universal RT microRNA PCR, RNA Spike-in kit (Exiqon) were added to all samples prior to isolation. Isolated small RNA (including miRNA) was stored at -80 °C until analysis.

### **NGS**

NGS of miRNAs from EDTA-plasma samples was performed by Exiqon. Briefly, RNA was isolated following quality control by RT-qPCR. Next, the miRNA library was prepared, followed by quality control *via* RT-qPCR and bioanalyzer. Finally, miRNAs were sequenced on a Nextseq500 (Illumina, San Diego, CA, United States) with 10 million reads per sample and 50 nucleotide single-end read. The annotation reference used was miRBase 20 (<http://mirbase.org/>). In the following data analyses, the reads were mapped and classified based on their sequence as: (1) Known miRNA; (2) Predicted (putative) miRNA; (3) Outmapped; (4) Unmapped; (5) Genome; and (6) Small RNA. In the NGS report from Exiqon, putative miRNAs were described as miRNAs predicted from the sequences that do not map to any organism found in miRBase or to other known RNA sequences. miRPara was used to analyze the potential folding of these sequences[32]. These results were combined to identify putative novel miRNAs. The differential expression analyses were done using the trimmed mean of *M*-value normalization method in the EdgeR statistical software package.

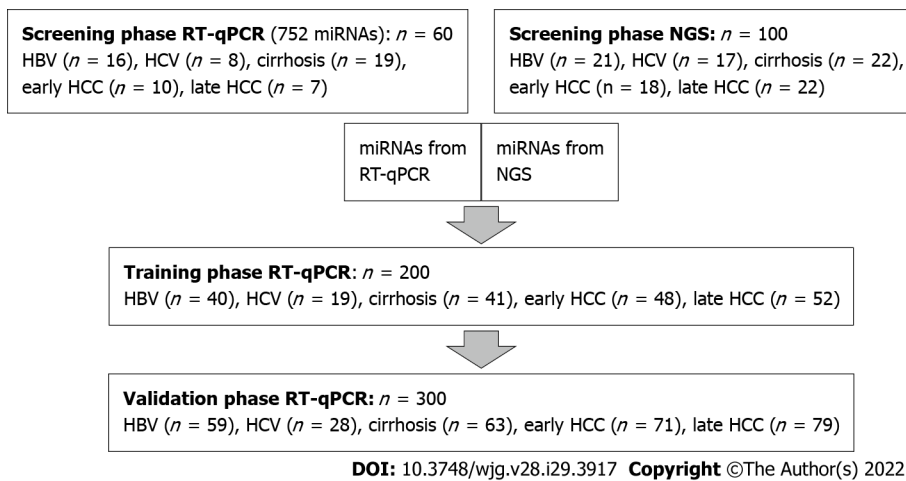


**Figure 1 Overview of study design.** HBV: Hepatitis B virus; HCC: Hepatocellular carcinoma; HCV: Hepatitis C virus; miRNA: Micro ribonucleic acid; NGS: Next-generation sequencing; RT-qPCR: Real-time quantitative PCR.

### Putative miRNA primer design

For the evaluation of the putative miRNA (put-miRs), the following RT-qPCR primers were designed using the Exiqon tool for primer design: put-miR-25, put-miR-46, put-miR-56, put-miR-66, put-miR-79, put-miR-99, put-miR-83, put-miR-86, put-miR-91, put-miR-100, put-miR-118 and put-miR-128. Three primer sets for each put-miR were tested in the three EDTA-plasma samples that had shown the highest expression for the respective put-miR in NGS. The put-miRs that showed a cycle threshold (Ct) lower than 35 were selected for clinical validation. The primer set with the lowest Ct of all three primer sets was used for the following RT-qPCR analyses. Details on the put-miRs and their corresponding chromosome location, chromosome strand, start and stop position, sequence and primer design-IDs from Exiqon can be found in the Supplementary materials (Supplementary Table 2).

### Reverse transcription and RT-qPCR

Reverse transcription and RT-qPCR were carried out using the Universal complementary DNA synthesis kit II for reverse transcription and the ExiLent SYBR Green master mix kit for RT-qPCR (Exiqon) according to the manufacturer's protocol. For quality control, spike-ins UniSp6 and cel-miR-39-3p from the miRCURY LNA Universal RT microRNA PCR, RNA Spike-in kit were added to all samples prior to reverse transcription. RT-qPCR analysis was performed for: (1) Individual miRNA primer sets; (2) Commercially available predefined ready-to-use panels: Human miRNome panel I and II, V4 which included primers for 752 known miRNAs; and (3) Customized ready-to-use panels [all primer sets and panels from miRCURY LNA Universal RT microRNA PCR Biofluids (Exiqon)]. RT-qPCR was performed on a LightCycler® 480 (Roche Diagnostics International Ltd, Rotkreuz, Switzerland). The following modifications to the manufacturer's protocol were made: (1) In both customized and predefined ready-to-use panels the amount of complementary DNA was doubled; and (2) After adding the PCR mastermix-complementary DNA mix to each well and centrifuging the plate, the reagents in the plate were mixed on a shaker for 20 s and then centrifuged again.

### Normalization and miRNA expression

Pre-processing of RT-qPCR data from the ready-to-use and customized panels was done using GenEx (MultiD Analyses AB, Gothenburg, Sweden) following the Exiqon Data Analysis Guide for the miRCURY LNA Universal RT microRNA Ready-to-Use PCR panels, V3. All Ct values < 35 were considered valid and included in further analyses. Normalization was done by applying the global mean (Human miRNome panel I and II, V4) or by normalizing to the expression of reference genes (customized panels). When conducting RT-qPCR analysis with only a small number of miRNAs, global mean normalization was not applicable. Therefore, a normalization to endogenous control miRNAs that show equal expression throughout all sample groups was necessary. Reference genes for normalization of customized panels were selected with GenEx NormFinder software by comparing their standard deviation (SD) and accumulated SD ( $\text{accumulated SD} = \frac{1}{n} \sqrt{\sum_{i=1}^n SD_i^2}$ ). Relative miRNA expression was calculated using a  $2^{-\Delta\Delta Ct}$  method.

### Serum protein assays measurements

AFP and PIVKA-II were measured using microchip capillary electrophoresis and a liquid-phase binding assay on the uTASWako i30 automated analyzer (Fujifilm Wako Pure Chemical Industries, Osaka, Japan).

### **Biostatistical analyses**

The statistical methods and analyses of this study were performed and reviewed by biostatisticians Dr. Martin Klammer and Vinzent Rolny of Roche Diagnostics GmbH.

### **Univariate analysis**

For each miRNA, two-sample Wilcoxon rank-sum testing was performed, and the *P* value was reported. Subsequently, the *P* values were corrected by means of Benjamini-Hochberg false discovery rate correction to account for multiple hypothesis testing (referred to as 'Q-values' in the tables).

In the initial global discovery of differentially expressed miRNAs, the raw *P* values (without false discovery rate correction) were used. Here, a higher false-positive rate was deliberately accepted for the sake of minimizing the risk of missing a potential biomarker candidate (*i.e.*, minimizing the false-negative rate).

### **Multivariate analysis**

To discover the optimal bivariate biomarker combination and reliably estimate its performance in future samples, a two-tier cross-validation workflow employing logistic regression was established. In the first (outer) tier with 200 Monte-Carlo cross-validation runs, the data set was randomly split into training and test set (80% and 20%, respectively) in each run, while maintaining the ratio of cases and controls. The optimal feature combination was then searched for in the second (inner) tier with five-fold cross-validation, where the training data were again split into an inner training and an inner test set. All possible two-marker combinations (exhaustive search) were then assessed by training a logistic regression model on the inner training data containing only information of the respective two markers (inner selected training data) and testing their performances by means of area under the curve (AUC) of the receiver operating characteristics curve with the respective inner test set (inner selected test data). The combination showing the best inner cross-validation results (*i.e.*, maximum mean AUC across the five cross-validation runs) was then selected and used to train a model in the outer tier. As with the inner tier, logistic regression was used, and the performance of the test set (selected test data) for each of the 200 Monte-Carlo cross-validation runs was then assessed; the mean AUC represented the estimated overall performance.

Since the feature selection procedure was part of the outer cross-validation tier, it was possible that different marker pairs were selected in the 200 Monte-Carlo cross-validation runs. However, it was necessary to select the one pair that would be used to train a model to predict future samples. This was achieved by subjecting the entire data set to the inner cross-validation tier (not only the training data, as was done for the performance evaluation) and receiving the final biomarker pair, which was subsequently used to train the final logistic regression model on the entire data set (Figure 2).

In the case of searching for a miRNA that best complements the protein marker (AFP or PIVKA-II), the protein marker itself was fixed as first feature in the feature selection process, and the optimal partner was determined as described above.

## **RESULTS**

### **Analysis of differentially expressed miRNAs yielded 26 potential biomarker candidates**

To find a suitable biomarker for the (early) diagnosis of HCC, a large number of miRNAs were screened, using two independent methods: RT-qPCR (752 predefined miRNAs) and NGS (resulting in 244 miRNAs). We analyzed whether miRNAs were differentially expressed between a group with (early stage) HCC and a control group with CLD (including patients with hepatitis B, hepatitis C and cirrhosis). The miRNAs identified in the screening were then analyzed as potential biomarkers for (early) diagnosis of HCC in an independent training panel using RT-qPCR and validated in an independent panel.

### **Global miRNome analysis of miRNAs by NGS and human miRNA panels**

Compared with RT-qPCR, NGS can identify all known and unknown miRNAs. First, miRNA was isolated from the plasma of 60 patients from the CLD control group (HBV, HCV and cirrhosis; see Supplementary Table 1) and 40 patients from the HCC groups (early and late stages), followed by a quality control *via* RT-qPCR. Six control samples did not pass the quality control and were excluded from NGS. Illumina Nextseq500 sequencing of the prepared library produced an average of 10.9 million accepted reads per sample. After data analysis, two additional outlier control samples were identified and excluded from further analysis. The miRNA expression was compared for the following groups: all HCC *vs* CLD and early HCC *vs* CLD, for known and unknown miRNAs, respectively (Supplementary Table 3). The 13 miRNAs with the smallest *P* value, highest AUC and largest fold change (approximately 1.2 or higher) were selected for validation *via* RT-qPCR (Table 1).

In the second discovery approach, RT-qPCR panels of preassigned assays for 752 known human miRNAs were applied for the screening of miRNA expression. miRNAs were investigated in the

**Table 1** Overview of the 26 selected known and putative microRNA candidates from next-generation sequencing and real-time quantitative PCR

Known miRNA	Fold change	AUC	P value (Wilcoxon)	Method	Comparison		
hsa-miR-185-5p	2.01	0.77	0.000099 <sup>c</sup>	NGS	All HCC <i>vs</i> CLD		
hsa-miR-320a <sup>1</sup>	1.52	0.74	0.000335 <sup>c</sup>				
hsa-miR-423-5p	-1.22	0.69	0.004126 <sup>b</sup>				
hsa-miR-664a-5p	1.38	0.69	0.005695 <sup>b</sup>				
hsa-miR-203a	-2.73	0.67	0.01167 <sup>a</sup>				
hsa-miR-320d	2.56	0.66	0.017151 <sup>a</sup>				
hsa-miR-21-5p <sup>1</sup>	1.34	0.66	0.020486 <sup>a</sup>				
hsa-miR-28-5p	-1.65	0.80	0.0004 <sup>c</sup>			RT-qPCR	Early HCC <i>vs</i> CLD
hsa-miR-21-5p <sup>1</sup>	1.59	0.79	0.0006 <sup>c</sup>				
hsa-miR-103a-3p	-1.65	0.78	0.012 <sup>a</sup>				
hsa-miR-301a-3p	-1.50	0.78	0.013 <sup>a</sup>				
hsa-miR-30b-5p	-1.63	0.75	0.0033 <sup>b</sup>				
hsa-miR-495-3p	-1.50	0.73	0.0068 <sup>b</sup>				
hsa-miR-320a <sup>1</sup>	1.37	0.72	0.0093 <sup>b</sup>				
hsa-miR-30a-3p	-1.60	0.72	0.008145 <sup>b</sup>				
hsa-miR-25-3p	1.75	0.71	0.01019 <sup>a</sup>				
hsa-miR-7706	1.67	0.69	0.02002 <sup>a</sup>				
hsa-miR-186-5p <sup>1</sup>	1.68	0.68	0.02364 <sup>a</sup>				
hsa-miR-15b-5p	4.21	0.97	< 0.0001 <sup>c</sup>				
hsa-miR-339-3p	-2.73	0.87	0.0006 <sup>c</sup>				
hsa-miR-10b-5p	2.81	0.86	0.0007 <sup>c</sup>				
hsa-miR-151a-5p	-2.25	0.85	0.0011 <sup>b</sup>				
hsa-miR-652-3p	-2.22	0.85	0.001 <sup>b</sup>				
hsa-miR-32-5p	2.03	0.85	0.001 <sup>b</sup>				
hsa-miR-221-3p	-2.96	0.83	0.0021 <sup>b</sup>				
hsa-miR-486-5p	2.43	0.82	0.0034 <sup>b</sup>				
hsa-miR-186-5p <sup>1</sup>	1.46	0.75	0.0215 <sup>a</sup>				
Putative miRNA	Fold change	AUC	P value (Wilcoxon)	Method	Comparison		
put-miR-6	3.63	0.68	0.001956 <sup>b</sup>	NGS	All HCC <i>vs</i> CLD		
put-miR-99	1.83	0.6	0.188			RT-qPCR	Early HCC <i>vs</i> CLD

<sup>1</sup>MicroRNAs detected in both next-generation sequencing and real-time quantitative PCR.

<sup>a</sup> $P < 0.05$ .

<sup>b</sup> $P < 0.01$ .

<sup>c</sup> $P < 0.001$ .

AUC: Area under the curve; CLD: Chronic liver disease; HCC: Hepatocellular carcinoma; miRNA: MicroRNA; NGS: Next-generation sequencing; RT-qPCR: Real-time quantitative PCR; miR: MicroRNA; put-miR: Putative microRNA.

independent sample panel ( $n = 60$ , see [Supplementary Table 1](#)). After global mean normalization, the miRNA expression was compared between the following groups: (1) All HCC *vs* CLD; and (2) Early HCC *vs* CLD ([Supplementary Table 4](#)). The 16 miRNAs with the smallest  $P$  value, highest AUC and largest fold change were selected for further analysis *via* RT-qPCR ([Table 1](#)). The AUCs and fold changes for the comparison of early HCC *vs* CLD were generally higher than the AUCs and fold changes when comparing all HCC *vs* CLD. Twenty-six miRNAs with the highest AUCs and fold changes, resulting from both discovery methods, were selected for further evaluation. Three miRNAs,

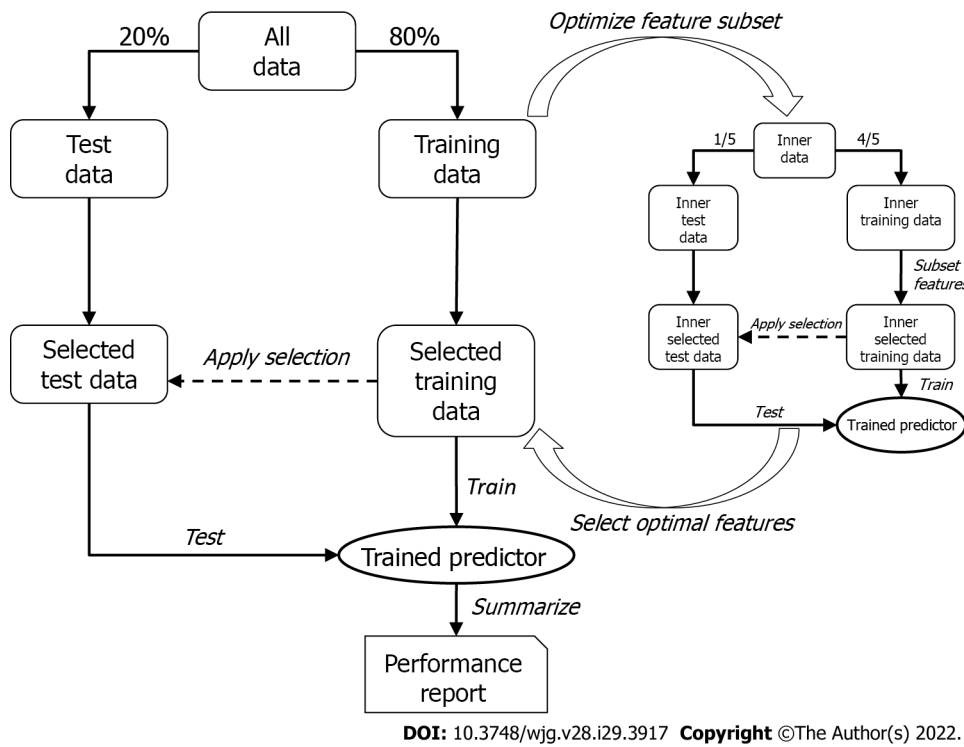


Figure 2 Overview of the two-tier cross-validation workflow employing logistic regression.

hsa-miR-320a (miR-320a), hsa-miR-421 (miR-421) and hsa-miR-21-5p (miR-21-5p), were identified by both independent methods (Supplementary Table 3).

**Selection of five endogenous control miRNAs for normalization**

The 26 selected miRNAs were then analyzed by RT-qPCR in an independent sample panel. As the number of examined miRNAs was very small, the normalization could not be based on the global mean value, which was used for the screening. To select endogenous miRNAs that could be used for normalization, GenEx software (MultiD) was used. Five miRNAs with the lowest SD and SDacc, hsa-let-7i-5p, hsa-miR-222-3p, hsa-miR-23a-3p, hsa-miR-30e-5p and hsa-miR-191-5p, were selected as endogenous controls for normalization (Table 2).

**Putative miRNA primer selection**

During NGS, sequences that could be potential miRNAs based on their length and structure were identified (= put-miR; Supplementary Table 2). Some showed different expression between the all/early-stage HCC and CLD groups. The 15 potential miRNAs with the smallest P values, highest AUCs and largest fold changes detected in the NGS were validated by RT-qPCR in an independent sample panel. For all 15 put-miRs identified, the three plasma samples with the highest expression of the respective put-miR in the NGS were selected, and RNA was isolated with the miRCURY isolation kit and subject to RT-qPCR analysis. In the RT-qPCR, two put-miRs (put-miR-6 and put-miR-99) reached Cts below the cut-off of 35, and their best primer pairs showed a mean Ct of 33.54 (put-miR-6) and 34.17 (put-miR-99). The remaining 13 put-miRs showed no expression. Put-miR-6 and put-miR-99 were further analyzed in the training and validation cohorts (Table 1).

**RT-qPCR analysis of training cohort: univariate analysis**

The 26 (24 known and 2 putative) miRNAs showing the best diagnostic performance and expression fold change in the NGS and RT-qPCR analysis (Table 1) were further validated by RT-qPCR in two independent sample panels: training cohort (200 samples) and validation cohort (300 samples). From the 24 previously selected known miRNAs, only three candidates (miR-21-5p, miR-320a and miR-186-5p) revealed themselves as potential biomarkers through both NGS and RT-qPCR analysis. miRNAs were analyzed alone (univariate) and as a combination of several miRNAs (signature, multivariate). miRNAs were also combined with known protein markers PIVKA-II and AFP (multivariate).

The training cohort consisted of the following plasma samples: HCC group (48 early stage and 52 late stage) and control group (100 HCV and HBV patients with and without cirrhosis). When comparing all HCC vs CLD controls in a univariate analysis, three miRNAs, namely miR-21-5p, hsa-miR-320d (miR-320d) and hsa-miR-423-5p (miR-423), could significantly distinguish ( $Q < 0.05$ ) between those two groups (Table 3, Supplementary Figure 1).

**Table 2 Individual standard deviation and accumulated standard deviation for consecutive microRNA reference genes**

miRNA	SD	SD <sub>acc</sub>
hsa-let-7i-5p	0.49	0.49
hsa-miR-222-3p	0.57	0.37
hsa-miR-23a-3p	0.63	0.33
hsa-miR-30e-5p	0.65	0.29
hsa-miR-191-5p	0.79	0.28

The lower the standard deviation/accumulated standard deviation, the more applicable microRNA/microRNA combination was as reference gene. These miRNAs were used as endogenous controls for the normalization of real-time quantitative PCR data. SD: Standard deviation; SD<sub>acc</sub>: Accumulated standard deviation; miRNA: MicroRNA; miR: MicroRNA.

For the comparison of early HCC *vs* CLD, none of the 26 miRNAs could significantly distinguish between early HCC and the control group. After a refined analysis of the control groups, hsa-miR-652-3p (miR-652) demonstrated itself to be a marker significantly distinguishing early HCC from the cirrhosis group (mixed HBV and HCV) (Table 3, Supplementary Figure 1).

#### **RT-qPCR analysis of training cohort: multivariate analysis and combination with protein biomarkers**

A combination of several miRNAs did not perform better than the single miRNAs (data not shown). MiRNA marker candidates from the univariate analysis of all HCC *vs* CLD were then combined with the protein marker PIVKA-II, which is a widely used marker for HCC[33]. As a result, two-tier cross-validation workflow (see Methods for details) was established, which employed logistic regression and combined two features (PIVKA-II and one of the 26 miRNAs) repeatedly to investigate the potential improvement of the diagnostic performance of PIVKA-II alone. The combined approach resulted in a higher AUC and specificity at 90% sensitivity than PIVKA-II or miR-21-5p alone (Table 4, Supplementary Figure 2A). miR-21-5p was selected as the best PIVKA-II partner in 86% of the cross-validation runs (Table 5), and PIVKA-II + miR-21-5p was selected as the final biomarker pair.

In the next step, the specificity of the combined approach was tested for early HCC *vs* CLD. The three best partners for PIVKA-II were miR-21-5p in 60%, miR-320d in 18% and miR-652 in 16% of the cross-validation runs (Table 5, Supplementary Figure 2B), and PIVKA-II + miR-21-5p was selected as the final biomarker pair.

For the differentiation between early HCC and cirrhotic control patients, the AUC and specificity at 90% sensitivity of the combination PIVKA-II with miRNAs was higher than for single markers (Table 4, Supplementary Figure 2C). The two best miRNA partners for PIVKA-II were miR-652 in 64% and hsa-miR-221 in 26% of the cross-validation runs (Table 5), and PIVKA-II + miR-652 was selected as the final biomarker pair.

The multivariate analyses of the miRNA marker candidates combined with protein marker AFP did not show any improvement in diagnostic performance (Supplementary Figure 3).

#### **RT-qPCR analysis of validation cohort: univariate analysis**

The validation cohort consisted of the following plasma samples: all HCC group (71 early stage and 79 late stage) and CLD control group [63 cirrhosis (HBV, HCV), 59 HBV and 28 HCV]. When comparing all HCC *vs* CLD, miR-21-5p and miR-423 were confirmed as possible biomarker candidates for the diagnosis of HCC. The performance of miR-21-5p was slightly worse in the validation cohort compared with the training cohort; miR-423 performance remained almost unchanged. The results from the training cohort for miR-320d could not be confirmed (Table 6, Supplementary Figure 4).

For the comparison of early HCC *vs* CLD with cirrhosis, miR-652 could not be confirmed as a possible biomarker, as seen in the training cohort (Table 6, Supplementary Figure 4).

#### **RT-qPCR analysis of validation cohort: multivariate analysis and combination with protein biomarkers**

As no combination of miRNAs could be identified in the training analysis, only PIVKA-II + miRNA combinations were validated here. However, the performance of PIVKA-II as a single marker could not be improved through combination with miRNAs selected in the training cohort for all data sets (Figure 3).

#### **No confirmation of put-miRs as potential biomarkers for HCC**

Put-miRs (put-miR-6 and put-miR-99) were tested in the training and validation panels. Put-miR-6 could only be detected in 2 samples, with a Ct of 31.24 in 1 of 200 samples in the training panel and a Ct of 34.00 in 1 of 300 samples in the validation panel. Put-miR-99 Cts between 34.00 and 34.97 (mean value

**Table 3 Univariate analysis of real-time quantitative PCR results for comparison**

miRNA	Wilcoxon Q-value	AUC	Specificity at 90% sensitivity
All HCC <i>vs</i> CLD			
hsa-miR-21-5p	0.000003 <sup>a</sup>	0.71	0.24
hsa-miR-320d	0.010872 <sup>b</sup>	0.63	0.25
hsa-miR-423-5p	0.046214 <sup>b</sup>	0.61	0.26
hsa-miR-221-3p	0.099403	0.60	0.27
hsa-miR-320a	0.109399	0.60	0.28
hsa-miR-339-3p	0.154338	0.58	0.29
hsa-miR-301a-3p	0.160690	0.57	0.30
hsa-miR-652-3p	0.160690	0.56	0.31
hsa-miR-30b-5p	0.160690	0.56	0.32
hsa-miR-25-3p	0.186436	0.57	0.33
Early HCC <i>vs</i> CLD			
hsa-miR-21-5p	0.113812	0.64	0.20
hsa-miR-320d	0.302365	0.61	0.16
hsa-miR-652-3p	0.382238	0.60	0.23
hsa-miR-320a	0.432100	0.58	0.01
hsa-miR-423-5p	0.432100	0.56	0.06
hsa-miR-301a-3p	0.432100	0.57	0.09
hsa-miR-15b-5p	0.432100	0.57	0.07
hsa-miR-186-5p	0.432100	0.57	0.15
hsa-miR-221-3p	0.432100	0.56	0.24
hsa-miR-25-3p	0.432100	0.56	0.15
Early HCC <i>vs</i> cirrhosis			
hsa-miR-652-3p	0.038792 <sup>b</sup>	0.69	0.34
hsa-miR-221-3p	0.094025	0.66	0.29
hsa-miR-151a-5p	0.201979	0.63	0.15
hsa-miR-21-5p	0.201979	0.63	0.24
hsa-miR-15b-5p	0.217324	0.61	0.10
hsa-miR-25-3p	0.217324	0.61	0.15
hsa-miR-320a	0.306457	0.59	0.00
hsa-miR-423-5p	0.306457	0.59	0.07
hsa-miR-320d	0.306457	0.59	0.15
hsa-miR-28-5p	0.306457	0.59	0.20

<sup>a</sup>Q-value < 0.001.

<sup>b</sup>Q-value < 0.05.

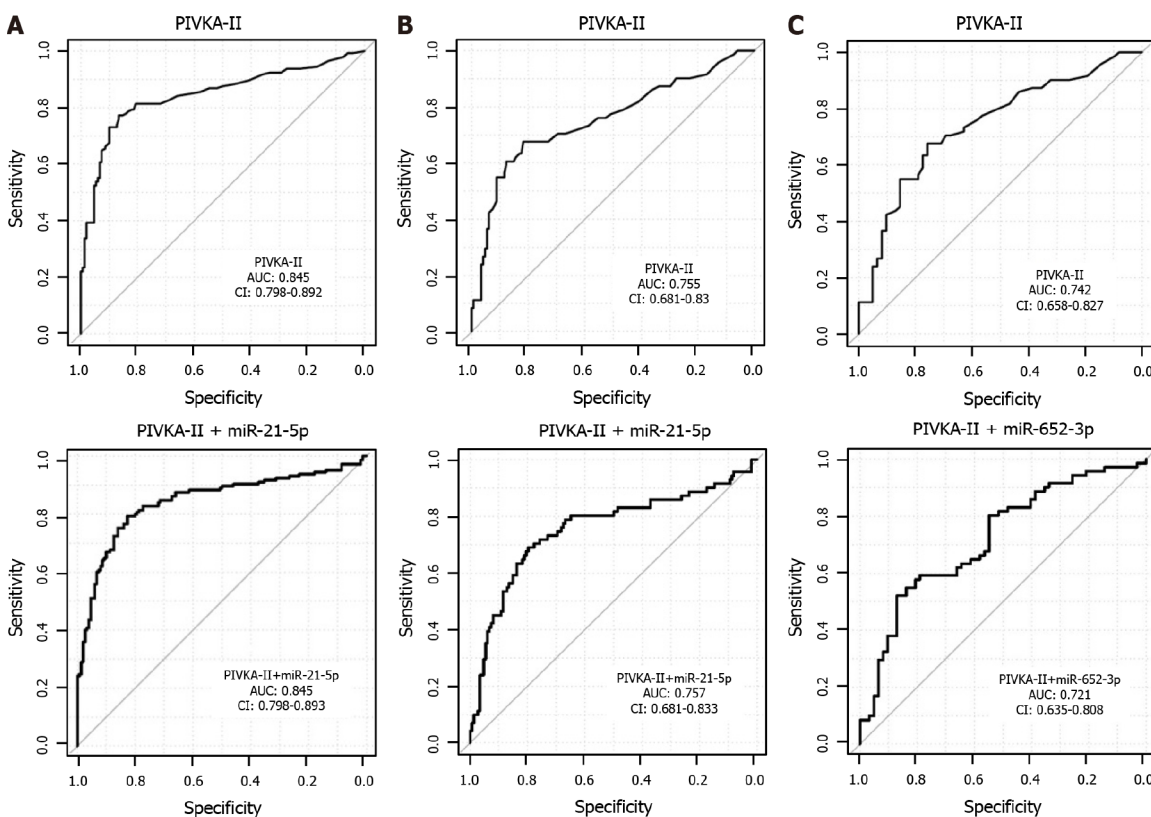
AUC: Area under the curve; CLD: Chronic liver disease; HCC: Hepatocellular carcinoma; miRNA: MicroRNA; miR: MicroRNA.

Ct = 34.41) could be detected in 3 of 200 samples in the training panel and Cts between 33.85 and 34.89 (mean Ct = 34.42) in 5 of 300 samples in the validation panel. All other samples showed no put-miR-6 and put-miR-99 expression, thus both put-miRs were excluded from further analysis.

**Table 4** Multivariate analysis of real-time quantitative PCR results for comparison

Marker	AUC	Specificity at 90% sensitivity	Comparison
PIVKA-II	0.83	34	All HCC <i>vs</i> CLD
PIVKA-II + miRNAs	0.87	48	
PIVKA-II	0.70	15	Early HCC <i>vs</i> CLD
PIVKA-II + miRNAs	0.74	29	
PIVKA-II	0.64	12	Early HCC <i>vs</i> cirrhosis
PIVKA-II + miRNAs	0.71	42	

Area under the curve and specificity at 90% sensitivity for Protein induced by vitamin K absence/antagonist-II alone and in combination with the 26 selected miRNAs, resulting from the logistic regression model. AUC: Area under the curve; CLD: Chronic liver disease; HCC: Hepatocellular carcinoma; miRNA: MicroRNA; PIVKA-II: Protein induced by vitamin K absence/antagonist-II.



DOI: 10.3748/wjg.v28.i29.3917 Copyright ©The Author(s) 2022.

**Figure 3** Receiver operating characteristics curves and area under the curve for multivariate analysis of real-time quantitative PCR results. A: Comparison of all hepatocellular carcinoma vs chronic liver disease; B: Early hepatocellular carcinoma vs chronic liver disease; C: Early hepatocellular carcinoma vs cirrhosis. Analyses were for the validation cohort. Upper panel: Protein induced by vitamin K absence/antagonist-II alone; Lower panel: Protein induced by vitamin K absence/antagonist-II in combination with the best miRNA (selected as final pair in the training analysis). AUC: Area under the curve; CI: Confidence interval; CLD: Chronic liver disease; HCC: Hepatocellular carcinoma; miR: MicroRNA; PIVKA-II: Protein induced by vitamin K absence/antagonist-II.

## DISCUSSION

HCC is a severe disease of the liver and one of the leading causes of cancer-related deaths worldwide [5]. As with all other cancers, early detection is crucial for successful treatment. Recommended detection methods include US, CT, magnetic resonance imaging and measurement of AFP and PIVKA-II. However, these methods are either cost-intensive, operator-dependent or not suitable for the detection of early HCC[6-8,11-13,15]. Previous publications show that single miRNAs, like miR-21, hsa-miR-26a and hsa-miR-101[34,35], as well as miRNA signatures (e.g., hsa-miR-3677, miR-421, hsa-miR-326, hsa-miR-424 and hsa-miR-511-2)[36,37] can improve detection of HCC. While these results are promising, the studies were conducted in small cohorts and/or the control group included healthy individuals who were not being screened regularly for HCC.

**Table 5 Fractions of characteristics (feature) selected during internal cross-validation for evaluating the two-marker combination performance**

Feature	Fraction selected in cross-validation
All HCC vs CLD	
PIVKA-II	1.00
hsa-miR-21-5p	0.86
hsa-miR-320d	0.10
hsa-miR-339-3p	0.02
hsa-miR-320a	0.01
hsa-miR-423-5p	0.00
Early HCC vs CLD	
PIVKA-II	1.00
hsa-miR-21-5p	0.60
hsa-miR-320d	0.18
hsa-miR-652-3p	0.16
hsa-miR-339-3p	0.02
hsa-miR-221-3p	0.01
hsa-miR-30b-5p	0.01
hsa-miR-10b-5p	0.00
hsa-miR-15b-5p	0.00
Early HCC vs cirrhosis	
PIVKA-II	1.00
hsa-miR-652-3p	0.64
hsa-miR-221-3p	0.26
hsa-miR-21-5p	0.05
hsa-miR-423-5p	0.04
hsa-miR-320a	0.01
hsa-miR-339-3p	0.01
hsa-miR-320d	0.00

CLD: Chronic liver disease; HCC: Hepatocellular carcinoma; PIVKA-II: Protein induced by vitamin K absence/antagonist-II; miR: MicroRNA.

Therefore, we carried out a comprehensive, prospective, multicenter, case-control study including patient samples with early-stage ( $n = 147$ ) and late-stage HCC ( $n = 160$ ), HBV ( $n = 136$ ), HCV ( $n = 72$ ) and cirrhosis with HBV and HCV ( $n = 145$ ). We analyzed plasma samples to evaluate the utility of circulating miRNAs alone and in combination with two established protein markers, PIVKA-II and AFP, as biomarkers for detection (including early detection) of HCC and performed multivariate analysis on the included miRNAs. When compared with other studies of circulating miRNAs, our study is unique for the following reasons. First, we screened a large number of plasma miRNAs *via* NGS and RT-qPCR, which enabled us to identify potential diagnostic markers independently of the detection method. Second, we included early-stage and late-stage HCC and for the control cohort included HBV and HCV patients with and without cirrhosis to find a miRNA that can diagnose HCC at an early stage and to validate a biomarker that would be applicable for most of the at-risk population. Third, we used a large sample size of 660 samples with four different independent sample panels to increase statistical power. Finally, we employed an empirically validated set of endogenous reference genes for the normalization of our data.

To find reliable miRNA biomarkers for HCC that were unbiased with respect to the detection method, we followed two different screening approaches (RT-qPCR and NGS) to assess a large number of miRNAs isolated from patient plasma. For each method, we used a different set of plasma samples to receive reproducible results by two independent techniques in a large set of samples. These factors

Table 6 Univariate analysis of real-time quantitative PCR results for comparison

miRNA	Wilcoxon Q-value	AUC	Specificity at 90% sensitivity	Comparison
hsa-miR-21-5p	0.00025 <sup>a</sup>	0.65	0.17	All HCC <i>vs</i> CLD
hsa-miR-423-5p	0.037 <sup>b</sup>	0.59	0.11	
hsa-miR-320d	0.078	0.57	0.11	
hsa-miR-652-3p	0.25	0.59	0.13	Early HCC <i>vs</i> cirrhosis

<sup>a</sup>Q-value < 0.001.<sup>b</sup>Q-value < 0.05.

AUC: Area under the curve; CLD: Chronic liver disease; HCC: Hepatocellular carcinoma; miRNA: MicroRNA; miR: MicroRNA.

could explain why we obtained only three miRNAs (miR-21-5p, miR-320a and miR-421) that showed high potential as diagnostic biomarkers for HCC in both screening approaches.

The 26 best miRNAs selected by both screening methods, including the three overlapping miRNAs, were then analyzed in two different sample panels (training and validation) and combined with the established protein markers PIVKA-II and AFP. In the training panel, miR-21-5p, miR-320d and miR-423 were the best single markers for distinguishing between the HCC and CLD groups. For the early detection of HCC, our data showed that miR-21-5p has the potential to improve the diagnostic performance of PIVKA-II. In the validation panel, the results from the training panel for the comparison of HCC *vs* CLD for miR-21-5p (AUC = 0.65) and miR-423 (AUC = 0.59) could be confirmed. However, the hypothesis of finding a miRNA signature specific for the detection of early HCC could not be confirmed, and the combination of all 26 miRNAs and AFP did not reveal greater diagnostic potential than AFP alone.

MiR-21-5p was one of the two miRNAs with significantly higher expression in the HCC group compared with the CLD group in both the training and validation cohorts. Other publications have shown similar results. Amr *et al*[38] demonstrated that the expression of serum miR-21 was increased in HCC compared with chronic hepatitis, while Gedawya *et al*[39] revealed overexpression of plasma miR-21 in an HCC group ( $P < 0.05$ ) compared with both CLD and healthy subjects from a cohort in Egypt. However, miR-21 was also reported as a circulating diagnostic biomarker for various other cancers[40] such as breast cancer[41], glioma[42] and non-small cell lung cancer[43]. MiR-21 has been described as an oncogene, targeting tumor suppressors like TP63, TP53, TGF- $\beta$  and PTEN, leading to the inhibition of apoptosis[44,45]. Furthermore, miR-21 contributes to the epithelial-to-mesenchymal transition in cervical cancer by modulating the expression of the *Rasa1* gene (RAS p21 protein activator 1). Therefore, by indirectly influencing the activity of Ras, miR-21 contributes to the migration potential of these cells. Another described oncogenic effect is that miR-21 modulates angiogenesis in prostate cancer cells[46]. Thus, the underlying biology of miR-21 supports its role in HCC development and its potential diagnostic value in HCC as well as other cancers.

MiR-423 also showed differential expression when comparing HCC and CLD in both the training and validation groups. Previously, it was revealed that the expression of miR-423 was significantly increased in HCC tissues compared with adjacent normal tissues[47,48]. In serum samples from HCC patients, miR-423 was also found to be significantly upregulated compared with a control group consisting of patients with cirrhosis or chronic hepatitis[49]. In the training and validation panels (total of 500 independent samples), miR-423 levels were elevated in the HCC group. MiR-423 expression has also been found to be upregulated in breast cancer tissue[50], human prostate cancer tissues and prostate cancer PC3 cells[51] and plasma of patients with oral squamous cell carcinoma[52]. This indicates that miR-423 is not limited to the detection of HCC and can also detect several other cancer types. It can act as an oncogene by enhancing the proliferation and migration of gastric cancer cells *in vitro* and *in vivo* when overexpressed[53]. Furthermore, when knocking down miR-423, proliferation of PC3 cells was inhibited, and apoptosis was promoted[51]. In summary, although miR-21 and miR-423 are upregulated in several diseases, their overexpression in a high-risk population could be indicative of early HCC development.

Our results indicate that miR-320d and miR-652 might not be robust biomarkers to diagnose (early) HCC as the results from the training cohort could not be validated. However, they seem to play a role in the development of cancer in general, which requires further investigation.

The 15 putative miRNAs detected by NGS in the screening phase that were differentially expressed between HCC and CLD could not be confirmed as potential biomarkers by RT-qPCR in the training and validation panel. Nonetheless, they could be detected in a small number of samples by both NGS and RT-qPCR. Though the putative miRNAs only showed a relatively low expression, they could be novel miRNAs and should be considered in further investigations.

In the training panel, the combination of the HCC biomarker PIVKA-II with the 26 miRNAs selected in the screening phase improved diagnostic capability, and AUC was increased compared with PIVKA-

II alone. However, this could not be confirmed in the validation panel, which included more samples than the training panel. The combination of AFP and miRNA also did not show any improvement in AFP diagnostic capability in the training panel and was therefore not analyzed in the validation panel. We observed that individual miRNAs identified the same set of patients as those identified by AFP, thus the miRNAs did not add any significant value in this case. However, as the performance of PIVKA-II in the same cohort was between 5% and 20% lower than the performance of AFP, the miRNAs therefore had higher additive value when combined with PIVKA-II. Our results demonstrate that the protein markers AFP and PIVKA-II are more robust biomarkers for HCC than miRNAs.

---

## CONCLUSION

In conclusion, our study found that two miRNAs (miR-21-5p and miR-423) demonstrated significant differential expression between the HCC group and CLD control group. However, the combination of miRNAs with established protein biomarkers (AFP and PIVKA-II) did not improve diagnostic performance of either protein. Further investigation of the molecular mechanisms by which miRNAs, specifically miR-21-5p and miR-423, support HCC development may help in diagnosing and treating this highly malignant tumor.

## ARTICLE HIGHLIGHTS

### **Research background**

Hepatocellular carcinoma (HCC) is the sixth most common cancer worldwide and a leading cause of cancer-related mortality. Current guidelines recommend the surveillance of high-risk patients every 6 mo using ultrasonography, but early-stage HCC detection is limited.

### **Research motivation**

Previous reports show that the expression level of human microRNAs (miRNAs) can serve as an early marker for HCC, even outperforming established biomarkers like alpha-fetoprotein (AFP) and protein induced by vitamin K absence/antagonist-II (PIVKA-II).

### **Research objectives**

To evaluate the diagnostic role of miRNAs in HCC as single markers, signatures or in combination with known protein biomarkers AFP and PIVKA-II in a prospective, multicenter, case-control study.

### **Research methods**

We employed two independent methods, real-time quantitative PCR and next-generation sequencing, to investigate miRNAs levels in the discovery cohort of 160 HCC and control patients. Selected miRNAs were subsequently analyzed for their univariate and multivariate performance in independent training ( $n = 200$ ) and validation cohorts ( $n = 300$ ).

### **Research results**

Real-time quantitative PCR and next-generation sequencing identified 26 miRNAs differentiating between HCC and chronic liver disease controls. Three miRNAs (miR-21, miR-320a and miR-186-5p) were selected by both methods. In the training cohort, only miR-21, miR-320d and miR-423 could significantly distinguish ( $Q < 0.05$ ) between the HCC and control groups. In the multivariate setting, miR-21 with PIVKA-II was selected as the best combination, resulting in an area under the curve of 0.87 for diagnosis and 0.74 for early diagnosis of HCC. miR-21 and miR-423 were confirmed as potential HCC biomarkers in the validation cohort. A combination of miRNAs did not perform better than any single miRNA. Improvement of AFP or PIVKA-II performance through combination with miRNAs was not confirmed in the validation panel.

### **Research conclusions**

Selected miRNA candidates in standalone or signature settings or in combination with biomarkers AFP and PIVKA-II did not improve the diagnostic performance of the protein biomarkers in identification of early-stage HCC.

### **Research perspectives**

Diagnostic superiority of microRNAs for detection of early HCC could not be confirmed, which was primarily due to the excellent and robust performance of the protein biomarkers AFP and PIVKA-II for this intended use. Therefore, miRNAs still carry diagnostic potential for application in other oncological diseases.

## ACKNOWLEDGEMENTS

The authors would like to acknowledge Heike Wegmeyer for her help with study protocol design and sample collection and Gloria Tabares for her help with study design and interpretation. LightCycler 480 is a trademark of Roche. All other product names and trademarks are the property of their respective owners.

## FOOTNOTES

**Author contributions:** Swiatek-de Lange M provided study supervision; Malik J and Swiatek-de Lange M contributed to project development; Chan HL-Y, Piratvisuth T, Tanwandee T, Thongsawat S, Sukeepaisarnjaroen W, Esteban JL, Bes M and Köhler B contributed to sample collection; Malik J contributed to development of methodology and collection of data; Malik J, Klammer M and Rolny V contributed to the biostatistical analysis of the data; Malik J, Klammer M, Rolny V and Swiatek-de Lange M contributed to the interpretation of the data; Malik J, Klammer M and Swiatek-de Lange wrote the manuscript; Malik J and Swiatek-de Lange M provided critical review and editing of the manuscript; All authors have read and approved the final manuscript.

**Institutional review board statement:** The study was approved by the following review boards: Siriraj Institutional Review Board; Research Ethics Committee of the Faculty of Medicine, Chiang Mai University; Joint Chinese University of Hong Kong - New Territories East Cluster Clinical Research Ethics Committee; Ethikkommission Medizinische Fakultät Heidelberg; Research Ethics Committee, Faculty of Medicine, Prince of Songkla University; Clinical Research Ethics Committee of Vall d'Hebron University Hospital; and Khon Kaen University Ethics Committee for Human Research.

**Informed consent statement:** Written informed consent was obtained from all participants.

**Conflict-of-interest statement:** Malik J, Klammer M, Rolny V and Swiatek-de Lange M are employees of Roche Diagnostics GmbH and shareholders in Roche Diagnostics.

**Data sharing statement:** No additional data are available.

**STROBE statement:** The authors have read the STROBE Statement – checklist of items, and the manuscript was prepared and revised according to the STROBE Statement – checklist of items.

**Open-Access:** This article is an open-access article that was selected by an in-house editor and fully peer-reviewed by external reviewers. It is distributed in accordance with the Creative Commons Attribution NonCommercial (CC BY-NC 4.0) license, which permits others to distribute, remix, adapt, build upon this work non-commercially, and license their derivative works on different terms, provided the original work is properly cited and the use is non-commercial. See: <https://creativecommons.org/licenses/by-nc/4.0/>

**Country/Territory of origin:** Germany

**ORCID number:** Juliane Malik 0000-0003-2306-3920; Martin Klammer 0000-0001-6426-0029; Vinzent Rolny 0000-0001-8229-0002; Henry Lik-Yuen Chan 0000-0002-7790-1611; Teerha Piratvisuth 0000-0002-5249-9208; Tawesak Tanwandee 0000-0001-7634-0843; Satawat Thongsawat 0000-0003-3302-3930; Wattana Sukeepaisarnjaroen 0000-0001-5065-9397; Juan Ignacio Esteban 0000-0001-5085-917X; Marta Bes 0000-0001-6103-072X; Bruno Köhler 0000-0002-7308-0377; Magdalena Swiatek-de Lange 0000-0003-1406-3232.

**S-Editor:** Chang KL

**L-Editor:** Filipodia

**P-Editor:** Chang KL

## REFERENCES

- 1 International Agency for Research on Cancer. Cancer today. [cited 1 January 2022]. Available from: <http://gco.iarc.fr/today/>
- 2 El-Serag HB, Rudolph KL. Hepatocellular carcinoma: epidemiology and molecular carcinogenesis. *Gastroenterology* 2007; **132**: 2557-2576 [PMID: 17570226 DOI: 10.1053/j.gastro.2007.04.061]
- 3 Sherman M. Hepatocellular carcinoma: epidemiology, surveillance, and diagnosis. *Semin Liver Dis* 2010; **30**: 3-16 [PMID: 20175029 DOI: 10.1055/s-0030-1247128]
- 4 El-Serag HB. Hepatocellular carcinoma. *N Engl J Med* 2011; **365**: 1118-1127 [PMID: 21992124 DOI: 10.1056/NEJMra1001683]
- 5 Wang CY, Li S. Clinical characteristics and prognosis of 2887 patients with hepatocellular carcinoma: A single center 14 years experience from China. *Medicine (Baltimore)* 2019; **98**: e14070 [PMID: 30681563 DOI: 10.1093/med/98.14.14070]

- 10.1097/MD.00000000000014070]
- 6 **European Association For The Study Of The Liver**; European Organisation For Research And Treatment Of Cancer. EASL-EORTC clinical practice guidelines: management of hepatocellular carcinoma. *J Hepatol* 2012; **56**: 908-943 [PMID: 22424438 DOI: 10.1016/j.jhep.2011.12.001]
  - 7 **Omata M**, Cheng AL, Kokudo N, Kudo M, Lee JM, Jia J, Tateishi R, Han KH, Chawla YK, Shiina S, Jafri W, Payawal DA, Ohki T, Ogasawara S, Chen PJ, Lesmana CRA, Lesmana LA, Gani RA, Obi S, Dokmeci AK, Sarin SK. Asia-Pacific clinical practice guidelines on the management of hepatocellular carcinoma: a 2017 update. *Hepatol Int* 2017; **11**: 317-370 [PMID: 28620797 DOI: 10.1007/s12072-017-9799-9]
  - 8 **Heimbach JK**, Kulik LM, Finn RS, Sirlin CB, Abecassis MM, Roberts LR, Zhu AX, Murad MH, Marrero JA. AASLD guidelines for the treatment of hepatocellular carcinoma. *Hepatology* 2018; **67**: 358-380 [PMID: 28130846 DOI: 10.1002/hep.29086]
  - 9 **European Association for the Study of the Liver**. EASL Clinical Practice Guidelines: Management of hepatocellular carcinoma. *J Hepatol* 2018; **69**: 182-236 [PMID: 29628281 DOI: 10.1016/j.jhep.2018.03.019]
  - 10 **Kokudo N**, Takemura N, Hasegawa K, Takayama T, Kubo S, Shimada M, Nagano H, Hatano E, Izumi N, Kaneko S, Kudo M, Iijima H, Genda T, Tateishi R, Torimura T, Igaki H, Kobayashi S, Sakurai H, Murakami T, Watadani T, Matsuyama Y. Clinical practice guidelines for hepatocellular carcinoma: The Japan Society of Hepatology 2017 (4th JSH-HCC guidelines) 2019 update. *Hepatol Res* 2019; **49**: 1109-1113 [PMID: 31336394 DOI: 10.1111/hepr.13411]
  - 11 **Singal A**, Volk ML, Waljee A, Salgia R, Higgins P, Rogers MA, Marrero JA. Meta-analysis: surveillance with ultrasound for early-stage hepatocellular carcinoma in patients with cirrhosis. *Aliment Pharmacol Ther* 2009; **30**: 37-47 [PMID: 19392863 DOI: 10.1111/j.1365-2036.2009.04014.x]
  - 12 **Jeong WK**. Surveillance of hepatocellular carcinoma: is only ultrasound enough? *Clin Mol Hepatol* 2017; **23**: 222-223 [PMID: 28942623 DOI: 10.3350/cmh.2017.0046]
  - 13 **Li Q**, Dhyani M, Grajo JR, Sirlin C, Samir AE. Current status of imaging in nonalcoholic fatty liver disease. *World J Hepatol* 2018; **10**: 530-542 [PMID: 30190781 DOI: 10.4254/wjh.v10.i8.530]
  - 14 **Tzartzeva K**, Obi J, Rich NE, Parikh ND, Marrero JA, Yopp A, Waljee AK, Singal AG. Surveillance Imaging and Alpha Fetoprotein for Early Detection of Hepatocellular Carcinoma in Patients With Cirrhosis: A Meta-analysis. *Gastroenterology* 2018; **154**: 1706-1718.e1 [PMID: 29425931 DOI: 10.1053/j.gastro.2018.01.064]
  - 15 **Gentile I**, Buonomo AR, Scotto R, Zappulo E, Carriero C, Piccirillo M, Izzo F, Rizzo M, Cerasuolo D, Borgia G, Cavalcanti E. Diagnostic Accuracy of PIVKA-II, Alpha-Fetoprotein and a Combination of both in Diagnosis of Hepatocellular Carcinoma in Patients Affected by Chronic HCV Infection. *In Vivo* 2017; **31**: 695-700 [PMID: 28652441 DOI: 10.21873/invivo.11115]
  - 16 **Bushati N**, Cohen SM. microRNA functions. *Annu Rev Cell Dev Biol* 2007; **23**: 175-205 [PMID: 17506695 DOI: 10.1146/annurev.cellbio.23.090506.123406]
  - 17 **Wienholds E**, Plasterk RH. MicroRNA function in animal development. *FEBS Lett* 2005; **579**: 5911-5922 [PMID: 16111679 DOI: 10.1016/j.febslet.2005.07.070]
  - 18 **Ruan K**, Fang X, Ouyang G. MicroRNAs: novel regulators in the hallmarks of human cancer. *Cancer Lett* 2009; **285**: 116-126 [PMID: 19464788 DOI: 10.1016/j.canlet.2009.04.031]
  - 19 **Nana-Sinkam SP**, Croce CM. Clinical applications for microRNAs in cancer. *Clin Pharmacol Ther* 2013; **93**: 98-104 [PMID: 23212103 DOI: 10.1038/clpt.2012.192]
  - 20 **Mitchell PS**, Parkin RK, Kroh EM, Fritz BR, Wyman SK, Pogosova-Agadjanyan EL, Peterson A, Noteboom J, O'Brian KC, Allen A, Lin DW, Urban N, Drescher CW, Knudsen BS, Stirewalt DL, Gentleman R, Vessella RL, Nelson PS, Martin DB, Tewari M. Circulating microRNAs as stable blood-based markers for cancer detection. *Proc Natl Acad Sci U S A* 2008; **105**: 10513-10518 [PMID: 18663219 DOI: 10.1073/pnas.0804549105]
  - 21 **Li L**, Zhu D, Huang L, Zhang J, Bian Z, Chen X, Liu Y, Zhang CY, Zen K. Argonaute 2 complexes selectively protect the circulating microRNAs in cell-secreted microvesicles. *PLoS One* 2012; **7**: e46957 [PMID: 23077538 DOI: 10.1371/journal.pone.0046957]
  - 22 **Lässer C**. Exosomal RNA as biomarkers and the therapeutic potential of exosome vectors. *Expert Opin Biol Ther* 2012; **12** Suppl 1: S189-S197 [PMID: 22506888 DOI: 10.1517/14712598.2012.680018]
  - 23 **Huang JT**, Liu SM, Ma H, Yang Y, Zhang X, Sun H, Xu J, Wang J. Systematic Review and Meta-Analysis: Circulating miRNAs for Diagnosis of Hepatocellular Carcinoma. *J Cell Physiol* 2016; **231**: 328-335 [PMID: 26291451 DOI: 10.1002/jcp.25135]
  - 24 **Murakami Y**, Yasuda T, Saigo K, Urashima T, Toyoda H, Okanou T, Shimotohno K. Comprehensive analysis of microRNA expression patterns in hepatocellular carcinoma and non-tumorous tissues. *Oncogene* 2006; **25**: 2537-2545 [PMID: 16331254 DOI: 10.1038/sj.onc.1209283]
  - 25 **Tan Y**, Ge G, Pan T, Wen D, Chen L, Yu X, Zhou X, Gan J. A serum microRNA panel as potential biomarkers for hepatocellular carcinoma related with hepatitis B virus. *PLoS One* 2014; **9**: e107986 [PMID: 25238238 DOI: 10.1371/journal.pone.0107986]
  - 26 **Borel F**, Konstantinova P, Jansen PL. Diagnostic and therapeutic potential of miRNA signatures in patients with hepatocellular carcinoma. *J Hepatol* 2012; **56**: 1371-1383 [PMID: 22314424 DOI: 10.1016/j.jhep.2011.11.026]
  - 27 **Yang W**, Zhou C, Luo M, Shi X, Li Y, Sun Z, Zhou F, Chen Z, He J. MiR-652-3p is upregulated in non-small cell lung cancer and promotes proliferation and metastasis by directly targeting Lgl1. *Oncotarget* 2016; **7**: 16703-16715 [PMID: 26934648 DOI: 10.18632/oncotarget.7697]
  - 28 **Sun X**, Dongol S, Qiu C, Xu Y, Sun C, Zhang Z, Yang X, Zhang Q, Kong B. miR-652 Promotes Tumor Proliferation and Metastasis by Targeting *RORA* in Endometrial Cancer. *Mol Cancer Res* 2018; **16**: 1927-1939 [PMID: 30093563 DOI: 10.1158/1541-7786.MCR-18-0267]
  - 29 **Li LM**, Hu ZB, Zhou ZX, Chen X, Liu FY, Zhang JF, Shen HB, Zhang CY, Zen K. Serum microRNA profiles serve as novel biomarkers for HBV infection and diagnosis of HBV-positive hepatocarcinoma. *Cancer Res* 2010; **70**: 9798-9807 [PMID: 21098710 DOI: 10.1158/0008-5472.CAN-10-1001]
  - 30 **Zhou J**, Yu L, Gao X, Hu J, Wang J, Dai Z, Wang JF, Zhang Z, Lu S, Huang X, Wang Z, Qiu S, Wang X, Yang G, Sun H,

- Tang Z, Wu Y, Zhu H, Fan J. Plasma microRNA panel to diagnose hepatitis B virus-related hepatocellular carcinoma. *J Clin Oncol* 2011; **29**: 4781-4788 [PMID: 22105822 DOI: 10.1200/JCO.2011.38.2697]
- 31 Piratvisuth T, Tanwandee T, Thongsawat S, Sukeepaisarnjaroen W, Esteban JI, Bes M, Köhler B, He Y, Swiatek-de Lange M, Morgenstern D, Chan HL. Multimarker Panels for Detection of Early Stage Hepatocellular Carcinoma: A Prospective, Multicenter, Case-Control Study. *Hepatol Commun* 2022; **6**: 679-691 [PMID: 34796691 DOI: 10.1002/hep4.1847]
- 32 Wu Y, Wei B, Liu H, Li T, Rayner S. MiRPara: a SVM-based software tool for prediction of most probable microRNA coding regions in genome scale sequences. *BMC Bioinformatics* 2011; **12**: 107 [PMID: 21504621 DOI: 10.1186/1471-2105-12-107]
- 33 Sengupta S, Parikh ND. Biomarker development for hepatocellular carcinoma early detection: current and future perspectives. *Hepat Oncol* 2017; **4**: 111-122 [PMID: 30191058 DOI: 10.2217/hep-2017-0019]
- 34 Qu KZ, Zhang K, Li H, Afdhal NH, Albitar M. Circulating microRNAs as biomarkers for hepatocellular carcinoma. *J Clin Gastroenterol* 2011; **45**: 355-360 [PMID: 21278583 DOI: 10.1097/MCG.0b013e3181f18ac2]
- 35 Zhuang C, Jiang W, Huang D, Xu L, Yang Q, Zheng L, Wang X, Hu L. Serum miR-21, miR-26a and miR-101 as potential biomarkers of hepatocellular carcinoma. *Clin Res Hepatol Gastroenterol* 2016; **40**: 386-396 [PMID: 26669589 DOI: 10.1016/j.clinre.2015.11.002]
- 36 Wen Y, Han J, Chen J, Dong J, Xia Y, Liu J, Jiang Y, Dai J, Lu J, Jin G, Wei Q, Shen H, Sun B, Hu Z. Plasma miRNAs as early biomarkers for detecting hepatocellular carcinoma. *Int J Cancer* 2015; **137**: 1679-1690 [PMID: 25845839 DOI: 10.1002/ijc.29544]
- 37 Lu M, Kong X, Wang H, Huang G, Ye C, He Z. A novel microRNAs expression signature for hepatocellular carcinoma diagnosis and prognosis. *Oncotarget* 2017; **8**: 8775-8784 [PMID: 28060739 DOI: 10.18632/oncotarget.14452]
- 38 Amr KS, Ezzat WM, Elhosary YA, Hegazy AE, Fahim HH, Kamel RR. The potential role of miRNAs 21 and 199-a in early diagnosis of hepatocellular carcinoma. *Gene* 2016; **575**: 66-70 [PMID: 26302751 DOI: 10.1016/j.gene.2015.08.038]
- 39 Gedawya GE, Obada M, Kelani A, El-Saida H, Ghanayem NM. Circulating MiRNA-21 and programmed cell death (PDCD) 4 gene expression in hepatocellular carcinoma (HCC) in Egyptian patients. *Egypt J Med Hum Genet* 2017; **18**: 137-145 [DOI: 10.1016/j.ejmhg.2016.04.007]
- 40 Wu K, Li L, Li S. Circulating microRNA-21 as a biomarker for the detection of various carcinomas: an updated meta-analysis based on 36 studies. *Tumour Biol* 2015; **36**: 1973-1981 [PMID: 25527152 DOI: 10.1007/s13277-014-2803-2]
- 41 Asaga S, Kuo C, Nguyen T, Terpenning M, Giuliano AE, Hoon DS. Direct serum assay for microRNA-21 concentrations in early and advanced breast cancer. *Clin Chem* 2011; **57**: 84-91 [PMID: 21036945 DOI: 10.1373/clinchem.2010.151845]
- 42 Ivo D'Urso P, Fernando D'Urso O, Damiano Gianfreda C, Mezzolla V, Storelli C, Marsigliante S. miR-15b and miR-21 as Circulating Biomarkers for Diagnosis of Glioma. *Curr Genomics* 2015; **16**: 304-311 [PMID: 27047250 DOI: 10.2174/1389202916666150707155610]
- 43 Zhao W, Zhao JJ, Zhang L, Xu QF, Zhao YM, Shi XY, Xu AG. Serum miR-21 Level: a potential diagnostic and prognostic biomarker for non-small cell lung cancer. *Int J Clin Exp Med* 2015; **8**: 14759-14763 [PMID: 26628958]
- 44 Buscaglia LE, Li Y. Apoptosis and the target genes of microRNA-21. *Chin J Cancer* 2011; **30**: 371-380 [PMID: 21627859 DOI: 10.5732/cjc.011.10132]
- 45 Papagiannakopoulos T, Shapiro A, Kosik KS. MicroRNA-21 targets a network of key tumor-suppressive pathways in glioblastoma cells. *Cancer Res* 2008; **68**: 8164-8172 [PMID: 18829576 DOI: 10.1158/0008-5472.CAN-08-1305]
- 46 Bica-Pop C, Ciojocneanu-Petric R, Magdo L, Raduly L, Gulei D, Berindan-Neagoe I. Overview upon miR-21 in lung cancer: focus on NSCLC. *Cell Mol Life Sci* 2018; **75**: 3539-3551 [PMID: 30030592 DOI: 10.1007/s00018-018-2877-x]
- 47 Sun X, Wang M, Liu H, Wang J. MicroRNA-423 enhances the invasiveness of hepatocellular carcinoma via regulation of BRMS1. *Am J Transl Res* 2017; **9**: 5576-5584 [PMID: 29312509]
- 48 Yu Z, Zhao H, Feng X, Li H, Qiu C, Yi X, Tang H, Zhang J. Long Non-coding RNA FENDRR Acts as a miR-423-5p Sponge to Suppress the Treg-Mediated Immune Escape of Hepatocellular Carcinoma Cells. *Mol Ther Nucleic Acids* 2019; **17**: 516-529 [PMID: 31351327 DOI: 10.1016/j.omtn.2019.05.027]
- 49 An Y, Gao S, Zhao WC, Qiu BA, Xia NX, Zhang PJ, Fan ZP. Novel serum microRNAs panel on the diagnostic and prognostic implications of hepatocellular carcinoma. *World J Gastroenterol* 2018; **24**: 2596-2604 [PMID: 29962816 DOI: 10.3748/wjg.v24.i24.2596]
- 50 Sun X, Huang T, Zhang C, Zhang S, Wang Y, Zhang Q, Liu Z. Long non-coding RNA LINC00968 reduces cell proliferation and migration and angiogenesis in breast cancer through up-regulation of PROX1 by reducing hsa-miR-423-5p. *Cell Cycle* 2019; **18**: 1908-1924 [PMID: 31213129 DOI: 10.1080/15384101.2019.1632641]
- 51 Lin H, Lin T, Lin J, Yang M, Shen Z, Liu H, Zou Z, Zheng Z. Inhibition of miR-423-5p suppressed prostate cancer through targeting GRIM-19. *Gene* 2019; **688**: 93-97 [PMID: 30415005 DOI: 10.1016/j.gene.2018.11.021]
- 52 Chang YA, Weng SL, Yang SF, Chou CH, Huang WC, Tu SJ, Chang TH, Huang CN, Jong YJ, Huang HD. A Three-MicroRNA Signature as a Potential Biomarker for the Early Detection of Oral Cancer. *Int J Mol Sci* 2018; **19** [PMID: 29518940 DOI: 10.3390/ijms19030758]
- 53 Yang H, Fu H, Wang B, Zhang X, Mao J, Li X, Wang M, Sun Z, Qian H, Xu W. Exosomal miR-423-5p targets SUFU to promote cancer growth and metastasis and serves as a novel marker for gastric cancer. *Mol Carcinog* 2018; **57**: 1223-1236 [PMID: 29749061 DOI: 10.1002/mc.22838]

## Retrospective Cohort Study

## Optimal timing of biliary drainage based on the severity of acute cholangitis: A single-center retrospective cohort study

Zhao-Qing Lu, Han-Yu Zhang, Chen-Fen Su, Yue-Yan Xing, Guo-Xing Wang, Chun-Sheng Li

**Specialty type:** Gastroenterology and hepatology**Provenance and peer review:**

Unsolicited article; Externally peer reviewed.

**Peer-review model:** Single blind**Peer-review report's scientific quality classification**Grade A (Excellent): 0  
Grade B (Very good): 0  
Grade C (Good): C, C, C  
Grade D (Fair): 0  
Grade E (Poor): 0**P-Reviewer:** Badessi G, Italy;

Emran TB, Bangladesh; Maieron A, Austria

**Received:** March 17, 2022**Peer-review started:** March 17, 2022**First decision:** April 11, 2022**Revised:** April 25, 2022**Accepted:** July 5, 2022**Article in press:** July 5, 2022**Published online:** August 7, 2022**Zhao-Qing Lu, Han-Yu Zhang, Chen-Fen Su, Yue-Yan Xing, Guo-Xing Wang,** Department of Emergency Medicine, Beijing Friendship Hospital, Capital Medical University, Beijing 100050, China**Chun-Sheng Li,** Emergency and Critical Care Center, Beijing Friendship Hospital, Capital Medical University, Beijing 100050, China**Corresponding author:** Chun-Sheng Li, PhD, Professor, Emergency and Critical Care Center, Beijing Friendship Hospital, Capital Medical University, No. 95 Yong'an Road, Xicheng District, Beijing 100050, China. [lscyyy@163.com](mailto:lscyyy@163.com)**Abstract****BACKGROUND**

Biliary decompression is well known to greatly decrease the risks of mortality in acute cholangitis (AC). Although early biliary drainage is recommended by the treatment guidelines for AC, the best time for performing this procedure is yet to be established. Furthermore, since the clinical outcomes of patients with severe AC vary dramatically, screening for patients that could benefit the most from early drainage would be more beneficial than the drainage performed based on the severity grade criteria.

**AIM**

To investigate the optimal drainage timing for AC patients with each disease severity grade and organ dysfunction.

**METHODS**

In this retrospective monocenter cohort analysis, we reviewed 1305 patients who were diagnosed with AC according to the Tokyo guidelines 2018 at a Chinese tertiary hospital between July 2016 and December 2020. Demographic characteristics including age and sex, clinical and laboratory characteristics, and imaging findings of each patient were obtained from electronic medical records. We investigated the all-cause in-hospital mortality (IHM), hospital length of stay (LOS), and hospitalization costs associated with the timing of biliary drainage according to the severity grading and different dysfunctioning organs and predictors [age, white blood cell (WBC) count, total bilirubin, albumin, lactate, malignant obstruction, and Charlton comorbidity index (CCI)].

**RESULTS**

Biliary drainage within 24 or 48 h in Grade III AC patients could dramatically decrease IHM (3.9% *vs* 9.0%,  $P = 0.041$ ; 4% *vs* 9.9%,  $P = 0.018$ , respectively), while increasing LOS and hospitalization costs. Multivariate logistic analysis revealed that neurological, respiratory, renal, and cardiovascular dysfunctions, hypoalbuminemia, and malignant obstruction were significantly associated with IHM (odds ratio = 5.32, 2.541, 6.356, 4.021, 5.655, and 7.522;  $P < 0.001$ ,  $P = 0.016$ ,  $P < 0.001$ ,  $P = 0.012$ ,  $P < 0.001$ , and  $P < 0.001$ ; respectively). Biliary decompression performed within 12 h of admission significantly decreased the IHM in AC patients with neurological dysfunction (0% *vs* 17.3%,  $P = 0.041$ ) or with serum lactate  $> 2$  mmol/L (0% *vs* 5.4%,  $P = 0.016$ ). In the subgroup of AC patients with renal dysfunction, abnormal WBC count, hyperbilirubinemia, or hypoalbuminemia, early drainage ( $< 24$  h) reduced the IHM (3.6% *vs* 33.3%,  $P = 0.004$ ; 1.9% *vs* 5.8%,  $P = 0.031$ ; 1.7% *vs* 5.0%,  $P = 0.019$ ; 0% *vs* 27%,  $P = 0.026$ ; respectively). The IHM was lower in patients with AC combined with hepatic dysfunction, malignant obstruction, or a CCI  $> 3$  who had undergone biliary drainage within 48 h (2.6% *vs* 20.5%,  $P = 0.016$ ; 3.0% *vs* 13.5%,  $P = 0.006$ ; 3.4% *vs* 9.6%,  $P = 0.021$ ; respectively).

### CONCLUSION

Biliary drainage within 12 h is beneficial for AC patients with neurological or cardiovascular dysfunction, while complete biliary decompression within 24 h of admission is recommended for treating patients with Grade III AC.

**Key Words:** Acute cholangitis; Endoscopic retrograde cholangiopancreatography; Mortality; Biliary drainage; Organ dysfunction

©The Author(s) 2022. Published by Baishideng Publishing Group Inc. All rights reserved.

**Core Tip:** This study aimed to investigate the optimal timing of drainage for patients with acute cholangitis (AC) with each grade and organ dysfunction. We first attempted to study whether AC patients with different organ dysfunction should undergo biliary drainage at distinct times. We believe that our study makes a significant contribution to the literature because we found that patients with severe AC should complete biliary decompression within 24 h of admission, while biliary drainage within 12 h was beneficial for AC patients with neurological or cardiovascular dysfunction.

**Citation:** Lu ZQ, Zhang HY, Su CF, Xing YY, Wang GX, Li CS. Optimal timing of biliary drainage based on the severity of acute cholangitis: A single-center retrospective cohort study. *World J Gastroenterol* 2022; 28(29): 3934-3945

**URL:** <https://www.wjgnet.com/1007-9327/full/v28/i29/3934.htm>

**DOI:** <https://dx.doi.org/10.3748/wjg.v28.i29.3934>

## INTRODUCTION

Acute cholangitis (AC) is a life-threatening condition that occurs in the presence of biliary obstruction. Although growing evidence confirms that biliary decompression can dramatically decrease the mortality rates associated with AC, the optimal time for biliary drainage remains controversial[1-3]. Most experts agree that the timeframe for biliary decompression is distinct for different severity grades based on the Tokyo guidelines 2018/2013 (TG18/13), which recommend early biliary drainage for Grade II AC and urgent biliary drainage for Grade III AC; however, the exact timeframe is unclear[4]. Moreover, the 2019 European Society of Gastrointestinal Endoscopy guidelines recommend biliary drainage as soon as possible in patients with Grade III AC and within 12 h for patients with septic shock, while within 48–72 h for patients with Grade II AC[2]. Meanwhile, the 2021 American Society of Gastrointestinal Endoscopy (ASGE) guidelines suggest endoscopic retrograde cholangiopancreatography (ERCP) within 48 h in AC patients, regardless of severity[1]. Some studies have demonstrated a “the earlier, the better” approach for the management of AC cases[5-8]. They deemed urgent biliary decompression necessary in severe cases. However, other studies have shown that ERCP can be safely delayed to allow for sufficient resuscitation[9-11]. In our clinical experience, the severity of Grade III AC varies dramatically, and we have observed that the optimal timing of biliary decompression may vary for different organ injuries.

So far, no relevant study has determined whether the clinical outcomes of Grade III AC patients vary with different organ injuries and whether AC patients with different organ dysfunction should undergo biliary drainage at distinct times. Consequently, this single-center retrospective study aimed to

investigate the relationship between drainage timing and in-hospital mortality (IHM) in patients with AC of different severities, and attempted to stratify patients with AC to identify the best decompression time.

## MATERIALS AND METHODS

### Patients

**Ethical compliance:** This retrospective cohort study was conducted according to the tenets of the Declaration of Helsinki, and approved by the Bioethics Committee of Beijing Friendship Hospital, Capital Medical University (Certification No. 2020-P2-224-01). After the review conducted by the Ethics Committee, the need for informed consent was waived.

**Sample size:** Based on the pre-experimental results, which revealed a 0.87% and 3% mortality rates for patients who did and did not undergo biliary drainage, respectively, we calculated the sample size using PASS 15.0 with Power = 0.8, Alpha = 0.05, and N1 = N2. The resultant sample size was 1306. On this basis, we expanded the sample size by 15% to exclude the reduction caused by data deficiency or diagnostic errors.

**Enrollment:** We searched the electronic medical record database of the Beijing Friendship Hospital for all adult (> 18 years) non-pregnant patients visiting the Emergency Department (ED) between July 2016 and December 2020 who were discharged with a diagnosis of AC. A total of 1498 patients were included in the study. All the medical records were reviewed and a diagnosis of AC was confirmed according to the TG18 diagnostic criteria[12]. Besides pregnant women and patients aged < 18 years, we also excluded patients transferred to other hospitals or outpatient departments for treatment and patients whose medical data were incomplete or missing. Finally, 1305 patients were enrolled (Figure 1).

### Data collection

Demographic data, including age and sex, were obtained for each patient. Clinical data, laboratory characteristics, and imaging findings were obtained from the electronic medical records. Clinical data included vital signs, fluid output, Glasgow coma score, the vasoactive drug dose, history of biliary disease, Charlton comorbidity index (CCI), etiology of AC, registration time at the ED, time and type of drainage, discharge time, complications of drainage, hospitalization cost, and IHM. Laboratory findings included white blood cell (WBC) count, platelet count, total bilirubin, albumin, aspartate transaminase, alanine transaminase, creatinine, amylase, prothrombin time-international normalized ratio, arterial blood oxygen pressure, and lactate. Computed tomography, magnetic resonance cholangiopancreatography, or ERCP findings were reviewed to determine the etiology of cholangitis. The time interval for biliary drainage was calculated as the difference between ED registration time and the time of ERCP or percutaneous transhepatic biliary drainage (PTBD). We used the TG18 severity criteria for grading the severity[12].

### Definition and indications

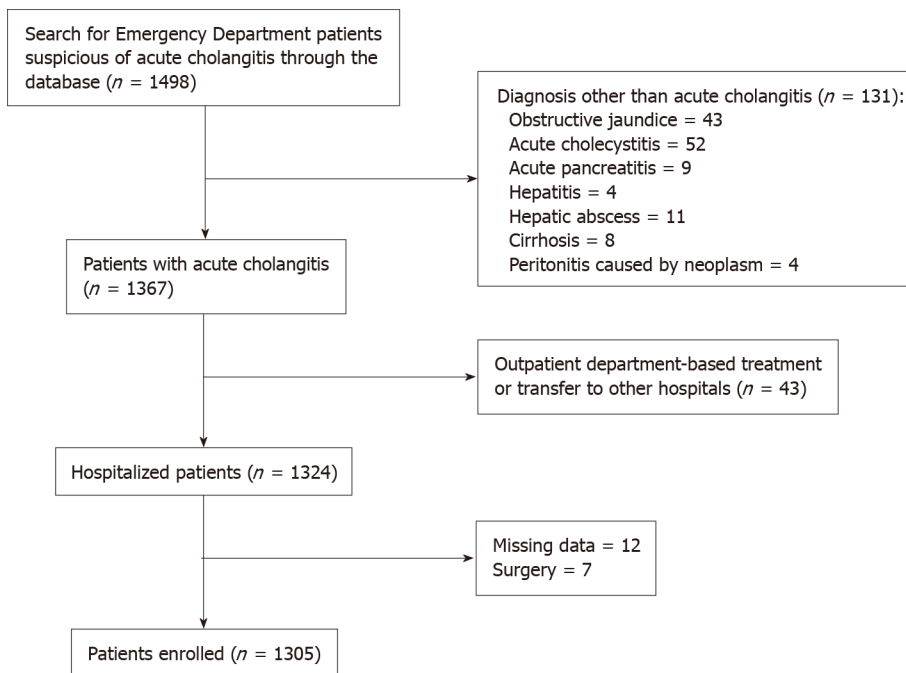
Benign stenosis was defined as stenosis in the biliary ducts without radiological findings of metastasis or malignant cells on histological examination. The indications of ERCP were AC combined with persistent extrahepatic biliary obstruction, and cases of anatomical derangement, failed ERCP, intrahepatic biliary obstruction underwent PTBD. The contraindications of ERCP included acute coronary syndrome, acute heart failure (New York Heart Association class III-IV), acute stroke occurring within 2 wk prior to enrollment, and acute pulmonary embolism complicated with the arterial PaO<sub>2</sub> <60 mmHg, while the contraindications of PTBD were platelet count < 50000/mm<sup>3</sup> or prothrombin activity < 60%. The adverse effects after drainage were based on the lexicon guidelines of the ASGE[13]. The second treatment included a second ERCP and a second PTBD for stone removal or stent placement. The need for a second therapeutic ERCP was assessed per the discretion of the experienced operators who performed the intervention and based on 2018 ERCP Guidelines for China[14]. All of the endoscopists had independently completed 300 ERCP interventions per year for 3 years.

### Study outcomes

Our primary outcome was IHM, and the secondary outcomes were hospital length of stay (LOS) and hospitalization costs. When analyzing the survivors' LOS and entailed cost, we excluded patients who died or were transferred to other hospitals. We investigated the primary and secondary outcomes relevant to the timing of biliary drainage according to severity grading and some predictors based on TG18 and other previous studies.

### Statistical analysis

Continuous variables were reported as medians with interquartile ranges (IQR) for not normally distributed; categorical variables were expressed as numbers and percentages. Comparisons between



DOI: 10.3748/wjg.v28.i29.3934 Copyright ©The Author(s) 2022.

Figure 1 A flowchart of the study population.

groups for continuous variables were evaluated using the Kruskal–Wallis test and Mann–Whitney *U* test, and for categorical variables, Fisher’s exact test was used. Univariate logistic regression analysis and multivariate logistic regression with stepwise variable selection were used to analyze the relationship between organ dysfunction or predictors and IHM. Odds ratios (ORs) and 95% confidence intervals were calculated. Statistical significance was set at  $P < 0.05$ . Statistical analyses were conducted using SPSS v22.

## RESULTS

The characteristics of the study population are shown in Tables 1 and 2. This cohort included 1305 patients, the majority of whom were men (60%). The median age of the group was 74 years (IQR, 63–82 years), and patients with Grade I AC were significantly younger ( $P < 0.001$ ). The CCI of individuals with Grade III cholangitis was significantly higher than that of patients with Grade I or II cholangitis ( $P < 0.001$ ). Choledocholithiasis (69.4%) was the most common cause of cholangitis, followed by malignant obstruction (18.5%). Among patients with cholangitis caused by malignancy, the number of patients with Grade II cholangitis was higher than that of patients with Grade I or III cholangitis. More patients with Grade II AC underwent biliary decompression ( $P = 0.006$ ), while the IHM and hospitalization costs were significantly higher in the Grade III AC group than in the Grade I and II AC groups (IHM:  $P < 0.001$ , hospitalization costs:  $P < 0.001$ ). Deaths tended to occur earlier in the disease course in patients with Grade III AC (median time 6 d).

A total of 915 patients in this cohort (70.1%) underwent biliary decompression, most of whom underwent endoscopic interventions (90.7%), while more patients underwent PTBD in the severe AC groups (Grade II: 37 cases, Grade III: 35 cases vs Grade I: 13 cases,  $P = 0.001$ ). One hundred and sixty patients with Grade III were treated with antibiotics and fluid infusion only (disagreement about procedures = 35 cases, including two of mortality; with contraindications = 24 cases, including five of death; not tolerable conditions = 14 cases, including eight of death; obstruction spontaneous relief = 67 cases, including seven of mortality; not persistent biliary obstruction with high risk to stone removal by ERCP = 15 cases without death; not persistent biliary obstruction with selective cholecystectomy = five cases without death). The median drainage time was 24 h. Nearly half of the patients underwent biliary drainage within 24 h (445/915, 48%), while 89 patients with Grade III underwent drainage within 12 h (29%), which was significantly higher than that in Grades I and II ( $P = 0.04$ ). Among the patients who underwent biliary drainage, more patients in Grade III underwent biliary drainage outside regular working hours (31.9%) and 478 patients (52.2%) required a second intervention for stone removal or stent placement, which exhibited no relationship with severity ( $P = 0.688$ ). Post-ERCP pancreatitis was the major adverse event (8.2%), and the incidence of adverse events was not significantly different among the three severity grades.

Table 1 Characteristics data for all patients

Characteristics, n (%)	Total (n = 1305)	Grade I (n = 433)	Grade II (n = 405)	Grade III (n = 467)	P value
Age (yr)-median (IQR)	74 (63-82)	66 (59-72.5)	79 (69-84)	77 (66-83)	< 0.001
Male, n (%)	783 (60)	276 (63.7)	240 (59.3)	267 (57.2)	0.123
CCI- median (IQR)	2 (1-4)	2 (1-3)	2 (1-4)	3 (1-5)	< 0.001
Etiology, n (%)					< 0.001
Cholelithiasis	906 (69.4)	315 (72.7)	252 (62.2)	339 (72.6)	
Malignant obstruction	242 (18.5)	73 (16.9)	97 (24.0)	72 (15.4)	
Benign stenosis	94 (7.2)	27 (6.2)	42 (10.4)	25 (5.4)	
Others	63 (4.8)	18 (4.2)	14 (3.5)	31 (6.6)	
Biliary drainage, n (%)	915 (70.1)	302 (69.7)	306 (75.6)	307 (65.7)	0.006
LOS (d)-median (IQR)	11 (8-14)	11 (8-14)	11 (7.5-14)	12 (7-15)	0.110
Hospitalization cost (CNY)-median (IQR)	38784.37 (22744.31-53278.63)	36536.36 (20851.37-47274.77)	38308.33 (23452.14-52847.29)	41832.19 (23355.98-58145.52)	< 0.001
IHM, n (%)	41 (3.1)	1 (0.2)	7 (1.7)	33 (7.1)	< 0.001
Survival time of dead (d)-median (IQR)	8 (3-23.5)	9	23 (13-46)	6 (3-17)	0.024
Organ dysfunction					
Neurological dysfunction	126	0	0	126	< 0.001
Respiratory dysfunction	227	0	0	227	< 0.001
Renal dysfunction	64	0	0	64	< 0.001
Cardiovascular dysfunction	39	0	0	39	< 0.001
Hematological dysfunction	149	0	0	149	< 0.001
Hepatic dysfunction	83	0	0	83	< 0.001
Temperature (°C)-median (IQR)	37.0 (36.6-38)	36.8 (36.6-37.8)	37 (36.6-38.25)	37.2 (36.6-38.3)	0.001
Laboratory values					
WBC (/mm <sup>3</sup> )-median (IQR)	10560 (7705-14305)	9120 (7160-11165)	12700 (8897-18441)	11140 (7870-15810)	< 0.001
T-Bil (mg/dL)-median (IQR)	99.81 (62.43-155.76)	69.28 (49.625-120.975)	121.74 (88.97-184.41)	1041.2 (67.74-156.31)	< 0.001
Albumin (g/L)-median (IQR)	35.4 (31.2-39.2)	37.5 (34.2-40.4)	34.9 (30.8-38.1)	33.6 (29.2-37.8)	< 0.001
Lactate (mmol/L)-median (IQR)	2.15 (1.6-3.4)	1.8 (1.4-2.7)	2.1 (1.5-2.8)	2.4 (1.7-4.1)	< 0.001

IQR: Interquartile range; CCI: Charlton Comorbidity Index; LOS: Length of stay; CNY: Chinese Yuan; IHM: In-hospital mortality; WBC: White blood cell count; T-Bil: Total bilirubin.

The association of the IHM, LOS, and hospitalization costs with the timing of biliary drainage in each severity grade has been presented in Table 3. Biliary drainage significantly decreased the IHM in all AC patients (13/915 vs 28/390,  $P < 0.001$ ). Among individuals with Grade III cholangitis, the IHM rate was significantly decreased in patients who had biliary drainage within 24 h or 48 h ( $P = 0.041$ ,  $P = 0.018$ ), while the LOS was significantly increased among those patients who underwent drainage within 12 h, 24 h, or 48 h ( $P < 0.001$ ,  $P < 0.001$ , and  $P < 0.001$ , respectively). Hospitalization costs significantly increased for all patients with biliary drainage, regardless of severity criteria. For patients with Grade I AC, IHM was not affected by the timing of drainage and there was no relationship between LOS and the timing of biliary drainage for the survivors, but LOS was significantly extended in all the patients who underwent biliary drainage within 24 h or 48 h ( $P = 0.004$ ,  $P = 0.002$ ).

Univariate and multivariate analyses of predictors, including TG18 severity grading factors, lactate, CCI, and etiology of malignant obstruction, are shown in Table 4. In the univariate analysis, organ dysfunction, abnormal WBC count, hypoalbuminemia, CCI > 3, and etiology of malignancy were significantly associated with IHM. In a multivariate analysis of organ dysfunction, only neurological, respiratory, renal, and cardiovascular dysfunction, hypoalbuminemia, and malignant obstruction were significantly positively associated with IHM (OR = 5.32, 2.541, 6.356, 4.021, 5.655, and 7.522;  $P < 0.001$ ,  $P = 0.016$ ,  $P < 0.001$ ,  $P = 0.012$ ,  $P < 0.001$ , and  $P < 0.001$ , respectively).

Table 2 Characteristics data for patients with drainage

Characteristics, n (%)	Total (n = 915)	Grade I (n = 302)	Grade II (n = 306)	Grade III (n = 307)	P value
Drainage method, n (%)					0.001
ERCP	830 (90.7)	289 (95.7)	269 (87.9)	272 (88.6)	
PTBD	85 (9.3)	13 (4.3)	37 (12.1)	35 (11.4)	
Timing of drainage (hours)- median (IQR), n (%)	24.0 (60.0)	26.4 (62.4)	26.4 (62.4)	21.6 (45.6)	0.001
Biliary drainage within, n (%)					0.001
12 h	212 (23.2)	54 (17.9)	69 (22.5)	89 (29.0)	
12-24 h	233 (25.5)	74 (24.5)	70 (22.9)	89 (29.0)	
24-48 h	172 (18.8)	71 (23.5)	54 (17.6)	47 (15.3)	
> 48 h	298 (32.6)	103 (34.1)	113 (36.9)	82 (26.7)	
Second intervention, n (%)	478 (52.2)	159 (52.6)	154 (50.3)	165 (53.7)	0.688
Drainage outside working hours, n (%)	207 (22.6)	49 (16.2)	60 (19.6)	98 (31.9)	< 0.001
Adverse events, n (%)					
Pancreatitis	75 (8.2)	23 (7.6)	23 (7.5)	29 (9.4)	0.643
Cholangitis	8 (0.9)	2 (0.7)	2 (0.7)	4 (1.3)	0.742
Perforation	7 (0.8)	1 (0.3)	2 (0.7)	0 (0)	0.440
Bile leak	4 (0.4)	2 (0.7)	1 (0.3)	1 (0.3)	0.701
Myocardial infarction	5 (0.5)	0 (0)	3 (1.0)	2 (0.7)	0.339

IQR: Interquartile range; ERCP: Endoscopic retrograde cholangiopancreatography; PTBD: Percutaneous transhepatic biliary drainage.

From the data presented in Table 4, the association between IHM and the timing of biliary drainage for each clinical predictor is reflected. Among patients with AC complicated with neurological dysfunction or hyperlactatemia, the IHM rate was significantly decreased in individuals who underwent biliary decompression within 12 h ( $P = 0.041$ ,  $P = 0.016$ ), while those patients complicated with neurological dysfunction who had drainage within 24 h or 48 h could not improve prognosis compared with those who underwent drainage after 24 or 48 h, as well as those who did not undergo biliary drainage after admission ( $P = 0.175$ ,  $P = 0.304$ ). In patients with renal dysfunction, abnormal WBC count, hyperbilirubinemia, hypoalbuminemia, or hyperlactatemia, who had biliary decompression within 24 h or 48 h, there were significantly lower IHM rates than those of the remaining patients in each subgroup. Among patients with AC complicated with hepatic dysfunction, higher CCI ( $> 3$ ), or malignancy, a lower IHM rate was significantly associated with early drainage ( $< 48$  h) ( $P = 0.016$ ,  $P = 0.006$ ,  $P = 0.021$ ).

## DISCUSSION

In this retrospective monocenter cohort analysis including 1305 AC patients stratified according to TG18 severity criteria, early drainage ( $< 24$  h) in Grade III AC patients had the greatest benefit, which could significantly reduce the all-cause IHM. It is worth noting that, in this subgroup, patients complicated with neurological dysfunction should be drained as early as possible ( $< 12$  h). Moreover, early drainage was also required for AC patients with lactate more than 2 mmol/L, abnormal WBC count, hyperbilirubinemia, or hypoalbuminemia. Although these patients may have no severe cholangitis, early drainage could significantly reduce IHM and benefit the most. However, it should be noted that our results did not prove that drainage reduced hospitalization costs compared to conservative treatment. Furthermore, early drainage increased hospitalization costs and LOS.

AC is a clinically heterogeneous disease with recent mortality rates ranging from 2.7% to 10%, which is considered as an improvement since these rates were as high as 50%-60% in severe cases[15,16]. Although it is well-accepted that biliary decompression can significantly decrease the mortality of AC, it is highly debatable as to what the optimal strategy is for performing biliary drainage procedures. Should drainage occur as early as possible or should the procedure be delayed until stabilization after adequate resuscitation, especially for Grade III AC patients? Our study showed that biliary drainage could significantly decrease the IHM of AC patients (1.4% vs 7.2%,  $P < 0.001$ ), and AC patients of Grade

**Table 3 Association of the clinical outcomes in relation to the timing of biliary drainage and severity grading by Tokyo guidelines 2018**

Severity of AC	Characteristic-median (IQR)	Drainage	Absence of drainage	P value	Drainage < 12 h	Drainage > 12 h or absence	P value	Drainage < 24 h	Drainage > 24 h or absence	P value	Drainage < 48 h	Drainage > 48 h or absence	P value
Grade I	IHM	0/302	1/131	0.303	0/54	1/379	1.000	0/128	1/305	1.000	0/199	1/234	1.000
	LOS (d)	11 (9-15)	7 (4-10)	< 0.001	11 (8-13.25)	10 (8-14)	0.778	11 (8-14)	10 (7-14)	0.004	11 (8-14)	10 (6-14)	0.002
	Survivors' LOS (d) (n = 387)	12 (9-15)	8 (5-11)	< 0.001	11 (8-13.25)	11 (8-14)	0.794	11 (9-14)	11 (8-14)	0.065	11 (9-14)	10 (8-14)	0.101
	Hospitalization cost (CNY)	42845.67 (33734.18-52209.23)	15763.10 (7737.32-23680.31)	< 0.001	43328.59 (32863.61-49384.19)	35317.71 (18848.59-46850.08)	0.001	44154.19 (35638.76-52219.56)	31292.68 (16269.75-44599.67)	< 0.001	42908.34 (33358.44-50564.68)	25519.43 (12347.06-42424.96)	< 0.001
	Survivors' hospitalization cost (CNY) (n = 387)	42957.18 (33973.58-52224.73)	16596.85 (9096.73-24755.65)	< 0.001	43462.72 (36174.00-49384.19)	36604.86 (21962.98-47554.27)	0.003	44443.3 (35988.02-52237.14)	33492.6 (46019.17-18880.26)	< 0.001	43264.07 (34606.54-51093.62)	29762.32 (16376.75-44463.21)	< 0.001
Grade II	IHM	2/306	5/99	0.011	0/69	7/336	0.608	0/139	7/266	0.101	1/193	6/212	0.125
	LOS (d)	11 (9-15)	7 (4-12)	< 0.001	11 (8-14)	11 (7-14)	0.684	11 (9-14)	10 (7-14)	0.122	11 (8-14)	10 (7-14.8)	0.190
	Survivors' LOS (d) (n = 349)	12 (9-15)	7.5 (4.75-11.25)	< 0.001	11.5 (9-14)	11 (8-14)	0.367	12 (10-14)	11 (7-14)	0.024	12 (9-14)	11 (7-14)	0.050
	Hospitalization cost (CNY)	44033.13 (31071.05-56134.72)	17626.20 (10037.69-25587.43)	< 0.001	45832.44 (36061.53-56949.37)	36132.93 (21795.89-51453.62)	< 0.001	46789.09 (35989.59-57723.15)	31505.72 (19948.31-47463.61)	< 0.001	45489.74 (33858.99-57600.43)	29275.30 (16928.45-46255.47)	< 0.001
	Survivors' hospitalization cost (CNY) (n = 349)	45004.20 (32631.09-56660.62)	16342.15 (10300.68-25017.80)	< 0.001	47938.00 (37937.29-58046.02)	36629.15 (22828.93-51509.37)	< 0.001	48254.61 (37937.29-58929.51)	31589.96 (20386.80-47062.76)	< 0.001	46564.37 (36191.07-57998.63)	29338.38 (17687.02-45685.12)	< 0.001
Grade III	IHM	11/307	22/160	< 0.001	3/89	30/378	0.168	7/178	26/289	0.041	9/225	24/242	0.018
	LOS (d)	13 (9-17)	8 (3-12)	< 0.001	13 (11-19)	11 (6-15)	< 0.001	13 (10-17)	10 (6-14)	< 0.001	13 (9-17)	9.5 (5-14)	< 0.001
	Survivors' LOS (d) (n = 351)	13 (11-18)	9.5 (7-13.25)	< 0.001	13 (12-19)	12 (9-16)	0.001	13 (11-17.75)	12 (9-15)	< 0.001	13 (11-17.75)	11 (8-15)	< 0.001
	Hospitalization cost	51583.64 (38985.47-64886.01)	20183.58 (11317.37-29525.99)	< 0.001	56599.94 (43260.73-70300.00)	38527.58 (21034.79-55279.53)	< 0.001	55121.49 (40428.29-67707.01)	31832.99 (17933.81-50037.89)	< 0.001	54295.52 (39252.57-65638.57)	28165.23 (15708.29-45478.26)	< 0.001
	Survivors' hospitalization cost (CNY) (n = 351)	53507.33 (41027.94-65312.29)	22909.77 (15594.93-31845.39)	< 0.001	57976.4 (50131.44-70333.71)	43241.54 (28347.56-57860.29)	< 0.001	55873.84 (46654.40-69946.73)	38973.06 (24292.41-53090.85)	< 0.001	55782.38 (43994.26-66493.67)	34748.29 (21379.37-50147.24)	< 0.001

AC: Acute cholangitis; IQR: Interquartile range; IHM: In-hospital mortality; LOS: Length of stay; CNY: Chinese Yuan.

Table 4 Univariate and multivariate analysis of predictors of mortality, and relationship of mortality with the timing of drainage for each predictor

Predictors (n = 1305)	Univariate analysis		Multivariate analysis		Mortality to the timing of drainage								
	OR (95%CI)	P value	OR (95%CI)	P value	< 12 h	> 12 h or absence	P value	< 24 h	> 24 h or absence	P value	< 48 h	> 48 h or absence	P value
Neurological dysfunction	8.377 (4.384-16.007)	< 0.001	5.32 (2.373-11.931)	< 0.001	0/22	18/104	0.041	3/42	15/84	0.175	5/51	13/75	0.304
Respiratory dysfunction	2.886 (1.491-5.497)	0.003	2.541 (1.189-5.43)	0.016	1/44	14/183	0.314	4/91	11/136	0.414	6/117	9/110	0.428
Renal dysfunction	11.043 (5.402-22.573)	< 0.001	6.356 (2.623-15.397)	< 0.001	1/15	12/49	0.269	1/28	12/36	0.004	1/31	12/33	0.001
Cardiovascular dysfunction	11.569 (5.078-26.357)	< 0.001	4.021 (1.361-11.88)	0.012	0/7	9/32	0.169	2/16	7/23	0.262	2/18	7/21	0.139
Hematological dysfunction	2.611 (1.253-5.441)	0.02	N/A		2/37	8/104	1	3/61	7/88	0.527	3/74	7/75	0.327
Hepatic dysfunction	5.263 (2.484-11.152)	< 0.001	N/A		0/15	10/68	0.196	1/30	9/53	0.086	1/39	9/44	0.016
Age (≥ 75 yr)	1.432 (0.765-2.680)	0.261	N/A		2/88	21/531	0.759	4/196	19/423	0.172	7/267	16/352	0.284
Temperature (≥ 39 °C)	0.390 (0.093-1.631)	0.197	N/A		0/43	2/106	1	1/75	1/74	1	1/85	1/64	1
WBC (> 12000/mm <sup>3</sup> , < 4000/mm <sup>3</sup> )	1.962 (1.043-3.688)	0.036	N/A		1/107	23/445	0.063	4/207	20/342	0.031	6/278	18/275	0.012
T-Bil (≥ 5 mg/dL)	1.711 (0.865-3.385)	0.123	N/A		3/143	26/626	0.333	5/292	24/477	0.019	8/407	21/362	0.007
Albumin (< STD*0.7)	10.715 (5.147-22.303)	< 0.001	5.655 (2.398-13.335)	< 0.001	0/8	12/51	0.188	0/15	12/44	0.026	1/24	11/35	0.018
Lactate (≥ 2 mmol/L)	1.450 (0.766-2.747)	0.254	N/A		0/105	16/298	0.016	2/186	14/217	0.008	4/227	12/176	0.018
Malignant obstruction	5.495 (2.924-10.325)	< 0.001	7.522 (3.504-16.149)	< 0.001	1/26	21/216	0.483	2/59	20/183	0.116	3/101	19/141	0.006
CCI (> 3)	4.080 (2.153-7.7340)	< 0.001	N/A		2/57	23/318	0.397	4/127	21/248	0.052	6/177	19/198	0.021

WBC: White blood cell count; T-Bil: Total bilirubin; STD: Lower limit of normal value; CCI: Charlton Comorbidity Index; OR: Odds ratio; CI: Confidence interval; N/A: Not applicable.

III underwent decompression within 24 h or 48 h had lower IHM (3.9% vs 9.0%,  $P = 0.041$ ; 4% vs 9.9%,  $P = 0.018$ ). These findings are in line with the results of a large sample size retrospective study, which showed that drainage within 48 h was associated with improved IHM (3.4% vs 10.2%,  $P = 0.019$ )[17], although it did not discuss drainage within 24 h. Another retrospective study of 6063 patients with AC conducted by Kiriya *et al*[3] reported a distinct result: decompression within 24 h or 48 h improved the 30-d mortality rate only among Grade II patients (drainage within 24 h vs. after 24 h or no drainage: 1.7% vs 3.4%,  $P < 0.05$ ; drainage within 48 h vs after 48 h or no drainage: 2.0% vs 3.7%,  $P < 0.05$ ), and the drainage timing did not influence 30-d mortality in patients with Grade I and Grade III. This dissimilarity may be because we reviewed the all-cause IHM, while Kiriya *et al*'s study observed 30-d cholangitis-caused mortality, and the mortality rate of Grade III AC patients was lower than that in our study (5.1% vs 9.4%), especially for subgroups of delayed decompression in which more patients died from malignancy[3]. In addition, as the number and grade of patients without drainage were not shown in the results of Kiriya *et al*[3], the proportion of patients without drainage in our study may be different from the group studied by Kiriya *et al*[3]. Since then, few researchers have tried to examine

the possibility of improving the prognosis of Grade III AC patients by undergoing biliary drainage more immediately [6,8]. Unfortunately, consistent with our results, there was no evidence that earlier decompression (within 12 h) benefited these severe patients.

Another multicenter retrospective net cohort study reported a novel finding in which delayed biliary decompression (> 12 h) was significantly associated with increased mortality in AC patients combined with septic shock [OR 3.40 (1.12-10.31)] [7]. These results suggest that it may be necessary to approach each organ's failure separately and that different types of organ dysfunction should be considered when determining the optimal drainage timing. This was verified by our multivariable analysis which showed that neurological, respiratory, renal, and cardiovascular dysfunction were significantly associated with IHM (OR = 5.32, 2.541, 6.356, 4.021, respectively), whereas hepatic and hematological dysfunction did not influence IHM. In addition to indicators affecting mortality recommended in TG18, we also analyzed CCL, malignancy, and lactate levels, which were previously reported to have an impact on the death rate [5,7,18]. Multivariate regression analysis showed that, in addition to organ dysfunction, hypoproteinemia and malignant obstruction significantly increased IHM. These outcomes were similar to those reported in a previous review [3].

In this study, we first attempted to stratify Grade III AC patients according to organ dysfunction to identify patients whose prognosis could most likely be improved by earlier decompression. According to our clinical experience, neurological dysfunction was the most severe complication and might affect drainage operation; therefore, AC patients with altered mental status require immediate biliary decompression. This was verified by our data that only undergoing drainage within 12 h could greatly improve IHM in this subgroup of individuals (0% *vs* 17.3%,  $P = 0.041$ ). For AC patients with renal dysfunction, performing drainage within 24 h could decrease the IHM. As a result, the renal injury was not only caused by infection but also induced by hypovolemia, which was provoked by fever, decreased appetite, early initiation of antibiotics, and aggressive fluid resuscitation to improve renal flow were more valuable for these patients. Unlike previous studies [7], we did not observe an association between drainage and IHM in AC patients with cardiovascular dysfunction. This may be because only 39 patients were included in this subgroup. Drainage within 12 h significantly reduced mortality in AC patients with increased lactate levels ( $\geq 2$  mmol/L), suggesting that decompression within 12 h might be beneficial for patients with cardiovascular dysfunction. Performing drainage within 48 h greatly reduced mortality in AC patients with hepatic dysfunction, because the amelioration of biliary stasis after drainage could directly rescue hepatic function and diminish inflammatory reaction, even if no significant association between hepatic injury and IHM was observed.

The influence of abnormal WBC count and hyperbilirubinemia on outcomes in AC has been previously described [9]. The underlying pathophysiologic mechanisms are known to result from sepsis; therefore, abnormal WBC count and hyperbilirubinemia are linked with an increased likelihood of poor prognosis. Hypoalbuminemia refers to malnutrition, which is linked to life-threatening infections and poor outcomes. For individuals in these subgroups, undergoing drainage within 24 h indicated a lower IHM.

Decompression within 12, 24, or 48 h in Grade III AC patients would extend the LOS, which was contrary to the findings of Aboelsoud *et al* [19] who demonstrated that drainage within 24 h or 48 h could decrease the LOS, compared with drainage after 24 h or 48 h (drainage within 24 h *vs* after 24 h: mean 7.71 *vs* 13.57 d,  $P = 0.001$ ; drainage within 48 h *vs* after 48 h: mean 8.61 *vs* 14.24 d,  $P = 0.002$ ). This was because their study only reviewed patients who underwent drainage, whereas our study included both patients who underwent drainage and those who did not. In addition, most of the Grade II and Grade III patients in this study received only endoscopic nasobiliary drainage or endoscopic retrograde biliary drainage treatment at the first ERCP intervention because of their serious condition, and 52.2% of them received a second endoscopic intervention for biliary stone removal or stent placement when their condition stabilized, thus increasing the LOS. Drainage within 12, 24, or 48 h was associated with increased hospital costs despite the severity of AC since endoscopic operation itself was expensive, and the delayed-drainage group contained non-drainage ones who spent little.

### Limits of study

Our analysis had certain limitations. First, it was retrospective in design, and as such, was susceptible to record bias and incomplete data. Second, because it is a single-center study, the study results only reflect the clinical status of our center and cannot represent the situation of all hospitals. Third, due to the limited sample size, especially the limited number of patients with cardiovascular dysfunction who underwent drainage within 48 h, some results were not statistically significant. In addition, the time from onset to initial treatment and the antibiotics and fluid resuscitation before admission to our hospital were not evaluated, which may have an impact on the outcome. A prospective multicenter study will be conducted to further explore a precise stratified model to guide drainage timing rather than TG18.

## CONCLUSION

To our knowledge, this is the first study to stratify patients with Grade III AC according to different organ dysfunctions and to recommend the optimal timing of biliary drainage accordingly. Biliary decompression significantly decreases the all-cause IHM rates in AC, and early biliary drainage (< 24 h) was shown to be beneficial for AC patients with Grade III severity. Severe cases with different organ dysfunctions have distinct prognoses, and cases complicated with either neurological or cardiovascular dysfunction should undergo drainage within 12 h of admission. For patients with mild or moderate cholangitis, early drainage increases the probability of a second treatment and increases the patients' injury, hospitalization cost, and LOS. A further multicenter prospective cohort study will be conducted to verify the result and investigate whether the optimal timing of drainage based on different organ dysfunctions can increase the 30-d mortality rates and decrease the readmission rate.

## ARTICLE HIGHLIGHTS

### **Research background**

Acute cholangitis (AC) is a life-threatening condition that occurs in the presence of biliary obstruction. Biliary decompression is well known to greatly decrease the risks of mortality in AC. Although early biliary drainage is recommended by the treatment guidelines for AC, the exact timeframe is yet to be established.

### **Research motivation**

We have observed that the clinical outcomes of severe AC patients vary dramatically. So, we first attempted to study whether AC patients with different organ dysfunction should undergo biliary drainage at distinct times and try to screen out patients that could benefit the most from earlier drainage.

### **Research objectives**

To investigate the optimal drainage timing for AC patients with each disease severity grade and organ dysfunction.

### **Research methods**

In this retrospective monocenter cohort analysis, we reviewed 1305 patients who were diagnosed with AC according to the Tokyo guidelines 2018 at a Chinese tertiary hospital for four years. We investigated the all-cause in-hospital mortality (IHM), hospital length of stay (LOS), and hospitalization costs associated with the timing of biliary drainage according to the severity grading and different dysfunctioning organs and critical predictors [age, white blood cell (WBC) count, total bilirubin, albumin, lactate, malignant obstruction, and Charlton comorbidity index (CCI)].

### **Research results**

Biliary drainage within 24 h in Grade III AC patients had the greatest benefit, which could significantly reduce the all-cause IHM, while increasing LOS and hospitalization costs. Multivariate logistic analysis revealed that neurological, respiratory, renal, and cardiovascular dysfunctions, hypoalbuminemia, and malignant obstruction were significantly associated with IHM. Furthermore, AC patients complicated with neurological dysfunction or with serum lactate > 2 mmol/L should be drained as early as possible (< 12 h) for it could significantly decrease the IHM. In the subgroup of AC patients with renal dysfunction, abnormal WBC count, hyperbilirubinemia, or hypoalbuminemia, drainage within 24 h reduced the IHM, while in the subgroup of AC patients with hepatic dysfunction, malignant obstruction, or a CCI > 3, biliary drainage should be performed within 48 h.

### **Research conclusions**

Biliary drainage within 12 h is beneficial for AC patients with neurological or cardiovascular dysfunction, while complete biliary decompression within 24 h of admission is recommended for treating patients with Grade III AC.

### **Research perspectives**

A further multicenter prospective cohort study will be conducted to verify the result and investigate whether the optimal timing of drainage based on different organ dysfunctions can increase the 30-d mortality rates and decrease the readmission rate.

---

## FOOTNOTES

**Author contributions:** Li CS designed the research study and made critical revisions to the article; Lu ZQ, Zhang HY, Xing YY, Su CF, and Wang GX performed the research and analyzed the data; Lu ZQ drafted the article; all authors have read and approved the final manuscript.

**Institutional review board statement:** This retrospective cohort study was conducted according to the tenets of the Declaration of Helsinki, and approved by the Bioethics Committee of Beijing Friendship Hospital, Capital Medical University (Certification No. 2020-P2-224-01).

**Informed consent statement:** Since we conducted a retrospective review of patient data obtained from the electronic medical records of our hospital, and as stated by the ethical standards of China, the Ethics Committee exempted the need for obtaining informed consent.

**Conflict-of-interest statement:** All the Authors have no conflict of interest related to the manuscript.

**Data sharing statement:** The datasets used during the current study are available from the corresponding author on reasonable request at [lscyy@163.com](mailto:lscyy@163.com).

**STROBE statement:** The authors have read the STROBE Statement – checklist of items, and the manuscript was prepared and revised according to the STROBE Statement – checklist of items.

**Open-Access:** This article is an open-access article that was selected by an in-house editor and fully peer-reviewed by external reviewers. It is distributed in accordance with the Creative Commons Attribution NonCommercial (CC BY-NC 4.0) license, which permits others to distribute, remix, adapt, build upon this work non-commercially, and license their derivative works on different terms, provided the original work is properly cited and the use is non-commercial. See: <https://creativecommons.org/licenses/by-nc/4.0/>

**Country/Territory of origin:** China

**ORCID number:** Zhao-Qing Lu 0000-0001-8895-1596; Han-Yu Zhang 0000-0001-5181-4619; Chen-Fen Su 0000-0002-7882-6975; Yue-Yan Xing 0000-0002-6162-3098; Guo-Xing Wang 0000-0003-1379-5749; Chun-Sheng Li 0000-0002-3161-4457.

**S-Editor:** Yan JP

**L-Editor:** A

**P-Editor:** Yan JP

---

## REFERENCES

- 1 **Buxbaum JL**, Buitrago C, Lee A, Elmunzer BJ, Riaz A, Ceppa EP, Al-Haddad M, Amateau SK, Calderwood AH, Fishman DS, Fujii-Lau LL, Jamil LH, Jue TL, Kwon RS, Law JK, Lee JK, Naveed M, Pawa S, Sawhney MS, Schilperoort H, Storm AC, Thosani NC, Qumseya BJ, Wani S. ASGE guideline on the management of cholangitis. *Gastrointest Endosc* 2021; **94**: 207-221.e14 [PMID: 34023065 DOI: 10.1016/j.gie.2020.12.032]
- 2 **Manes G**, Paspatis G, Aabakken L, Anderloni A, Arvanitakis M, Ah-Soune P, Barthet M, Domagk D, Dumonceau JM, Gigot JF, Hritz I, Karamanolis G, Laghi A, Mariani A, Paraskeva K, Pohl J, Ponchon T, Swahn F, Ter Steege RWF, Tringali A, Vezakis A, Williams EJ, van Hooft JE. Endoscopic management of common bile duct stones: European Society of Gastrointestinal Endoscopy (ESGE) guideline. *Endoscopy* 2019; **51**: 472-491 [PMID: 30943551 DOI: 10.1055/a-0862-0346]
- 3 **Kiriyama S**, Takada T, Hwang TL, Akazawa K, Miura F, Gomi H, Mori R, Endo I, Itoi T, Yokoe M, Chen MF, Jan YY, Ker CG, Wang HP, Wada K, Yamaue H, Miyazaki M, Yamamoto M. Clinical application and verification of the TG13 diagnostic and severity grading criteria for acute cholangitis: an international multicenter observational study. *J Hepatobiliary Pancreat Sci* 2017; **24**: 329-337 [PMID: 28419764 DOI: 10.1002/jhbp.458]
- 4 **Miura F**, Okamoto K, Takada T, Strasberg SM, Asbun HJ, Pitt HA, Gomi H, Solomkin JS, Schlossberg D, Han HS, Kim MH, Hwang TL, Chen MF, Huang WS, Kiriyama S, Itoi T, Garden OJ, Liau KH, Horiguchi A, Liu KH, Su CH, Gouma DJ, Belli G, Dervenis C, Jagannath P, Chan ACW, Lau WY, Endo I, Suzuki K, Yoon YS, de Santibañes E, Giménez ME, Jonas E, Singh H, Honda G, Asai K, Mori Y, Wada K, Higuchi R, Watanabe M, Rikiyama T, Sata N, Kano N, Umezawa A, Mukai S, Tokumura H, Hata J, Kozaka K, Iwashita Y, Hibi T, Yokoe M, Kimura T, Kitano S, Inomata M, Hirata K, Sumiyama Y, Inui K, Yamamoto M. Tokyo Guidelines 2018: initial management of acute biliary infection and flowchart for acute cholangitis. *J Hepatobiliary Pancreat Sci* 2018; **25**: 31-40 [PMID: 28941329 DOI: 10.1002/jhbp.509]
- 5 **Navaneethan U**, Gutierrez NG, Jegadeesan R, Venkatesh PG, Butt M, Sanaka MR, Vargo JJ, Parsi MA. Delay in performing ERCP and adverse events increase the 30-day readmission risk in patients with acute cholangitis. *Gastrointest Endosc* 2013; **78**: 81-90 [PMID: 23528654 DOI: 10.1016/j.gie.2013.02.003]
- 6 **Khamaysi I**, Taha R. ERCP for severe acute cholangitis: The earlier, the better. *Turk J Gastroenterol* 2020; **31**: 78-79 [PMID: 32009619 DOI: 10.5152/tjg.2020.19103]
- 7 **Karvellas CJ**, Abalde JG, Zepeda-Gomez S, Moffat DC, Mirzanejad Y, Vazquez-Grande G, Esfahani EK, Kumar A; Cooperative Antimicrobial Therapy of Septic Shock (CATSS) Database Research Group. The impact of delayed biliary

- decompression and anti-microbial therapy in 260 patients with cholangitis-associated septic shock. *Aliment Pharmacol Ther* 2016; **44**: 755-766 [PMID: 27506331 DOI: 10.1111/apt.13764]
- 8 **Becq A**, Chandnani M, Bartley A, Nuzzo A, Bilal M, Bharadwaj S, Cohen J, Gabr M, Berzin TM, Pleskow DK, Sawhney MS. ERCP within 6 or 12 h for acute cholangitis: a propensity score-matched analysis. *Surg Endosc* 2022; **36**: 2418-2429 [PMID: 33977378 DOI: 10.1007/s00464-021-08523-w]
  - 9 **Schwed AC**, Boggs MM, Pham XD, Watanabe DM, Bermudez MC, Kaji AH, Kim DY, Plurad DS, Saltzman DJ, de Virgilio C. Association of Admission Laboratory Values and the Timing of Endoscopic Retrograde Cholangiopancreatography With Clinical Outcomes in Acute Cholangitis. *JAMA Surg* 2016; **151**: 1039-1045 [PMID: 27557050 DOI: 10.1001/jamasurg.2016.2329]
  - 10 **Tabibian JH**, Yang JD, Baron TH, Kane SV, Enders FB, Gostout CJ. Weekend Admission for Acute Cholangitis Does Not Adversely Impact Clinical or Endoscopic Outcomes. *Dig Dis Sci* 2016; **61**: 53-61 [PMID: 26391268 DOI: 10.1007/s10620-015-3853-z]
  - 11 **Inamdar S**, Sejpal DV, Ullah M, Trindade AJ. Weekend vs. Weekday Admissions for Cholangitis Requiring an ERCP: Comparison of Outcomes in a National Cohort. *Am J Gastroenterol* 2016; **111**: 405-410 [PMID: 26782818 DOI: 10.1038/ajg.2015.425]
  - 12 **Kiriyama S**, Kozaka K, Takada T, Strasberg SM, Pitt HA, Gabata T, Hata J, Liao KH, Miura F, Horiguchi A, Liu KH, Su CH, Wada K, Jagannath P, Itoi T, Gouma DJ, Mori Y, Mukai S, Giménez ME, Huang WS, Kim MH, Okamoto K, Belli G, Dervenis C, Chan ACW, Lau WY, Endo I, Gomi H, Yoshida M, Mayumi T, Baron TH, de Santibañes E, Teoh AYB, Hwang TL, Ker CG, Chen MF, Han HS, Yoon YS, Choi IS, Yoon DS, Higuchi R, Kitano S, Inomata M, Deziel DJ, Jonas E, Hirata K, Sumiyama Y, Inui K, Yamamoto M. Tokyo Guidelines 2018: diagnostic criteria and severity grading of acute cholangitis (with videos). *J Hepatobiliary Pancreat Sci* 2018; **25**: 17-30 [PMID: 29032610 DOI: 10.1002/jbhp.512]
  - 13 **Cotton PB**, Eisen GM, Aabakken L, Baron TH, Hutter MM, Jacobson BC, Mergener K, Nemcek A Jr, Petersen BT, Petrini JL, Pike IM, Rabeneck L, Romagnuolo J, Vargo JJ. A lexicon for endoscopic adverse events: report of an ASGE workshop. *Gastrointest Endosc* 2010; **71**: 446-454 [PMID: 20189503 DOI: 10.1016/j.gie.2009.10.027]
  - 14 **ERCP group of Digestive Endoscopy Branch of Chinese Medical Association**; Biliopancreology Group of Gastroenterologist Branch of Chinese Medical Association, National Clinical Research Center for Digestive Diseases. ERCP Guidelines for China (2018). *Zhonghua Xiaohua Beijing Zazhi* 2018; **35**: 777-813
  - 15 **Andrew DJ**, Johnson SE. Acute suppurative cholangitis, a medical and surgical emergency. A review of ten years experience emphasizing early recognition. *Am J Gastroenterol* 1970; **54**: 141-154 [PMID: 5458220]
  - 16 **Shimada H**, Nakagawara G, Kobayashi M, Tsuchiya S, Kudo T, Morita S. Pathogenesis and clinical features of acute cholangitis accompanied by shock. *Jpn J Surg* 1984; **14**: 269-277 [PMID: 6436560 DOI: 10.1007/bf02469641]
  - 17 **Mulki R**, Shah R, Qayed E. Early vs late endoscopic retrograde cholangiopancreatography in patients with acute cholangitis: A nationwide analysis. *World J Gastrointest Endosc* 2019; **11**: 41-53 [PMID: 30705731 DOI: 10.4253/wjge.v11.i1.41]
  - 18 **Lee F**, Ohanian E, Rheem J, Laine L, Che K, Kim JJ. Delayed endoscopic retrograde cholangiopancreatography is associated with persistent organ failure in hospitalised patients with acute cholangitis. *Aliment Pharmacol Ther* 2015; **42**: 212-220 [PMID: 25997554 DOI: 10.1111/apt.13253]
  - 19 **Abolsoud M**, Siddique O, Morales A, Seol Y, Al-Qadi M. Early biliary drainage is associated with favourable outcomes in critically-ill patients with acute cholangitis. *Prz Gastroenterol* 2018; **13**: 16-21 [PMID: 29657606 DOI: 10.5114/pg.2018.74557]

## Retrospective Study

## Incidence and clinical characteristics of hypertriglyceridemic acute pancreatitis: A retrospective single-center study

Xue-Yan Lin, Yi Zeng, Zheng-Chao Zhang, Zhi-Hui Lin, Lu-Chuan Chen, Zai-Sheng Ye

**Specialty type:** Gastroenterology and hepatology**Provenance and peer review:** Invited article; Externally peer reviewed.**Peer-review model:** Single blind**Peer-review report's scientific quality classification**Grade A (Excellent): A  
Grade B (Very good): B, B  
Grade C (Good): C, C, C  
Grade D (Fair): D  
Grade E (Poor): 0**P-Reviewer:** Cho E, South Korea; Fujimori N, Japan; Gupta R, India; Kitamura K, Japan; Trna J, Czech Republic**Received:** December 6, 2021**Peer-review started:** December 6, 2021**First decision:** April 16, 2022**Revised:** April 25, 2022**Accepted:** June 30, 2022**Article in press:** June 30, 2022**Published online:** August 7, 2022**Xue-Yan Lin, Zhi-Hui Lin,** Department of Gastroenterology, Fujian Provincial Hospital, Fujian Medical University Provincial of Clinical Medicine, Fuzhou 350001, Fujian Province, China**Yi Zeng, Lu-Chuan Chen, Zai-Sheng Ye,** Department of Gastrointestinal Surgical Oncology, Fujian Cancer Hospital, Fujian Medical University Cancer Hospital, Fuzhou 350014, Fujian Province, China**Zheng-Chao Zhang,** Department of Emergency Surgery, Fujian Provincial Hospital, Fujian Medical University Provincial of Clinical Medicine, Fuzhou 350001, Fujian Province, China**Corresponding author:** Zai-Sheng Ye, PhD, Attending Doctor, Surgical Oncologist, Teacher, Department of Gastrointestinal Surgical Oncology, Fujian Cancer Hospital, Fujian Medical University Cancer Hospital, No. 420 Fuma Road, Fuzhou 350014, Fujian Province, China. [flyingengel@sina.cn](mailto:flyingengel@sina.cn)**Abstract****BACKGROUND**

The incidence of hypertriglyceridemic acute pancreatitis (HTG-AP) has increased yearly, but updated population-based estimates on the incidence of HTG-AP are lacking. Reducing serum triglyceride (TG) levels quickly is crucial in the early treatment of HTG-AP. Decreased serum TG levels are treated by non-invasive methods, which include anti-lipidemic agents, heparin, low-molecular weight heparin, and insulin, and invasive methods, such as blood purification including hemoperfusion (HP), plasmapheresis, and continuous renal replacement therapy. However, authoritative guidelines have not been established. Early selection of appropriate treatment is important and beneficial in controlling the development of HTG-AP.

**AIM**

To evaluate the effect between patients treated with intravenous insulin (INS) and HP to guide clinical treatment.

**METHODS**

We retrospectively reviewed 371 patients with HTG-AP enrolled in the Department of Fujian Provincial Hospital from April 2012 to March 2021. The inpatient medical and radiologic records were reviewed to determine clinical features, severity, complications, mortality, recurrence rate, and treatment. Multivariate logistic regression analyses were used to analyze risk factors for

severe HTG-AP. Propensity score matching was used to compare the clinical outcomes of INS and HP.

## RESULTS

A total of 371 patients met the HTG-AP criteria. The incidence of HTG-AP was increased by approximately 2.6 times during the 10 years (8.4% in April 2012-March 2013 and 22.3% in April 2020-March 2021). The highest incidence rate of acute pancreatitis was observed for men in the age group of 30-39 years. The amylase level was elevated in 80.1% of patients but was only three times the normal value in 46.9% of patients. The frequency of severe acute pancreatitis (26.9%), organ failure (31.5%), rate of recurrence (32.9%), and mortality (3.0%) of HTG-AP was high. Improved Marshall score, modified computed tomography severity index score, baseline TG, baseline amylase, C-reactive protein (CRP), albumin, aspartate aminotransferase, low-density lipoprotein cholesterol, urea nitrogen, creatinine, calcium, hemoglobin, free triiodothyronine, admission to intensive care unit, and mortality were significantly different between patients with different grades of severity ( $P < 0.050$ ). Multivariate logistic regression analysis confirmed that high CRP [ $P = 0.005$ , odds ratio (OR) = 1.011, 95%CI: 1.003-1.019], low calcium ( $P = 0.003$ , OR = 0.016, 95%CI: 0.001-0.239), and low albumin ( $P = 0.023$ , OR = 0.821, 95%CI: 0.693-0.973) were risk factors of severe HTG-AP. After propensity score matching adjusted by sex, age, severity of HTG-AP, and baseline TG, the serum TG significantly decreased in patients treated with INS ( $P < 0.000$ ) and HP ( $P < 0.000$ ) within 48 h. However, the clearance rate of TG ( $57.24 \pm 33.70\%$  vs  $56.38 \pm 33.61\%$ ,  $P = 0.927$ ) and length of stay ( $13.04 \pm 7.92$  d vs  $12.35 \pm 6.40$  d,  $P = 0.730$ ) did not differ between the two groups.

## CONCLUSION

The incidence of HTG-AP exhibited a significant increase, remarkable severity, and recurrent trend. Patients with mild and moderately severe acute pancreatitis can be treated effectively with INS safely and effectively without HP.

**Key Words:** Hypertriglyceridemic acute pancreatitis; Triglyceride; Improved Marshall score; Severity of acute pancreatitis; Intravenous insulin; Hemoperfusion

©The Author(s) 2022. Published by Baishideng Publishing Group Inc. All rights reserved.

**Core Tip:** We assessed the clinical characteristics of hypertriglyceridemic acute pancreatitis, determined factors related to grades of severity, and evaluated differences in clinical outcomes between patients treated with intravenous insulin and hemoperfusion to guide clinical diagnosis and treatment.

**Citation:** Lin XY, Zeng Y, Zhang ZC, Lin ZH, Chen LC, Ye ZS. Incidence and clinical characteristics of hypertriglyceridemic acute pancreatitis: A retrospective single-center study. *World J Gastroenterol* 2022; 28(29): 3946-3959

**URL:** <https://www.wjgnet.com/1007-9327/full/v28/i29/3946.htm>

**DOI:** <https://dx.doi.org/10.3748/wjg.v28.i29.3946>

## INTRODUCTION

Acute pancreatitis (AP) is an inflammatory condition of the pancreas that originates within the pancreatic acinar cells and causes pancreatic necrosis, systemic inflammatory response syndrome, and multiple organ failure[1], with a mortality rate for severe cases as high as 20%-25%[2]. The great majority of AP is driven by gallstones (40%-70%) and alcohol (25%-35%)[3]. With the change of people's diet structure and lifestyle, the incidence and mortality of hypertriglyceridemic (HTG)-AP are increasing year by year and has surpassed alcohol as the second leading cause of AP in China[4]. The standardized incidence rate of HTG-AP increased from 0.7 to 1.7 per 100000 person-years from 2008 to 2019 in Denmark[5], and the incidence has increased by 2.4 times in 10 years. However, the increasing number of HTG-AP incidence remains unclear in China.

The mechanism by which severe HTG precipitates to AP remains unknown. Studies have shown that pancreatic lipase hydrolyses excess triglyceride (TG) with accumulation of free fatty acids, thereby inducing the production of acinar cell and pancreatic capillary injury; chylomicrons lead to increased blood viscosity and local tissue ischemia[6,7]. Therefore, early detection of serum TG and active treatment measures to reduce serum TG are crucial for the prognosis of AP. Some scholars believe that

rapid reduction of serum triglyceride levels within 48 h before the onset of HTG-AP is the key to treatment[8]. Effective treatments of reducing serum TG levels include anti-lipidemic agents, insulin, heparin, low-molecular weight heparin, and blood purification, such as hemoperfusion (HP), plasmapheresis (PE), and continuous renal replacement therapy[6,9]; however, no HTG-AP treatment guideline has been established. At present, selecting routine treatment or blood purification for patients with HTG-AP after admission remains controversial.

In view of the increasing incidence of HTG-AP in recent years and its short and long-term harmful effects on patients, families, and society, scholars have focused on preventing and effectively blocking HTG-AP as well as on its diagnosis and treatment. However, the causes remain unknown[10-12]; the low elevation of amylase (AMY) levels[13] and other characteristics[14] lead to the early misdiagnosis of HTG-AP. In addition, HTG-AP is prone to young age of onset[10], many complications[15], higher chance of systemic inflammatory response syndrome and cardiopulmonary and renal insufficiency[16], severe tendency[17], and lack of unified clinical treatment standards, which bring some difficulties to clinical treatment.

This study aims to improve the clinical diagnosis rate of HTG-AP by summarizing the clinical characteristics of HTG-AP and developing appropriate and cost-effective treatments for patients with HTG-AP.

## MATERIALS AND METHODS

### Patients

From April 2012 to March 2021, AP was diagnosed in 2206 patients in the Fujian Provincial Hospital. A total of 371 hospitalized patients who met the diagnostic criteria of HTG-AP were retrospectively studied, and 219 patients met the inclusion and exclusion criteria that were used to explore risk factors for severe HTG-AP. Fifty-two patients were included after propensity score matching (PSM) was adjusted by sex, age, grades of severity, and baseline TG. Clinical outcomes were compared between the 52 patients treated with intravenous insulin (INS) and HP (Figure 1). The Ethics Committee of Fujian Provincial Hospital approved the study (K2021-02-007).

The inclusion criteria were as follows: (1) Diagnosis of HTG-AP; (2) Admission within 72 h after onset; (3) Age older than 18 years; (4) Assessment of the first episode (for patients with multiple episodes of AP); and (5) Serum TG detected within 24 h after admission.

The exclusion criteria were as follows: (1) Did not undergo serum lipid detection within 48 h after treatment upon hospitalization; (2) AP due to other etiologies (including gallstones, alcohol, autoimmune, drug-induced, hypercalcemia, hyperparathyroidism, pancreatic tumor-related etiology of AP); (3) Treatment in another hospital; and (4) Incomplete information.

### Grouping methods

According to the grades of severity standard in the Revised Atlanta Classification, patients were classified into the mild acute pancreatitis (MAP) group, moderately severe acute pancreatitis (MSAP) group, and severe acute pancreatitis (SAP) groups.

Patients were divided into the INS group and HP group according to treatment method. All patients were given basic support treatment including abrosia, gastrointestinal decompression, enema, fluid resuscitation, water maintenance, electrolyte and acid-base balance, lactulose to improve intestinal function, low molecular weight heparin, proton pump inhibitors for gastric acid secretion, and somatostatin/octreotide inhibitor pancreatic secretion. The INS group was given INS. The HP group was treated with HP. Blood access was established by puncture of the femoral vein or internal jugular vein. HP was performed with a resin irrigator (HA330, Zhuhai Lizhu Group, Biological Material Co, Ltd., China) for 2 h every 24 h with a blood flow of 150-250 mL/min. During the procedure, heparin was used to flush the infusion tube. After the procedure, coagulation markers were monitored. For those with prolonged coagulation times, 10-15 mg protamine was given to neutralize the effect of heparin. For patients with bleeding tendency, low molecular weight heparin was chosen, or the dose of heparin was appropriately reduced.

### Definition

The diagnosis of AP was in accordance with the Revised Atlanta Definitions[18]. AP was diagnosed when two of the following three characteristics were met: (1) Abdominal pain consistent with AP (acute onset of a persistent, severe, epigastric pain often radiating to the back); (2) At least three times higher levels of AMY and/or lipase above the upper limit of the normal value; and (3) Abdominal imaging (including computed tomography, magnetic resonance imaging, or transabdominal ultrasonography) consistent with changes in AP.

HTG-AP was considered in patients with AP when the level of serum TG was: (1) Over 1000 mg/dL; and (2) Between 500 and 1000 mg/dL with lactescent serum at admission[19].

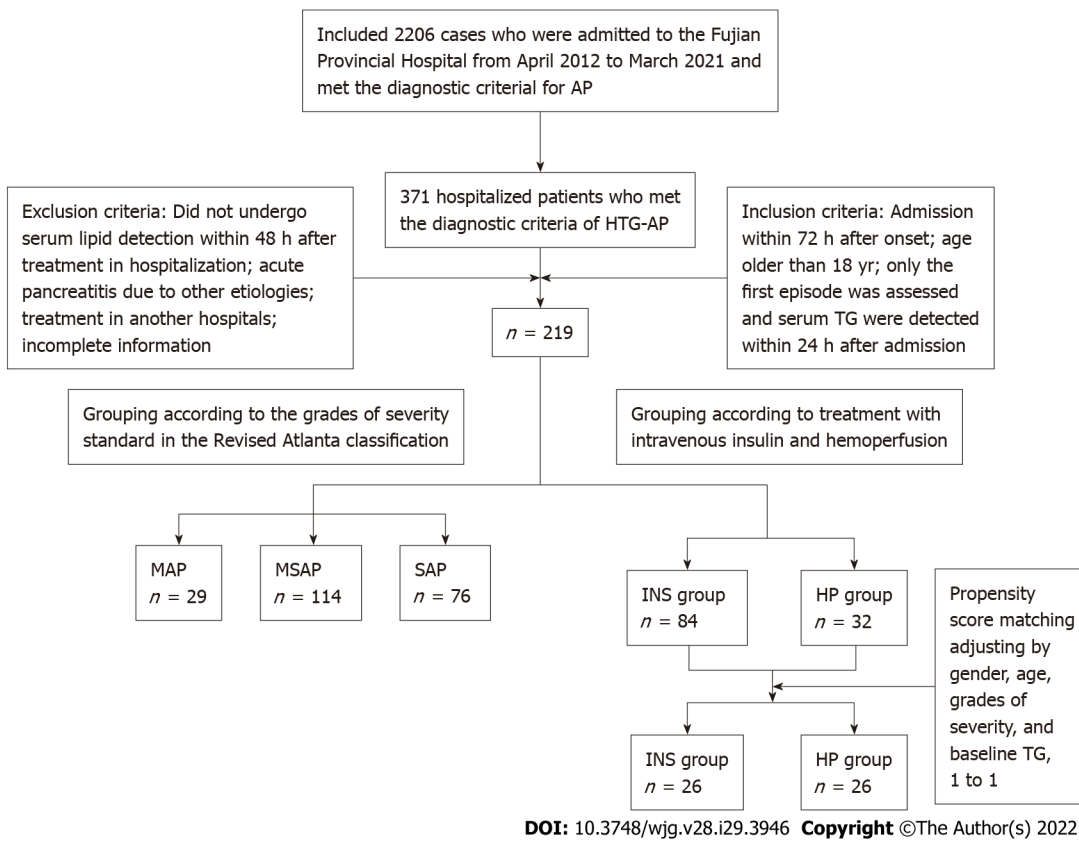


**Figure 1 Research sample screening and grouping process.** HTG-AP: Hypertriglyceridemic acute pancreatitis; MAP: Mild acute pancreatitis; MSAP: Moderately severe acute pancreatitis; SAP: Severe acute pancreatitis; TG: Triglyceride; INS: Insulin; HP: Hemoperfusion; AP: Acute pancreatitis.

The severity of AP was graded according to the Revised Atlanta Definitions[18]: MAP, MSAP, and SAP. MAP was defined by the absence of organ failure and the absence of local or systemic complications. MSAP was defined by the presence of transient (< 48 h) organ failure or local or systemic complications in the absence of persistent organ failure. SAP was defined by persistent (> 48 h) organ failure.

Organ failure was determined according to the improved Marshall score standard in the Revised Atlanta classification[18]. Three organ systems were assessed to define organ failure: respiratory, cardiovascular, and renal. For respiratory (PaO<sub>2</sub>/FiO<sub>2</sub>), 301 mmHg ≤ PaO<sub>2</sub>/FiO<sub>2</sub> ≤ 400 mmHg was scored as 1 point, 201 mmHg ≤ PaO<sub>2</sub>/FiO<sub>2</sub> ≤ 300 mmHg was scored as 2 points, 101 mmHg ≤ PaO<sub>2</sub>/FiO<sub>2</sub> ≤ 200 mmHg was scored as 3 points, and PaO<sub>2</sub>/FiO<sub>2</sub> ≤ 101 mmHg was scored as 4 points. For renal serum creatinine (SCR), 134 μmol/L ≤ SCR ≤ 169 μmol/L was scored as 1 point, 170 μmol/L ≤ SCR ≤ 310 μmol/L was scored as 2 points, 311 μmol/L ≤ SCR ≤ 439 μmol/L was scored as 3 points, and SCR > 439 μmol/L was scored as 4 points. For cardiovascular systolic blood pressure (BP), BP < 90 mmHg and fluid responsive was scored as 1 point, BP < 90 mmHg without fluid responsive was scored as 2 points, BP < 90 mmHg and pH < 7.3 was scored as 3 points, and BP < 90 mmHg and pH < 7.2 was scored as 4 points. A score of 2 or more in any system defined the presence of organ failure.

**Data collection**

Data were obtained from the patients’ medical records and hospital electronic database records. Sex, age, and comorbidities were collected. Clinical manifestations, improved Marshall score[18], modified computed tomography severity index (MCTSI) score[20], organ failure[18], laboratory and imaging data, treatments, intensive care unit admission, length of stay, and prognosis during hospitalization were recorded. All laboratory data were measured within 24 h after admission. Baseline TG and serum AMY were measured using the first tested values since onset. Serum lipids were reviewed within 48 h after administering lipid-lowering treatment.

**Statistical analysis**

SPSS 25.0 (IBM Corp., Armonk, NY, United States) was used for data analysis, and GraphPad Prism7.0 was used for mapping. Measurement data in normal distribution were expressed as mean ± SD and analyzed with Student’s *t*-test or analysis of variance. Otherwise, variables were described as medians and interquartile ranges and analyzed by Mann-Whitney *U* test or Kruskal-Wallis test. Categorical variables were presented as absolute numbers and proportions and tested by χ<sup>2</sup> or Fisher’s exact test.

Paired *t* test was used for continuous variables before and after treatment. Multivariate logistic regression analysis was used to identify independent risk factors with odds ratios (ORs) and 95% CIs. In addition, 1-1 PSM was performed, followed by univariate analysis.  $P < 0.05$  was considered statistically significant.

## RESULTS

### Trends in incidence of HTG-AP

For nearly a decade, 371 patients were diagnosed with HTG-AP in Fujian Provincial Hospital. The total number of patients with HTG-AP in our hospital increased, and the incidence of HTG-AP was increased by approximately 2.6 times over the past 10 years and ranged from 8.4% to 22.3% (Figure 2).

### Clinical characteristics of HTG-AP

A total of 371 patients were diagnosed with HTG-AP, the mean age of the patients with HTG-AP was  $39.86 \pm 10.20$  years, and most of the patients (approximately 93.8%) were young and middle-aged individuals, with a male/female ratio of 2.0 (247/124). The highest incidence rate of AP was observed for men in the age group of 30-39 years (Figure 3).

The mean serum baseline TG values in HTG-AP were significantly high ( $2544.59 \pm 2305.37$  mg/dL). The serum AMY elevated levels were higher than normal in 80.1% of the patients with HTG-AP but only three times greater than normal in 46.9% of patients (Table 1).

About 90.6% of patients with HTG-AP had comorbidity with fatty liver disease, and 11 women (3.0%) had an HTG-AP attack during pregnancy. About 54.7% of the cases were related to diet (high fatty acid) and/or drinking (beer). Patients with HTG-AP had a high frequency of SAP (100, 26.9%), organ failure (117, 31.5%), recurrence (122, 32.9%), and high MCTSI score ( $5.00 \pm 1.83$ ). Eleven patients (3.0%) died during hospitalization (Table 1).

### Comparisons of different grades of severity of HTG-AP

A total of 219 patients met the inclusion and exclusion criteria divided into the MAP group ( $n = 29$ ), MSAP group ( $n = 114$ ), and SAP group ( $n = 76$ ).

Table 2 shows that the more severe HTG-AP was, the more frequent blood purification was used. Improved Marshall score ( $P < 0.000$ ), MCTSI score ( $P < 0.000$ ), baseline TG ( $P = 0.035$ ), baseline AMY ( $P < 0.000$ ), CRP ( $P < 0.000$ ), albumin ( $P < 0.000$ ), aspartate aminotransferase ( $P < 0.000$ ), low-density lipoprotein-cholesterol ( $P = 0.003$ ), urea nitrogen ( $P < 0.000$ ), creatinine ( $P < 0.000$ ), calcium ( $P < 0.000$ ), hemoglobin ( $P = 0.010$ ), free triiodothyronine ( $P = 0.018$ ), admission to the intensive care unit ( $P < 0.000$ ), and mortality ( $P < 0.000$ ) were significantly different between patients with different grades of severity.

Multivariate logistic regression analysis confirmed that high CRP ( $P = 0.005$ , OR = 1.011, 95% CI: 1.003-1.019), low calcium ( $P = 0.003$ , OR = 0.016, 95% CI: 0.001-0.239), and low albumin ( $P = 0.023$ , OR = 0.821, 95% CI: 0.693-0.973) were risk factors of severe HTG-AP (Table 3).

### Comparisons between INS and HP treatments

Of the 219 patients, 84 patients were treated with INS in the INS group and 32 patients were treated with HP in the HP group. The entire cohort showed that the grades of severity of HTG-AP ( $P = 0.002$ ) and baseline TG ( $P = 0.037$ ) were significantly different between patients treated with INS and HP (Table 4).

Given the large severity and baseline TG gap between the two groups, patients were selected for further analysis using PSM, adjusted by sex, age, grades of severity, and baseline TG. After matching, 26 patients were in the INS group and 26 patients were in the HP group (1:1, match tolerance = 0.02). No significant differences in sex ( $P = 0.184$ ), age ( $P = 0.895$ ), grades of severity ( $P = 0.755$ ), improved Marshall score ( $P = 0.186$ ), MCTSI score ( $P = 0.127$ ), and baseline TG ( $P = 0.734$ ) were found between the two groups (Table 4).

In patients with MAP and MSAP, the serum TG level significantly decreased in patients treated with INS ( $P < 0.000$ ) and HP ( $P < 0.000$ ) within 48 h (Figure 4). The clearance rates of TG were  $57.24\% \pm 33.70\%$  and  $56.38\% \pm 33.61\%$ , respectively ( $P = 0.927$ ). However, the clearance rate of TG ( $P = 0.927$ ) and length of stay ( $13.04 \pm 7.92$  d vs  $12.35 \pm 6.40$  d,  $P = 0.730$ ) did not differ between the two groups (Table 4).

## DISCUSSION

### Trends in incidence of HTG-AP

AP has many etiologies, and previous studies reported that HTG as an etiologic factor is between 1.3% and 6.9% [21,22]. However, HTG-AP increased at a fast rate in the Asian region during recent years. Taiwan reported that the frequency of HTG as an etiologic factor in patients with AP ranged from 6.3% to 12.3% [23]. A study reported that the incidence of HTG-AP reached 25.6% in 2013 [14]. Zheng *et al* [24]

**Table 1** Clinical characteristics of hypertriglyceridemic acute pancreatitis

Characteristic	All (n = 371)
Sex, n (%)	
Male	247 (66.6)
Female	124 (33.4)
Age, yr	39.86 ± 10.20
BMI (kg/m <sup>2</sup> )	25.99 ± 3.18
Causes, n (%)	203 (54.7)
Diet (high fatty acid)	127 (34.2)
Drinking (beer)	55 (14.8)
Mixed	21 (5.7)
Complications, n (%)	
Diabetes mellitus	115 (31.0)
Hypertension	62 (16.7)
Fatty liver disease	336 (90.6)
Pregnancy	11 (3.0)
Recurrence, n (%)	122 (32.9)
Grades of severity, n (%)	
MAP	63 (17.0)
MSAP	208 (56.1)
SAP	100 (26.9)
Improved Marshall score	1.30 ± 1.77
Organ failure, n (%)	117 (31.5)
MCTSI score	5.00 ± 1.83
Lipid-lowering treatment, n (%)	
Intravenous insulin	144 (38.8)
HP	32 (8.6)
CRRT/HP + CRRT	77 (20.8)
Only anti-lipemic	118 (31.8)
Baseline TG, mg/dL	2544.59 ± 2305.37
Baseline AMY (nUNL)	5.00 ± 6.47
> UNL, n (%)	297 (80.1)
≥ 3UNL, n (%)	174 (46.9)
Admission to ICU, n (%)	126 (34.0)
Death, n (%)	11 (3.0)

BMI: Body mass index; MAP: Mild acute pancreatitis; MSAP: Moderately severe acute pancreatitis; SAP: Severe acute pancreatitis; MCTSI: Modified computed tomography severity index; HP: Hemoperfusion; CRRT: Continuous renal replacement therapy; TG: Triglyceride; AMY: Amylase; UNL: Upper limit of normal; ICU: Intensive care unit.

retrospectively analyzed 2461 patients with AP in Beijing during a 5-year period and reported that the causes of AP included biliary (55.75%), alcoholism (10%), hypertriglyceridemia (10.36%), and others (23.89%); however, this work did not mention the rate of increase in HTG-AP.

The standardized incidence rate of HTG-AP increased from 0.7 to 1.7 per 100000 person-years from 2008 to 2019 in Denmark, and the incidence has increased by 2.4 times over the past 10 years[5]. Another study from Guangdong showed that the incidence of HTG-AP in 2000 to 2005 was 2.6 times higher than that in 1990 to 1994 (8.9% *vs* 3.4%, *P* < 0.05)[25]. Based on recent observations from China[26], the

**Table 2 Comparisons of clinical characteristics and laboratory parameters with different grades of severity of hypertriglyceridemic acute pancreatitis**

Characteristic	All (n = 219)	MAP group (n = 29)	MSAP group (n = 114)	SAP group (n = 76)	P value
Sex, n (%)					0.111
Male	140 (63.9)	23 (79.3)	67 (58.8)	50 (65.8)	
Female	79 (36.1)	6 (20.7)	47 (41.2)	26 (34.2)	
Age, yr	38.92 ± 10.02	38.66 ± 9.73	38.96 ± 10.12	38.96 ± 10.12	0.941
BMI (kg/m <sup>2</sup> )	26.13 ± 3.30	26.20 ± 1.56	25.58 ± 3.54	28.51 ± 2.97	0.097
Complications, n (%)					
Diabetes mellitus	109 (49.8)	14 (48.3)	58 (50.9)	37 (48.7)	0.982
Fatty liver disease	205 (93.6)	25 (86.2)	106 (93.0)	74 (97.4)	0.112
Lipid-lowering treatment, n (%)					< 0.001
Intravenous insulin	84 (38.4)	14 (48.3)	69 (60.5)	1 (1.3)	
HP	32 (14.6)	1 (3.4)	26 (22.8)	5 (6.6)	
CRRT/HP + CRRT	60 (27.4)	0 (0.0)	1 (0.9)	59 (77.6)	
Only anti-lipemic	43 (19.6)	14 (48.3)	18 (15.8)	11 (14.5)	
Improved Marshall score	1.00 (0.00, 3.00)	0.00 (0.00, 0.00)	0.00 (0.00, 1.00)	3.00 (3.00, 4.75)	< 0.001
MCTSI score	5.11 ± 1.70	2.14 ± 0.92	5.14 ± 1.06	6.18 ± 1.35	< 0.001
Baseline TG, mg/dL	2713.82 ± 2458.65	1895.15 ± 1685.17	2480.80 ± 2040.458	3386.29 ± 3081.51	0.035
Baseline AMY (nUNL)	2.92 (1.43, 6.41)	2.81 (1.47, 5.21)	2.22 (0.98, 5.08)	5.28 (2.21, 8.66)	< 0.001
CRP, mg/L	196.36 ± 121.97	143.17 ± 97.51	178.65 ± 103.25	247.12 ± 143.73	< 0.001
Albumin, g/L	32.66 ± 5.99	36.48 ± 4.96	34.46 ± 5.16	28.49 ± 5.16	< 0.001
TBIL, mmol/L	16.60 (10.80, 22.90)	18.91 (13.02, 23.68)	15.35 (10.69, 22.46)	16.57 (10.60, 24.92)	0.511
ALT, U/L	20.00 (13.60, 30.70)	21.30 (14.90, 35.75)	20.25 (13.00, 31.93)	19.75 (14.03, 27.30)	0.648
AST, U/L	25.00 (17.50, 39.50)	21.30 (17.00, 28.05)	20.00 (16.08, 30.63)	36.55 (25.00, 56.80)	< 0.001
Total cholesterol, mmol/L	8.58 ± 4.56	7.47 ± 2.96	8.82 ± 4.53	8.64 ± 5.06	0.522
HDL-C, mmol/L	0.82 (0.61, 1.10)	0.88 (0.75, 1.17)	0.86 (0.66, 1.16)	0.69 (0.52, 0.99)	0.241
LDL-C, mmol/L	2.92 ± 1.55	3.77 ± 1.41	2.91 ± 1.58	2.62 ± 1.46	0.003
Glucose, mmol/L	10.50 ± 3.64	9.47 ± 3.70	10.34 ± 3.54	11.13 ± 3.69	0.100
Urea nitrogen, mmol/L	4.73 ± 3.31	4.56 ± 1.63	3.66 ± 1.76	6.40 ± 4.64	< 0.001
Creatinine, μmol/L	83.03 ± 66.48	71.90 ± 18.03	65.46 ± 19.11	113.63 ± 103.46	< 0.001
Calcium, mmol/L	1.93 ± 0.31	2.16 ± 0.18	2.00 ± 0.21	1.75 ± 0.37	< 0.001
WBC, × 10 <sup>9</sup> /L	11.67 ± 4.10	11.22 ± 3.64	11.99 ± 4.06	11.37 ± 4.33	0.351
PLT, × 10 <sup>9</sup> /L	200.19 ± 69.19	194.69 ± 73.58	208.67 ± 65.17	189.57 ± 72.51	0.159
Hb, g/L	141.11 ± 24.52	143.69 ± 19.12	136.87 ± 22.76	146.49 ± 27.78	0.010
STSH, mIU/L	0.28 (0.16, 0.65)	0.49 (0.28, 0.98)	0.28 (0.14, 0.66)	0.24 (0.16, 0.62)	0.188
FT3, pmol/L	2.29 ± 1.00	2.90 ± 0.77	2.36 ± 0.86	2.89 ± 1.18	0.018
FT4, pmol/L	12.56 ± 3.70	12.83 ± 2.10	12.88 ± 3.95	12.11 ± 3.68	0.302
Admission to ICU, n (%)	98 (44.7)	1 (3.4)	27 (23.7)	70 (92.1)	< 0.001
Death, n (%)	9 (4.1)	0 (0.0)	0 (0.0)	9 (11.8)	< 0.001

MAP: Mild acute pancreatitis; MSAP: Moderately severe acute pancreatitis; SAP: Severe acute pancreatitis; BMI: Body mass index; HP: Hemoperfusion; CRRT: Continuous renal replacement therapy; MCTSI: Modified computed tomography severity index; TG: Triglyceride; AMY: Amylase; UNL: Upper

limit of normal; CRP: C-reactive protein; TBIL: Total bilirubin; ALT: Alanine aminotransferase; AST: Aspartate transaminase; HDL-C: High-density lipoprotein cholesterol; LDL-C: Low-density lipoprotein cholesterol; WBC: White blood cell; PLT: Blood platelet; Hb: Hemoglobin; STSH: Sensitive thyrotropin; FT3: Free triiodothyronine; FT4: Free thyroxine; ICU: Intensive care unit.

**Table 3 Factors associated with severe hypertriglyceridemic acute pancreatitis according to multivariate logistic regression analysis**

Variable	B	OR	OR (95%CI)	P value
Baseline TG	0.023	1.023	(0.991-1.056)	0.159
Baseline AMY	0.345	1.412	(0.916-2.175)	0.118
CRP	0.110	1.011	(1.003-1.019)	0.005
Albumin	-0.197	0.821	(0.693-0.973)	0.023
AST	0.018	1.018	(0.975-1.063)	0.423
LDL-C	-0.173	0.814	(0.556-1.272)	0.412
Urea nitrogen	-0.334	0.709	(0.462-1.086)	0.114
Creatinine	0.025	1.026	(0.988-1.065)	0.186
Calcium	-4.152	0.016	(0.001-0.239)	0.003
Hb	0.008	1.008	(0.975-1.043)	0.621
FT3	-1.324	0.266	(0.055-1.281)	0.099

OR: Odds ratio; TG: Triglyceride; AMY: Amylase; CRP: C-reactive protein; AST: Aspartate transaminase; LDL-C: Low-density lipoprotein cholesterol; Hb: Hemoglobin; FT3: Free triiodothyronine.

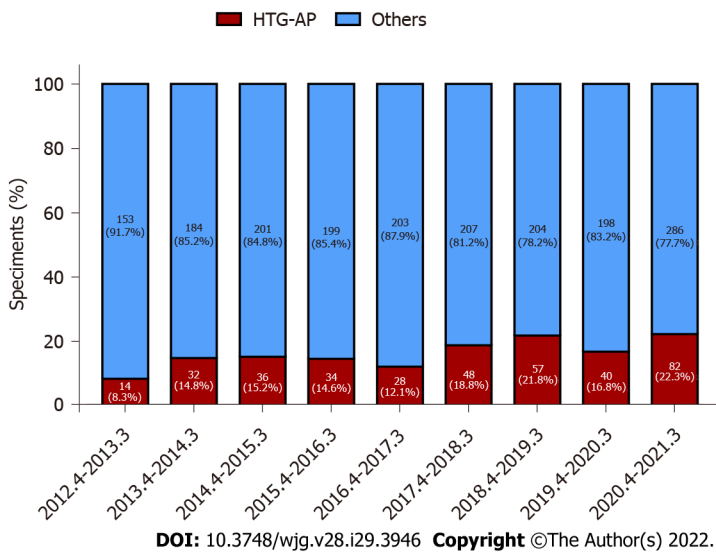


**Figure 2 The total number of patients with hypertriglyceridemic acute pancreatitis and other acute pancreatitis in Fujian Provincial Hospital increased significantly during nearly 10 years.** HTG-AP: Hypertriglyceridemic acute pancreatitis.

proportion of patients with HTG-AP increased from 14.0% to 34.0% during a 16-year period in a tertiary hospital setting. Our study found that the incidence of HTG-AP increased by approximately 2.6 times and ranged from 8.4% to 22.3% during nearly 10 years, with a significant increase detected after 2017. Our results are similar to previously reported data.

At present, updated population-based estimates on the incidence of HTG-AP are lacking. Some studies have shown that the incidence and mortality of HTG-AP were increasing year by year, which was related to the change of people’s diet structure and lifestyle[4]. At the same time, the availability of the detection of serum TG also improved the diagnosis of HTG-AP. For example, the emergency of our hospital began testing serum TG in 2017, and Figure 1 shows the incidence of HTG-AP has increased since 2017.

**Table 4 Comparisons of clinical characteristics and laboratory parameters with different treatment between intravenous insulin and hemoperfusion before and after propensity score matching**

Characteristic	Entire cohort		P value	PSM		P value
	INS group (n = 84)	HP Group (n = 32)		INS group (n = 26)	HP group (n = 26)	
Sex, n (%)			0.626			0.184
Male	51 (60.7)	21 (65.6)		20 (76.9)	16 (61.5)	
Female	33 (39.3)	11 (34.4)		6 (23.1)	10 (38.5)	
Age, yr	39.99 ± 10.36	36.44 ± 11.60	0.965	36.81 ± 10.79	36.42 ± 10.10	0.895
Grades of severity, n (%)			0.002			0.755 <sup>a</sup>
MAP	14 (16.7)	1 (3.1)		1 (3.8)	1 (3.8)	
MSAP	69 (82.1)	26 (81.3)		25 (96.2)	25 (96.2)	
SAP	1 (1.2)	5 (15.6)		0 (0.0)	0 (0.0)	
Improved Marshall score	0.00 (0.00, 1.00)	1.00 (1.00, 2.00)	< 0.001	0.00 (0.00, 1.00)	1.00 (0.00, 1.00)	0.186 <sup>a</sup>
MCTSI score	4.67 ± 1.59	5.75 ± 0.84	< 0.001	5.15 ± 1.29	5.62 ± 0.80	0.127 <sup>a</sup>
Baseline TG, mg/dL	2493.20 ± 1958.06	3443.88 ± 1676.31	0.037	3484.64 ± 2275.248	3264.91 ± 2375.37	0.734 <sup>a</sup>
Treated TG within 48 h, mg/dL	946.25 ± 769.05	1145.60 ± 699.05	0.205	1108.39 ± 856.76	1040.16 ± 686.65	0.753
Clearance rate of TG within 48 h, %	47.65 ± 34.64	63.91 ± 23.32	0.005	57.24 ± 33.70	56.38 ± 33.61	0.927 <sup>a</sup>
CRP, mg/L	184.75 ± 99.84	198.43 ± 94.00	0.552	214.612 ± 119.22	198.28 ± 97.09	0.629
Albumin, g/L	34.05 ± 4.81	32.50 ± 6.39	0.219	34.56 ± 5.03	32.53 ± 6.58	0.218
TBIL, mmol/L	17.80 ± 8.96	19.83 ± 13.61	0.439	18.70 ± 9.38	20.87 ± 14.41	0.523
ALT, U/L	24.55 ± 17.77	23.15 ± 18.15	0.705	24.58 ± 16.69	21.81 ± 16.47	0.550
AST, U/L	25.70 ± 14.23	30.85 ± 26.87	0.187	24.84 ± 12.40	32.10 ± 29.44	0.252
Total cholesterol, mmol/L	8.38 ± 3.89	8.93 ± 4.37	0.511	9.84 ± 4.91	8.52 ± 4.58	0.318
Glucose, mmol/L	11.08 ± 3.65	10.83 ± 3.42	0.739	11.71 ± 2.74	10.07 ± 3.22	0.057
Urea nitrogen, mmol/L	4.02 ± 1.86	3.83 ± 2.27	0.652	3.54 ± 1.76	3.34 ± 1.94	0.688
Creatinine, mmol/L	63.73 ± 18.23	67.72 ± 24.01	0.338	65.00 ± 12.33	67.00 ± 23.36	0.702
Calcium, mmol/L	1.98 ± 0.25	1.90 ± 0.28	0.100	2.03 ± 0.23	1.89 ± 0.31	0.063
WBC, × 10 <sup>9</sup> /L	11.79 ± 4.20	12.33 ± 4.37	0.541	12.40 ± 4.00	12.51 ± 4.44	0.920
PLT, × 10 <sup>9</sup> /L	205.39 ± 68.44	204.34 ± 65.98	0.941	201.66 ± 59.77	197.38 ± 57.91	0.795
Hb, g/L	137.48 ± 23.67	138.12 ± 27.60	0.902	143.44 ± 19.50	135.38 ± 27.50	0.230
Length of stay, d	11.88 ± 6.37	11.93 ± 6.01	0.965	13.04 ± 7.92	12.35 ± 6.40	0.730
Death, n (%)	0 (0.0)	0 (0.0)		0 (0.0)	0 (0.0)	

<sup>a</sup>P value changed after propensity score matching.

PSM: Propensity score matching; INS: Intravenous insulin; HP: Hemoperfusion; MAP: Mild acute pancreatitis; MSAP: Moderately severe acute pancreatitis; SAP: Severe acute pancreatitis; MCTSI: Modified computed tomography severity index; TG: Triglyceride; CRP: C-reactive protein; TBIL: Total bilirubin; ALT: Alanine aminotransferase; AST: Aspartate transaminase; WBC: White blood cell; PLT: Blood platelet; Hb: Hemoglobin.

Figure 1 showed the decrease in the incidence of HTG-AP from April 2016 to March 2017 and from April 2019 to March 2020, which coincided with the opening of the South Hospital of Fujian Provincial Hospital and the outbreak of coronavirus disease 2019 in China, leading to the diversion and reduction of the number of patients with AP and HTG-AP.

#### Clinical feature of HTG-AP

This study also found that the clinical manifestations of patients with HTG-AP included the most common abdominal pain and abdominal distension as well as nausea, vomiting, and anhelation without

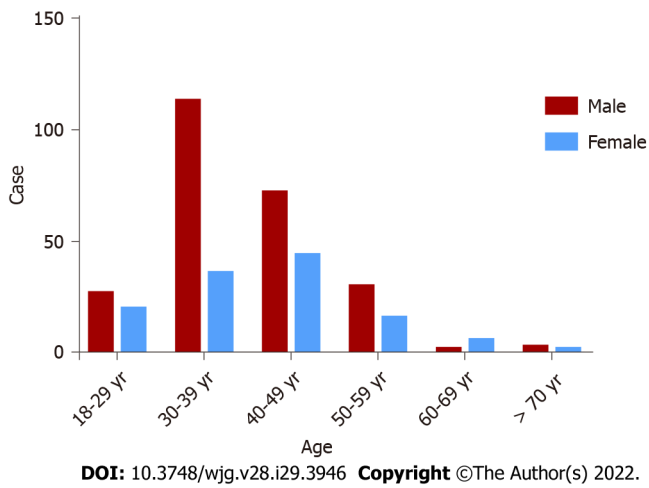


Figure 3 Incidence rates of hypertriglyceridemic acute pancreatitis stratified by age and sex.

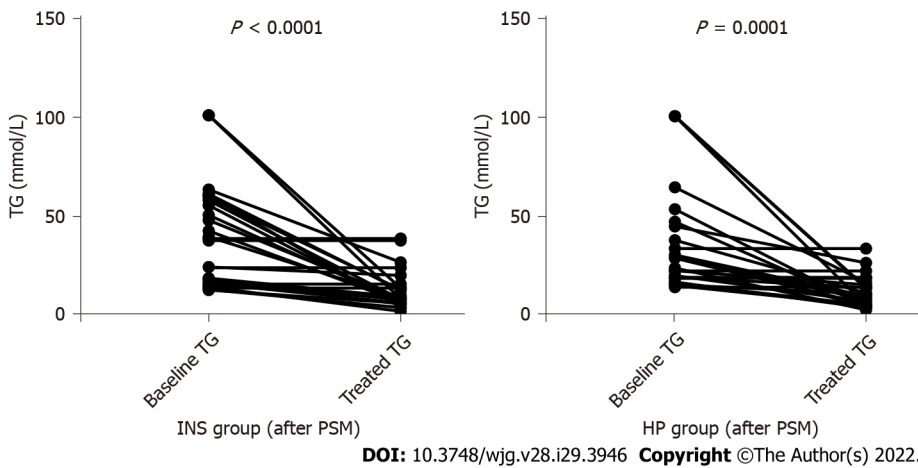


Figure 4 Changes of serum triglyceride levels in both groups before and after treatment. TG: Triglyceride; INS: Insulin; PSM: Propensity score matching; HP: Hemoperfusion.

specificity. However, patients with HTG-AP have some clinical characteristics, such as serum TG level ( $2544.59 \pm 2305.37$  mg/dL) that was significantly higher than normal values at the onset of disease. Hence, serum TG level  $\geq 1000$  mg/dL is the most important characteristic of HTG-AP[19]. Thus, we can improve the diagnosis rate of HTG-AP by improving the early detection rate of serum TG in clinical work.

We found that the mean age of patients with HTG-AP was  $39.86 \pm 10.20$  years. The highest incidence rate of AP was observed for men in the age group of 30-39 years, and the male/female ratio was 2.0 (247/124). Li *et al*[10] reported that patients with HTG-AP were younger (40 *vs* 51,  $P < 0.01$ ) and were mostly males (214/91 *vs* 242/183,  $P < 0.01$ ) compared with patients with biliary AP.

Sekimoto *et al*[27] stated that the average age for HTG-AP was lower than that for other causes. Zheng *et al*[24] reported a higher proportion of alcoholic and HTG-AP in men than in women and in patients younger than 50 years. Olesen *et al*[5] reported that the highest incidence rate of severe HTG was observed for men in the age group of 40-49 years, and severe HTG is a well-known risk factor for AP. Therefore, HTG-AP is becoming more prevalent among younger individuals.

AMY was elevated to levels higher than the normal value in 80.1% of patients but only three times higher than the normal in 46.9% of patients. About 50% of patients with HTG-AP showed no significant increase in serum and urine AMY levels[13], which may be due to the presence of AMY activity inhibitors in their plasma; these inhibitors can enter the urine through the kidneys and inhibit urinary AMY activity. In addition, increased TG levels directly affected the determination of AMY. Therefore, the early diagnosis of HTG-AP is more difficult. The diagnostic accuracy of lipase for HTG-AP was 91.83%, while that of AMY was only 40.38%[14]. Thus, we can improve the diagnosis rate of HTG-AP by combining serum AMY and lipase.

In this study, the frequency of SAP (26.9%), organ failure (31.5%), rate of recurrence (32.9%), and mortality (3.0%) of HTG-AP was high. A large multicenter study in China showed higher incidences of

local complication (34.13% *vs* 15.72%,  $P < 0.000$ ) and MSAP (28.85% *vs* 12.95%,  $P < 0.000$ ) in patients with HTG-AP than in patients without HTG-AP[14]. HTG-AP varied in severity between mild (41%), moderate (26%), and severe (33%)[17]. A foreign study showed that patients with HTG-AP had significantly higher percentages of multiple organ dysfunction syndrome (24.1% *vs* 12.1%,  $P = 0.009$ ) and cardiovascular failure (17.6% *vs* 4.6%,  $P < 0.001$ ) compared with biliary AP[26].

Some reports showed a more severe course of AP induced by HTG compared with other causes, whereas other scholars seemed to favor no significant difference in disease severity[28]. Vipperla *et al* [17] reported that the risk of recurrent AP attacks was 32%, often in patients with poorly controlled diabetes, alcoholism, and TG levels. Our study showed that the recurrence rate of MSAP was higher than that of SAP, which may be due to insufficient attention and medical care. Different studies reported that the mortality rate of HTG-AP ranged from 0.48% to 7.9%[10,14,26], but the mortality rate for severe cases reached as high as 20%-25%[2].

The high frequency rates of fatty liver disease, diabetes mellitus, and hypertension were found in patients with HTG-AP, with values of 90.6%, 31.0%, and 16.7%, respectively. Patients with HTG-AP were often complicated with metabolic diseases such as diabetes mellitus and obesity, and patients with type 2 diabetes mellitus had an elevated risk of AP compared with patients without diabetes[15].

### Comparisons of different grades of severity of HTG-AP

A comparison was conducted among patients with MAP, MSAP, and SAP to investigate the association of the severity of HTG-AP with clinical data and laboratory indicators. Table 2 showed that age and sex had no difference among the three groups (all  $P > 0.050$ ). Improved Marshall score, MCTSI score, baseline TG, baseline AMY, CRP, albumin, aspartate aminotransferase, low-density lipoprotein-cholesterol, urea nitrogen, creatinine, calcium, hemoglobin, and free triiodothyronine were significantly different among patients with different grades of severity of HTG-AP (all  $P < 0.050$ ). Multivariate logistic regression analysis confirmed that high CRP ( $P = 0.005$ , OR = 1.011, 95% CI: 1.003-1.019), low calcium ( $P = 0.003$ , OR = 0.016, 95% CI: 0.001-0.239), and low albumin ( $P = 0.023$ , OR = 0.821, 95% CI: 0.693-0.973) were risk factors of severe HTG-AP.

CRP, serum calcium, and serum albumin are well-known predictors of severe AP with non-HTG-AP and are widely used in its early detection. Experts suggested that CRP levels  $> 150$  mg/L 48 h after the onset of symptoms have a high sensitivity for predicting the severity of AP[29]. Yu *et al*[30] reported that patients with HTG-AP had lower serum ionized calcium associated with a higher risk of developing SAP. Chen *et al*[31] confirmed that low serum albumin ( $P = 0.004$ , OR = 3.362, 95% CI: 1.492-8.823) and high CRP ( $P = 0.005$ , OR = 3.061, 95% CI: 1.407-6.659) were risk factors of moderately severe to severe HTG-AP.

Our study showed that the predictors of SAP with HTG-AP were similar to those of AP with other etiologies including alcoholic and biliary AP.

### Comparisons among different treatments

Reducing serum TG levels quickly is crucial in the early treatment of HTG-AP. This method mainly includes two categories of routine treatment, and blood purification had been implemented for the patients with HTG-AP. Currently, the TG levels should be reduced to below 500 mg/dL as soon as possible; when follow-up TG levels were  $< 500$  mg/dL, an associated reduction in the risk of clinical events and decrease in health care resource use and costs were observed[32]. However, selecting routine treatment or blood purification for patients with HTG-AP after admission to obtain economic cost effectiveness remains controversial. Routine treatments, such as insulin, heparin, and anti-HTG drugs, are effective in reducing TG and have the advantages of non-invasiveness and low cost.

Blood purification includes HP, PE, and continuous renal replacement therapy, which have the disadvantages of invasiveness and expensive. Compared with HP and PE, continuous renal replacement therapy can not only reduce TG rapidly but also remove inflammatory mediators and is more accurate for systemic inflammatory response syndrome control[9]. However, selecting routine treatment or blood purification for patients with HTG-AP after admission in order to obtain economic cost effectiveness remains controversial. Therefore, this study mainly compared the effect of INS and HP on lowering serum TG.

Among patients with MAP and MSAP, a significant decrease in serum TG was found in patients treated with INS ( $P < 0.000$ ) and HP ( $P < 0.000$ ) within 48 h. The clearance rates of TG were  $57.24\% \pm 33.70\%$  and  $56.38\% \pm 33.61\%$ , respectively ( $P = 0.927$ ). This rate of decline was similar to a report[33] wherein 22 episodes of HTG-AP had a calculated fall in serum TG of 69.8% within 48 h by conservative management. This finding is also similar to that reported in an HP case series, which demonstrated 49%-80% reductions in serum TG after a single session[34,35]. These reports showed no difference in the rate of TG decline between patients managed with or without HP. This study also showed that length of stay ( $13.04 \pm 7.92$  d *vs*  $12.35 \pm 6.40$  d,  $P = 0.730$ ) did not differ between the two treatments. A large multicenter retrospective study collected 1159 patients with SAP, which included 30 patients with HTG-AP, and 10 patients treated with PE compared with 20 patients treated with routine therapy; no additional reduction in TG levels and no improvement in clinical outcomes were detected[36].

**Study strengths and limitations**

The strengths of this study are the high accuracy of data due to the strict inclusion and exclusion criteria and the use of PSM to avoid test errors. At present, few studies have reported on how to choose the treatment mode of HTG-AP, which is the innovation of this study.

Our study has some important limitations. This study adopted a single-center retrospective design. The incidence of HTG-AP is not universal and can only reflect the situation of our hospital. Data such as body mass index, urine AMY, blood lipase, and blood gas analysis were missing. The choice of treatment had selection bias.

**CONCLUSION**

The incidence of HTG-AP exhibited a significant increase, remarkable severity, and recurrent trend. By understanding the characteristics of HTG-AP, we can improve the clinical diagnosis rate and identify patients who are likely to develop severe disease early. Patients with MAP and MSAP can be treated with INS safely and effectively without HP. This work provides a basis for doctors to choose an appropriate treatment plan for patients.

**ARTICLE HIGHLIGHTS****Research background**

The incidence of hypertriglyceridemic acute pancreatitis (HTG-AP) has increased yearly, but updated population-based estimates on the incidence of HTG-AP are lacking. Reducing serum triglyceride (TG) levels quickly is crucial in the early treatment of HTG-AP. Currently, there are many treatments to reduce TG levels, but there is still a lack of authoritative guidelines.

**Research motivation**

We wanted to explore appropriate treatments to block the progression of HTG-AP.

**Research objectives**

To explore the clinical characteristics to reduce the missed diagnosis rate of HTG-AP and to identify the patients who would develop severe acute pancreatitis early. To compare the clinical outcomes of intravenous insulin (INS) and hemoperfusion (HP) and guide the choice of treatment for patients.

**Research methods**

We retrospectively reviewed the incidence and clinical characteristics of 371 patients with HTG-AP in our hospital from the past 10 years. Then, 219 patients who met the inclusion and exclusion criteria were further screened and divided to different groups according to grades of severity of HTG-AP and treatments. Multivariate logistic regression analyses were used to identify the independent risk factors for severe HTG-AP. Propensity score matching was used to compare the clinical outcomes of INS and HP.

**Research results**

The incidence of HTG-AP increased by approximately 2.6 times during the 10 years and ranged from 8.4% to 22.3% (8.4% in April 2012–March 2013 and 22.3% in April 2020–March 2021). Multivariate logistic regression analysis confirmed that high C-reactive protein [ $P = 0.005$ , odds ratio (OR) = 1.011, 95%CI: 1.003-1.019], low calcium ( $P = 0.003$ , OR = 0.016, 95%CI: 0.001-0.239), and low albumin ( $P = 0.023$ , OR = 0.821, 95%CI: 0.693-0.973) were risk factors of severe HTG-AP. After propensity score matching with sex, age, grades of severity, and baseline TG, there was a significant decrease in serum TG in patients treated with INS ( $P < 0.0001$ ) and HP ( $P = 0.0001$ ) within 48 h. However, the clearance rate of TG and length of stay did not differ between the two groups.

**Research conclusions**

The incidence of HTG-AP exhibited a significant increase. Patients with mild and moderately severe acute pancreatitis can be treated with INS safely and effectively without HP.

**Research perspectives**

Identifying patients with a severe tendency at the early stage of HTG-AP and choosing cost-effective treatments is the future direction of this research.

## FOOTNOTES

**Author contributions:** Lin XY, Zeng Y, and Zhang ZC contributed equally to the work; Lin XY, Zeng Y, and Zhang ZC designed the study, collected and analyzed the data, and wrote the manuscript; Lin ZH, Chen LC, and Ye ZS made contributions to conception, design, and coordination of the study and gave final approval of the version to be published; All authors read and approved the final manuscript.

**Institutional review board statement:** The Ethics Committee of Fujian Provincial Hospital approved the study (K2021-02-007).

**Informed consent statement:** Informed written consent was obtained from the patient for publication of this report and any accompanying images.

**Conflict-of-interest statement:** The authors declare that they have no conflict of interest.

**Data sharing statement:** Participants gave informed consent for data sharing.

**Open-Access:** This article is an open-access article that was selected by an in-house editor and fully peer-reviewed by external reviewers. It is distributed in accordance with the Creative Commons Attribution NonCommercial (CC BY-NC 4.0) license, which permits others to distribute, remix, adapt, build upon this work non-commercially, and license their derivative works on different terms, provided the original work is properly cited and the use is non-commercial. See: <https://creativecommons.org/licenses/by-nc/4.0/>

**Country/Territory of origin:** China

**ORCID number:** Xue-Yan Lin 0000-0002-3397-0498; Yi Zeng 0000-0001-9144-8414; Zheng-Chao Zhang 0000-0003-3291-2947; Zhi-Hui Lin 0000-0001-6595-7952; Lu-Chuan Chen 0000-0003-3362-447x; Zai-Sheng Ye 0000-0001-9881-6400.

**S-Editor:** Zhang H

**L-Editor:** Filipodia CL

**P-Editor:** Zhang H

## REFERENCES

- 1 **Crockett SD**, Wani S, Gardner TB, Falck-Ytter Y, Barkun AN; American Gastroenterological Association Institute Clinical Guidelines Committee. American Gastroenterological Association Institute Guideline on Initial Management of Acute Pancreatitis. *Gastroenterology* 2018; **154**: 1096-1101 [PMID: 29409760 DOI: 10.1053/j.gastro.2018.01.032]
- 2 **Johnson CD**, Abu-Hilal M. Persistent organ failure during the first week as a marker of fatal outcome in acute pancreatitis. *Gut* 2004; **53**: 1340-1344 [PMID: 15306596 DOI: 10.1136/gut.2004.039883]
- 3 **Khatua B**, El-Kurdi B, Singh VP. Obesity and pancreatitis. *Curr Opin Gastroenterol* 2017; **33**: 374-382 [PMID: 28719397 DOI: 10.1097/MOG.0000000000000386]
- 4 **Carr RA**, Rejowski BJ, Cote GA, Pitt HA, Zyromski NJ. Systematic review of hypertriglyceridemia-induced acute pancreatitis: A more virulent etiology? *Pancreatology* 2016; **16**: 469-476 [PMID: 27012480 DOI: 10.1016/j.pan.2016.02.011]
- 5 **Olesen SS**, Harakow A, Krogh K, Drewes AM, Handberg A, Christensen PA. Hypertriglyceridemia is often under recognized as an aetiological risk factor for acute pancreatitis: A population-based cohort study. *Pancreatology* 2021; **21**: 334-341 [PMID: 33608229 DOI: 10.1016/j.pan.2021.02.005]
- 6 **Tsuang W**, Navaneethan U, Ruiz L, Palascak JB, Gelrud A. Hypertriglyceridemic pancreatitis: presentation and management. *Am J Gastroenterol* 2009; **104**: 984-991 [PMID: 19293788 DOI: 10.1038/ajg.2009.27]
- 7 **Ewald N**, Hardt PD, Kloer HU. Severe hypertriglyceridemia and pancreatitis: presentation and management. *Curr Opin Lipidol* 2009; **20**: 497-504 [PMID: 19770656 DOI: 10.1097/MOL.0b013e3283319a1d]
- 8 **Dominguez-Muñoz JE**, Malfertheiner P, Ditschuneit HH, Blanco-Chavez J, Uhl W, Büchler M, Ditschuneit H. Hyperlipidemia in acute pancreatitis. Relationship with etiology, onset, and severity of the disease. *Int J Pancreatol* 1991; **10**: 261-267 [PMID: 1787337]
- 9 **Guo YY**, Li HX, Zhang Y, He WH. Hypertriglyceridemia-induced acute pancreatitis: progress on disease mechanisms and treatment modalities. *Discov Med* 2019; **27**: 101-109 [PMID: 30939294]
- 10 **Li X**, Ke L, Dong J, Ye B, Meng L, Mao W, Yang Q, Li W, Li J. Significantly different clinical features between hypertriglyceridemia and biliary acute pancreatitis: a retrospective study of 730 patients from a tertiary center. *BMC Gastroenterol* 2018; **18**: 89 [PMID: 29914404 DOI: 10.1186/s12876-018-0821-z]
- 11 **Devlin JW**, Lau AK, Tanios MA. Propofol-associated hypertriglyceridemia and pancreatitis in the intensive care unit: an analysis of frequency and risk factors. *Pharmacotherapy* 2005; **25**: 1348-1352 [PMID: 16185179 DOI: 10.1592/phco.2005.25.10.1348]
- 12 **Durval A**, Zamidei L, Bettocchi D, Luzzio MG, Consales G. Hyperlipidemic acute pancreatitis: a possible role of antiretroviral therapy with entecavir. *Minerva Anestesiol* 2011; **77**: 1018-1021 [PMID: 21242955]
- 13 **Yadav D**, Pitchumoni CS. Issues in hyperlipidemic pancreatitis. *J Clin Gastroenterol* 2003; **36**: 54-62 [PMID: 12488710 DOI: 10.1097/00004836-200301000-00016]

- 14 **Yin G**, Cang X, Yu G, Hu G, Ni J, Xiong J, Hu Y, Xing M, Chen C, Huang Y, Tang M, Zhao Y, Cheng G, Wan R, Wang S, Wang X. Different Clinical Presentations of Hyperlipidemic Acute Pancreatitis: A Retrospective Study. *Pancreas* 2015; **44**: 1105-1110 [PMID: 26348469 DOI: 10.1097/MPA.0000000000000403]
- 15 **Girman CJ**, Kou TD, Cai B, Alexander CM, O'Neill EA, Williams-Herman DE, Katz L. Patients with type 2 diabetes mellitus have higher risk for acute pancreatitis compared with those without diabetes. *Diabetes Obes Metab* 2010; **12**: 766-771 [PMID: 20649628 DOI: 10.1111/j.1463-1326.2010.01231.x]
- 16 **Bosques-Padilla FJ**, Vázquez-Elizondo G, González-Santiago O, Del Follo-Martínez L, González OP, González-González JA, Maldonado-Garza HJ, Garza-González E. Hypertriglyceridemia-induced pancreatitis and risk of persistent systemic inflammatory response syndrome. *Am J Med Sci* 2015; **349**: 206-211 [PMID: 25545390 DOI: 10.1097/MAJ.0000000000000392]
- 17 **Vipperla K**, Somerville C, Furlan A, Koutroumpakis E, Saul M, Chennat J, Rabinovitz M, Whitcomb DC, Slivka A, Papachristou GI, Yadav D. Clinical Profile and Natural Course in a Large Cohort of Patients With Hypertriglyceridemia and Pancreatitis. *J Clin Gastroenterol* 2017; **51**: 77-85 [PMID: 27322530 DOI: 10.1097/MCG.0000000000000579]
- 18 **Banks PA**, Bollen TL, Dervenis C, Gooszen HG, Johnson CD, Sarr MG, Tsiotos GG, Vege SS; Acute Pancreatitis Classification Working Group. Classification of acute pancreatitis--2012: revision of the Atlanta classification and definitions by international consensus. *Gut* 2013; **62**: 102-111 [PMID: 23100216 DOI: 10.1136/gutjnl-2012-302779]
- 19 **Wang Q**, Wang G, Qiu Z, He X, Liu C. Elevated Serum Triglycerides in the Prognostic Assessment of Acute Pancreatitis: A Systematic Review and Meta-Analysis of Observational Studies. *J Clin Gastroenterol* 2017; **51**: 586-593 [PMID: 28682990 DOI: 10.1097/MCG.0000000000000846]
- 20 **Zhao K**, Adam SZ, Keswani RN, Horowitz JM, Miller FH. Acute Pancreatitis: Revised Atlanta Classification and the Role of Cross-Sectional Imaging. *AJR Am J Roentgenol* 2015; **205**: W32-W41 [PMID: 26102416 DOI: 10.2214/AJR.14.14056]
- 21 **Fortson MR**, Freedman SN, Webster PD 3rd. Clinical assessment of hyperlipidemic pancreatitis. *Am J Gastroenterol* 1995; **90**: 2134-2139 [PMID: 8540502]
- 22 **Gullo L**, Migliori M, Oláh A, Farkas G, Levy P, Arvanitakis C, Lankisch P, Beger H. Acute pancreatitis in five European countries: etiology and mortality. *Pancreas* 2002; **24**: 223-227 [PMID: 11893928 DOI: 10.1097/00006676-200204000-00003]
- 23 **Chen CH**, Dai CY, Hou NJ, Chen SC, Chuang WL, Yu ML. Etiology, severity and recurrence of acute pancreatitis in southern taiwan. *J Formos Med Assoc* 2006; **105**: 550-555 [PMID: 16877234 DOI: 10.1016/S0929-6646(09)60149-2]
- 24 **Zheng Y**, Zhou Z, Li H, Li J, Li A, Ma B, Zhang T, Liao Q, Ye Y, Zhang Z, Yang Y, Wang Z, Yang J, Li F. A multicenter study on etiology of acute pancreatitis in Beijing during 5 years. *Pancreas* 2015; **44**: 409-414 [PMID: 25438072 DOI: 10.1097/MPA.0000000000000273]
- 25 **Huang YX**, Jia L, Jiang SM, Wang SB, Li MX, Yang BH. Incidence and clinical features of hyperlipidemic acute pancreatitis from Guangdong, China: a retrospective multicenter study. *Pancreas* 2014; **43**: 548-552 [PMID: 24717803 DOI: 10.1097/MPA.000000000000069]
- 26 **Jin M**, Bai X, Chen X, Zhang H, Lu B, Li Y, Lai Y, Qian J, Yang H. A 16-year trend of etiology in acute pancreatitis: The increasing proportion of hypertriglyceridemia-associated acute pancreatitis and its adverse effect on prognosis. *J Clin Lipidol* 2019; **13**: 947-953.e1 [PMID: 31735687 DOI: 10.1016/j.jacl.2019.09.005]
- 27 **Sekimoto M**, Takada T, Kawarada Y, Hirata K, Mayumi T, Yoshida M, Hirota M, Kimura Y, Takeda K, Isaji S, Koizumi M, Otsuki M, Matsuno S; JPN. JPN Guidelines for the management of acute pancreatitis: epidemiology, etiology, natural history, and outcome predictors in acute pancreatitis. *J Hepatobiliary Pancreat Surg* 2006; **13**: 10-24 [PMID: 16463207 DOI: 10.1007/s00534-005-1047-3]
- 28 **Scherer J**, Singh VP, Pitchumoni CS, Yadav D. Issues in hypertriglyceridemic pancreatitis: an update. *J Clin Gastroenterol* 2014; **48**: 195-203 [PMID: 24172179 DOI: 10.1097/01.mcg.0000436438.60145.5a]
- 29 **Dervenis C**. Assessments of severity and management of acute pancreatitis based on the Santorini Consensus Conference report. *JOP* 2000; **1**: 178-182 [PMID: 11856859]
- 30 **Yu S**, Wu D, Jin K, Yin L, Fu Y, Liu D, Zhang L, Yu X, Xu J. Low Serum Ionized Calcium, Elevated High-Sensitivity C-Reactive Protein, Neutrophil-Lymphocyte Ratio, and Body Mass Index (BMI) Are Risk Factors for Severe Acute Pancreatitis in Patients with Hypertriglyceridemia Pancreatitis. *Med Sci Monit* 2019; **25**: 6097-6103 [PMID: 31413252 DOI: 10.12659/MSM.915526]
- 31 **Chen L**, Huang Y, Yu H, Pan K, Zhang Z, Man Y, Hu D. The association of parameters of body composition and laboratory markers with the severity of hypertriglyceridemia-induced pancreatitis. *Lipids Health Dis* 2021; **20**: 9 [PMID: 33573658 DOI: 10.1186/s12944-021-01443-7]
- 32 **Christian JB**, Arondekar B, Buysman EK, Johnson SL, Seeger JD, Jacobson TA. Clinical and economic benefits observed when follow-up triglyceride levels are less than 500 mg/dL in patients with severe hypertriglyceridemia. *J Clin Lipidol* 2012; **6**: 450-461 [PMID: 23009781 DOI: 10.1016/j.jacl.2012.08.007]
- 33 **Berberich AJ**, Ziada A, Zou GY, Hegele RA. Conservative management in hypertriglyceridemia-associated pancreatitis. *J Intern Med* 2019; **286**: 644-650 [PMID: 31077464 DOI: 10.1111/joim.12925]
- 34 **Galán Carrillo I**, Demelo-Rodríguez P, Rodríguez Ferrero ML, Anaya F. Double filtration plasmapheresis in the treatment of pancreatitis due to severe hypertriglyceridemia. *J Clin Lipidol* 2015; **9**: 698-702 [PMID: 26350817 DOI: 10.1016/j.jacl.2015.07.004]
- 35 **Valdivielso P**, Ramírez-Bueno A, Ewald N. Current knowledge of hypertriglyceridemic pancreatitis. *Eur J Intern Med* 2014; **25**: 689-694 [PMID: 25269432 DOI: 10.1016/j.ejim.2014.08.008]
- 36 **Miyamoto K**, Horibe M, Sanui M, Sasaki M, Sugiyama D, Kato S, Yamashita T, Goto T, Iwasaki E, Shirai K, Oe K, Sawano H, Oda T, Yasuda H, Ogura Y, Hirose K, Kitamura K, Chiba N, Ozaki T, Oshima T, Yamamoto T, Nagata K, Mine T, Saito K, Sekino M, Furuya T, Matsuda N, Hayakawa M, Kanai T, Mayumi T. Plasmapheresis therapy has no triglyceride-lowering effect in patients with hypertriglyceridemic pancreatitis. *Intensive Care Med* 2017; **43**: 949-951 [PMID: 28233051 DOI: 10.1007/s00134-017-4722-3]

## Retrospective Study

## Radiomics for differentiating tumor deposits from lymph node metastasis in rectal cancer

Yong-Chang Zhang, Mou Li, Yu-Mei Jin, Jing-Xu Xu, Chen-Cui Huang, Bin Song

**Specialty type:** Radiology, nuclear medicine and medical imaging**Provenance and peer review:** Unsolicited article; Externally peer reviewed.**Peer-review model:** Single blind**Peer-review report's scientific quality classification**Grade A (Excellent): 0  
Grade B (Very good): B, B  
Grade C (Good): 0  
Grade D (Fair): 0  
Grade E (Poor): 0**P-Reviewer:** Gnetti L, Italy; Hwang KH, South Korea**Received:** December 29, 2021**Peer-review started:** December 29, 2021**First decision:** March 10, 2022**Revised:** March 28, 2022**Accepted:** July 6, 2022**Article in press:** July 6, 2022**Published online:** August 7, 2022**Yong-Chang Zhang**, Department of Radiology, Chengdu Seventh People's Hospital, Chengdu 610213, Sichuan Province, China**Yong-Chang Zhang, Mou Li, Yu-Mei Jin, Bin Song**, Department of Radiology, West China Hospital, Sichuan University, Chengdu 610041, Sichuan Province, China**Jing-Xu Xu, Chen-Cui Huang**, Department of Research Collaboration, R&D center, Beijing Deepwise & League of PHD Technology Co., Ltd, Beijing 100080, China**Corresponding author:** Bin Song, MD, PhD, Chief Doctor, Professor, Department of Radiology, West China Hospital, Sichuan University, No. 37 Guoxue Alley, Chengdu 610041, Sichuan Province, China. [songlab\\_radiology@163.com](mailto:songlab_radiology@163.com)**Abstract****BACKGROUND**

Tumor deposits (TDs) are not equivalent to lymph node (LN) metastasis (LNM) but have become independent adverse prognostic factors in patients with rectal cancer (RC). Although preoperatively differentiating TDs and LNM is helpful in designing individualized treatment strategies and achieving improved prognoses, it is a challenging task.

**AIM**

To establish a computed tomography (CT)-based radiomics model for preoperatively differentiating TDs from LNM in patients with RC.

**METHODS**

This study retrospectively enrolled 219 patients with RC [TDs<sup>+</sup>LNM<sup>-</sup> ( $n = 89$ ); LNM<sup>+</sup> TDs<sup>-</sup> ( $n = 115$ ); TDs<sup>-</sup>LNM<sup>+</sup> ( $n = 15$ )] from a single center between September 2016 and September 2021. Single-positive patients (*i.e.*, TDs<sup>+</sup>LNM<sup>-</sup> and LNM<sup>+</sup>TDs<sup>-</sup>) were classified into the training ( $n = 163$ ) and validation ( $n = 41$ ) sets. We extracted numerous features from the enhanced CT (region 1: The main tumor; region 2: The largest peritumoral nodule). After deleting redundant features, three feature selection methods and three machine learning methods were used to select the best-performing classifier as the radiomics model (Rad-score). After validating Rad-score, its performance was further evaluated in the field of diagnosing double-positive patients (*i.e.*, TDs<sup>+</sup>LNM<sup>+</sup>) by outlining all peritumoral nodules with diameter (short-axis) > 3 mm.

## RESULTS

Rad-score 1 (radiomics signature of the main tumor) had an area under the curve (AUC) of 0.768 on the training dataset and 0.700 on the validation dataset. Rad-score 2 (radiomics signature of the largest peritumoral nodule) had a higher AUC (training set: 0.940; validation set: 0.918) than Rad-score 1. Clinical factors, including age, gender, location of RC, tumor markers, and radiological features of the largest peritumoral nodule, were excluded by logistic regression. Thus, the combined model was comprised of Rad-scores of 1 and 2. Considering that the combined model had similar AUCs with Rad-score 2 ( $P = 0.134$  in the training set and 0.594 in the validation set), Rad-score 2 was used as the final model. For the diagnosis of double-positive patients in the mixed group [TDs+LNM<sup>+</sup> ( $n = 15$ ); single-positive ( $n = 15$ )], Rad-score 2 demonstrated moderate performance (sensitivity, 73.3%; specificity, 66.6%; and accuracy, 70.0%).

## CONCLUSION

Radiomics analysis based on the largest peritumoral nodule can be helpful in preoperatively differentiating between TDs and LNM.

**Key Words:** Radiomics; Tumor deposits; Lymph node metastasis; Rectal cancer; Computed tomography; Differential diagnosis

©The Author(s) 2022. Published by Baishideng Publishing Group Inc. All rights reserved.

**Core Tip:** In this study, a radiomics model based on the largest peritumoral nodule was developed to preoperatively differentiate tumor deposits (TDs) from lymph node (LN) metastasis in patients with rectal cancer. This model demonstrated good performance in both the training and validation cohorts. However, its performance decreased with the diagnosis of the double-positive patients. In summary, this model can be helpful for differentiating TDs from LN metastasis.

**Citation:** Zhang YC, Li M, Jin YM, Xu JX, Huang CC, Song B. Radiomics for differentiating tumor deposits from lymph node metastasis in rectal cancer. *World J Gastroenterol* 2022; 28(29): 3960-3970

**URL:** <https://www.wjgnet.com/1007-9327/full/v28/i29/3960.htm>

**DOI:** <https://dx.doi.org/10.3748/wjg.v28.i29.3960>

## INTRODUCTION

Colorectal cancer (CRC) ranks third in terms of incidence and second in terms of mortality[1], and RC accounts for approximately 30% of CRC[2]. Tumor deposits (TDs) in RC are defined as discontinuous extramural extensions or focal aggregates of adenocarcinoma located in the perirectal region, without histological evidence of residual lymph node (LN) or vascular/neural structures[3,4]. As a factor for poor prognosis, TDs have attracted widespread attention in recent years[4,5]. A review published in 2017 confirmed that TDs were independently associated with lower overall and disease-free survival according to data available in the literature[4].

Clearly, TDs are not equivalent to LN metastasis (LNM) in terms of biology and prognosis. Among patients with LNM, the occurrence of TDs can lead to a worse prognosis[4,5], strongly indicating that their impact on prognosis is independent and additive. Therefore, TDs must be reported separately from LNM[6]. However, TDs and LNM can only be determined through pathological examinations of surgical specimens[7]. Presently, it is difficult to preoperatively differentiate TDs from LNM using computed tomography (CT).

Radiomics is a rapidly developing field of research that involves the extraction of numerous quantitative features from medical images. These features can capture characteristics of volume of interest (VOI), such as heterogeneity, and it may, alone or in combination with other data, be used to solve clinical problems[8]. Recently, some studies have reported the involvement of TDs in RC[6,9,10]. However, some previous studies did not focus on the differentiation of TDs from LNM[9,10], and Atre *et al*[6] used only texture analysis and lacked the construction and validation of a model. Therefore, we aimed to establish a CT-based radiomics model to preoperatively differentiate TDs from LNM in patients with RC.

## MATERIALS AND METHODS

### Patients

This retrospective study was approved by the institutional review board (No. 1159) of the authors' hospital. Given the retrospective design and use of anonymized patient data, requirements for informed consent were waived.

Patient data collected between September 2016 and September 2021 were reviewed by searching radiological and pathological databases. A total of 219 patients [single-positive, 112 male, 92 female; mean  $\pm$  SD age,  $60 \pm 12$  years (range, 32-92 years); double-positive, 6 male, 9 female; mean age,  $60 \pm 13$  years (range, 37-83 years)] were enrolled. The inclusion criteria were as follows: Diagnosis of rectal adenocarcinoma on pathology; single positive result (*i.e.*, TDs<sup>+</sup> or LNM<sup>+</sup>); and 15 randomly selected patients who were TDs<sup>+</sup>LNM<sup>+</sup>. The exclusion criteria were as follows: No peritumoral nodules with short-axis diameter  $> 3$  mm on enhanced CT images ( $n = 22$ ); incomplete clinical data, such as tumor markers ( $n = 36$ ); patients who did not undergo surgery ( $n = 5$ ); treatment before CT examination ( $n = 2$ ); and poor-quality CT images ( $n = 4$ ). [Figure 1](#) shows the flow diagram of patient recruitment. [Figure 2](#) shows the workflow of this radiomics study. Clinical characteristics, including age, gender, location of RC, tumor markers, pTN stage, extramural vascular invasion (EMVI), histological grade, and radiological features of the largest peritumoral nodule, are summarized in [Table 1](#).

### Reference standard

Pathological confirmation reports based on surgically resected specimens were obtained from the hospital's electronic medical database. From these reports, pathological information about the main tumor and peritumoral nodules (status and number of TDs and LNMs) were obtained.

### Image acquisition and evaluation

Chest-abdomen-pelvis enhanced CT can detect not only the primary tumor but also suspected metastases. The main scanning parameters of CT are described in the [Supplementary Table 1](#).

Two experiential radiologists reviewed the CT images and recorded the radiological features while blinded to clinical and pathological information. As shown in [Table 1](#), the tumor location and radiological features of the largest peritumoral nodule, such as size, morphology, spiculation, and CT value, was confirmed by summarizing the results of these two radiologists (disagreements were resolved by consensus discussion).

### Feature extraction and model-building

The reliability of the radiomics features was tested in twenty patients. The features with intra-/inter-class correlation coefficients (ICCs)  $> 0.75$  were considered stable[11]. Thereafter, the radiologists independently segmented the main tumor and largest peritumoral nodule by manually drawing three-dimensional VOI ([Figure 2](#)). All images were resampled to pixel spacing of 1 mm in all three dimensions. Several transformation methods, such as wavelet filter and Laplace of Gaussian filter, were applied to the original images. PyRadiomics was used to extract features from the original and filtered images[12]. [Figure 2](#) shows the types of the features. The correlation analysis was performed to remove redundant features. In detail, if the correlation coefficient between two features was  $> 0.4$ , the one with a lower coefficient was removed. Subsequently, three feature selection methods and three machine learning methods were tested to select the best performing classifier as the radiomics model (*i.e.*, Rad-score). Statistically significant factors from univariate and multivariate logistic regression analyses were used to develop the combined model.

### Model evaluation

Receiver operating characteristic (ROC) curves of the models were performed to assess and compare their performance in identifying TDs<sup>+</sup>LNM<sup>-</sup> patients. Moreover, the performance of the models in diagnosing double-positive (*i.e.*, TDs<sup>+</sup>LNM<sup>+</sup>) patients were further evaluated by outlining all peritumoral nodules with short-axis diameters  $> 3$  mm in the mixed group [TDs<sup>+</sup>LNM<sup>+</sup> ( $n = 15$ ); randomly selected single-positive patients from the training or validation sets ( $n = 15$ )]. If there were two different results (TD<sup>+</sup> or LNM<sup>+</sup>) in all the outlined peritumoral nodules of each patient, double-positive patients were considered to be diagnosed correctly.

### Statistical analysis

Statistical analyses were performed using SPSS (IBM Corporation, Armonk, NY, United States), Stata (StataCorp LP, College Station, TX, United States), and MedCalc software. In [Table 1](#), continuous variables were analyzed using *t*-test or Mann-Whitney *U* test, and categorical variables were compared using the chi-squared test or Fisher's exact test. The areas under the curve (AUCs) of the models were compared using DeLong's test.

**Table 1** Baseline and clinical characteristics of the included patients

Characteristics	TDs <sup>+</sup> LNM <sup>-</sup> (n = 89)	LNM <sup>+</sup> TDs <sup>-</sup> (n = 115)	P value	Training set (n = 163)	Validation set (n = 41)	P value
Age (mean ± SD, yr)	59 ± 12	61 ± 12	0.268	60 ± 12	60 ± 11	0.965
Gender (man/woman)	49/40	63/52	0.969	94/69	18/23	0.113
Location (middle-low/high)	65/24	74/41	0.187	107/56	32/9	0.128
Neoadjuvant therapy (+/-)	34/55	43/72	0.906	62/101	15/26	0.864
CEA (+/-) (positive ≥ 5 ng/mL)	42/47	43/72	0.159	75/88	10/31	0.012
CA19-9 (+/-) (positive ≥ 30 U/mL)	23/66	18/97	0.072	34/129	7/34	0.589
CA125 (+/-) (positive ≥ 24 U/mL)	13/76	14/101	0.611	21/142	6/35	0.767
pT stage (T1/T2/T3/T4)	0/9/70/10	4/12/93/6	0.063	4/17/127/15	0/4/36/1	0.894
pN stage (1a/1b/1c/2a/2b)	0/0/89/0/0	52/39/0/15/9	< 0.001	37/33/71/13/9	15/6/18/2/0	0.115
Histologic EMVI (+/-)	33/56	16/99	< 0.001	41/122	8/33	0.450
Histologic grade (G1/G2/G3)	1/63/25	0/76/39	0.299	0/113/50	1/26/14	0.901
Peritumoral nodule						
Shape (irregular/regular)	12/77	2/113	0.003	11/152	3/38	0.898
Spiculation (+/-)	7/82	2/113	0.077	7/156	2/39	0.871
Size (mm <sup>2</sup> ) (median)	72.7	41.2	< 0.001	54	43	0.886
CT value (HU)	61 ± 22	65 ± 23	0.258	64 ± 23	63 ± 23	0.858
Rad-score 1 (median)	0.71	0.39	< 0.001	0.44	0.71	0.002
Rad-score 2 (median)	0.89	0.13	< 0.001	0.39	0.62	0.561

Rad-score 1: Rad-score of the main tumor; Rad-score 2: Rad-score of the largest peritumoral nodule; CT: Computed tomography; TDs: Tumor deposits; LNM: Lymph node metastasis; CEA: Carcinoembryonic antigen; CA19-9: Carbohydrate antigen 19-9; CA125: Carbohydrate antigen 125; pT stage: Pathological T stage; pN stage: Pathological N stage; EMVI: Extramural vascular invasion.

## RESULTS

### Patient characteristics

A total of 219 patients with RC [TDs<sup>+</sup>LNM<sup>-</sup> (n = 89); LNM<sup>+</sup>TDs<sup>-</sup> (n = 115); TDs<sup>+</sup>LNM<sup>+</sup> (n = 15)] were enrolled in this study. Clinical factors, including pathological N stage, pathological EMVI, and the size and shape of the largest peritumoral nodule, were found significantly different between the TDs<sup>+</sup>LNM<sup>-</sup> group and LNM<sup>+</sup>TDs<sup>-</sup> group. No statistical differences were found in age, gender, location of RC, tumor markers, pathological T stage, histological grade, and other features of the peritumoral nodule (spiculation and CT values) between the TDs<sup>+</sup>LNM<sup>-</sup> group and LNM<sup>+</sup>TDs<sup>-</sup> group. The patients were classified into a training set (n = 163) and a validation set (n = 41). Except for carcinoembryonic antigen (P = 0.012), no significant differences were found in the other clinical factors between the training and validation sets (Table 1).

### Feature selection and model building

After evaluating the reliability, a large number of radiomics features remained (n = 1490 extracted from the tumor and 1252 from the largest peritumoral nodule), with ICCs of > 0.75. After excluding redundant radiomics features, we selected features using the L1-based method and established Rad-score using a logistic regression analysis. Features included in Rad-score are reported in the Supplementary Tables 2 and 3. Rad-score of the main tumor (Rad-score 1) and that of the largest peritumoral nodule (Rad-score 2) were independent risk factors for differentiating TDs from LNM [odds ratio (OR) = 3.267 and 14.396, respectively]. Regarding clinical factors, although the size and shape of the largest peritumoral nodule had significant difference between the TDs<sup>+</sup> group and LNM<sup>+</sup> group, they were all deleted in the logistic regression (P = 0.314 and 0.948, respectively; Table 2). Furthermore, a combined model integrating Rad-scores of 1 and 2 was established using the logistic regression.

**Table 2 Univariate and multivariate logistic regression analysis**

Variables	Univariate		Multivariate	
	OR	P value	OR	P value
Age	0.995	0.693	-	-
Gender	0.820	0.534	-	-
Location	0.819	0.282	-	-
CEA	1.546	0.171	-	-
CA19-9	1.613	0.217	-	-
CA125	1.503	0.384	-	-
Peritumoral nodule				
Shape	14.918	0.011	0.915	0.948
Spiculated (+/-)	8.400	0.051	-	-
Size (mm <sup>2</sup> )	1.009	0.001	0.999	0.314
CT value (HU)	0.994	0.364	-	-
Rad-score 1	2.946	< 0.001	3.267	< 0.001
Rad-score 2	11.979	< 0.001	14.396	< 0.001

Rad-score 1: Rad-score of the main tumor; Rad-score 2: Rad-score of the largest peritumoral nodule; CEA: Carcinoembryonic antigen; CA19-9: Carbohydrate antigen 19-9; CA125: Carbohydrate antigen 125; CT: Computed tomography; OR: Odds ratio.

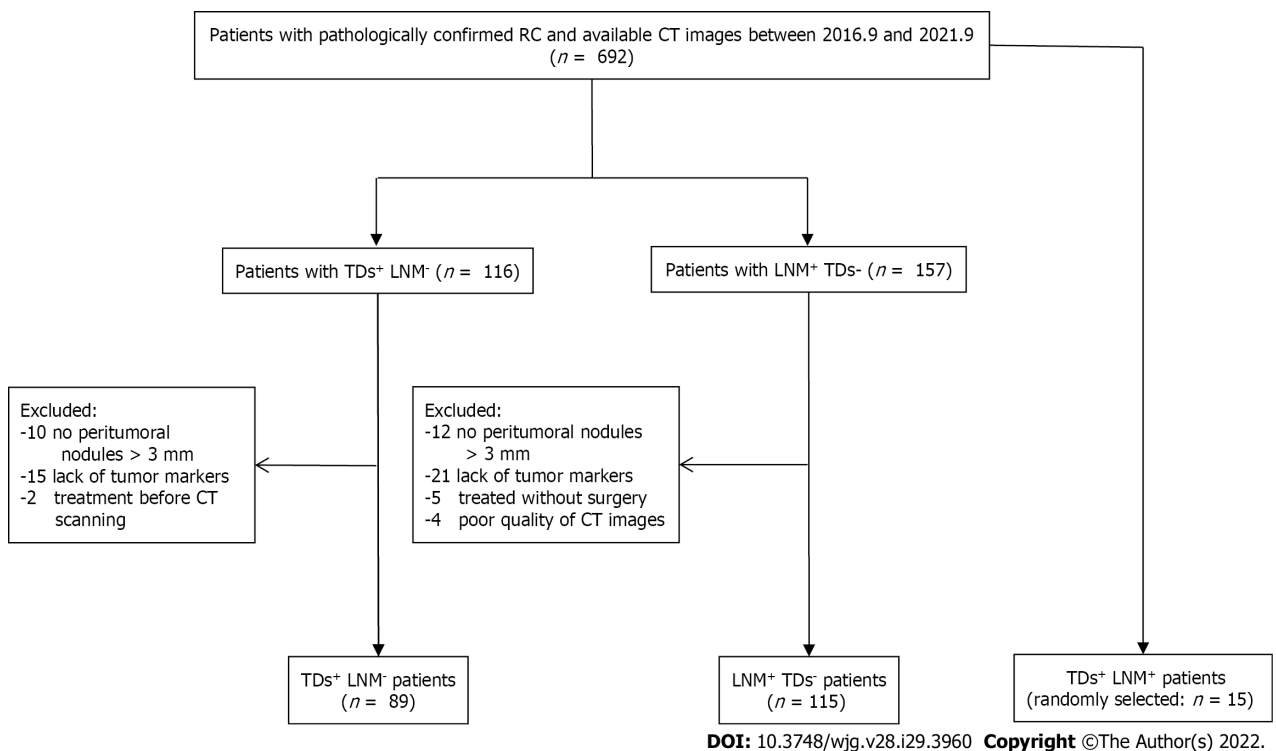


**Figure 1 Flowchart of patients' recruitment pathway.** RC: Rectal cancer; CT: Computed tomography; TDs: Tumor deposits; LNM: Lymph node metastasis.

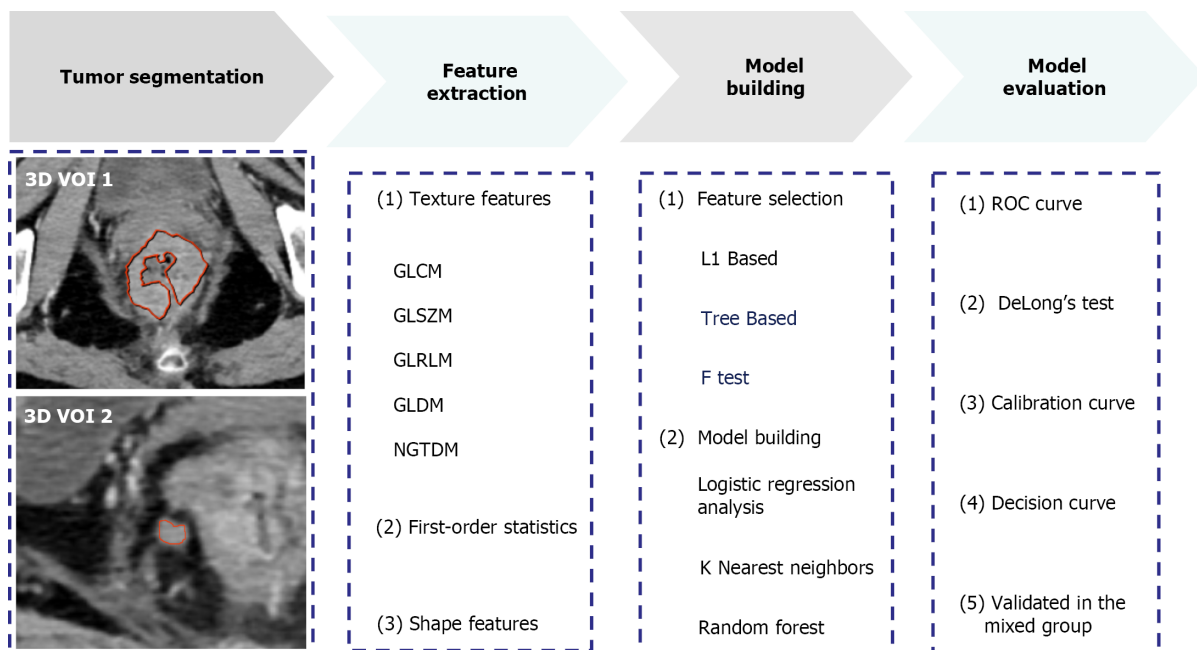
**Model evaluation**

For classification results, the AUC for Rad-score 1 was 0.768 [95% confidence interval (CI): 0.695-0.830] in the training set and 0.700 (95%CI: 0.537-0.833) in the validation set. Rad-score 2 achieved improved performance, with an AUC of 0.940 (95%CI: 0.892-0.971) in the training set and 0.918 (95%CI: 0.789-0.981) in the validation set. The combined model (Rad-scores 1 + 2) had similar AUCs to Rad-score 2 in both the training and validation sets, as shown in Table 3 and Figure 3A and B. Thus, Rad-score 2 (Rad-

Table 3 Comparisons of the models in the training, validation, and mixed groups

	Training set				Validation set				Mixed group		
	AUC	SEN	SPE	P value	AUC	SEN	SPE	P value	SEN	SPE	Accuracy
Rad-score 1	0.768 (95%CI: 0.695-0.830)	66.2%	70.7%	< 0.001	0.700 (95%CI: 0.537-0.833)	77.8%	47.8%	0.032	-	-	-
Combined model	0.955 (95%CI: 0.910-0.981)	83.1%	88.0%	0.134	0.930 (95%CI: 0.805-0.986)	94.4%	82.6%	0.594	66.6%	73.3%	70.0%
Rad-score 2	0.940 (95%CI: 0.892-0.971)	83.1%	84.8%		0.918 (95%CI: 0.789-0.981)	83.3%	82.6%		73.3%	66.6%	70.0%

The mixed group consisted of 15 double-positive (TDs<sup>+</sup>LNM<sup>+</sup>) and 15 single-positive (11 TDs<sup>+</sup>LNM<sup>-</sup> and 4 LNM<sup>+</sup>TDs<sup>-</sup>) patients. P value: compared with Rad-score 2 by DeLong's test. Rad-score 1: Rad-score of the main tumor; Rad-score 2: Rad-score of the largest peritumoral nodule; TDs: Tumor deposits; LNM: Lymph node metastasis; AUC: Area under the curve; SEN: Sensitivity; SPE: Specificity.



DOI: 10.3748/wjg.v28.i29.3960 Copyright ©The Author(s) 2022.

**Figure 2 Radiomics workflow.** 3D VOI: Three-dimensional volume of interest; GLCM: Gray level co-occurrence matrix; GLSZM: Gray level size zone matrix; GLRLM: Gray level run length matrix; GLDM: Gray level dependence matrix; NGTDM: Neighbouring gray tone difference matrix; ROC: Receiver operating characteristic curve.

score of the largest peritumoral nodule) was used as the final model owing to its simplicity.

In the calibration curve for Rad-score 2, the solid line was close to the reference line (dotted line), indicating that Rad-score 2 demonstrated good agreement between the prediction (x-axis) and observation (y-axis) (Figure 3C). However, Rad-score 2 still overestimated the actual risk for TDs<sup>+</sup> (approximately 10%, at most). A decision curve was constructed to evaluate the clinical utility of Rad-score 2 in differentiating TDs from LNM. The net benefit can be measured along the y-axis. Figure 3D shows that Rad-score 2 yielded more benefit than “treat all”, “treat none”, and Rad-score 1. A case example is shown in Figure 4.

Moreover, all peritumoral nodules with short-axis diameter > 3 mm were delineated in each patient in the mixed group [TDs<sup>+</sup>LNM<sup>+</sup> ( $n = 15$ ); single-positive ( $n = 15$ )] to evaluate the performance of the models in predicting double-positive (*i.e.*, TDs<sup>+</sup>LNM<sup>+</sup>) patients. Of the 30 patients, 134 peritumoral nodules were delineated. Rad-score 2 had a moderate accuracy of 70% (sensitivity, 73.3%; specificity, 66.6%). Because the combined model had the same accuracy of 70% as Rad-score 2, it confirmed the use of Rad-score 2 as the final model.

### Subgroup analysis

In view of the prognostic difference between the upper and middle-lower RC[13], we performed a subgroup analysis indicating that Rad-score 2 had high AUCs in both the upper [0.941 (95%CI: 0.853-

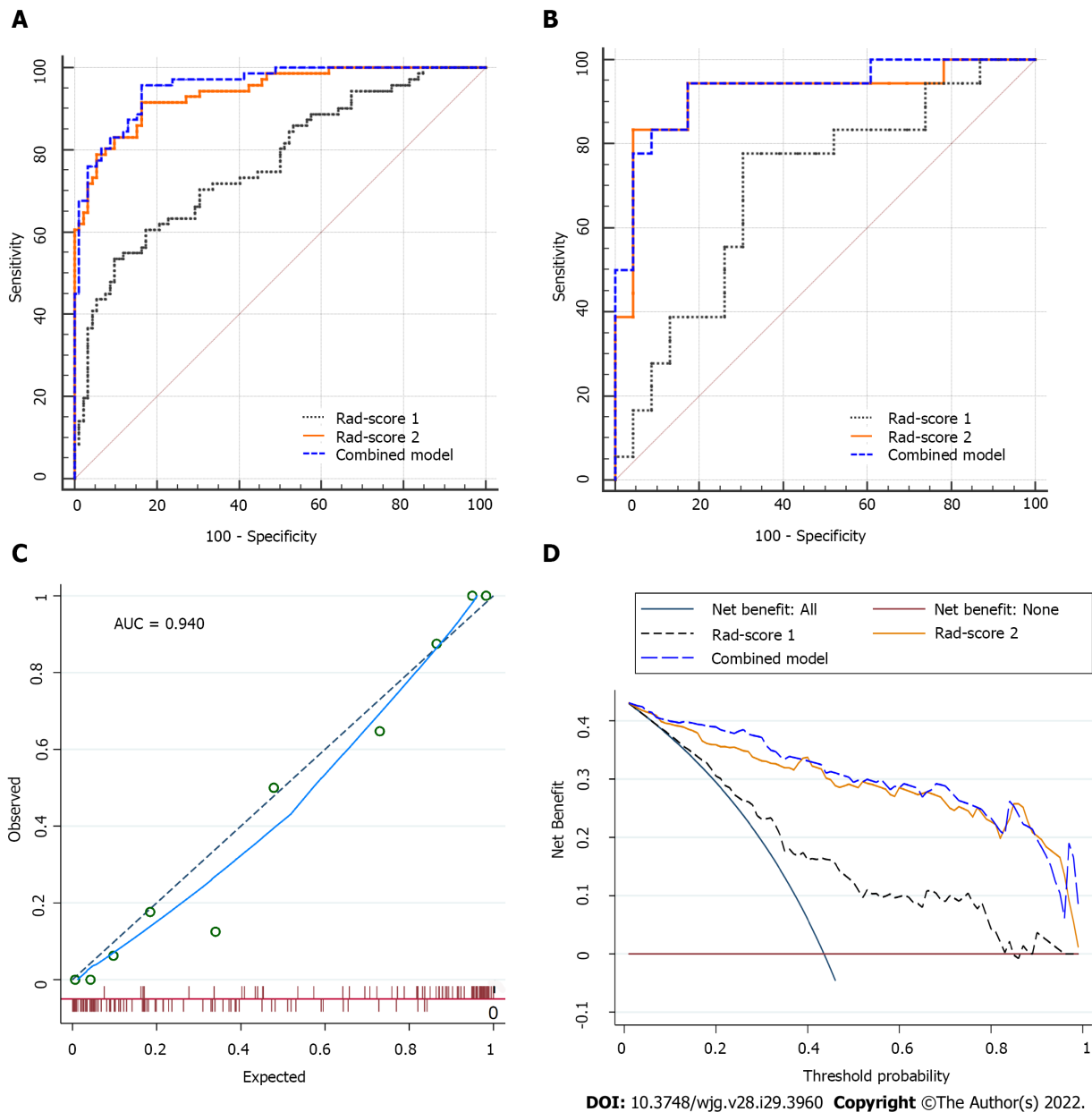


**Figure 3 Comparisons of the receiver operating characteristic curves, and fit and usefulness evaluation of Rad-score 2.** A: In the training set: Area under the curve (AUC) = 0.768 for Rad-score 1, 0.955 for the combined model, and 0.940 for Rad-score 2; B: In the validation set: AUC = 0.700 for Rad-score 1, 0.930 for the combined model, and 0.918 for Rad-score 2; C: The calibration curve of Rad-score 2 shows good agreement between the predicted and observed risks in the training cohort; D: The decision curve demonstrates that Rad-score 2 obtains more benefit than “treat all”, “treat none”, and Rad-score 1. Rad-score 1: Rad-score of the main tumor; Rad-score 2: Rad-score of the largest peritumoral nodule; AUC: Area under the curve.

0.984)] and middle-lower [0.931 (95%CI: 0.875-0.967)] RC groups. For patients receiving neoadjuvant chemoradiotherapy (nCRT), Rad-score 2 also had high AUCs, as shown in Table 4. In these subgroup analyses, Rad-score 2 outperformed Rad-score 1.

The American Joint Committee on Cancer (AJCC) tumor-node-metastasis (TNM) staging system has not correlated a higher number of TDs with staging, unlike LNs (*e.g.*, N1, 1-3 and N2, ≥ 4 regional LNs) [14]. Several authors have found that patients with ≥ 3 TDs have a significantly worse prognosis than those with 1-2 TDs[15]. However, in this study, the values of Rad-scores 1 and 2 were not significantly different between the ≥ 3 TDs group and the 1-2 TDs group ( $P = 0.838$  for Rad-score 1, and  $P = 0.309$  for Rad-score 2) (Table 4).

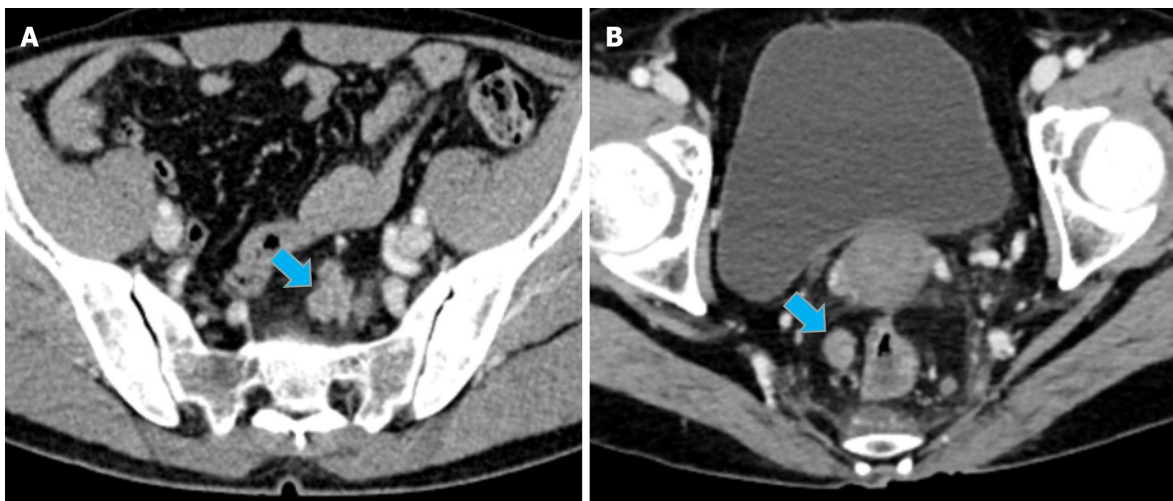
## DISCUSSION

Our study established a new radiomics signature (Rad-score 2) based on 11 features extracted from the largest peritumoral nodule, demonstrating the potential for preoperatively differentiating TDs from

**Table 4** Subgroup analyses of the models in single-positive patients

Subgroups	Rad-score 1			Rad-score 2			P value
	AUC	SEN (%)	SPE (%)	AUC	SEN (%)	SPE (%)	
nCRT							
With ( <i>n</i> = 77)	0.740 (95%CI: 0.628-0.833)	73.5%	74.4%	0.897 (95%CI: 0.806-0.954)	73.5%	90.7%	0.014
Without ( <i>n</i> = 127)	0.753 (95%CI: 0.668-0.825)	60%	86.1%	0.957 (95%CI: 0.905-0.985)	89.1%	93.1%	< 0.001
Location							
Mid-low ( <i>n</i> = 139)	0.782 (95%CI: 0.704-0.848)	75.4%	62.2%	0.931 (95%CI: 0.875-0.967)	86.2%	82.4%	< 0.001
High ( <i>n</i> = 65)	0.643 (95%CI: 0.515-0.758)	54.2%	73.2%	0.941 (95%CI: 0.853-0.984)	83.3%	85.4%	< 0.001
Number of TDs	1-2 ( <i>n</i> = 50)	≥ 3 ( <i>n</i> = 39)	<i>P</i> = 0.838	1-2 ( <i>n</i> = 50)	≥ 3 ( <i>n</i> = 39)	<i>P</i> = 0.309	
Value	0.64 ± 0.24	0.65 ± 0.22		0.83 ± 0.22	0.77 ± 0.26		

Rad-score 1: Rad-score of the main tumor; Rad-score 2: Rad-score of the largest peritumoral nodule; TDs: Tumor deposits; AUC: Area under the curve; SEN: Sensitivity; SPE: Specificity; nCRT: Neoadjuvant chemoradiotherapy.



DOI: 10.3748/wjg.v28.i29.3960 Copyright ©The Author(s) 2022.

**Figure 4 Case presentation.** A: A 56-year-old man with upper RC, the nodule of TDs (size: 24 mm × 16 mm) had an irregular shape; B: A 44-year-old man with lower RC, the nodule of TDs (size: 14 mm × 11 mm) had a regular oval shape. It is difficult to distinguish TDs and LNM from conventional imaging findings. For these two patients, Rad-score of the largest peritumoral nodule achieved correct diagnosis (values = 0.98 and 0.97, respectively). RC: Rectal cancer; TDs: Tumor deposits; LNM: Lymph node metastasis.

LNM. Moreover, Rad-score 2 outperformed Rad-score 1 (based on the main tumor) in this field [0.918 *vs* 0.700 (*P* = 0.032) in the validation set]. However, this model had a minor overestimation of TDs<sup>+</sup> probability for most of the included patients.

The 8<sup>th</sup> AJCC TNM staging system incorporates a N1c category for RC patients with TDs<sup>+</sup>LNM. The N1c category represents 5% to 10% of RC with TDs (TDs<sup>+</sup>LNM<sup>-</sup> and TDs<sup>+</sup>LNM<sup>+</sup>) observed in approximately 20% of all rectal adenocarcinomas[5]. Although many authors have speculated on the origin of TDs, the phenomenon remains unclear. However, some authors have found that a significant proportion of TDs cannot be traced back to the LN[16]. Goldstein *et al*[17] reported that, after performing experiments on deeper sections, most TDs (up to 90%) exhibited signs of > 1 origin. Currently, the only method to determine the status of peritumoral nodules is the histopathologic examination of the resected specimens. The preoperative differentiation of TDs and LNM facilitates the design of individualized treatment strategies and evaluation of prognosis.

Unlike CT and magnetic resonance imaging (MRI), radiomics may solve clinical problems by extracting an enormous number of features which can quantify invisible differences in tissues for the human eye. Several radiomics studies investigating TDs[6,9,10] and LNM[18-21] have been reported in

RC. There were, however, some differences in our study. First, in contrast to most previous models (predicting single factor positive TDs[9,10] or LNM[18-21]), our model can be used to predict the status of both TDs and LNM. When a peritumoral nodule with a short-axis diameter > 3 mm was found on CT images, we could then use our model to predict the classification of this nodule (TDs<sup>+</sup> or LNM<sup>+</sup>) and further identify the patient as TDs<sup>+</sup> only, LNM<sup>+</sup> only, or double positive. Second, we delineated the main tumor and the largest peritumoral nodule, while previous authors delineated the tumor and whole peritumoral fat[10] or only the main tumor[9]. Third, our study included a larger sample size of TDs<sup>+</sup> patients ( $n = 89$ ) and had a higher AUC (0.918 in the validation set) than those reported by Chen *et al*[10] [TDs<sup>+</sup> ( $n = 40$ ); AUC 0.795], Yang *et al*[9] [TDs<sup>+</sup> ( $n = 23$ ); AUC 0.820], and Atre *et al*[6] [TDs<sup>+</sup> ( $n = 25$ ); AUC 0.810]. Finally, although Atre *et al*[6] could also predict both TDs<sup>+</sup> and LNM<sup>+</sup>, they only performed texture analysis, which was clearly different from the analysis in our study.

Notably, double-positive patients had a worse prognosis than those with TDs<sup>+</sup> or LNM<sup>+</sup> only. One positive LN 5-year survival rate was 62% without TDs, *vs* 44% with TDs[4]. Thus, preoperative diagnosis of double-positive patients is of great clinical significance. However, the performance of the model decreased (accuracy, 70%) when used to diagnose double-positive patients. We speculated that this may be related to the following factors. First, we established a model based on the largest peritumoral nodule. When diagnosing double-positive patients, we used all peritumoral nodules (> 3 mm). Thus, the mean size in the mixed group was smaller than that in the training set. Second, the sample size of the mixed group was small. Third, among the double-positive patients, some LNMs were incorrectly evaluated as TDs. In these lesions, the value of wavelet-HLH\_firstorder\_Median (a radiomics feature) decreased. In the future, we will include a larger sample to improve the applicability of the model in double-positive patients.

Nevertheless, the nature of TDs after neoadjuvant therapy remains unclear. Regarding the 77 patients who underwent nCRT in our study, the AUC for the Rad-score 2 did not decrease significantly (0.897), indicating that the model was stable. Regarding the tumor location, the AUCs of the model were also similar between the upper and middle-lower RC. Our model failed to differentiate between groups with  $\geq 3$  TDs and 1-2 TDs ( $P = 0.309$ ).

Our study had several limitations. Firstly, because this was a retrospective study, selection bias may have been introduced. Secondly, to directly compare peritumoral nodules, we especially selected a sample comprising TDs<sup>+</sup>LNM<sup>-</sup> and LNM<sup>+</sup>TDs<sup>-</sup> and outlined the largest peritumoral nodule. However, it was still possible to identify benign peritumoral nodules. Thirdly, this was a single-center analysis. In the future, it will be necessary to conduct an external validation to confirm the versatility of the model.

## CONCLUSION

A radiomics signature based on the largest peritumoral nodule is established in this article. This signature can facilitate the preoperative differentiation of TDs from LNM.

## ARTICLE HIGHLIGHTS

### Research background

Tumor deposits (TDs) are not equivalent to lymph node (LN) metastasis (LNM) but have become independent adverse prognostic factors in patients with rectal cancer (RC). If TDs can be differentiated from LNM before therapy, individualized treatment and patient prognosis may greatly improve.

### Research motivation

Currently, preoperative differentiation of TDs and LNM can be challenging.

### Research objectives

To establish a radiomics model for preoperatively differentiating between TDs and LNM in patients with RC.

### Research methods

The present study retrospectively enrolled 219 patients with RC [TDs<sup>+</sup>LNM<sup>-</sup> ( $n = 89$ ); LNM<sup>+</sup>TDs<sup>-</sup> ( $n = 115$ ); TDs<sup>+</sup>LNM<sup>+</sup> ( $n = 15$ )] from a single center between September 2016 and September 2021. Single-positive patients (TDs<sup>+</sup>LNM<sup>-</sup> and LNM<sup>+</sup>TDs<sup>-</sup>) were classified into training ( $n = 163$ ) and validation ( $n = 41$ ) sets. Rad-scores were established based on the main tumor and largest peritumoral nodule. After validating Rad-score, we further evaluated its performance for diagnosing double-positive patients (*i.e.*, TDs<sup>+</sup>LNM<sup>+</sup>) by outlining all peritumoral nodules with diameters > 3 mm (short axis).

### Research results

Rad-score 1 (radiomics signature of the main tumor) had an area under the curve (AUC) of 0.768 on the training dataset and 0.700 on the validation dataset. Rad-score 2 (radiomics signature of the largest peritumoral nodule) had a higher AUC (training set: 0.940; validation set: 0.918) than Rad-score 1. For the diagnosis of double-positive patients in the mixed group [TDs+LNM<sup>+</sup> ( $n = 15$ ); single-positive ( $n = 15$ )], Rad-score 2 demonstrated moderate performance (sensitivity, 73.3%; specificity, 66.6%; and accuracy, 70%).

### Research conclusions

The radiomics signature of the largest peritumoral nodule could provide individualized preoperative differentiation of TDs and LNM. Moreover, it was helpful in diagnosing patients who were TDs+LNM<sup>+</sup>.

### Research perspectives

To improve the model, surgeons, radiologists, and pathologists should collaborate through prospective research to achieve node-to-node correspondence between CT images and pathological examinations in the future.

---

## FOOTNOTES

**Author contributions:** Song B designed the research; Zhang YC and Jin YM collected the data; Li M, Xu JX, and Huang CC analyzed the data; Zhang YC and Li M wrote the paper; all authors have read and approved the final manuscript.

**Institutional review board statement:** This study was reviewed and approved by the Ethics Committee of West China Hospital of Sichuan University, No. 1159.

**Informed consent statement:** Patients were not required to give informed consent to the study because the analysis used anonymous clinical data that were obtained after each patient agreed to treatment by written consent.

**Conflict-of-interest statement:** Authors Jing-Xu Xu and Chen-Cui Huang are employed by the company Beijing Deepwise & League of PHD Technology Co., Ltd; the remaining authors declare no conflicts-of-interest related to this article.

**Data sharing statement:** No additional data are available.

**Open-Access:** This article is an open-access article that was selected by an in-house editor and fully peer-reviewed by external reviewers. It is distributed in accordance with the Creative Commons Attribution NonCommercial (CC BY-NC 4.0) license, which permits others to distribute, remix, adapt, build upon this work non-commercially, and license their derivative works on different terms, provided the original work is properly cited and the use is non-commercial. See: <https://creativecommons.org/licenses/by-nc/4.0/>

**Country/Territory of origin:** China

**ORCID number:** Yong-Chang Zhang 0000-0003-0402-2525; Mou Li 0000-0002-7101-5942; Yu-Mei Jin 0000-0001-6606-8049; Jing-Xu Xu 0000-0003-1079-7378; Chen-Cui Huang 0000-0003-3307-6872; Bin Song 0000-0002-7269-2101.

**S-Editor:** Chen YL

**L-Editor:** A

**P-Editor:** Chen YL

---

## REFERENCES

- 1 **Sung H**, Ferlay J, Siegel RL, Laversanne M, Soerjomataram I, Jemal A, Bray F. Global Cancer Statistics 2020: GLOBOCAN Estimates of Incidence and Mortality Worldwide for 36 Cancers in 185 Countries. *CA Cancer J Clin* 2021; **71**: 209-249 [PMID: 33538338 DOI: 10.3322/caac.21660]
- 2 **Bailey CE**, Hu CY, You YN, Bednarski BK, Rodriguez-Bigas MA, Skibber JM, Cantor SB, Chang GJ. Increasing disparities in the age-related incidences of colon and rectal cancers in the United States, 1975-2010. *JAMA Surg* 2015; **150**: 17-22 [PMID: 25372703 DOI: 10.1001/jamasurg.2014.1756]
- 3 **Maguire A**, Sheahan K. Controversies in the pathological assessment of colorectal cancer. *World J Gastroenterol* 2014; **20**: 9850-9861 [PMID: 25110416 DOI: 10.3748/wjg.v20.i29.9850]
- 4 **Lord AC**, D'Souza N, Pucher PH, Moran BJ, Abulafi AM, Wotherspoon A, Rasheed S, Brown G. Significance of extranodal tumour deposits in colorectal cancer: A systematic review and meta-analysis. *Eur J Cancer* 2017; **82**: 92-102 [PMID: 28651160 DOI: 10.1016/j.ejca.2017.05.027]

- 5 **Benoit O**, Svrcek M, Creavin B, Bouquet M, Challine A, Chafai N, Debove C, Voron T, Parc Y, Lefevre JH. Prognostic value of tumor deposits in rectal cancer: A monocentric series of 505 patients. *J Surg Oncol* 2020; **122**: 1481-1489 [PMID: 32789859 DOI: 10.1002/jso.26165]
- 6 **Atre ID**, Eurboonyanun K, Noda Y, Parakh A, O'Shea A, Lahoud RM, Sell NM, Kunitake H, Harisinghani MG. Utility of texture analysis on T2-weighted MR for differentiating tumor deposits from mesorectal nodes in rectal cancer patients, in a retrospective cohort. *Abdom Radiol (NY)* 2021; **46**: 459-468 [PMID: 32700214 DOI: 10.1007/s00261-020-02653-w]
- 7 **Jin M**, Frankel WL. Lymph Node Metastasis in Colorectal Cancer. *Surg Oncol Clin N Am* 2018; **27**: 401-412 [PMID: 29496097 DOI: 10.1016/j.soc.2017.11.011]
- 8 **Mayerhoefer ME**, Materka A, Langs G, Häggström I, Szczypiński P, Gibbs P, Cook G. Introduction to Radiomics. *J Nucl Med* 2020; **61**: 488-495 [PMID: 32060219 DOI: 10.2967/jnumed.118.222893]
- 9 **Yang YS**, Feng F, Qiu YJ, Zheng GH, Ge YQ, Wang YT. High-resolution MRI-based radiomics analysis to predict lymph node metastasis and tumor deposits respectively in rectal cancer. *Abdom Radiol (NY)* 2021; **46**: 873-884 [PMID: 32940755 DOI: 10.1007/s00261-020-02733-x]
- 10 **Chen LD**, Li W, Xian MF, Zheng X, Lin Y, Liu BX, Lin MX, Li X, Zheng YL, Xie XY, Lu MD, Kuang M, Xu JB, Wang W. Preoperative prediction of tumour deposits in rectal cancer by an artificial neural network-based US radiomics model. *Eur Radiol* 2020; **30**: 1969-1979 [PMID: 31828415 DOI: 10.1007/s00330-019-06558-1]
- 11 **Benchofi M**, Matzner-Lober E, Molinari N, Jannot AS, Soyer P. Interobserver agreement issues in radiology. *Diagn Interv Imaging* 2020; **101**: 639-641 [PMID: 32958434 DOI: 10.1016/j.diii.2020.09.001]
- 12 **van Griethuysen JJM**, Fedorov A, Parmar C, Hosny A, Aucoin N, Narayan V, Beets-Tan RGH, Fillion-Robin JC, Pieper S, Aerts HJWL. Computational Radiomics System to Decode the Radiographic Phenotype. *Cancer Res* 2017; **77**: e104-e107 [PMID: 29092951 DOI: 10.1158/0008-5472.CAN-17-0339]
- 13 **Clancy C**, Flanagan M, Marinello F, O'Neill BD, McNamara D, Burke JP. Comparative Oncologic Outcomes of Upper Third Rectal Cancers: A Meta-analysis. *Clin Colorectal Cancer* 2019; **18**: e361-e367 [PMID: 31445919 DOI: 10.1016/j.clcc.2019.07.004]
- 14 **Amin MB**, Greene FL, Edge SB, Compton CC, Gershenwald JE, Brookland RK, Meyer L, Gress DM, Byrd DR, Winchester DP. The Eighth Edition AJCC Cancer Staging Manual: Continuing to build a bridge from a population-based to a more "personalized" approach to cancer staging. *CA Cancer J Clin* 2017; **67**: 93-99 [PMID: 28094848 DOI: 10.3322/caac.21388]
- 15 **Puppa G**, Maisonneuve P, Sonzogni A, Masullo M, Capelli P, Chilosi M, Menestrina F, Viale G, Pelosi G. Pathological assessment of pericolonic tumor deposits in advanced colonic carcinoma: relevance to prognosis and tumor staging. *Mod Pathol* 2007; **20**: 843-855 [PMID: 17491597 DOI: 10.1038/modpathol.3800791]
- 16 **Wünsch K**, Müller J, Jähnig H, Herrmann RA, Arnholt HM, Märkl B. Shape is not associated with the origin of pericolonic tumor deposits. *Am J Clin Pathol* 2010; **133**: 388-394 [PMID: 20154277 DOI: 10.1309/AJCPAWOLX7ADZQ2K]
- 17 **Goldstein NS**, Turner JR. Pericolonic tumor deposits in patients with T3N+MO colon adenocarcinomas: markers of reduced disease free survival and intra-abdominal metastases and their implications for TNM classification. *Cancer* 2000; **88**: 2228-2238 [PMID: 10820343]
- 18 **Chen LD**, Liang JY, Wu H, Wang Z, Li SR, Li W, Zhang XH, Chen JH, Ye JN, Li X, Xie XY, Lu MD, Kuang M, Xu JB, Wang W. Multiparametric radiomics improve prediction of lymph node metastasis of rectal cancer compared with conventional radiomics. *Life Sci* 2018; **208**: 55-63 [PMID: 29990485 DOI: 10.1016/j.lfs.2018.07.007]
- 19 **Zhou X**, Yi Y, Liu Z, Zhou Z, Lai B, Sun K, Li L, Huang L, Feng Y, Cao W, Tian J. Radiomics-Based Preoperative Prediction of Lymph Node Status Following Neoadjuvant Therapy in Locally Advanced Rectal Cancer. *Front Oncol* 2020; **10**: 604 [PMID: 32477930 DOI: 10.3389/fonc.2020.00604]
- 20 **Li J**, Zhou Y, Wang X, Zhou M, Chen X, Luan K. An MRI-based multi-objective radiomics model predicts lymph node status in patients with rectal cancer. *Abdom Radiol (NY)* 2021; **46**: 1816-1824 [PMID: 33241428 DOI: 10.1007/s00261-020-02863-2]
- 21 **Zhu H**, Zhang X, Li X, Shi Y, Zhu H, Sun Y. Prediction of pathological nodal stage of locally advanced rectal cancer by collective features of multiple lymph nodes in magnetic resonance images before and after neoadjuvant chemoradiotherapy. *Chin J Cancer Res* 2019; **31**: 984-992 [PMID: 31949400 DOI: 10.21147/j.issn.1000-9604.2019.06.14]

## Retrospective Study

## Effects of microwave ablation on serum Golgi protein 73 in patients with primary liver cancer

Zheng-Ju Xu, Mei-Juan Wei, Xiao-Man Zhang, Hui-Guo Liu, Jin-Piao Wu, Jin-Fa Huang, Yong-Fei Li, Zhi-Jie Huang, Yan-Yan Yan

**Specialty type:** Gastroenterology and hepatology

**Provenance and peer review:**

Unsolicited article; Externally peer reviewed.

**Peer-review model:** Single blind

**Peer-review report's scientific quality classification**

Grade A (Excellent): 0  
Grade B (Very good): 0  
Grade C (Good): C, C, C  
Grade D (Fair): 0  
Grade E (Poor): 0

**P-Reviewer:** Koganti S, United States; Sultana N, Bangladesh; Zhang X, United States

**Received:** February 21, 2022

**Peer-review started:** February 21, 2022

**First decision:** April 16, 2022

**Revised:** April 30, 2022

**Accepted:** July 5, 2022

**Article in press:** July 5, 2022

**Published online:** August 7, 2022



**Zheng-Ju Xu, Hui-Guo Liu, Jin-Piao Wu, Jin-Fa Huang, Yong-Fei Li, Zhi-Jie Huang, Yan-Yan Yan,** The Liver Disease Center, The 910<sup>th</sup> Hospital of the PLA Joint Logistics Support Force, Quanzhou 362000, Fujian Province, China

**Mei-Juan Wei,** Central Laboratory, Decheng Hospital, Quanzhou 362104, Fujian Province, China

**Xiao-Man Zhang,** Central Laboratory of Clinical Hepatology, The 910<sup>th</sup> Hospital of the PLA Joint Logistics Support Force, Quanzhou 362000, Fujian Province, China

**Corresponding author:** Zheng-Ju Xu, MD, Chief Doctor, The Liver Disease Center, The 910<sup>th</sup> Hospital of the PLA Joint Logistics Support Force, No. 180 Huayuan Road, Fengze District, Quanzhou 362000, Fujian Province, China. [h180@163.com](mailto:h180@163.com)

## Abstract

### BACKGROUND

Microwave ablation (MWA) is an effective treatment option for patients with primary liver cancer. However, it has been reported that the MWA procedure induces a hepatic inflammatory response and injury, which may negatively affect the efficacy of MWA. As such, the discovery of reliable markers to monitor the patient's response to MWA is needed. Golgi protein 73 (GP73) has been shown to be associated with chronic liver disease. To date, the potential value of serum GP73 in the dynamic monitoring during MWA of liver cancer remains unclear.

### AIM

To examine the effects of MWA on the serum levels of GP73 in patients with primary liver cancer.

### METHODS

A total of 150 primary liver cancer patients with a single small lesion ( $\leq 3$  cm in diameter) were retrospectively enrolled spanning the period between January 2016 and October 2018. All of the patients received MWA for the treatment of primary liver cancer. Serum GP73, alpha-fetoprotein (AFP), and widely used liver biochemical indicators [serum albumin, total bilirubin (TBIL), alanine aminotransferase (ALT), and aspartate aminotransferase (AST)] were compared before MWA and at different time points, including 1, 2, and 4 wk following the ablation procedure.

## RESULTS

Complete tumor ablation was achieved in 95.33% of the patients at 1 mo after MWA. The 1-, 2-, and 3-year disease-free survival rates were 74.67%, 59.33%, and 54.00%, respectively. The serum AFP levels were significantly decreased at 1, 2, and 4 wk after MWA; they returned to the normal range at 12 wk after MWA; and they remained stable thereafter during follow-up in those cases without recurrence. In contrast, the serum GP73 levels were significantly increased at 1 and 2 wk after MWA. The serum GP73 levels reached the peak at 2 wk after MWA, started to decline after hepatoprotective treatment with glycyrrhizin and reduced glutathione, and returned to the pretreatment levels at 12 and 24 wk after MWA. Notably, the changes of serum GP73 in response to MWA were similar to those of TBIL, ALT, and AST.

## CONCLUSION

Serum GP73 is markedly increased in response to MWA of liver cancer. Thus, serum GP73 holds potential as a marker to monitor MWA-induced inflammatory liver injury in need of amelioration.

**Key Words:** Liver cancer; Microwave ablation; Ablation therapy; Golgi protein 73; Biomarker; Liver injury

©The Author(s) 2022. Published by Baishideng Publishing Group Inc. All rights reserved.

**Core Tip:** Microwave ablation (MWA) has become an effective modality of cancer treatment, including primary liver cancer. However, the MWA procedure induces a hepatic inflammatory response and injury, which may diminish the efficacy of MWA. Therefore, the discovery of reliable markers to monitor the response to MWA is still needed. In this study, we examined the effects of MWA on the serum levels of Golgi protein 73 (GP73). The resulting data suggest that serum GP73 is markedly elevated in response to the MWA procedure. Importantly, our novel findings may have the clinical implication that serum GP73 could be a potential marker to monitor MWA-induced inflammatory liver injury.

**Citation:** Xu ZJ, Wei MJ, Zhang XM, Liu HG, Wu JP, Huang JF, Li YF, Huang ZJ, Yan YY. Effects of microwave ablation on serum Golgi protein 73 in patients with primary liver cancer. *World J Gastroenterol* 2022; 28(29): 3971-3980

**URL:** <https://www.wjgnet.com/1007-9327/full/v28/i29/3971.htm>

**DOI:** <https://dx.doi.org/10.3748/wjg.v28.i29.3971>

## INTRODUCTION

Liver cancer is one of the most common malignant tumors throughout the world, and its incidence is relatively high in Asian countries and Pacific islands[1,2]. In China, nearly 500000 cases of primary liver cancer are newly diagnosed annually, accounting for approximately 50% of all new primary liver cancer cases worldwide, mainly due to a particularly high prevalence of hepatitis B virus (HBV) infection[1-3]. Primary liver cancer mainly includes hepatocellular carcinoma (HCC), intrahepatic cholangiocarcinoma (ICC), and combined hepatocellular-cholangiocarcinoma, of which HCC makes up 75%-85% and ICC accounts for 10%-15% of all primary liver cancer cases[4]. For patients with primary liver cancer at an early stage, ablation therapy has been shown to be an effective treatment option. Microwave ablation (MWA) is an ablation modality that destroys cancer cells by using heat from microwave energy. Over the last decade, extensive studies have shown that MWA is effective and safe for treating small primary liver cancer, which is usually less than 3 cm in diameter[5-9]. However, it has been reported that the MWA procedure induces a hepatic inflammatory response and injury, which may negatively affect its efficacy[10]. Therefore, the discovery of reliable markers to monitor the patient's response to MWA is still needed.

Golgi protein 73 (GP73) is a transmembrane glycoprotein with a molecular weight of 73 kDa. Under normal conditions in the liver, GP73 is mainly expressed in the epithelial cells of the bile duct, while its expression in hepatocytes is considerably lower[11]. Previous studies have shown that hepatic GP73 expression is upregulated in a variety of acute and chronic liver diseases[12]. Our previous study also has demonstrated that GP73 is expressed in the cytoplasm of hepatocytes, but not in the infiltrating inflammatory cells in patients with chronic HBV infection, and that changes in the hepatic and serum levels of GP73 are positively correlated with hepatic necroinflammatory activity in CHB patients[13]. Few hepatocytes expressed GP73, and the serum GP73 levels were low in patients with chronic HBV infection but without indications of liver injury. However, once hepatic necrosis was triggered, the affected hepatocytes started to release more GP73 into the blood, resulting in elevated hepatic and

serum levels of GP73. Our previous study also found that elevated serum GP73 levels were positively associated with a higher hepatic necroinflammatory activity grade[14]. To date, the potential value of serum GP73 in the dynamic monitoring and assessment of patient response to MWA during the treatment of liver cancer remains to be further investigated.

Intrigued by our previous findings, we aimed to examine the effects of MWA of liver cancer on the serum GP73 levels before and at different time points after ablation therapy in patients with primary liver cancer. The findings may help to identify potential markers to be used in the dynamic monitoring of the response to MWA for the treatment of primary liver cancer.

## MATERIALS AND METHODS

### **Study subjects**

A total of 150 patients with primary liver cancer were retrospectively enrolled from the Liver Disease Center at the 910<sup>th</sup> Hospital of the PLA Logistics Support Force between January 2016 and October 2018. All of the study subjects were diagnosed as having primary liver cancer, in accordance with the Guidelines for the Diagnosis and Treatment of Primary Liver Cancer in China (2019 edition) issued by the National Health and Health Commission of the People's Republic of China[15], and fulfilled the following inclusion criteria: (1) Age > 18 years old; (2) A single lesion ≤ 3 cm in diameter; and (3) No invasion into the portal vein, hepatic vein, or extrahepatic distant metastasis on imaging examinations [e.g., color Doppler ultrasound, computed tomography (CT), or magnetic resonance imaging (MRI)]. All of the 150 patients with primary liver cancer had a history of HBV infection. Chronic hepatitis B (CHB) and CHB-associated liver cirrhosis were diagnosed in accordance with the diagnostic criteria as reported in the Guidelines of Prevention and Treatment for Chronic Hepatitis B (2019 version)[16]. The exclusion criteria were as follows: (1) Age ≤ 18 years old; (2) The number of lesions ≥ 2 or the size > 3 cm in diameter; (3) The tumor invaded adjacent organs or extrahepatic metastases occurred; (4) Child-Pugh score of grade C; (5) Uncorrectable coagulation dysfunction; (6) Complicated with active infection; (7) Massive ascites and cachexia; (8) Major organ failure (heart, brain, lung, kidney, or other important organs); (9) Eastern Cooperative Oncology Group (ECOG) score > 2; and (10) Disorders of consciousness or inability to cooperate with medical treatments. Among the 150 patients with primary liver cancer, 143 patients with space-occupying lesions with typical imaging features of liver cancer did not receive a liver biopsy, and the remaining 7 patients underwent a liver biopsy and had a pathological diagnosis of primary HCC. In terms of the status of the background liver, 115 patients had background liver cirrhosis, and 35 patients showed no clinical signs of liver cirrhosis.

This study was approved by the Ethics Committee of the 910<sup>th</sup> Hospital of the PLA Joint Logistics Support Force (Quanzhou, Fujian Province, China). All of the patients provided a signed informed consent.

### **MWA of liver cancer**

All of the patients refused liver resection surgery and were willing to undergo MWA of liver cancer on a microwave therapeutic apparatus (Nanjing, Jiangsu Province, China). The procedure was performed under the guidance of CT or color Doppler ultrasound. The power and ablation time were designed for each patient based on the size of the liver cancer and the surrounding tissues. The ablation zone size was 0.5-1 cm to the margin of the tumor.

### **Effectiveness of MWA and follow-up**

Enhanced CT or MRI examinations were performed on the patients at 1 mo after MWA to determine the complete or partial tumor ablation rate. The patients were followed up for more than 3 years, during which the patients were scheduled for enhanced CT or MRI to determine the cumulative recurrence rate, survival time, local tumor progression, presence of new tumors, disease-free survival (DFS), and overall survival (OS). Complete tumor ablation was defined as no residual tumor on enhanced CT or MRI within the ablation zone and adequate ablation margins of 0.5-1.0 cm. Partial tumor ablation was defined as the presence of a residual tumor on enhanced CT or MRI in the zone of ablation.

### **Quantitative enzyme-linked immunosorbent assay of serum GP73 levels**

Enzyme-linked immunosorbent assay (ELISA) was performed to determine the serum GP73 levels at the Laboratory of Liver Diseases, the 910<sup>th</sup> Hospital of the PLA Joint Logistics Support Force. The GP73 ELISA detection kit was purchased from Hotgen Biotech Co. Ltd. (Beijing, China) and used for the determination of serum GP73 levels on a Model 680 Microplate Reader (BIO-RAD, United States), according to the manufacturer's protocol. A serum GP73 concentration of 45 mg/L was used as a cut-off value for the general healthy population.

### **Serum alpha-fetoprotein and liver biochemical tests**

Serum alpha-fetoprotein (AFP) was examined using an AFP detection kit (Roche Diagnostics, Basel,

Switzerland), and a value of < 7 mg/L was considered to be normal. Liver biochemical tests, including serum albumin (ALB), total bilirubin (TBIL), alanine aminotransferase (ALT), and aspartate aminotransferase (AST), were determined on a TBA120FR automatic biochemistry analyzer (Toshiba Medical System Co., Ltd., Japan) in the Clinical Laboratory of the 910<sup>th</sup> Hospital of the PLA Joint Logistics Support Force (Quanzhou, Fujian Province, China).

### Statistical analysis

Statistical analysis was performed using GraphPad Prism 5.0 software (Graphpad Software Inc., La Jolla, CA, United States). Count data were expressed as percentages (%). Continuous variables were presented as the median (25%, 75%). For paired data following a normal distribution, a paired *t*-test was used to evaluate differences between the pairs. For non-normally distributed data, a paired Wilcoxon signed-rank test was applied to determine the difference between matched samples. The Kaplan–Meier method was used for survival analysis. *P* < 0.05 indicated that the difference was statistically significant. The statistical methods of this study were reviewed by Zhu YL from the Department of Medical Statistics, Huaqiao University.

## RESULTS

### Characteristics of the enrolled patients with primary liver cancer

The study cohort was comprised of 150 primary liver cancer patients with one small lesion (average size, 2.03 cm in diameter; range, 0.7–3 cm), including 130 men (86.67%) and 20 women (13.33%), and the median age was 56.00 years old. All of the enrolled patients had a medical history of chronic HBV infection, of which 97 patients (97/150, 64.7%) were positive for the HBV e antigen. Of note, 91 patients (91/150, 60.7%) received antiviral treatment with entecavir or tenofovir disoproxil fumarate for more than 1 year before undergoing MWA and had an HBV DNA concentration of < 500 IU/L, while the remaining 59 patients (59/150, 39.33%) who did not receive the antiviral treatment had an average HBV DNA level of 6.32 (4.52, 7.15) log<sub>10</sub> IU/L. Of the enrolled primary liver cancer patients, 115 patients had compensated liver cirrhosis, accounting for 76.7% of the study subjects. Prior to MWA, the 150 patients with primary liver cancer had an ECOG Performance Status score of 0 and a Child–Pugh classification of Class A. The majority of the patients with primary liver cancer had abnormally high levels of AFP, accounting for 68.00% (102/150) of the study subjects. The liver biochemical characteristics, including serum ALB, TBIL, ALT, and AST, as well as the AFP and serum GP73 Levels of the study subjects before MWA are summarized in [Table 1](#).

All of the patients received MWA for primary liver cancer, and the effectiveness was evaluated, including the complete tumor ablation rate at 1 mo after MWA, recurrence rate, and survival time. At 1 month after MWA, enhanced CT/MRI examinations showed that 143 patients (143/150, 95.33%) achieved complete tumor ablation. A small proportion of the patients (7/150, 4.67%) who had partial tumor ablation underwent reablation treatment with MWA and achieved complete tumor ablation. All of the 150 patients were followed up for more than 3 years, and the results were as follows: 134 patients (134/150, 89.33%) survived and 16 patients (16/150, 10.67%) died due to gastrointestinal bleeding in 5 patients (5/150, 3.33%) and liver failure in 11 patients (11/150, 7.33%). The OS rates at 1, 2, and 3 years after MWA were 100.00%, 96.00%, and 89.33%, respectively. In terms of tumor recurrence, cumulative recurrence occurred in 69 patients (69/150, 46.00%) at 3 years after MWA, including 13 patients (13/150, 8.67%) with local tumor progression and 57 patients (57/150, 37.33%) with a new tumor. Among the 69 patients with tumor recurrence, the overall 1-, 2-, and 3-year recurrence rates after MWA were 55.07% (38/150), 33.33% (23/150), and 11.59% (8/150), respectively. As presented in [Figure 1](#), the 1-, 2-, and 3-year DFS rates after MWA were 74.67%, 59.33%, and 54.00%, respectively, in the patients with MWA treatment of primary liver cancer.

### Changes of liver biochemical indicators before and after MWA in the enrolled patients with primary liver cancer

MWA for primary liver cancer may cause some adverse effects, including inflammatory injury in the liver. We analyzed the effects of MWA treatment on the widely used liver biochemical indicators ALB, TBIL, ALT, and AST by comparing their values of the enrolled patients before MWA and at different time points (1, 2, and 4 wk) after the treatment procedure. As shown in [Table 1](#), the serum levels of ALB were significantly decreased, while the levels of serum TBIL, ALT, and AST were significantly increased at 1 wk after MWA treatment compared with those levels prior to MWA as a control (all *P* < 0.001). We found that increases in the biochemical indicators (TBIL, ALT, and AST) were related to the hepatocyte injury in response to MWA treatment. There were no significant differences in ALB, TBIL, ALT, or AST between before and at 2 or 4 wk after the MWA treatment ([Table 1](#)), which was mainly attributed to the implementation of hepatoprotective therapy using the active compounds glycyrrhizin and reduced glutathione for nearly 2 wk.

**Table 1 Liver biochemical tests in the primary liver cancer patients before and after microwave ablation treatment**

	ALB (g/L)	TBIL (μmol/L)	ALT (U/L)	AST (U/L)	GP73 (mg/L)	AFP (mg/L)
Cases	150	150	150	150	150	102 <sup>1</sup>
Before MWA	42.10 (38.83, 45.20)	16.20 (12.70, 23.35)	30.10 (20.55, 41.55)	28.30 (22.05, 35.40)	90.83 (54.49, 110.60)	110.40 (32.71, 267.30)
1 wk after MWA	38.40 (36.65, 41.15) <sup>a</sup>	24.80(16.25, 30.60) <sup>a</sup>	102.20(88.65, 166.30) <sup>a</sup>	81.70(68.25, 91.30) <sup>a</sup>	127.10(84.66, 175.50) <sup>a</sup>	37.61(23.30, 95.48) <sup>a</sup>
2 wk after MWA	40.30 (38.36, 42.00)	15.00 (12.90, 18.05)	29.40 (25.65, 36.85)	29.00 (24.10, 36.05)	130.70 (88.39, 163.60)	27.34 (6.32, 81.59) <sup>b</sup>
4 wk after MWA	43.75 (37.12, 47.31)	17.35 (13.62, 25.76)	33.21 (21.57, 43.82)	26.29 (19.70, 40.61)	102.20 (59.15, 121.90)	7.32 (3.87, 16.25) <sup>c</sup>
<sup>a</sup> t/W	7.037 (t)	3.991 (t)	6.703 (t)	5.768 (t)	5.150 (t)	-157 (W)
<sup>a</sup> P	< 0.001	< 0.001	< 0.001	< 0.001	< 0.001	< 0.001

<sup>1</sup>Cases with significantly elevated alpha-fetoprotein.

<sup>a</sup>P < 0.001 vs before microwave ablation (MWA) as a control.

<sup>b</sup>P < 0.001 (W = -190) versus before MWA as a control.

<sup>c</sup>P < 0.001 (W = -253) versus before MWA as a control.

t from the paired t-test for normally distributed data and W from the paired Wilcoxon signed-rank test for non-normally distributed data.

MWA: Microwave ablation; ALB: Serum albumin; TBIL: Total bilirubin; ALT: Alanine aminotransferase; AST: Aspartate aminotransferase; AFP: Alpha-fetoprotein; GP73: Golgi protein 73.

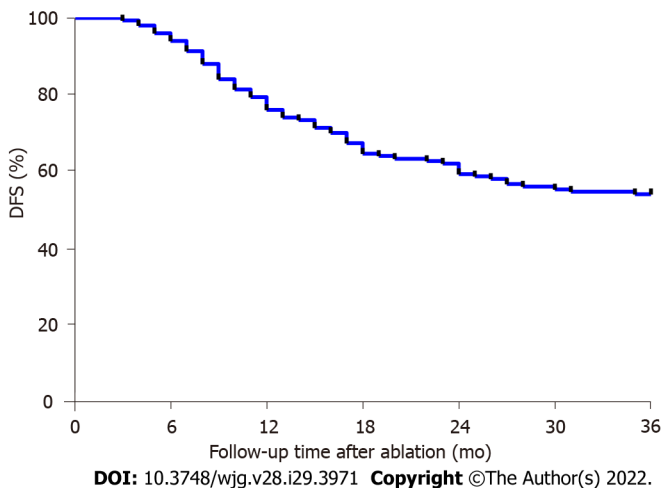


**Figure 1 Disease-free survival rates of the patients with primary liver cancer after treatment with microwave ablation.** The disease-free survival (DFS) rates were analyzed at 6, 12, 18, 24, 30, and 36 mo after microwave ablation (MWA) for primary liver cancer in the patients. The 1-, 2-, and 3-year DFS rates after MWA were 74.67%, 59.33%, and 54.00%, respectively. DFS: Disease-free survival.

**Changes of serum AFP before and after MWA treatment in the enrolled patients with primary liver cancer**

We examined the effects of MWA on the serum AFP levels before and after MWA treatment in the enrolled patients with primary liver cancer. As illustrated in Figure 2 and Table 1, the patients had an abnormally high AFP level of 110.40 (32.71, 267.30) mg/L before MWA treatment (pre-MWA), which was decreased sharply to 37.61 (23.30, 95.48) mg/L at 1 wk after MWA treatment. Notably, the AFP level continued to decrease at 2 and 4 wk, returned to the normal range at 12 wk after MWA, and remained stable thereafter during follow-up in those cases without recurrence (Figure 2, Table 1). Statistical analysis revealed that the serum AFP levels at all time points after the MWA treatment were significantly lower compared with the value prior to MWA treatment as a control (all P < 0.001). For the recurrent cases with primary liver cancer, however, the serum AFP levels started to increase at 12 wk post MWA; the values were 75.85 mg/L (range, 38.32-86.70 mg/L), 54.17 mg/L (range, 37.83-82.60 mg/L), 67.80 mg/L (range, 37.67-97.32 mg/L), 43.20 mg/L (range, 29.80-58.96 mg/L), 38.05 mg/L (range, 30.85-93.93 mg/L), and 66.73 mg/L (range, 51.90-81.56 mg/L) at 24, 48, 72, 96, 120, and 144 wk following the MWA treatment, respectively (Figure 2).

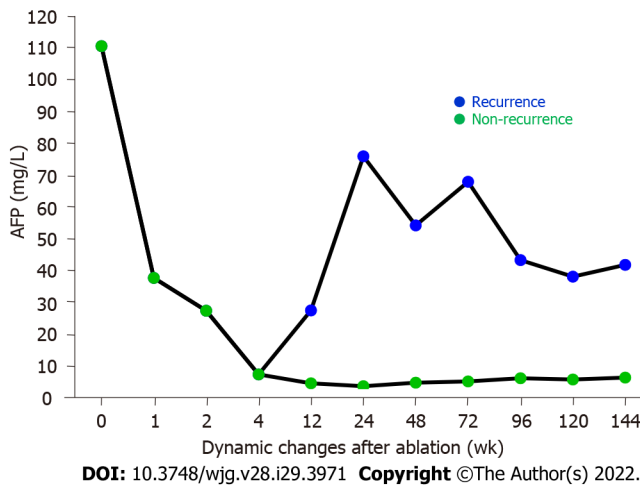


**Figure 2** Effects of microwave ablation treatment on the serum alpha-fetoprotein levels in patients with primary liver cancer. The serum alpha-fetoprotein (AFP) levels were examined in the primary liver cancer patients before microwave ablation (MWA) treatment and at different time points after the treatment. The average serum AFP level was 110.4 mg/L before MWA treatment (pre-MWA), decreased sharply to 37.61 mg/L at 1 wk after MWA treatment, continued to decrease, returned to the normal range at 12 wk after MWA, and remained stable thereafter during follow-up in those cases without recurrence. For the recurrent cases with primary liver cancer, however, the serum AFP levels started to increase at 12 wk following the MWA treatment. AFP: Alpha-fetoprotein.

**Comparison of serum GP73 levels in the primary liver cancer patients with or without liver cirrhosis**

We compared the serum GP73 levels in the enrolled liver cancer patients with *vs* without background liver cirrhosis. As shown in Figure 3, the average level of serum GP73 in the 115 patients with liver cirrhosis was 97.76 mg/L (range, 70.65-133.10 mg/L), which was significantly greater than 69.02 mg/L (range, 45.48-101.40 mg/L) in the 35 patients without liver cirrhosis ( $t = 2.477, P < 0.05$ ) (Figure 3).

**Changes of serum GP73 before and after MWA treatment in the enrolled patients with primary liver cancer**

To evaluate the potential value of serum GP73 measurement for inflammatory injury associated with MWA treatment, we analyzed the serum GP73 levels in the primary liver cancer patients before and at different times after the MWA treatment. As shown in Figure 4 and Table 1, the average serum GP73 level was 90.83 mg/L (range, 54.49-110.6 mg/L) before MWA, which was increased to 127.1 mg/L (range, 84.66-175.50 mg/L) and 130.70 mg/L (range, 88.39-163.60 mg/L) at 1 and 2 wk following the MWA treatment, respectively. Notably, the serum GP73 level started to decline after hepatoprotective treatment with glycyrrhizin and reduced glutathione at 4 wk post MWA; the values were 102.20 mg/L (range, 59.15-121.90 mg/L), 85.73 mg/L (range, 61.42-105.70 mg/L), and 76.09 mg/L (range, 59.26-102.66 mg/L) at 8, 12, and 24 wk following the MWA treatment, respectively (Figure 4). Statistical analysis revealed that the serum GP73 levels were significantly greater at 1 and 2 wk after the MWA procedure *vs* before MWA (1 wk after MWA *vs* before MWA:  $t = 5.150, P < 0.001$ ; 2 wk after MWA *vs* before MWA:  $t = 6.182, P < 0.001$ ) (Figure 4). It is worth noting that the serum GP73 level reached the peak at 2 wk after MWA and then started to decline at 4 wk after MWA (Figure 4). During the follow-up of the patients at 12 and 24 wk following the MWA treatment, the serum GP73 levels were similar to the pretreatment level (Figure 4).

**DISCUSSION**

This retrospective study has the following major findings: (1) MWA was highly efficacious in treating patients with small primary liver cancer, with as high as 95.33% of the patients achieving complete tumor ablation at 1 mo after MWA; (2) The serum AFP level was significantly decreased following the MWA treatment and returned to the normal range at 3 mo after MWA, which was in agreement with the observation for the complete tumor ablation rate; (3) The serum GP73 levels were significantly elevated at 1 and 2 wk following MWA, with the peak reached at 2 wk after completion of the treatment; (4) The serum GP73 level declined starting at 4 wk after MWA and continued to decrease to the pretreatment level at 12 and 24 wk after MWA; and (5) The effect of MWA on the serum GP73 level was similar to those of TBIL, ALT, and AST. These findings suggest that measurement of the serum GP73 level has the potential to monitor MWA-mediated inflammatory injury in patients with primary liver cancer.

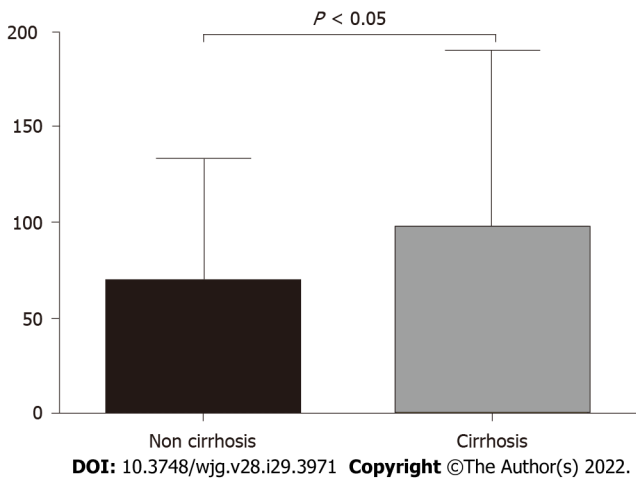


**Figure 3 Comparison of serum Golgi protein 73 levels in the primary liver cancer patients with vs without liver cirrhosis.** The serum Golgi protein 73 levels were examined in the primary liver cancer patients with compensated liver cirrhosis ( $n = 115$ ) vs those without liver cirrhosis ( $n = 35$ ).  $P < 0.05$ . GP73: Golgi protein 73.

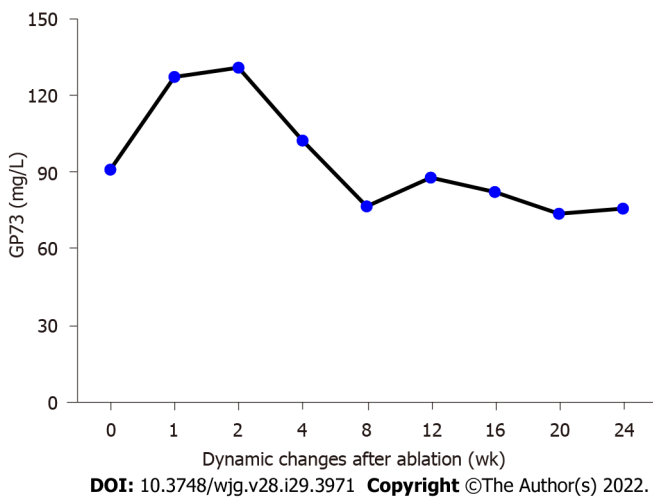


**Figure 4 Effects of microwave ablation treatment on serum Golgi protein 73 levels in the enrolled patients with primary liver cancer.** The serum Golgi protein 73 (GP73) levels were examined in the primary liver cancer patients before and after microwave ablation (MWA) treatment. The serum GP73 levels were increased 1 and 2 wk after MWA. The serum GP73 levels reached the peak at 2 wk after MWA, then progressively decreased, and returned to the pretreatment levels 12 and 24 wk following the MWA treatment. GP73: Golgi protein 73.

In the last decade, percutaneous ablation therapy has been used as a radical treatment method for treating patients with liver cancer[6,17]. In contrast to other types of ablation therapy, MWA has a number of advantages (*e.g.*, a faster ablation time, the capability of simultaneous ablation of multiple lesions, and larger tumor ablation volumes)[18]. Compared with traditional radiofrequency ablation for the treatment of small primary liver cancer nodules, MWA is less affected by the heat sink effect[19-21]. Therefore, MWA is widely accepted as an effective nonsurgical treatment option for liver cancer of a small size and at an early stage[19-23]. Of note, MWA has been demonstrated to completely destroy tumor cells and has been proposed as a radical treatment for small primary liver cancer ( $\leq 3$  cm in diameter) with a single lesion[6,22,24]. In addition, Zhang *et al*[25] performed a meta-analysis of 1480 patients and showed that the therapeutic effectiveness of MWA was superior to that of surgical resection for the treatment of small liver cancer ( $< 3$  cm in diameter). There were no significant differences in the OS, DFS rate, and recurrence rate between MWA and surgical resection for small liver cancer. Our results revealed a high therapeutic effectiveness of MWA for primary liver cancer as supported by several lines of evidence, including 95.33% of patients reaching complete tumor ablation at 1 mo after MWA, high OS rates (1- and 3-year OS rates of 100.00% and 89.33%, respectively), and high DFS rates (1-, 2-, and 3-year DFS rates of 74.67%, 59.33%, and 54.00%, respectively), which were similar to those values previously reported for surgical resection[26]. Despite the high therapeutic effectiveness of MWA for small primary liver cancer, the procedure may trigger an inflammatory response and cause liver injury, which will need to be monitored and alleviated properly.

It merits attention that the serum GP73 level in the present study was significantly elevated at 1 wk after MWA, reached the peak at 2 wk after completion of the procedure, and then declined at 4 wk following MWA. During follow-up of the patients with primary liver cancer at 12 and 24 wk after MWA, the serum GP73 levels nearly returned to the pretreatment level. Consistent with the increase of the serum GP73 levels at 2 and 4 wk after MWA, the serum TBIL, ALT, and AST levels were also significantly increased. Moreover, previous studies have reported that MWA is associated with liver injury due to the high temperature generated in the procedure, induction of hepatocyte apoptosis, and stimulation of the intrahepatic macrophage-related inflammatory response [10,21]. After the MWA-mediated liver injury was alleviated with the implementation of hepatoprotective therapy using the active compounds glycyrrhizin and reduced glutathione for nearly 2 wk, the serum GP73 level was significantly decreased and returned to a level similar to that before MWA. The change of the serum GP73 level in the early response to MWA as well as anti-inflammatory and hepatoprotective therapy using glycyrrhizin and reduced glutathione suggests that serum GP73 is related to the aseptic inflammatory injury of hepatocytes after MWA. The results of this study are also in agreement with those of our previous study demonstrating that the serum GP73 level is increased in liver inflammatory injury [13,14]. Therefore, these findings suggest that the serum GP73 level could be a useful diagnostic approach to monitor the liver inflammatory injury caused by MWA during the treatment of primary liver cancer.

This study does have some limitations that must be addressed. For instance, this was a retrospective study that selected liver cancer patients with one small lesion ( $\leq 3$  cm); therefore, bias in patient selection may have occurred. In addition, due to the retrospective nature of this study, we were unable to examine the correlation between the initial level of GP73 after MWA and the AFP level, recurrence rate, or survival rate. Further prospective studies are needed in the future to validate the interesting findings and to assess the diagnostic accuracy of serum GP73 for monitoring liver injury following MWA treatment for primary liver cancer.

## CONCLUSION

Taken together, this study demonstrated that serum GP73 is markedly elevated in response to MWA treatment for primary liver cancer. Therefore, the findings have a clinical implication that measurement of serum GP73 holds promise for monitoring MWA-induced inflammatory liver injury that requires alleviation.

## ARTICLE HIGHLIGHTS

### **Research background**

Microwave ablation (MWA) has been proven to be highly effective in treatment of small primary liver cancer. However, the procedure may trigger an inflammatory response and cause liver injury in primary liver cancer patients undergoing MWA. As such, it is needed to find reliable markers to monitor and evaluate patient response to MWA. Previous studies have shown that Golgi protein 73 (GP73) are associated with liver inflammatory injury.

### **Research motivation**

This study was designed to test our hypothesis that serum GP73 levels altered in response to MWA in patients with primary liver cancer, and thereby could be used as a potential marker for MWA-induced liver inflammation and injury.

### **Research objectives**

The main objective of this study was to examine effects of MWA on the serum levels of GP73 before and at different time points after the ablation procedure in patients with primary liver cancer.

### **Research methods**

Patients with primary liver cancer ( $\leq 3$  cm in diameter) receiving MWA were retrospectively enrolled in this study. Serum GP73 levels were compared before and 1, 2, and 4 wk after the ablation procedure.

### **Research results**

The serum GP73 levels were significantly elevated at 1 and 2 wk after MWA with the peak at 2 wk after completion of the treatment. The serum GP73 levels decreased starting at 4 wk after MWA and continued to decline to the pretreatment level at 12 and 24 wk after MWA. It was worthy to note that the alterations of serum GP73 levels in response to MWA were similar to those of liver biochemical indicators.

### Research conclusions

The findings of this study have demonstrated that serum GP73 levels altered in response to MWA in patients with primary liver cancer, and thereby measurement of serum GP73 level holds potential as a biomarker for monitoring and assessment of MWA-mediated inflammatory injury in patients with primary liver cancer.

### Research perspectives

Future prospective studies are needed to validate the findings and to assess the diagnostic accuracy of serum GP73 for monitoring liver injury following MWA treatment for primary liver cancer.

---

## FOOTNOTES

**Author contributions:** Xu ZJ carried out the design, coordination of experimental work, manuscript writing, and also performed the microwave ablation procedure; Wei MJ and Zhang XM participated in the study design and data analysis; Liu HG, Wu JP, Huang JF, Li YF, Huang ZJ, and Yan YY participated in data collection and analysis; all authors read and approved the final manuscript.

**Supported by** the Military Medical Science and Technology Committee of China, No. 14MS095; and the Quanzhou Science and Technology Planning Project, No. 2017Z018.

**Institutional review board statement:** The study was reviewed and approved by the 910th Hospital of the PLA Joint Logistics Support Force Institutional Review Board.

**Informed consent statement:** All study participants or their legal guardian provided informed written consent about personal and medical data collection prior to study enrolment.

**Conflict-of-interest statement:** Xu ZJ has received research funding from the Military Medical Science and Technology Committee of China, No. 14MS095, and grants from the Quanzhou Science and Technology Planning Project, No. 2017Z018, during the conduct of the study.

**Data sharing statement:** Technical appendix and dataset available from the corresponding author at "[h180@163.com](mailto:h180@163.com)". Participants gave informed consent for data sharing.

**Open-Access:** This article is an open-access article that was selected by an in-house editor and fully peer-reviewed by external reviewers. It is distributed in accordance with the Creative Commons Attribution NonCommercial (CC BY-NC 4.0) license, which permits others to distribute, remix, adapt, build upon this work non-commercially, and license their derivative works on different terms, provided the original work is properly cited and the use is non-commercial. See: <https://creativecommons.org/licenses/by-nc/4.0/>

**Country/Territory of origin:** China

**ORCID number:** Zheng-Ju Xu [0000-0002-2250-5013](https://orcid.org/0000-0002-2250-5013); Mei-Juan Wei [0000-0003-1639-7244](https://orcid.org/0000-0003-1639-7244); Xiao-Man Zhang [0000-0001-7525-2972](https://orcid.org/0000-0001-7525-2972); Hui-Guo Liu [0000-0003-4314-9836](https://orcid.org/0000-0003-4314-9836); Jin-Piao Wu [0000-0001-5160-2894](https://orcid.org/0000-0001-5160-2894); Jin-Fa Huang [0000-0001-5287-1607](https://orcid.org/0000-0001-5287-1607); Yong-Fei Li [0000-0002-7742-8203](https://orcid.org/0000-0002-7742-8203); Zhi-Jie Huang [0000-0002-3479-5791](https://orcid.org/0000-0002-3479-5791); Yan-Yan Yan [0000-0002-6164-8260](https://orcid.org/0000-0002-6164-8260).

**S-Editor:** Yan JP

**L-Editor:** A

**P-Editor:** Yan JP

---

## REFERENCES

- 1 **Sung H**, Ferlay J, Siegel RL, Laversanne M, Soerjomataram I, Jemal A, Bray F. Global Cancer Statistics 2020: GLOBOCAN Estimates of Incidence and Mortality Worldwide for 36 Cancers in 185 Countries. *CA Cancer J Clin* 2021; **71**: 209-249 [PMID: [33538338](https://pubmed.ncbi.nlm.nih.gov/33538338/) DOI: [10.3322/caac.21660](https://doi.org/10.3322/caac.21660)]
- 2 **Bosch FX**, Ribes J, Diaz M, Cléries R. Primary liver cancer: worldwide incidence and trends. *Gastroenterology* 2004; **127**: S5-S16 [PMID: [15508102](https://pubmed.ncbi.nlm.nih.gov/15508102/) DOI: [10.1053/j.gastro.2004.09.011](https://doi.org/10.1053/j.gastro.2004.09.011)]
- 3 **Fung J**, Lai CL, Yuen MF. Hepatitis B and C virus-related carcinogenesis. *Clin Microbiol Infect* 2009; **15**: 964-970 [PMID: [19874379](https://pubmed.ncbi.nlm.nih.gov/19874379/) DOI: [10.1111/j.1469-0691.2009.03035.x](https://doi.org/10.1111/j.1469-0691.2009.03035.x)]
- 4 **Bray F**, Ferlay J, Soerjomataram I, Siegel RL, Torre LA, Jemal A. Global cancer statistics 2018: GLOBOCAN estimates of incidence and mortality worldwide for 36 cancers in 185 countries. *CA Cancer J Clin* 2018; **68**: 394-424 [PMID: [30207593](https://pubmed.ncbi.nlm.nih.gov/30207593/) DOI: [10.3322/caac.21492](https://doi.org/10.3322/caac.21492)]
- 5 **Hasegawa K**, Aoki T, Ishizawa T, Kaneko J, Sakamoto Y, Sugawara Y, Kokudo N. Comparison of the therapeutic outcomes between surgical resection and percutaneous ablation for small hepatocellular carcinoma. *Ann Surg Oncol* 2014; **21** Suppl 3: S348-S355 [PMID: [24566865](https://pubmed.ncbi.nlm.nih.gov/24566865/) DOI: [10.1245/s10434-014-3585-x](https://doi.org/10.1245/s10434-014-3585-x)]

- 6 **Liang P**, Yu J, Lu MD, Dong BW, Yu XL, Zhou XD, Hu B, Xie MX, Cheng W, He W, Jia JW, Lu GR. Practice guidelines for ultrasound-guided percutaneous microwave ablation for hepatic malignancy. *World J Gastroenterol* 2013; **19**: 5430-5438 [PMID: 24023485 DOI: 10.3748/wjg.v19.i33.5430]
- 7 **Shibata T**, Iimuro Y, Yamamoto Y, Maetani Y, Ametani F, Itoh K, Konishi J. Small hepatocellular carcinoma: comparison of radio-frequency ablation and percutaneous microwave coagulation therapy. *Radiology* 2002; **223**: 331-337 [PMID: 11997534 DOI: 10.1148/radiol.2232010775]
- 8 **Vogl TJ**, Nour-Eldin NA, Hammerstingl RM, Panahi B, Naguib NNN. Microwave Ablation (MWA): Basics, Technique and Results in Primary and Metastatic Liver Neoplasms - Review Article. *Rofo* 2017; **189**: 1055-1066 [PMID: 28834968 DOI: 10.1055/s-0043-117410]
- 9 **Shiina S**, Sato K, Tateishi R, Shimizu M, Ohama H, Hatanaka T, Takawa M, Nagamatsu H, Imai Y. Percutaneous Ablation for Hepatocellular Carcinoma: Comparison of Various Ablation Techniques and Surgery. *Can J Gastroenterol Hepatol* 2018; **2018**: 4756147 [PMID: 29974040 DOI: 10.1155/2018/4756147]
- 10 **Zhou H**, Sun Y, Wang Q, Li Z, Zhong W, Wang X, Dai X, Kong L. N-acetylcysteine alleviates liver injury by suppressing macrophage-mediated inflammatory response post microwave ablation. *Int Immunopharmacol* 2020; **85**: 106580 [PMID: 32438077 DOI: 10.1016/j.intimp.2020.106580]
- 11 **Kladney RD**, Bulla GA, Guo L, Mason AL, Tollefson AE, Simon DJ, Koutoubi Z, Fimmel CJ. GP73, a novel Golgi-localized protein upregulated by viral infection. *Gene* 2000; **249**: 53-65 [PMID: 10831838 DOI: 10.1016/s0378-1119(00)00136-0]
- 12 **Liu X**, Wan X, Li Z, Lin C, Zhan Y, Lu X. Golgi protein 73(GP73), a useful serum marker in liver diseases. *Clin Chem Lab Med* 2011; **49**: 1311-1316 [PMID: 21663469 DOI: 10.1515/CCLM.2011.640]
- 13 **Xu Z**, Liu L, Pan X, Wei K, Wei M, Yang H, Liu Q. Serum Golgi protein 73 (GP73) is a diagnostic and prognostic marker of chronic HBV liver disease. *Medicine (Baltimore)* 2015; **94**: e659 [PMID: 25816035 DOI: 10.1097/MD.0000000000000659]
- 14 **Xu Z**, Shen J, Pan X, Wei M, Liu L, Wei K, Yang H, Huang J. Predictive value of serum Golgi protein 73 for prominent hepatic necroinflammation in chronic HBV infection. *J Med Virol* 2018; **90**: 1053-1062 [PMID: 29424455 DOI: 10.1002/jmv.25045]
- 15 **Department of Medical Administration**, National Health and Health Commission of the People's Republic of China. . [Guidelines for diagnosis and treatment of primary liver cancer in China (2019 edition)]. *Zhonghua Gan Zang Bing Za Zhi* 2020; **28**: 112-128 [PMID: 32164061 DOI: 10.3760/cma.j.issn.1007-3418.2020.02.004]
- 16 **Chinese Society of Infectious Diseases**; Chinese Medical Association. ; Chinese Society of Hepatology, Chinese Medical Association. [The guidelines of prevention and treatment for chronic hepatitis B (2019 version)]. *Zhonghua Gan Zang Bing Za Zhi* 2019; **27**: 938-961 [PMID: 31941257 DOI: 10.3760/cma.j.issn.1007-3418.2019.12.007]
- 17 **Hinshaw JL**, Lubner MG, Ziemlewicz TJ, Lee FT Jr, Brace CL. Percutaneous tumor ablation tools: microwave, radiofrequency, or cryoablation--what should you use and why? *Radiographics* 2014; **34**: 1344-1362 [PMID: 25208284 DOI: 10.1148/rg.345140054]
- 18 **Poulou LS**, Botsa E, Thanou I, Ziakas PD, Thanos L. Percutaneous microwave ablation vs radiofrequency ablation in the treatment of hepatocellular carcinoma. *World J Hepatol* 2015; **7**: 1054-1063 [PMID: 26052394 DOI: 10.4254/wjh.v7.i8.1054]
- 19 **Ierardi AM**, Giorlando F, Piacentino F, Fontana F, Novario R, Angileri SA, Duka E, Carrafello G. Factors predicting outcomes of microwave ablation of small hepatocellular carcinoma. *Radiol Med* 2017; **122**: 81-87 [PMID: 27744607 DOI: 10.1007/s11547-016-0694-6]
- 20 **Poggi G**, Tosoratti N, Montagna B, Picchi C. Microwave ablation of hepatocellular carcinoma. *World J Hepatol* 2015; **7**: 2578-2589 [PMID: 26557950 DOI: 10.4254/wjh.v7.i25.2578]
- 21 **Bhardwaj N**, Dormer J, Ahmad F, Strickland AD, Gravante G, West K, Dennison AR, Lloyd DM. Microwave ablation of the liver: a description of lesion evolution over time and an investigation of the heat sink effect. *Pathology* 2011; **43**: 725-731 [PMID: 22027742 DOI: 10.1097/PAT.0b013e32834c356c]
- 22 **Luo W**, Zhang Y, He G, Yu M, Zheng M, Liu L, Zhou X. Effects of radiofrequency ablation versus other ablating techniques on hepatocellular carcinomas: a systematic review and meta-analysis. *World J Surg Oncol* 2017; **15**: 126 [PMID: 28693505 DOI: 10.1186/s12957-017-1196-2]
- 23 **Wang ZL**, Liang P, Dong BW, Yu XL, Yu DJ. Prognostic factors and recurrence of small hepatocellular carcinoma after hepatic resection or microwave ablation: a retrospective study. *J Gastrointest Surg* 2008; **12**: 327-337 [PMID: 17943391 DOI: 10.1007/s11605-007-0310-0]
- 24 **Rao Z**, Ling W, Dai X, Zhang H, Pu L, Wu J, Zhu D, Yang X, Li Z, Lu L, Wang X, Zhou H, Kong L. Precoagulation with microwave ablation for hepatic parenchymal transection during liver partial resection. *Int J Hyperthermia* 2019; **36**: 146-150 [PMID: 30484720 DOI: 10.1080/02656736.2018.1540799]
- 25 **Zhang M**, Ma H, Zhang J, He L, Ye X, Li X. Comparison of microwave ablation and hepatic resection for hepatocellular carcinoma: a meta-analysis. *Oncotargets Ther* 2017; **10**: 4829-4839 [PMID: 29042794 DOI: 10.2147/OTT.S141968]
- 26 **Zhang EL**, Yang F, Wu ZB, Yue CS, He TY, Li KY, Xiao ZY, Xiong M, Chen XP, Huang ZY. Therapeutic efficacy of percutaneous microwave coagulation vs liver resection for single hepatocellular carcinoma ≤3 cm with Child-Pugh A cirrhosis. *Eur J Surg Oncol* 2016; **42**: 690-697 [PMID: 26995115 DOI: 10.1016/j.ejso.2016.02.251]

## Observational Study

# Evaluating the best treatment for multifocal hepatocellular carcinoma: A propensity score-matched analysis

Matteo Risaliti, Ilenia Bartolini, Claudia Campani, Umberto Arena, Carlotta Xodo, Valentina Adotti, Martina Rosi, Antonio Taddei, Paolo Muiasan, Amedeo Amedei, Giacomo Batignani, Fabio Marra

**Specialty type:** Gastroenterology and hepatology

**Provenance and peer review:** Invited article; Externally peer reviewed.

**Peer-review model:** Single blind

**Peer-review report's scientific quality classification**

Grade A (Excellent): 0  
Grade B (Very good): B  
Grade C (Good): C  
Grade D (Fair): 0  
Grade E (Poor): 0

**P-Reviewer:** Gorrell MD, Australia; Nakano M, Japan

**Received:** February 1, 2022

**Peer-review started:** February 1, 2022

**First decision:** February 24, 2022

**Revised:** March 9, 2022

**Accepted:** July 6, 2022

**Article in press:** July 6, 2022

**Published online:** August 7, 2022



Matteo Risaliti, Ilenia Bartolini, Claudia Campani, Umberto Arena, Carlotta Xodo, Valentina Adotti, Martina Rosi, Antonio Taddei, Paolo Muiasan, Amedeo Amedei, Giacomo Batignani, Fabio Marra, Department of Experimental and Clinical Medicine, AOU Careggi, Florence 50134, Italy

**Corresponding author:** Fabio Marra, MD, Professor, Department of Experimental and Clinical Medicine, AOU Careggi, Largo Brambilla 3, Florence 50134, Italy. [fabio.marra@unifi.it](mailto:fabio.marra@unifi.it)

## Abstract

### BACKGROUND

Hepatocellular carcinoma (HCC) is a common tumour often diagnosed with a multifocal presentation. Patients with multifocal HCC represent a heterogeneous group. Although Trans-Arterial ChemoEmbolization (TACE) is the most frequently employed treatment for these patients, previous data suggested that liver resection (LR) could be a safe and effective procedure.

### AIM

To compare LR and TACE in patients with multifocal HCC in terms of procedure-related morbidity and oncologic outcomes.

### METHODS

All patients with multifocal HCC who underwent LR or TACE as the first procedure between May 2011 and March 2021 were enrolled. The decision to perform surgery or TACE was made after a multidisciplinary team evaluation. Only patients in Child-Pugh class A or B7 and stage B (according to the Barcelona Clinic Liver Cancer staging system, without severe portal hypertension, vascular invasion, or extrahepatic spread) were included in the final analysis. Propensity score matching was used to adjust the baseline differences between patients undergoing LR and the TACE group [number and diameter of lesions, presence of cirrhosis, alpha-fetoprotein (AFP) levels, and Model for End-Stage Liver Disease score]. The Kaplan-Meier method was used to estimate overall survival (OS) and disease-free survival (DFS). The outcomes of LR and TACE were compared using the log-rank test.

### RESULTS

After matching, 30 patients were eligible for the final analysis, 15 in each group. Morbidity rates were 42.9% and 40% for LR and TACE, respectively ( $P = 0.876$ ).

Median OS was not different in the LR and TACE groups (53 mo *vs* 18 mo,  $P = 0.312$ ), while DFS was significantly longer with LR (19 mo *vs* 0 mo,  $P = 0.0001$ ). Subgroup analysis showed that patients in the Italian Liver Cancer (ITA.LI.CA) B2 stage, with AFP levels lower than 400 ng/mL, less than 3 lesions, and lesions bigger than 41 mm, benefited more from LR in terms of DFS. Patients classified as ITA.LI.CA B3, with AFP levels higher than 400 ng/mL and with more than 3 lesions, appeared to receive more benefit from TACE in terms of OS.

### CONCLUSION

In a small cohort of patients with multifocal HCC, LR confers longer DFS compared with TACE, with similar OS and post-procedural morbidity.

**Key Words:** Hepatocellular carcinoma; Multifocal hepatocellular carcinoma; Liver resection; Trans-arterial chemoembolization; Guidelines; Liver tumour management

©The Author(s) 2022. Published by Baishideng Publishing Group Inc. All rights reserved.

**Core Tip:** Hepatocellular carcinoma (HCC) is a leading cause of death and often presents in a multifocal form. Trans-Arterial ChemoEmbolization (TACE) is the most frequently employed treatment for this patient category. As patients with multifocal HCC are a heterogeneous group, previous data suggested that liver resection (LR) could be a safe and effective procedure. A propensity score-matched analysis has been performed to compare LR and TACE in terms of post-procedure morbidity and survival. Despite the limited number of patients, LR conferred longer disease-free survival with similar overall survival compared to TACE. Subgroup analyses identified the patients benefiting more from a specific treatment.

**Citation:** Risaliti M, Bartolini I, Campani C, Arena U, Xodo C, Adotti V, Rosi M, Taddei A, Muiesan P, Amedei A, Batignani G, Marra F. Evaluating the best treatment for multifocal hepatocellular carcinoma: A propensity score-matched analysis. *World J Gastroenterol* 2022; 28(29): 3981-3993

**URL:** <https://www.wjgnet.com/1007-9327/full/v28/i29/3981.htm>

**DOI:** <https://dx.doi.org/10.3748/wjg.v28.i29.3981>

## INTRODUCTION

Hepatocellular carcinoma (HCC) is the most frequent primary liver cancer worldwide, accounting for approximately 90% of cases[1]. HCC incidence has grown over the last two decades, with more than 900.000 new cases *per* year. Moreover, it is expected to further increase in the next few years due to the exponential growth in nonalcoholic fatty liver disease[2]. Despite the improvements in diagnosis and management, HCC is detected in a multinodular form in 35%-40% of cases[3,4] with a reported 5-year survival rate of 19.5%[5].

Over the years, various staging systems have been proposed to overcome the limitations of the tumour-node-metastasis system, which only considers tumour burden[6]. Currently, the Barcelona Clinic Liver Classification (BCLC) is one of the most widely used staging systems for HCC, and includes variables related to tumour status, liver function, and performance status (PS), and recommends one or more specific treatment modalities for each disease stage[7].

Several additional efforts have been made to deal with the heterogeneity of the BCLC-B or intermediate stage of this classification. The Italian Liver Cancer (ITA.LI.CA) group recently proposed a new staging system and prognostic score, based on the BCLC staging system, which includes tumour burden, liver function, and other patient-related variables, and provides a subclassification of this stage [8].

Surgical treatments, including liver resection (LR) and liver transplantation, are considered the best choice for survival and quality of life whenever feasible, while Trans-Arterial ChemoEmbolization (TACE) is not a curative treatment and should be used for patients with well-defined, multifocal HCC, a preserved portal flow, and adequate liver function and PS. TACE outcomes are poor, and several lines of information about the safety and effectiveness of surgery in selected patients for whom TACE is usually recommended have been reported[9-12]. Finally, liver transplantation could also have a central role for these patients, especially after successful downstaging[7], but organ shortage and increased demand for organ transplantation could lead to high drop-out rates.

The debate concerning whether selected patients with multinodular HCC may benefit from surgery rather than TACE remains unsolved.

In this study, a propensity-score matching analysis was used to compare procedure-related morbidity and oncological outcomes in multifocal HCC patients classified as BCLC-B who underwent LR or TACE to determine if one treatment should be given priority over the other.

## MATERIALS AND METHODS

### **Study design and patients**

A retrospective analysis was conducted on patients with multifocal HCC who had undergone surgical resection or TACE as first-line treatment between May 2011 and March 2021. The following exclusion criteria were considered: Age < 18 years, Child-Pugh score > 7, vascular invasion or extrahepatic spread, and hepatic venous pressure gradient > 15 mmHg. HCC was diagnosed histologically or by imaging techniques [magnetic resonance imaging and/or triphasic computed tomography (CT)] according to the available EASL guidelines version. Before LR or TACE, an evaluation of age, comorbidities, blood chemistry, tumour number and size (major radiological diameter of the largest lesion from the last available imaging test), ITA.LI.CA. stage and Eastern Cooperative Oncology Group PS.

The decision to perform surgery or TACE was taken by the local multidisciplinary team who considered patients and tumour features, including lesion location and relation with the pedicles, and the volume of the future liver remnant. During surgery, intraoperative ultrasound sonography (IOUS) was routinely performed to confirm preoperative planning. Whenever feasible, anatomic resections were preferred. Both conventional, lipiodol-based TACE and TACE with drug-eluting beads were included. The patients' response was evaluated one month after the procedure with a CT scan. For patients who did not achieve a complete response, data and the effectiveness of each subsequent TACE were also recorded.

Post-treatment morbidity was evaluated according to the Clavien-Dindo (CD) classification[13].

All patients underwent a standardised follow-up programme that included blood tests with alpha-fetoprotein (AFP), and a triple phase-contrast enhanced CT scan every three months for the first year and then biannually for 5 years after surgery (starting 3 mo after surgery or 1 mo after TACE). Recurrence was diagnosed in the case of radiological evidence of HCC.

### **Statistical analysis**

Quantitative data were expressed as mean  $\pm$  SD or median and range, as appropriate. Qualitative data are reported as absolute and relative frequencies. Satterthwait's test or the Mann-Whitney test was used according to the Shapiro-Wilk test and F-Test, respectively, for normality distribution and homoscedasticity to assess the difference in quantitative variables between treatment groups t-test. The chi-square test or Fisher's test were used as appropriate to verify the association between qualitative variables and treatment groups. The propensity score matching (PSM) method was used to compare similar treatment groups for known prognostic factors (AFP levels as a dichotomous variable with a cut-off set at 400 ng/dL, presence or not of cirrhosis, Child-Pugh and Model for End-Stage Liver Disease (MELD) score, number, and diameter of lesions). An AFP level > 400 ng/mL was considered a prognostic factor of poor outcome, as suggested by recent guidelines[14]. A diagnosis of cirrhosis was established based on the presence of one or more of the following: Compatible histology, imaging showing compatible hepatic morphology, liver stiffness > 15 kPa by vibration-controlled transient elastography, clinical or endoscopic or imaging signs of portal hypertension. The propensity score was calculated by a multiple logistic regression model with a backward selection method. The nearest neighbour method was used to match the two groups with a 1:1 ratio.

Overall survival (OS) was calculated from the date of the first treatment to death of any cause or the last follow-up. As TACE patients could need more than one treatment to achieve a complete response, disease-free survival (DFS) was calculated from the date of the effective treatment to the date of first radiological recurrence. Survival was expressed as the median and 95% confidence interval.

The Kaplan-Meier curve method and the log-rank test were used to evaluate the difference in OS and DFS between the groups.

Subgroup survival analyses were performed comparing the results of the different treatment modalities and stratifying patients by the different grades of the ITA.LI.CA classification, the AFP levels (using 400 ng/mL as cut-off), and by the different number and size of HCC (dividing them into two groups using the median value as a cut-off). A *P* value < 0.05 was considered statistically significant.

All the analyses were conducted using SAS, version 9.2 (SAS Corporation, Cary, NC, United States), and revised by a biomedical statistician.

## RESULTS

### **Patient clinical characteristics**

A total of 50 patients with multifocal HCC were included in the study, 25 underwent LR while 25

underwent TACE. The distribution of the factors used for the PSM in the general population is reported in [Table 1](#). All patients belonging to the TACE group had cirrhosis, whereas, among those who underwent LR, cirrhosis was absent in 36% of cases ( $P = 0.002$ ). The number of lesions was higher among patients who underwent TACE, whereas resected patients usually had more extensive tumours. No significant differences were found between the two groups regarding Child-Pugh score and AFP levels. In contrast, the MELD score tended to be higher in patients who underwent TACE compared with the resected patients. After the PSM, only 30 patients were eligible for the final analysis, 15 from each subgroup.

The general baseline clinical characteristics are shown in [Table 2](#), while data regarding liver function aspects, tumour characteristics, and patient distribution according to the Up-to-7 criteria[15] and ITA.LI.CA classification are reported in [Table 3](#). No statistical differences were found in baseline characteristics. The median age was 69 years, and more than two-thirds of patients were male. The most common cause of liver disease was viral hepatitis, followed by NASH and alcohol use disorder. Lower platelet counts and higher bilirubin levels were present in the TACE group. There was also a trend towards a higher presence of varices in the TACE group. No significant differences across the Up-to-7 criteria in or out and ITA.LI.CA. staging distribution were found.

### Postoperative short-term outcomes and survival analysis

Patients in the TACE group received a significantly higher number of treatments ([Table 4](#),  $P = 0.001$ ). Post-procedure complications were not significantly different between patients who underwent LR and TACE ([Table 4](#)). In the surgery group, complications classified as grade 1 and 2 of CD included fever, pneumonia, or the need for blood transfusion. Only one patient developed bile leakage classified as grade 3 according to CD and was treated with percutaneous drainage.

In the TACE group, complications classified as grade 1 and 2 of CD included mostly transient alterations in liver biochemistry and/or fever. Only one patient developed temporary liver failure and required percutaneous drainage due to an abdominal effusion.

The median follow-up was 19 mo (range 3-62). The estimated global median OS and DFS were 31 and 5 mo, respectively ([Figure 1](#)). There were no significant differences in OS and DFS for the global population stratified by the ITA.LI.CA classification. Median OS for B1, B2, and B3 groups were 31, 31, and 14 mo, respectively ( $P = 0.803$ ), while median DFS for B1, B2, and B3 groups were 5, 14.5, and 1.5 mo, respectively ( $P = 0.516$ ).

No differences in OS were observed when the two treatment groups were compared. A significantly longer DFS was found in resected patients compared with those undergoing TACE (19 mo *vs* 0 mo, respectively,  $P = 0.0001$ ) ([Figure 2](#)).

Subgroup analyses were also performed to evaluate the possible differences in OS or DFS according to AFP levels, size, lesion number, Up-to-7 criteria, and ITA.LI.CA staging between each treatment group.

A significant difference was found in both OS and DFS ( $P < 0.0001$  and  $P = 0.0001$ , respectively, [Figure 3A](#)), with patients presenting with lower levels of AFP showing the best prognosis, in both treatment groups. Furthermore, patients with AFP levels higher than 400 ng/mL and receiving surgery showed a poor OS compared to the TACE group.

No difference in OS was found when comparing treatment modalities in patients stratified according to the Up-to-7 criteria. On the contrary, DFS was higher in the LR group ( $P = 0.002$ ) ([Figure 3B](#)).

The results of different treatment modalities for patients stratified by the ITA.LI.CA classification are reported in [Figure 3C](#). Similar to the previous analysis, a significant difference was found in both OS and DFS ( $P = 0.047$  and  $P = 0.001$ , respectively), with patients classified as B2 and receiving resection, showing the best prognosis, while those classified as B3 and receiving resection had the worst prognosis.

Although no significant differences were found in OS, the 4 patients with more than 3 lesions receiving TACE showed a 1, 3, and 5-year OS of 75%, 25%, and 25%, respectively. Among the surgery group, patients with less than 3 lesions had a significantly higher DFS compared with those with 3 or more lesions ( $P = 0.001$ ). Conversely, no differences in terms of OS and DFS were found in the TACE group stratified by the number of lesions ([Figure 3D](#)). Similar results were obtained when the treatment groups were stratified according to the size of the more extensive lesion ([Figure 3E](#)). Patients with smaller lesions in the surgery group had a better DFS.

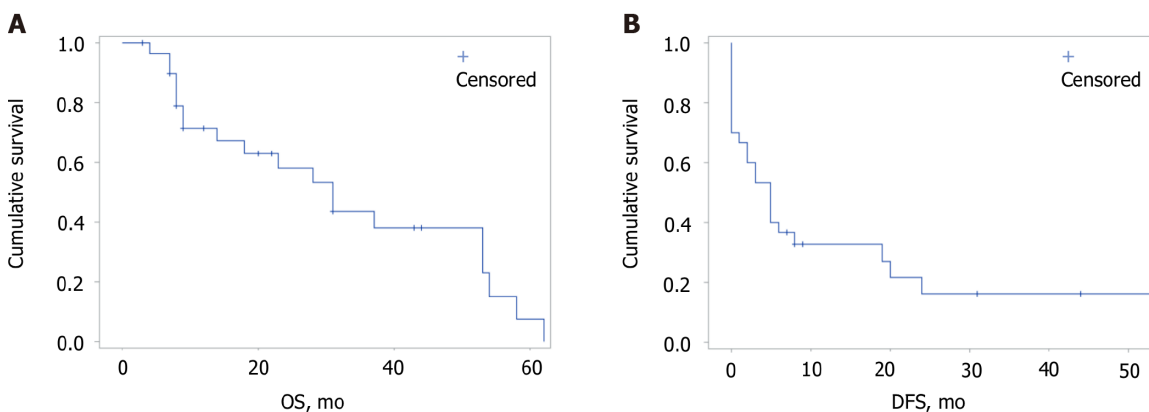
## DISCUSSION

HCC is the most common primary liver tumour. Despite recent advantages in terms of follow-up, early diagnosis, and treatment, a considerable percentage of patients are still diagnosed in multiple or advanced forms and global mortality remains high with poor long-term prognosis[16]. The term multifocal HCC comprises patients presenting with a broad disease spectrum, ranging from small, oligonodular tumours to diffuse disease. The accompanying liver cirrhosis, portal hypertension, and liver function impairment should be considered, as they are related to high post-procedure morbidity

**Table 1** Distribution of the factors used in the propensity score matching in the general population ( $n = 50$ ),  $n$  (%)

	Resection, $n = 25$	TACE, $n = 25$	Total, $n = 50$	<i>P</i> value
AFP, $n$ (%)				0.243
< 400 ng/mL	20 (90.9)	17 (73.9)	37 (82.2)	
> 400 ng/mL	2 (9.1)	6 (26.1)	8 (17.8)	
Missing	3	2	5	
Cirrhosis, $n$ (%)				0.002
No	9 (36)	0	9 (18)	
Yes	16 (64)	25 (100)	41 (82)	
Child-Pugh score, $n$ (%)				0.840
A5	12 (48)	10 (40)	22 (44)	
A6	9 (36)	11 (44)	20 (40)	
B7	4 (16)	4 (16)	8 (16)	
MELD	$8.4 \pm 2.7$	$9.7 \pm 2.2$	$9 \pm 2.5$	0.069
Number of lesions	2 (2-10)	4 (2-7)	2.5 (2-10)	0.008
Tumor diameter (mm)	$69.5 \pm 52.2$	$41.9 \pm 17$	$55.7 \pm 40.9$	0.018

TACE: Trans-Arterial ChemoEmbolization; AFP: Alpha-fetoprotein; MELD: Model for End-Stage Liver Disease.



DOI: 10.3748/wjg.v28.i29.3981 Copyright ©The Author(s) 2022.

**Figure 1** Kaplan–Meier curves of global overall survival and disease-free survival. The median overall survival (OS) and disease-free survival (DFS) were 31 mo [95% confidence interval (CI): 14-53] and 5 mo (95%CI: 1-8), respectively. 1-, 3 and 5-yr OS rates were 71.4%, 43.6%, and 7.6%, respectively. 1-, and 3-yr DFS rates were 32.6%, and 16.3%, respectively. A: OS; B: DFS. OS: Overall survival; DFS: Disease-free survival.

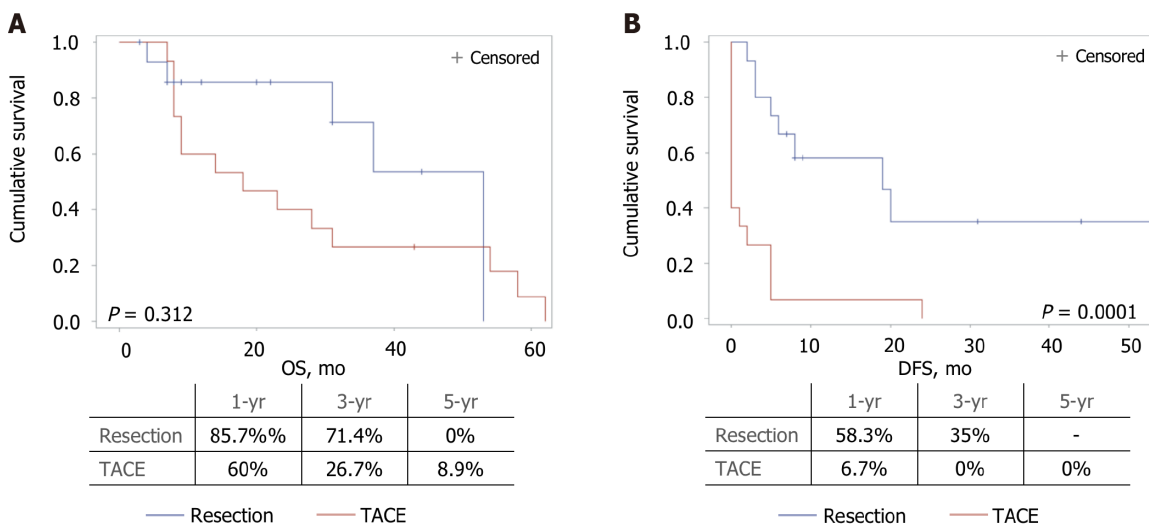
and mortality. Therefore, a tailored approach is mandatory for each patient, and the decisional role of a specialised multidisciplinary team has been highlighted and encouraged in the last version of the BCLC classification[7].

The BCLC algorithm recommends TACE as the primary treatment modality for multinodular HCC, but whether a subset of patients may benefit from a surgical approach remains unestablished. We conducted a retrospective analysis using the PSM, a method that may provide high-quality evidence in conditions when randomised clinical trials are unethical or unfeasible. For the PSM analysis, both indicators of liver function and tumour burden and aggressiveness were used. Although the Child-Pugh and MELD scores could be considered outdated after the last published version of the BCLC staging system[7], these data are still commonly used in clinical practice. Wang *et al*[5] showed that patients with gradual deterioration in CP score had shorter survival times and worse prognosis (5-year OS rates of 31.1%, 2.4%, and 0.9% for CP A, B, and C, respectively). AFP is a well-established independent risk factor for survival in HCC patients and levels greater than 400 ng/mL are generally considered diagnostic for HCC, in the presence of appropriate radiologic findings[5,17]. Finally, the number and dimension of the nodules are two of the major prognostic factors, and the most used guidelines underscore their importance in treatment allocation[7,8,14,18].

**Table 2** General baseline characteristics after propensity score matching (*n* = 30)

	Resection, <i>n</i> = 15	TACE, <i>n</i> = 15	Total, <i>n</i> = 30	<i>P</i> value
Age (yr)	68.9 ± 9.2	70.5 ± 9.9	69.7 ± 9.5	0.651
Gender, <i>n</i> (%)				0.651
Male	13 (86.7)	11 (73.3)	24 (80)	
Female	2 (13.3)	4 (26.7)	6 (20)	
BMI (kg/m <sup>2</sup> )	26.1 ± 4.3	26.3 ± 7.7	26.2 ± 5.9	0.927
Hepatitis Etiology, <i>n</i> (%)				0.300
Viral	4 (28.6)	9 (60)	13 (44.8)	
Alcoholic	0	1 (6.7)	1 (3.5)	
Dysmetabolic	3 (21.4)	1 (6.7)	4 (13.8)	
Mixed	3 (21.4)	1 (6.7)	4 (13.8)	
Other	4 (28.6)	3 (20)	7 (24.1)	
Missing	1	-	1	
Diabetes, <i>n</i> (%)				0.700
No	9 (60)	11 (73.3)	20 (66.7)	
Yes	6 (40)	4 (26.7)	10 (33.3)	
Heart disease, <i>n</i> (%)				0.330
No	11 (73.3)	14 (93.3)	25 (83.3)	
Yes	4 (26.7)	1 (6.7)	5 (16.7)	

TACE: Trans-Arterial ChemoEmbolization; BMI: Body mass index.



DOI: 10.3748/wjg.v28.i29.3981 Copyright ©The Author(s) 2022.

**Figure 2** Kaplan–Meier curves of overall and disease-free survival comparing the results of the different treatment modalities (*P* = 0.312 and *P* = 0.0001, respectively). Median overall survival (OS) and disease-free survival (DFS) for the resection group were 53 [95% confidence interval (CI): 31–53] and 19 mo (95%CI: 3–Not Evaluable), respectively. Median OS and DFS for the Trans-Arterial ChemoEmbolization group were 18 (95%CI: 8–31) and 0 (95%CI: 0–2) months, respectively. A: OS; B: DFS. OS: Overall survival; DFS: Disease-free survival; TACE: Trans-Arterial ChemoEmbolization.

TACE is considered the standard treatment for BCLC-B patients, as evidence from randomised clinical trials and meta-analyses indicates that TACE provides better survival outcomes compared to the best supportive care with a 1-year mortality rate of 34.1% [19-21]. On the other hand, guidelines do not recommend LR for BCLC-B patients, due to the unfavourable prognostic impact of multinodular presentation and high postoperative morbidity[18]. Moreover, LR for multifocal HCC is a challenging

**Table 3** Liver function test and disease burden after propensity score matching (*n* = 30)

	Resection, <i>n</i> = 15	TACE, <i>n</i> = 15	Total, <i>n</i> = 30	<i>P</i> value
INR	1.2 ± 0.1	1.3 ± 0.3	1.2 ± 0.2	0.185
Bilirubin (mg/dL)	0.75 ± 0.5	1.2 ± 0.6	0.99 ± 0.6	0.026
Platelets (10 <sup>3</sup> /μL)	245 ± 118	95 ± 31	163 ± 111	0.003
Creatinine (mg/dL)	1.37 ± 0.8	0.78 ± 0.2	1.08 ± 1.19	0.188
AFP, <i>n</i> (%)				1.000
< 400 ng/mL	13 (86.7)	12 (80)	25 (83.3)	
> 400 ng/mL	2 (13.3)	3 (20)	5 (16.7)	
Varices, <i>n</i> (%)				0.081
No	8 (80)	4 (36.4)	12 (57.1)	
Yes	2 (20)	7 (63.6)	9 (42.9)	
Missing	5	4	9	
Cirrhosis, <i>n</i> (%)				0.100
No	4 (26.7)	0	4 (13.3)	
Yes	11 (73.3)	15 (100)	26 (86.7)	
Child-Pugh score, <i>n</i> (%)				0.556
A5	8 (53.3)	5 (33.3)	13 (43.3)	
A6	6 (40)	7 (46.7)	13 (43.3)	
B7	1 (6.7)	3 (20)	4 (13.4)	
MELD score	9.1 ± 3.2	9.9 ± 2.4	9.5 ± 2.8	0.473
Number of lesions	2 (2-5)	3 (2-5)	2 (2-5)	0.101
Diameter (mm)	46.3 ± 3	47 ± 5	46.9 ± 12.9	0.793
Up-to-7 criteria, <i>n</i> (%)				0.456
In	10 (66.7)	8 (53.3)	18 (60)	
Out	5 (33.3)	7 (46.7)	12 (40)	
ITA.LI.CA classification, <i>n</i> (%)				0.868
B1	10 (66.7)	8 (53.3)	18 (60)	
B2	3 (20)	5 (33.3)	8 (26.7)	
B3	2 (13.3)	2 (13.3)	4 (13.3)	

TACE: Trans-Arterial ChemoEmbolization; INR: International normalized ratio; AFP: Alpha-fetoprotein; MELD: Model for End-Stage Liver Disease.

surgery as wide and/or multiple resections are needed, possibly leading to bile leaks and/or postoperative liver failure.

Advances in surgical techniques, including extensive use of IOUS, better coagulation devices, and wider application of minimally invasive surgery, together with better perioperative management, have contributed to improving the results of LR in this difficult-to-treat population. Remarkably, the comparison between different studies is limited by variations in the modalities of detection and reporting of post-procedural complications.

In the present series, we did not find any differences in post-procedure morbidity when comparing resection and TACE. According to the CD classification, only three patients undergoing LR and one patient in the TACE group had a clinically relevant event. However, it should be documented that TACE patients often required more than one treatment to achieve the best response, thus partially explaining the lower morbidity rate of the procedure. Conflicting results on morbidity were previously reported. Zhong *et al*[22] showed a complication rate of 35% and 21% for resection and TACE, respectively[22]. On the contrary, a meta-analysis did not find any difference in post-procedure morbidity between these two treatment modalities[23].

**Table 4 Postoperative morbidity and recurrence status (n = 30)**

	Resection, n = 15	TACE, n = 15	Total, n = 30	P value
Number of treatments	1 ± 0	2.4 ± 1.1	1.7 ± 1.1	0.001
Complications, n (%)				0.876
No	8 (57.1)	9 (60)	17 (58.6)	
Yes	6 (42.9)	6 (40)	12 (41.4)	
Missing	1	-	1	
Complications, n (%)				0.545
CD 1-2	5 (83.3)	5 (83.3)	10	
CD 3-4	1 (16.7)	1 (16.7)	2 (16.7)	
Hospital stay (days)	7 ± 3	5 ± 5	6 ± 4.3	0.224
Recurrence, n (%)				0.006
No	7 (46.7)	0	7 (23.3)	
Yes	8 (53.3)	15 (100)	23 (76.7)	

TACE: Trans-Arterial ChemoEmbolization; CD: Clavien-Dindo classification grade.

While only a nonsignificant trend towards better OS was observed with surgery, we found that DFS was significantly longer in resected patients. These results confirm and extend previous studies conducted on patients with multinodular HCC. Favourable results with surgery were originally reported by non-controlled studies[10,24]. In a multicentric study including 736 BCLC-B patients, Torzilli *et al*[24] reported a 5-year survival rate of 57% and a DFS of 27%. The survival benefit of LR compared with TACE in BCLC-B patients has been previously reported in the meta-analysis by Liu *et al* [23], and similar conclusions were reached in a randomised controlled trial enrolling 173 patients[25].

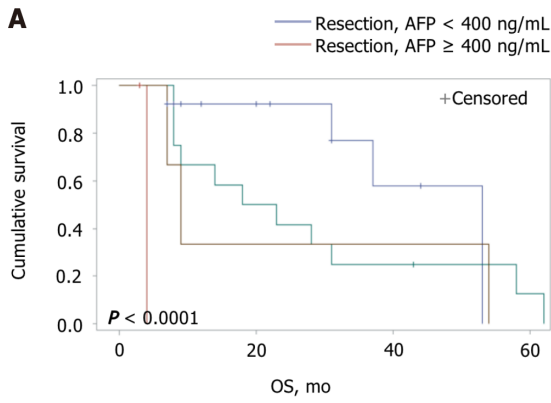
Considering the marked population heterogeneity of patients with multinodular HCC, subgroup analyses may provide additional clues for better selection of the treatment modality. Not surprisingly, patients with lower AFP levels had the best prognosis. An exciting result was the observation that patients with high AFP levels benefit more from TACE in terms of OS, and further studies are needed to confirm these data and investigate the possible mechanisms thereof. Another aspect which deserves further investigation is to what extent some of these patients with multinodular HCC could benefit from new systemic combination treatments which include the use of immunotherapy with excellent results [26].

Interesting results were also provided by patient stratification according to the ITA.LI.CA classification. Patients in the B2 subgroup, characterised by nodules of smaller size or lower number, showed the best prognosis when receiving LR. In contrast, those classified as B3, *i.e.*, with larger nodules and higher numbers, had the worst prognosis when resected. Patients with two HCC nodules had a more significant benefit from LR compared with TACE in terms of DFS. These data emphasise the relevance of the number of nodules, which is considered a poor prognostic factor and a predictor of early recurrence.

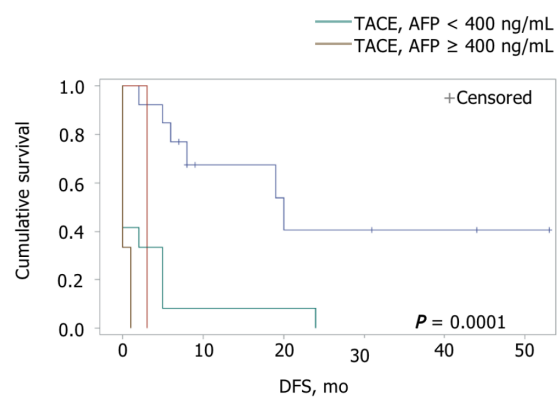
Nonetheless, a clear cut-off value for the number of nodules beyond which resection is contraindicated has not been determined[10,12,25,27]. Furthermore, although using the same parameters of the Up-to-7 criteria (number of lesions and a maximum diameter of the bigger lesions), the ITA.LI.CA classification showed better ability in patient stratification.

We also evaluated the impact of nodule size on survival in our series. Interestingly, patients with lesions larger than 41 mm had an even more significant benefit from LR in terms of DFS. Previously published studies reported that patients with large solitary HCC had better survival rates when treated with resection than TACE[28,29]. Furthermore, conflicting results have been reported regarding the potential role of tumour diameter as a prognostic factor. While some studies indicated that tumour size alone was not a predictor of poor prognosis[24,30], other reports mentioned tumour dimension as a predictor of survival[31-33]. In particular, in the analysis of 2887 HCC patients, tumour size was an independent prognostic factor of poor survival at multivariate analysis[5], and Wada *et al*[12] concluded that while size alone was not a contraindication for resection, a diameter lower than 5 cm was a favourable factor[12].

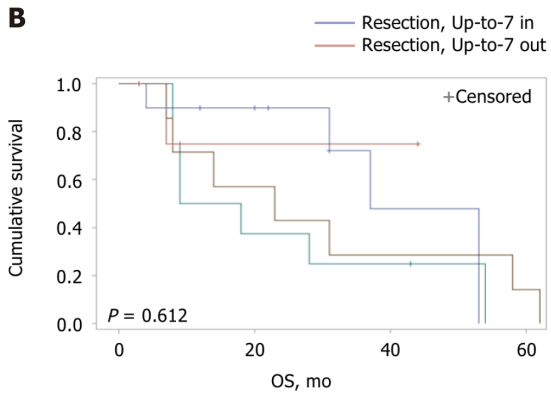
Several limitations of this study must be acknowledged, including its retrospective nature with the inherent selection bias. Moreover, the fact that a limited number of patients from a single centre were enrolled should lead to caution in the general applicability of the results. In addition, the relatively long period of enrollment could have been associated with differences due to modifications in the HCC



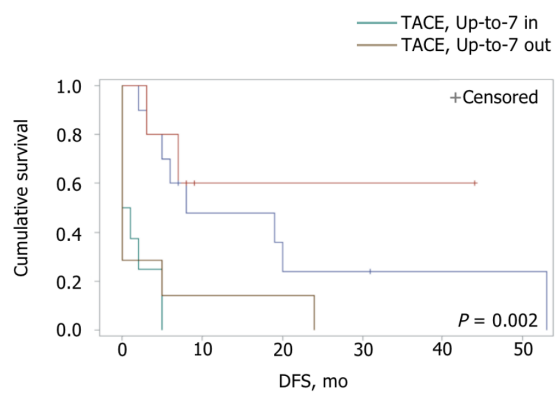
	1-yr	3-yr	5-yr	Median OS (m)
Resection				
AFP < 400 ng/mL (n = 13)	92.3%	76.9%	0%	53 (31-53)
AFP ≥ 400 ng/mL (n = 2)	0%	0%	0%	4 (N.E.-N.E.)
TACE				
AFP < 400 ng/mL (n = 12)	66.7%	25%	12.5%	21 (8-58)
AFP ≥ 400 ng/mL (n = 3)	55.6%	11.1%	0%	9 (7-54)



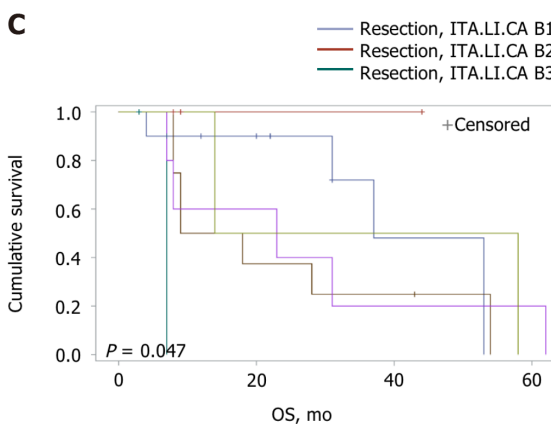
	1-yr	3-yr	5-yr	Median DFS (m)
Resection				
AFP < 400 ng/mL (n = 13)	67.3%	40.4%	-	20 (6-N.E.)
AFP ≥ 400 ng/mL (n = 2)	0%	0%	0%	3 (N.E.-N.E.)
TACE				
AFP < 400 ng/mL (n = 12)	8.3%	0%	0%	0 (0-24)
AFP ≥ 400 ng/mL (n = 3)	0%	0%	0%	0 (0-1)



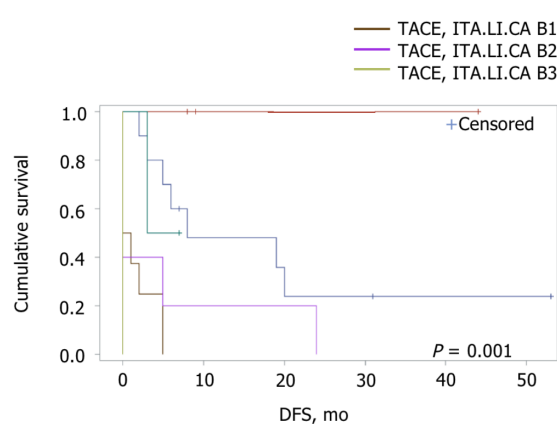
	1-yr	3-yr	5-yr	Median OS (m)
Resection				
In (n = 10)	90%	72%	0%	37 (4-53)
Out (n = 5)	75%	75%	-	N.E.
TACE				
In (n = 8)	50%	25%	0%	14 (8-54)
Out (n = 7)	71%	29%	14%	23 (7-58)



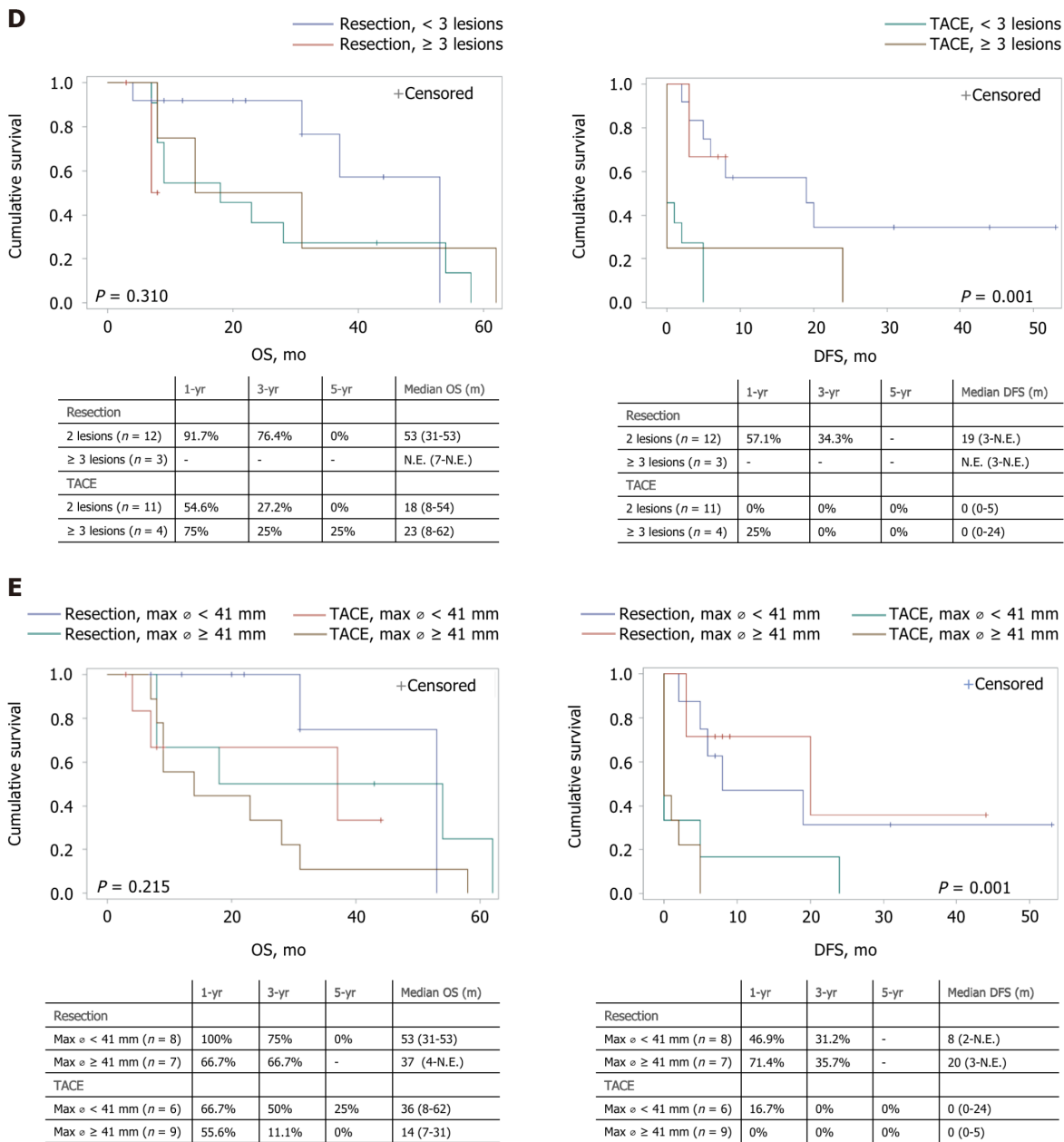
	1-yr	3-yr	5-yr	Median DFS (m)
Resection				
In (n = 10)	48%	24%	-	8 (2-N.E.)
Out (n = 5)	60%	60%	-	N.E. (3-N.E.)
TACE				
In (n = 8)	0%	0%	0%	0.5 (0-5)
Out (n = 7)	14%	0%	0%	0 (0-5)



	1-yr	3-yr	5-yr	Median OS (m)
Resection				
ITA.LI.CA B1 (n = 10)	90%	72%	0%	37 (4-53)
ITA.LI.CA B2 (n = 3)	100%	100%	-	N.E.
ITA.LI.CA B3 (n = 2)	0%	0%	0%	7 (N.E.-N.E.)
TACE				
ITA.LI.CA B1 (n = 8)	50%	25%	0%	14 (8-54)
ITA.LI.CA B2 (n = 5)	60%	20%	20%	23 (7-62)
ITA.LI.CA B3 (n = 2)	100%	50%	0%	36 (14-58)



	1-yr	3-yr	5-yr	Median DFS (m)
Resection				
ITA.LI.CA B1 (n = 10)	48%	24%	-	8 (2-N.E.)
ITA.LI.CA B2 (n = 3)	100%	100%	-	N.E.
ITA.LI.CA B3 (n = 2)	-	-	-	N.E.
TACE				
ITA.LI.CA B1 (n = 8)	0%	0%	0%	0.5 (0-5)
ITA.LI.CA B2 (n = 5)	20%	0%	0%	0 (0-24)
ITA.LI.CA B3 (n = 2)	0%	0%	0%	0 (N.E.-N.E.)



DOI: 10.3748/wjg.v28.i29.3981 Copyright ©The Author(s) 2022.

**Figure 3** Kaplan–Meier curves of overall and disease-free survival comparing the results of the different treatment modalities for patients stratified by different parameters (n = 30). A: Stratification by alpha-fetoprotein levels, lower or higher than 400 ng/mL [overall survival (OS):  $P < 0.0001$  and disease-free survival (DFS):  $P = 0.0001$ ]; B: Stratification by the Up-to-7 criteria, in or out (OS:  $P = 0.612$  and DFS:  $P = 0.002$ ); C: Stratification by the ITA.LI.CA classification (OS:  $P = 0.047$  and DFS:  $P = 0.001$ ); D: Stratification by the number of lesions, 2 lesions or more than 3 lesions (OS:  $P = 0.310$  and DFS:  $P = 0.001$ ); E: Stratification by the maximum diameter of the lesion, smaller or bigger than 41 mm (OS:  $P = 0.215$  and DFS:  $P = 0.001$ ). Median survival is expressed as months and 95% confidence interval. OS: Overall survival; DFS: Disease-free survival; AFP: Alpha-fetoprotein; N.E.: Not Evaluable; TACE: Trans-Arterial ChemoEmbolization.

management. On the other hand, we performed a rigorous matching using a powerful statistical tool such as the propensity score, although some additional variables not included in the score could have influenced the outcomes.

## CONCLUSION

Although the small sample analysed should lead to careful interpretation of the results, after a propensity score matching analysis, patients with multinodular HCC appear to significantly benefit from a surgical approach over TACE in terms of DFS. These results are more evident in the sub-population belonging to the less advanced B2 subgroup according to the ITA.LI.CA. classification, with AFP levels lower than 400 ng/mL, 2 lesions, and with lesions bigger than 41 mm. Patients classified as

ITA.LI.CA B3, with AFP levels higher than 400 ng/mL, and more than 3 lesions had higher benefits from TACE in terms of OS. Future studies are needed to confirm these results in a larger population and to identify other HCC subgroups of patients who would benefit from personalised treatment.

## ARTICLE HIGHLIGHTS

### Research background

Hepatocellular carcinoma (HCC) is the most frequent primary liver tumour and a leading cause of death. Despite follow-up programmes for cirrhotic patients, HCC is diagnosed in a multifocal form in up to 40% of the patients. Although being a heterogeneous group, the existing classifications consider together the patients with multifocal HCC and generally recommend Trans-Arterial ChemoEmbolization (TACE) as the main treatment. Considering the progress in perioperative care, a growing body of literature has started to propose liver resection (LR) in selected cases, which has shown the best long-term oncological results.

### Research motivation

A consensus and detailed guidelines that also consider LR for these patients have not yet been proposed. Moreover, the characteristics of the patients that could benefit more from LR have still to be determined. Defining these aspects could help clinicians in patient management and potentially improve their prognosis.

### Research objectives

A comparison between LR and TACE as the first main treatment in terms of post-procedural results and long-term oncological outcomes was performed in patients with multifocal HCC.

### Research methods

To reduce the influence of the well-known prognostic factors [*i.e.*, Alpha-fetoprotein (AFP) levels as a dichotomous variable with a cut-off set at 400 ng/dL, presence or absence of cirrhosis, Child-Pugh and Model for End-Stage Liver Disease score, number, and diameter of lesions], a propensity score-matched analysis was performed. Two homogeneous groups (with a 1:1 ratio) were compared to assess the difference in short- and long-term post-procedural results.

### Research results

After matching, 30 patients were eligible for the final analysis. Morbidity rates were 42.9% and 40% for LR and TACE, respectively ( $P = 0.876$ ). Median overall survival (OS) was not different when comparing LR and TACE (53 mo *vs* 18 mo,  $P = 0.312$ ), while disease-free survival (DFS) was significantly longer with LR (19 mo *vs* 0 mo,  $P = 0.0001$ ). Subgroup analysis showed that patients in the Italian Liver Cancer (ITA.LI.CA) B2 stage, with AFP levels lower than 400 ng/mL, 2 lesions, and lesions bigger than 41 mm benefited more from LR in terms of DFS. Patients classified as ITA.LI.CA B3, with AFP levels higher than 400 ng/mL and more than 3 lesions appeared to receive more benefit from TACE in terms of OS. However, not all patients with multifocal HCC are amenable to treatment with LR or TACE. Consequently, only a small sample of patients resulted in being eligible for the analysis. Therefore, these results should be considered with caution and further studies are needed.

### Research conclusions

There are subgroups of patients with multifocal HCC that seem to benefit more from LR than TACE.

### Research perspectives

Further studies are needed to include LR in the guidelines as a potential treatment to be offered to specific subgroups of patients with multifocal HCC.

## FOOTNOTES

**Author contributions:** All authors contributed to the conceptualization and design of the study; Risaliti M, Bartolini I and Campani C wrote the original draft; all authors contributed to critical revision of the article and final approval of the version to be published; Amedei A, Batignani G and Marra F supervised the work.

**Institutional review board statement:** The study was approved by the Ethical Committee Area Vasta Centro (Florence), No. 12254/22.

**Informed consent statement:** All study participants or their legal guardian provided informed written consent for

personal and medical data collection prior to study enrolment.

**Conflict-of-interest statement:** All the authors report no relevant conflicts of interest for this article.

**Data sharing statement:** No additional data are available.

**STROBE statement:** The authors have read the STROBE Statement – checklist of items, and the manuscript was prepared and revised according to the STROBE Statement – checklist of items.

**Open-Access:** This article is an open-access article that was selected by an in-house editor and fully peer-reviewed by external reviewers. It is distributed in accordance with the Creative Commons Attribution NonCommercial (CC BY-NC 4.0) license, which permits others to distribute, remix, adapt, build upon this work non-commercially, and license their derivative works on different terms, provided the original work is properly cited and the use is non-commercial. See: <https://creativecommons.org/licenses/by-nc/4.0/>

**Country/Territory of origin:** Italy

**ORCID number:** Matteo Risaliti 0000-0001-8476-2536; Ilenia Bartolini 0000-0003-0387-2042; Claudia Campani 0000-0003-3842-782X; Umberto Arena 0000-0002-8839-1506; Carlotta Xodo 0000-0002-7975-5865; Valentina Adotti 0000-0003-3639-0509; Martina Rosi 0000-0001-6601-4737; Antonio Taddei 0000-0003-2963-4085; Paolo Muijesan 0000-0002-7389-6691; Amedeo Amedei 0000-0002-6797-9343; Giacomo Batignani 0000-0001-8369-6418; Fabio Marra 0000-0001-8629-0878.

**S-Editor:** Fan JR

**L-Editor:** Webster JR

**P-Editor:** Chen YX

## REFERENCES

- 1 Llovet JM, Kelley RK, Villanueva A, Singal AG, Pikarsky E, Roayaie S, Lencioni R, Koike K, Zucman-Rossi J, Finn RS. Hepatocellular carcinoma. *Nat Rev Dis Primers* 2021; **7**: 6 [PMID: 33479224 DOI: 10.1038/s41572-020-00240-3]
- 2 Younossi ZM, Henry L. Epidemiology of non-alcoholic fatty liver disease and hepatocellular carcinoma. *JHEP Rep* 2021; **3**: 100305 [PMID: 34189448 DOI: 10.1016/j.jhepr.2021.100305]
- 3 Fukami Y, Kaneoka Y, Maeda A, Kumada T, Tanaka J, Akita T, Kubo S, Izumi N, Kadoya M, Sakamoto M, Nakashima O, Matsuyama Y, Kokudo T, Hasegawa K, Yamashita T, Kashiwabara K, Takayama T, Kokudo N, Kudo M; Liver Cancer Study Group of Japan. Liver Resection for Multiple Hepatocellular Carcinomas: A Japanese Nationwide Survey. *Ann Surg* 2020; **272**: 145-154 [PMID: 30672806 DOI: 10.1097/SLA.0000000000003192]
- 4 Roayaie S, Jibara G, Tabrizian P, Park JW, Yang J, Yan L, Schwartz M, Han G, Izzo F, Chen M, Blanc JF, Johnson P, Kudo M, Roberts LR, Sherman M. The role of hepatic resection in the treatment of hepatocellular cancer. *Hepatology* 2015; **62**: 440-451 [PMID: 25678263 DOI: 10.1002/hep.27745]
- 5 Wang CY, Li S. Clinical characteristics and prognosis of 2887 patients with hepatocellular carcinoma: A single center 14 years experience from China. *Medicine (Baltimore)* 2019; **98**: e14070 [PMID: 30681563 DOI: 10.1097/MD.00000000000014070]
- 6 Brierley JD, Gospodarowicz MK, Wittekind C. TNM Classification of Malignant Tumours, 8 th edition due December 2016. *J Clin Pathol* 1998; **1**: 84 [DOI: 10.1136/jcp.43.4.350-e]
- 7 Reig M, Forner A, Rimola J, Ferrer-Fàbrega J, Burrel M, Garcia-Criado Á, Kelley RK, Galle PR, Mazzaferro V, Salem R, Sangro B, Singal AG, Vogel A, Fuster J, Ayuso C, Bruix J. BCLC strategy for prognosis prediction and treatment recommendation: The 2022 update. *J Hepatol* 2022; **76**: 681-693 [PMID: 34801630 DOI: 10.1016/j.jhep.2021.11.018]
- 8 Farinati F, Vitale A, Spolverato G, Pawlik TM, Huo TL, Lee YH, Frigo AC, Giacomini A, Giannini EG, Ciccarese F, Piscaglia F, Rapaccini GL, Di Marco M, Caturelli E, Zoli M, Borzio F, Cabibbo G, Felder M, Sacco R, Morisco F, Biasini E, Foschi FG, Gasbarrini A, Svegliati Baroni G, Virdone R, Masotto A, Trevisani F, Cillo U; ITA. LI.CA study group. Development and Validation of a New Prognostic System for Patients with Hepatocellular Carcinoma. *PLoS Med* 2016; **13**: e1002006 [PMID: 27116206 DOI: 10.1371/journal.pmed.1002006]
- 9 Ruzzenente A, Capra F, Pachera S, Iacono C, Piccirillo G, Lunardi M, Pistoso S, Valdegamberi A, D'Onofrio M, Guglielmi A. Is liver resection justified in advanced hepatocellular carcinoma? *J Gastrointest Surg* 2009; **13**: 1313-1320 [PMID: 19418103 DOI: 10.1007/s11605-009-0903-x]
- 10 Ishizawa T, Hasegawa K, Aoki T, Takahashi M, Inoue Y, Sano K, Imamura H, Sugawara Y, Kokudo N, Makuuchi M. Neither multiple tumors nor portal hypertension are surgical contraindications for hepatocellular carcinoma. *Gastroenterology* 2008; **134**: 1908-1916 [PMID: 18549877 DOI: 10.1053/j.gastro.2008.02.091]
- 11 Kamiyama T, Orimo T, Wakayama K, Shimada S, Nagatsu A, Yokoo H, Kamachi H, Yamashita K, Shimamura T, Taketomi A. Survival outcomes of hepatectomy for stage B Hepatocellular carcinoma in the BCLC classification. *World J Surg Oncol* 2017; **15**: 156 [PMID: 28830473 DOI: 10.1186/s12957-017-1229-x]
- 12 Wada H, Eguchi H, Noda T, Ogawa H, Yamada D, Tomimaru Y, Tomokuni A, Asaoka T, Kawamoto K, Gotoh K, Marubashi S, Umeshita K, Nagano H, Doki Y, Mori M. Selection criteria for hepatic resection in intermediate-stage (BCLC stage B) multiple hepatocellular carcinoma. *Surgery* 2016; **160**: 1227-1235 [PMID: 27395761 DOI: 10.1016/j.surg.2016.05.023]
- 13 Clavien PA, Barkun J, de Oliveira ML, Vauthey JN, Dindo D, Schulick RD, de Santibañes E, Pekolj J, Slankamenac K,

- Bassi C, Graf R, Vonlanthen R, Padbury R, Cameron JL, Makuuchi M. The Clavien-Dindo classification of surgical complications: five-year experience. *Ann Surg* 2009; **250**: 187-196 [PMID: 19638912 DOI: 10.1097/SLA.0b013e3181b13ca2]
- 14 **European Association for the Study of the Liver.** EASL Clinical Practice Guidelines: Management of hepatocellular carcinoma. *J Hepatol* 2018; **69**: 182-236 [PMID: 29628281 DOI: 10.1016/j.jhep.2018.03.019]
- 15 **Mazzaferro V,** Llovet JM, Miceli R, Bhoori S, Schiavo M, Mariani L, Camerini T, Roayaie S, Schwartz ME, Grazi GL, Adam R, Neuhaus P, Salizzoni M, Bruix J, Forner A, De Carlis L, Cillo U, Burroughs AK, Troisi R, Rossi M, Gerunda GE, Lerut J, Belghiti J, Boin I, Gugenheim J, Rochling F, Van Hoek B, Majno P; Metroticket Investigator Study Group. Predicting survival after liver transplantation in patients with hepatocellular carcinoma beyond the Milan criteria: a retrospective, exploratory analysis. *Lancet Oncol* 2009; **10**: 35-43 [PMID: 19058754 DOI: 10.1016/S1470-2045(08)70284-5]
- 16 **Pecorelli A,** Lenzi B, Gramenzi A, Garuti F, Farinati F, Giannini EG, Ciccarese F, Piscaglia F, Rapaccini GL, Di Marco M, Caturelli E, Zoli M, Borzio F, Sacco R, Cabibbo G, Felder M, Morisco F, Gasbarrini A, Baroni GS, Foschi FG, Biasini E, Masotto A, Virdone R, Bernardi M, Trevisani F; Italian LiverCancer (ITA. LI.CA) group. Curative therapies are superior to standard of care (transarterial chemoembolization) for intermediate stage hepatocellular carcinoma. *Liver Int* 2017; **37**: 423-433 [PMID: 27566596 DOI: 10.1111/liv.13242]
- 17 **Bai DS,** Zhang C, Chen P, Jin SJ, Jiang GQ. The prognostic correlation of AFP level at diagnosis with pathological grade, progression, and survival of patients with hepatocellular carcinoma. *Sci Rep* 2017; **7**: 12870 [PMID: 28993684 DOI: 10.1038/s41598-017-12834-1]
- 18 **Llovet JM,** Brú C, Bruix J. Prognosis of hepatocellular carcinoma: the BCLC staging classification. *Semin Liver Dis* 1999; **19**: 329-338 [PMID: 10518312 DOI: 10.1055/s-2007-1007122]
- 19 **Llovet JM,** Bruix J. Systematic review of randomized trials for unresectable hepatocellular carcinoma: Chemoembolization improves survival. *Hepatology* 2003; **37**: 429-442 [PMID: 12540794 DOI: 10.1053/jhep.2003.50047]
- 20 **Llovet JM,** Real MI, Montaña X, Planas R, Coll S, Aponte J, Ayuso C, Sala M, Muchart J, Solà R, Rodés J, Bruix J; Barcelona Liver Cancer Group. Arterial embolisation or chemoembolisation vs symptomatic treatment in patients with unresectable hepatocellular carcinoma: a randomised controlled trial. *Lancet* 2002; **359**: 1734-1739 [PMID: 12049862 DOI: 10.1016/S0140-6736(02)08649-X]
- 21 **Lo CM,** Ngan H, Tso WK, Liu CL, Lam CM, Poon RT, Fan ST, Wong J. Randomized controlled trial of transarterial lipiodol chemoembolization for unresectable hepatocellular carcinoma. *Hepatology* 2002; **35**: 1164-1171 [PMID: 11981766 DOI: 10.1053/jhep.2002.33156]
- 22 **Zhong JH,** Peng NF, You XM, Ma L, Li LQ. Hepatic resection is superior to transarterial chemoembolization for treating intermediate-stage hepatocellular carcinoma. *Liver Int* 2017; **37**: 1083-1084 [PMID: 27797424 DOI: 10.1111/liv.13290]
- 23 **Liu W,** Zhou JG, Sun Y, Zhang L, Xing BC. Hepatic Resection Improved the Long-Term Survival of Patients with BCLC Stage B Hepatocellular Carcinoma in Asia: a Systematic Review and Meta-Analysis. *J Gastrointest Surg* 2015; **19**: 1271-1280 [PMID: 25943910 DOI: 10.1007/s11605-015-2811-6]
- 24 **Torzilli G,** Belghiti J, Kokudo N, Takayama T, Capussotti L, Nuzzo G, Vauthey JN, Choti MA, De Santibanes E, Donadon M, Morengi E, Makuuchi M. A snapshot of the effective indications and results of surgery for hepatocellular carcinoma in tertiary referral centers: is it adherent to the EASL/AASLD recommendations? *Ann Surg* 2013; **257**: 929-937 [PMID: 23426336 DOI: 10.1097/SLA.0b013e31828329b8]
- 25 **Yin L,** Li H, Li AJ, Lau WY, Pan ZY, Lai EC, Wu MC, Zhou WP. Partial hepatectomy vs. transcatheter arterial chemoembolization for resectable multiple hepatocellular carcinoma beyond Milan Criteria: a RCT. *J Hepatol* 2014; **61**: 82-88 [PMID: 24650695 DOI: 10.1016/j.jhep.2014.03.012]
- 26 **Finn RS,** Qin S, Ikeda M, Galle PR, Ducreux M, Kim TY, Kudo M, Breder V, Merle P, Kaseb AO, Li D, Verret W, Xu DZ, Hernandez S, Liu J, Huang C, Mulla S, Wang Y, Lim HY, Zhu AX, Cheng AL; IMbrave150 Investigators. Atezolizumab plus Bevacizumab in Unresectable Hepatocellular Carcinoma. *N Engl J Med* 2020; **382**: 1894-1905 [PMID: 32402160 DOI: 10.1056/NEJMoa1915745]
- 27 **Donadon M,** Fontana A, Procopio F, Del Fabbro D, Cimino M, Viganò L, Palmisano A, Torzilli G. Dissecting the multinodular hepatocellular carcinoma subset: is there a survival benefit after hepatectomy? *Updates Surg* 2019; **71**: 57-66 [PMID: 30852806 DOI: 10.1007/s13304-019-00626-3]
- 28 **Liu PH,** Su CW, Hsu CY, Hsia CY, Lee YH, Huang YH, Lee RC, Lin HC, Huo TI. Solitary Large Hepatocellular Carcinoma: Staging and Treatment Strategy. *PLoS One* 2016; **11**: e0155588 [PMID: 27176037 DOI: 10.1371/journal.pone.0155588]
- 29 **Hong SK,** Lee KW, Hong SY, Suh S, Hong K, Han ES, Lee JM, Choi Y, Yi NJ, Suh KS. Efficacy of Liver Resection for Single Large Hepatocellular Carcinoma in Child-Pugh A Cirrhosis: Analysis of a Nationwide Cancer Registry Database. *Front Oncol* 2021; **11**: 674603 [PMID: 33996606 DOI: 10.3389/fonc.2021.674603]
- 30 **Chang WT,** Kao WY, Chau GY, Su CW, Lei HJ, Wu JC, Hsia CY, Lui WY, King KL, Lee SD. Hepatic resection can provide long-term survival of patients with non-early-stage hepatocellular carcinoma: extending the indication for resection? *Surgery* 2012; **152**: 809-820 [PMID: 22766361 DOI: 10.1016/j.surg.2012.03.024]
- 31 **Delis SG,** Bakoyiannis A, Tassopoulos N, Athanassiou K, Kelekis D, Madariaga J, Dervenis C. Hepatic resection for hepatocellular carcinoma exceeding Milan criteria. *Surg Oncol* 2010; **19**: 200-207 [PMID: 19500972 DOI: 10.1016/j.suronc.2009.05.003]
- 32 **Truant S,** Boleslawski E, Duhamel A, Bouras AF, Louvet A, Febvay C, Leteurtre E, Huet G, Zerbib P, Dharancy S, Hebbbar M, Pruvot FR. Tumor size of hepatocellular carcinoma in noncirrhotic liver: a controversial predictive factor for outcome after resection. *Eur J Surg Oncol* 2012; **38**: 1189-1196 [PMID: 22863304 DOI: 10.1016/j.ejso.2012.07.112]
- 33 **Bartolini I,** Nelli T, Russolillo N, Cucchetti A, Pesi B, Moraldi L, Ferrero A, Ercolani G, Grazi G, Batignani G. Multiple hepatocellular carcinoma: Long-term outcomes following resection beyond actual guidelines. An Italian multicentric retrospective study. *Am J Surg* 2021; **222**: 599-605 [PMID: 33546852 DOI: 10.1016/j.amjsurg.2021.01.023]

## Observational Study

# Structure of the myenteric plexus in normal and diseased human ileum analyzed by X-ray virtual histology slices

Bela Veress, Niccolò Peruzzi, Marina Eckermann, Jasper Frohn, Tim Salditt, Martin Bech, Bodil Ohlsson

**Specialty type:** Gastroenterology and hepatology**Provenance and peer review:**

Unsolicited article; Externally peer reviewed.

**Peer-review model:** Single blind**Peer-review report's scientific quality classification**Grade A (Excellent): 0  
Grade B (Very good): B  
Grade C (Good): C  
Grade D (Fair): 0  
Grade E (Poor): 0**P-Reviewer:** Goldstein AM, United States; Natale G, Italy**Received:** April 28, 2022**Peer-review started:** April 28, 2022**First decision:** May 11, 2022**Revised:** May 18, 2022**Accepted:** July 11, 2022**Article in press:** July 11, 2022**Published online:** August 7, 2022**Bela Veress**, Department of Pathology, Skåne University Hospital, Malmö 205 02, Sweden**Niccolò Peruzzi, Martin Bech**, Medical Radiation Physics, Department of Clinical Sciences, Lund University, Lund 221 00, Sweden**Marina Eckermann, Jasper Frohn, Tim Salditt**, Institute for X-Ray Physics, University of Göttingen, Göttingen 37077, Germany**Marina Eckermann, Tim Salditt**, Cluster of Excellence "Multiscale Bioimaging: from Molecular Machines to Networks of Excitable Cells" (MBExC), University of Göttingen, Göttingen 37077, Germany**Marina Eckermann**, ESRF, The European Synchrotron, Grenoble 38043, France**Bodil Ohlsson**, Department of Internal Medicine, Skåne University Hospital, Lund University, Malmö S-205 02, Sweden**Corresponding author:** Bodil Ohlsson, MD, PhD, Full Professor, Department of Internal Medicine, Skåne University Hospital, Lund University, 15 Jan Waldenströms Street, Malmö S-205 02, Sweden. [bodil.ohlsson@med.lu.se](mailto:bodil.ohlsson@med.lu.se)

## Abstract

### BACKGROUND

The enteric nervous system (ENS) is situated along the entire gastrointestinal tract and is divided into myenteric and submucosal plexuses in the small and large intestines. The ENS consists of neurons, glial cells, and nerves assembled into ganglia, surrounded by telocytes, interstitial cells of Cajal, and connective tissue. Owing to the complex spatial organization of several interconnections with nerve fascicles, the ENS is difficult to examine in conventional histological sections of 3-5  $\mu\text{m}$ .

### AIM

To examine human ileum full-thickness biopsies using X-ray phase-contrast nanotomography without prior staining to visualize the ENS.

### METHODS

Six patients were diagnosed with gastrointestinal dysmotility and neuropathy based on routine clinical and histopathological examinations. As controls, full-thickness biopsies were collected from healthy resection ileal regions after

hemicolectomy for right colon malignancy. From the paraffin blocks, 4- $\mu$ m thick sections were prepared and stained with hematoxylin and eosin for localization of the myenteric ganglia under a light microscope. A 1-mm punch biopsy (up to 1 cm in length) centered on the myenteric plexus was taken and placed into a Kapton<sup>®</sup> tube for mounting in the subsequent investigation. X-ray phase-contrast tomography was performed using two custom-designed laboratory setups with micrometer resolution for overview scanning. Subsequently, selected regions of interest were scanned at a synchrotron-based end-station, and high-resolution slices were reported. In total, more than 6000 virtual slices were analyzed from nine samples.

## RESULTS

In the overview scans, the general architecture and quality of the samples were studied, and the myenteric plexus was localized. High-resolution scans revealed details, including the ganglia, interganglionic nerve fascicles, and surrounding tissue. The ganglia were irregular in shape and contained neurons and glial cells. Spindle-shaped cells with very thin cellular projections could be observed on the surface of the ganglia, which appeared to build a network. In the patients, there were no alterations in the general architecture of the myenteric ganglia. Nevertheless, several pathological changes were observed, including vacuolar degeneration, autophagic activity, the appearance of sequestosomes, chromatolysis, and apoptosis. Furthermore, possible expulsion of pyknotic neurons and defects in the covering cellular network could be observed in serial slices. These changes partly corresponded to previous light microscopy findings.

## CONCLUSION

The analysis of serial virtual slices could provide new information that cannot be obtained by classical light microscopy. The advantages, disadvantages, and future possibilities of this method are also discussed.

**Key Words:** Enteric nervous system; Immunohistochemistry; Neuropathy; Synchrotron; Virtual histology; X-ray phase-contrast nanotomography

©The Author(s) 2022. Published by Baishideng Publishing Group Inc. All rights reserved.

**Core Tip:** Full-thickness biopsies of 1 mm diameter and up to 1 cm length from the human ileum were scanned using two laboratory-based  $\mu$ -computed tomography setups to study the architecture of the enteric nervous system (ENS) and further scanned by a synchrotron-based end-station for histopathological studies, without any staining. Several pathological neuronal changes, such as vacuolar degeneration, autophagic activity, appearance of sequestosomes, chromatolysis, and apoptosis, were identified in diseased patients. Phenomena that were undetectable by light microscopy were observed. The relationships among various tissue components could be followed in all directions. Thus, this method provides a unique analysis of the ENS.

**Citation:** Veress B, Peruzzi N, Eckermann M, Frohn J, Salditt T, Bech M, Ohlsson B. Structure of the myenteric plexus in normal and diseased human ileum analyzed by X-ray virtual histology slices. *World J Gastroenterol* 2022; 28(29): 3994-4006

**URL:** <https://www.wjgnet.com/1007-9327/full/v28/i29/3994.htm>

**DOI:** <https://dx.doi.org/10.3748/wjg.v28.i29.3994>

## INTRODUCTION

The neurons of the enteric nervous system (ENS) assemble into ganglia, forming the submucosal and myenteric plexuses[1]. The ganglia, which also contain glial cells, are connected by nerve fascicles and are surrounded by telocytes and interstitial cells of Cajal (ICC), as well as by other cells and fibers of connective tissue. Various diseases of the ENS may lead to severe bowel motility dysfunction in the form of chronic intestinal pseudo-obstruction (CIPO) and enteric dysmotility (ED)[2,3]. Enteric neuropathy is seldom studied because only a few centers are available for the evaluation of gastrointestinal motility, access to the myenteric plexus requires full-thickness bowel biopsies, and pathologists subspecializing in neuromuscular diseases of the ENS are scarce. Subsequently, the neuropathy diagnosis may be ignored or delayed for several years, which prevents proper healthcare of the patients[4].

We recently presented a methodology to use X-ray phase-contrast nanotomography to study the volume and structure of the ENS[5]. Neurons and surrounding structures are visible using this method without any prior staining, allowing the possibility to study large sample volumes[5,6]. The aim of the present qualitative analysis of virtual slices was to describe in detail the structure of human ileal myenteric ganglia in the normal human ileum as well as in patients with CIPO or ED.

## MATERIALS AND METHODS

### *Patients and samples*

Six patients with severe gastrointestinal pain and dysmotility were examined using esophageal manometry, gastric emptying scintigraphy, antroduodenjejunal manometry, and colonic transit time, after exclusion of organic disease. Patients were diagnosed with CIPO when they fulfilled the following three criteria: a medical history compatible with pseudo-obstruction, documented events or chronic signs mimicking mechanical obstruction (bowel dilatation and/or air/fluid levels), and absence of mechanical obstruction or other organic causes for these symptoms and findings[3]. The criteria for ED were documented abnormal contractile activity, but no history of episodes or current signs mimicking mechanical obstruction and the absence of any medication that could lead to the observed motor abnormalities[2].

A previously described laparoscopy-assisted technique for ileal full-thickness biopsies and the preparation of biopsies was used[4,7]. Briefly, 1.0 cm × 1.5 cm large full-thickness biopsies were cut from the ileum and embedded in paraffin. Transversal and horizontal 3-5-mm thick serial sections were stained according to the protocol for CIPO analysis[8]. Histopathological findings were evaluated by a pathologist (B.V.) and classified as previously described[9]. The criteria for neuropathies were based on criteria suggested by the Gastro 2009 International Working Group for Gastrointestinal Neuromuscular Pathology[10]. The histopathological diagnoses and various stains, such as CD117 for ICC, CD34 for telocytes, S100 for Schwann cells, periodic acid-Schiff (PAS) with or without diastase (PAS-D) for carbohydrates or their compounds (*e.g.*, glycogen and mucin), and p62 for sequestosome, were obtained from the medical records (Table 1). For all patients, the disease initially presented when they were adults without any known heredity. Genetic analysis was not performed. There was no correlation between the varying histopathological findings described in Table 1 and the clinical presentation or other functional findings of patients (data not shown).

Three men aged 45, 54, and 82 years were used as controls, all of whom had undergone hemicolectomy due to malignancy in the right colon. A full-thickness biopsy specimen was collected and stained from the healthy resection region of the ileum. The sample size was adopted based on the beam time available in the laboratory.

### *Sample preparation*

From the paraffin blocks of these nine individuals, 4- $\mu$ m thick sections were prepared and stained with hematoxylin and eosin (H&E) for the localization of the myenteric ganglia under a light microscope. A biopsy punch of 1 mm diameter and up to 1 cm in length centered on the myenteric plexus was taken from the paraffin blocks of patients and controls and placed into a Kapton<sup>®</sup> tube (Paramount, Indiana, United States) for mounting in the subsequent tomographic investigation[11].

### *X-ray phase-contrast tomography*

X-ray phase-contrast tomography was performed on two custom-designed laboratory setups with micrometer resolution, located at the Institute for X-Ray Physics, University of Göttingen, Göttingen, Germany[11] and a Gottingen Instrument for Nano-Imaging with X-rays (GINIX), installed at the P10/PETRAIII beamline (Hamburg, Germany) with sub-micron resolution[12]. All setups used propagation-based, phase-contrast methods, in which the sample is placed between the source and detector, and the phase information is obtained by free-space propagation and self-interference of the coherent X-ray beam without the need for additional optical elements. Phase retrieval is necessary to correctly extract phase information before tomographic reconstruction[13-15].

The two laboratory setups were installed at a liquid metal jet source (Excillum, Kista, Sweden) or a microfocus rotating anode (mm007, Rigaku, Austin, TX, United States). Both setups used high-resolution scintillator-based detectors (Xsight, Rigaku) and employed broad bandpass radiation peaking at the characteristic lines of Ga Ka (9.25 keV) and Cu (8.05 keV) for the liquid jet and rotating anode sources, respectively. Phase retrieval was performed using the Bronnikov-aided correction algorithm[11, 15,16]. As a result, these home-built setups allowed us to image the whole 1-mm wide and several-mm long sample with an isotropic effective voxel size of approximately 1  $\mu$ m (approximately 15 h scan time per sample), enabling identification of the neural tissue structure (further information about the experimental parameters is provided in Table 2). The two systems could run in parallel and were used to optimize time consumption.

**Table 1 Basic characteristics of subjects**

Age, sex	Disease (years)	Clinical diagnosis	Histopathological findings	Histopathological diagnosis	X-ray
45, M	NA	Control	Normal neurons	Healthy	Healthy
54, M	NA	Control	Normal neurons	Healthy	Healthy
82, M	NA	Control	Normal neurons	Healthy	Healthy
27, W	4	ED/type 1 diabetes	Vacuolated, apoptotic neurons, chromatolysis	Lymphocytic ganglioneuritis	Vacuolated, shrunken neurons, chromatolysis, autophagia
27, W	6	Idiopathic ED	Vacuolated neurons, chromatolysis	Degenerative neuropathy	Pre-apoptotic and dead nucleus
32, W	2	Drug-induced CIPO	Vacuolated, shrunken, chromatolysis, hyperplasia ICC	Visceral degenerative neuropathy with axon vacuolization, hyperplasia, and vacuolization of ICCs, and hypertrophy of the longitudinal and internal circular muscle layers	Only fascicle, no ganglia for evaluation
43, W	3	Idiopathic ED	Amphophilic shrunken neurons, Vacuolated neurons, chromatolysis	Lymphocytic ganglioneuritis with neurondegeneration	Amphophilic degeneration, vacuolated neurons
52, W	4	Idiopathic ED	Vacuolated, shrunken neurons, hypoplasia of ICC	Lymphocytic ganglioneuritis	Vacuolated, shrunken neurons, chromatolysis
56, W	50	ED/Ehlers-Danlos	Vacuolated neurons, chromatolysis, hyperplasia ICC	Lymphocytic ganglioneuritis with vacuolar neurodegeneration and hyperplasia of the ICC	Severe atrophy with reduced volume

Data obtained from the medical records; disease duration assessed in years. CIPO: Chronic intestinal pseudo-obstruction; ED: Enteric dysmotility; ICC: Interstitial cells of Cajal; M: Man; W: Woman; NA: Not available.

**Table 2 Experimental and reconstruction parameters**

Scan configuration	Effective pixel size ( $\mu\text{m}$ )	Energy (keV)	Number of projections <sup>1</sup>	Phase retrieval scheme	Phase retrieval parameter	Ring removal algorithm
Laboratory setup (liquid metal jet)	0.920 <sup>2</sup>	9.25 (K $\alpha$ )	1 × 1000 (50 s) or 1 × 700 (40 s)	BAC	$\alpha = 0.008, \beta = 0.160$	Wavelet
Laboratory setup (rotating anode)	1.072	8.05 (K $\alpha$ )	1 × 1000 (50 s) or 1 × 700 (40 s)	BAC	$\alpha = 0.07, \beta = 0.16$	Wavelet
GINIX waveguide (all samples except for ED/Ehlers-Danlos patient)	0.169	8.00	4 × 1500 (1 s) or 3 × 1500 (1 s)	Non-linear Tikhonov <sup>3</sup>	$\delta/\beta = 50, \text{lim1} = 8e-3, \text{lim2} = 0.5$	Additive
GINIX waveguide (ED/Ehlers-Danlos patient)	0.176	7.50	4 × 1000 (2 s)	Non-linear Tikhonov <sup>3</sup>	$\delta/\beta = 50, \text{lim1} = 1e-4, \text{lim2} = 0.1$	Additive

<sup>1</sup>Due to time constraints, some samples were scanned with a lower number of projections and shorter exposure times (in the overview scans) or with less distances (in the high-resolution scans of the drug-induced chronic intestinal pseudo-obstruction patient and of the 40 years old control).

<sup>2</sup>After voxel binning of  $2 \times 2 \times 2$ .

<sup>3</sup>No support, no restriction on phase shift.

GINIX: Gottingen Instrument for Nano-Imaging with X-rays; ED: Enteric dysmotility.

Selected regions of interest (ROIs) of  $320 \mu\text{m} \times 320 \mu\text{m} \times 320 \mu\text{m}$  were scanned with an isotropic effective voxel size of 169 nm at the synchrotron-based end-station (approximately 2.5-3.0 h scan time), using inline holography based on a coherent divergent beam [8 keV, Si (111) monochromator] exiting from an X-ray waveguide[11,12]. Holographic phase retrieval based on contrast-transfer-function (CTF) approach, ring removal, and tomographic reconstructions were performed using in-house reconstruction pipelines[16]. Further details can be found in Table 2.

Complete information regarding the experimental setups and reconstruction pipelines, which were performed by physicists unaware of the diagnosis, is provided in a previous publication[5]. The analysis of the slices reported in this paper was performed on the data acquired at the synchrotron end-station, on the high-resolution scans.

### Image analysis

All the obtained volumetric datasets were digitally sectioned along any arbitrary slicing plane, enabling virtual histology of the samples. In the histological evaluation, the term “spindle-shaped cells” was used to describe the cells around the ganglia, which represented either telocytes, ICCs, or fibroblasts/cytes because no differentiation could be made without immunohistochemistry. In cases where identification can be made from double immunohistochemical staining of the same regions[17], the cells are called telocytes or ICC. In total, more than 6000 virtual slices were analyzed from the nine samples.

## RESULTS

In the overview scans performed with the laboratory setup, the general architecture of the bowel samples was examined with respect to the quality of the sample and the presence and localization of the myenteric plexus. High-resolution scans revealed details of the myenteric plexus, including the ganglia, interganglionic nerve fascicles, and surrounding tissue.

### Normal structure of the ileal myenteric plexus

**Ganglion:** The shape of the ganglia was uneven toward both the muscle layers and interganglionic nerve fascicles. The smaller or larger irregularities contained one or more neurons and glial cells (Figures 1, 2A, 4A-D, and 5).

In the surface view of the ganglia, a parallel arrangement of telocytes with long thin “primary” telopodes originating directly from the cellular bodies could be observed, from which shorter “secondary” telopodes radiated sidewise, building up a network (Figures 1A-C, 3B, 4A and B). Occasionally, at the optimal transverse view of the ganglion, a double layer of thin cytoplasmic projections was present (Figure 2B), corresponding to the immunohistochemical demonstration of telocytes and ICCs[17].

Both larger and smaller neurons had mostly rounded nuclei and nucleoli, where larger neurons had finely granulated cytoplasm with a paler network between the granules, whereas the smaller neurons had slightly denser and more homogeneous cytoplasm (Figures 2B and 3B-D). Axons were occasionally observed (Figure 2A). Small glial cells were present around and between the neurons (Figures 2A, 3C and D). No degenerating neurons were found in either of the two younger individuals. In the 82-year-old control, however, one neuron with a shrunken, dark body, pyknotic small almost black nucleus and larger autophagic vacuoles could be observed in addition to numerous normal neurons (not shown).

### Nerve fascicles and spindle-shaped cell layer

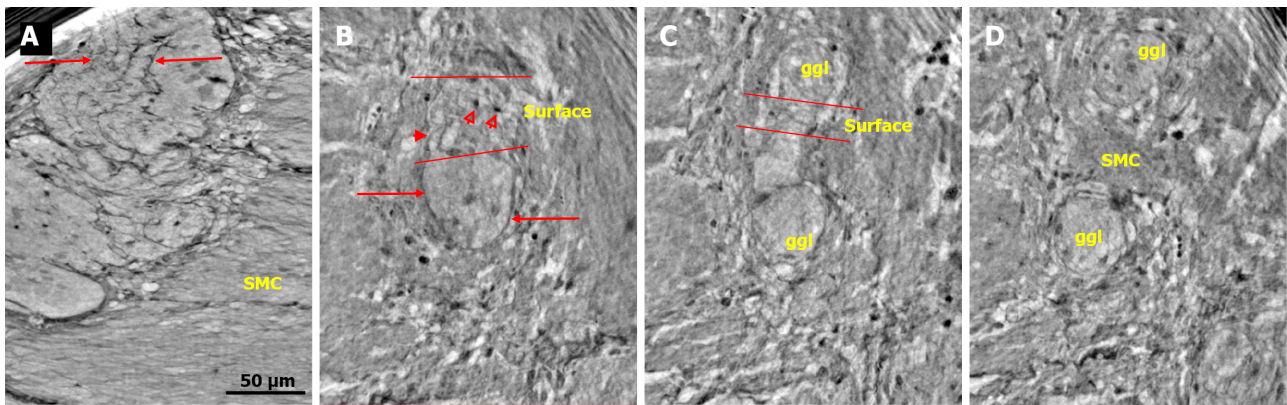
The nerve fascicles had normal architecture. Parallel thin telopodes separated the individual axons (Figures 2C and 3A-C). Some spindle-shaped cells had very thin, dark nuclei, whereas the nuclei of others were larger and cigar-like.

### Pathological findings of the ileal myenteric plexus

Four patients had lymphocytic ganglioneuritis or lymphocytic neuritis, and two patients had only visceral degenerative neuropathy. No alterations were observed in the general architecture of the myenteric ganglia. Nevertheless, several pathological changes could be observed, partly corresponding to the light microscopic findings, as shown in the insets of the figures. Cellular changes occurred in all six patients with dysmotility. Suspected lymphocytes were found within the ganglion only in one patient. The lack of lymphocytic attack on the ganglion in other patients can be explained by the focal nature of inflammation.

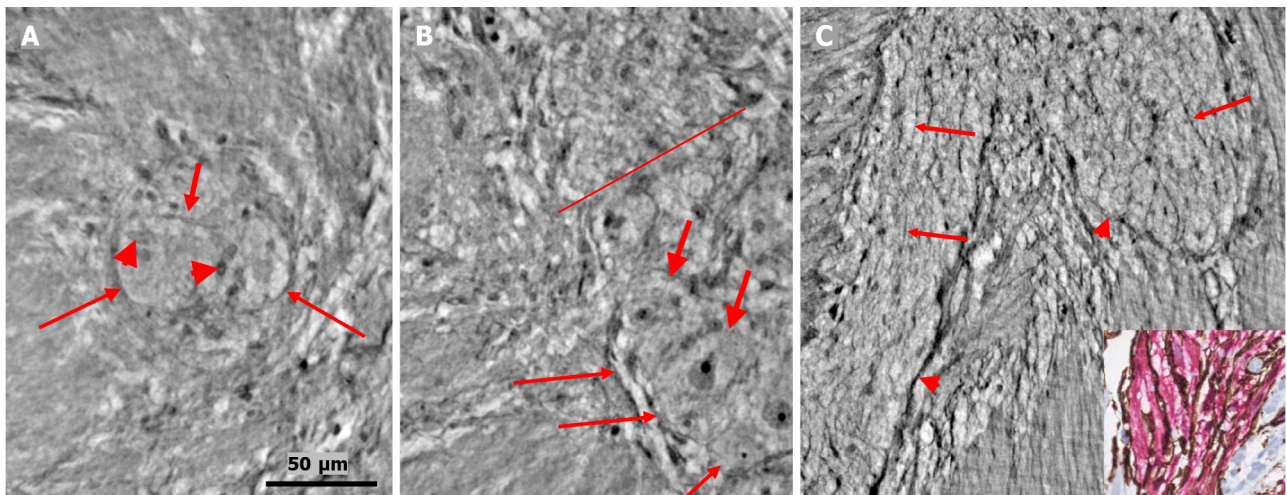
### Pathological neuronal changes

The cytoplasm of several neurons contained vacuoles. Many of the vacuoles contained small dark granules (Figure 5A, C, and D) (autophagic vacuoles/Lipofuscin; 5D-inset: PAS-D<sup>+</sup>). In one patient, several neurons exhibited pale cytoplasm (Figure 4A-D) (chromatolysis), and a large homogeneous irregular dark area was present (Figure 4F) (4F-inset: Sequestosome p62<sup>+</sup>). Apoptotic shrunken neurons had compact, dark cytoplasm with small, irregular, pyknotic nuclei (Figures 4C-E, 5B and 6) (4E-inset H&E; 5B-inset: Apoptosis H&E). These neurons were observed in three patients at the ganglion border without telopodes in a few virtual slices (Figure 4B-D), possibly representing the ejection of a dead neuron (Figures 4B-D and 6). Very dense dark inclusions with similar substructures were found in two patients, which are foreign structures for the normal ganglion; one of these bodies is shown in serial virtual slices (Figure 4A-C) (4A-C: Hyaline bodies; 4A and B-insets: PAS-D<sup>+</sup>). At 6.8 μm in Figure 4A, an inner structure with a central pale area surrounded by an irregular dark ring can be seen within the body (Figure 4B). When viewing 4.0 μm deeper, there is a semi-dense “half-moon” at the edge of the hyaline body (Figure 4C).



DOI: 10.3748/wjg.v28.i29.3994 Copyright ©The Author(s) 2022.

**Figure 1 Ganglion from healthy human ileum.** A: Part of the myenteric ganglion in two portions. Quite regular, almost parallel, thin cytoplasmic projections of telocytes (telopodes) with short, thin "spines" on the surface are observed (between arrows). The scale bar (50 µm) was applied to all subfigures; B: A small portion of the ganglion containing two neurons. On the surface of the ganglion (between the two lines), the cellular nuclei of the two telocytes were observed as dark spots (empty arrowheads). Telopodes radiate from their body. Arrows indicate the telopodes around the ganglion. A telopode can be followed toward the surface (arrowhead); C: 16.9 µm deeper from Figure B, two portions appeared with thin telopodes on the surface; D: 10.1 µm deeper from Figure C, SMCs are observed between the two portions. B-D are representative virtual slices from a series covering 27.0 µm thickness of the ganglion. Ggl: Ganglion; SMC: Smooth muscle cells.



DOI: 10.3748/wjg.v28.i29.3994 Copyright ©The Author(s) 2022.

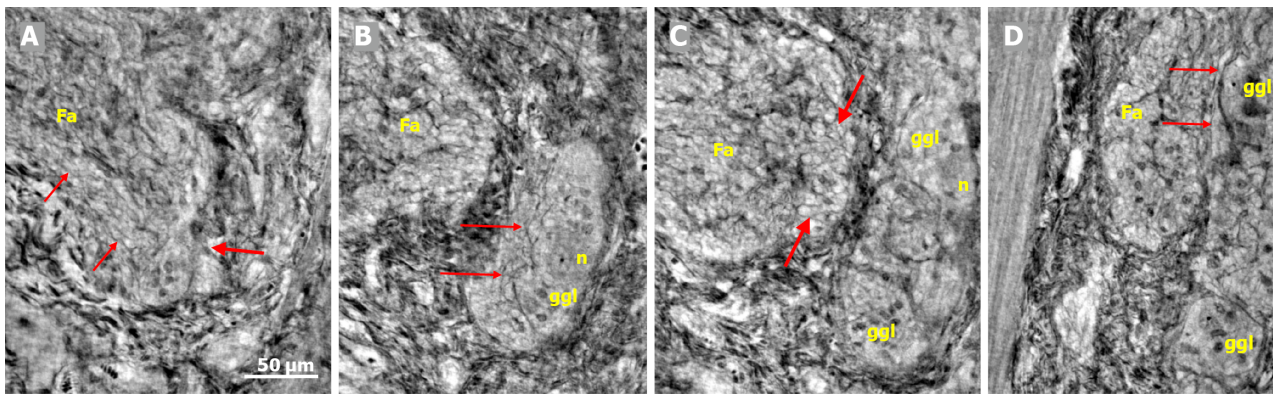
**Figure 2 Ganglion and fascicle from healthy human ileum.** A: Within a portion of the ganglion, there is a neuron with an axon (thick arrow). Arrowheads indicate glial cells. Thin arrows indicate a single layer of telopodes at the border of the ganglion. The scale bar (50 µm) was applied to all subfigures; B: Part of a ganglion with several large (thick arrows) and medium-large (short thin arrow) neurons. The nuclei contain dark nucleoli. The cytoplasm is slightly granulated. Above the straight line, a small area of the neuropil was observed. Long thin arrows indicate the double-cell layer at the border; C: Normal nerve fascicle and thicker nerve with telopodes separating axons (arrows). Note the single layer of telopodes around the fascicle and nerve (arrowheads). Inset: Normal nerve fascicles stained with double immunohistochemistry. Telocytes run parallel to Schwann cells (light microscopy; S100: Schwann cells red; CD34: Telocytes brown).

### Pathological change of the nerve fascicles and periganglionic spindle-shaped cell layer

In one patient who was diagnosed with lymphocytic ganglioneuritis, a segment of the periganglionic spindle-shaped cell layer showed vacuolization and/or was absent within a 19.9 µm distance along the length axis of the bowel sample (Figure 5). The largest window in this absence was 16.1 µm in the virtual slices (Figure 5B). At a 7.8 µm deeper level (Figure 5C), a double layer of thin cellular projections appeared at the border of the defect, whereas at an additionally 4.7 µm deeper, one intact layer of cellular projections was again present between the ganglion and the surrounding tissue (Figure 5D).

### Video-film

In the video film from one patient, more than one dozen neurons and glial cells could be observed (Supplementary material). Almost all the neurons showed various types of degeneration. Furthermore, one pre-apoptotic neuron in the lower part of the ganglion was probably in contact with the tip of the incomplete septum, and hence, extended into the surrounding tissue (Supplementary material).



DOI: 10.3748/wjg.v28.i29.3994 Copyright ©The Author(s) 2022.

**Figure 3** Series of virtual slices covering 113.6  $\mu\text{m}$  thickness at the border between the nerve fascicle and the ganglion. A: Thick fascicle with parallel telopodes (thin arrows). There is a small peripheral part of the ganglion (thick arrow); B: 62.2  $\mu\text{m}$  deeper from Figure A. Connective tissue cells between the fascicle and the superficial part of the ganglion. Normal large neurons and nuclei of several glial cells in the ganglion. A network of telopodes is present on the surface of the ganglion (arrows); C: 11.5  $\mu\text{m}$  deeper from Figure B. The thickness of the connective tissue is diminished between the fascicle and the periphery of the ganglion, with two neurons and small glial cells. Transversally cut vesicle-like axons (between the arrows) on the right end of the fascicle; D: 39.9  $\mu\text{m}$  deeper from Figure C, the fascicle and ganglion are united. Thin arrows show telopodes. The scale bar (50  $\mu\text{m}$ ) applies to all the subfigures. Fa: Fascicle; ggl: Ganglion; n: Neuron.

## DISCUSSION

The main qualitative finding in the present study was that X-ray phase-contrast nanotomography could analyze the different cellular components of the myenteric plexus in more than 6000 serial virtual slices, which could reveal minor changes not seen under the light microscope. We could image large volumes with finer sampling resolution with shorter distances between sections along the sample direction, that is, below the standard thickness of a histological scan.

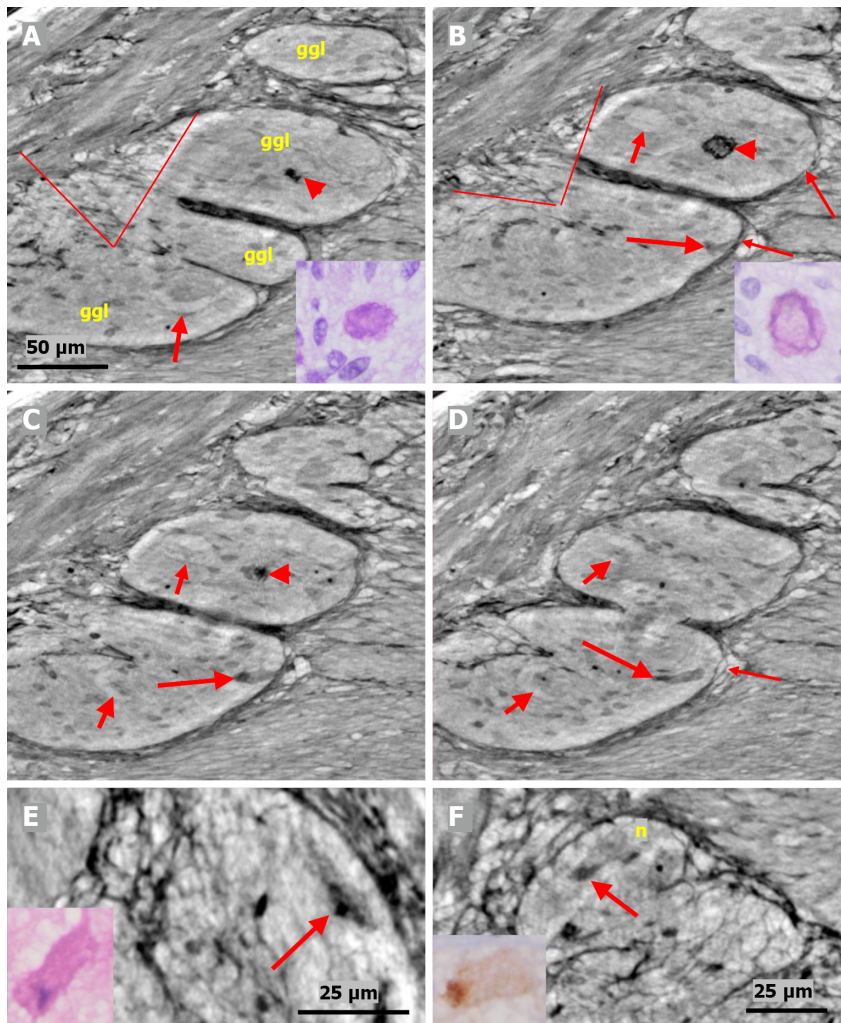
A study of the normal ganglia revealed that their shape is not usually seen in the transverse sections under a light microscope with a well-defined border. In serial virtual slices, the ganglia have smaller or larger irregularities, with one or a few neurons and glial cells protruding into the muscle layers or the intermyenteric connective tissue. Within the ganglia, neurons of various sizes and glial cells could be clearly differentiated. The absence of thin cytoplasmic projections in the neuropil corroborates our previous finding in the ileal ganglia, namely the lack of telopodes in the ileum in contrast to the colon [17]. The presence of one degenerating neuron in the 82-year-old control may be the result of aging starting at around 40-50 years of age [18].

The optimal transverse sections showed two clear layers of cellular projections surrounding the ganglion, in accordance with our previous immunohistochemical findings [17]. The inner layer consisted of cytoplasmic projections of telocytes called telopodes, which were situated almost parallel to each other, in agreement with immunohistochemical observations [17]. The outer layer is composed of an ICC [17].

Pathological changes from the patients revealed different types of neuronal degeneration (vacuolization, autophagic vacuoles/Lipofuscin, chromatolysis, and apoptosis) and the presence of a hyaline body within the ganglion, as observed under a light microscope by the golden standard of various staining techniques [8]. Furthermore, p62+ sequestosomes were also observed in accordance with the findings of Alafuzoff *et al* [19].

Three new phenomena were discovered with the present phase-contrast nanotomography, which cannot be observed under a light microscope because of the thickness of the paraffin sections. First, the presence of a semi-dense “half-moon” attached to the hyaline body could hypothetically be one of the end stages of cellular death. Second, the phenomenon of a probable expulsion of dead neurons could be followed in the virtual serial slices because of the occurrence of a short “opening” of the telopode-layer between the surrounding connective tissue and shrunken apoptotic neurons. Third, the total absence of the single telopode layer within the 16.1  $\mu\text{m}$  “window” could possibly have negatively affected the stability of the ganglion.

The virtual histology of the myenteric ganglion using X-ray nanotomography has advantages, disadvantages, and future possibilities. The main advantage is that the method can exactly measure the volumes of chosen tissue components following segmentation, as have been previously published [5]. The second advantage is the possibility to analyze several hundred serial virtual slices at subcellular, isotropic resolution, and through this, discover “nano-changes” which cannot be seen using the light microscope. Because the neuron size is 15-40  $\mu\text{m}$ , the ENS is difficult to examine in conventional histological sections of 3-5  $\mu\text{m}$ . Slow videos make it possible to follow the relationships between the various tissue components. The third advantage is the flexibility in sample preparation; samples can be examined with or without paraffin embedding (*e.g.*, in liquid or epoxy resin) or staining. Thus, the

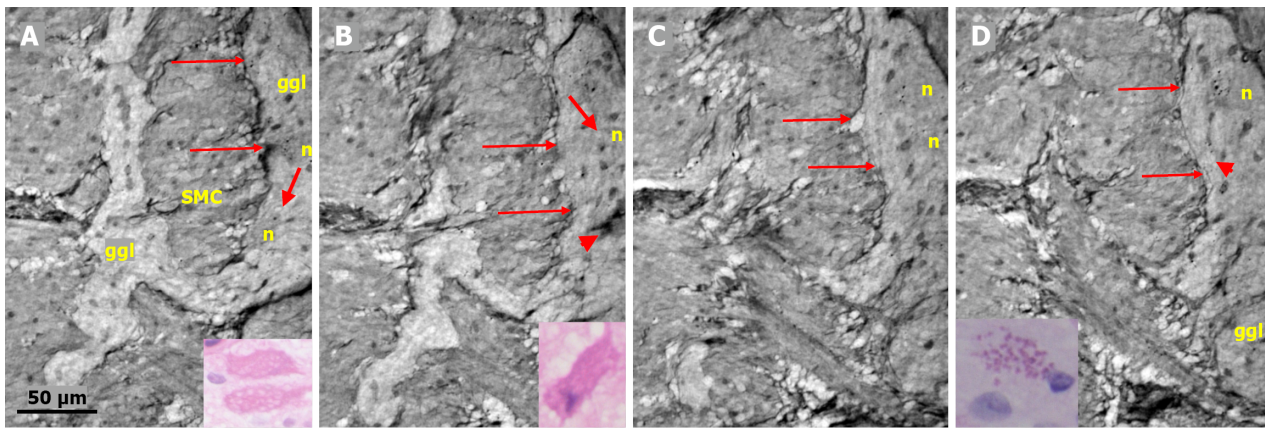


DOI: 10.3748/wjg.v28.i29.3994 Copyright ©The Author(s) 2022.

**Figure 4** Series of virtual slices covering 17.2  $\mu\text{m}$  thickness of the ganglion from one patient. A: Four portions of the ganglion. There is a dark body at the center of one of these areas (arrowheads). An arrow indicates a neuron with a very pale homogeneous cytoplasm below the nucleus. Between the straight lines, a network of telopodes is observed on the ganglion surface. Incomplete septa between portions. Scale bar (50  $\mu\text{m}$ ) is applied to subfigures A-D. Inset: Hyaline body in the ganglion [1<sup>st</sup> level of serial sections; light microscopy; periodic acid-Schiff with diastase (PAS-D) staining]; B: 6.8  $\mu\text{m}$  from Figure A., three portions of the ganglia are completely separated, and the surface area is smaller (between straight lines). The central dark body shows an irregular dense outer layer and central light area (arrowhead). A new neuron with pale cytoplasm is seen in the middle portion (short arrow). Intact telopodes form the border between the ganglion and the periganglionic connective tissue rim (thin arrows). An almost triangle-shaped moderately dense area is seen below the telopode corresponding to an apoptotic neuron (long arrow; see also C and D). Inset: The central region of the hyaline body is negative, whereas the outer layer is positive with PAS-D staining (2<sup>nd</sup> level of serial sections, light microscopy; PAS-D); C: 4.0  $\mu\text{m}$  from Figure B. The hyaline body is without a central pale area (arrowhead), with a semi-dense irregular half-moon to the left. The two neurons had a pale cytoplasm (short arrows). A dark pyknotic nucleus appeared in the semi-dense cytoplasm at the border showing an apoptotic neuron corresponding to the "dark triangle" in Figure B (long arrow); D: 6.4  $\mu\text{m}$  deeper from Figure C. Two of the portions are united. Nuclei are present in neurons with pale cytoplasm (short arrows). Intact telopodes are present between the degenerated apoptotic cells (long arrow) and the periganglionic space (thin arrow); E: Digital magnification of a shrunken neuron with a darker cytoplasm, small vacuoles, and enlarged nucleolus. Scale bar: 25  $\mu\text{m}$  Inset: Pre-apoptotic neurons with pyknotic nucleus and vacuole-containing amphophilic cytoplasm (light microscopy; H&E staining); F: There is a homogeneous circumscribed "inclusion" in the neuron, suggesting a sequestosome, as seen in the inset (arrow). Scale bar: 25  $\mu\text{m}$ . Inset: Large p62<sup>+</sup> aggregates in neurons (arrow; light microscopy; p62 immunohistochemistry). Scale bars of 50 or 25  $\mu\text{m}$  included. Ggl: Ganglion; n: Neuron; PAS-D: Periodic acid-schiff with diastase.

samples require less handling and fewer preparation steps[20].

The current established method to diagnose enteric neuropathy uses immunohistochemistry with a wide range of staining according to a standardized protocol[8,21]. The strength of this method lies in the exact identification of different cell types and tissue structures. The weakness is that there is a wide range of different molecules and structures that can vary in abundance among different patients with the same diagnosis. We do not know whether these changes are causal or primary, or whether they are secondary or compensatory. Due to the large variation between patients, no uniform pattern has been determined for the diagnosis of enteric neuropathy, and thus, some of the information did not add substantial value to the examination. The current description of neurons, glial cells, and spindle-shaped cells appears to be sufficient for diagnosis.



DOI: 10.3748/wjg.v28.i29.3994 Copyright ©The Author(s) 2022.

**Figure 5** Series of virtual slices covering 19.9  $\mu\text{m}$  thickness of the ganglion from one patient. A: Two portions of the ganglion with smooth muscle cells between them. Long arrows indicate the continuous layer of telopodes with tiny vesicles bordering the ganglion. A string of glial cell nuclei was present within the left portion. The thick arrow shows the vacuole above the nucleus of the neuron. Four small dark granules were present in the other neurons. Inset: Several vacuoles fill the cytoplasm of the two degenerating neurons (light microscopy and H&E staining); B: 7.4  $\mu\text{m}$  deeper from Figure A. Between the thin arrows there is no continuous layer of telopodes, instead some vesicles are seen. The left portion has disappeared. The remaining portion is part of a pre-apoptotic neuron with a dark cytoplasm and pyknotic nucleus (arrowhead). Above this neuron is the nuclei of normal glial cells. The thick arrow indicates a vacuole in the neuron. Inset: Apoptotic neurons with strongly amphophilic cytoplasm and rest of the pyknotic nuclei (light microscopy; H&E staining); C: 7.8  $\mu\text{m}$  deeper from Figure B. The defect of the telopodes (between the thin arrows) was shorter. Double layer of telopodes below the defect. In the upper part of the ganglion, there is a large neuron with a few small dark, dense dots, whereas the pre-apoptotic neuron from the middle of the ganglion is no longer present; D: 4.7  $\mu\text{m}$  deeper from Figure C. There is a continuous layer of telopodes (between arrows) with a "remnant" of the double layer, as shown in Figure C. The dark granules in the neurons were larger and more numerous. Arrowhead shows a neuron with both dark granules and vacuoles. Inset: The cytoplasm of the neurons was filled with diastase-resistant PAS+ lipofuscin granules (light microscopy; PAS-D staining). The scale bar (50  $\mu\text{m}$ ) applies to all the subfigures. Ggl: Ganglion; H&E: Hematoxylin & eosin; n: Neuron; PAS: Periodic acid-Schiff; PAS-D: Periodic acid-Schiff with diastase; SMC: Smooth muscle cells.

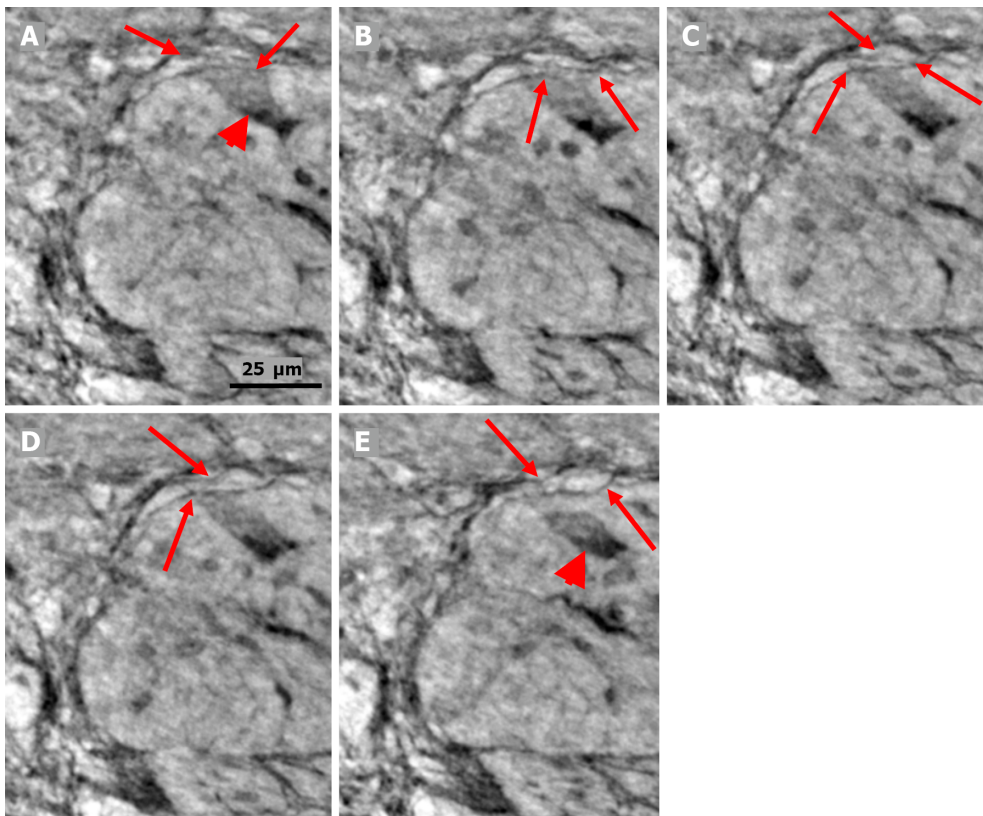
Fluorescence confocal microscopy has been performed with serial sectioning to mimic three-dimensional (3D) imaging; however, the maximal thickness of viewing is still limited, and the space between sections is larger[22-25]. Recently, another method using immunohistochemistry and confocal microscopy was developed for the quantitative analysis of full-thickness bowel biopsies[26]. These different efforts to improve the analysis of ENS prove the importance of clinicians obtaining more information about the function and dysfunction of the gastrointestinal tract.

Among the disadvantages were the limited access to synchrotron beamtime and the cost of the entire process in terms of money and manpower. Furthermore, because the ganglia of the ENS are very sparse, especially in patients with dysmotility, and the myenteric plexus can fold and curve beneath what is visible on the surface of the block, it is very difficult to correctly punch the tissue of interest based on a histological section. Hence, multi-scale X-ray phase-contrast tomography, which involves scanning a tissue block with a mm-sized field-of-view at  $\mu\text{m}$ -resolution and then imaging specific features of interest in greater detail using local nanotomography on the full block (instead of extracting biopsy punches as in this work), would be preferable and has been proven to be feasible at different synchrotron beamlines, such as TOMCAT[27,28] and P10/GINIX[29-31].

In the future, the combination of immunohistochemistry with X-ray phase-contrast nanotomography, such as immuno-electron microscopy[32], or with joint X-ray phase-contrast tomography and focused ion beam scanning electron microscopy (FIB-SEM) could provide unique possibilities to study targeted cells and their internal and external relationships[33]. In addition, this technique can determine the exact volume of the target tissue components[5].

## CONCLUSION

Virtual sectioning by X-ray phase-contrast nanotomography is a method that provides a unique analysis of the myenteric ganglion, revealing minor pathological changes that cannot be discovered using light microscopy or other two-dimensional scanning methods to study the relationship between various tissue components.



DOI: 10.3748/wjg.v28.i29.3994 Copyright ©The Author(s) 2022.

**Figure 6** Series of virtual slices covering 6.4  $\mu\text{m}$  thickness of the ganglion from one patient. A: Neuron with shrunken pyknotic nucleus and dark cytoplasm containing vacuoles at the edge of the ganglion (arrowhead). A part of the cytoplasm of the pre-apoptotic neuron is present between the telopodes (arrows); B: 2.0  $\mu\text{m}$  deeper from Figure A. The lower telopode was discontinuous (arrows); C: 0.7  $\mu\text{m}$  deeper from Figure B. The two telopodes are intact, and almost all of the cytoplasm between them has disappeared; D: 0.7  $\mu\text{m}$  deeper from Figure C. Pre-apoptotic neurons seem to be in contact with the lower telopode; E: 3.0  $\mu\text{m}$  deeper from Figure D. The pre-apoptotic neuron (arrowhead) lies within the ganglion, without contact with the telopodes. Arrows point to two telopodes on the figures. The scale bar (25  $\mu\text{m}$ ) applies to all the subfigures.

## ARTICLE HIGHLIGHTS

### Research background

The enteric nervous system (ENS) is difficult to study because of its deep localization in the intestinal wall. The limited sections visualized by light microscopy cannot show the size of the neurons or the interconnection between different parts of the ENS or different cell types.

### Research motivation

Since the ENS is difficult to examine, patients with gastrointestinal dysmotility are not properly examined, diagnosed, and treated. They can experience symptoms for several years before a proper diagnosis is established.

### Research objectives

The main objective of this study was to examine whether X-ray phase-contrast tomography could improve the visualization of the ENS. We realized that the ENS could be visualized without any prior staining, and the information provided was superior to conventional light microscopy in some respects. Thus, this method should be further evaluated in future studies.

### Research methods

Full-thickness biopsies from the ileum of patients with dysmotility and controls were examined using X-ray phase-contrast tomography. For comparison, the same samples were examined using immunohistochemistry. This is the first time that bowel biopsies have been examined using X-ray tomography, and the histopathology has been described in detail.

### Research results

This study showed that X-ray phase-contrast tomography can be used to study the ENS in detail to describe normal and pathological cells and tissue structures. The interconnections between the cells and

structures can be visualized. Some new findings could not have been observed using conventional light microscopy.

### **Research conclusions**

Virtual sectioning by X-ray phase-contrast nanotomography provides a unique analysis of the myenteric ganglion, revealing minor pathological changes that cannot be discovered by light microscopy, to follow the relationship between various tissue components.

### **Research perspectives**

This method needs to be further studied in larger cohorts, with scanning of whole paraffin blocks combined with different staining methods to try to improve the identification of different cell types and tissue structures. More healthy controls should be examined to obtain reference values for health and disease.

---

## **ACKNOWLEDGEMENTS**

The authors thank Maria Teresa Moreira Jara and Maria Nilsson for their technical assistance and the pathologists for control sample collection. The valuable discussion with Anca Dragomir, MD, PhD, Uppsala University, regarding possible artifacts, is greatly appreciated.

---

## **FOOTNOTES**

**Author contributions:** Veress B performed the histochemical and pathological analyses of the X-ray data and wrote the initial draft together with Ohlsson B; Peruzzi N, Eckermann M, and Frohn J scanned the samples; Peruzzi N analyzed the technical data; all authors planned and designed the study, contributed to intellectual analysis of the results, and approved the final version of the manuscript.

**Supported by** the Development Foundation of Region Skåne, No. REGSKANE-818781 and No. 2018-Projekt0024; and the Foundation Skåne University Hospital, No. 2020-0000028.

**Institutional review board statement:** The study was reviewed and approved by the Regional Ethics Review Board at Lund University (2009/209, Date of approval 28/04/2009; 2012/527, Date of approval 16/10/2012 and 2018/132, Date of approval 02/08/2018) and the Swedish Biobank Act.

**Informed consent statement:** All study participants provided informed written consent prior to study enrollment.

**Conflict-of-interest statement:** There are no conflicts of interest to report.

**Data sharing statement:** No additional data is available.

**STROBE statement:** The authors have read the STROBE Statement – checklist of items, and the manuscript was prepared and revised according to the STROBE Statement – checklist of items.

**Open-Access:** This article is an open-access article that was selected by an in-house editor and fully peer-reviewed by external reviewers. It is distributed in accordance with the Creative Commons Attribution NonCommercial (CC BY-NC 4.0) license, which permits others to distribute, remix, adapt, build upon this work non-commercially, and license their derivative works on different terms, provided the original work is properly cited and the use is non-commercial. See: <https://creativecommons.org/licenses/by-nc/4.0/>

**Country/Territory of origin:** Sweden

**ORCID number:** Bela Veress 0000-0001-9529-6809; Niccolò Peruzzi 0000-0002-2929-4247; Marina Eckermann 0000-0001-6418-4310; Jasper Frohn 0000-0003-3849-6032; Tim Salditt 0000-0003-4636-0813; Bodil Ohlsson 0000-0002-9142-5244.

**Corresponding Author's Membership in Professional Societies:** UEG; Swedish Society of Gastroenterology.

**S-Editor:** Chen YL

**L-Editor:** A

**P-Editor:** Chen YL

## REFERENCES

- 1 **Furness JB**, Callaghan BP, Rivera LR, Cho HJ. The enteric nervous system and gastrointestinal innervation: integrated local and central control. *Adv Exp Med Biol* 2014; **817**: 39-71 [PMID: [24997029](#) DOI: [10.1007/978-1-4939-0897-4\\_3](#)]
- 2 **Wingate D**, Hongo M, Kellow J, Lindberg G, Smout A. Disorders of gastrointestinal motility: towards a new classification. *J Gastroenterol Hepatol* 2002; **17** Suppl: S1-14 [PMID: [12000590](#) DOI: [10.1046/j.1440-1746.17.s1.7.x](#)]
- 3 **Keller J**, Bassotti G, Clarke J, Dinning P, Fox M, Grover M, Hellström PM, Ke M, Layer P, Malagelada C, Parkman HP, Scott SM, Tack J, Simren M, Törnblom H, Camilleri M; International Working Group for Disorders of Gastrointestinal Motility and Function. Expert consensus document: Advances in the diagnosis and classification of gastric and intestinal motility disorders. *Nat Rev Gastroenterol Hepatol* 2018; **15**: 291-308 [PMID: [29622808](#) DOI: [10.1038/nrgastro.2018.7](#)]
- 4 **Hammar O**, Ohlsson B, Veress B, Alm R, Fredrikson GN, Montgomery A. Depletion of enteric gonadotropin-releasing hormone is found in a few patients suffering from severe gastrointestinal dysmotility. *Scand J Gastroenterol* 2012; **47**: 1165-1173 [PMID: [22835010](#) DOI: [10.3109/00365521.2012.706826](#)]
- 5 **Peruzzi N**, Veress B, Dahlin LB, Salditt T, Andersson M, Eckermann M, Frohn J, Robisch AL, Bech M, Ohlsson B. 3D analysis of the myenteric plexus of the human bowel by X-ray phase-contrast tomography - a future method? *Scand J Gastroenterol* 2020; **55**: 1261-1267 [PMID: [32907418](#) DOI: [10.1080/00365521.2020.1815079](#)]
- 6 **Eckermann M**, Peruzzi N, Frohn J, Bech M, Englund E, Veress B, Salditt T, Dahlin LB, Ohlsson B. 3d phase-contrast nanotomography of unstained human skin biopsies may identify morphological differences in the dermis and epidermis between subjects. *Skin Res Technol* 2021; **27**: 316-323 [PMID: [33022848](#) DOI: [10.1111/srt.12974](#)]
- 7 **Törnblom H**, Lindberg G, Nyberg B, Veress B. Full-thickness biopsy of the jejunum reveals inflammation and enteric neuropathy in irritable bowel syndrome. *Gastroenterology* 2002; **123**: 1972-1979 [PMID: [12454854](#) DOI: [10.1053/gast.2002.37059](#)]
- 8 **Lindberg G**, Törnblom H, Iwarzon M, Nyberg B, Martin JE, Veress B. Full-thickness biopsy findings in chronic intestinal pseudo-obstruction and enteric dysmotility. *Gut* 2009; **58**: 1084-1090 [PMID: [19136514](#) DOI: [10.1136/gut.2008.148296](#)]
- 9 **Knowles CH**, Veress B, Kapur RP, Wedel T, Farrugia G, Vanderwinden JM, Geboes K, Smith VV, Martin JE, Lindberg G, Milla PJ, De Giorgio R. Quantitation of cellular components of the enteric nervous system in the normal human gastrointestinal tract--report on behalf of the Gastro 2009 International Working Group. *Neurogastroenterol Motil* 2011; **23**: 115-124 [PMID: [21175997](#) DOI: [10.1111/j.1365-2982.2010.01657.x](#)]
- 10 **Knowles CH**, De Giorgio R, Kapur RP, Bruder E, Farrugia G, Geboes K, Lindberg G, Martin JE, Meier-Ruge WA, Milla PJ, Smith VV, Vanderwinden JM, Veress B, Wedel T. The London Classification of gastrointestinal neuromuscular pathology: report on behalf of the Gastro 2009 International Working Group. *Gut* 2010; **59**: 882-887 [PMID: [20581236](#) DOI: [10.1136/gut.2009.200444](#)]
- 11 **Töpperwien M**, van der Meer F, Stadelmann C, Salditt T. Three-dimensional virtual histology of human cerebellum by X-ray phase-contrast tomography. *Proc Natl Acad Sci U S A* 2018; **115**: 6940-6945 [PMID: [29915047](#) DOI: [10.1073/pnas.1801678115](#)]
- 12 **Salditt T**, Osterhoff M, Krenkel M, Wilke RN, Priebe M, Bartels M, Kalbfleisch S, Sprung M. Compound focusing mirror and X-ray waveguide optics for coherent imaging and nano-diffraction. *J Synchrotron Radiat* 2015; **22**: 867-878 [PMID: [26134789](#) DOI: [10.1107/S1600577515007742](#)]
- 13 **Cloetens P**, Ludwig W, Baruchel J, Van Dyck D, Landuyt JV, Guigay JP, Schlenker M. Holotomography: Quantitative phase tomography with micrometer resolution using hard synchrotron radiation x rays. *Appl Phys Lett* 1999; **75**: 2912 [DOI: [10.1063/1.125225](#)]
- 14 **Groso A**, Stampanoni M, Abela R, Schneider P, Linga S, Müller R. Phase contrast tomography: An alternative approach. *Appl Phys Lett* 2006; **88**: 214104 [DOI: [10.1063/1.2207221](#)]
- 15 **De Witte Y**, Boone M, Vlassenbroeck J, Dierick M, Van Hoorebeke L. Bronnikov-aided correction for x-ray computed tomography. *J Opt Soc Am A Opt Image Sci Vis* 2009; **26**: 890-894 [PMID: [19340263](#) DOI: [10.1364/josaa.26.000890](#)]
- 16 **Lohse LM**, Robisch AL, Töpperwien M, Maretzke S, Krenkel M, Hagemann J, Salditt T. A phase-retrieval toolbox for X-ray holography and tomography. *J Synchrotron Radiat* 2020; **27**: 852-859 [PMID: [32381790](#) DOI: [10.1107/S1600577520002398](#)]
- 17 **Veress B**, Ohlsson B. Spatial relationship between telocytes, interstitial cells of Cajal and the enteric nervous system in the human ileum and colon. *J Cell Mol Med* 2020; **24**: 3399-3406 [PMID: [31983076](#) DOI: [10.1111/jcmm.15013](#)]
- 18 **Hanewinkel R**, Drenthen J, van Oijen M, Hofman A, van Doorn PA, Ikram MA. Prevalence of polyneuropathy in the general middle-aged and elderly population. *Neurology* 2016; **87**: 1892-1898 [PMID: [27683845](#) DOI: [10.1212/WNL.0000000000003293](#)]
- 19 **Alafuzoff I**, Popova SN, Veress B. Neuronal protein alteration in enteric dysmotility syndrome. *J Alzheimers Dis Parkinsonism* 2016; **6**: 212-216 [DOI: [10.4172/2161-0460.1000212](#)]
- 20 **Eckermann M**, van der Meer F, Cloetens P, Ruhwedel T, Möbius W, Stadelmann C, Salditt T. Three-dimensional virtual histology of the cerebral cortex based on phase-contrast X-ray tomography. *Biomed Opt Express* 2021; **12**: 7582-7598 [PMID: [35003854](#) DOI: [10.1364/BOE.434885](#)]
- 21 **Lehtonen HJ**, Sipponen T, Tojkander S, Karikoski R, Järvinen H, Laing NG, Lappalainen P, Aaltonen LA, Tuupainen S. Segregation of a missense variant in enteric smooth muscle actin  $\gamma$ -2 with autosomal dominant familial visceral myopathy. *Gastroenterology* 2012; **143**: 1482-1491.e3 [PMID: [22960657](#) DOI: [10.1053/j.gastro.2012.08.045](#)]
- 22 **Vanderwinden JM**, Rumessen JJ, De Laet MH, Vanderhaeghen JJ, Schiffmann SN. CD34+ cells in human intestine are fibroblasts adjacent to, but distinct from, interstitial cells of Cajal. *Lab Invest* 1999; **79**: 59-65 [PMID: [9952111](#)]
- 23 **Toma H**, Nakamura K, Kuraoka A, Tanaka M, Kawabuchi M. Three-dimensional structures of c-Kit-positive cellular networks in the guinea pig small intestine and colon. *Cell Tissue Res* 1999; **295**: 425-436 [PMID: [10022963](#) DOI: [10.1007/s004410051249](#)]
- 24 **Cobine CA**, Hennig GW, Kurahashi M, Sanders KM, Ward SM, Keef KD. Relationship between interstitial cells of Cajal, fibroblast-like cells and inhibitory motor nerves in the internal anal sphincter. *Cell Tissue Res* 2011; **344**: 17-30 [PMID: [21337122](#) DOI: [10.1007/s00441-011-1138-1](#)]

- 25 **Grover M**, Bernard CE, Pasricha PJ, Parkman HP, Abell TL, Nguyen LA, Snape W, Shen KR, Sarr M, Swain J, Kendrick M, Gibbons S, Ordog T, Farrugia G. Platelet-derived growth factor receptor  $\alpha$  (PDGFR $\alpha$ )-expressing "fibroblast-like cells" in diabetic and idiopathic gastroparesis of humans. *Neurogastroenterol Motil* 2012; **24**: 844-852 [PMID: 22650155 DOI: 10.1111/j.1365-2982.2012.01944.x]
- 26 **Graham KD**, López SH, Sengupta R, Shenoy A, Schneider S, Wright CM, Feldman M, Furth E, Valdivieso F, Lemke A, Wilkins BJ, Naji A, Doolin EJ, Howard MJ, Heuckeroth RO. Robust, 3-Dimensional Visualization of Human Colon Enteric Nervous System Without Tissue Sectioning. *Gastroenterology* 2020; **158**: 2221-2235.e5 [PMID: 32113825 DOI: 10.1053/j.gastro.2020.02.035]
- 27 **Norvik C**, Westöö CK, Peruzzi N, Lovric G, van der Have O, Mokso R, Jeremiasen I, Brunnström H, Galambos C, Bech M, Tran-Lundmark K. Synchrotron-based phase-contrast micro-CT as a tool for understanding pulmonary vascular pathobiology and the 3-D microanatomy of alveolar capillary dysplasia. *Am J Physiol Lung Cell Mol Physiol* 2020; **318**: L65-L75 [PMID: 31596108 DOI: 10.1152/ajplung.00103.2019]
- 28 **Westöö C**, Norvik C, Peruzzi N, van der Have O, Lovric G, Jeremiasen I, Tran PK, Mokso R, de Jesus Perez V, Brunnström H, Bech M, Galambos C, Tran-Lundmark K. Distinct types of plexiform lesions identified by synchrotron-based phase-contrast micro-CT. *Am J Physiol Lung Cell Mol Physiol* 2021; **321**: L17-L28 [PMID: 33881927 DOI: 10.1152/ajplung.00432.2020]
- 29 **Frohn J**, Pinkert-Leetsch D, Missbach-Güntner J, Reichardt M, Osterhoff M, Alves F, Salditt T. 3D virtual histology of human pancreatic tissue by multiscale phase-contrast X-ray tomography. *J Synchrotron Radiat* 2020; **27**: 1707-1719 [PMID: 33147198 DOI: 10.1107/S1600577520011327]
- 30 **Reichardt M**, Frohn J, Khan A, Alves F, Salditt T. Multi-scale X-ray phase-contrast tomography of murine heart tissue. *Biomed Opt Express* 2020; **11**: 2633-2651 [PMID: 32499949 DOI: 10.1364/BOE.386576]
- 31 **Eckermann M**, Schmitzer B, van der Meer F, Franz J, Hansen O, Stadelmann C, Salditt T. Three-dimensional virtual histology of the human hippocampus based on phase-contrast computed tomography. *Proc Natl Acad Sci U S A* 2021; **118** [PMID: 34819378 DOI: 10.1073/pnas.2113835118]
- 32 **Goodarzi N**, Akbari Bazm M, Poladi S, Rashidi F, Mahmoudi B, Abumandour MMA. Histology of the small intestine in the common pheasant (*Phasianus colchicus*): A scanning electron microscopy, histochemical, immunohistochemical, and stereological study. *Microsc Res Tech* 2021; **84**: 2388-2398 [PMID: 33908129 DOI: 10.1002/jemt.23794]
- 33 **Eckermann M**, Ruhwedel T, Möbus W, Salditt T. Towards correlative imaging of neuronal tissue by phase-contrast x-ray tomography and SEM. *Proceedings of the SPIE* 2021; **11840**: 29-36 [DOI: 10.1117/12.2596133]

## Recurrence rates after endoscopic resection of large colorectal polyps: A systematic review and meta-analysis

Carola Rotermund, Roupen Djinbachian, Mahsa Taghiakbari, Markus D Enderle, Axel Eickhoff, Daniel von Renteln

**Specialty type:** Gastroenterology and hepatology

**Provenance and peer review:** Invited article; Externally peer reviewed.

**Peer-review model:** Single blind

**Peer-review report's scientific quality classification**

Grade A (Excellent): A  
Grade B (Very good): 0  
Grade C (Good): C  
Grade D (Fair): 0  
Grade E (Poor): 0

**P-Reviewer:** Gao W, China; Yu T, China

**Received:** March 30, 2022

**Peer-review started:** March 30, 2022

**First decision:** April 25, 2022

**Revised:** May 11, 2022

**Accepted:** July 8, 2022

**Article in press:** July 8, 2022

**Published online:** August 7, 2022



**Carola Rotermund, Markus D Enderle**, Research and Basic Technologies, ERBE Elektromedizin GmbH, Tuebingen 72072, Germany

**Roupen Djinbachian**, Division of Internal Medicine, Montreal University Hospital Center, Montreal QC H2X 3E4, Canada

**Mahsa Taghiakbari, Daniel von Renteln**, Montreal University Hospital Research Center, Montreal University Hospital Center, Montreal QC H2X 3E4, Canada

**Axel Eickhoff**, Department of Internal Medicine II, Klinikum Hanau, Hanau 63450, Germany

**Corresponding author:** Daniel von Renteln, MD, Associate Professor, Montreal University Hospital Research Center, Montreal University Hospital Center, 1051 Rue Sanguinet, Montreal QC H2X 3E4, Canada. [danielrenteln@gmail.com](mailto:danielrenteln@gmail.com)

### Abstract

#### BACKGROUND

Complete polyp resection is the main goal of endoscopic removal of large colonic polyps. Resection techniques have evolved in recent years and endoscopic submucosal dissection (ESD), endoscopic mucosal resection (EMR) with margin ablation, cold snare polypectomy (CSP), cold EMR, and underwater EMR have been introduced. Yet, efficacy of these techniques with regard to local recurrence rates (LRRs) *vs* traditional hot snare polypectomy and standard EMR remains unclear.

#### AIM

To analyze LRR of large colonic polyps in a systematic review and meta-analysis.

#### METHODS

MEDLINE, EMBASE, EBM Reviews, and CINAHL were searched for prospective studies reporting LRR or incomplete resection rate (IRR) after colonic polypectomy of polyps  $\geq 10$  mm, published between January 2011 and July 2021. Primary outcome was LRR for polyps  $\geq 10$  mm.

#### RESULTS

Six thousand nine hundred and twenty-eight publications were identified, of which 34 prospective studies were included. LRR for polyps  $\geq 10$  mm at up to 12 mo' follow-up was 11.0% (95%CI, 7.1%-14.8%; 15 studies; 4904 polyps). ESD

(1.7%; 95% CI, 0%-3.4%; 3 studies, 221 polyps) and endoscopic mucosal resection with margin ablation (3.3%; 95% CI, 2.2%-4.5%; 2 studies, 947 polyps) significantly reduced LRR *vs* standard EMR without (15.2%; 95% CI, 12.5%-18.0%; 4 studies, 650 polyps) or with unsystematic margin ablation (16.5%; 95% CI, 15.2%-17.8%; 6 studies, 3031 polyps).

### CONCLUSION

LRR is significantly lower after ESD or EMR with routine margin ablation; thus, these techniques should be considered standard for endoscopic removal of large colorectal polyps. Other techniques, such as CSP, cold EMR, and underwater EMR require further evaluation in prospective studies before their routine implementation in clinical practice can be recommended.

**Key Words:** Colonoscopy; Adenoma; Polyp; Endoscopic mucosal resection; Colorectal cancer

©The Author(s) 2022. Published by Baishideng Publishing Group Inc. All rights reserved.

**Core Tip:** Complete polyp resection is the main goal of endoscopic removal of large colonic polyps. Resection techniques have evolved in recent years and endoscopic submucosal dissection, endoscopic mucosal resection (EMR) with margin ablation, cold snare polypectomy, cold EMR, and underwater EMR have been introduced. Yet, efficacy of these techniques with regard to local recurrence rates (LRRs) *vs* traditional hot snare polypectomy and standard EMR remains unclear. We aimed to analyze LRR of large colonic polyps in a systematic review and meta-analysis.

**Citation:** Rotermund C, Djinbachian R, Taghiakbari M, Enderle MD, Eickhoff A, von Renteln D. Recurrence rates after endoscopic resection of large colorectal polyps: A systematic review and meta-analysis. *World J Gastroenterol* 2022; 28(29): 4007-4018

**URL:** <https://www.wjgnet.com/1007-9327/full/v28/i29/4007.htm>

**DOI:** <https://dx.doi.org/10.3748/wjg.v28.i29.4007>

## INTRODUCTION

Complete endoscopic polyp removal is especially important for large colorectal polyps in order to prevent local polyp recurrence and progression to colorectal cancer[1]. Evidence is growing that polyp removal is frequently incomplete, putting patients at risk of developing post-colonoscopy cancer[2-4]. A meta-analysis published in 2020 found that after snare resection, 15.9% of diminutive and small polyps and 20.8% of polyps 10-19 mm are removed incompletely[5]. For polyps 20 mm or larger, a meta-analysis published in 2014 demonstrated a recurrence rate of 15% after endoscopic mucosal resection (EMR)[6].

In recent years, different techniques for endoscopic resection of large colorectal polyps have evolved or been developed. Cold snare polypectomy (CSP) has been introduced and its use expanded to include the removal of large colorectal polyps[7]. Endoscopic submucosal dissection (ESD) has gained traction in Western countries and EMR has undergone technical modifications by introducing margin ablation or underwater EMR[8,9].

These developments have sparked our interest in providing an up-to-date meta-analysis of local recurrence rates (LRRs) and incomplete resection rates (IRRs) for large ( $\geq 10$  mm) colorectal polyps, and to evaluate the impact of the novel or modified endoscopic resection techniques on LRRs.

## MATERIALS AND METHODS

The analysis was conducted adhering to the Preferred Reporting Items for Systematic Reviews and Meta-analysis statement[10].

### Literature search

A systematic literature search was performed within MEDLINE, EMBASE, EBM Reviews, and CINAHL databases. All articles published between January 2011 and July 2021 reporting on IRR and/or LRR for colorectal polyps 10 mm or larger removed by endoscopic resection techniques were included in the search. For specific search terms, see [Supplementary Table 1](#). Additionally, a secondary search was performed to identify further records using article reference crosscheck, manual searching, and expert contact.

### Article selection

Articles retrieved by the systematic search were collected and duplicates removed. Two researchers (Rotermund C and Taghiakbari M) assessed all articles independently and decided upon inclusion and exclusion. In cases of disagreement, a third researcher (von Renteln D) was consulted.

Inclusion criteria were full-text articles of prospectively performed clinical studies reporting on either LRR or IRR evaluated by margin assessment or margin biopsy of endoscopically removed polyps  $\geq 10$  mm. Even though often of larger sample size, publications with retrospective study design were excluded from the analysis, as risk for selection bias and risk for missed data is usually higher.

Exclusion criteria were retrospective study design, polyps  $< 10$  mm, IRR evaluated by visual margin assessment, data from first follow-up that exceeded 12 mo, publications solely evaluating difficult polypectomies, publication languages other than English, articles reporting on training of a certain technique, and articles in which results from different polypectomy techniques were not clearly distinguishable.

### Data extraction

Relevant data retrieved from the evaluated study included author, year of publication, country, study type, study quality, polyp size, polyp morphology, polyp histology, polyp resection method and adjunct therapy, LRR, IRR, IRR assessment method, submucosal injection rate and solution, *en bloc* resection rate, and endoscopist number and experience level. For analyses, polyps were subdivided according to size: 10–19 mm,  $\geq 20$  mm (not including polyps  $< 20$  mm), and all polyps  $\geq 10$  mm (including polyps  $\geq 20$  mm). Data were retrieved by one author (Rotermund C) and correct retrieval confirmed by a second author (Djinbachian R).

### Outcomes

Primary outcome was LRR for polyps  $\geq 10$  mm. Local recurrence was defined as the presence of recurrent polyp at the resection site, detected during follow-up examination. Publications, in which the appointments for follow-up examinations exceeded 12 mo between the different patients, were excluded from the analysis. Secondary outcomes were IRR evaluated by either margin assessment or margin biopsy for polyps  $\geq 10$  mm, as well as factors influencing LRR and IRR, including polyp resection technique [hot snare polypectomy (HSP), CSP, hot and cold EMR, underwater EMR, ESD], adjunct therapy, margin assessment method, submucosal injection status, polyp size, polyp morphology and histology, endoscopist experience and number of endoscopists involved. IRR assessment method was defined as (1) Biopsy from the resection margin (=“margin biopsy”); (2) Histologic assessment of polyp margin (= “margin assessment”); and (3) *En bloc* resection and histologic assessment of polyp margin (= “*en bloc* and margin assessment”). Endoscopist experience was defined as (1) Less experienced for EMR, when a fellow was included in the study or  $< 2000$  colonoscopies had been performed by the endoscopist; (2) Experienced for EMR, when only expert endoscopists ( $> 2000$  colonoscopies) were involved; (3) Less experienced for ESD, when fellows for ESD ( $< 200$  cases) were included in the study; and (4) Experts for ESD ( $> 200$  cases).

### Quality assessment and publication bias

Study quality was assessed independently by two researchers (Taghiakbari M and Rotermund C). In cases of disagreement, a third researcher (von Renteln D) was consulted. For evaluation, National Institutes of Health quality assessment forms for case series and randomized controlled trials (RCTs) were used[11]. For RCTs (maximum score: 14), a score of 11–14 was rated as good, a score of 8–10 as fair, and a score below 8 as poor quality. For prospective case series (maximum score: 9), a score of 7–9 was rated as good, a score of 4–6 as fair, and a score below 4 as poor quality. Detailed information on criteria for low and high quality are given in [Supplementary Tables 2 and 3](#).

A sensitivity analysis was performed to determine the effects of excluding poor-quality studies and publication bias was assessed using funnel plots ([Supplementary Figure 1](#)). The graph was plotted as proportion vs. sample size instead of log odds vs 1/standard error, as this method has been shown to be more accurate in predicting risk of publication bias for meta-analyses of proportions[12].

### Statistical analysis

Proportions were meta-analyzed using the metaprop command of Stata version 16 (StataCorp, College Station, TX, United States), and tests of heterogeneity were performed using the  $I^2$  statistic. Either a random-effects model or a fixed-effect model was used for the analyses. Proportions were reported with their associated 95% confidence intervals (CIs) with an alpha level of  $< 0.05$  used for statistical significance.

## RESULTS

### Literature search and study characteristics

Systematic literature search yielded 6922 hits and 6 additional records were identified through reference crosscheck, manual search, and expert contact (Figure 1, Supplementary Table 1). After removal of duplicates, 5010 publications remained. Of these, 4070 were excluded based on title and 672 based on abstract, so that 268 full-text records were evaluated for eligibility. Ultimately, 34 publications were included in the analysis, with 19 reporting on IRR, 13 on LRR, and 2 on both (Figure 1). All studies were prospective and 14 were RCTs.

### Quality assessment and publication bias

Included studies showed symmetrical distribution for both assessments of LRR and IRR, with no publication bias detected (Supplementary Figure 1). Quality assessment revealed 23 studies of good quality, 10 studies of fair quality, and 1 study of poor quality (Supplementary Tables 2 and 3). Sensitivity analyses did not show statistically different results or decreased heterogeneity when excluding poor- or fair-quality studies (Supplementary Figures 2 and 3).

### Local recurrence rate

A total of 15 studies reported on LRR after removal of large colonic polyps  $\geq 10$  mm. Of these, 15 studies stated LRR obtained during follow-up examinations up to 12 mo, 7 during follow-up up to 24 mo, and 3 from follow-up after more than 24 mo (Supplementary Table 4). Definitions of LRR given in the original studies are presented in Supplementary Table 5. Mean overall LRR at up to 12 mo' follow-up was 11.0% (95%CI, 7.1%–14.8%; 4904 polyps) (Figure 2A). Overall LRR for follow-up up to 24 mo was 14.6% (95%CI, 8.4%–20.8%; 7 studies) (Supplementary Figure 4).

**Local recurrence rate up to 12 mo' follow-up: Influence of resection method:** Resection method was found to exhibit major influence on LRR of polyps  $\geq 10$  mm (Figure 2B, Table 1). ESD (1.7%; 95%CI, 0–3.4%; 3 studies) and EMR with margin ablation (3.3%; 95%CI, 2.2%–4.5%; 2 studies) significantly reduced LRR compared with EMR in which margin ablation was not performed (15.2%; 95%CI, 12.5%–18.0%; 4 studies) or only used in some cases (16.5%; 95%CI, 15.2%–17.8%; 6 studies). No prospective studies were found evaluating LRR after HSP, CSP, or cold EMR within the search period. Two studies evaluated LRR after underwater EMR; however, heterogeneity between studies was high, so that a valid analysis could not be performed.

Similarly, when only results for polyps  $\geq 20$  mm were evaluated, ESD and EMR with margin ablation yielded lower LRRs compared with EMR without margin ablation (Table 1). No prospective studies were found evaluating HSP, CSP, or cold EMR.

**Local recurrence rate up to 12 mo' follow-up: further influencing factors:** Polyp size did not influence LRR ( $\geq 10$  mm: 11.0%; 95%CI, 7.1%–14.8%; 15 studies *vs*  $\geq 20$  mm: 11.2%; 95%CI, 6.8%–15.6%; 12 studies) (Table 1). Similarly, expert status of the endoscopist was not found to influence LRR (Table 1); however, as only two expert studies were found, the data set was small. The data set was also insufficient for analysis of the influence of polyp morphology or histology on LRR. Only one study included pedunculated polyps (12.1% of all resected polyps); however, the reported LRR was comparable to the rate observed in other studies[13]. Most studies included sessile serrated adenoma/polyps (SSA/Ps). One study compared LRR after EMR removal of SSA/Ps *vs* conventional adenomas and reported significantly reduced LRR for SSA/Ps[14].

### Incomplete resection rate

A total of 21 studies reported on IRR after removal of large colonic polyps  $\geq 10$  mm, using either margin assessment or margin biopsy for evaluation (Supplementary Table 6). Mean overall IRR for all polyps  $\geq 10$  mm was 14.9% (95%CI, 11.4%–18.4%; 21 studies; 3563 polyps) (Figure 3). Twelve studies indicated IRR for polyps 10–19 mm, resulting in a mean IRR of 16.0% (95%CI, 10.4–21.7%) (Supplementary Figure 5), and 14 studies reported IRR for polyps  $\geq 20$  mm, yielding a mean IRR of 11.7% (95%CI, 7.5%–15.8%; 1739 polyps) (Supplementary Figure 6).

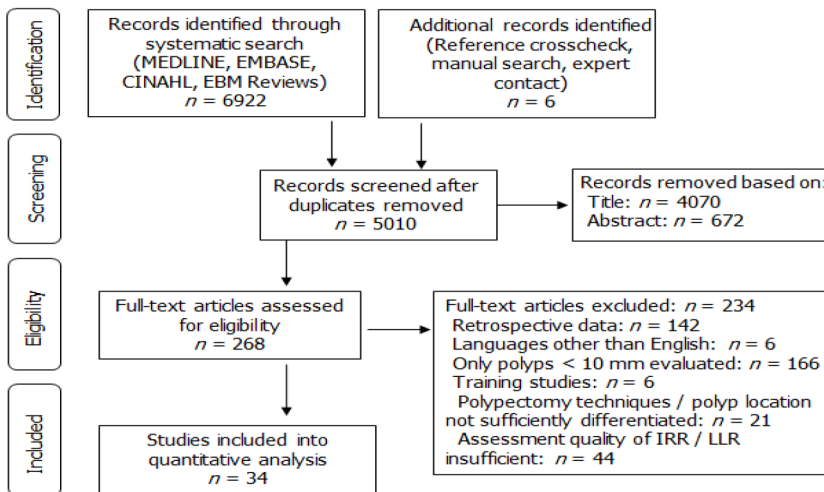
**Incomplete resection rate: Influence of resection method:** Resection method was not found to significantly influence IRR of polyps 10–19 mm, comparing hot EMR (18.5%; 95%CI, 8.9%–28.1%; 8 studies), HSP (16.2%; 95%CI, 10.6%–21.7%; 2 studies), underwater EMR (25.5%; 95%CI, 18.9%–32.2%; 2 studies), and cold EMR (14.0%; 95%CI, 1.8%–26.3%; 3 studies), with studies on cold EMR exhibiting high variability (Table 2). Only two studies evaluated CSP, showing high heterogeneity, so that a valid analysis could not be performed.

Comparison of ESD and EMR for polyps  $\geq 20$  mm showed a lower IRR for ESD (12.5%; 95%CI, 6.2%–18.8%; 9 studies) than for EMR (29.3%; 95%CI, 19.3%–39.2%; 3 studies) (Table 2). Only two studies evaluated IRR for polyps  $\geq 20$  mm with HSP, yielding high heterogeneity, so that a valid analysis could not be performed. No data were found reporting IRR after CSP or cold EMR for polyps  $\geq 20$  mm.

**Table 1** Factors influencing local recurrence for polyps ≥ 10 mm at 0–12 mo' follow-up

Subgroups	LRR % (95%CI)	P %	Studies, n	Polyps, n
Resection method, polyps ≥ 10 mm				
Hot EMR, no margin ablation	15.2 (12.5–18.0)	0	4	650
Hot EMR, some margin ablation	16.5 (15.2–17.8)	0	6	3013
Hot EMR, with margin ablation	3.3 (2.2–4.5)	NA	2	947
ESD	1.7 (0.0–3.4)	NA	3	221
Resection method, polyps ≥ 20 mm				
Hot EMR, no margin ablation	14.8 (11.0–18.5)	NA	2	334
Hot EMR, some margin ablation	16.5 (15.2–17.8)	0	6	3013
Hot EMR, with margin ablation	3.3 (2.2–4.5)	NA	2	947
ESD	2.4 (0–5.7)	NA	2	83
Polyp size				
≥ 10 mm	11.0 (7.1–14.8)	95.6	15	4904
≥ 20 mm	11.2 (6.8–15.6)	95.8	12	4431
Expert level				
Only expert endoscopists	13.3 (11.1–15.6)	NA	2	3712
Including non-expert endoscopists	11.8 (6.8–16.8)	95.8	9	837
Not defined	9.2 (1.5–16.9)	93.7	4	524

NA: Number of studies insufficient for estimation; EMR: Endoscopic mucosal resection; ESD: Endoscopic submucosal dissection; LRR: Local recurrence rate.



DOI: 10.3748/wjg.v28.i29.4007 Copyright ©The Author(s) 2022.

**Figure 1** Literature search strategy.

**Incomplete resection rate: Further influencing factors:** For polyps sized 10–19 mm, submucosal injection status did not influence IRR. Mean IRR after resection with submucosal injection was 20.0% (95%CI, 11.9%–28.0%; 10 studies) compared with 14.4% (95%CI, 5.4%–23.3%; 6 studies) after resection without submucosal injection (Table 2). For polyps ≥20 mm, IRR was lower after resection with prior submucosal injection (Table 2). Mean IRR after submucosal injection was 12.6% (95%CI 7.7–17.6; 13 studies), compared to 32.4% (95%CI, 0-76.3%; 3 studies) after resection without injection.

The solution used for submucosal injection was not found to influence IRR, yielding comparable results for saline solution (15.8%, 95%CI, 7.1%–24.8%; 6 studies) and hyaluronic acid (16.3%, 95%CI, 8.5%–24.1%; 8 studies) (Table 2).

**Table 2** Factors influencing incomplete resection

Subgroups	IRR % (95%CI)	P %	Studies, n	Polyps, n
Resection method, polyps 10–19 mm				
Hot EMR	18.5 (8.9–28.1)	93.2	8	655
HSP	16.2 (10.6–21.7)	NA	2	167
U-EMR	25.5 (18.9–32.2)	NA	2	160
Cold EMR <sup>1</sup>	14.0 <sup>1</sup> (1.8–26.3)	NA	3	334
Resection method, polyps ≥ 20 mm				
ESD	12.5 (6.2–18.8)	95.0	9	1452
Hot EMR	29.3 (19.3–39.2)	NA	3	88
Submucosal injection, polyps 10–19 mm				
No injection	14.4 (5.4–23.3)	95.8	6	836
Injection	20.0 (11.9–28.0)	93.9	10	989
Submucosal injection, polyps ≥ 20 mm				
No injection	32.4 (0–76.3)	96.2	3	124
Injection	12.6 (7.7–17.6)	94.4	13	1614
Injection solution, polyps ≥ 10 mm				
Saline solution	15.8 (7.1–24.6)	95.6	6	774
Hyaluronic acid	16.3 (8.5–24.1)	95.1	8	916
Expert level				
Only expert endoscopists	7.0 (3.5, 10.4)	93.7	8	1451
Including non-expert endoscopists	20.3 (13.5–27.1)	96.0	13	2092
Method of margin evaluation, polyps 10–19 mm				
Margin assessment	18.6 (10.9, 26.2)	75.1	5	380
Margin biopsy	5.7 (1.1, 10.3)	95.1	5	1150
Method of margin evaluation, polyps ≥ 20 mm				
Margin assessment	21.8 (9.4–34.2)	92.1	4	429
Margin assessment and <i>en bloc</i> resection	14.1 (5.7–22.6)	96.0	7	1106
Margin biopsy	0.4 (0–2.5)	55.8	3	203

<sup>1</sup>Data exhibit high variance; calculated mean should be handled with care.

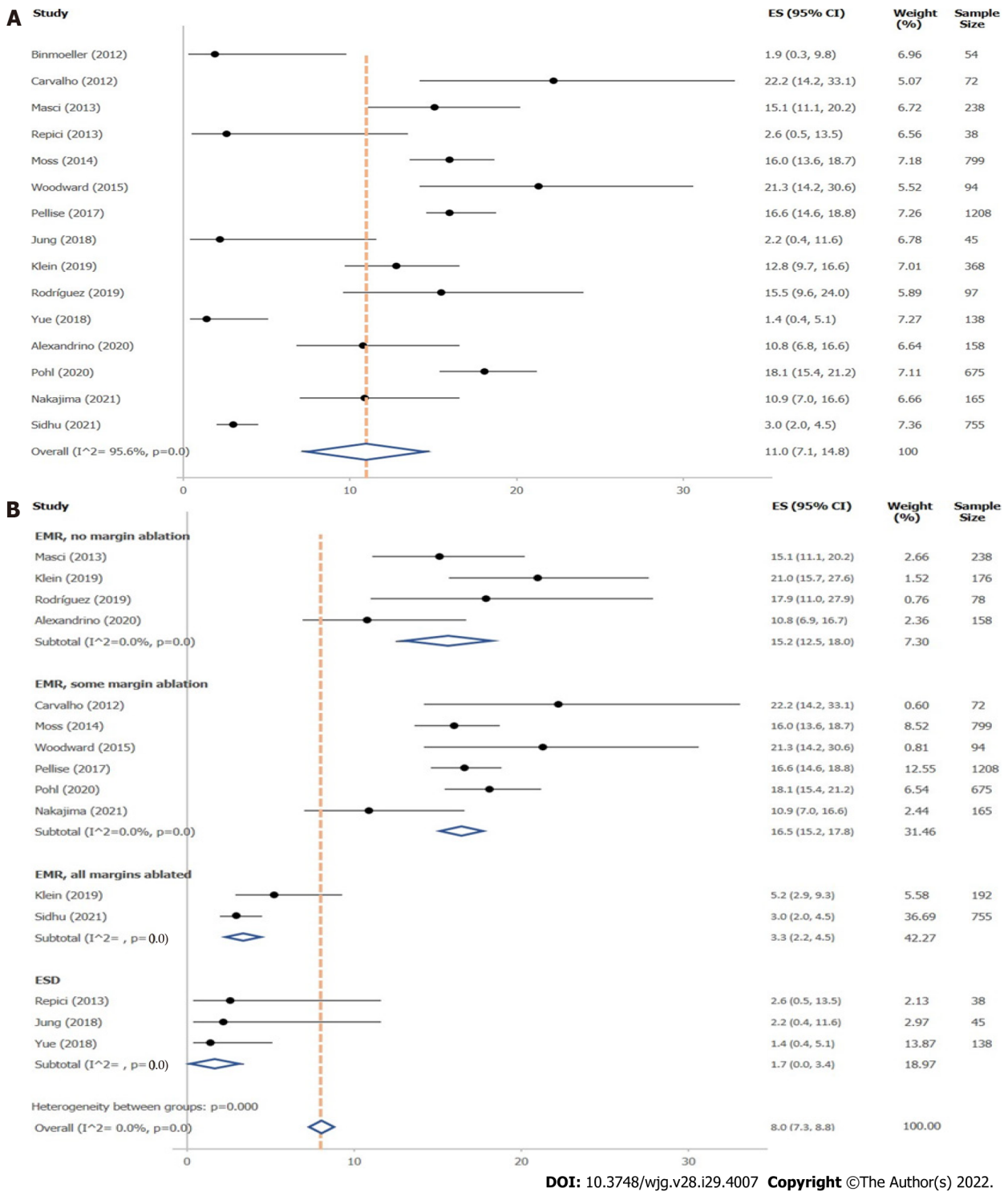
NA: Number of studies insufficient for estimation; EMR: Endoscopic mucosal resection; ESD: Endoscopic submucosal dissection; HSP: Hot snare polypectomy; IRR: Incomplete resection rate; U-EMR: Underwater endoscopic mucosal resection.

There was a strong trend toward lower IRR when considering endoscopist experience (Table 2, Supplementary Figure 7). The mean IRR was 7.0% (95%CI, 3.5%–10.4%; 8 studies) when only expert endoscopists were involved in the study, and 20.3% (95%CI, 13.5%–27.1%; 13 studies) when non-experts were included.

Insufficient data were available for analysis of the influence of polyp morphology or histology on IRR. Three studies included around 50% or more pedunculated polyps; two analyzed hot EMR[15,16], and the third analyzed hot and cold EMR and CSP[17]. Three further studies included smaller numbers of pedunculated polyps, using cold EMR[18], ESD[19], and underwater EMR[20]. Most studies included 10% or less SSA/Ps, while two studies investigating CSP and cold EMR evaluated results from SSA/Ps only[21,22]. The latter two studies reported exceptionally low IRR of less than 1.5%.

## DISCUSSION

This meta-analysis confirms the high risk for recurrence after standard EMR resection of large colonic



DOI: 10.3748/wjg.v28.i29.4007 Copyright ©The Author(s) 2022.

Figure 2 Local recurrence rate at < 12 mo' follow-up. A: For polyps ≥ 10 mm; B: For polyps ≥ 10 mm, stratified by resection method.

polyps. When standard EMR without routine margin ablation is used, we found a 12-month recurrence rate of 15.2%. This is comparable to the results found in the two available meta-analyses published in 2014 and 2021, which reported recurrence rates of 15% [6] and 10% [23], respectively. However, since then, many new or modified endoscopic removal techniques have been developed. These novel developments include cold EMR, hot snare with margin ablation, and an increasing body of literature on ESD for colorectal polyps coming from Asian, European and North American centers. We found that two of these modalities resulted in significantly lower LRRs compared with standard EMR. ESD was associated with an LRR of only 1.7%, and the LRR after EMR with routine ablation of the complete margin was 3.3%. However, ESD requires advanced endoscopy skills, adequate training, and the technique is associated with an increased risk for complications [24-26]. Furthermore, significant differences in safety and efficacy of ESD have been shown between Asian and non-Asian countries [27], so that EMR has remained the standard for large polyp resection in Western countries to date.

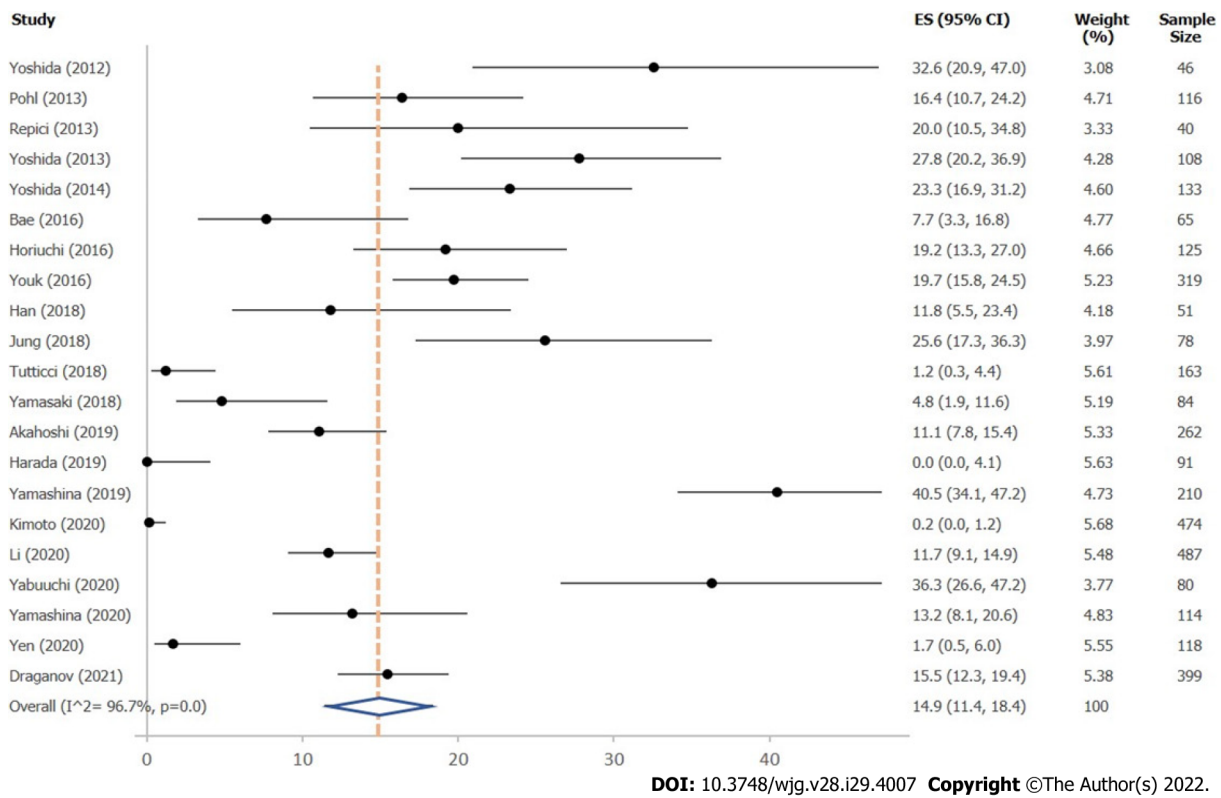


Figure 3 Incomplete resection rate for polyps ≥ 10 mm, independent of resection method.

The other modality that shows significantly reduced recurrence rates is the combination of hot EMR with routine margin ablation[9,28]. Thus, ESD or EMR with routine margin ablation currently seem to be the best approaches for endoscopic removal of large colorectal polyps in order to avoid recurrence. We found that systematic margin ablation after EMR can reduce the LRR to rates similar to those of ESD. These results originate from two recent Australian prospective studies, in which snare tip soft coagulation (STSC) was routinely performed after EMR[9,28]. As these studies included only polyps ≥ 20 mm further studies evaluating the effect of margin ablation on polyps sized 10-19 mm may be of additional value. The positive effect of margin ablation has also been shown in a retrospective US study, evaluating systematic application of argon plasma coagulation (APC) after EMR in 246 patients[29]. The authors found an LRR of 5% at < 12 mo FU, which is comparable to the rates found by Klein (5%) [9] and Sidhu (3%)[28]. However, the results for using APC margin ablation still need to be confirmed by prospective studies. A recently completed prospective, multicenter study evaluating resection of large colonic lesions ≥ 20 mm in 76 patients using EMR and hybrid APC for margin and base ablation found a LRR of 2.2%[30]. This indicates that APC ablation can reduce local recurrence comparable to ESD and EMR with STSC.

Importantly, margin ablation should be performed systematically and completely, as visual margin assessment may underestimate incomplete resection[4]. This is confirmed by our analysis, which showed that studies using unsystematic or incomplete margin ablation were not able to reduce the LRR [9,14,31].

Notably, even though use of cold snare resection techniques for large colonic polyps is increasingly reported, at present no prospective studies have been published reporting LRR for CSP or cold EMR for large colorectal polyps. Furthermore, recent retrospective studies have indicated that these techniques might potentially increase the risk for local recurrence. In the largest retrospective series published to date, Suresh *et al*[32] reported an LRR of 34.8% after cold EMR. Therefore, caution is warranted for routine use of cold EMR outside of clinical studies until data from ongoing RCTs comparing hot with cold EMR become available.

For polyps 10–19 mm, follow-up examination is often performed years after the index colonoscopy. Therefore, data on LRR for 10–19 mm colorectal polyps are sparse, and we used IRR to estimate the risk of local recurrence for this subgroup. In our analysis, overall IRR for polyps sized 10–19 mm was 16.0%. This rate was similar to the IRR found in a previous meta-analysis (20.8%)[5] and in one of the landmark studies on IRR (CARE study)[4]. The CARE study reported that even though endoscopists rated resection as complete by visual assessment, 10.1% of cases showed residual tissue on margin biopsy. Compared with the previous meta-analysis, our analysis included more data, especially regarding cold snare resection techniques[5]. However, adding the recently published data on cold snare resection did not significantly alter overall IRR of polyps 10–19 mm. Furthermore, IRR of EMR, cold EMR, HSP, and

underwater EMR were similar[17,18,21]. Only two prospective studies evaluated IRR for large colonic polyps after CSP resection[17,21]. These studies showed high variability in IRR, and while one study found rates comparable to those obtained with other techniques[17], rates reported in the second were extremely low[21]. This is likely based on the fact that in this study only expert endoscopists were involved and only SSA/Ps were removed by wide-field style cold snare resection. A previous meta-analysis has already demonstrated that expert endoscopists achieve lower IRRs[5], and this was confirmed in our analysis, with an IRR of 7.0% for expert endoscopists and 20.3% for those studies in which less experienced endoscopists were included. Furthermore, the exclusive inclusion of SSA/Ps introduced a further bias into the study, as removal of SSA/Ps generally yields better results[14]. This renders the generalizability of CSP to general clinical practice difficult, and more prospective studies are needed to establish IRR, and especially LRR risk, after CPS and cold EMR removal of large colorectal polyps including all pathology types.

For polyps  $\geq 20$  mm, the mean IRR was 11.7% in this analysis. Interestingly, this rate is lower than the results obtained for polyps sized 10–19 mm (16.0%). This effect was based on the good results obtained with ESD, and is most likely also associated with the fact that 10–19 mm polyps are usually resected in general endoscopic practice, whereas polyps  $\geq 20$  mm are often referred for expert resection.

Recent guidelines recommend HSP, EMR [European Society of Gastrointestinal Endoscopy, American Gastroenterological Association (AGA)][33,34] and CSP (AGA)[34] for resection of 10–19 mm polyps. Our data show that EMR with margin ablation is an important new development that warrants further study. For lesions  $\geq 20$  mm, guidelines recommend ESD in specific cases, and the need for a skilled endoscopist to perform the procedure is highlighted[25,26,35]. The importance of endoscopist skill level is also supported by our data. Furthermore, our data suggest that EMR with systematic and complete margin ablation may be an appropriate alternative to ESD, especially considering the low complication rates reported in the available studies[9,28,29].

However, safety profiles should also be taken into account when evaluating different polypectomy techniques. Known complications occurring during and after polypectomy are immediate and delayed bleeding as well as perforation and post-coagulation syndrome[33,34]. A meta-analysis from 2016 evaluating endoscopic resection of polyps  $\geq 20$  mm found perforation occurring in 1.5% and bleeding in 6.5% of polyps. Mortality was indicated as 0.08%[36]. Yet, an up-to-date analysis comparing safety profiles of CSP, HSP, EMR with and without margin ablation, underwater EMR, and ESD still has to be performed.

Our analysis has several strengths, including the robustness of the literature search with a large number of publications screened (6928 publications). Of these, 34 prospective studies with a total of 10268 polyp resections were included. As only prospective data were evaluated, we were able to perform a high-quality analysis, as retrospective studies reporting on LRR and IRR are unsystematic in the ascertainment of the main outcomes, thus having a high likelihood of bias. Furthermore, the retrieval of granular data allowed us to perform multiple analyses.

The main limitation of the study is that by exclusion of retrospective studies, the data set was reduced. Furthermore, publications were excluded in which IRR was determined by visual assessment or in which appointments for follow-up examinations for LRR assessment exceeded 12 mo. While this reduced the amount of studies included into the analysis, it ensured a better overview of the high-quality data available in the literature. Additionally, it shows that for some techniques data of sufficient quality is sparse and that there is a need for further studies. Second, expert endoscopist status was difficult to determine, as there is no published consensus definition, and some studies do not clarify the expertise of the involved endoscopists. However, expert and non-expert status were systematically assessed and discussed for this meta-analysis. Third, as assessment for IRR is not standardized, different methods, including margin assessment and margin biopsy, are used for its estimation. However, margin assessment is likely to overestimate IRR, as lesions resected in piecemeal fashion may be resected completely, but will appear with positive resection margins. Margin biopsy, on the other hand, is likely to underestimate IRR, as only sample parts of the margins are examined[37]. Therefore, true IRR will be located somewhere in between the values found with margin biopsy and margin assessment. Another limitation is the elevated heterogeneity in some reported outcomes. For LRR, most of the observed heterogeneity was due to combining different resection techniques into the same analysis. When stratifying for resection technique and use of margin ablation, we found very low heterogeneity in the reported outcomes. For IRR, the differing use of wide field resection before biopsies and the number of margin biopsies taken could explain some of the heterogeneity reported.

---

## CONCLUSION

---

In conclusion, we found that local recurrence after resection of large colonic polyps occurs frequently when standard EMR is used. Local polyp recurrence can be reduced by performing ESD or EMR with routine and complete margin ablation. Other techniques, such as CSP, cold EMR, and underwater EMR require further evaluation in prospective studies before their routine implementation in clinical practice can be recommended.

## ARTICLE HIGHLIGHTS

### Research background

Complete resection is the aim of endoscopic therapy for large colonic polyps. Endoscopic mucosal resection (EMR) is the most common endoscopic treatment for such polyps. In recent years, endoscopic resection techniques have evolved, including cold snare polypectomy (CSP), cold EMR, EMR with margin ablation, underwater EMR, and endoscopic submucosal dissection (ESD).

### Research motivation

Efficacy of these newer polypectomy techniques with regard to local recurrence rates (LRRs) *vs* traditional hot snare polypectomy and standard EMR remains unclear.

### Research objectives

These developments have sparked our interest in providing an up-to-date meta-analysis of LRRs and incomplete resection rates (IRRs) for large ( $\geq 10$  mm) colorectal polyps, and to evaluate the impact of the novel or modified endoscopic resection techniques on LRRs.

### Research methods

A systematic literature search was performed within MEDLINE, EMBASE, EBM Reviews, and CINAHL databases. All articles published between January 2011 and July 2021 reporting on IRR and/or LRR for colorectal polyps 10 mm or larger removed by endoscopic resection techniques were included in the search.

### Research results

LRR were lowest when EMR with systematic margin ablation (3.3%) or ESD (1.7%) were used for endoscopic removal of large ( $> 10$  mm) colorectal polyps. When standard EMR (without margin ablation) or with partial margin ablation were used, LRRs were high (15.2% and 16.5%, respectively).

### Research conclusions

Local recurrence after resection of large colonic polyps occurs frequently when standard EMR is used, but can be reduced by performing ESD or EMR with routine and complete margin ablation. Other techniques, such as CSP, cold EMR, and underwater EMR require further evaluation in prospective studies before their routine implementation in clinical practice can be recommended.

### Research perspectives

ESD or EMR with margin ablation should be considered standard of care for endoscopic removal of large colorectal polyps in order to avoid recurrence. At present, cold snare resection techniques or underwater EMR should only be performed within clinical trials, pending the availability of high-quality evidence.

## FOOTNOTES

**Author contributions:** von Renteln D designed the research study; von Renteln D, Rotermund C, Djinbachian R, Taghiakbari M, Enderle MD, and Eickhoff A performed the research; von Renteln D, Rotermund C, Djinbachian R, and Taghiakbari M analyzed the data; and von Renteln D, Rotermund C, and Djinbachian R wrote the manuscript; and All authors have read and approve the final manuscript.

**Conflict-of-interest statement:** All authors report no relevant conflicts of interest for this article.

**PRISMA 2009 Checklist statement:** The authors have read the PRISMA 2009 Checklist, and the manuscript was prepared and revised according to the PRISMA 2009 Checklist.

**Open-Access:** This article is an open-access article that was selected by an in-house editor and fully peer-reviewed by external reviewers. It is distributed in accordance with the Creative Commons Attribution NonCommercial (CC BY-NC 4.0) license, which permits others to distribute, remix, adapt, build upon this work non-commercially, and license their derivative works on different terms, provided the original work is properly cited and the use is non-commercial. See: <https://creativecommons.org/licenses/by-nc/4.0/>

**Country/Territory of origin:** Canada

**ORCID number:** Daniel von Renteln 0000-0002-6125-0068.

**S-Editor:** Ma YJ

L-Editor: A

P-Editor: Ma YJ

---

**REFERENCES**


---

- 1 **Pohl H**, Anderson JC, Aguilera-Fish A, Calderwood AH, Mackenzie TA, Robertson DJ. Recurrence of Colorectal Neoplastic Polyps After Incomplete Resection. *Ann Intern Med* 2021; **174**: 1377-1384 [PMID: [34370514](#) DOI: [10.7326/M20-6689](#)]
- 2 **Hassan C**, Antonelli G, Dumonceau JM, Regula J, Bretthauer M, Chaussade S, Dekker E, Ferlitsch M, Gimeno-Garcia A, Jover R, Kalager M, Pellisé M, Pox C, Ricciardiello L, Rutter M, Helsingen LM, Bleijenberg A, Senore C, van Hoof JE, Dinis-Ribeiro M, Quintero E. Post-polypectomy colonoscopy surveillance: European Society of Gastrointestinal Endoscopy (ESGE) Guideline - Update 2020. *Endoscopy* 2020; **52**: 687-700 [PMID: [32572858](#) DOI: [10.1055/a-1185-3109](#)]
- 3 **Gupta S**, Lieberman D, Anderson JC, Burke CA, Dominitz JA, Kaltenbach T, Robertson DJ, Shaikat A, Syngal S, Rex DK. Recommendations for Follow-Up After Colonoscopy and Polypectomy: A Consensus Update by the US Multi-Society Task Force on Colorectal Cancer. *Gastrointest Endosc* 2020; **91**: 463-485.e5 [PMID: [32044106](#) DOI: [10.1016/j.gie.2020.01.014](#)]
- 4 **Pohl H**, Srivastava A, Bensen SP, Anderson P, Rothstein RI, Gordon SR, Levy LC, Toor A, Mackenzie TA, Rosch T, Robertson DJ. Incomplete polyp resection during colonoscopy-results of the complete adenoma resection (CARE) study. *Gastroenterology* 2013; **144**: 74-80.e1 [PMID: [23022496](#) DOI: [10.1053/j.gastro.2012.09.043](#)]
- 5 **Djinbanchian R**, Itratni R, Durand M, Marques P, von Renteln D. Rates of Incomplete Resection of 1- to 20-mm Colorectal Polyps: A Systematic Review and Meta-Analysis. *Gastroenterology* 2020; **159**: 904-914.e12 [PMID: [32437747](#) DOI: [10.1053/j.gastro.2020.05.018](#)]
- 6 **Belderbos TD**, Leenders M, Moons LM, Siersema PD. Local recurrence after endoscopic mucosal resection of nonpedunculated colorectal lesions: systematic review and meta-analysis. *Endoscopy* 2014; **46**: 388-402 [PMID: [24671869](#) DOI: [10.1055/s-0034-1364970](#)]
- 7 **Thoguluva Chandrasekar V**, Spadaccini M, Aziz M, Maselli R, Hassan S, Fuccio L, Duvvuri A, Frazzoni L, Desai M, Fugazza A, Jegadeesan R, Colombo M, Dasari CS, Hassan C, Sharma P, Repici A. Cold snare endoscopic resection of nonpedunculated colorectal polyps larger than 10 mm: a systematic review and pooled-analysis. *Gastrointest Endosc* 2019; **89**: 929-936.e3 [PMID: [30639542](#) DOI: [10.1016/j.gie.2018.12.022](#)]
- 8 **Binmoeller KF**, Weilert F, Shah J, Bhat Y, Kane S. "Underwater" EMR without submucosal injection for large sessile colorectal polyps (with video). *Gastrointest Endosc* 2012; **75**: 1086-1091 [PMID: [22365184](#) DOI: [10.1016/j.gie.2011.12.022](#)]
- 9 **Klein A**, Tate DJ, Jayasekaran V, Hourigan L, Singh R, Brown G, Bahin FF, Burgess N, Williams SJ, Lee E, Sidhu M, Byth K, Bourke MJ. Thermal Ablation of Mucosal Defect Margins Reduces Adenoma Recurrence After Colonic Endoscopic Mucosal Resection. *Gastroenterology* 2019; **156**: 604-613.e3 [PMID: [30296436](#) DOI: [10.1053/j.gastro.2018.10.003](#)]
- 10 **Page MJ**, McKenzie JE, Bossuyt PM, Boutron I, Hoffmann TC, Mulrow CD, Shamseer L, Tetzlaff JM, Akl EA, Brennan SE, Chou R, Glanville J, Grimshaw JM, Hróbjartsson A, Lalu MM, Li T, Loder EW, Mayo-Wilson E, McDonald S, McGuinness LA, Stewart LA, Thomas J, Tricco AC, Welch VA, Whiting P, Moher D. The PRISMA 2020 statement: An updated guideline for reporting systematic reviews. *J Clin Epidemiol* 2021; **134**: 178-189 [PMID: [33789819](#) DOI: [10.1016/j.jclinepi.2021.03.001](#)]
- 11 **National Institutes of Health**. NIH Study Quality Assessment Tool 2021. Available from: <https://www.nhlbi.nih.gov/health-topics/study-quality-assessment-tools>
- 12 **Hunter JP**, Saratzis A, Sutton AJ, Boucher RH, Sayers RD, Bown MJ. In meta-analyses of proportion studies, funnel plots were found to be an inaccurate method of assessing publication bias. *J Clin Epidemiol* 2014; **67**: 897-903 [PMID: [24794697](#) DOI: [10.1016/j.jclinepi.2014.03.003](#)]
- 13 **Woodward T**, Crook JE, Raimondo M, Wallace M. Improving complete EMR of colorectal neoplasia: a randomized trial comparing snares and injectate in the resection of large sessile colon polyps. *Gastrointest Endosc* 2015; **81**: 673-681 [PMID: [25708754](#) DOI: [10.1016/j.gie.2014.10.010](#)]
- 14 **Pellise M**, Burgess NG, Tutticci N, Hourigan LF, Zanati SA, Brown GJ, Singh R, Williams SJ, Raftopoulos SC, Ormonde D, Moss A, Byth K, P'Ng H, Mahajan H, McLeod D, Bourke MJ. Endoscopic mucosal resection for large serrated lesions in comparison with adenomas: a prospective multicentre study of 2000 lesions. *Gut* 2017; **66**: 644-653 [PMID: [26786685](#) DOI: [10.1136/gutjnl-2015-310249](#)]
- 15 **Han SJ**, Jung Y, Cho YS, Chung IK, Kim JY, Eun JY, Lee SH, Ko GB, Lee TH, Park SH, Cho HD, Kim SJ. Clinical Effectiveness of Submucosal Injection with Indigo Carmine Mixed Solution for Colon Endoscopic Mucosal Resection. *Dig Dis Sci* 2018; **63**: 775-780 [PMID: [29383606](#) DOI: [10.1007/s10620-018-4918-6](#)]
- 16 **Yoshida N**, Saito Y, Hirose R, Ogiso K, Inada Y, Yagi N, Naito Y, Otake Y, Nakajima T, Matsuda T, Yanagisawa A, Itoh Y. Endoscopic mucosal resection for middle and large colorectal polyps with a double-loop snare. *Digestion* 2014; **90**: 232-239 [PMID: [25532080](#) DOI: [10.1159/000368044](#)]
- 17 **Li D**, Wang W, Xie J, Liu G, Wang R, Jiang C, Ye Z, Xu B, He X, Hong D. Efficacy and safety of three different endoscopic methods in treatment of 6-20 mm colorectal polyps. *Scand J Gastroenterol* 2020; **55**: 362-370 [PMID: [32150478](#) DOI: [10.1080/00365521.2020.1732456](#)]
- 18 **Yabuuchi Y**, Imai K, Hotta K, Ito S, Kishida Y, Yoshida M, Kawata N, Kakushima N, Takizawa K, Ishiwatari H, Matsubayashi H, Aizawa D, Oishi T, Imai T, Ono H. Efficacy and safety of cold-snare endoscopic mucosal resection for colorectal adenomas 10 to 14 mm in size: a prospective observational study. *Gastrointest Endosc* 2020; **92**: 1239-1246 [PMID: [32464143](#) DOI: [10.1016/j.gie.2020.05.019](#)]

- 19 **Draganov PV**, Aihara H, Karasik MS, Ngamruengphong S, Aadam AA, Othman MO, Sharma N, Grimm IS, Rostom A, Elmunzer BJ, Jawaid SA, Westerveld D, Perbtani YB, Hoffman BJ, Schlachterman A, Siegel A, Coman RM, Wang AY, Yang D. Endoscopic Submucosal Dissection in North America: A Large Prospective Multicenter Study. *Gastroenterology* 2021; **160**: 2317-2327.e2 [PMID: [33610532](#) DOI: [10.1053/j.gastro.2021.02.036](#)]
- 20 **Yamashina T**, Uedo N, Akasaka T, Iwatsubo T, Nakatani Y, Akamatsu T, Kawamura T, Takeuchi Y, Fujii S, Kusaka T, Shimokawa T. Comparison of Underwater vs Conventional Endoscopic Mucosal Resection of Intermediate-Size Colorectal Polyps. *Gastroenterology* 2019; **157**: 451-461.e2 [PMID: [30981791](#) DOI: [10.1053/j.gastro.2019.04.005](#)]
- 21 **Kimoto Y**, Sakai E, Inamoto R, Kurebayashi M, Takayanagi S, Hirata T, Suzuki Y, Ishii R, Konishi T, Kanda K, Negishi R, Takita M, Ono K, Minato Y, Muramoto T, Ohata K. Safety and Efficacy of Cold Snare Polypectomy Without Submucosal Injection for Large Sessile Serrated Lesions: A Prospective Study. *Clin Gastroenterol Hepatol* 2022; **20**: e132-e138 [PMID: [33152541](#) DOI: [10.1016/j.cgh.2020.10.053](#)]
- 22 **Tutticci NJ**, Hewett DG. Cold EMR of large sessile serrated polyps at colonoscopy (with video). *Gastrointest Endosc* 2018; **87**: 837-842 [PMID: [29133196](#) DOI: [10.1016/j.gie.2017.11.002](#)]
- 23 **Lim XC**, Nistala KRY, Ng CH, Lin SY, Tan DJH, Ho KY, Chong CS, Muthiah M. Endoscopic submucosal dissection vs endoscopic mucosal resection for colorectal polyps: A meta-analysis and meta-regression with single arm analysis. *World J Gastroenterol* 2021; **27**: 3925-3939 [PMID: [34321855](#) DOI: [10.3748/wjg.v27.i25.3925](#)]
- 24 **Fuccio L**, Hassan C, Ponchon T, Mandolesi D, Farioli A, Cucchetti A, Frazzoni L, Bhandari P, Bellisario C, Bazzoli F, Repici A. Clinical outcomes after endoscopic submucosal dissection for colorectal neoplasia: a systematic review and meta-analysis. *Gastrointest Endosc* 2017; **86**: 74-86.e17 [PMID: [28254526](#) DOI: [10.1016/j.gie.2017.02.024](#)]
- 25 **Tanaka S**, Kashida H, Saito Y, Yahagi N, Yamano H, Saito S, Hisabe T, Yao T, Watanabe M, Yoshida M, Saitoh Y, Tsuruta O, Sugihara KI, Igarashi M, Toyonaga T, Ajioka Y, Kusunoki M, Koike K, Fujimoto K, Tajiri H. Japan Gastroenterological Endoscopy Society guidelines for colorectal endoscopic submucosal dissection/endoscopic mucosal resection. *Dig Endosc* 2020; **32**: 219-239 [PMID: [31566804](#) DOI: [10.1111/den.13545](#)]
- 26 **Draganov PV**, Wang AY, Othman MO, Fukami N. AGA Institute Clinical Practice Update: Endoscopic Submucosal Dissection in the United States. *Clin Gastroenterol Hepatol* 2019; **17**: 16-25.e1 [PMID: [30077787](#) DOI: [10.1016/j.cgh.2018.07.041](#)]
- 27 **Daoud DC**, Suter N, Durand M, Bouin M, Faulques B, von Renteln D. Comparing outcomes for endoscopic submucosal dissection between Eastern and Western countries: A systematic review and meta-analysis. *World J Gastroenterol* 2018; **24**: 2518-2536 [PMID: [29930473](#) DOI: [10.3748/wjg.v24.i23.2518](#)]
- 28 **Sidhu M**, Shahidi N, Gupta S, Desomer L, Vosko S, Arnout van Hattem W, Hourigan LF, Lee EYT, Moss A, Raftopoulos S, Heitman SJ, Williams SJ, Zanati S, Tate DJ, Burgess N, Bourke MJ. Outcomes of Thermal Ablation of the Mucosal Defect Margin After Endoscopic Mucosal Resection: A Prospective, International, Multicenter Trial of 1000 Large Nonpedunculated Colorectal Polyps. *Gastroenterology* 2021; **161**: 163-170.e3 [PMID: [33798525](#) DOI: [10.1053/j.gastro.2021.03.044](#)]
- 29 **Raju GS**, Lum P, Abu-Sbeih H, Ross WA, Thirumurthi S, Miller E, Lynch P, Lee J, Bhutani MS, Shafi M, Weston B, Rashid A, Wang Y, Chang GJ, Carlson R, Hagan K, Davila M, Stroehlein J. Cap-fitted endoscopic mucosal resection of  $\geq 20$  mm colon flat lesions followed by argon plasma coagulation results in a low adenoma recurrence rate. *Endosc Int Open* 2020; **8**: E115-E121 [PMID: [32010742](#) DOI: [10.1055/a-1012-1811](#)]
- 30 **Motchum L**, Levenick J, Djinbanchian R, Moyer M, Bouchard S, Taghiakbari M, Repici A, Deslandres E, Renteln D von. Endoscopic mucosal resection combined with hybrid argon plasma coagulation to prevent recurrence of large nonpedunculated colorectal polyps. *Gastrointestinal Endoscopy*, under Revision 2022 [PMID: [35724695](#) DOI: [10.1016/j.gie.2022.06.018](#)]
- 31 **Pohl H**, Grimm IS, Moyer MT, Hasan MK, Pleskow D, Elmunzer BJ, Khashab MA, Sanaei O, Al-Kawas FH, Gordon SR, Mathew A, Levenick JM, Aslanian HR, Antaki F, von Renteln D, Crockett SD, Rastogi A, Gill JA, Law RJ, Elias PA, Pellise M, Mackenzie TA, Rex DK. Effects of Blended (Yellow) vs Forced Coagulation (Blue) Currents on Adverse Events, Complete Resection, or Polyp Recurrence After Polypectomy in a Large Randomized Trial. *Gastroenterology* 2020; **159**: 119-128.e2 [PMID: [32173478](#) DOI: [10.1053/j.gastro.2020.03.014](#)]
- 32 **Suresh S**, Zhang J, Ahmed A, Abu Ghanimeh M, Elbanna A, Kaur R, Isseh M, Watson A, Dang DT, Chathadi KV, Pompa R, Singla S, Piraka C, Zuchelli T. Risk factors associated with adenoma recurrence following cold snare endoscopic mucosal resection of polyps  $\geq 20$  mm: a retrospective chart review. *Endosc Int Open* 2021; **9**: E867-E873 [PMID: [34079869](#) DOI: [10.1055/a-1399-8398](#)]
- 33 **Ferlitsch M**, Moss A, Hassan C, Bhandari P, Dumonceau JM, Paspatis G, Jover R, Langner C, Bronzwaer M, Nalankilli K, Fockens P, Hazzan R, Gralnek IM, Gschwantler M, Waldmann E, Jeschek P, Penz D, Heresbach D, Moons L, Lemmers A, Paraskeva K, Pohl J, Ponchon T, Regula J, Repici A, Rutter MD, Burgess NG, Bourke MJ. Colorectal polypectomy and endoscopic mucosal resection (EMR): European Society of Gastrointestinal Endoscopy (ESGE) Clinical Guideline. *Endoscopy* 2017; **49**: 270-297 [PMID: [28212588](#) DOI: [10.1055/s-0043-102569](#)]
- 34 **Kaltenbach T**, Anderson JC, Burke CA, Dominitz JA, Gupta S, Lieberman D, Robertson DJ, Shaikat A, Syngal S, Rex DK. Endoscopic Removal of Colorectal Lesions-Recommendations by the US Multi-Society Task Force on Colorectal Cancer. *Gastroenterology* 2020; **158**: 1095-1129 [PMID: [32122632](#) DOI: [10.1053/j.gastro.2019.12.018](#)]
- 35 **Pimentel-Nunes P**, Dinis-Ribeiro M, Ponchon T, Repici A, Vieth M, De Ceglie A, Amato A, Berr F, Bhandari P, Bialek A, Conio M, Haringsma J, Langner C, Meisner S, Messmann H, Morino M, Neuhaus H, Piessevaux H, Rugge M, Saunders BP, Robaszkiewicz M, Seewald S, Kashin S, Dumonceau JM, Hassan C, Deprez PH. Endoscopic submucosal dissection: European Society of Gastrointestinal Endoscopy (ESGE) Guideline. *Endoscopy* 2015; **47**: 829-854 [PMID: [26317585](#) DOI: [10.1055/s-0034-1392882](#)]
- 36 **Hassan C**, Repici A, Sharma P, Correale L, Zullo A, Bretthauer M, Senore C, Spada C, Bellisario C, Bhandari P, Rex DK. Efficacy and safety of endoscopic resection of large colorectal polyps: a systematic review and meta-analysis. *Gut* 2016; **65**: 806-820 [PMID: [25681402](#) DOI: [10.1136/gutjnl-2014-308481](#)]
- 37 **Djinbanchian R**, Renteln DV. Endoscopic Polypectomy: How Should We Determine Complete Resection Status? *Clin Gastroenterol Hepatol* 2022; **20**: 242-243 [PMID: [33309986](#) DOI: [10.1016/j.cgh.2020.12.006](#)]



Published by **Baishideng Publishing Group Inc**  
7041 Koll Center Parkway, Suite 160, Pleasanton, CA 94566, USA  
**Telephone:** +1-925-3991568  
**E-mail:** [bpgoffice@wjgnet.com](mailto:bpgoffice@wjgnet.com)  
**Help Desk:** <https://www.f6publishing.com/helpdesk>  
<https://www.wjgnet.com>

